Friedrich-Schiller-Universität Jena

Chemisch-Geowissenschaftliche Fakultät

Tailor-made polymers as nanocarriers for drug and gene delivery

Dissertation

(kumulativ)

zur Erlangung des akademischen Grades

doctor rerum naturalium (Dr. rer. nat.)

vorgelegt dem Rat der Chemisch-Geowissenschaftlichen Fakultät

der Friedrich-Schiller-Universität Jena

von Alexandra C. Rinkenauer

M.sc. Molecular Biology and Biochemistry

geboren am 04.06.1986 in Friedrichshafen

Gutachter:

1. Prof. Dr. Ulrich S. Schubert (Universität Jena)
2. Prof. Dr. Michael Bauer (Universitätsklinikum Jena)
3. Prof. Dr. Achim Göpferich (Universität Regensburg)

Tag der öffentlichen Verteidigung: 08.04.2016

Table of contents

Documentation of authorship

This section contains a list of the individual author contributions to the publications reprinted in this thesis.

P1)	A. C. Rinkenauer,[1] S. Schubert,[2] A. Taeger,[3] U. S. Schubert,[4] Influence of polymer architecture on *in vitro* pDNA delivery, *J. Mater. Chem. B* **2015**, *3*, 7477-7493.			
Author	**1**	**2**	**3**	**4**
Conceptual development	x			
Preparation of the manuscript	x			
Correction of the manuscript		x	x	x
Supervision of A. C. Rinkenauer			x	x
Proposed publication equivalent	0.5			

P2)	M. Wagner,[1] A. C. Rinkenauer,[2] A. Schallon,[3] U. S. Schubert,[4] Opposites attract: Influence of the molar mass branched poly(ethylene imine) on biophysical characteristics of siRNA-based polyplexes, *RSC Adv.* **2013**, *3*, 12774-12785.			
Author	**1**	**2**	**3**	**4**
Conceptual development	x		x	
Physico-chemical characterization	x			
Biological studies		x		
Preparation of the manuscript	x	x		
Correction of the manuscript			x	x
Supervision of M. Wagner			x	
Supervision of A. C. Rinkenauer			x	x
Proposed publication equivalent		0.5		

P3) A. C. Rinkenauer,[1#] L. Tauhardt,[2#] F. Wendler,[3] K. Kempe,[4] M. Gottschaldt,[5] A. Traeger,[6] U. S. Schubert,[7] A cationic poly(2-oxazonline) with high *in vitro* transfection efficiency identified by a library approach, *Macromol. Biosci.* **2015**, *15*, 414-425.

# Both authors contributed equally

Author	**1**	**2**	**3**	**4**	**5**	**6**	**7**
Conceptual development	x	x		x		x	
Polymer synthesis & characterization		x	x				
Biological studies	x						
Preparation of the manuscript	x	x					
Correction of the manuscript				x	x	x	x
Supervision of L. Tauhardt				x			
Supervision of A. C. Rinkenauer						x	x
Proposed publication equivalent	1.0						

P4) A. C. Rinkenauer,[1#] A. Vollrath,[2#] A. Schallon,[3] L. Tahuhardt,[4] K. Kempe,[5] S. Schubert,[6] D. Fischer,[7] U. S. Schubert,[8] Parallel high-throughput screening of polymer vectors for nonviral gene delivery: evaluation of structure-property relationships of transfection, *ACS Comb. Sci.* **2013**, *15*, 475-482.

# Both authors contributed equally

Author	**1**	**2**	**3**	**4**	**5**	**6**	**7**	**8**
Conceptual development	x	x	x					
Scientific discussion							x	
Polymer synthesis & characterization				x	x			
Biological studies	x							
Polyplex preparation & DLS measurement		x						
Preparation of the manuscript	x	x	x					
Correction of the manuscript				x	x	x	x	x
Supervision of A. Vollrath						x		x
Supervision of A. C. Rinkenauer			x					x
Proposed publication equivalent	1.0							

P5) A. C. Rinkenauer,[1] A. Schallon,[2] U. Günther,[3] M. Wagner,[4] E. Betthausen,[5] U. S. Schubert,[6] F. H. Schacher,[7] A paradigm change: Efficient transfection of human leukemia cells by stimuli-responsive multicompartment micelles, *ACS Nano* **2013**, *7*, 9624-9631.

Author	**1**	**2**	**3**	**4**	**5**	**6**	**7**
Conceptual development	x	x					x
Polymer synthesis & characterization					x		
Biological studies	x						
Cryo-TEM measurements			x				
AF4, ultracentrifugation, DLS, zeta potential				x			
Preparation of the manuscript	x	x					
Correction of the manuscript				x		x	x
Supervision of U. Günther							x
Supervision of A. C. Rinkenauer		x				x	
Proposed publication equivalent	1.0						

P6) M. J. Barthel,[1#] A. C. Rinkenauer,[2#] M. Wagner,[3] U. Mansfeld,[4] S. Höppner,[5] J. A. Czaplewska,[6] M. Gottschaldt,[7] A. Traeger,[8] F. H. Schacher,[9] U. S. Schubert,[10] Small but powerful: Co-assembly of polyether-based triblock terpolymer into sub-30 nm micelles and synergistic effects on cellular interactions, *Biomacromolecules* **2014**, *15*, 2426-2439.
# Both authors contributed equally

Author	**1**	**2**	**3**	**4**	**5**	**6**	**7**	**8**	**9**	**10**
Conceptual development	x	x						x	x	
Polymer synthesis & characterization	x									
Biological studies		x								
AF4, DLS, zeta potential, electrophoretic studies		x	x							
Cryo-TEM measurements				x	x					
Synthesis of acetylated thiogalatose						x				
Preparation of the manuscript	x	x								
Correction of the manuscript			x				x	x	x	x
Supervision of M. J. Barthel									x	x
Supervision of A. C. Rinkenauer								x		x
Proposed publication equivalent		0.5								

P7) T. Yildrim,[1] A. C. Rinkenauer,[2] C. Weber,[3] A. Traeger,[4] S. Schubert,[5] U. S. Schubert,[6] RAFT made methacrylate copolymers for reversible pH-responsive nanoparticles, *J. Polym. Sci. Part A: Polym. Chem.* **2015**, *53*, 2711-2721.

Author	**1**	**2**	**3**	**4**	**5**	**6**
Conceptual development	x			x	x	
Scientific discussions			x			
Polymer synthesis & characterization	x					
Biological studies		x				
Preparation of the manuscript	x					
Correction of the manuscript		x	x	x	x	x
Supervision of T. Yildrim					x	x
Supervision of A. C. Rinkenauer				x		x
Proposed publication equivalent		0.25				

P8) A. C. Rinkenauer,[1#] A. T. Press,[2#] M. Raasch,[3] C. Pietsch,[4] S. Schweizer,[5] S. Schwörer,[6] K. L. Rudolph,[7] A. Mosig,[8] M. Bauer,[9] A. Traeger,[10] U. S. Schubert,[11] Comparison of the uptake of methacrylate-based nanoparticles in static and dynamic *in vitro* systems as well as *in vivo*, *J. Controll. Release* **2015**, *216*, 158-168.
# Both authors contributed equally

Author	**1**	**2**	**3**	**4**	**5**	**6**	**7**	**8**	**9**	**10**	**11**
Conceptual development	x	x									
Scientific discussion								x		x	
Polymer synthesis & characterization				x							
Nanoparticle preparation & characterization	x			x	x						
In vitro investigations	x										
Dynamic cell culture			x								
In vivo investigations		x									
Preparation of the manuscript	x	x									
Correction of the manuscript			x	x	x	x	x	x	x	x	x
Supervision of A. T. Press									x		
Supervision of M. Raasch								x			
Supervision of A. C. Rinkenauer										x	x
Proposed publication equivalent	0.5										

Erklärung zu den Eigenanteilen des Promovenden/der Promovendin sowie der weiteren Doktoranden/Doktorandinnen als Koautoren an den Publikationen und Zweitpublikationsrechten bei einer kumulativen Dissertation

Für alle in dieser kumulativen Dissertation verwendeten Manuskripte liegen die notwendigen Genehmigungen der Verlage („Reprint permissions“) für die Zweitpublikation vor.

Die Co-Autoren der in dieser kumulativen Dissertation verwendeten Manuskripte sind sowohl über die Nutzung als auch über die oben angegebenen Eigenanteile informiert und stimmen dem zu.

Die Anteile der Co-Autoren an den Publikationen sind in den vorausgehenden Tabellen (Documentation of authorship) aufgeführt.

Ich bin mit der Abfassung der Dissertation als publikationsbasiert, d.h. kumulativ, einverstanden und bestätige die vorstehenden Angaben. Eine entsprechend begründete Befürwortung mit Angabe des wissenschaftlichen Anteils des Doktoranden/der Doktorandin an den verwendeten Publikationen werde ich parallel an den Rat der Fakultät der Chemisch-Geowissenschaftlichen Fakultät richten.

Prof. Dr. Ulrich S. Schubert ……2015 Jena_____

Alexandra C. Rinkenauer ……2015 Jena_____

1 Introduction

Over the last 30 years nanomedicine represents a rapidly growing new field of research. This arising topic is very promising as there is a relatively high chance for the translation into clinical trials.[1] Only symptomatic treatment of genetic disorders like cystic fibrosis, Parkinson or cancer is possible when hazarding the detrimental side effects. For instance, the enormous side effects of therapeutics due to off-target delivery represent a severe drawback. Nanocarriers represent an ideal approach to avoid such problems. They have the possibility by encapsulation to reduce side effects and further enhance the bioavailability of poorly soluble drugs. A mitotic inhibitor, Paclitaxel, shows a high potential as chemotherapeutics, but is restricted due to its low water solubility.[2] Nanocarriers can be applied for drug and gene delivery, whereas the distinction is mainly based on the differences of their chemical properties. As a consequence, the nanocarrier material has to show properties which fits to the delivered substrate. The delivery of drugs *via* nanocarriers can be achieved by various strategies, *e.g.* by encapsulation, covalent attachment or physical adsorption. In this thesis the focus will be on encapsulation strategies of hydrophobic drugs or drug models. Therein, spherical micelles and nanoparticles are frequently used, as they can provide a hydrophobic interior (Figure 1.1). On the other hand, gene delivery *via* nanocarriers can transport diverse nucleic acids, like small interfering RNA (siRNA) or plasmid DNA (pDNA). Besides physical differences of siRNA and pDNA like the size or flexibility, also the site of action in cells differs. In the case of siRNA, a suppression of the protein expression occurs on the mRNA level in the cytoplasm. pDNA encodes a specific sequence for a protein and results in protein production, starting with the transcription of the pDNA in the cell nuclei. For the delivery of pDNA *via* nanocarriers, which will be discussed in this thesis, cationic charges are required to provide a sufficient interaction with the negatively charged phosphates of the pDNA. In this case, cationic polymers as well as cationic micelles can be applied (Figure 1.1). The mainly used materials

for nanocarriers represent lipid and polymer based systems, whereas polymers show a high tuning potential as they can be synthesized with varying physical and chemical properties (*e.g.* architectures, monomer class and functionalization).[3, 4] The biological challenges for nanocarriers and different polymer features like architecture are described in detail in **Chapter 2**.

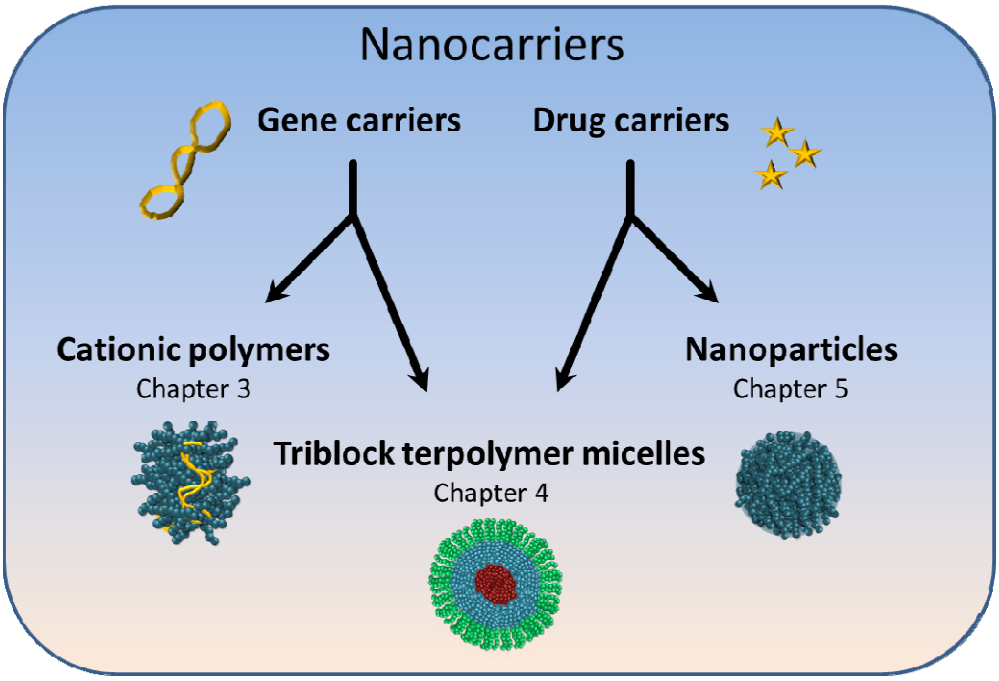

Figure 1.1: Schematic depiction of a possible subdivision of the nanocarriers discussed in this thesis.

Polymer-based gene delivery, also called transfection, is less pronounced in clinical trials in contrast to polymer-based drug delivery. A more detailed understanding of the transfection mechanism is necessary, starting from the impact of different polymer properties *in vitro*. In particular, cationic polymer systems like poly(ethylenimine) (PEI), poly(2-(dimethylamino)ethyl methacrylate (PDMAEMA) or poly(L-lysin) (PLL) are commonly used and well characterized concerning their delivery potential.[5] Herein, PEI represents the gold standard for polymer based transfection agents *in vitro*, due to high transfection efficiency and commercial availability.[6] However, PEI shows high cytotoxicity and reduced transfection efficiency compared to viruses, restricting the *in vivo* application. In the last years PEI is often used as template for numerous polymer modifications. For instance, the

functionalization with biocompatible polymers like poly(ethylene glycol) (PEG) or poly(2-oxazoline)s (POx) reduce the cytotoxicity and unspecific protein interactions.[7, 8] However, this benefit of PEGylated or POxylated polymers accompanies with a decreased efficiency.[8, 9] The opportunities to design tailor-made nanocarriers are manifold from the perspective of polymer chemistry. Varying the chain length, composition, functionalization, or architecture leads to different properties and, therefore, to other efficiencies. For example the effect of molar mass of polymers (chain length) was investigated in detail and was presented as one main aspect for an efficient pDNA delivery and a low cytotoxicity.[10] Detailed information concerning PEI as gene delivery agent and how to overcome the drawbacks of POx on cellular uptake are given in **Chapter 3**.

The polymer architecture and the self-assembled structures have an important role on the delivery performance; spherical micelles show a high potential for the delivery of pDNA as well as of drugs. The main polymer topology to self-assemble into highly ordered structures like spherical micelles is based on amphiphilic block copolymers. The ratio of the hydrophobic to hydrophilic segments is the driving force for self-assembly in aqueous solutions. The main application of spherical micelles as nanocarriers is the delivery of drugs, due to the fact that the hydrophobic interior represents an ideal environment for hydrophobic drugs.[11] In addition, the minor size of drugs allows the formation of spherical micelles with small diameters. Spherical micelles for pDNA delivery have to carry positive charges to enable the polyplex formation. Thus, the balance on charges represents a criterion, but it can be also a promising tool for efficient delivery. Triblock terpolymers are well suited for this requirement. In **Chapter 4** the application potential of triblock terpolymers-based spherical micelles will be discussed for gene and drug delivery by using 200 and 30 nm micelles, respectively.

Besides micelles also polymer-based nanoparticles represent promising systems as nanocarriers for drug delivery. Poly(lactic-*co*-glycolic acid) (PLGA), poly(ε-caprolactone)

(PCL) and poly(methyl methacrylate (PMMA) derivatives are frequently used polymer systems for nanoparticle preparation. Although, nanoparticles often enter clinical trials, the main challenge is the gap between the *in vitro* and *in vivo* behavior. In particular, *in vitro* screenings reveal no information concerning the biodistribution or interaction with the reticuloendothelial system (RES). The bloodstream induces mechanical force on endothelial cells, which are abundant in the inner layer of the blood vessels. This influences the cell biology like morphology, cytoskeleton, surface proteins, cellular interactions and, in the end, the nanoparticle uptake. A promising technique is the microfluidically-supported dynamic cell culture, which allows investigations concerning different shear stress. **Chapter 5** provides detailed information how methacrylate-based nanoparticles of different charges can be used as drug carrier to systematically investigate the differences of static and dynamic *in vitro* systems as well as *in vivo* models.

2 Biological challenges for polymer-based nanocarriers

Parts of this chapter have been published in: **P1)** A C. Rinkenauer, S. Schubert, A. Traeger, U. S. Schubert, Influence of polymer architecture on *in vitro* pDNA delivery, *J. Mater. Chem. B* **2015**, *3*, 7477-7493.

For the treatment of many different diseases with nanocarriers two main approaches can be pursued, namely drug and gene delivery. Herein, polymer-based nanocarriers show high potential, for example they can increase the bioavailability. Drugs and genes differ particularly in their chemical properties, which result in different requirements of the encapsulation strategies. In detail, drugs are small molecules either with hydrophobic or hydrophilic character: (i) Hydrophobic drugs can be encapsulated into nanoparticles and micelles, whereas, (ii) the encapsulation of hydrophilic drugs can be realized just in nanoparticles. The main differences between micelles and nanoparticles are the used polymers. Micelles are mainly formed by spontaneously self-organization of amphiphilic block copolymers. A defined and ordered inner structure can be achieved and their size depends directly on the polymer chain length. In contrast, nanoparticles are often based on hydrophobic homo- or statistical copolymers with hard spheres (between the water phase and the nanoparticle). The formation of defined nanoparticles is frequently realized *via* emulsification techniques and nanoprecipitation.[12, 13] In both cases spherical nanoparticles can be obtained with tunable sizes and small dispersities. The advantage of nanoprecipitation is the absence of surfactants, which are necessary for the stabilization of the nanoparticles prepared *via* the emulsion technique in aqueous solutions.[12] The double emulsion technique allows the encapsulation of hydrophilic drugs. The frequently used polymers for nanoparticle preparation, like PLGA, PCL and PMMA derivatives, are featured by a hydrophobic character (Figure 2.1).[14] In contrast to common drugs, the application of pDNA is limited in emulsification techniques, because the mechanical force by sonication and their exposure to organic solvent might damage the pDNA.[15] Therefore, pDNA delivery is based on the formation of complexes with electrostatic interactions, called polyplexes.

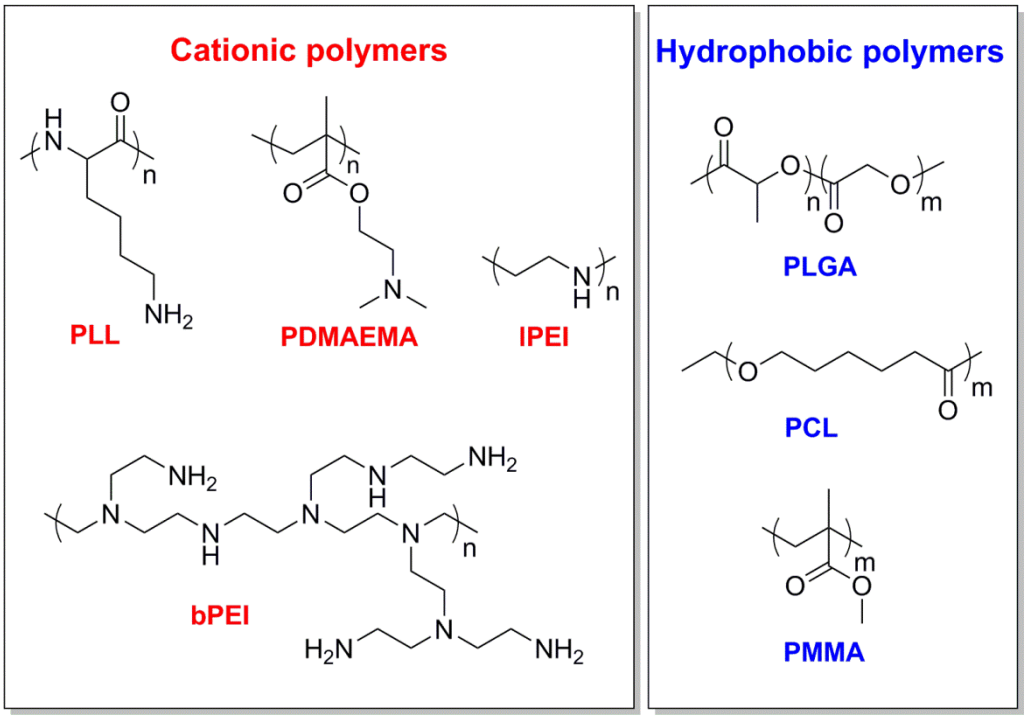

Figure 2.1: Schematic representation of the chemical structures of selected cationic and hydrophobic polymers (lPEI = linear PEI, bPEI = branched PEI).

In order to complex pDNA a polymer needs to contain cationic charges on the polymer chain; PEI, PLL as well as PDMAEMA represent the most frequently investigated cationic polymers (Figure 2.1). The formation of polyplexes between positive charged polymers and the negative charged pDNA is driven by the gain of entropy due to the release of the small counter ions.[16, 17] The binding capacity of the polymer represents an important factor, as a balance of strong binding for an enhanced polyplex stability under physiological conditions and a weak binding for the later release of the genetic material has to be carefully considered.[18]

After the formation of nanocarriers (drug carriers or polyplexes) the biological barriers have to be overcome (Figure 2.2). The interaction between the positive charged nanocarriers and the negative charged cell membrane is enhanced, if compared to the utilization of negative charged carriers. However, positive charges can induce membrane destabilization and subsequently mostly local, the destruction results in an increased cytotoxicity.[10, 19]

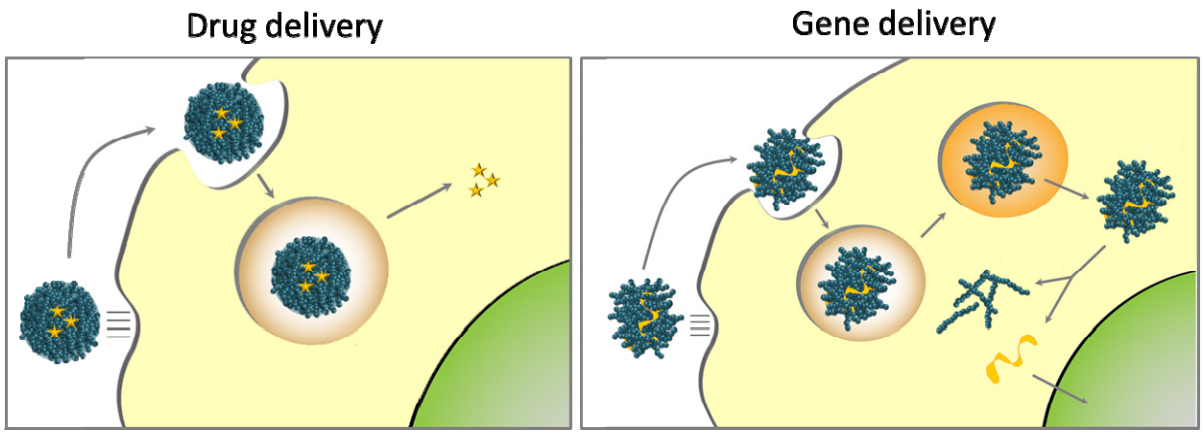

Figure 2.2: Schematic depiction of the delivery of genes or drugs *via* nanocarriers, *in vitro*.

The cellular interaction and internalization is mainly based on endocytosis[20] and this process is well–known to be size dependent and additionally varies between different cell types. In general, nanocarriers with diameters between 50 and 200 nm are taken up *via* endocytosis.[21] Up to now, the mechanisms underlying on endocytosis are in detail not fully understood and can be divided into phagocytosis, clathrin- and caveolin-mediated endocytosis as well as macropinocytosis.[20] Concerning the internalization of polyplexes, different uptake mechanisms and intracellular trafficking are observed, depending on the polymer class and structure.[22] For example, PEI polyplexes show caveolin- and clathrin-mediated endocytosis.[23] After efficient internalization *via* endocytosis, the nanocarriers have to escape from the endosome to prevent digestion in the lysosome or excretion by exocytosis.[24] In case of drug delivery the release of drugs from the nanocarrier can occur already in the endosome, because most hydrophobic drugs can passively diffuse through the endosomal membrane (Figure 2.2).[25] Subsequently, the drugs diffuse to their site of action like microtubule in case of Paclitaxel. Possible mechanisms to release drugs are the swelling of the nanoparticles or degradation of the polymer backbone.[26] On the other hand, pDNA is too large and charged for such passive diffusion, which makes an endosomal escape triggered by nanocarriers indispensable (Figure 2.2). Cationic polymers like PEI are known for its high buffer capacity. The caused influx of protons and chloride ions in the endosome leads to an osmotic swelling, resulting in a disruption of the endosomal membrane, named

proton sponge effect.[27-29] When the pDNA is released in the cytoplasm, it has to enter the cell nuclei for the transcription mechanism and efficient protein production. The mechanisms for polyplex dissociation and how the pDNA enters the cell nuclei are up to now only barely investigated.[30] There is evidence that the polyplex dissociation occurs at the same time as the endosomal release indicating a transfer of the pure pDNA into the nuclei.[31] In other studies polyplexes were also detected in the nuclei.[32] An increased transfection efficiency in cells with a high division rate was observed, confirming the entry of pDNA into the nuclei during mitosis.[33] However, it was shown that the entry of pDNA can occur through nuclear pores.[34] Since the first polymers were used as transfection agent numerous studies helped to understand the relying mechanism for most of the biological barriers. Concerning the polymer properties, different strategies and design rules were developed to overcome the transfection steps (Figure 2.3). For example the pKa value is one characteristic criterion of cationic polymers and is responsible for the degree of protonation, influencing the complexation behavior as well as the endosomal escape.[35] Figure 2.3 depicts an overview of general polymer features showing an influence on the pDNA delivery performance of cationic polymers.

Figure 2.3: Overview of set screws of selected polymer properties for an efficient pDNA delivery.

The complexity of the pDNA transfection mechanism results in defined requirements for the used polymers. For this purpose, living and controlled polymerization techniques like reversible addition-fragmentation chain transfer (RAFT) polymerization, cationic ring opening polymerization (CROP) or living anionic polymerization enable the synthesis of polymers in a controlled or living manner. Tailor-made polymers with defined chain length (degree of polymerization (DP)), composition, and architecture can be realized. In general, polymers can be classified by their composition and/or topology. Polymer compositions meaning the order of repeating units and can be divided into homopolymers, statistical, gradient-, alternated-, and block copolymers.[36, 37] In contrast to homopolymers, copolymers contain at least two different monomers. Copolymers can be beneficial in order to tune the polymer characteristics towards a high transfection and a low cytotoxicity. For instance, an increased polyplex stability of methacrylate-based polymers can be achieved by using

tertiary and primary amines in the same polymer chain.[38] These effects can be attributed to a higher charge density of the primary amines at physiological pH values. Furthermore, the copolymerization with hydrophobic monomers leads to an increased internalization efficiency and endosomal escape, resulting in enhanced transfection efficiency.[39] Concerning the tuning potential of polymers for drug delivery, the drug release of PLGA-based nanoparticles can be tuned by molar mass and the ratio of lactic to glycolic acid.[26] Regarding the polymer topology, a distinction is drawn between linear, branched, graft (combs and brushes), and star-shaped polymers. The most frequently used polymers for drug delivery have a linear topology. Branched polymers, like branched PEI (bPEI) or dendrimers, are composed of polymer chains with at least two branching points and more than four end-groups. Other topologies like graft polymers or star-shaped polymer represent an upcoming strategy for gene delivery.[40, 41] A further possibility is the formation of self-assembled structures of amphiphilic polymers in solution, meaning the arrangement into highly ordered structures by non-covalent interactions. For instance, spherical or worm-like micelles and vesicular structures can be realized and are applied as nanocarriers. The responsible principles for the mechanism of self-assembly depend on several factors starting from the used solvent to the block ratios.[42] Spherical micelles are often used for the delivery of hydrophobic drugs.[11] Concerning the micellar structures for pDNA delivery, it should be distinguished if preformed spherical micelles are used for polyplex formation or so called polyion complex (PIC) micelles are applied (Figure 2.4). In detail, a block copolymer can consist of a cationic and a hydrophilic segment which probably form polyplex micelles with pDNA due to electrostatical interactions (Figure 2.4a). Thus, the pDNA is located in the core and the hydrophilic part in the shell.[43] K. Kataoka firstly presented this concept of PIC micelles in 1990.[44, 45] Preformed micelles are only rarely used for pDNA delivery. The size of the micelle plays an important role, because two different polyplex formations can occur regarding the pDNA size (Figure 2.4b and c). Small micelles of around 20 nm in diameter probably results in polyplexes consisting of multiple micelles surrounding the pDNA (Figure

2.4c).[46] In contrast large micelles provide the opportunity that the pDNA is wrapped around in the shell (Figure 2.4b). A deeper insight is given in Chapter 4. Another study pointed out that larger micelles of around 200 nm show a higher transfection efficiency than 90 nm micelles. Herein, the question arises if the higher transfection efficiency can be attributed to the higher amount of cationic charges (based on the longer polymer chains) or to the micellar size and the resulting polyplex properties.[47]

Furthermore, micelles can provide pH responsive shape changes, which are – concerning biological applications – a promising strategy for an enhanced uptake or a low cytotoxicity. A fine-tuning of the pH dependent membrane destabilizing character can lead to an enhanced endosomal escape and a higher transfection efficiency.[46] In addition, the delivery of drugs and genes at the same time, called multidrug nanocarriers, can be realized by a hydrophobic core and a cationic shell. [38, 48, 49]

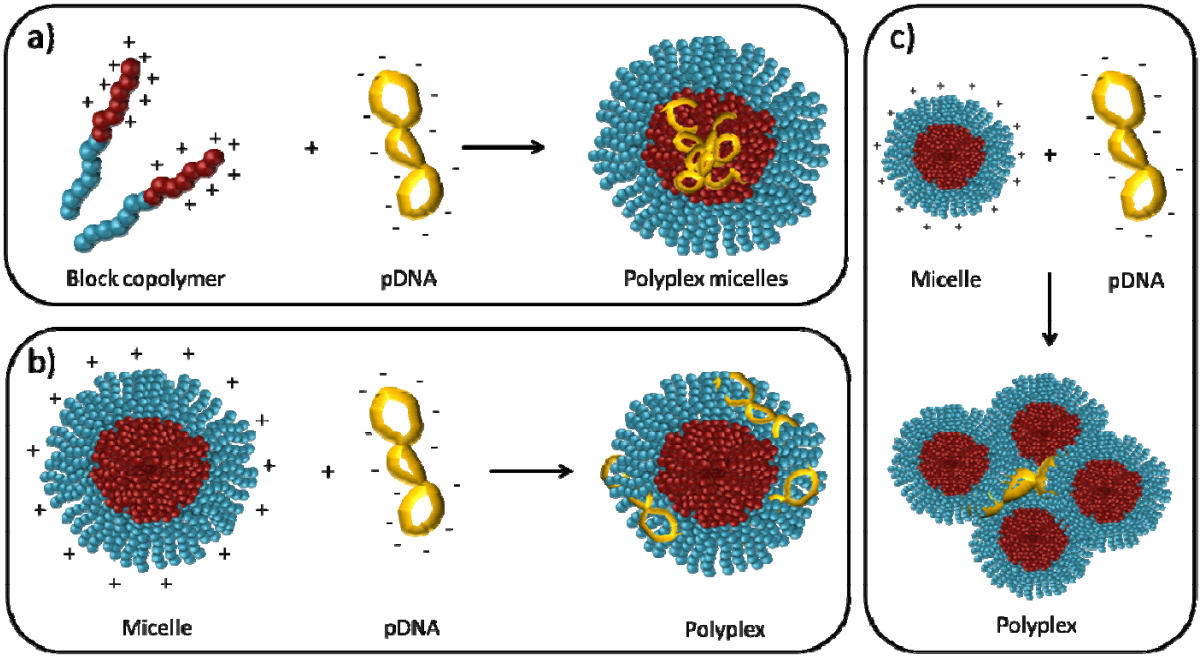

Figure 2.4: Polyplex micelles (a) *vs.* polyplexes formed with large (b) and small (c) preformed micelles and pDNA. (+) Represents the cationic charges of the block copolymers or the surface charges of the preformed micelles and (–) represents the negative charges of the pDNA.

Nowadays, nanoparticle-based drug delivery has the obstacles mainly *in vivo*, besides drug encapsulation efficiency and drug release. In particular, the biodistribution and bioavailability represent important factors and are influenced by the nanoparticle characteristics. The biodistribution is influenced by the RES because nanoparticles once in the blood circulation interact with various plasma proteins influencing their fate in different manner.[50] These factors are mainly influenced by the nanoparticle characteristics like particle size, surface charge, modification and hydrophobicity.[51]

3 Linear cationic polymers as nanocarriers for gene delivery

Parts of this chapter have been published in: **P2)** M. Wagner, A. C. Rinkenauer, A. Schallon, U. S. Schubert, Opposites attract: Influence of the molar mass branched poly(ethylene imine) on biophysical characteristics of siRNA-based polyplexes, *RSC Advances* **2013**, *3*, 12774-12785; **P3)** A. C. Rinkenauer, L. Tauhardt, F. Wendler, K. Kempe, M. Gottschaldt, A. Traeger, U. S. Schubert, A cationic poly(2-oxazonline) with high *in vitro* transfection efficiency identified by a library approach, *Macromol. Biosci.* **2015**, *15*, 414-425; **P4)** A. C. Rinkenauer, A. Vollrath, A. Schallon, L. Tauhardt, K. Kempe, S. Schubert, D. Fischer, U. S. Schubert, Parallel high-throughput screening of polymer vectors for nonviral gene delivery: Evaluation of strucutre-property relationships of transfection, *ACS Comb. Sci.* **2013**, *15*, 475-482.

Nanocarriers for gene delivery based on cationic polymers have to combine low cytotoxicty and high transfection efficiency.[52, 53] PEI represents the most intensively applied agent for pDNA delivery, in particular for *in vitro* investigations. The high transfection efficiency and commercial availability of branched and linear PEI are the main reasons for this dominance.[54] In addition, a wide range of molar masses are available. The above mentioned reasons lead to the application of PEI as control polymer, beside other commercial transfection agents like Lipofectamine (liposome based) or FuGENE (dendrimer based). However, PEI shows cytotoxic effects and, therefore, some modifications with other polymers like PEG or POx were realized and investigated. These modifications lead to a negative impact on the transfection efficiency, which implies further modifications like the introduction of hydrophobic moieties into the polymer chain. PEI is excelled by its high charge density due to the high amino content. In contrast to lPEI (only secondary amines), bPEI contains primary, secondary and tertiary amines.[55, 56] It is known that the architecture, with respect to the different amino types, as well as the molar mass influence the transfection efficiency. However, more insights into the performance during the single transfections steps are necessary. In a first step, the polyplex formation of diverse PEIs was investigated and in general high molar masses bPEIs (≥ 10 kDa) show an enhanced complexation ability, compared to high molar masses lPEI (≥ 10 kDa). This can be

attributed to the presence of primary amines in bPEI, due to the fact that these amino types show an enhanced pDNA interaction/complexation.[57] The impact of the molar mass is evidenced by an insufficient polyplex formation either due to the inability to complex pDNA or to the reduced polyplex stability in the presence of heparin in the case of low molar mass PEI (< 10 kDa). Another criterion is the escape from the endosome; PEI is known for its good buffer capacity due to the proton sponge effect. With regard to this, the pKa values of different molar mass bPEI were investigated (Figure 3.1a). The pKa values of bPEI decrease slightly from 10 to 8 with increasing molar mass. In detail, the high molar mass bPEI (10 and 25 kDa) differ from the low molar mass bPEIs. However, the buffer capacity at pH values around 7 is similar for all polymers. Furthermore, no significant differences between bPEI 25kDa (pKa 8.3) and lPEI 25kDa (pKa 8.6) are reported.[55]

The cytotoxicity represents one crucial characteristic for a transfection agent. Herein, the molar mass shows a high impact; with increasing molar mass the cytotoxicity increases (Figure 3.1b). The molar masses influence also the transfection efficiency. Low molar mass PEI show lower transfection efficiency compared to high molar mass PEI independent on the used architecture.

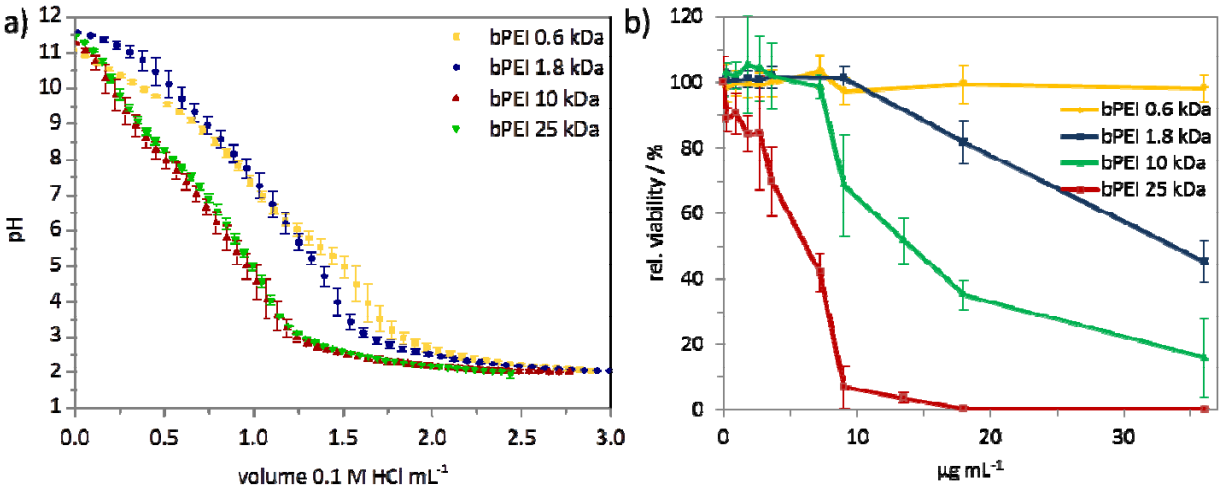

Figure 3.1: Titration curve of bPEI of different molar masses in water against HCl (a) and cytotoxicity of different bPEI at various end concentrations (b).

The main requirements for transfection agents are an efficient delivery, combined with a low cytotoxicity. High molar mass PEI reveals cytotoxic effects at concentrations around 10 µg mL^{-1} (Figure 6b). An often used approach to overcome this drawback is the functionalization with biocompatible compounds like PEG or POx. Both polymers are known for the so called "stealth effect".[7, 8] The resulting copolymers lead to an enhanced permeability and retention *in vivo* as well as a reduced cytotoxicity. POx, in particular poly(2-ethyl-2-oxazoline), (PEtOx) and poly(2-methyl-2-oxazoline), (PMeOx), have been intensively investigated as PEG alternative. However, it was demonstrated that the functionalization with hydrophilic POx can also result in an inefficient delivery, due to a reduced interaction with the genetic material as well as the cellular membranes caused by the cell- and protein-repellent character of the polymers.[8] One possibility to increase the pDNA interaction as well as cellular uptake is the introduction of hydrophobic groups.[39] In order to investigate the influence of hydrophobicity and amino type (primary *versus* tertiary) in a systematically way, a library of POx copolymer was synthesized. In total 18 statistical copolymers either based on poly((2-methyl-2-oxazoline)-*co*-(2-(3-butenyl)-2-oxazoline), (P(MeOx-*co*-ButEnOx)) or poly((2-methyl-2-oxazoline)-*co*-(2-(9-decenyl)-2-oxazoline), (P(MeOx-*co*-DecEnOx)) were synthesized, varying the amount of hydrophobic content of 10, 20, 30 and 40 mol% (Figure 3.2). A DP of 200 was chosen to achieve a successful pDNA complexation. The cationic character, required for pDNA binding, was acquired by functionalization of ButEnOx or DecEnOx with either primary or tertiary amine (Figure 3.2). The library was then systematically investigated with regard to: (i) The ability to form stable polyplexes, (ii) the cytotoxicty and (iii) the transfection efficiency.

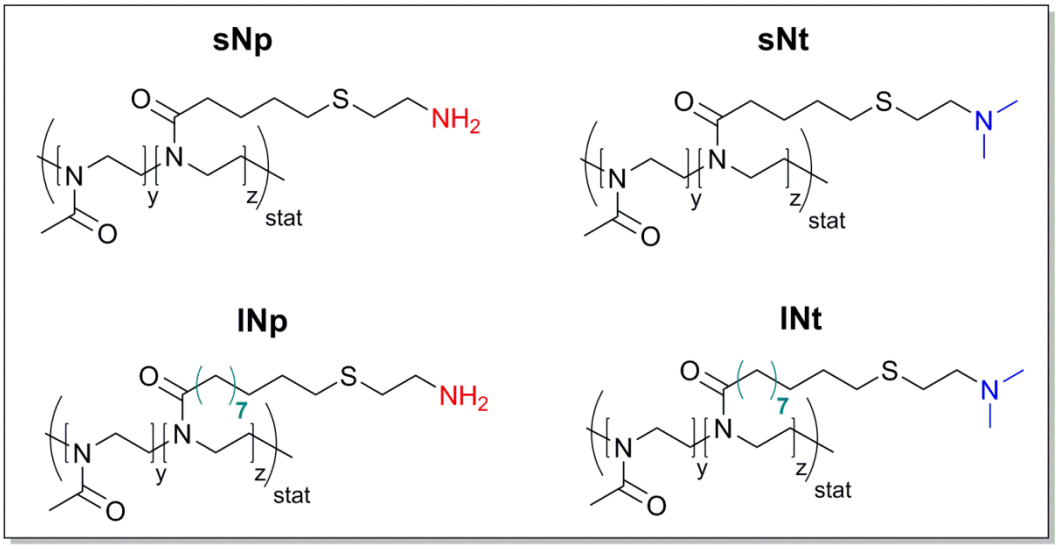

Figure 3.2: Schematic representation of the chemical structures of the poly(oxazolines) library based on functionalized P(MeOx-*co*-ButEnOx)$_{stat}$ and P(MeOx-*co*-DecEnOx)$_{stat}$. Product terms: s = short butyl side chain, l = long decenyl side chain, N = amino content in mol%, p = primary amine, t = tertiary amine.

The ability to form polyplexes was investigated *via* ethidium bromide exclusion assay (EBA)[58] and physiochemical analysis like dynamic light scattering (DLS) and zeta potential measurements. In case of the EBA, all 18 polymers lead to a decrease in ethidium bromide (EB) fluorescence intensity, indicating polyplex formation (Figure 3.3). The following structure-activity relationships could be observed: (i) For the longer side chains the amino type shows a high impact on the polyplex formation (primary amines leads to an increased exclusion of EB), (ii) the amount of amines and the degree of hydrophobicity correlates with the pDNA condenstation, (iii) polymers with longer side chain increase the pDNA complexation. Based on the obtained data the impact of hydrophobicity is more pronounced as compared to the amino type. With regard to the size and zeta potential all polymers show a positive zeta potential and acceptable sizes, except the copolymers with 10 mol% indicating an insufficient polyplex formation (Figure 3.3). The reasons for that behavior are the low amino contents.

Another investigated parameter is the polyplex stability, where an optimum between strong and weak binding has to be found. This can be analyzed with negatively charged heparin that competes against the pDNA binding. Compared to the polyplexes formed of polymers

with short side chains (**sNp** and **sNt**), the ones of long side chain (**INp** and **INt**) are more stable, as indicated by the higher used heparin concentrations to release the pDNA (Figure 3.3). This is in particular the case for **I40p**, where 50 U mL^{-1} of heparin is required to dissociate the polyplexes, which correlates with the strong pDNA condensation. In contrast, the **s40p** polyplexes release the pDNA already at heparin concentration of 10 U mL^{-1}. This indicates a stronger binding of **I40p** and could result in an inefficient release of pDNA in the cytoplasm and, probably, a low transfection efficiency. It was further found that for **sNt** and **INt** polyplexes a low amount of heparin is necessary for polyplex dissociation compared to their counterparts with primary amines. This is another indication that the interaction of the genetic material with polymers with tertiary amines are weaker and that the polymers are probably not able to protect the pDNA from degradation.

		mol%	EBA [%]	Size [nm]	ZP [mV]	Toxic	Hemolytic	LDH-Release	Uptake [%]	Heparin [U mg^{-1}]	TE [%]	comments
Short hydrophobic side chain (x = 1)	primary amines	10	80	255	-4	no	no	-	-	0	0	no polyplex formation
		20	72	178	22	no	no	-	-	3	8	labile polyplex
		30	72	110	40	no	no	-	-	10	6	low TE
		40	60	94	23	no	no	no	90	10	31	**best performer!**
		50	60	51	47	yes	-	-	-	30	24	increased toxicity
	teriary amines	10	82	151	-6	no	no	-	-	0	1	no polyplex formation
		20	68	158	19	no	no	-	-	3	8	labile polyplex
		30	64	124	29	no	no	-	-	5	5	low TE
		40	57	105	29	no	no	no	60	5	3	inefficient uptake
x = 1		40	-	-	-	yes	-	-	-	-	8	hexamethylene spacer, toxic
Long hydrophobic side chain (x = 7)	primary amines	10	69	152	-17	yes	no	-	-	3	0	no polyplex formation
		20	46	105	28	yes	yes	-	-	10	6	toxic
		30	36	84	29	yes	yes	-	-	20	4	toxic
		40	30	97	34	yes	yes	yes	80	50	6	toxic
	teriary amines	10	76	152	-9	no	no	-	-	0	0	no polyplex formation
		20	60	113	26	yes	yes	-	-	10	3	toxic
		30	50	84	30	yes	yes	-	-	20	6	toxic
		40	41	67	27	yes	yes	yes	-	20	2	toxic
LPEI200			45	-	-	yes	-	no	90	-	31	good performer but toxic

Figure 3.3: Overview of all copolymers regarding their characteristics and bottlenecks for the transfection process. Probable reasons for transfection failure or drawbacks are described as comments.

Further investigations showed that **sNp** and **sNt** polymers have no cytotoxicity or hemolytic activity at the tested concentrations (Figure 3.3). In contrast, cytotoxic and hemolytic effects were observed for polymers with long side chains (**INp** and **INt**), showing furthermore a dependency on the amino content and the amino type. An increased amino

content leads to an increased cytotoxicity; the primary amine systems show higher cytotoxic effects. IC_{50} values of 4 to 14 µg mL^{-1} were obtained, meaning a comparable cytotoxicity to lPEI200 (lPEI DP = 200), (Figure 3.3). The hemolytic activity can be ascribed to strong membrane interactions of the more hydrophobic side chains leading to membrane destruction, as also reported elsewhere.[59] Due to their low amino/side chain content the **l10p** and **l10t** copolymers did not cause any hemolytic effect. All together, the results showed that the interaction between the polymers and membranes is much more influenced by the hydrophobic nature of the polymers than by the amino type and content. This is in accordance with the results of the pDNA condensation study (EBA). Moreover, the **lNp** copolymers are more hemolytic compared to **lNt**, which also indicates an enhanced interaction of primary amines with the negative cellular membrane or their proteins. In contrast to the **lNp** copolymers, where **l40p** showed a lower cytotoxicity than **l30p**, an increasing cytotoxicity with increasing amino content was observed for the **lNt** copolymers. The decreased toxicity of **l40p** might be caused by (electrostatic) interactions with serum components and will be investigated in further studies. In summary, the alkyl content and the hydrophobicity of the side chains showed again a high impact on the interaction of the polymers with cellular membranes.

Often, a paradigm exists, namely high transfection efficiency is associated with high cytotoxicity, which is *e.g.* the case for PEI. Interestingly, the polymer **s40p**, showed transfection efficiency (30.5 ± 7.6%) similar to lPEI (31.2 ± 1.7%) without cytotoxic effects, whereas all other polymers revealed lower transfection efficiencies (below 10%), (Figure 3.4). The comparable transfection efficiency of **s40p** and lPEI is surprising, since the same DP was used and, hence, **s40p** exhibits a much lower amino content (only 80 of 200 repeating units bear an amino group).

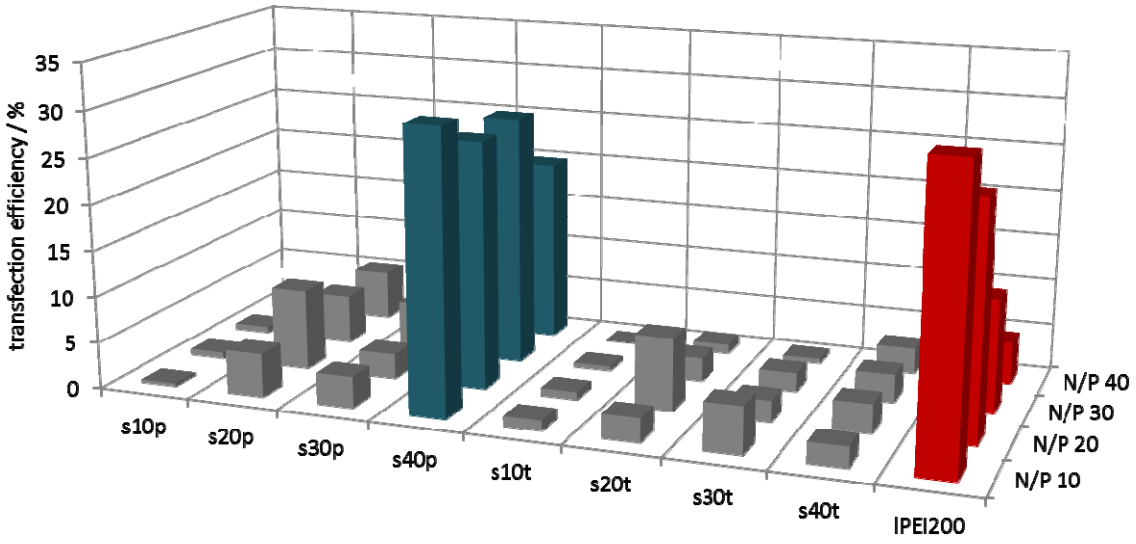

Figure 3.4: Transfection efficiency of all copolymers with short side chains (sNp and sNt) and lPEI200 for adherent HEK293 (human embryonic kidney) cells in serum reduced media at the indicated NP ratios. Values represent the mean (n = 3).

The question arises if higher amino contents over 40 mol% lead to a further increased transfection efficiency. Thus, a polymer with a short side chain and 50 mol% of primary amines was synthesized (**s50p**). Again, the transfection efficiency and the cytotoxicity were investigated. For this polymer (**s50p**), the transfection efficiency was slightly lower but showed no significant differences to the **s40p** polymer. However, it was cytotoxic at higher concentration, whereas no cytotoxicity was observed for **s40p** (Figure 3.4). Obviously, the polymer **s40p** represents an optimal combination of cationic charges, hydrophobicity and biocompatible monomers for an enhanced cellular interaction and a high transfection efficiency as well as a reduced cytotoxicity.

Based on a 18-membered 2-oxazoline-functionalized library the promising copolymer **s40p** was identified due to the screening of different parameter, such as the hydrophobicity, the type as well as the content of amino groups. It was found that independent of the amino content, long hydrophobic side chains enhance the pDNA condensation to the genetic material but interrupt the cellular membranes, leading to a higher cytotoxicity, hemolysis, and lactate dehydrogenase (LDH) release. POx with short side chains and an amino content

below 50 mol% were found to be biocompatible at all studied concentrations. In addition, primary amines are more suitable for an efficient polyplex formation and a high polyplex stability. Further investigations, like polyplex uptake or LDH release assay studies, provided more information for the possible failure of some polymers (Figure 3.3). All in all, the best performer **s40p** showed no cytotoxic effects and similar transfection efficiency to lPEI200.

This study demonstrates the importance to understand the interplay between different parameters for the development of non-toxic cationic polymers used as non-viral vectors in gene delivery applications. However, the screening of a polymer library is time consuming with standard techniques for the investigation of biological properties of polymers. Therefore, a high-throughput (HT) workflow for the investigation of cationic polymers for gene delivery applications would provide faster insights into structure-activity relationships, *e.g.* regarding the biological activity. For this purpose, various PEI polymers were used as representative cationic polymers and investigated *via* HT-assays in a 96-well plate format, starting from polyplex preparation up to the examination of the transfection process. In detail, automated polyplex preparation, complex size determination, DNA binding affinity, polyplex stability, cytotoxicity, and transfection efficiency were performed in the well plate format. The transfection efficiency of the polyplexes was quantified using EGFP as reporter protein in a fluorescence plate reader, allowing a fast and facile screening, in contrast to flow cytometry or microscopy (Figure 3.5a) The polymers can be ranked from high to low transfection efficiency: lPEI600 $>$ lPEI200 $>$ bPEI200 $>$ bPEI600 $>$ bPEI20 $>$ lPEI20 (numbers denote the DP), whereby the obvious increase in standard derivation compared to the flow cytometry measurements must be taken into account. Another example for the benefit of HT is the heparin assay: It can be used for 23 polymers at four different NP ratios resulting in 92 samples plus controls (n = 1). By using only one NP ratio, a further increase in polymer samples up to 30 (triplicate), 46 (duplicate), or 94 (single) is possible

(Figure 3.5b). The HT investigation showed trends and are eligible for a suitable approach to spot high potential candidates, which can subsequently be investigated in depth.

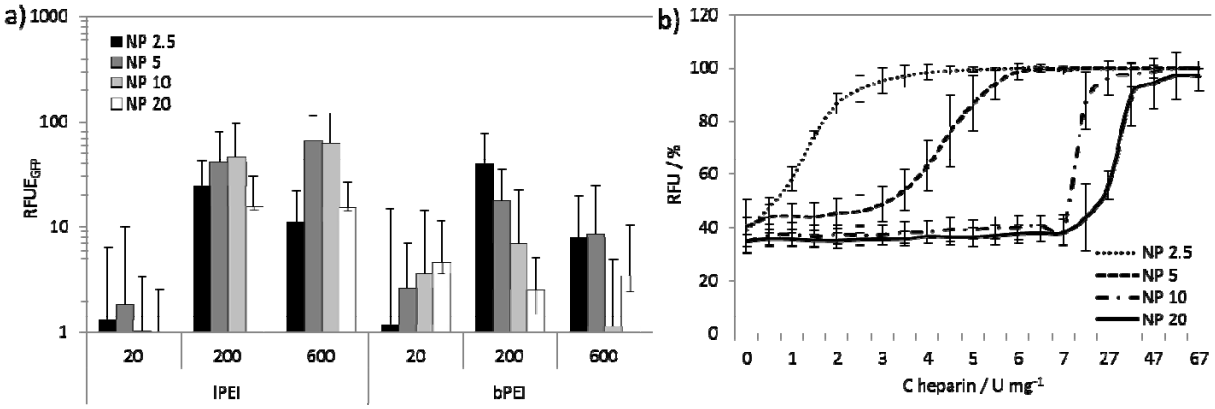

Figure 3.5: Transfection efficiency by fluorescence intensity measurements, HEK293 cells transfected with PEI of different molar mass and architecture (a). pDNA release of lPEI600 based polyplexes at different NP ratios after automated titration with heparin (b).

To proof whether the developed workflow is applicable for polymers systems or not, the obtained results were compared with literature and data obtained *via* the classical way (handmade). Furthermore, conditions enabling a fast and efficient screening in terms of important vector parameters, such as polyplex formation, transfection and release, were found. The possible screening of polymer libraries for the best transfection candidate will help to elucidate the main polymer characteristics and to understand why some polymers are high performers and others not. Thus, an enhanced development of more efficient polymers and polyplexes can be realized.

In summary, the characterization of PEI demonstrated the paradigm between transfection efficiency and cytotoxicity, particularly for high molar mass polymers. Combinations with POx-based copolymers, which are functionalized with hydrophobic and cationic moieties, were investigated regarding their delivery potential. By screening the copolymer library, one polymer was identified with superior performance, namely **s40p**, showing a low cytotoxicity and a high transfection efficiency. In addition, an HT approach was evaluated to allow a screening of such polymer libraries in a fast and efficient way.

4 Triblock terpolymer based micelles as nanocarriers

Parts of this chapter have been published in: **P5)** A C. Rinkenauer, A. Schallon, U. Günther, M. Wagner, E. Betthausen, U. S. Schubert, F. H. Schacher, A Paradigm Change: Efficient transfection of human leukemia cells by stimuli-responsive multicompartment micelles, *ACS Nano* **2013**, *7*, 9624-9631; **P6)** M. J. Barthel, A. C. Rinkenauer, M. Wagner, U. Mansfeld, S. Höppner, J. A. Czaplewska, M. Gottschaldt, A. Traeger, F. H. Schacher, U. S. Schubert, Small but powerful: Co-assembly of polyether-based triblock terpolymer into sub-30 nm micelles and synergistic effects on cellular interactions, *Biomacromolecules* **2014**, *15*, 2426-2439.

The most frequently used nanocarriers for drug and gene delivery represent nanoparticles and linear cationic polymers, respectively. However, the self-assembly of amphiphilic block copolymers into micellar structures of defined size, shape, and composition is a further active field of research.[42, 60, 61] Triblock terpolymers represent an ideal platform to study the biological applications of self-assembled multicompartment micelles. This topology is also favored for the introduction of different functionalities, like amino or carboxy groups, to achieve a stimuli-responsive behavior. The subdivision of the micelle into core, shell and corona allows the usage of simultaneously loading with different payloads like drugs or pDNA.[62] Typically, each segment of the ABC triblock terpolymers is attributed to a specific "task" in solution: The first block A often represents a hydrophobic segment leading to an amphiphilic character together with the blocks B and C, which are also used to achieve stimuli-responsive behavior or allow the introduction of different functionalizations, *e.g.* PEGylation (Figure 4.1). The size of the spherical micelles can be tuned by the polymer chain length. The here used polymers with low DP results in small micelles of around 30 nm, whereas with high DP micelles with diameter of 200 nm can be obtained (Figure 4.1).

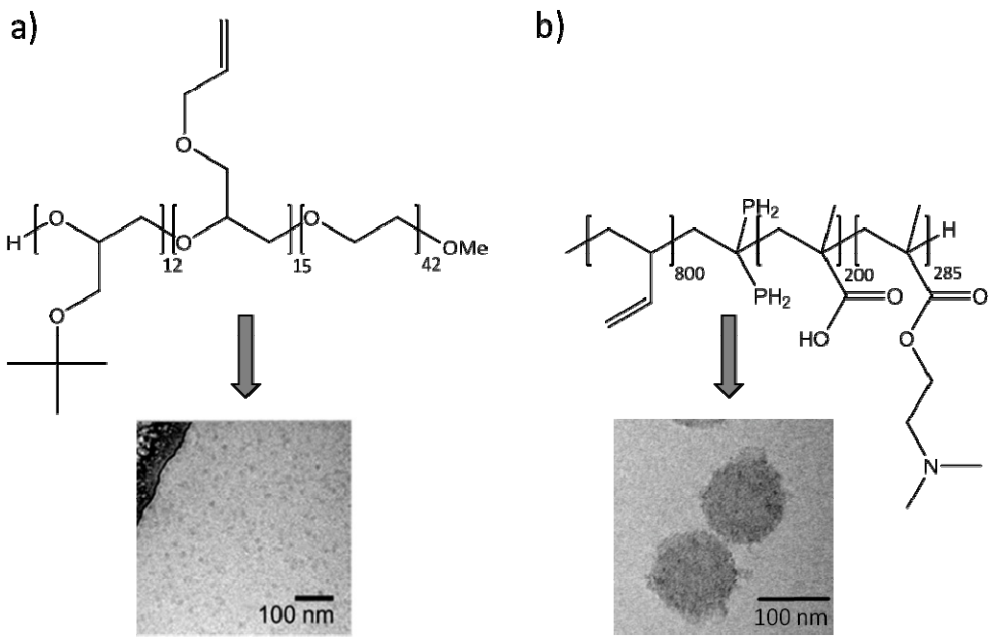

Figure 4.1: Schematic representation of the chemical structures of ABC triblock terpolymers and cyro-TEM micrographs of the corresponding micelles. a) Poly(ethylene oxide)-*block*-poly(allyl glycidyl ether)-*block*-poly(*tert*-butyl glycidyl ether) and b) poly(butadiene-*block*-poly(methacrylic acid)-*block*-poly(2-(dimethylamino)ethyl methacrylate).

Commonly, nanocarriers with diameters between 50 to 200 nm are used, because endocytosis can be assumed as a predominant internalization process. The interaction with the immune system is reduced, and glomerular filtration can be avoided.[63, 64] In contrast, polymeric micelles with sizes below 50 nm are rare in literature and, up to now, barely studied with regard to interactions with biological matter. In this context, spherical core-shell micellar structures of approximately 30 nm were found to effectively penetrate poorly permeable tumor membranes.[65] Hydrophobic drugs are well suited for encapsulation into such small micellar cores. In contrast, pDNA cannot be encapsulated into nanocarriers below 50 nm due to its large size. Moreover, a direct control over the charge balance in nanocarriers can be a promising strategy to balance cellular interactions, an efficient uptake, and simultaneously to suppress non-specific interactions and lower cytotoxicity.[66] This can be achieved, *e.g. via* the combination of positively and negatively charged segments within one block copolymer.

For pDNA delivery a multicompartment micelle based on stimuli-responsive triblock terpolymers, poly(butadiene-*block*-poly(methacrylic acid)-*block*-poly(2-(dimethylamino)ethyl methacrylate) (**BMAAD**), was used (Figure 4.1b). The polymer and the corresponding micelle with a diameter of around 200 nm exhibits a pH dependency concerning shape, size and surface charge, due to the PMAA and PDMAEMA block.[67] At an endosomal pH value (~ 5), PMAA is uncharged and PDMAEMA forms a cationic corona, whereas at pH 10, PDMAEMA is uncharged, collapsed, and merely PMAA now forms a negatively charged corona (Figure 4.2). Under physiological conditions both blocks are charged, leading to the formation of an intra-micellar interpolyelectrolyte complexed (*im*-IPEC) shell. Hence, the micellar surface is patchy, featuring both charge neutral (*im*-IPEC) and cationic domains (the DP of PDMAEMA is higher than for the PMAA segment, resulting in an excess positive net charge).

In contrast to this relative large micelle another triblock terpolymer poly(ethylene oxide)-*block*-poly(allyl glycidyl ether)-*block*-poly(*tert*-butyl glycidyl ether) (PEO-*b*-PAGE-*b*-P*t*BGE) with different functionalities was used for drug delivery experiments (Figure 4.1). Here, very small spherical micelles with diameters below 30 nm were achieved allowing the encapsulation of hydrophobic compounds inside the core.

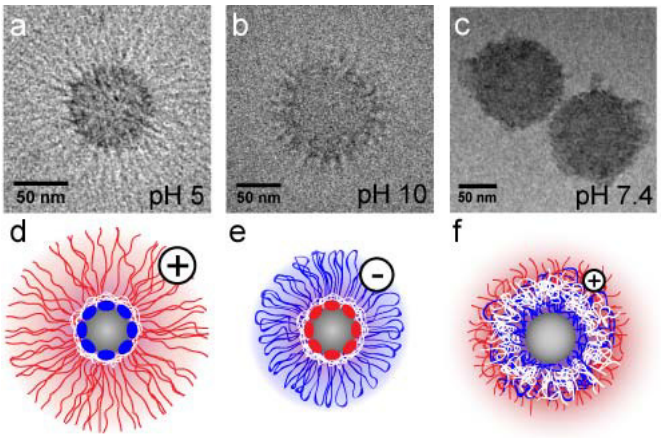

Figure 4.2: Cryo-TEM micrographs (a-c) and corresponding schematic depictions (d-f) of BMAAD micelles at indicated pH values.

As first step, transfection studies of **BMAAD** with pDNA under serum reduced conditions as well as with media containing 10% bovine serum were performed in adherent HEK293 cells, using lPEI 25 kDa and PDMAEMA 30 kDa as control. The **BMAAD** micelles showed enhanced transfection efficiency, compared to lPEI 25 kDa and PDMAEMA under both conditions (Figure 4.3b). The fact that **BMAAD** performs even better under serum conditions (74 $\pm$ 8%) is remarkable as in general serum leads to unspecific interactions and lower transfection efficiencies for cationic polymers. Next, the transfection of suspension Jurkat T cells, a model cell line for human leukemia cells and known to be hard to transfect with pDNA, was evaluated. Again, the **BMAAD** micelles demonstrate superior transfection efficiency, 5-fold higher than lPEI 25kDa (Figure 4.3c). With regard to cytotoxic effects, **BMAAD** show no cytotoxicity up to the tested concentrations (320 µg mL^{-1}), in contrast to PDMAEMA and lPEI 25 kDa, which show IC_{50} values of 30 µg mL^{-1} and 6 µg mL^{-1}, respectively (Figure 4.3a). This can be attributed to the PMAA block of **BMAAD** and the patchy surface featuring cationic domains and neutral charged *im*-IPECs. This remarkable performance of the **BMAAD** micelles, showing high transfection efficiency and no cytotoxicity, was further investigations concerning the underlying mechanism. Therefore, the physicochemical properties of the polyplexes were investigated using EBA and DLS experiments. **BMAAD** and the control polymers lead to a decrease in EB fluorescence intensity, indicating the successful formation of polyplexes. At physiological pH value all investigated polyplexes exhibit a positive net charge, as it is shown in zeta potential measurements. Hydrodynamic diameters of 64 nm (lPEI 25 kDa), 237 nm (**BMAAD**), and 52 nm (PDMAEMA) can be observed. For **BMAAD**, the formed polyplexes are of comparable size to the "bare" micelles (212 nm), which can be explained by a rather tight wrapping of pDNA around the particles (see also to Chapter 2). The results could also be confirmed by asymmetric flow field flow fractionation, where an R_g of 97 nm was obtained for **BMAAD** and 111 nm for the corresponding polyplex. With decreasing pH value, the

zeta potential as well as the hydrodynamic diameter increases from 16.5 mV and 237 nm to 30.3 mV and 420 nm indication a stretching of the PDMAEMA block.

To achieve a successful transfection of human leukemia cells an enhanced cellular interaction and uptake of the cells has to be realized. This was accessed *via* the sedimentation rate of the polyplexes, as determined by analytical ultracentrifugation. Presumably, larger particles with higher sedimentation coefficients lead to an increased particle uptake in case of *in vitro* transfections. Indeed, a higher sedimentation rate of the **BMAAD** polyplexes (6480 S) compared to lPEI 25kDa (3140 S) and PDMAEMA (230 S) was obtained, most probably due to the rather dense PB core. This might lead to longer and more intensive interactions between the cells and the polyplexes and, an increased internalization, *in vitro*.[68, 69]

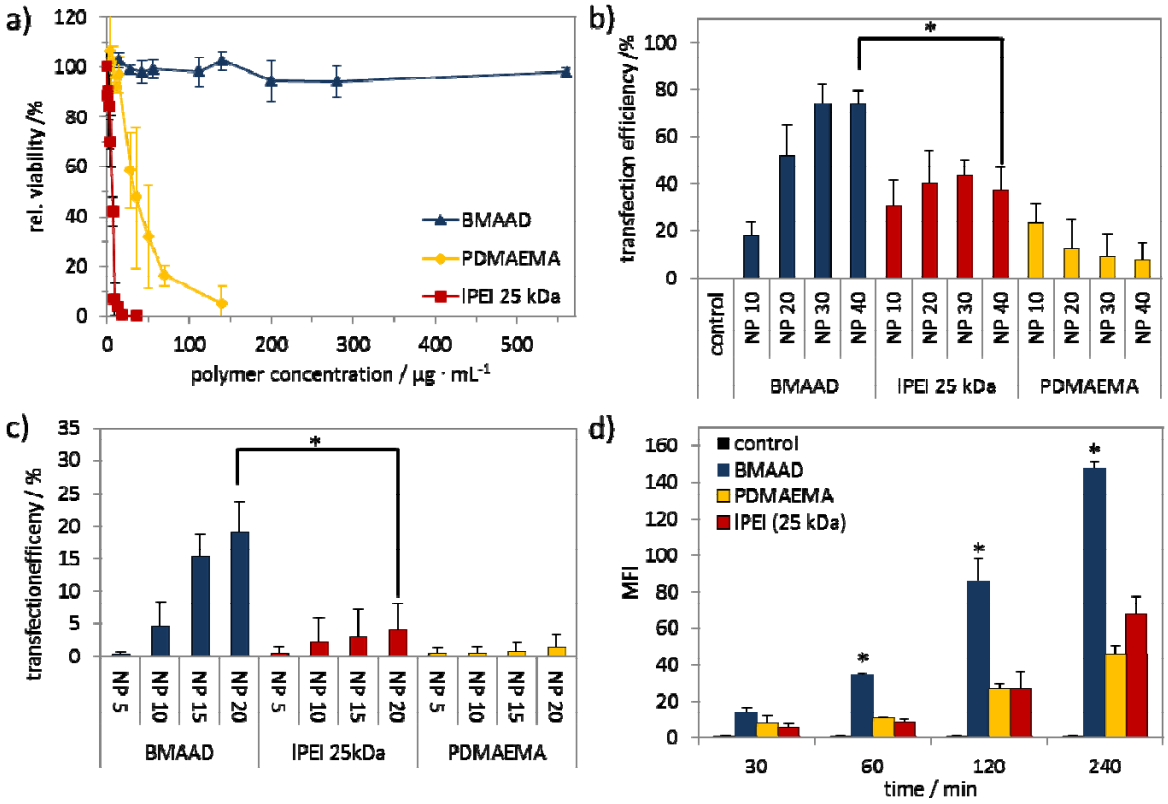

Figure 4.3: Cytotoxicity of BMAAD, lPEI 25 kDa and PDMAEMA 30 kDa tests using L929 cells (a). Transfection efficiency for adherent HEK293 cells in serum-containing media (b) and human leukemia cell (Jurkat T cells) (c) at different NP ratios. Mean fluorescence intensity (MFI) of HEK293 cells transfection with YOYO-1 labeled pDNA for indicated time points using BMAAD, lPEI 25 kDa and PDMAEMA (d). Values represent the mean ± S.D; * represents a significant difference ($p < 0.05$) to lPEI 25 kDa and PDMAEMA 30 kDa.

Further investigations concerning the polyplex uptake were performed using YOYO-1 labeled pDNA in a time dependent manner. The labeled pDNA complexed with **BMAAD** show an impressive behavior. Beside a faster uptake also the overall amount is enhanced compared to lPEI 25 kDa and PDMAEMA (Figure 4.3d). The uptake kinetics of the polyplexes was investigated, but, due to the relative large size of the micelle and their corresponding polyplexes the relying uptake mechanism was questionable. Thus, transfections at 4 °C and with bafilomycin (an inhibitor for the ATPases in the endosome and therefore prevention of an acidification) were performed. In both cases, the transfection efficiency of **BMAAD** is significantly decreased from around 70% to less than 20%. This indicates that the uptake of **BMAAD** polyplexes occur *via* endocytosis. To further confirm the uptake mechanism, localization of transported pDNA was investigated using confocal laser scanning microscopy (CLSM). Interestingly, already after 1 h no co-localization of the labeled **BMAAD** polyplexes with the late endosome and lysosome was detected, in contrast to lPEI 25 kDa and PDMAEMA polyplexes (Figure 4.4). However, the polyplexes were observed in early endosome, indicating a fast and efficient escape from the endosome within 30 min.

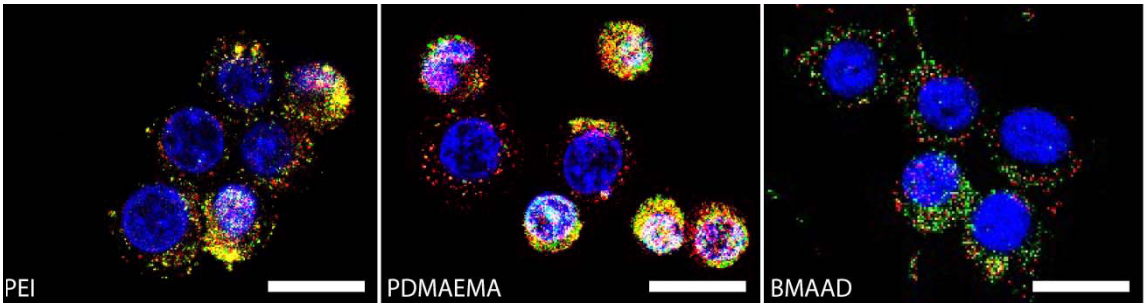

Figure 4.4: CLSM images of HEK293 cells transfected with indicated polymer based polyplexes and YOYO-1 labled pDNA (green); late endosome/lysosome were stained with lysoTracker Red (red), and cell nuclei were stained with Hoechst 33342 (blue). Each scale bar represents 20 µm; colocalization of pDNA and endosomal compartments are depicted in yellow.

For lPEI 25kDa, a rather high buffer capacity is known, causing the proton sponge effect. In contrast to lPEI 25 kDa, PDMAEMA has lower buffer capacities,[70] which might explain the lower transfection efficiency of the linear homopolymer PDMAEMA but not the outstanding

performance of **BMAAD**. Here, the stimuli-responsive behavior of **BMAAD** is the key factor, an increased amount of positive charges at pH value of 5 lead to strong interactions with cellular membranes and, potentially, a destabilization. This was confirmed both for the polymers and the polyplexes by a hemolysis assay at different pH values.

Once the polyplexes are released into the cytoplasm, their dissociation is of great importance; this behavior was investigated using the heparin assay. Typically, heparin concentrations of 10 U mL^{-1} are necessary to achieve a total release of pDNA from PEI-based polyplexes,[71] whereas 50 U mL^{-1} were required for linear PDMAEMA, which is a further explanation for the lower transfection efficiency. Although, **BMAAD** and PDMAEMA showed comparable binding affinities, the addition of only 10 U mL^{-1} heparin led to an almost complete release of pDNA from the **BMAAD** -based polyplexes. This can be attributed to the PMAA block acting as a competing polyanion.

The structure of the formed polyplexes was further investigated using cryo-TEM measurements at different pH-values (Figure 4.5). At pH 7.4, the **BMAAD** micelles are close to their isoelectric point and polyplex formation with pDNA leads to rather homogeneous structures of spherical shape. The observed clustering can be explained by the rather low zeta potential of 16.5 mV. A decreased pH value of 5 leads to full protonation and stretching of the PDMAEMA corona ($pK_a \sim 7.7$, zeta potential of 30.3 mV). Afterwards, severe structural changes occur, as shown in Figure 4.5b. Parts of the micellar core are covered by collapsed PMAA patches (blue) and, in addition, the polyplexes formed of PDMAEMA (red) and pDNA (black) appear more dense and rigid, as seen in the protrusions connecting several micellar structures.[67]

These observations and the data provided by hemolysis support the assumption of an endosomal burst at acidic conditions. Subsequently, if the polyplex is released from the endosome, the pH value within the cytoplasm rises to approximately 7.4, which was also

simulated for the same polyplex solution (Figure 4.5c). The cryo-TEM micrograph now shows polyplexes with the combined characteristics of Figure 4.5 and Figure 4.5b: PMAA is resolubilized *via* deprotonation, leading to a more homogeneous overall appearance, and the rather rigid PDMAEMA/pDNA strands are still present, interconnecting several micelles. The latter can be explained by a closer look at the linear homopolymer of PDMAEMA, showing a rather strong binding between PDMAEMA and pDNA. Since the polyplex is formed, neither an increase in the pH value nor the addition of heparin facilitated an easy release of pDNA. Hence, in the case of the **BMAAD** the negatively charged PMAA block acts as a competing polyelectrolyte, presumably reducing the binding between PDMAEMA and pDNA, and enabling the release of genetic material in the cytoplasm.

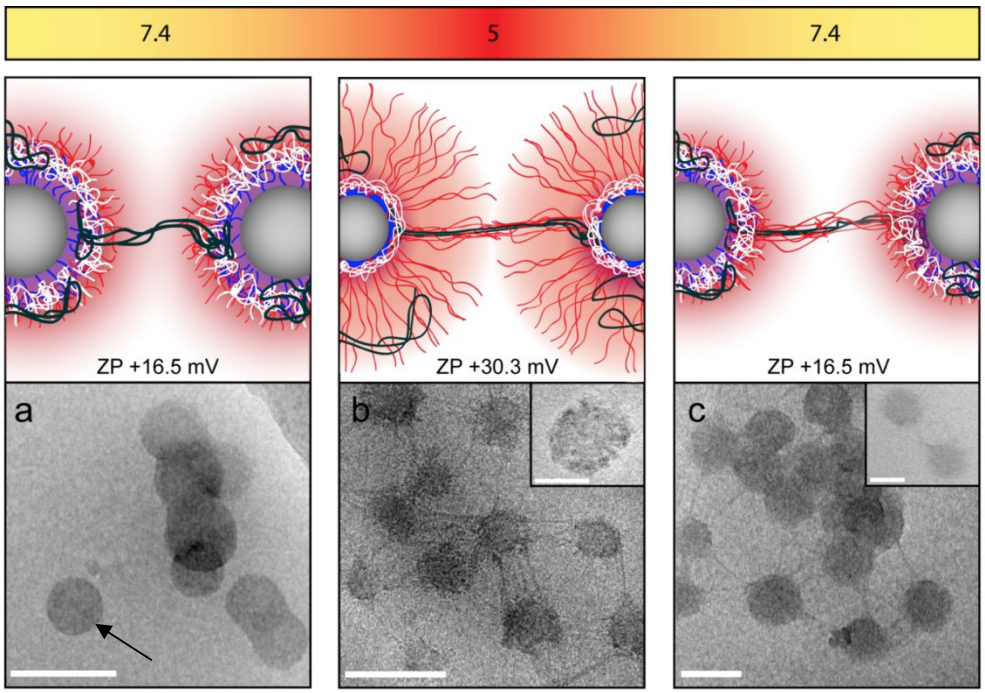

Figure 4.5: Schematic depiction of the proposed polyplex structure and the corresponding cryo-TEM micrographs at pH 7.4, the black arrow indicates the presence of *im*-IPEC (a), pH 5 (b), and pH 7.4 (c). Zeta potentials (ZP) of BMAAD polyplexes at pH 7.4 (16.5 mV) and pH 5 (30.3 mV). Color code: Grey (PB), blue (PMAA), red (PDMAEMA), white (*im*-IPEC), and black (pDNA-polyplex). Scale bars indicate 200 nm and 50 nm in the insets.

The detailed investigations of the underlying mechanism revealed a number of advantages for the **BMAAD** micelle. The dense core leads to higher sedimentation rates and a superior cellular uptake. Furthermore, the neutral charged *im*-IPECs probably lead to reduced serum

aggregation, unaffected viability, enhanced cellular uptake, and an improved pDNA release. In addition, under acidic conditions PDMAEMA provokes an increase in size and zeta potential, responsible for membrane destabilization and the release of the polyplex from the endosome.

The **BMAAD** micelle demonstrates the importance of control over the charge balance in (block co-) polymer nanostructures. Resulting in a promising strategy to balance cellular interactions, efficient uptake, and to simultaneously suppress non-specific interactions and reduced cytotoxicity.

Besides the combination of positively and negatively charged segments within one block copolymer the simple mixing of different charged block copolymers during micelle formation represents an alternative approach. For this purpose, a small library of structurally similar ABC triblock terpolymers (PEO-*b*-PAGE-*b*-P*t*BGE = **EAT**) (Figure 4.1a) with different functional groups being present within the segment B were synthesized. In detail, the pendant double bonds of the PAGE block were functionalized to introduce galactose (**EGT**), amino groups to provide positive charges (**ENT**), as well as carboxylic groups to generate negative charges (**ECT**) (Figure 4.6). Galactose was chosen to enable selective cellular uptake into hepatocytes, as an interaction with the asialoglycoprotein receptor can be assumed.[72] The obtained triblock terpolymers were subsequently used for the co-assembly into well-defined spherical core-shell-corona micelles with diameters below 30 nm and precisely adjustable charge and composition. In addition, nile red, a hydrophobic red fluorescent dye, was encapsulated into the hydrophobic P*t*BGE core. Nile red is poorly soluble in water and exhibits a strong fluorescence in hydrophobic environment, herein it was used as model drug.[73] The characterization *via* DLS, cryo-TEM (Figure 4.6) as well as AF4 measurements, confirmed the assembly into spherical micelles with hydrodynamic diameter between 10 and 34 nm.

To create mixed micelles the co-assembly of the different triblock terpolymers was performed leading to the formation of core-shell-corona micelles. Here, a PEO corona and a hydrophobic P*t*BGE core formed by identical segments (A and C) should be achieved. The shell (B segment) should be composed of a combination of different functional groups, depending on which materials are used. Mixed micelles formed of two different triblock terpolymers (**ENT** and **ECT**) as well as ternary micelles (**ENT**, **ECT** and **EGT**) were assembled. Moreover, the binary mixed micelles were formed with different ratios, an excess of positive charges **(ENT/ECT)**$_{3.5:1}$, a slight excess of positive charges **(ENT/ECT)**$_{1.2:1}$, and an excess of negative charges **(ENT/ECT)**$_{1:2.6}$. Here, the superscripts represent the mixing ratio regarding the functional groups of the involved triblock terpolymers. For the ternary systems, two ratios were prepared *via* co-assembly: **(ENT/ECT/EGT)**$_{3.5:1:0.5}$ and **(ENT/ECT/EGT)**$_{3.4:1:2.3}$, featuring almost identical charge ratios and mainly differing in the amount of incorporated galactose. In all cases, evaluation by DLS and cryo-TEM led to comparable results to the pure micelles, regarding size and shape of both binary and ternary mixed micelles, also supported by AF4 measurements.

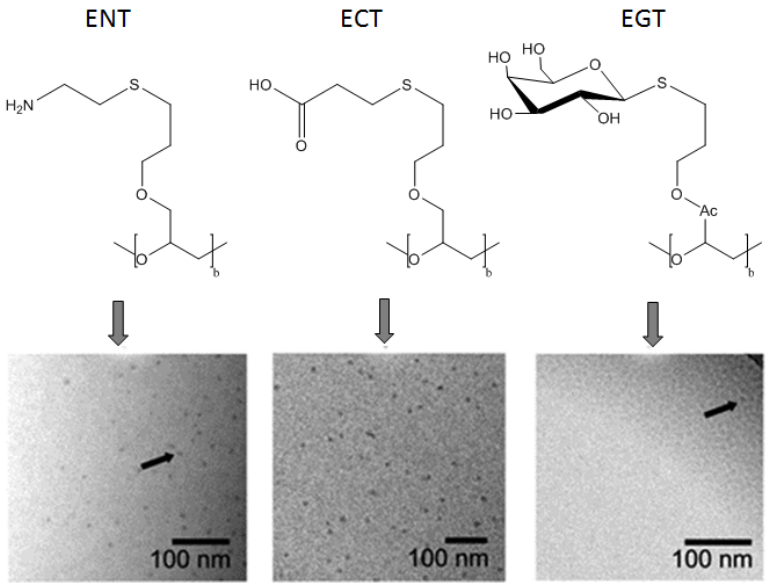

Figure 4.6: Schematic representation of the co-assembly of functionalized triblock terpolymers and the corresponding cyro-TEM micrographs of the prepared micelles. Due to the rather low contrast an arrow highlights representative ENT and EGT micellar cores.

Subsequently, further characterization of the micelles and mixed micelles was necessary. In particular, if two separate populations of micelles composed of only one polymer exist or if the co-assembly was successful. For this purpose, the zeta potential was analyzed (Figure 4.7b). As expected, a negative value is found for **ECT** (–36 mV) whereas the zeta potential for **ENT** is positive (48 mV). Both **EAT** and **EGT** revealed negative values (–10 and -27 mV), which can be attributed to the complexation of ions within the PEO corona or charge-dipole and dipole-dipole interactions, which are both known to influence the zeta potential. For binary mixed micelles **(ENT/ECT)**, a clear dependence of the zeta potential on the mixing ratio can be observed, as with increasing amount of **ENT** the zeta potential increases (from –24 mV for **(ENT/ECT)**$_{1:2.6}$ to 14 mV for **(ENT/ECT)**$_{3.5:1}$). Thus, zeta potential measurements indicate that mixed micelles are formed. If the co-assembly in case of, *e.g.* **(ENT/ECT)**$_{3.5:1}$, would lead to two separate populations of **ENT** and **ECT**, aggregation of oppositely charged micelles due to electrostatic interactions might be expected. In this case, an increase of the aggregates size and, presumably, precipitation might occur. Moreover, the ternary mixed micelles exhibit a decreased zeta potential if compared to the binary **(ENT/ECT)**$_{3.5:1}$ structures with 6 mV for **(ENT/ECT/EGT)**$_{3.5:1:0.5}$ and 7 mV for **(ENT/ECT/EGT)**$_{3.4:1:2.3}$, thus, indicating the presence of **EGT** within the structures. In this case the zeta potential measurements confirm again that mixed micelles are formed.

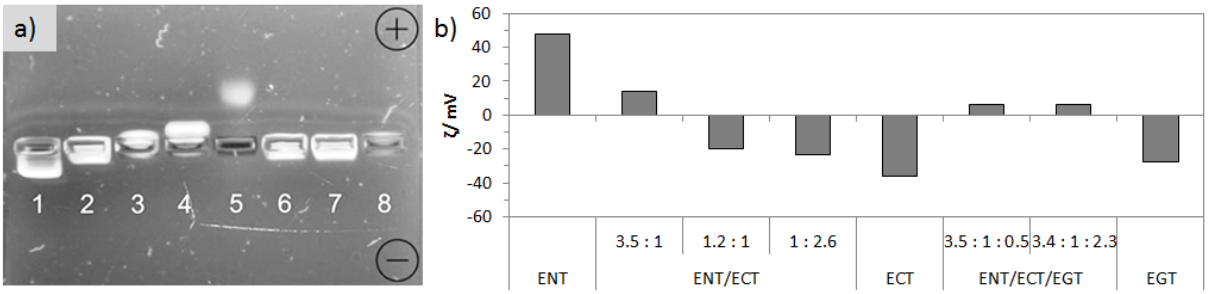

Figure 4.7: Gel electrophoresis using 1% agarose gel and TBE buffer (1 = ENT, 2 = (ENT/ECT)$_{3.5:1}$, 3 = (ENT/ECT)$_{1.2:1}$, 5 = ECT, 6 = (ENT/ECT/EGT)$_{3.5:1:0.5}$, 7 = (ENT/ECT/EGT)$_{3.4:1:2.3}$, 8 = (EGT). Zeta potential of different tribock terpolymer micelles and mixed micelles diluted in water.

Beside zeta potential measurements, gel-electrophoresis is another method for the investigation of charged macromolecules (*e.g.* DNA). Here, the samples are placed in an agarose gel and an electrical field is applied. The electrical field induces movements within the gel towards the positive or negative pole, depending on the charge of the sample. An advantage of this method is the visualization of the material depending on its charge and size. It was anticipated that mixed micelles should feature only one band, as additional confirmation of the zeta potential measurements. As shown in Figure 4.7a, micelles formed by **ENT** reveal the highest shift to the negative pole, whereas **ECT** moved towards the positive pole. The bands observed for **ENT/ECT** mixed micelles of different mixing ratios can be found in between, in accordance with their zeta potential. As only one band is visible for all samples, we regard this as another indication for an efficient co-assembly. In addition, ternary **ENT/ECT/EGT** exhibited movement towards the negative pole, again confirming the results from zeta potential measurements. **EGT** did not show any movement in gel electrophoresis.

Aiming for a later use of such triblock terpolymer micelles in targeting and/or delivery applications, their cytotoxicity was investigated. At first, triblock terpolymer micelles formed *via* the self-assembly of one kind of polymer were investigated. Micelles formed of **EAT**, **ECT** or **EGT** did not show any cytotoxic effects for concentrations up to 0.5 mg mL^{-1}, only in case of the **ENT** the situation was different (Figure 4.8a). Regarding **EAT**, **ECT**, and **EGT** these results are in accordance with literature report as all structures exhibited negative zeta potentials. For micelles based on **ENT**, the IC_{50} of 300 µg mL^{-1} can be explained by the presence of cationic charges within the shell (zeta potential of +47.5 mV), which could lead to stronger interactions with or even destabilization of the cell membrane. This was also confirmed by an increased hemolytic activity. These results can be taken as further proof that the functionalization of the middle block (PAGE) significantly influences interactions of such micelles with biological matter, even though all structures feature a

rather long PEO corona (compared to the degrees of polymerization for PAGE and P*t*BGE). Furthermore, the internalization efficiency of micelles from **EAT**, **ENT**, **ECT**, and **EGT** into HEK293 cells, a model cell line for unspecific uptake studies, was analyzed under serum reduced and serum containing conditions (Figure 4.8b). From this data set it becomes obvious that **ENT** revealed the best uptake into 79.7 ± 4.5% cells (at 10 µg mL^{-1}). This can be attributed to the presence of positive charges in the shell and an increased interaction with the cell membrane. Compared to **ENT**, the decreased uptake of **ECT** and **EGT** can be explained by the negative zeta potential of these particles, resulting in decreased interactions with the cells. Nevertheless, the introduction of charges (COOH) or targeting units (galactose) enhanced the uptake if compared to **EAT** (1 ± 1.11%). As the presence of a PEO corona has been shown in many examples to prevent unspecific protein adsorption ("stealth effect"), the uptake was also analyzed in the presence of serum (Figure 4.8b). Here, only the uptake of **ENT** decreased significantly from 86 ± 11% to 13 ± 0.6% at 10 µg mL^{-1}, presumably due to stronger interactions with the negatively charged serum proteins. However, the uptake of both, **ENT** and **ECT**, is significantly higher compared to **EAT**. The internalization of **EGT** is similar to **EAT**, thus, also reduced from 15 to 2.9% in the presence of serum proteins. As the functionalization with galactose is supposed to result in a specific uptake into liver cells, the internalization efficiency of the **EGT** micelles was investigated in HepG2 cells. Unfortunately, no increased uptake at low concentrations (3.9% ± 5 at 10 µg mL^{-1}) could be detected, which would hint towards a targeted internalization process. One explanation might be that the galactose side chains are not sufficiently exposed at the surface and, thus, the interaction with the asialoglycoprotein receptor, specific for galactose in HepG2 cells, is hampered. As the pure micelles (**EAT**, **ENT**, **ECT**, and **EGT**) already showed significant differences regarding cellular uptake and cytotoxicity, the influence of the composition in binary and ternary mixed micelles on the cytotoxicity was studied. **(ENT/ECT)**$_{3.5:1}$ exhibited a positive zeta potential and a similar cytotoxicity (IC_{50} of 350 µg mL^{-1}), if compared to **ENT** (Figure 4.8a

and c). In case of **(ENT/ECT)**$_{1.2:1}$ and **(ENT/ECT)**$_{1:2.6}$, no cytotoxicity was observed, in accordance with the negative zeta potential. Interestingly, both ternary mixed micelles, **(ENT/ECT/EGT)**$_{3.5:1:0.5}$ and **(ENT/ECT/EGT)**$_{3.4:1:2.3}$, which feature the same charge ratio as **(ENT/ECT)**$_{3.5:1}$ and exhibited positive zeta potentials, did not show any cytotoxicity at all tested concentrations (Figure 4.8c). This is indeed remarkable, and can be attributed to the presence of **EGT** terpolymer chains in the micelles. With regard to the uptake, the **(ENT/ECT)**$_{3.5:1}$ demonstrated an outstanding uptake compared to the other samples. Under serum containing conditions already 75% $\pm$ 11.5 (10 µg mL^{-1}) of the cells showed an internalization of **(ENT/ECT)**$_{3.5:1}$ (Figure 4.8d). These results are comparable to **ENT** micelles under serum reduced conditions, thus indicating decreased non-specific interactions of **(ENT/ECT)**$_{3.5:1}$ with serum proteins. For the other binary and ternary micelles a reduced uptake (compared to **(ENT/ECT)**$_{3.5:1}$) was found (Figure 4.8d). In the case of ternary micelles, the decreased uptake compared to **(ENT/ECT)**$_{3.5:1}$, can be attributed to the presence of **EGT**. Further increase of the galactose content leads to even the lower values, which is in accordance with lower uptake of **EGT** compared to **ECT** and **ENT**. Nevertheless, it should be noted that, in contrast to **(ENT/ECT)**$_{3.5:1}$, both ternary micelles did not show any observable cytotoxicity. In summary, by adjusting the micellar composition *via* co-assembly of **ENT**, **ECT**, and **EGT** both cellular uptake and cytotoxicity can be controlled and optimized. Thus, by fine tuning the charges in the shell either higher uptake rates or reduced cytotoxicity can be achieved.

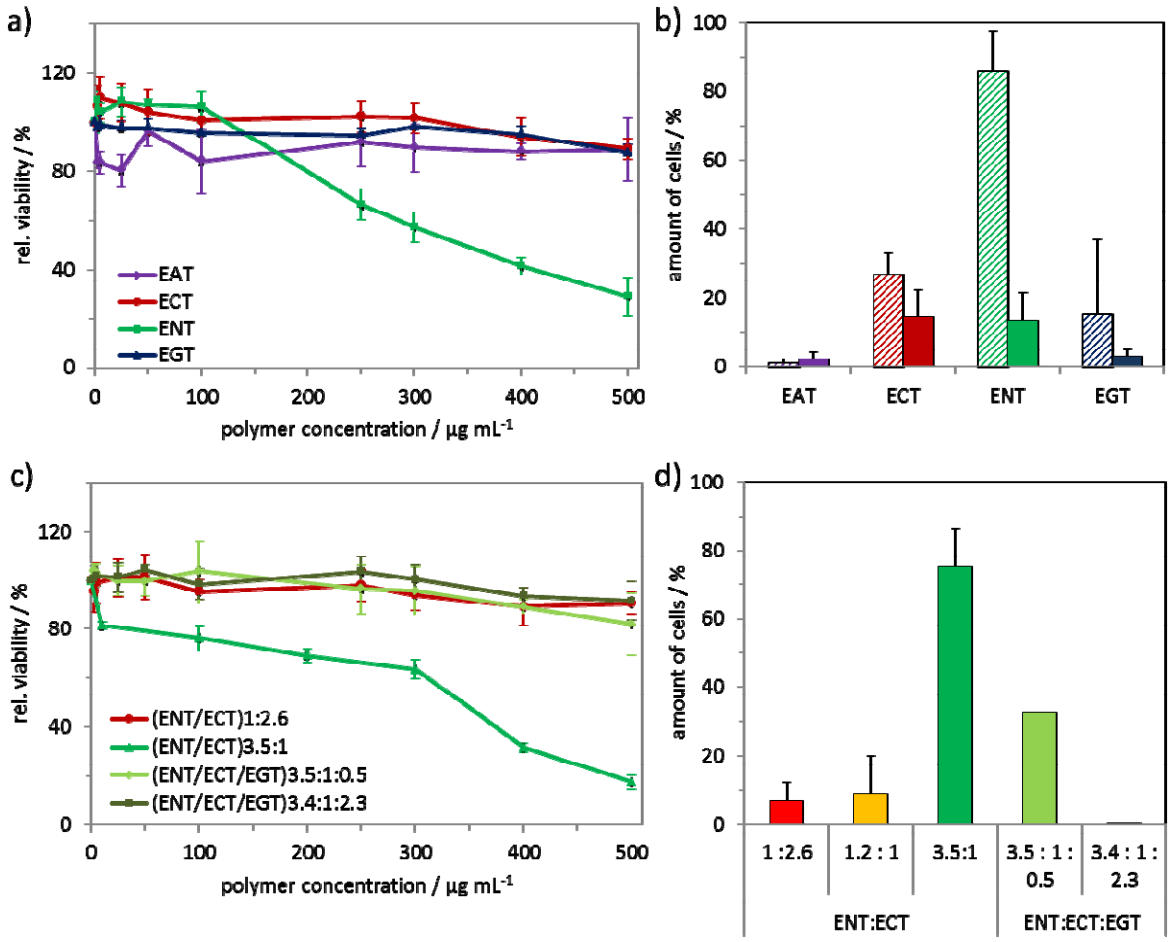

Figure 4.8: Cytotoxicity of the indicated triblock terpolymer micelles (a) and mixed micelles (c) using L929 cells and cellular uptake in HEK293 cells at concentration of 10 µg mL^{-1} under serum reduced conditions (dashed bar) and serum containing conditions (filled bars) (b and d). Values represent the mean ± SD.

Triblock terpolymers based micelles are very promising nanocarriers for drug and gene delivery. It was demonstrated that large micelles allow a wrapping around the pDNA, which results in a superior performance. In all transfection steps beneficial properties were obtained, which can be attributed to the pH dependent stimuli-responsiveness and the patchy surface of this micelle. In contrast, very small micelles were demonstrated as possible drug delivery agents. Based on a polymer toolbox, the tuning of the charges, in the shell, results in synergistic effects, whereby the cytotoxicity and uptake efficiency can be controlled.

5 Polymer-based nanoparticles for drug delivery

Parts of this chapter will be published in: **P7)** T. Yildrim, A. C. Rinkenauer, C. Weber, A. Traeger, S. Schubert, U. S. Schubert, RAFT made methacrylate copolymers for reversible pH-responsive nanoparticles, *J. Polym. Sci, Part A: Polym. Chem.* **2015**, *53*, 2711-2721; **P8)** A. C. Rinkenauer, A. T. Press, M. Raasch, C. Pietsch, S. Schweizer, S. Schwörer, K. L. Rudolph, A. Mosig, M. Bauer, A. Traeger, U. S. Schubert, Comparison of the uptake of methacrylate-based nanoparticles in static and dynamic *in vitro* systems as well as *in vivo*, *J. Controll. Release* **2015**, *216*, 158-168.

Nanocarriers applied for drug delivery are based either on spherical micelles or on nanoparticles. In both cases pH-dependent stimuli-responsiveness can be one feature of the polymers for enhanced uptake or drug release. Besides PLGA, PMMA derivates are the commonly used hydrophobic polymers for nanoparticle preparation. The statistical P(MMA-*co*-MAA) copolymers are applied *e.g.* as coating material (EUDRAGIT-S100), because it shows a pH dependency behavior, no cytotoxicity and a good biocompatibility.[74] In addition, PMMA derivatives can be used for the preparation of well-defined nanoparticle *via* nanoprecitpitation.[74] These polymers are non-biodegradable and, thus, particularly suited to analyze the internalization behavior depending on the structural properties of nanoparticles, *e.g.* the surface charge or the nanoparticle size. Detailed investigations of nanoparticle efficiencies result in numerous factors which affect their uptake *in vitro*. However, direct translation of their uptake efficiency to their behavior *in vivo* is challenging. In particular, the prediction concerning the biodistribution and the interaction with the RES remains a challenge.[75] Thus, cost and time consuming *in vivo* experiments are applied to evaluate new nanoparticle systems and to answer the question, whether they improve the biodistribution and the availability of a compound to the target cell. Microfluidically-supported cell cultures represent promising new developments to model physiological relevant conditions more accurately by mimicking key-features (*e.g.* the shear stress).[76] In blood vessels the inner

layer – exposed to the bloodstream are endothelial cells. As a consequence, their cell biology morphology, permeability, and the expression of other important features are affected by shear stress.[77] This mechanical force evolved to an important factor investigating physiological processes in the context of endothelial and substance interaction and internalization. First results demonstrate the impact of shear stress on the nanoparticle uptake.[78-81]

To gain more insight into the impact of shear stress and co-cultivation in microfluidically-supported dynamic cell cultures, PMMA derivatives-based nanoparticles were applied. The copolymers were synthesized *via* the RAFT polymerization technique to obtain polymers with narrow molar mass distributions and tailored polymer properties.[82, 83] Here, pH dependent copolymers were synthesized consisting on the one hand of negatively charged MAA groups at basic conditions and on the other hand of cationic charges (DMAEMA units) at acidic conditions. A fine-tuning of the pH dependency, which goes hand in hand with the negative charges (-COOH groups), as well as the hydrophobicity (MMA units) was realized by synthesizing statistical copolymer libraries with a systematic variation in the compositions. Thus, MAA amounts of 3, 5, 8 and 13%, as well as 20% of DMAEMA were used as a comonomer in the polymerization procedure.

As a first step, nanoparticles were prepared by nanoprecipitation with subsequent solvent evaporation without any need of stabilizers/surfactants.[12] In this study nanoparticles of around 200 nm in diameter were chosen due to the size dependent cellular internalization *via* endocytosis. In order to obtain such nanoparticles, with defined size the "dropping method" was applied (polymer diluted in acetone and dropped into water). The characterization of diameter and shape of the nanoparticles were performed using DLS as well as SEM measurements (Figure 5.1a-c). Spherical nanoparticles with diameters of 190 to 210 nm were obtained. The zeta potential measurements confirmed the negative surface charges of nanoparticles consisting of PMMA-*co*-PMAA (**3**, **5**, **8**, **13% PMAA**

nanoparticles) and positive charges for PMMA-*co*-PDMAEMA (**20% PDMAEMA** nanoparticle) nanoparticles, indicating a high colloidal stability.[84] In case of PDMAEMA-based nanoparticles a pH-responsive behavior under acidic condition can be assumed due to the pKa value of 7.5 of PDMAEMA.[35, 85] Thus, the pH-response behavior was investigated by DLS measurements of nanoparticle suspensions at various pH values (Figure 5.1d). The **20% PDMAEMA** nanoparticles did not show any instability at pH 7, whereas, at pH values of 3.4 to 5, the nanoparticles are protonated and show a disassembling or swelling. This protonation was detected by an increased zeta potential, and furthermore the disassembly or swelling can be explained by increase of the dispersity.

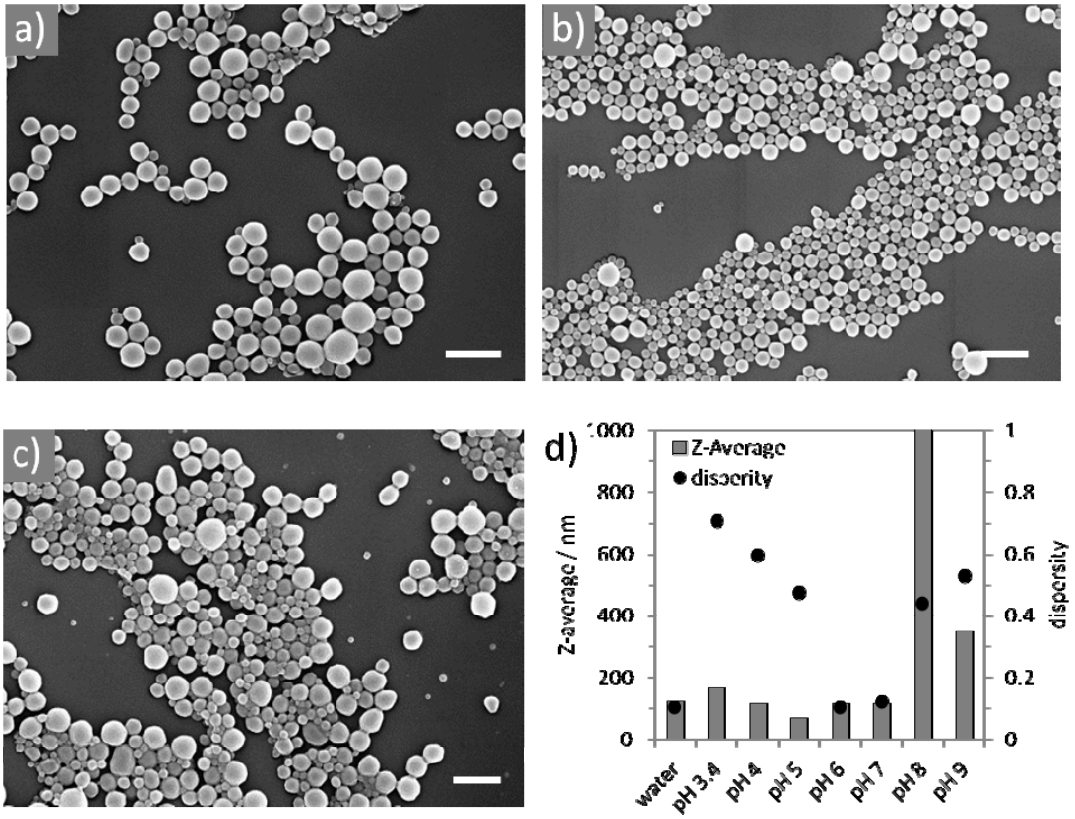

Figure 5.1: SEM micrographs of methacrylate based nanoparticles a) 3% PMAA, b) 13% PMAA and c) 20% PDMAEMA. Scale bar = 500 nm. d) Z-Average diameter (represented up to 1000 nm) and nanoparticle dispersity values of 20% PDMAEMA nanoparticles as a function of the pH value.

Initially, the nanoparticles were investigated regarding their internalization in HEK293 cells. A clear correlation of cellular internalization rates depending on the PMAA amount of the nanoparticles was observed. Increasing amounts of PMAA resulted in an increased uptake of

the nanoparticles (Figure 5.2a). In particular, the differences in the uptake behavior of **3% PMAA** (rel. SSC/FSC = 1.2) and **13% PMAA** (rel. SSC/FSC = 1.7) are remarkable. The differences in polymer composition and related negative charge increase of the particle surface as well as a decreased hydrophobicity appear to be beneficial for the cellular uptake. The cationic charged nanoparticles (**20% PDMAEMA**) showed the highest cellular uptake (rel. SSC/FSC = 2). This increased internalization rate can be explained by the cationic charges that are known to be beneficial for interactions with the cell membrane.[86] Nanoparticles carrying negative as well as positive charges show an adsorption of serum proteins that impact their uptake efficiency.[50, 51] The nanoparticle uptake of **3% PMAA**, **13% PMAA** and **20% PDMAEMA** was tested in the presence of fetal calf serum (FCS) in the cell culture medium (Figure 5.2b). No impact of FCS on the internalization of **13% PMAA** and **20% PDMAEMA** nanoparticles was found. In contrast to this observation, an increased cellular uptake of **3% PMAA** in the absence of FCS was observed. It can be assumed that the differences in cellular uptake of **3%** and **13% PMAA** nanoparticles are attributed to the presence of serum proteins. The dependency of nanoparticle uptake on the protein coronas is known, but is hard to investigate due to its complexity.[87, 88] First hints concerning the impact of the protein corona on the nanoparticle uptake were given by SDS-PAGE. The **3% PMAA** nanoparticles show in contrast to both other nanoparticles an increased protein adsorption, indicating a negative impact on the uptake. Furthermore, cell line and type independent uptake trends support the assumption of an impact of the protein corona on the internalization efficiency.

Besides, the nanoparticle uptake measurement *via* flow cytometry, also confocal microscopy was performed to proof the internalization of the nanoparticles (Figure 5.2c-d). For this purpose, nile red as hydrophobic dye was encapsulated. All investigated nanoparticles were detectable inside the cells. **20% PDMAEMA** showed higher fluorescence intensity and a

more diffuse distribution compared to PMAA nanoparticles. This supports the swelling and disassembly of nanoparticles under acidic conditions within the endosome and the release of nile red.

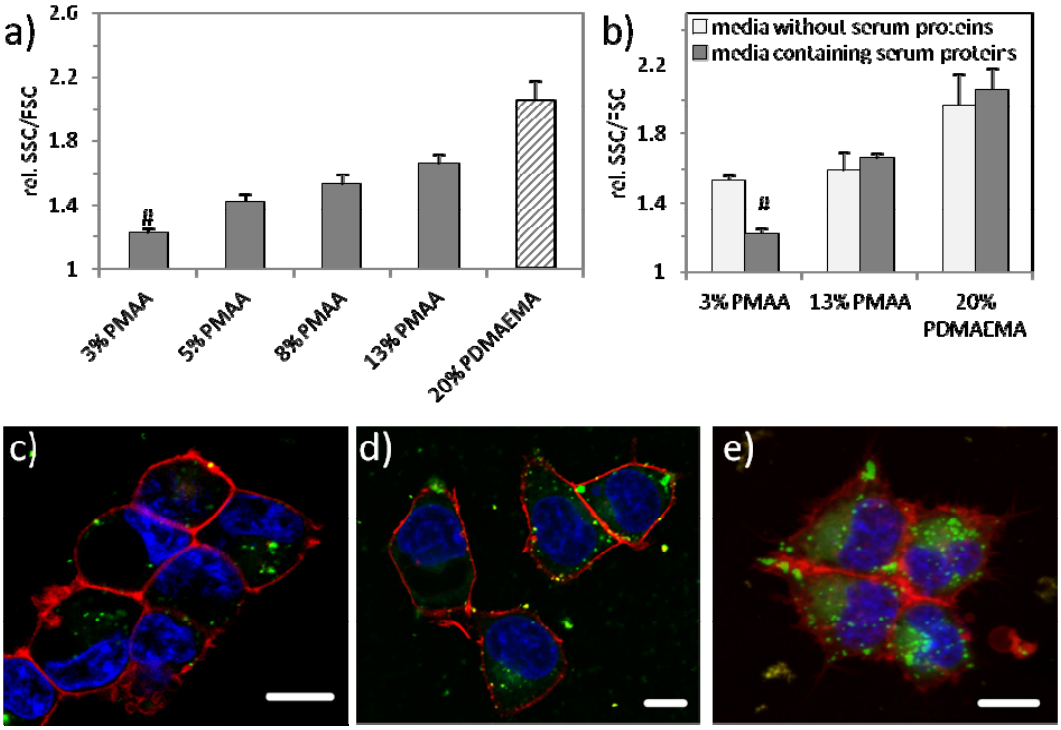

Figure 5.2: Internalization of methacrylate-based nanoparticles in HEK293 cells treated for 24 h with 100 µg mL^{-1} nanoparticle in media containing serum proteins, rel. SSC/FSC regarding the control. a) Negative and cationic charged nanoparticle uptake # represent significant difference compared to 20% PDMAEMA and b) comparison of nanoparticle uptake in media with and without serum. Internalization of 3% PMAA (c), 13% PMAA (d) and 20% PDMAEMA (e) in HEK293 cells stained with Hoechst for DNA-staining (blue) and CellMask DeepRed (red) for plasma membrane staining previous to the addition of nanoparticles (green). Images were taken 25 to 30 min after addition of nanoparticles. Scale bar = 10 µm. a, b) bars show mean + s.e.m (n = 3), significance tested a) using Two-way ANOVA with post-hoc Turkey test and b), using Kruskal-Wallis Anova in combination with Dunn's multiple comparison test,# $p<0.05$.

Taken together, static *in vitro* studies depict relevant properties of the nanoparticles: (i) Uptake effectiveness depending on nanoparticle characteristics, (ii) crucial assays to understand the interaction of nanoparticles with soluble molecules of, *e.g.* serum proteins , and (iii) first assessment of nanoparticle toxicity. In addition, by analyzing the cellular uptake in different cell types as well as in co-cultivation of primary human umbilical vein endothelial cells (HUVEC) and primary human macrophages (MΦ) the same trend concerning an enhanced uptake of charged nanoparticles was observed. Interaction of

particles and proteins were shown by SDS-PAGE, indicating serum interaction as one aspect of the internalization of nanoparticles. However, static cell culture conditions provide sedimentation effect which are strongly altered under dynamic condition, *e.g.* in the blood stream.[89]

Cell culture under dynamic conditions allows the investigation of nanoparticle binding and internalization under physiologically relevant conditions *in vitro*. HUVEC were dynamically cultured with physiological stimulation by shear stress. Shear stress values from 0.7, 3.0, 6.0 and 10.0 dyn cm^{-2} were applied. Interestingly, increasing shear stress positively correlates with the total amount of internalized nanoparticles (Figure 5.3). Similar to PMAA-based nanoparticles **20% PDMAEMA** show a positive correlation of the cellular uptake efficiency with applied shear stress in the dynamic cell culture. This indicates that nanoparticle cell interactions are sufficient to induce adhesion and internalization even at shear stress. However, in case of **20% PDMAEMA** a plateau for the cellular uptake was already reached at 3 dyn cm^{-2}. The findings of the methacrylate-based nanoparticles concerning shear stress can be attributed to a higher frequency of nanoparticle interaction per cell compared to static *in vitro* conditions. In addition, dynamic microfluidically-supported cell cultures revealed different nanoparticle uptake tendencies as seen under static *in vitro* conditions: The uptake rate of **20% PDMAEMA** under flow conditions is reduced to comparable levels to **13% PMAA** (Figure 5.3). This might be due to an activation of HUVEC under dynamic conditions leading to a different surface receptor expression pattern and, thus, different nanoparticle-cell interaction.[79, 90]

Additionally, HUVECs were co-cultured with MΦ under dynamic conditions to investigate cell-cell interactions, which are known to influence cellular physiology. MΦ are known to be responsible for the clearance of cell debris and circulating nanoparticles in the blood stream by phagocytosis.[91] MΦ in general exhibited a higher uptake rate compared to HUVEC for the methacrylate-based nanoparticles (Figure 5.3). The investigations in static and dynamic

cell culture conditions lead to the assumptions that the **13% PMAA** as well as the **20% PDMAEMA** could be also taken up by macrophages *in vivo*. With regard to the uptake-tendencies between the different nanoparticles in the co-culture experiments, similar patterns were obtained under static and dynamic conditions at 3 and 6 dyn cm^{-2}, respectively. However, at 0.7 dyn cm^{-2}, which is assumed to be present in hepatic sinusoids, the uptake of **13% PMAA** and **20% PDMAEMA** did not significantly differ in contrast to the results obtained under static conditions.

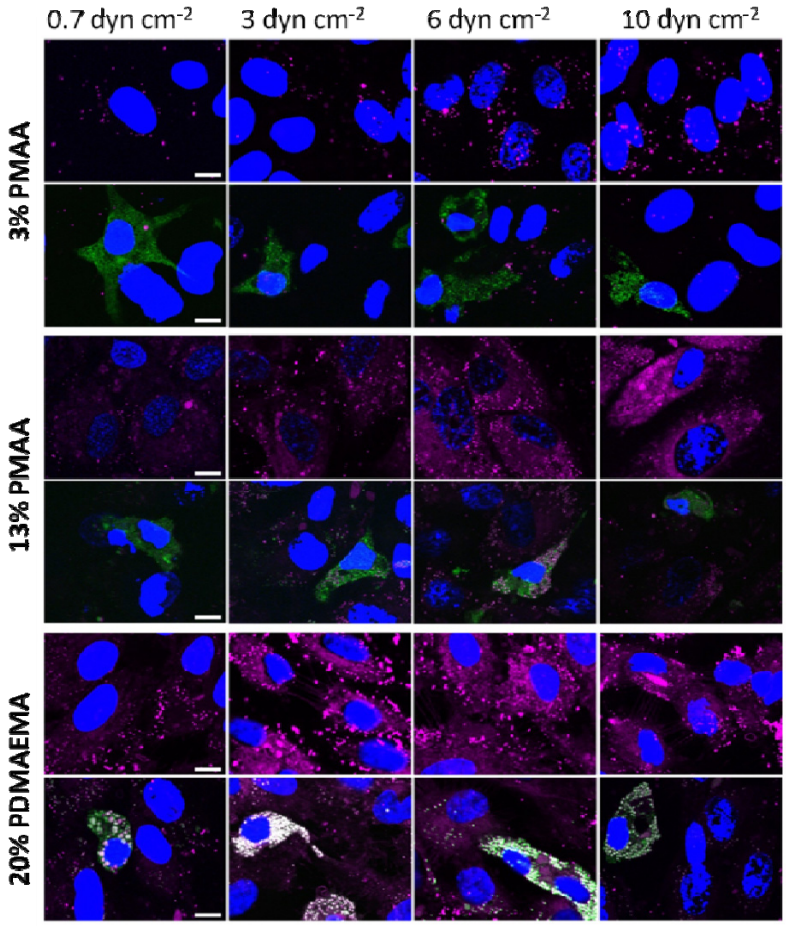

Figure 5.3: Different nanoparticles in the microfluidically-assisted cell culture. Uptake of methacrylate-based nanoparticles containing nile red in a HUVEC monoculture or a co-culture with MΦ which were subjected to different shear stress (0.7, 3, 7 or 10 dyn cm^{-2}) were analyzed after 60 min. Uptake and distribution of nanoparticles (orange) in the HUVEC mono-culture (upper panels) and co-culture (lower panels) with MΦ. Cells were subsequently stained with DAPI (blue) and macrophages were stained using CMFDA (green). All scale bars = 10 µm.

The liver plays an important role for drug- and nanoparticle clearance. In particular Kupffer cells, the local tissue-macrophages, possess endocytic activity against blood-borne materials

entering the liver and contribute to tissue modulation and regulation of the immune system in response to stimulants. For a rational drug development, possible immune-modulatory effects as well as nanoparticle clearance are key factors that need to be investigated under physiological conditions. Using intravital microscopy the cellular distribution of **3%**, **13% PMAA** and **20% PDMAEMA** nanoparticles in the liver could be observed. *In vivo* Kupffer cells mainly cleared all tested nanoparticles in the liver. However to a lower extend also endothelial cells took up **13% PMAA** and **20% PDMAEMA** nanoparticles (Figure 5.4a).

Beside the differences in the cellular distribution also the speed and kinetic of nanoparticle uptake varies between the different nanoparticles. Charged cationic **20% PDMAEMA** were taken up fastest followed by the **13% PMAA** nanoparticles (Figure 5.4b). The slowest uptake was shown by the lower charged **3% PMAA** nanoparticles. These different uptake kinetics and cellular distributions represent the different abilities to unspecifically interact with cellular membranes and to subsequently activate endocytotic or phagocytotic pathways. The uptake of all nanoparticles reached a plateau after 30 to 60 min reflecting a saturation of the processes or a clearance of the nanoparticles in the body (Figure 5.4b). The MFI of **20% PDMAEMA** even decreased constantly by 0.5% per min after 30 min within the time of observation, implying a release of nile red from **20% PDMAEMA**. Finally the comparison between the nanoparticle uptake in Kupffer cells *in vivo* reveals that **13% PMAA** and **20% PDMAEMA** are cleared more effective by the liver than the **3% PMAA** and that Kupffer cells showed a higher nanoparticle uptake than the endothelial cells. However, higher charged nanoparticles excerpt a smaller difference between the uptake in Kupffer cells and endothelial lining (Figure 5.4c). Beside the relevance of shear stress and surface charge also the cellular distribution between certain cell types can be compared. Here, the uptake of different nanoparticles (represented by the MFI) in endothelial lining and Kupffer cells was assessed.

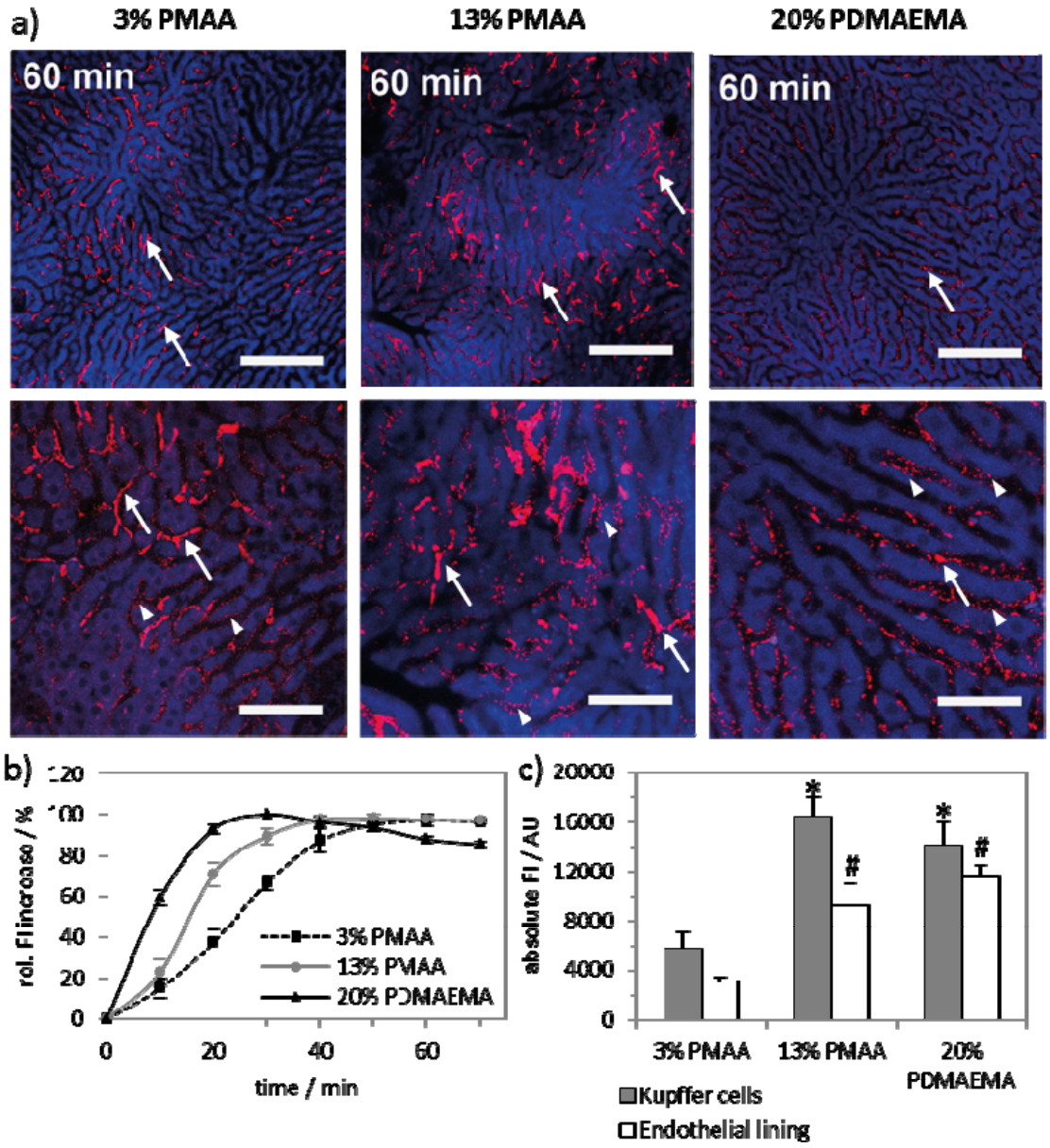

Figure 5.4. a) Intravital microscopy of different nanoparticles in the liver (liver architecture: blue, nile red containing nanoparticles red) showing accumulation of nanoparticles mostly in Kupffer cells (examples marked with a white arrows) and only little in endothelial cells (examples marked with a white triangle); scale bar upper column 250 µm, lower column 50 µm. Contrast of all images were harmonized. b) Uptake kinetic of nile red containing nanoparticles in Kupffer cells *in vivo*; graph show mean ± s.e.m. of three independent experiments. c) Maximal fluorescence intensity of PMAA and PDMAEMA-nanoparticles containing nile red in murine Kupffer cells and endothelial lining in the liver 60 min after administration; bars show mean + s.e.m. of the MFI-corrected FI of three independent experiments; significance was testes using a two-way ANOVA with Tukey post-hoc test performed on three independent experiments * $p<0.01$ between 13% PMAA or 20% PDMAEMA and 3% PMAA within one cell type. # $p<0.01$ between both cell types of one nanoparticle.

Altogether, methods for pre-screening of nanoparticle internalization under physiological relevant conditions are required. Static cultures represent a fast and useful tool to assess

nanoparticle uptake in general. However, the impact of flow conditions on the nanoparticle-cell interaction as well as different cell phenotypes can not be comprehended. The microfluidically-supported cell culture mimics shear stress as one key-factor influencing the nanoparticle uptake in general and might represent an important screening option for cell-type specific nanoparticle uptake. Since animal experiments are cost and time consuming, new models and automated systems for dynamic cell culture should be developed for screening purposes to increase the success of new animal studies.

6 Summary

The treatment of genetic disorders like cystic fibrosis, Parkinson or cancer by therapeutics is nowadays still challenging. The major drawbacks like side effects and decreased bioavailability of therapeutic substances can be reduced or overcome using nanocarriers. The most used materials for nanocarriers represent lipid and polymer based systems, whereas polymers show a high tuning potential due to the fact that they can be synthesized with varying physical and chemical properties (*e.g.* topology or functionalization). Nanocarriers are distinguished regarding their delivered substances; either they can be applied for genes, like plasmid DNA (pDNA) delivery, or for drugs, *e.g.* chemotherapeutics. Based on the different chemical properties different encapsulation strategies have to be used. As a consequence, the nanocarrier material has to fit to the desired substrate.

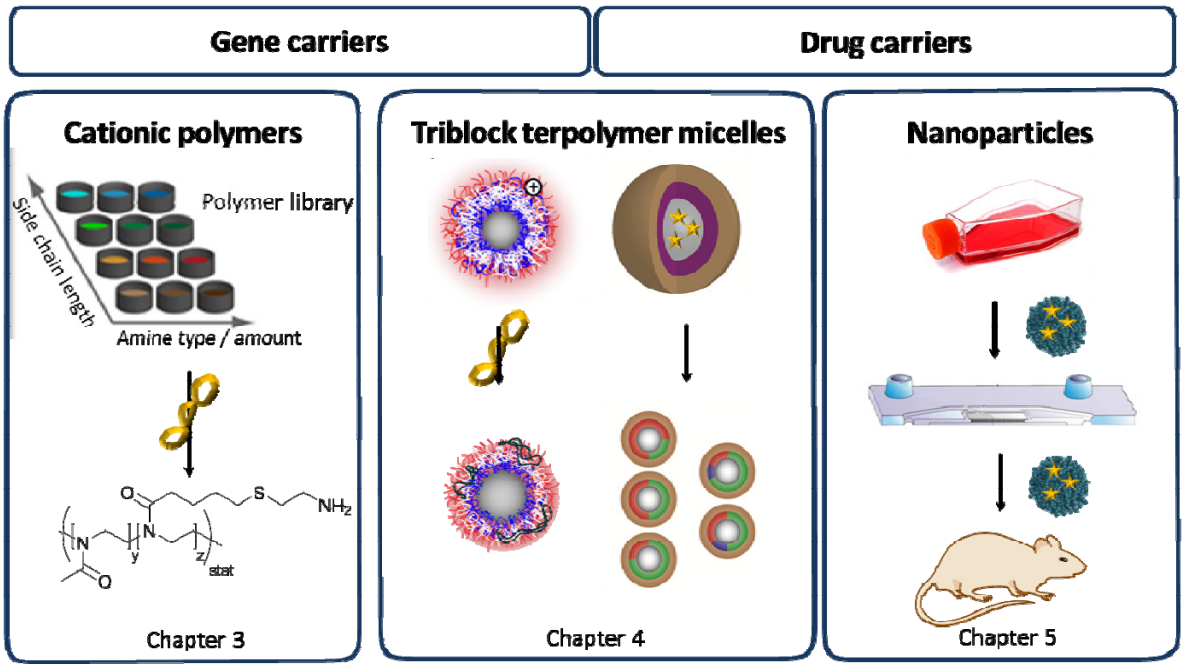

Figure 6.1: Overview about the presented polymer-based nanocarriers for potential gene and drug delivery application.

pDNA delivery is commonly based on the formation of complexes, called polyplexes, by the interaction of negatively charged phosphates and cationic polymer charges. Up to now, polymer-based pDNA transfection shows less success in clinical trials, demonstrating the

need to understand the transfection mechanism *in vitro*. In particular, poly(ethylenimine) (PEI) are frequently used and well characterized concerning its delivery potential. For instance, the high buffer capacity, which is based on high amino amount, results in an enhanced endosomal escape. However, the cytotoxic effects of PEI restrict its *in vivo* application. Thus, PEI is often used as template for numerous new polymer modifications like the functionalization with biocompatible polymers *e.g.* poly(2-oxazoline)s (POx). Here, a reduced cytotoxicity and decrease of unspecific protein interactions can be achieved, but on the other hand also a reduced transfection efficiency was observed. One possibility to overcome this drawback is the functionalization with hydrophobic units. For this purpose a library of 18 copolymers either poly((2-methyl-2-oxazoline)-*co*-(2-(3-butenyl)-2-oxazoline), (P(MeOx-*co*-ButEnOx)) or poly((2-methyl-2-oxazoline)-*co*-(2-(9-decenyl)-2-oxazoline), (P(MeOx-*co*-DecEnOx)) as precursor polymer was synthesized, varying the amount of hydrophobicity (10, 20, 30 and 40 mol%). ButEnOx and DecEnOx were then functionalized with either primary or tertiary amines for pDNA binding. Based on detailed investigations concerning the single transfection steps, like polyplex formation, stability and cytotoxicity, one polymer was identified with superior performance. Beside, transfection efficiencies similar to PEI (linear PEI DP = 200) no cytotoxic effects were detected. The screening of such polymer libraries is time consuming with conventional methods, thus a HT approach was established, starting with an automated polyplex formation.

Besides cationic polymers, cationic preformed micelles provide also the opportunity for pDNA delivery. Herein, spherical micelles based on triblock terpolymers represent promising candidates. The assembly of poly(butadiene-*b*-poly(methacrylic acid)-*b*-poly(2-(dimethylamino)ethyl methacrylate) (BMAAD) results in micelles of around 200 nm in diameter and both segments of poly(2-(dimethylamino)ethyl methacrylate) (PMAA) and poly(2-(dimethylamino)ethyl methacrylate (PDMAEMA) lead to pH dependent shapes. A patchy surface containing intra-micellar interpolyelectrolyte complexed (*im*-IPEC) at

physiological pH values leads to superior cell interaction and internalization also at the presence of serum proteins. Moreover, the expansion of the PDMAEMA block under acidic conditions results in an enhanced endosomal escape by explosion of the positively charged block. In total, the single hurdles of the transfection procedure can be overcome by this micelle resulting in high transfection efficiencies and no cytotoxicity. In contrast to such a relative large micelles, a small one with diameter below 30 nm was demonstrated as possible drug delivery carrier. The balance of charges is a promising tuning possibility and beside uptake efficiencies also the cytotoxicity can be influenced. For this purpose, spherical micelles based on poly(ethylene oxide)-*block*-poly(allyl glycidyl ether)-*block*-poly(*tert*-butyl glycidyl ether) (PEO-*b*-PAGE-*b*-P*t*BGE) were prepared. In addition, the PAGE block was functionalized with different groups to introduce cationic, anionic or targeting units. Simple mixing of the block copolymers prior micelle preparation results in mixed micelles. On the one hand binary micelles, consisting of two polymer and on the other hand ternary micelles were obtained with different polymer ratios. The resulting fine tuning of charges in the shell leads to synergistic effects, because either the internalization can be enhanced or the cytotoxicity might be reduced.

The main challenge for drug delivery *via* nanoparticles is the translation of the efficiency from *in vitro* to *in vivo*. In general, the prediction of the biodistribution, interaction with the reticuloendothelial system (RES) and the behavior under flow conditions is not possible. Thus, methacrylate-based nanoparticles were systematically investigated concerning their uptake under static and dynamic *in vitro* conditions as well as *in vivo*. The screening of different nanoparticle uptake ratios, the influence of serum proteins as well as the cytotoxicity can be efficiently and fast assessed by static *in vitro* investigations. Based on different charged methacrylate-based nanoparticles the influence of the charge on the uptake was observed. Subsequently, the microfluidically-supported dynamic cell culture was used to investigate the impact of shear stress on the nanoparticle uptake properties. Under

dynamic cell culture conditions, a shear stress dependent increased uptake was observed, indicating a sufficient interaction of the nanoparticle with the cells. Furthermore, the nanoparticle uptake in primary endothelial cells is significantly influenced by physiological shear stress and differs to the tendencies obtained under static conditions. In the co-culture of macrophages and endothelial cells an increased uptake of the nanoparticles by macrophages compared to endothelial cells were observed. Additionally, at a shear stress of 0.7 dyn cm^{-2} less pronounced differences between the dynamic co-cultivation and *in vivo* is observed in contrast to static conditions. Thus, shear stress represents a key-factor influencing nanoparticle uptake in general and might represent an important screening option for nanoparticle uptake and design.

Altogether, polymer-based nanocarriers represent an ideal tool to deliver different therapeutics, like pDNA or drugs. The continuous development in polymer science, biology and medicine are the basis for the design of new delivery systems. Based on the delivered substrate, genes and drugs, different encapsulation strategies are applied and, as a consequence, resulting in different bottlenecks. In the case of gene delivery, the main bottleneck is the performance of polymer-based nanocarriers *in vitro*. In contrast to that, drug delivery *via* nanocarriers is beyond this *in vitro* restriction and shows limits in the transfer from *in vitro* to *in vivo*. This thesis presents insight in new promising gene delivery carriers based on cationic charged polymers as well as cationic charged spherical micelles. In addition, new possible drug delivery systems based on small micelles were presented. In the end the microfluidically-supported dynamic cell culture was demonstrated as a powerful technique to obtain more information about the behavior of nanoparticles under physiological relevant conditions.

7 Zusammenfassung

Heutzutage stellt die Therapie genetisch bedingter Erkrankungen, wie beispielsweise zystische Fibrose, Parkinson oder Krebs, noch immer eine der größten Herausforderung der Medizin dar. Als Ursache gelten unter anderem die hohen Nebenwirkungen und die geringe Bioverfügbarkeit heutiger Arzneimittel. Neuartige Formulierungen auf Basis nanoskaliger Trägermaterialien sollen hier helfen, diese Nachteile zu reduzieren bzw. vollständig zu überwinden. Für die Trägermaterialien haben sich vor allem lipid- und polymerbasierte Systeme als vielversprechend herausgestellt. Polymere Systeme bieten zudem den Vorteil, dass ihre chemischen und physikalischen Eigenschaften, aufgrund ihrer vielen Variationsmöglichkeiten, an die aktuelle Problemstellung angepasst werden können. Neben dem Trägermaterial unterscheidet man derartige Systeme nach der Art, der zu transportierenden Substanz. Einerseits können genetische Strukturen, z.B. basierend auf Plasmid-Desoxyribonukleinsäure (pDNS) und andererseits Wirkstoffe, wie zum Beispiel Chemotherapeutika transportiert werden (Abbildung 7.1). Die zu transportierende Substanz ist hierbei der limitierende Faktor für die Anforderungen, die an das Trägermaterial und die entsprechenden Verkapselungsstrategien gestellt werden. Im Falle von pDNS, stellt die Bildung von Polymer-pDNS-Komplexen, sog. Polyplexe, die bisherige Grundlage für aktuelle Strategien dar. Diese Komplexbildung beruht auf den Wechselwirkungen zwischen den negativ geladenen Phosphatgruppen der pDNS und den positiven Ladungen des Polymers. Der bisher ausbleibende Erfolg derartiger Systeme in klinischen Studien zeigt allerdings die Notwendigkeit, die zugrunde liegenden Mechanismen, *in vivo* und *in vitro*, besser zu verstehen und aufzuklären.

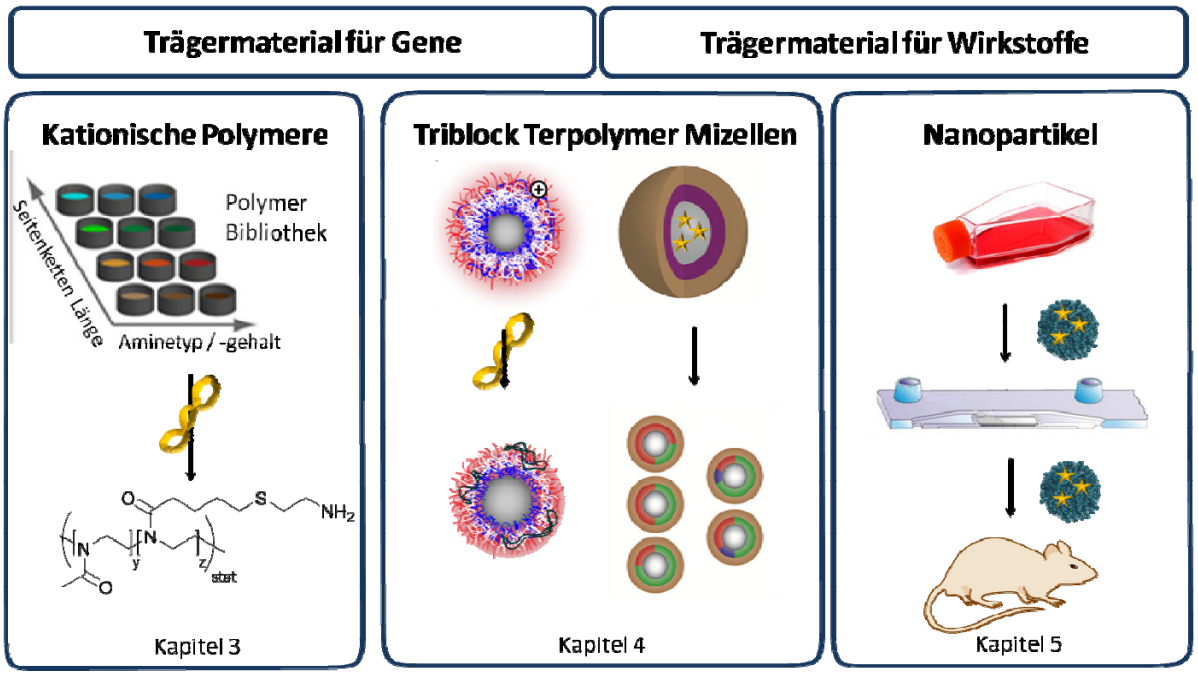

Abbildung 7.1: Übersicht über die vorgestellten Polymer-basierten nanoskalierten Trägermaterialien für die potenzielle Anwendung von Gene-und Wirkstoff-Transport.

Zur Zeit ist Poly(ethylenimin) (PEI), das am besten für solche Zwecke untersuchte Polymer, wodurch sein Potential als Trägermaterial detailliert charakterisiert ist. Vor allem die hohe Pufferkapazität, welche auf dem hohen Gehalt an Amino-Gruppen basiert, führt, im Vergleich zu anderen Polymeren, zu einer verbesserten Freisetzung aus dem Endosom. Jedoch zeigt PEI bei relevanten Konzentrationen zytotoxische Effekte, wodurch seine *in vivo* Anwendung stark einschränkt ist. Dies hat zur Folge, dass PEI oft als Baustein für neue Homo- oder Copolymere verwendet wird. So führt beispielsweise die Einführung von Poly(2-oxazolin) (POx) zu einer Reduktion der Zytotoxizität, sowie zur Unterdrückung unspezifischer Proteininteraktionen. Die Transfektionseffizienz sinkt jedoch im gleichen Maß. Eine Möglichkeit, die Verringerung der Transfektionseffizienz zu umgehen, ist die Funktionalisierung mit hydrophoben Gruppen. Aus diesem Grund wurde eine Polymerbibliothek aus insgesamt 18 Copolymeren, bestehend aus Poly((2-methyl-2-oxazolin)-*co*-(2-(3-butenyl)-2-oxazolin) (P(MeOx-*co*-ButEnOx)) und Poly((2-methyl-2-oxazolin)-*co*-(2-(9-decenyl)-2-oxazolin) (P(MeOx-*co*-DecEnOx)) hergestellt. Dabei wurde der jeweils hydrophobe Anteil, variiert (ButEnOx bzw. DecEnOx je 10, 20, 30 und

40 mol%) und um eine effiziente Interaktion mit pDNS zu gewährleisten, wurden ButEnOx und DecEnOx mit primären oder tertiären Aminen (kationischer Charakter) funktionalisiert. Auf der Grundlage detaillierter Untersuchungen der einzelnen Transfektionsschritte, welche auch die Polyplexbildung, die Polyplexstabilität und die Zytotoxizität umfassten, konnte ein Polymer identifiziert werden, welches herausragende Transfektionseffizienzen zeigt. Auf diese Weise wurden Transfektionseffizienzen, vergleichbar zu PEI (lineares PEI DP = 200) erzielt, während zytotoxische Effekte ausblieben. Da Forschungen an solch einer Polymerbibliothek mit konventionellen Methoden sehr zeitaufwendig sind, wurde in der vorliegenden Arbeit ebenfalls ein passendes Hochdurchsatzverfahren (high-throughput approach) etabliert.

Neben kationischen Polymeren eignen sich auch kationische Mizellen als Trägermaterial für pDNS. Vor allem sphärische Mizellen basierend auf dem Triblock Terpolymer Polybutadien-*block*-poly(methacrylsäure)-*block*-poly(2-(dimethylamino)ethyl methacrylat) (BMAAD) wurden im Rahmen dieser Arbeit als ein vielversprechender Kandidat identifiziert. BMAAD bildet in wässriger Umgebung sphärische Mizellen mit einem Durchmesser von ca. 200 nm, wobei sich, bedingt durch die beiden Blocksegmente Poly(methacrylsäure) (PMAA) und Poly(2-(dimethylamino)ethyl methacrylat (PDMAEMA), pH-abhängige Variationen bezüglich Geometrie und Größe ergeben können. Bei einem neutralen pH Wert entsteht eine ungleichmäßige Oberfläche, welche intra-mizellare Interpolyelektrolytkomplexe (im-IPEC) enthält, welche in Gegenwart von Serumproteinen zu einer herausragenden Zellinteraktion und -aufnahme führen. Unter sauren Bedingungen dehnt sich der kationisch geladenen PDMAEMA-Block aus, was zu einer effizienten Freisetzung der Polyplexe aus dem Endsom führt. Weiterhin konnte in der vorliegenden Arbeit gezeigt werden, dass dieses System die einzelnen Hürden einer erfolgreichen Transfektion überwinden kann und sehr hohe Transfektionseffizienzen ohne zytotoxische Effekte erzielt.

Im Rahmen dieser Arbeit wurden neben Mizellen im oberen Bereich der Nanometerskala, auch deutlich kleinere Systeme als potentieller Wirkstoffträger untersucht (Durchmesser < 30 nm). Wie mehrfach gezeigt (Kapitel 4), spielt das Gleichgewicht der positiven und negativen Ladungen eine Schlüsselrolle zur Steuerung der Zellaufnahme und Zytotoxizität. Aus diesem Grund wurden sphärische Mizellen basierend auf Poly(ethylen oxid)-*block*-poly(allyl glycidyl ether)-*block*-poly(*tert*-butyl glycidyl ether) (PEO-*b*-PAGE-*b*-PtBGE) hergestellt. Zusätzlich wurde der PAGE Block mit kationischen (Aminogruppen), anionischen (Carboxgruppen) oder zuckerbasierten (zur zielgerichteten Aufnahme, sog. „Targeting“) Gruppen funktionalisiert. Neben den Untersuchungen der klassischen Mizellen, welche aus jeweils einem Polymertyp bestehen, wurde durch Mischen der unterschiedlichen Polymertypen vor der Mizellbildung auch sog. Mix-Mizellen hergestellt. Dabei wurden binäre Mizellen (zwei unterschiedlichen Polymertypen) sowie ternäre Mizellen (drei unterschiedlichen Polymertypen) hergestellt und charakterisiert. Es konnte gezeigt werden, dass es durch eine entsprechende Justierung der Mischverhältnisse und damit der Ladungen in der Schale der Mizelle zu synergistischen Effekten in Bezug auf die Zellaufnahme und Zytotoxizität kommt.

Eine weitere große Herausforderung für nanoskalige Trägermaterialien für den Wirkstofftransport stellt der Analogieschluss und der Wissenstransfer zwischen *in vivo* und *in vitro* Versuchen dar. Grundsätzlich ist es nicht möglich, auf Grundlage von statischen *in vitro* Ergebnissen eine Vorhersage über die Bioverteilung, die Interaktionen mit dem retikuloendothelialen System (RES) und dem Verhalten unter Flussbedingen zu treffen. Aus diesem Grund wurden Methacrylat-basierte Nanopartikel systematisch auf ihre Zellaufnahme unter statischen und dynamischen *in vitro* Bedingungen untersucht und mit deren *in vivo* Verhalten verglichen. Statische *in vitro* Experimente eigenen sich besonders für ein Screening der Zellaufnahme geeigneter Nanopartikel in Abhängigkeit von deren physikalisch-chemischen Eigenschaften, der Anwesenheit bestimmter Serumproteine und der

Zytotoxizität. Im vorliegenden Fall konnte dabei unter anderem eine Ladungsabhängigkeit der Zellaufnahme beobachtet werden. Anschließend wurden diese Nanopartikel, im Hinblick auf Scherspannungs-abhängige Einflüsse, in der Mikrofluidik-unterstützten, dynamischen Zellkultur untersucht. Neben einer Scherspannungs-abhängigen Aufnahme, welche eine ausreichende Interaktion zwischen den Zellen und den Nanopartikeln wiederspiegelt, konnte in den Experimenten mit primären Endothelzellen unterschiedliche Aufnahmetendenzen zwischen den Nanopartikeln im Vergleich zu statischen Bedingungen festgestellt werden. In Co-Kulturexperimenten wurde eine erhöhte Aufnahme in Makrophagen festgestellt, welche einherging mit einer verringerten Aufnahme in den Endothelzellen. Makrophagen, vor allem Kupfferzellen, sind für die Beseitigung von Fremdkörpern und -partikeln in der Leber verantwortlich. Zudem stellte sich scherspannungs-abhängig nur ein gering ausgeprägter Unterschied in den Aufnahmetendenzen der Nanopartikel zu *in vivo* heraus, im Gegensatz zu dem statistisch System. Die Scherspannung stellt ein Schlüsselfaktor dar, der die Aufnahme von Nanopartikeln stark beeinflusst und somit als Screening Option für Nanopartikel Design herangezogen werden sollte.

Zusammenfassend konnte im Rahmen dieser Arbeit gezeigt werden, das polymerbasierte, nanoskalige Trägermaterialien eine ideale Plattform für den Transport von unterschiedlichen Therapeutika, wie pDNS, bilden. Basierend auf der zu transportierenden Substanz müssen unterschiedliche Verkapselungsstrategien verfolgt und deren individuelle Hürden überwunden werden. Im Falle von pDNS sind die größten Herausforderungen derzeit in den Transfektionseffizienzen der Polymere in *in vitro* Versuchen zu finden. Wohingegen der Schwerpunkt bei verkapselten Wirkstoffen im limitierten Transfer der Ergebnisse zwischen *in vitro* und *in vivo* Experimenten liegt.

In dieser Arbeit konnten neue Erkenntnisse in Bezug auf moderne, vielversprechende Transportsysteme basierend auf kationischen Polymeren und kationischen, sphärischen Mizellen gewonnen werden. Weiterhin wurden, basierend auf kleinen Mizellen, neue multi-

komponenten Wirkstofftransportsysteme untersucht. Am Ende wurde die mikrofluidik-unterstützte, dynamische Zellkultur als vielversprechende Technik aufgezeigt um mehr Informationen über das Verhalten von Nanopartikeln unter physiologisch relevanten Bedingung zu erlangen.

8 References

[1] A. Z. Wang, R. Langer, O. C. Farokhzad, *Annu. Rev. Med.* **2012**, *63*, 185-198.

[2] P. Ma, R. J. Mumper, *J. Nanomed. Nanotechnol.* **2013**, *4*, 1000164.

[3] A. Aied, U. Greiser, A. Pandit, W. X. Wang, *Drug Discov.Today* **2013**, *18*, 1090-1098.

[4] H. Yin, R. L. Kanasty, A. A. Eltoukhy, A. J. Vegas, J. R. Dorkin, D. G. Anderson, *Nat. Rev. Genet.* **2014**, *15*, 541-555.

[5] S. K. Samal, M. Dash, S. Van Vlierberghe, D. L. Kaplan, E. Chiellini, C. van Blitterswijk, L. Moroni, P. Dubruel, *Chem. Soc. Rev.* **2012**, *41*, 7147-7194.

[6] E. V. van Gaal, R. van Eijk, R. S. Oosting, R. J. Kok, W. E. Hennink, D. J. Crommelin, E. Mastrobattista, *J. Controll. Release* **2011**, *154*, 218-232.

[7] K. Knop, R. Hoogenboom, D. Fischer, U. S. Schubert, *Angew. Chem. Int. Ed.* **2010**, *49*, 6288-6308.

[8] J. H. Jeong, S. H. Song, D. W. Lim, H. Lee, T. G. Park, *J. Controll. Release* **2001**, *73*, 391-399.

[9] G. F. Walker, C. Fella, J. Pelisek, J. Fahrmeir, S. Boeckle, M. Ogris, E. Wagner, *Mol. Ther.* **2005**, *11*, 418-425.

[10] J. G. Cai, Y. A. Yue, D. Rui, Y. F. Zhang, S. Y. Liu, C. Wu, *Macromolecules* **2011**, *44*, 2050-2057.

[11] H. Cabral, K. Kataoka, *Sci. Technol. Adv. Mater.* **2010**, *11*.

[12] A. Vollrath, S. Schubert, U. S. Schubert, *J. Mater. Chem. B* **2013**, *1*, 1994-2007.

[13] S. Schubert, J. T. Delaney, U. S. Schubert, *Soft Matter* **2011**, *7*, 1581-1588.

[14] A. Kumari, S. K. Yadav, S. C. Yadav, *Colloid Surface B* **2010**, *75*, 1-18.

[15] Y. Lee, K. Kataoka, *Adv. Polym. Sci.* **2012**, *249*, 95-134.

[16] Y. Yue, C. Wu, *Biomater. Sci.* **2013**, *1*, 152-170.

[17] J. Ziebarth, Y. Wang, *Biophys. J.* **2009**, *97*, 1971-1983.

[18] C. L. Grigsby, K. W. Leong, *J. R. Soc. Interface* **2010**, *7*, 67-82.

[19] D. Fischer, Y. Li, B. Ahlemeyer, J. Krieglstein, T. Kissel, *Biomaterials* **2003**, *24*, 1121-1131.

[20] S. Xiang, H. Tong, Q. Shi, J. C. Fernandes, T. Jin, K. Dai, X. Zhang, *J. Controll. Release* **2012**, *158*, 371-378.

[21] V. Mailander, K. Landfester, *Biomacromolecules* **2009**, *10*, 2379-2400.

[22] K. M. Fichter, N. P. Ingle, P. M. McLendon, T. M. Reineke, *ACS Nano* **2013**, *7*, 347-364.

[23] J. Rejman, A. Bragonzi, M. Conese, *Mol. Ther.* **2005**, *12*, 468-474.

[24] D. Lechardeur, A. S. Verkman, G. L. Lukacs, *Adv. Drug Deliv. Rev.* **2005**, *57*, 755-767.

[25] H. J. Kuh, S. H. Jang, M. G. Wientjes, J. R. Weaver, J. L. S. Au, *J. Pharmacol. Exp. Ther.* **1999**, *290*, 871-880.

[26] S. Fredenberg, M. Wahlgren, M. Reslow, A. Axelsson, *Int. J. Pharm.* **2011**, *415*, 34-52.

[27] A. Akinc, M. Thomas, A. M. Klibanov, R. Langer, *J. Gene Med.* **2005**, *7*, 657-663.

[28] A. K. Varkouhi, M. Scholte, G. Storm, H. J. Haisma, *J. Controll. Release* **2011**, *151*, 220-228.

[29] T. Merdan, K. Kunath, D. Fischer, J. Kopecek, T. Kissel, *Pharm. Res.* **2002**, *19*, 140-146.

[30] Y. W. Cho, J. D. Kim, K. Park, *J. Pharm. Pharmacol.* **2003**, *55*, 721-734.

[31] Z. U. Rehman, D. Hoekstra, I. S. Zuhorn, *ACS Nano* **2013**, *7*, 3767-3777.

[32] W. T. Godbey, M. A. Barry, P. Saggau, K. K. Wu, A. G. Mikos, *J. Biomed. Mater. Res.* **2000**, *51*, 321-328.

[33] J. D. Larsen, N. L. Ross, M. O. Sullivan, *J. Gene Med.* **2012**, *14*, 580-589.

[34] M. Gillard, Z. Jia, J. J. Hou, M. Song, P. P. Gray, T. P. Munro, M. J. Monteiro, *Biomacromolecules* **2014**, *15*, 3569-3576.

[35] P. van de Wetering, E. E. Moret, N. M. E. Schuurmans-Nieuwenbroek, M. J. van Steenbergen, W. E. Hennink, *Bioconjugate Chem.* **1999**, *10*, 589-597.

[36] K. Matyjaszewski, *Science* **2011**, *333*, 1104-1105.

[37] K. Matyjaszewski, N. V. Tsarevsky, *Nat. Chem.* **2009**, *1*, 276-288.

[38] J.-L. Zhu, H. Cheng, Y. Jin, S.-X. Cheng, X.-Z. Zhang, R.-X. Zhuo, *J. Mater. Chem.* **2008**, *18*, 4433-4441.

[39] S. Han, H. Wan, D. Lin, S. Guo, H. Dong, J. Zhang, L. Deng, R. Liu, H. Tang, A. Dong, *Acta Biomater.* **2014**, *10*, 670-679.

[40] T. K. Georgiou, *Polym. Int.* **2014**, *63*, 1130-1133.

[41] H. Wei, J. A. Pahang, S. H. Pun, *Biomacromolecules* **2013**, *14*, 275-284.

[42] Y. Y. Mai, A. Eisenberg, *Chem. Soc. Rev.* **2012**, *41*, 5969-5985.

[43] N. Nishiyama, Y. Bae, K. Miyata, S. Fukushima, K. Kataoka, *Drug Discov.Today: Tech.* **2005**, *2*, 21-26.

[44] K. Kataoka, H. Togawa, A. Harada, K. Yasugi, T. Matsumoto, S. Katayose, *Macromolecules* **1996**, *29*, 8556-8557.

[45] N. Wiradharma, Y. Zhang, S. Venkataraman, J. L. Hedrick, Y. Y. Yang, *Nano Today* **2009**, *4*, 302-317.

[46] M. J. Manganiello, C. Cheng, A. J. Convertine, J. D. Bryers, P. S. Stayton, *Biomaterials* **2012**, *33*, 2301-2309.

[47] Y. Li, X. Lei, H. Dong, T. Ren, *RSC Adv.* **2014**, *4*, 8165-8176.

[48] M. S. Aw, M. Kurian, D. Losic, *Chem. Eur. J.* **2013**, *19*, 12586-12601.

[49] C. Liu, F. Liu, L. Feng, M. Li, J. Zhang, N. Zhang, *Biomaterials* **2013**, *34*, 2547-2564.

[50] P. Aggarwal, J. B. Hall, C. B. McLeland, M. A. Dobrovolskaia, S. E. McNeil, *Adv. Drug Deliv. Rev.* **2009**, *61*, 428-437.

[51] M. J. Ernsting, M. Murakami, A. Roy, S. D. Li, *J. Controll. Release* **2013**, *172*, 782-794.

[52] H. T. Lv, S. B. Zhang, B. Wang, S. H. Cui, J. Yan, *J. Controll. Release* **2006**, *114*, 100-109.

[53] S. Choksakulnimitr, S. Masuda, H. Tokuda, Y. Takakura, M. Hashida, *J. Controll. Release* **1995**, *34*, 233-241.

[54] M. Neu, D. Fischer, T. Kissel, *J. Gene Med.* **2005**, *7*, 992-1009.

[55] I. Richard, M. Thibault, G. De Crescenzo, M. D. Buschmann, M. Lavertu, *Biomacromolecules* **2013**, *14*, 1732-1740.

[56] M. A. Mintzer, E. E. Simanek, *Chem. Rev.* **2009**, *109*, 259-302.

[57] C. Zhu, S. Jung, G. Si, R. Cheng, F. Meng, X. Zhu, T. G. Park, Z. Zhong, *J. Polym. Sci., Part A: Polym. Chem.* **2010**, *48*, 2869-2877.

[58] M. J. Waring, *J. Mol. Biol.* **1965**, *13*, 269-282.

[59] C. J. Waschinski, V. Herdes, F. Schueler, J. C. Tiller, *Macromol. Biosci.* **2005**, *5*, 149-156.

[60] F. H. Schacher, P. A. Rupar, I. Manners, *Angew. Chem. Int. Ed.* **2012**, *51*, 7898-7921.

[61] A. H. Groschel, F. H. Schacher, H. Schmalz, O. V. Borisov, E. B. Zhulina, A. Walther, A. H. E. Muller, *Nat. Commun.* **2012**, *3*.

[62] T. P. Lodge, A. Rasdal, Z. B. Li, M. A. Hillmyer, *J. Am. Chem. Soc.* **2005**, *127*, 17608-17609.

[63] H. Dong, N. Dube, J. Y. Shu, J. W. Seo, L. M. Mahakian, K. W. Ferrara, T. Xu, *ACS Nano* **2012**, *6*, 5320-5329.

[64] F. Alexis, E. Pridgen, L. K. Molnar, O. C. Farokhzad, *Mol. Pharm.* **2008**, *5*, 505-515.

[65] H. Cabral, Y. Matsumoto, K. Mizuno, Q. Chen, M. Murakami, M. Kimura, Y. Terada, M. R. Kano, K. Miyazono, M. Uesaka, N. Nishiyama, K. Kataoka, *Nat. Nanotechnol.* **2011**, *6*, 815-823.

[66] Y. Lee, T. Ishii, H. Cabral, H. J. Kim, J. H. Seo, N. Nishiyama, H. Oshima, K. Osada, K. Kataoka, *Angew. Chem. Int. Ed.* **2009**, *48*, 5309-5312.

[67] E. Betthausen, M. Drechsler, M. Fortsch, F. H. Schacher, A. H. E. Muller, *Soft Matter* **2011**, *7*, 8880-8891.

[68] D. Luo, W. M. Saltzman, *Nat. Biotechnol.* **2000**, *18*, 893-895.

[69] C. T. de Ilarduya, Y. Sun, N. Duezguenes, *Eur. J. Pharm. Sci.* **2010**, *40*, 159-170.

[70] J. Y. Cherng, *J. Pharm. Pharm. Sci.* **2009**, *12*, 346-356.

[71] M. Breunig, U. Lungwitz, R. Liebl, A. Goepferich, *Proc. Natl. Acad. Sci. U. S. A.* **2007**, *104*, 14454-14459.

[72] K. Babiuch, D. Pretzel, T. Tolstik, A. Vollrath, S. Stanca, F. Foertsch, C. R. Becer, M. Gottschaldt, C. Biskup, U. S. Schubert, *Macromol. Biosci.* **2012**, *12*, 1190-1199.

[73] P. Greenspan, E. P. Mayer, S. D. Fowler, *J. Cell Biol.* **1985**, *100*, 965-973.

[74] A. Vollrath, A. Schallon, C. Pietsch, S. Schubert, T. Nomoto, Y. Matsumoto, K. Kataoka, U. S. Schubert, *Soft Matter* **2013**, *9*, 99-108.

[75] J. W. Nichols, Y. H. Bae, *Nano Today* **2012**, *7*, 606-618.

[76] S. H. Au, M. D. Chamberlain, S. Mahesh, M. V. Sefton, A. R. Wheeler, *Lab Chip* **2014**, *14*, 3290-3299.

[77] M. Raasch, K. Rennert, T. Jahn, S. Peters, T. Henkel, O. Huber, I. Schulz, H. Becker, S. Lorkowski, H. Funke, A. Mosig, *Biofabrication* **2015**, *7*, 015013.

[78] H. Yang, F. L. Zhao, Y. Li, M. M. Xu, L. Li, C. H. Wu, H. Miyoshi, Y. Y. Liu, *Int. J. Nanomed.* **2013**, *8*.

[79] S. P. Samuel, N. Jain, F. O'Dowd, T. Paul, D. Kashanin, V. A. Gerard, Y. K. Gun'ko, A. Prina-Mello, Y. Volkov, *Int. J. Nanomed.* **2012**, *7*, 2943-2956.

[80] A. T. Press, A. Traeger, C. Pietsch, A. Mosig, M. Wagner, M. G. Clemens, N. Jbeily, N. Koch, M. Gottschaldt, N. Beziere, V. Ermolayev, V. Ntziachristos, J. Popp, M. M. Kessels, B. Qualmann, U. S. Schubert, M. Bauer, *Nat. Commun.* **2014**, *5*.

[81] K. S. Vellonen, M. Malinen, E. Mannermaa, A. Subrizi, E. Toropainen, Y. R. Lou, H. Kidron, M. Yliperttula, A. Urtti, *J. Controll. Release* **2014**, *190*, 94-114.

[82] J. Chiefari, Y. K. Chong, F. Ercole, J. Krstina, J. Jeffery, T. P. T. Le, R. T. A. Mayadunne, G. F. Meijs, C. L. Moad, G. Moad, E. Rizzardo, S. H. Thang, *Macromolecules* **1998**, *31*, 5559-5562.

[83] G. Moad, E. Rizzardo, S. H. Thang, *Aust. J. Chem.* **2009**, *62*, 1402-1472.

[84] A. Shalviri, H. K. Chan, G. Raval, M. J. Abdekhodaie, Q. Liu, H. Heerklotz, X. Y. Wu, *Colloid Surface B* **2013**, *101*, 405-413.

[85] S. Agarwal, Y. Zhang, S. Maji, A. Greiner, *Mater. Today* **2012**, *15*, 388-393.

[86] J. Voigt, J. Christensen, V. P. Shastri, *Proc. Natl. Acad. Sci. U. S. A.* **2014**, *111*, 2942-2947.

[87] S. Tenzer, D. Docter, J. Kuharev, A. Musyanovych, V. Fetz, R. Hecht, F. Schlenk, D. Fischer, K. Kiouptsi, C. Reinhardt, K. Landfester, H. Schild, M. Maskos, S. K. Knauer, R. H. Stauber, *Nat. Nanotechnol.* **2013**, *8*, 772-781.

[88] S. Ritz, S. Schottler, N. Kotman, G. Baier, A. Musyanovych, J. Kuharev, K. Landfester, H. Schild, O. Jahn, S. Tenzer, V. Mailander, *Biomacromolecules* **2015**, *16*, 1311-1321.

[89] E. C. Cho, Q. Zhang, Y. N. Xia, *Nat. Nanotechnol.* **2011**, *6*, 385-391.

[90] M. Raasch, K. Rennert, T. Jahn, S. Peters, T. Henkel, O. Huber, I. Schulz, H. Becker, S. Lorkowski, H. Funke, A. Mosig, *Biofabrication* **2015**, *7*.

[91] M. A. Dobrovolskaia, P. Aggarwal, J. B. Hall, S. E. McNeil, *Mol. Pharm.* **2008**, *5*, 487-495.

List of abbreviations

AF4 – Asymmetric flow field-flow fractionation

BMAAD – poly(butadiene-*b*-poly(methacrylic acid)-*b*-poly(2-(dimethylamino)ethyl methacrylate)

bPEI – branched poly(ethylenimine)

CLSM – confocal laser scanning microscopy

CROP – cationic ring opening polymerization

DLS – dynamic light scattering

DP – degree of polymerization

EAT – PEO_{42}-*b*-$PAGE_{15}$-*b*-P*t*BGE_{12}

EB – ethidium bromid

EBA – ethidium bromide assay

ECT – PEO_{42}-*b*-$PAGE_{15,COOH}$-*b*-P*t*BGE_{12}

EGT – PEO_{42}-*b*-($PAGE_{10,Gal}$-*co*-$PAGE_{5}$)-*b*-P*t*BGE_{12}

ENT – PEO_{42}-*b*-($PAGE_{8,NH2}$-*co*-$PAGE_{7}$)-*b*-P*t*BGE_{12}

HT – high-throughput

im-IPEC – intra-micellar interpolyelectrolyte complexed

LDH – lactate dehydrogenase

lPEI – linear poly(ethylenimine)

lNp – l = long decenyl side chain, N = amino content in mol%, p = primary amine,

lNt – l = long decenyl side chain, N = amino content in mol%, t = tertiary amine.

MΦ –primary human macrophages

PDMAEMA – poly(2-(dimethylamino)ethyl methacrylate

pDNA – plasmid DNA

PCL – poly(ε-caprolactone)

PEG – poly(ethylene glycol)

PEI – poly(ethylenimine)

PEO-*b*-PAGE-*b*-PtBGE – poly(butadiene-*block*-poly(methacrylic acid)-*block*-poly(2-(dimethylamino)ethyl methacrylate)

PIC – polyion complex

PLGA – poly(lactic-*co*-glycolic acid)

PLL – poly(L-lysin)

PMAA – poly(methacrylic acid)

PMeOx – poly(2-methyl-2-oxazoline)

P(MeOx-*co*-ButEnOx) – poly((2-methyl-2-oxazoline)-*co*-(2-(3-butenyl)-2-oxazoline))

P(MeOx-*co*-DecEnOx) – poly((2-methyl-2-oxazoline)-*co*-(2-(9-decenyl)-2-oxazoline))

PMMA – poly(methyl methacrylate)

POx – poly(2-oxazoline)

RAFT – reversible addition-fragmentation chain transfer

RES – reticuloendothelial system

siRNA – small interfering RNA

sNp – s = short decenyl side chain, N = amino content in mol%, p = primary amine,

sNt – s = short decenyl side chain, N = amino content in mol%, t = tertiary amine.

Curriculum vitae

Alexandra C. Rinkenauer

Date of birth	04.06.1986
Place of birth	Friedrichshafen
Citizenship	German

Education

01/2012 – present **PhD-student,** Friedrich Schiller University Jena, Germany
Laboratory of Organic and Macromolecular Chemistry (IOMC)
"Tailor-made polymers as nanocarriers for drug and gene delivery"
Supervisor: Prof. Dr. Ulrich S. Schubert

05 – 11/2011 **Master Thesis**, University Bayreuth, Germany,
Chair for process biotechnology
"*Polycationic transfection of siRNA"*
Supervisor: Prof. Dr. Ruth Freitag

10/2009 – 11/2011 **Molecular Biology and Biochemistry, M. Sc**. University Bayreuth, Germany
Specialization: Methods of Biochemistry, Molecular Modeling, Cell cycle and Cancer, Neurobiology, Self-assembly of biopolymers

10/2006 –08/2009 **Molecular Biology, B. Sc.**, University Bayreuth, Germany
Bachelor Thesis: *"Cloning of the formaldehyd dehydrogenase promoter of Hyphomicrobium zavarzinii ZV 580"*

08/1996 - 06/2005 **University entrance qualification**: Abitur (A-Level)
Goethe Gymnasium Ludwigsburg, Germany

Jena, ……..

_____

Alexandra C. Rinkenauer

Publication list

Peer-reviewed publications

C. von der Ehe, A. C. Rinkenauer, C. Weber, D. Szamosvari, M. Gottschaldt, U. S. Schubert, Selective uptake of a fructose glycopolymer prepared by RAFT polymerization into human breast cancer cells, *Macromol. Biosci.* **2016**, *16*, 508-521.

A.T. Press, L. Ungelenk, A. C. Rinkenauer, M. Gröger, F. D. Lehmann, A. Mosig, U. S. Schubert, M. G. Clemens, M. Bauer, A new fluorescent dye for cell tracing and mitochondrial imaging *in vitro* and *in vivo*, *J. Biophotonics* **2015**, DOI: 10.1002/jbio.201500190.

A. C. Rinkenauer, A. T. Press, M. Raasch, C. Pietsch, S. Schweizer, S. Schwörer, K. L. Rudolph, A. Mosig, M. Bauer, A. Traeger, U. S. Schubert, Comparison of the uptake of methacrylate-based nanoparticles in static and dynamic *in vitro* systems as well as *in vivo*, *J. Controll. Release* **2015**, *216*, 158-168.

T. Yildrim, A. C. Rinkenauer, C. Weber, A. Traeger, S. Schubert, U. S. Schubert, RAFT made methacrylate copolymers for reversible pH-responsive nanoparticles, *J. Polym. Sci. Part A: Polym. Chem.* **2015**, *53*, 2711-2721.

A. C. Rinkenauer, S. Schubert, A. Taeger, U. S. Schubert, Influence of polymer architecture on *in vitro* pDNA delivery, *J. Mater. Chem. B* **2015**, *3*, 7477-7493.

A. C. Rinkenauer, L. Tauhardt, F. Wendler, K. Kempe, M. Gottschaldt, A. Traeger, U. S. Schubert, A cationic poly(2-oxazonline) with high *in vitro* transfection efficiency identified by a library approach, *Macromol. Biosci.* **2015**, *15*, 414-425.

M. J. Barthel, A. C. Rinkenauer, M. Wagner, U. Mansfeld, S. Höppner, J. A. Czaplewska, M. Gottschaldt, A. Traeger, F. H. Schacher, U. S. Schubert, Small but powerful: Co-assembly of polyether-based triblock terpolymer into sub-30 nm micelles and synergistic effects on cellular interactions, *Biomacromolecules* **2014**, *15*, 2426-2439.

A. C. Rinkenauer, A. Schallon, U. Günther, M. Wagner, E. Betthausen, U. S. Schubert, F. H. Schacher, A paradigm change: Efficient transfection of human leukemia cells by stimuli-responsive multicompartment micelles, *ACS Nano* **2013**, *7*, 9624-9631.

A. C. Rinkenauer, A. Vollrath, A. Schallon, L. Tauhardt, K. Kempe, S. Schubert, D. Fischer, U. S. Schubert, Parallel high-throughput screening of polymer vectors for nonviral gene delivery: evaluation of structure-property relationships of transfection, *ACS Comb. Sci.* **2013**, *15*, 475-482.

M. Wagner, A. C. Rinkenauer, A. Schallon, U. S. Schubert, Opposites attract: Influence of the molar mass branched poly(ethylene imine) on biophysical characteristics of siRNA-based polyplexes, *RSC Adv.* **2013**, *3*, 12774-12785.

.

Poster presentations

A. C. Rinkenauer, A. Schallon, U. Freier, E. Betthausen, M. Wagner, F. H. Schacher, U. S. Schubert, Efficient transfection of suspension cells by triblock terpolymer micelles….. **NanoConSens Annual Meeting**, Jena, Germany, September **2012**.

A. C. Rinkenauer, A. Vollrath, A. Schallon, U. S. Schubert, Parallel high-throughput screening of polymer vectors for non-viral gene delivery: Evaluation of structure-property-relationship of transfection **ESACT**, Lille, France, Juli **2013**.

Acknowledgement / Danksagung

An dieser Stelle bedanke ich mich bei allen, die mich bei der Erstellung dieser Arbeit unterstützt haben. Zu allererst richtet sich mein Dank an Prof. Dr. Ulrich S. Schubert, für die Möglichkeit und das Vertrauen als Biochemikerin in einer chemisch ausgeprägten Arbeitsgruppe promovieren zu dürfen. Neben den neuen und großzügigen Biolaboren war die interdisziplinäre Arbeit durch die unterschiedlichsten Polymere immer eine tolle Herausforderung an der ich sehr gewachsen bin. Ein weiterer besonderer Dank gilt Jun.-Prof. Dr. Felix H. Schacher für viele Diskussion und die „Eva“ Mizelle, sie hat mich bis heute noch kein einziges Mal enttäuscht. Zusätzlich ist ein äußerst großer Danke meiner direkten Betreuerin Dr. Anja Träger geschuldet, für die vielen, vielen produktiven Diskussion und die Unterstützung.

Weiterhin bedanke ich mich bei der gesamten Arbeitsgruppe und Kooperationspartnern für die gute und effiziente Zusammenarbeit. Hierbei bedanke ich mich im Besonderen bei Dr. Markus Barthel, neben den super Mizellen fand ich dein Interesse an den Bio-assays super. Auch bedanke ich mich bei Dr. Lutz Tauhardt und Dr. Antje Vollrath für die tolle Zusammenarbeit, was wirklich high-throughput genannt werden kann. Weiterhin danke ich Adrian Press für den im letzten Jahr neu gewonnen Einblick in die Medizin bzw. *in vivo* Mausversuche. Dr. Michael Wagner und Turgay Yildrim sei an dieser Stelle auch ausdrücklich gedankt.

Mein Dank gilt natürlich der kompletten Biogruppe, Dr. Anja Träger, Carolin Fritzsche, Dr. David Pretzel, Tanja Bus und Elisabeth Preußger. Die Zeit in unserem kleinen aber feinen TO Biolab war super, welches sich in den neuen ZAF Laboren nicht geändert hat. Besonders ist Carolin Fritzsche hervorzuheben für die fantastische Zusammenarbeit und Unterstützung. Hier komme ich gleich wieder zurück auf das TO. Besonderen Dank gilt der „TO-Crew“, für die tolle und freundliche Aufnahme in die Arbeitsgruppe, die mir den Start

in Jena sehr erleichtert hat. Nicht zu vergessen ist Ulrike Günther, für die vielen tollen Abende an denen wir die Inkubationszeiten zusammen verbracht haben. Dies bringt mich auch gleich zu den neu gewonnen bzw. vertieften Freundschaften im ZAF, Dr. Christine Weber, Dr. Stephanie Höppner und Dr. Uwe Köhn, danke euch. Aber auch allen anderen „neuen“ ZAFianern danke ich für die tolle Atmosphäre und morgendliche Grüße ins Aquarium. Auch meinen Büro- bzw. Aquariumskollegen, Dr. Stephanie Schubert, Dr. Anja Träger, Dr. Michael Wagner, Dr. Antje Vollrath, Tanja Bus und Turgay Yildrim, danke für die fantastische Atmosphäre und wissenschaftlichen Diskussionen.

Zuletzt bedanke ich mich noch im Besonderen bei Dr. Michael Wagner, Sarah Crotty und Dr. Anja Träger sowie Adrian Press. Neben den wissenschaftlichen Diskussionen seid ihr mir in den letzten Jahren sehr ans Herz gewachsen und ohne euch wäre die Zeit hier in Jena nicht dieselbe gewesen.

Der Größte Dank gilt meiner Familie und Pietscher für die Unterstützung und den Rückhalt in all den Jahren. Danke für alles!

Declaration of authorship / Selbstständigkeitserklärung

Hiermit erkläre ich, dass ich die vorliegende Arbeit selbständig angefertigt, nicht anderweitig zu Prüfungszwecken vorgelegt und keine anderen als die angegebenen Hilfsmittel verwendet habe. Sämtliche wissentlich verwendete Textausschnitte, Zitate oder Inhalte anderer Verfasser wurden ausdrücklich als solche gekennzeichnet.

I hereby certify that the work disclosed here is, to the best of my knowledge, original and the result of my own investigations, except as acknowledged, and has not been submitted, either in part or whole, for a degree at this or any other university.

Jena, den …….

_____

Alexandra C. Rinkenauer

Publication P1 to P8

P1 *J. Mater. Chem. B* **2015**, DOI: 10.1039/C5TB00782H. Reproduced by permission of The Royal Society of Chemistry.

P2 *RSC Advances* **2013**, *3*, 12774-12785. Reproduced by permission of The Royal Society of Chemistry.

P3 Reprinted by permission from *Macromol. Biosci.* **2015**, *15*, 414-425. Copyright 2014 Wiley-VCH.

P4 Reprinted by permission from *ACS Comb. Sci.* **2013**, *15*, 475-482. Copyright 2013 American Chemical Society.

P5 Reprinted by permission from *ACS Nano* **2013**, *7*, 9624-9631. Copyright 2013 American Chemical Society.

P6 Reprinted by permission from *Biomacromolecules* **2014**, *15*, 2426-2439. Copyright 2014 American Chemical Society.

P7 Reprinted by permission from *J. Polym. Sci. Part A: Polym. Chem.* **2015**, DOI: 10.1002/pola.27734. Copyright 2015 Wiley Periodicals.

P8 Reprinted with permission from *J. Controll. Release* **2015**, *216*, 158-168. Copyright 2015 Elsevier.

Publication P1

Influence of polymer architecture on *in vitro* pDNA delivery

A. C. Rinkenauer, S. Schubert, A. Taeger, U. S. Schubert

J. Mater. Chem. B **2015**, *3*, 7477-7493.

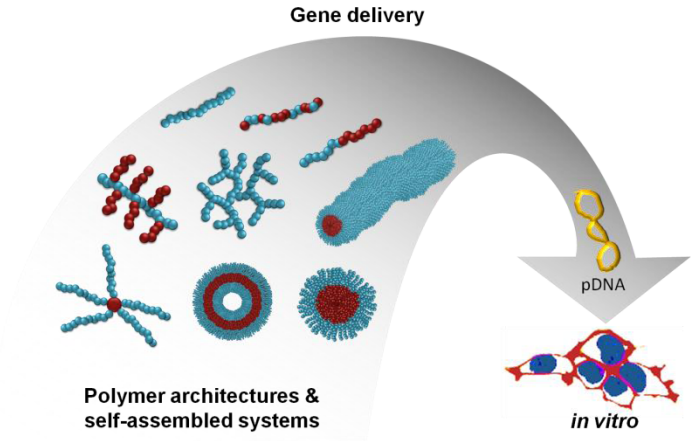

Journal of
Materials Chemistry B

REVIEW

View Article Online
View Journal | View Issue

Cite this: J. Mater. Chem. B, 2015, 3, 7477

The influence of polymer architecture on *in vitro* pDNA transfection

Alexandra C. Rinkenauer,[ab] Stephanie Schubert,[bc] Anja Traeger*[ab] and Ulrich S. Schubert*[ab]

Received 27th April 2015,
Accepted 22nd July 2015

DOI: 10.1039/c5tb00782h

www.rsc.org/MaterialsB

In 2012, the first gene therapy agent was approved by the Europe Medicines Agency leading to increased interest in this research field. Beside viruses, non-viral agents based on lipids or polymers represent aspiring alternatives to deliver the genetic material. Different hurdles have to be overcome depending on the kind of nucleic acid used, where plasmid DNA (pDNA) and small interfering RNA represent the common ones. The main challenge for transfection agents, in particular for pDNA delivery, is the transfer to the cell and into the cell nuclei. Within the group of transfection vesicles, cationic polymers show promising features and variability, as they can be synthesized with tailor-made physical and chemical properties (architectures and functionalisation). In the field of polymer-based gene delivery, the tuning potential of polymers by using different architectures like graft and star-shaped polymers as well as self-assembled block copolymers is immense. In particular, in the last few years numerous new polymer designs showed enhanced transfection properties in combination with good biocompatibility. Furthermore, new insights into the transfection mechanism demonstrated the continuous progress in this field. Polymer architecture influences the polyplex characteristics and the latter has an impact on the transfection mechanism, *e.g.* the interaction with the cellular membrane depends on the polyplex shape. Moreover, polyplex dissociation can be easily influenced by the polymer chemistry, thus biodegradable linkers lead to well suited polymers with reduced toxicity and high delivery potential, and are also promising for *in vivo* applications. This review focuses on the influence of polymer architectures for pDNA transfection *in vitro*, showing recent developments and insights. The theoretical background concerning the biological challenges for cationic polymers and the impact of graft- or star-shaped architectures as well as self-assembled structures will be presented in detail.

1 Introduction

Nowadays, genetic disorder diseases like cystic fibrosis, Parkinson's disease or cancer[1] can be treated only with low success rates. Since 1995, causal treatment on the genetic level has come into focus and gene therapy has become a prominent matter of research.[2,3] However, several drawbacks had to be overcome, for instance the tragic history of young children, who developed leukemia as a consequence of gene therapy.[4] The missing success of gene delivery vesicles in clinical trials also supports the attitudes of gene therapy criticism. However, in 2012 the first gene therapy agent was approved by the Europe Medicines Agency, and a revival started.[2,5] For gene therapy, two main routes can be applied, namely viral and non-viral delivery. Using viruses, very high efficiency can be achieved due to their evolutionary development. However, besides the risk of causing immune response after repeated administration the limited DNA packing capacity has also to be taken into consideration.[4,6] Thus, non-viral delivery methods are promising tools as alternative delivery vehicles to viruses. Herein, cationic lipids or polymers can be applied *in vitro* but also *in vivo*. In the field of gene delivery, diverse genetic materials are applied for instance plasmid DNA (pDNA) or small interfering RNA (siRNA). Besides physical differences such as size or flexibility, the site of action in cells also differs. In case of siRNA, down regulation of proteins occurs on the mRNA level in the cytoplasm. pDNA delivery results in protein production, starting with the transcription of the pDNA in the cell nuclei. It should be noted that the large size of pure pDNA (hydrodynamic diameter of 300 to 400 nm) and the short half-life in the presence of serum proteins make it indispensable to pack and protect pDNA in vesicles and particles.[7,8] However, the main challenge is their delivery to the desired site of action *in vitro* and *in vivo*. Cationic polymers show a high tuning potential as they can be synthesized with varying physical and

[a] Laboratory of Organic and Macromolecular Chemistry (IOMC), Friedrich Schiller University Jena, Humboldtstrasse 10, 07743 Jena, Germany
[b] Jena Center for Soft Matter (JCSM), Friedrich Schiller University Jena, Philosophenweg 7, 07743 Jena, Germany. E-mail: ulrich.schubert@uni-jena.de, anja.traeger@uni-jena.de
[c] Institute of Pharmacy, Department of Pharmaceutical Technology, Friedrich Schiller University Jena, Otto-Schott-Str. 41, 07745 Jena, Germany

chemical properties (functionalisation and architectures).[6,9] In particular cationic polymer systems like polyethylenimine (PEI), poly(2-(dimethylamino)ethyl methacrylate) (PDMAEMA) or poly(L-lysin) (PLL) are commonly used and well characterized concerning their delivery potential. Herein, PEI represents the gold standard for polymer based transfection agents *in vitro*, due to high efficiency and commercial availability.[10] Drawbacks like a low transfection efficiency compared to viruses and a high cytotoxicity restricted so far the *in vivo* application of cationic polymers. Significant research on pDNA delivery was triggered leading to numerous polymer modifications in the last few years. For instance, functionalisation with biocompatible polymers like poly(ethylene glycol) (PEG) reduces the cytotoxicity and unspecific protein interactions.[11,12] Nevertheless, this benefit of PEGylated polymers includes a decreased efficiency.[13,14] Therefore, the journey of identifying the perfect polymer for pDNA delivery did not end. The opportunities are manifold from the perspective of polymer chemistry. Varying the chain length, composition, functionalisation, or architecture leads to different properties and efficiencies. For example, the effect of the molar mass of the polymers was investigated in detail and was presented as one main aspect of an efficient pDNA delivery but also cytotoxic properties.[9,15,16] Beside, it was elucidated that the polymer architecture has an important impact. This may be one of the most promising opportunities to design efficient delivery polymers, as high efficiency is not always linked with an increased cytotoxicity. Moreover, also viruses like adenovirus (spherical shape) or ebola (worm like shape) represent different shapes.[17,18] In particular in the last five years, architectures like star-shaped polymers or filamentous micelles were presented as efficient pDNA delivery vehicles.[19–21]

This review addresses the influence of the molecular polymer architectures as well as of self-assembled structures concerning

Alexandra C. Rinkenauer

Alexandra C. Rinkenauer was born in 1986 in Friedrichshafen (Germany) and studied molecular biology and biochemistry at the University of Bayreuth (Germany; 2006–2011). She accomplished her master's thesis in 2011 at the chair for process biotechnology and started her PhD studies in 2012 at the Friedrich Schiller University Jena (Germany) in the Laboratory of Organic and Macromolecular Chemistry. In her PhD studies, supervised by Prof. Ulrich S. Schubert, she focused on the biological applications of new polymer-based nanocarriers for drug and gene delivery.

Stephanie Schubert

Stephanie Schubert (née Hornig) was born in 1981 in Zwickau (Germany). She obtained her MS in chemistry at the Fridrich Schiller University Jena (Germany) in 2005. After reteach activities at Virginia Tech (Blacksburg, USA), she finished her PhD studies in 2008 in the field of polysaccharide chemistry. During a postdoctoral training with J. M. J. Frechét at Berkeley UC (USA), she gained further experience in polymers as gene delivery devices. She currently is working on projects related to nanoparticles for drug delivery and sensor application in the Pharmaceutical Technology Department at the Friedrich Schiller University Jena.

Anja Traeger

Anja Traeger (née Schallon) was born in 1982 in Beeskow (Germany) and studied biochemistry at the University of Bayreuth (Germany; 2002–2007) with a stay at the University of York (UK). After her PhD studies (2007–2011) at the chair for process biotechnology at the University of Bayreuth, where she started to work with polymers for gene delivery, she moved to the Friedrich Schiller University Jena in 2011 for her postdoctoral training under the supervision of Prof. Ulrich S. Schubert. Her research interests are the characterization and biological application of polymer-based nanomaterials with a main focus on gene and drug delivery.

Ulrich S. Schubert

Ulrich S. Schubert was born in Tübingen (Germany) in 1969. He studied chemistry in Frankfurt and Bayreuth (both Germany) and at the Vorginia Commonwealth University, Richmond (USA). His PhD studies were performed at the Universities of Bayreuth and South Florida. After postdoctoral training with J.-M. Lehn at the University of Strasbourg (France), he moved to the TU Munich (Germany) and obtained his Habilitation in 1999. During 1999–2000 he was a professor at the University of Munich, and during 2000–2007 he was a Full-Professor at TU Eindhoven. Since April 2007, he is a Full-Professor at the Friedrich Schiller University Jena, Germany.

pDNA transfection properties. More precisely, the recent achievements in *in vitro* transfection, utilizing the most important synthetic polymer systems PEI, PLL and PDMAEMA of different architectures, will be highlighted. For this purpose, the theoretical background concerning the biological challenges for cationic polymers and the different possible polymer architectures as well as self-assembled structures will be summarized. The main characteristics of linear and branched systems will be only briefly addressed as they were recently reviewed in detail elsewhere.[22,23] The focus will be on graft and star-shaped as well as self-assembled polymer systems as they have emerged as efficient delivery systems in the last few years.

1.1 Biological challenges for cationic polymers

Polymer science meets biology when discussing barriers that have to be overcome for efficient gene transfection. The major obstacles of transfection polymers are efficiency and cytotoxicity. Unfortunately, the desired high efficiency is often combined with a high cytotoxicity. In the last couple of decades, scientists have been trying to overcome this paradigm. Nevertheless, a perfect polymer for *in vivo* gene therapy has yet to be developed. The transfection process can be divided into several steps starting from the formation of complexes of the positively charged polymer and the negatively charged pDNA, named polyplexes. The complexation is driven by the gain of entropy due to the release of small counter ions from the pDNA and the polymer.[22,24] The balance between the polyplex stability under physiological conditions and the release of the genetic material for the transcription mechanism has to be found.[25] After polyplex formation, cellular interaction followed by internalisation takes place, mainly *via* endocytosis.[26] Due to the negatively charged cell membrane, the interaction and internalisation with cationically charged polymer or polyplexes is enhanced. However, the cationic polymer can also induce membrane destabilisation resulting in membrane destructive effects and, thus a high cytotoxicity.[15,27] Up to now, the mechanisms relying on endocytosis are not yet understood in detail. There are basically phagocytosis, clathrin- and caveolin-mediated endocytosis as well as macropinocytosis. Concerning the internalisation of polyplexes, different uptake mechanisms and intracellular trafficking dependent on the polymer class and architecture were observed.[28] For example, PEI polyplexes show caveolin- and clathrin-mediated endocytosis.[29] After efficient internalisation *via* endocytosis, the polyplexes have to escape from the endosome to prevent digestion of the pDNA in the lysosome or exocytosis.[30] Due to the high buffer capacity of PEI, the influx of protons and chloride ions lead to an osmotic swelling of the endosome and disruption of the endosomal membrane, the so called proton sponge effect.[31–33] In the last few years, it was found that the proton-sponge effect is not the only reason for the endosomal release of the polyplexes.[34] A combination of swelling and local mechanical disruption is assumed.[35] Released in the cytoplasm, the pDNA has to enter the cell nuclei for the transcription mechanism and efficient protein production. The mechanism of polyplex dissociation and in particular how the pDNA enters the cell nuclei is only barely investigated to date.[36] There are hints that polyplex dissociation occurs at the same time as the endosomal release[35] but polyplexes were also detected in the nuclei.[37] An increased transfection efficiency in cells with a high division rate was observed, confirming the entry of pDNA into the nuclei during mitosis.[38] Due to the breakdown of the nuclear envelope, the pDNA can enter the transcription mechanism more easily. However, it was also shown that the entry can occur through nuclear pores.[39] The introduction of a nuclear localisation sequence was also presented as a possible route to enhance the active transport of genetic materials into the nuclei.[40]

Since the first polymers were used as transfection agents, a large number of studies were performed to understand the relying mechanism, successful for most of the steps. Different strategies were developed to overcome the transfection barriers (Fig. 1). For example the pK_a value is one characteristic of cationic polymers responsible for the degree of protonation and, thus, influencing the complexation behavior as well as the endosomal escape.[41] Fig. 1 depicts an overview of general polymer properties showing an influence on the main characteristics of the polymer vectors. However, a number of questions need to be solved. For this purpose studies have to be performed in detail to adjust the ideal polymer properties.

1.2 Polymer architecture

The use of controlled and living polymerisation techniques like reversible addition-fragmentation chain transfer (RAFT) polymerisation, atom-transfer radical polymerisation (ATRP), cationic ring opening polymerisation (CROP) or living anionic polymerisation enable the synthesis of polymers in a controlled manner. More precisely, tailor-made polymers with defined chain length (characterized by the degree of polymerisation (DP)), composition, and architecture can be realized. A detailed overview about the synthesis strategy of polymers for gene delivery concerning their architecture was recently published.[42] In general, polymers can be classified by their composition and topology. Polymer compositions, meaning the order of repeating units, include homopolymers and statistical, gradient-, periodic-, and block copolymers (Fig. 2).[43,44] In contrast to homopolymers, copolymers contain at least two different monomers with the advantage of combining different monomer properties in one polymer chain. For instance, cationic units, which are necessary for the pDNA complexation, can be combined with hydrophobic units that can be responsible for an enhanced internalisation.[45,46] Hydrophilic monomers like ethylene glycol or ethyl oxazolines can be used to introduce the so-called stealth effect and to reduce cytotoxicity.[47] In contrast to statistical copolymers, block copolymers are built up by at least two different block segments. Regarding the polymer topology, a distinction is drawn between linear, branched, graft (comb and brushes), and star-shaped polymers (Fig. 2). Branched polymers, like branched PEI (bPEI) or dendrimers, are composed of polymer chains with at least two branching points. These specific end-groups can be used for multiple end-functionalisation. Graft polymers, or more specified, comb- or brush-like polymers, comprise of several block segments that were grafted through, onto or from a main chain,

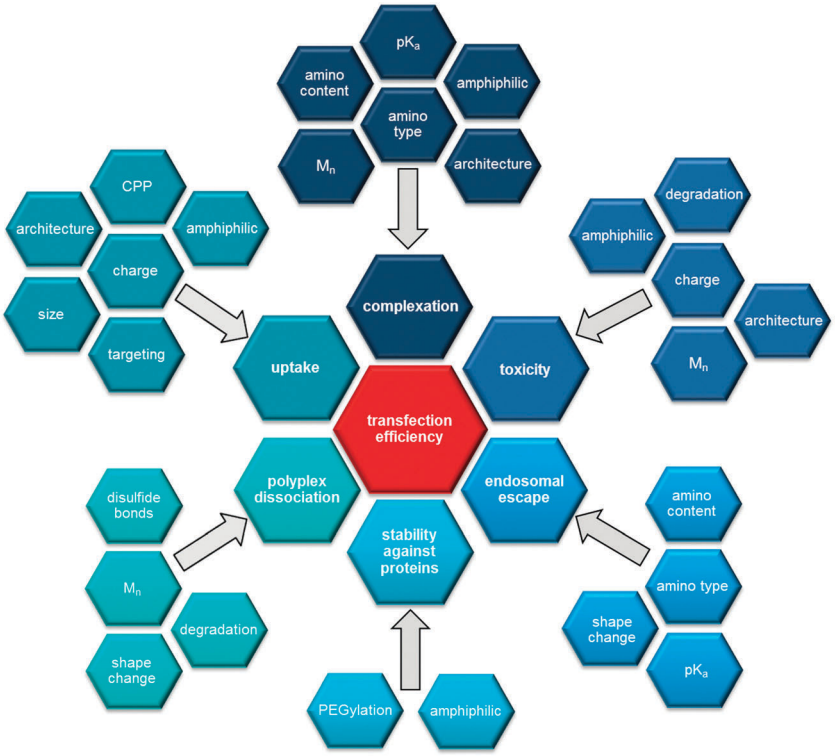

Fig. 1 Overview of the set screws of selected polymer properties for an efficient pDNA delivery.

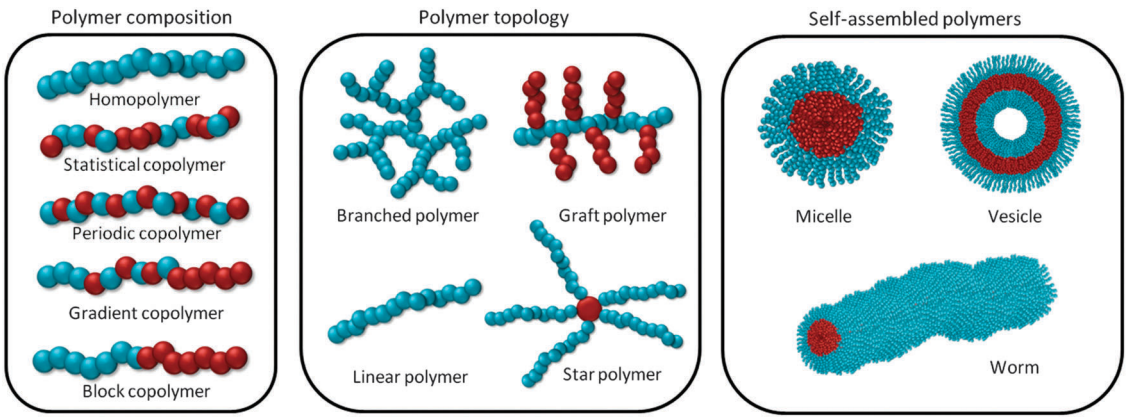

Fig. 2 Possible polymer architectures and self-assembled systems: polymer composition (left), topology (middle), and self-assembled structures (right).

the backbone. Comb- or brush-like polymers are often used to mimic a branched character but are formed of low molar mass segments.

Star-shaped polymers are formed by several linear chains (arms), which are attached to a central core.[43] In case of the arm-first approach, the linear polymer chains are synthesized first and then attached to the core. In the core-first method, the arm chains are synthesized from initiation sites at the core.[42] A third approach represents the utilisation of conjugation/coupling reactions with multifunctional coupling agents as cores.[19,48] As branching points multifunctional cores or crosslinking agents like ethylene glycol dimethacrylate (EGDMA) can be used. Star-shaped polymers based on a crosslinking agent rather present a star-like structure, and the characterisation of them is more difficult.[19] There are several possibilities to prepare star-shaped polymers. An overview of possible cores used for star-shaped polymers for pDNA delivery is presented in Table 1. It should be noted that one benefit of star-shaped polymers is the utilisation of multifunctional cores, which reveals a stimuli-response behaviour. For instance, porphyrin exhibits photosensitizer abilities; more precisely the absorption of light leads to chemical or physical changes and can induce cytotoxicity due to membrane disruption. This characteristic of porphyrin is often used in photodynamic therapy for the treatment of cancer.[49] Furthermore, a photochemical internalisation (PCI) can be realized for example by a porphyrin core,

Table 1 Selected cores for the synthesis of star polymers with regard to the polymer class, number of arms, polymerisation techniques and polymerisation strategy

Cores	Cationic polymers	Number of arms	Polymerisation technique	Polymerisation strategy	Ref.
PEG	PEI	3 to 6	Coupling reaction	Arm-first	54 and 55
PEG–PCL	PEI	5	Coupling reaction	Arm-first	56
Porphyrin	PLL	4	Coupling reaction	Arm-first	50 and 57
Cyclodextrin	PLL	7	Coupling reaction	Arm-first	52
PPI dendrimer (G2-5)	PLL	8 to 64	ROP	Core-first	58
POSS	PDMAEMA	8	ATRP	Core-first	59
Silica nanoparticle	PDMAEMA	20	ATRP	Core-first	60
Cyclodextrin	PDMAEMA	4, 7, 14, 21	ATRP	Core-first	61
Glucose	PDMAEMA	3	ATRP	Core-first	62
Saccharose	PDMAEMA	5	ATRP	Core-first	62
Cyclodextrin	PAMAM	7	Coupling reaction	Arm-first	63 and 64
Cyclodextrin	PGEA	4	ATRP	Core-first	65
Crosslinking substances					
EGDMA	PDMAEMA	—	GTP/ATRP	Arm-first	66–69
Glutharaldehyde	PLL	—	ROP	Arm-first	70
BAC	PDMAEMA	—	ATRP	Arm-first	71

PCL – poly(caprolactone), PPI – poly(propylenimine), POSS – poly(hedral oligomeric silesquioxane); PGEA – ethanolamine functionalised poly(glycidyl methacrylate), GTP – group transfer polymerisation; ROP – ring opening polymerisation; BAC – *N*,*N*-bis(acryloyl cystamine).

meaning an increased release behaviour from endosome/lysosome into the cytoplasm.[49,50] PCI is already successfully applied in clinical studies phase II for drug delivery in combination with bleomycin (anticancer agent).[51] Cyclodextrin-based systems are often applied due to the biodegradability and reduced cytotoxic effects. In addition, a co-delivery of pDNA and drugs can be realized due to the hydrophobic cavity.[52,53]

Furthermore, block copolymers can form self-assembled structures in solution, meaning the arrangement into highly ordered structures by non-covalent interactions. For instance, spherical or worm-like micelles and vesicular structures can be realized (Fig. 2). In particular, block copolymers with hydrophobic and hydrophilic segments are capable to self-assemble, due to their amphiphilic character.[43] The principles responsible for the mechanism of self-assembly depend on several factors starting from the used solvents to the block ratios.[72] Concerning biological applications, one crucial factor is the critical micelle concentration (cmc), meaning the concentration at which the polymers disassemble. For pDNA delivery often very low concentrations are applied, in particular with respect to *in vivo* applications, where high dilution occurs in the bloodstream post administration. Crosslinking of the micellar core can stabilize the structures.[20]

2 Linear polymers

Linear polymers, classified into homopolymers, statistical, random, gradient and block copolymers (polymer composition) represent the most commonly used polymer-based non-viral gene delivery agents with a high annual number of publications and clinical trials. In particular, PLL, linear PEI (lPEI), and PDMAEMA were often applied as homopolymers for the delivery of pDNA, as already investigated and reviewed in detail in the last few years.[22,23,73–75] Fig. 3 depicts the chemical structures of several linear cationic polymers, which are used for gene delivery. PLL is a cationic polymer based on the biodegradable natural compound L-lysine and can be synthesized in a controlled manner *via* ring-opening polymerisation. A molar mass of 3000 Da is at least necessary for an efficient polyplex formation.[1] However, 20 kDa PLL shows higher transfection efficiency but also significant cytotoxic effects compared to low molar mass PLL (PLL 36 kDa, IC_{50} = 38 μg mL^{-1}).[27] The high cytotoxicity is probably caused by the disruption of the cell membrane, which leads to apoptotic cell death.[27,76] PLL has only primary amines (pK_a of ε-amine in lysine is around 10.8),[75] which are mostly protonated at physiological pH values leading to a low buffer capacity, maybe resulting in an inefficient endosomal release.[23] In contrast to PLL, linear PEI(lPEI) comprises of mainly secondary amines. The synthesis of lPEI can be realized *via* hydrolysis of poly(2-ethyl-2-oxazoline) (PEtOx), which can be obtained *via* CROP. The unique feature of lPEI is a pK_a of 8.44 and the high amine density; every third atom in the polymer chain can be protonated leading to a high buffer capacity.[77] In fact, more than 70% of the amine residues of lPEI are protonated at physiological pH values.[78] Beside the high transfection efficiency, lPEI also shows cytotoxic effects (lPEI 22 kDa IC_{50} = 6.4 μg mL^{-1})[79] due to membrane destabilisation.[41] Another commonly used linear polymer system is PDMAEMA, a cationic methacrylate. PDMAEMA can be synthesized by free radical polymerisation as well as by ATRP, RAFT, and anionic polymerisation. To achieve acceptable transfection efficiencies molar masses of around 30 kDa are necessary.[1] In contrast to PLL or lPEI, PDMAEMA contains only tertiary amines (pK_a = 7.5) with adequate buffer capacity.[41,74] Nevertheless, also PDMAEMA shows cytotoxic effects (PDMAEMA 112 kDa, IC_{50} = 10 μg mL^{-1}).[80]

Based on the studies of the homopolymers PLL,[76] PEI[81] and PDMAEMA,[15,62] it generally can be assumed that with increasing molar mass the transfection efficiency and cytotoxicity both increase at the same time. For instance, low molar mass polymers (<5 kDa) are insufficient in polyplex formation/stability and high molar mass polymers (≥10 kDa) can show significant cytotoxic effects.[81]

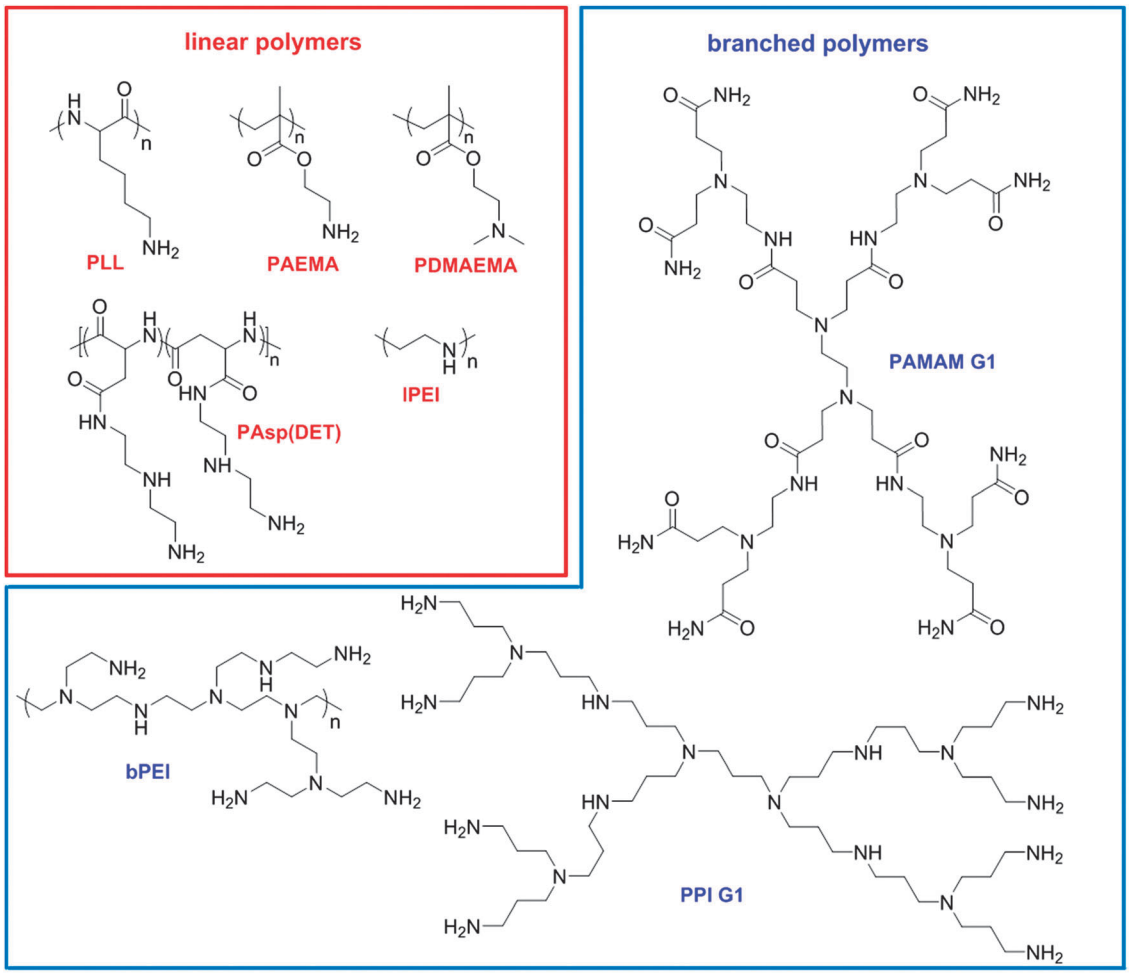

Fig. 3 Schematic representation of chemical structures of selected cationic polymers used for non-viral gene delivery. PAsp(DET) – poly(*N*-(*N*-(2-aminoethyl)-2-aminoethyl)aspartamide), PAMAM – poly(amidoamine).

The use of copolymers can therefore be beneficial in order to tune the polymer characteristics to high transfection rates with low cytotoxicity issues. For instance, an increased polyplex stability of methacrylate-based polymers can be achieved by using tertiary and primary amines in the same polymer chain.[82] This was realized by the synthesis of poly(2-(dimethylamino)-ethyl methacrylate-*stat*-aminoethyl methacrylate) (PDMAEMA-*stat*-PAEMA). Increased pDNA condensation combined with increased transfection efficiency was observed. These effects can be attributed to the higher charge density of the primary amines at physiological pH values.[82] Furthermore, the copolymerisation with 2-hydroxyethyl methacrylate (HEMA), which has hydrophobic properties, leads to an increased internalisation efficiency and endosomal escape, resulting in enhanced transfection efficiency.[83] Another example is partially hydrolysed PEtOx and the influence on the transfection efficiency compared to lPEI. In this study, different degrees of hydrolysation were analysed. In contrast to the 70% hydrolysed PEtOx, the 50% hydrolysed PEtOx shows no cytotoxicity but also no transfection efficiency.[84] To sum up, statistical copolymers are suitable for analysing the influence of different monomer properties like hydrophobicity or amine type as well as biocompatibility.

Block copolymers have the advantages of a defined structure in block segments compared to statistical polymers. A frequently used approach is the combination of a PEG block and a cationic block, resulting in reduced cytotoxicity and stealth behaviour. But this combination also often leads to a decreased transfection efficiency, probably due to decreased cell interactions.[7,85] However, this can be also used to prevent non-specific interactions and allow specific internalisation due to targeting moieties at the same time, in particular *in vivo*.[86] To avoid serum interactions, the utilisation of zwitterionic units represents an alternative to PEG. A block copolymer comprising of PDMAEMA-*b*-PMPDSAH (poly-(*N*(3-(methacryloylamino)propyl)-*N*,*N*-dimethyl-*N*-(3-sulfopropyl)ammonium hydroxide)) shows decreased cytotoxicity and increased transfection efficiency in the presence of serum proteins. The reduced cytotoxicity compared to the PDMAEMA homopolymer can be attributed to a lower amount of cationic charges per polymer at the same concentration.[87] Another example uses a decreased charge density while achieving efficient transfection and low cytotoxicity, also *in vivo*, by using

hydrophobic units.[88] The benefit of reducing the cationic charge was further demonstrated by decationisation of the polymer after polyplex formation while preserving the polyplex stability by crosslinking of the polyplexes *via* disulfide bonds.[89] A recent study deals with block copolymers *versus* statistical copolymers with the same composition (PDMAEMA-*co*-PAEMA). They showed that diblock copolymers form polyplexes with a higher colloidal stability compared to statistical ones.[90] This can be attributed to a more likely condensed pDNA in the core of the polyplex. In contrast, more looser complexation occurs with the statistical counterpart. In addition, block copolymers are able to self-assemble into spherical or worm-like micellar structures. These properties will be discussed in detail in Section 6.

3 Branched polymers

Similar to the linear topology also branched polymers represent a large group of polymer systems used and investigated for pDNA delivery. Herein, the main investigations were performed with dendrimers like poly(amidoamine) (PAMAM) and bPEI (Fig. 3). In contrast to dendrimers like PAMAM, branched polymers like bPEI possess a broad molar mass distribution ($Đ$) and a randomly branched architecture. However, they are easy to synthesize in large scale, also in a one-step process.[91] bPEI is synthesized *via* acid-catalyzed ring-opening polymerisation of aziridine and contains primary, secondary and tertiary amines in a 1 : 2 : 1 ratio independent of its molar mass.[41,92] With regard to its transfection efficiency, high efficiency is again accompanied by high cytotoxicity for 25 kDa bPEI (IC_{50} = 4.9 μg mL^{-1}).[79] The high delivery efficiency of bPEI can be attributed to a high buffer capacity of the secondary and tertiary amines as well as to a good ability to complex pDNA, as primary amines condense nucleic acids in a more efficient way than other amines.[93] Numerous efforts were performed regarding the decrease of the cytotoxic effects *via* modification of bPEI.[93] For instance, the inability of low molar mass bPEI (1.8 kDa) to form stable complexes with pDNA was solved by modifications with hydrophobic groups.[94] Another study presents 25 kDa bPEI functionalized with PMPC (poly(2-methacryloyloxethyl phosphorylcholine)), leading to reduced non-specific protein interactions, increased transfection efficiency and reduced cytotoxicity due to the zwitterionic character.[95] Very recently, biodegradable, branched PDMAEMA polymers were presented and the influence of the degree of branching was examined. Copolymerisation of DMAEMA and BADS (bis(2-acryloyl)oxyethyl disulfide) leads to biodegradation into short primary-chain molecules. Beside a decreased cytotoxicity also an enhanced transfection efficiency was observed using polymers with a higher degree of branching.[96]

Dendrimers are perfectly branched polymers with a specific tree-like structure and monodispersity ($Đ$ = 1.0).[22,97] In the convergent way they are engineered stepwise in generations, meaning the branching is constructed by "single layers". Based on this unique structure, high numbers of generations are hard to synthesize due to sterical hindrance. A high number of generations decreases the flexibility unfavourable for pDNA condensation. The most commonly used dendrimer families for pDNA delivery are PAMAM and poly(propylenimine) (PPI).[97] In the case of PAMAM, the primary amines at the surface lead to a high ability of pDNA condensation, and the tertiary amines in the interior are responsible for good buffer capacity.[98] PAMAM dendrimers with generations of 5 to 10 show the best transfection efficiency.[99] One interesting feature of PAMAM dendrimers is the generation or expansion of holes in cell membranes. In the case of PAMAM dendrimers of the 7th generation, hole formation in the cell membrane of around 15 to 40 nm diameter was detected. In contrast, PAMAM dendrimers of the 5th generation lead to expansion of existing holes.[100] Furthermore, the multivalent properties due to the high degree of surface functionalities was investigated in detail, in particular with PAMAM dendrimers of the 5th generation.[101] It is interesting to know that degraded dendrimers with an imperfect shape show a higher transfection efficiency.[102] A comparative study investigated the differences between linear, hyperbranched and dendritic PLL concerning their transfection potential. Herein, the most promising architecture concerning the transfection efficiency was the hyperbranched structure, as a transfection efficiency comparable to lPEI was achieved. With regard to cytotoxicity, the linear polymer shows less cytotoxic effects compared to the branched systems.[103] Based on the results, the higher delivery potential can be attributed to an increased adhesion of the hyperbranched polyplexes at the cell surface and also an increased buffer capacity. This can be ascribed to the fact that the hyperbranched polymers contain ε- and α-amino groups in contrast to the linear or dendritic PLL with only ε- or α-amino groups.[91]

4 Graft polymers

The main motivation for synthesizing graft, comb- or brush-like polymers is the imitation of the beneficial properties of branched polymers by using low molar mass segments as linear side chains (Fig. 4). Moreover, it is possible to synthesize graft polymers in a controlled manner, meaning that the polymers show a narrow molar mass distribution.[104] An overview of the applied polymers or oligoamines used as the backbone or as side chains is depicted in Fig. 4. One of the first examples imitating degradable high molar mass polymers was demonstrated by W. E. Hennink and his group, using a PHEMA backbone (DP ~ 110) grafted with low molar mass PDMAEMA (DP ~ 50). Higher transfection efficiencies and reduced cytotoxicities compared to PEI or linear PDMAEMA were achieved. The comb copolymers have carbonate esters as biodegradable linkers at the branching points, thus PDMAEMA side chains can be slowly cleaved off under physiological conditions.[105] Another example for PDMAEMA-based comb-like polymers consists of a ethanolamine/cystamine-functionalised poly(glycidyl methacrylate) backbone, at which PDMAEMA side chains of different DP values (14 to 57) are linked by disulfide bonds. Higher transfection efficiency and lower cytotoxicity values compared to PEI were observed also in this case. In addition, the known trend regarding the molar mass was observed: with increasing DP of the

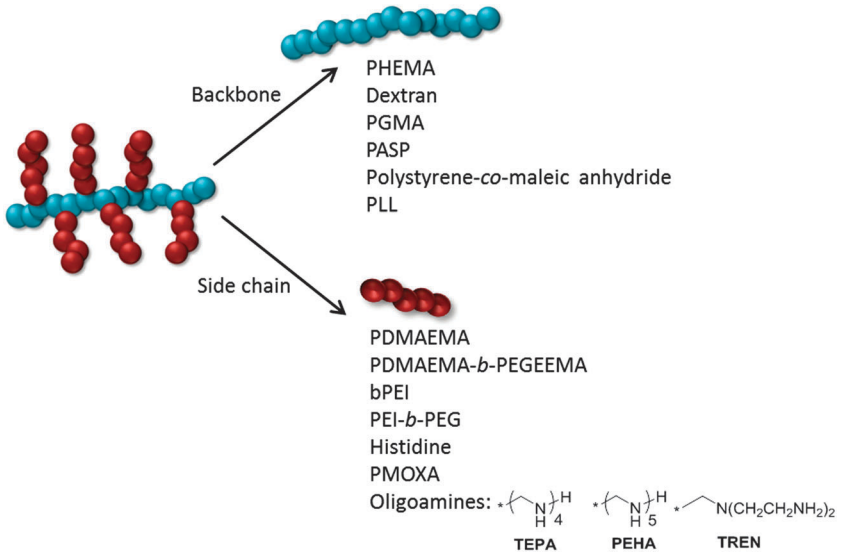

Fig. 4 Schematic representation of selected polymers used for the preparation of comb- and brush-like polymers.

PDMAEMA side chains, transfection efficiency and cytotoxicity increased. However, it should be noted that lower cytotoxicity was obtained compared to 25 kDa bPEI although the molar mass increased to 78 kDa. The usage of disulfide bonds enables an increased polyplex dissociation under reducing conditions.[106] Another study investigated PDMAEMA of different DPs linked *via* disulfide bonds to dextran as the main chain. Here, higher DP values (12 to 42) lead to an increased cytotoxicity, but the introduction of poly(ethylene glycol)ethyl ether methacrylate (PEGEEMA) segments at the end of the PDMAEMA side chains reduced the cytotoxicity and increased the transfection efficiency compared to PEI.[107] Beside PDMAEMA, also PEI was used to create comb-like polymers, which showed higher transfection efficiencies or at least less cytotoxicity than high molar mass PEI. Furthermore, a poly(glycidyl methacrylate) (P(GMA)) backbone was synthesised with varying DP (50 and 100) and functionalised with different oligoamines, tetraethylenepentamine (TEPA), pentaethylenehexamine (PEHA) and tris(2-aminoethylamine) (TREN) (Fig. 4). The polymer with a shorter backbone (DP 50) and TEPA and PEHA (carrying primary and secondary amines) in the side chain shows comparable transfection efficiencies like PEI with reduced cytotoxicity. This study demonstrates the important relationship of complexation and disassembly. In particular the TREN (primary and tertiary amines) functionalised polymer shows the most efficient binding, probably leading to an insufficient polyplex dissociation.[108] Using another backbone, polyaspartamide (PASP), and different oligoamines as side chains, reduced cytotoxicity and similar transfection efficiencies were obtained compared to PEI.[109] An impressive example of using low molar mass bPEI (800 Da) in the side chain was demonstrated with a poly(styrene-*co*-maleic anhydride) backbone. A twofold transfection efficiency of the gold standard bPEI was achieved. bPEI of 800 Da is usually not able to condense pDNA, but the comb like polymers (23.6 kDa) show a high transfection efficiency combined with a reduced cytotoxicity. These investigations demonstrate the successful mimic of high molar mass bPEI. The amphiphilic character of the polymer is probably also beneficial because the enhanced transfection efficiency can be related to an increased internalisation efficiency.[110] Another example confirming the benefit of comb-like architectures is a PHEMA-*g*-(PEI-*b*-PEG) polymer. An increased internalisation, reduced cytotoxicity and comparable or even higher transfection efficiency compared to PEI were observed depending on the cell type.[111] A different polymer class, namely PLL, was used to synthesise a comb-like polymer. In this study PLL was used as a backbone substituted with histidine residues in order to circumvent the low buffer capacity of PLL, by the introduction of histidine. The authors showed an increased transfection efficiency with reduced cytotoxicity compared to the PLL homopolymers.[112] Also, different oligoaminoethanes were coupled to a PLL backbone. The benefit of comb-like architecture could be demonstrated again, as the comb-shaped polymers were internalised in a more efficient way than their linear counterpart. Moreover, the so-called even–odd effect was observed.[113] To introduce stealth behaviour, a PLL backbone was functionalised with poly(2-methyl-2-oxazoline) (PMOXA) with different grafting density. Only polymers with a low grafting density (10%) show higher transfection efficiency than the homopolymer PLL. In the case of higher grafting density, the transfection efficiency is decreased, which can be attributed to the stealth effect. Nevertheless, by adjusting favourable conditions the polyplex stability can be enhanced for an increased transfection efficiency.[114]

In order to investigate the influence of the polyplex shape on the transfection efficiency, $PHEMA_{150}$-*co*-PLL comb-like polymers were applied. The utilisation of two polymers with the same composition and molar mass but different side chain length (DP of 10 or 15) leads to different polyplex structures. Short side chains result in rectangular particles ($\sim$25 by $\sim$74 nm), and higher DP leads to longer, rod-like (width of $\sim$18 nm, length of $\sim$102 nm), toroid, and twisted structures. A decreased internalisation efficiency and endosomal/lysosomal accumulation as well as a delayed nuclear delivery could be observed for the

longer rod-like particles. However, the uptake mechanism, intracellular trafficking, or the decomplexation behaviour of the two polymers is similar, indicating the internalisation efficiency as a critical factor.[115,116]

All together, one advantage of graft polymers is the easy introduction of biodegradable properties. On the one hand biodegradable or compatible backbones can be applied or on the other hand low molar mass side chains can be connected to the backbone *via* degradable linkers.[117,118] This degradation into low molar mass segments reduces the cytotoxicity and enhances the polyplex dissociation and is, therefore, beneficial to overcome these two barriers for efficient transfection. With regard to the main characteristics of comb-like polymers, three principles can be pointed out:

(i) If backbones with high DPs (>100 DP) are applied, it is beneficial to connect the side chains *via* degradable linkers, in order to enhance the intracellular polyplex dissociation;

(ii) if short backbones (<50 DP) are applied the length of the side chains and the type of amines have to be adjusted to achieve an efficient polyplex formation; and

(iii) relatively low DPs of the side chain are beneficial (DP between 10 and 50), to maintain a low cytotoxicity.

These principles are somewhat limited in their implementation as always three variables have to be considered: the length of the backbone, the length of the side chains, and monomer characteristics.[98] In case of the overall molar mass, the optimum seems to be between 25 and 50 kDa, but these values have to be handled with care due to mentioned variables. Graft polymers are very promising candidates as gene delivery agents due to the fact that higher transfection efficiency and lower cytotoxicity compared to the current gold standard PEI can be obtained.

5 Star-shaped polymers

About one decade ago the first star-shaped polymer was investigated with pDNA transfection efficiency ability.[66] The idea was to transfer and improve the preferred properties of dendritic and branched polymers to star-shaped polymers for transfection. In contrast to dendritic structures, star-shaped polymers show a higher flexibility, which may result in better pDNA complexation properties.[42,59] In addition, star-shaped polymers are suitable for the introduction of targeting units *via* diverse end functionalities. There are multitude studies about PDMAEMA-based stars. PDMAEMA can be synthesized *via* controlled radical polymerisation techniques like RAFT and ATRP, which show a higher tolerance against functional groups. In particular, T. K. Georgiou demonstrated the benefit of PDMAEMA stars as transfection agents. By using EGDMA as a bifunctional coupling agent, a star-like polymer comprising different PDMAEMA chain lengths (DP 10 to 100) was developed for performing GTP.[66] In addition, star-like polymers consisting of PDMAEMA-*co*-PMAA[68] and poly-(2-(dimethylamino)ethyl methacrylate)-*co*-hexa(ethylene glycol)-methacrylate (PDMAEMA-*co*-HEGMA)[67] were investigated concerning their transfection efficiency. Regarding the PDMAEMA homopolymer an increase of DP leads to an increased cytotoxicity.[66] The introduction of PMAA and HEGMA showed a decrease of cytotoxicity while maintaining the transfection efficiency. In addition, the position of either PMAA or HEGMA in the PDMAEMA based block copolymers was varied, resulting in different performance. In the case of PDMAEMA-*b*-PMAA star-like polymers, higher transfection efficiencies were obtained in which PMAA is located in the exterior. In contrast, higher transfection efficiency of PDMAEMA-*b*-HEGMA star-like polymers was achieved with HEGMA in the interior of the star. Additionally, a trend of an increased cytotoxicity combined with longer arm length of PDMAEMA was found, this was further confirmed by the group of A. H. E. Müller. In one approach, star-shaped polymers comprising of a glucose or a saccharose core functionalised with different PDMAEMA arm lengths were investigated. The number of arms as well as the arm length were varied. Interestingly, less cytotoxicity of the star-shaped polymers with the same molar mass but a higher amount of arms was found.[62] The influence of molar mass, arm length and number of arms was further investigated utilising a cyclodextrin core. On one hand, a higher cytotoxicity was observed when keeping the arm length constant and increasing the number of arms (4, 7, 14, 21), thus, also increasing the molar mass. On the other hand, a decrease in cytotoxicity was observed when keeping the molar mass constant and increasing the number of arms while decreasing the arm length (23, 34, 70, 140 DP).[61] A star-shaped polymer comprising of a silsesquioxane core and 20 PDMAEMA arms with a DP of 230 was synthesised showing superior transfection efficiency even in hard-to-transfect Jurkat T-cells and primary T-lymphocytes.[60] Star-shaped polymers provide a good opportunity to introduce biodegradable bonds. Their advantage regarding the cytotoxicity and the polyplex dissociation was demonstrated by using a POSS(SS-PDMAEMA$_{15-24}$)$_8$ star. The star-shaped polymer without disulfide bonds showed a reduced transfection efficiency compared to the polymer containing disulfide bonds, with transfection efficiencies higher than PEI.[59] The POSS core further allows the loading with drugs like paclitaxel.[119] Another approach for the construction of star-shaped polymers is based on cyclodextrin (CD) cores. Here, the hydroxyl groups can be modified to be used as initiators for ATRP.[120] The advantage of using cyclodextrin is the cub-shaped structure with a hydrophilic exterior and a hydrophobic interior. Moreover, the bioavailability is improved due to enhanced cell membrane adsorption.[53] By using ß-CD as a core, a 4-arm star was synthesized with either PDMAEMA homopolymers or PDMAEMA-*b*-PEGEEMA copolymers. The homo-star polymers show transfection efficiencies like PEI, however, the block copolymers result in superior transfection efficiencies, although PEGEEMA is known to reduce cell interactions.[121] Grafting of four PDMAEMA (DP 20, 30, 40) chains from a ß-CD core *via* disulfide bonds results in a bioreducible behaviour. Moreover, the star-shaped polymer with the highest DP showed the highest transfection efficiency even higher compared to PEI. Adamantane end-functionalised PEGEEMA was assembled to the CD core, resulting in higher transfection efficiency and lower cytotoxicity. The increased efficiency can be attributed to a higher stability against serum proteins leading to an enhanced internalisation.[53]

PDMAEMA can also be used as a core, as shown for PDMAEMA crosslinked with EGDMA and PEG as a shell. An increased transfection efficiency was demonstrated combined with a reduced cytotoxicity.[69]

Another example of a biodegradable star-like polymer is based on a mPEG-SS-PLL_{15} block copolymer crosslinked with glutaraldehyde. The star-like architecture results in efficient pDNA condensation and an enhanced buffer capacity, in contrast to the corresponding linear block copolymers. Moreover, the degradable disulfide bonds enhance the polyplex dissociation in the cytoplasm.[70] A star-shaped polymer based on a porphyrin core with four PLL dendron (G3) arms shows an enhanced transfection efficiency after irradiation due to the photochemical internalisation behaviour of a porphyrin core.[50] In another approach, a star-shaped polymer was constructed by using a PPI dendrimer of different generations (G2-5) as a core, with different amounts of PLL_{40} arms. This study demonstrates the benefit of high charge density per molecule: the star-shaped polymers with a high generation in the core showed an increased ability for pDNA complexation as well as a higher transfection efficiency compared to PLL. The spherical shape is also beneficial for internalisation of the polyplexes.[58] The driving force for PEI-based star-shaped polymers can be realized by using a multifunctional PEG core and low molar mass PEI as arms. An example was already demonstrated by the group of T. Kissel in 2002 wherein multi-stars (4- and 8-arm) composed of a PEG core and bPEI with different molar masses (600 and 800 Da) were synthesized.[54] In contrast to the single linear homopolymers, the star-shaped polymers are able to condense the pDNA into polyplexes with sizes between 100 and 200 nm. Unfortunately, there are no data available concerning their cytotoxicity and transfection efficiency. In another study, star-shaped polymers were synthesized with a multi-arm PEG core and 3 as well as 6 arms of 2500 Da lPEI. In particular, the 6-arm star with a total molar mass of 25 kDa showed comparable or even higher transfection efficiencies combined with lower cytotoxicity values compared to the 25 kDa lPEI.[55] Another example for mimicking high molar mass PEI by utilizing the low molar mass one was realized by Ladewig *et al.* using a PEG or PEG–PCL core and lPEI arms. A decreased cytotoxicity while maintaining the transfection efficiency was demonstrated.[56] In the case of PAMAM dendrimers, a star-shaped architecture was synthesized using a ß-CD core functionalized with 7 PAMAM ($G = 4$) arms. Due to the higher flexibility as compared to dendrimers of higher generations, a twofold transfection efficiency and a reduced cytotoxicity was achieved.[63,64]

As a summary it can be said that transferring the branched structure to star-shaped polymers can result in promising transfection properties while the cytotoxicity can be reduced and the transfection efficiency can be maintained or even increased. This behaviour can be attributed to a superior pDNA condensation, resulting in spherical polyplexes, where the pDNA is located in the polyplex core ensuring an efficient protection against enzymatical degradation.[19,58] Such spherical structures are beneficial for the internalisation efficiency. An increased buffer capacity and charge density can be realized due to the star-shaped architecture in case of PLL-shaped stars.[50,58] The introduction of bioreducible linkers like disulfide bonds results in a lower cytotoxicity and a higher transfection efficiency.[65] The decreased intracellular compatibility of the polymers results from degraded low molar mass segments with reduced cytotoxicity. Another advantage of degradable linkers is the enhanced polyplex dissociation in the cytoplasm. Concerning the molar mass, a trend can be observed as already known for linear polymers: with increasing molar mass the cytotoxicity increases.[19] Nevertheless, these aspects have to be handled with care as cytotoxicity and transfection efficiency depends on the number of arms and the arm length.[19] It is advantageous to use few arms, *e.g.*, 4 and low DP values ($\sim$40 to 50 DP) or many arms (20 or higher) with higher DP values (around 200). The final optimal molar masses are between 50 and 100 kDa.[19] Keeping the *in vivo* application in mind, the strategy of using less arms and low DP combined with disulfide bonds might be the most promising strategy.

6 Self-assembly of polymers

Beside dendritic, star-like, or graft polymers, in particular linear block copolymers represent the main polymer structure to self-assemble into highly-ordered structures. The hydrophobicity and hydrophilicity of at least two block segments can be tuned in a way to self-assemble in aqueous solution.[72] Possible architectures include worm-like or vesicular micellar structures as well as spherical micelle formation.

The main application of micelles is the delivery of drugs, due to the fact that the hydrophobic interior represents an ideal environment for hydrophobic drugs.[122] In addition, the use as multidrug delivery vehicle, meaning the delivery of drugs and genes at the same time, can be realized.[123,124] Concerning micellar structures for pDNA delivery it should be mentioned that preformed spherical micelles are used for polyplex formation or self assembly of block copolymers with plasmid DNA leads to so-called polyplex micelles (Fig. 5). In detail, a block copolymer built up of a cationic and a hydrophilic segment probably forms polyplex micelles with pDNA due to electrostatical interactions of the pDNA and the cationic segment (Fig. 5a). Thus, the pDNA is located in the core and the hydrophilic part in the shell.[125] K. Kataoka first presented the concept of so called polyionic (PIC) micelles in 1990.[126,127] In the following years the behaviour of this system was investigated in detail. One finding is that the size of the polyplex micelles can be tuned by the length of the hydrophilic segments. Thus, smaller polyplex micelles were obtained by increasing the hydrophilic part. This can be attributed to a sterical hindrance during the micelle association.[127–129] In particular, PEG-*b*-PAsp(DET) (poly(*N*-(*N*-(2-aminoethyl)-2-aminoethyl)aspartamide)) (Fig. 3) polyplex micelles showed high efficiency in delivering pDNA and represent systems, which are studied and reviewed in detail.[129] Further modifications were performed based on this initial structure, like the investigations of ternary complexes. In that case different polymers were mixed for complexation.[130]

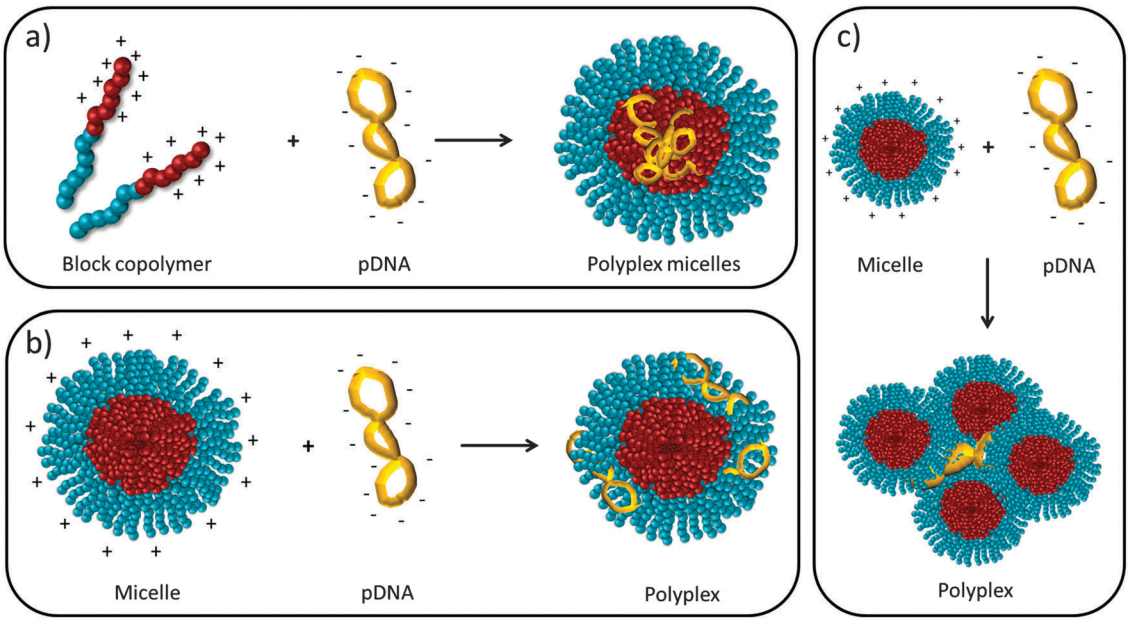

Fig. 5 Polyplex micelles (a) *vs.* polyplexes formed with preformed micelles and pDNA (b and c). (+) Represents the cationic charges of the block copolymers or the surface charges of the preformed micelles and (−) represents the negative charges of the pDNA.

Pre-formed micelles are only rarely used for pDNA delivery (Fig. 5b and c). In one approach, amphiphilic PDMAEMA star-like and linear polymers were investigated regarding their self-assembly and transfection efficiency behaviour. Beside the comparison of linear and star-shaped polymers, also different hydrophobic blocks were examined, namely poly(styrene) (PS) and poly(*n*-butyl acrylate) (PBuA). Both polymer systems form spherical micelles or micellar structures with hydrodynamic radii of around 60 to 90 nm. The spherical micelles formed of PS containing polymers show a stiff and glassy core in contrast to the micelles with PBuA, with a more rubbery core. The highest transfection efficiency was obtained with spherical micelles formed of the linear PDMAEMA-*b*-PBuA-*b*-PDMAEMA block copolymers. The authors attributed this behaviour to an inability of the PS containing polymer to sufficient complex pDNA based on the restricted core. Unfortunately, no detailed polyplex analysis concerning size, shape and micelle stability was presented.[131] In another study, biodegradable poly-((*N*-methyldietheneamine sebacate)-*co*-((cholesteryl oxocarbonyl-amido ethyl)methyl bis(ethylene)ammonium bromid)sebacate)) was used for the formation of spherical micelles. Micelles of around 100 nm (diameter) were obtained showing a positive zeta potential. With these preformed micelles higher transfection efficiency and less cytotoxicity compared to bPEI were obtained.[132] One advantage of micellar structures is the co-delivery of drugs and pDNA due to the hydrophobic core and the cationic shell.[123,124,133] Such a multidrug delivery agent was realized with poly(3-caprolactone)-*b*-poly(*N*,*N*-dimethylamino-2-ethylmethacrylate) (PCL-SS-PDMAEMA) based micelles. An enhanced release mechanism of the drug doxorubicin due to the disulfide bridges could be realized as well as a higher transfection efficiency compared to PEI in human oral carcinoma cells. The polymers with higher DP of PDMAEMA form larger micelles. Thus, PCL_{80}-SS-$PDMAEMA_{155}$ results in spherical micelles of around 205 nm in diameter, whereas PCL_{80}-SS-$PDMAEMA_{115}$ forms micelles with sizes of around 93 nm. The larger the micelles are, the higher is the transfection efficiency (with a maximum diameter of 205 nm). The authors attributed this to the higher PDMAEMA content.[134] Anyhow, the question arises, how the polyplexes are formed and if this influences the transfection efficiency. In the case of the micelles with a diameter of 205 nm rather a wrapping around of the pDNA occurs in contrast to the polyplexes obtained with the smaller micelles (Fig. 5b and c). Unfortunately, also in this case no detailed polyplex characterisation was performed. In contrast to these relatively large micelles, small spherical micelles of around 20 nm in diameter were achieved by using $PDMAEMA_{47}$-*b*-P(DEAMA-*co*-BMA)$_n$ polymers. Studies at different pH values showed an impact of the BMA content and a possible tuning ability from spherical micelles to the unimers depending on the pH value. Hence, higher BMA content leads to a shift of the transition to lower pH values. The pH dependent conformational change was also analyzed regarding the hemolytic activity. It was demonstrated that at a pH value of 7.4 none of the micelles are hemolytic. In contrast to this, hemolytic activity was achieved at lower pH values of around 5.8. The best pH dependent transfection behaviour is shown for the polymer with a BMA content of 40%, because fast transition from micelles to unimers could be observed at a pH value of 6.6. Concerning the transfection efficiency, the most promising candidates are the polymers containing 30% and 40% BMA, better performing than lipofectamine. The complexation with pDNA results in polyplexes of around 250 nm in diameter, suggesting polyplexes formed by multiple micelles and pDNA (Fig. 5c).[135] Another example for polyplexes formed by spherical micelles is based on

poly(butadiene)-*b*-poly(methacrylic acid)-*b*-poly(2-(dimethylamino)ethyl methacrylate) (PB-*b*-PMAA-*b*-PDMAEMA) triblock terpolymers. The polymers self-assemble into spherical micelles of around 200 nm in diameter. Higher transfection efficiency and no detectable cytotoxicity compared to lPEI were demonstrated. Due to the pH dependent protonation/deprotonation behaviour of the PDMAEMA and the PMAA block, an increased endosomal escape is achieved. At physiological pH values both blocks are partially charged leading to a patchy surface with neutral and cationic charged domains. At decreased pH values in the endosome, the PMAA blocks collapse partially to the corona and the PDMAEMA blocks are stretched, forming the corona. This stimuli-responsive behaviour leads to an enhanced endosomal membrane destabilisation resulting in a release to the cytoplasm. Concerning the polyplex properties, it was assumed that the pDNA is wrapped around the micelle (Fig. 5b), which is confirmed by Cryo-TEM and DLS investigations.[136] Beside block copolymers, also dendritic structures were used for the self-assembly into complex architectures, as recently reported in detail.[137] A few examples of pre-formed spherical micelles demonstrate the potential of these architectures for the pDNA delivery. However, it is obvious that polyplexes formed of spherical micellar structures have to be divided into three groups (Fig. 5) to investigate the influence on the transfection mechanism in more detail. The limited data set does not enable us to conclude general findings yet.

Polymersomes or vesicular structures have the advantage of a lower permeability compared to liposomes. By tuning the properties of the copolymers, also a higher mechanical stability can be achieved. However, most polymersomes are only applied for drug delivery.[122,138–140] G. Battaglia and his group mainly work on polymersomes or vesicles for gene delivery, such as poly(2-(methacryloyloxy)ethyl-phosphorylcholine)-*co*-poly(2-(diisopropylamino)ethyl methacrylate). One way to encapsulate DNA into 200 to 400 nm (diameter) polymersomes is the use of a pH transition. At a low pH value of 6 the polymer exists as a unimer. If the pH value is increased, the polymers assemble into polymersomes and the DNA is partially encapsulated. The second fraction of pDNA is aggregated into general polyplexes that are hard to remove from the solution. Nevertheless, much higher transfection efficiencies can be obtained compared to lipofectamine demonstrating the benefit of vesicular structures.[141]

Other interesting classes are worm-like micellar structures, which showed unique features of biological application. The inspiration for filamentous polymer-based systems arises from nature as for instance the ebola viruses represent this structure. However, the examples are rare in the literature concerning pDNA delivery. One of the rare but very impressive examples is a PEG–PPA (poly(phoramidate)) block copolymer. Herein, pDNA was used as a template to generate different shapes depending on the solvent polarity (Fig. 6a–e). In addition to worm-like micellar structures, also rod-like and spherical micelles were obtained. The stabilisation of the different shapes also in water was realized by disulfide bridges. Concerning transfection efficiency, worm-like micelles (average length: 581 nm) show the highest gene expression in liver followed by rod like (130 nm) structures and spherical micelles (diameter 40 nm) (Fig. 6f).[20]

7 Conclusion and perspective

The progress in understanding the performance of polymer-based gene delivery *in vitro* is still ongoing and results in numerous studies of new polymer designs. The ongoing development of controlled polymerisation techniques, but also molecular biological techniques like high resolution microscopy,

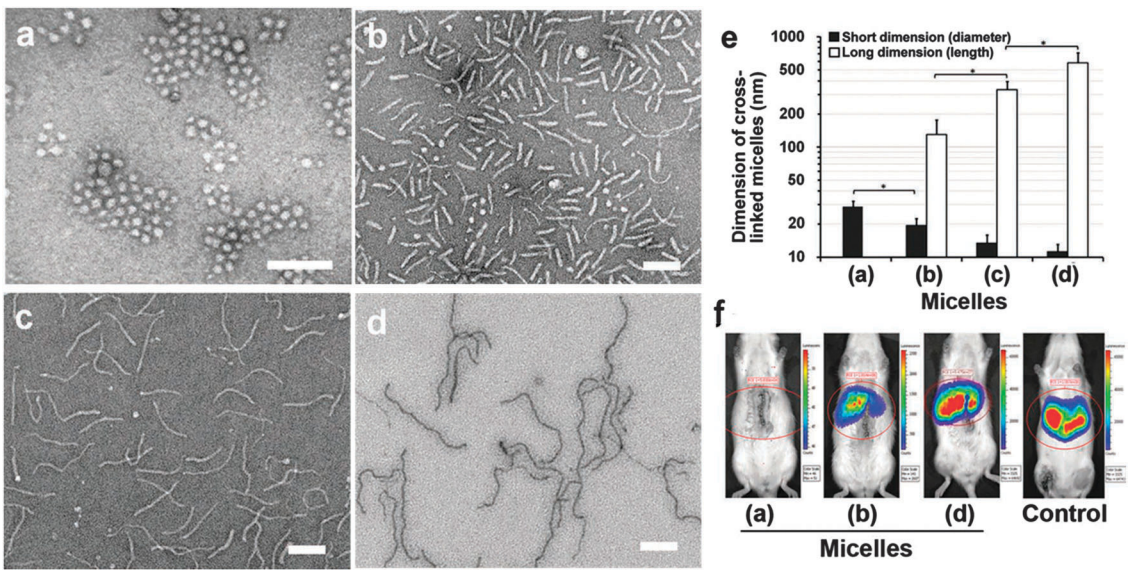

Fig. 6 PEG-*b*-PPA/DNA micelles. TEM images of crosslinked micelles obtained by different DMF–water mixtures, all scale bars represent 200 nm (a–d), average length and diameter of micelles (e), luciferase expression *in vivo* after 4 h with indicated micelles, control as benchmark expression level after hydrodynamic infusion of pDNA (f) (adopted from ref. 17).

allows us to provide more and more insights into the behaviour of polymers *in vitro* in order to conclude several findings also for *in vivo* applications. In the last few years, in particular more polymer architectures come into focus of research dealing with pDNA transfection. Linear homopolymers are well suited for the investigation of basic properties like pDNA complexation or buffer capacity. Statistical polymers can be applied to investigate "easy" combinations of various monomers. However, the rather different performance of statistical and block copolymers should be always kept in mind. In particular, the polyplex formation and properties thereof can vary significantly. Irregular branching seems to be beneficial showing that the polymer flexibility is advantageous for polyplex formation. The main goal to reduce the cytotoxicity of linear or branched systems without harming the transfection efficiency can be achieved by reducing the cationic charge and introducing at the same time an ampholytic or amphiphilic character that ensures polyplex stability and cellular internalisation. Also more complex architectures like brush- or comb-like polymers were presented in the last few years as promising vectors. This can be attributed to an enhanced polyplex formation and the possibility to introduce a biodegradable linker between backbone and side chain, which is responsible for the reduced cytotoxicity. A similar behaviour can be observed for star-shaped polymers, as here the transfer of dendritic structures can be achieved while maintaining a flexible behaviour. In case of the self-assembled structures, different polyplex types have to be considered meaning if polyplexes in micelles are applied or preformed spherical micelles interact with the pDNA. The rare examples of preformed micelles show the potential to outperform the gold standard PEI. Beside spherical, also worm-like micelles are investigated, here, in particular the *in vivo* behaviour is outstanding (Fig. 6).

All together, the usage of different architectures in the field of polymer-based gene delivery is immense and, in particular, the different polyplex properties seem to be a crucial factor. For this purpose, further investigations concerning the polyplex characteristics and their impact on the transfection mechanism are required. It was demonstrated that the interaction with the cellular membrane depends on the polyplex shape. Moreover, the paradigm between polyplex stability and dissociation can be successfully overcome by using biodegradable linkers like disulfide bonds because the intracellular polyplex dissociation is enhanced due to the degradation into low molar mass segments. The utilization of this strategy appears very promising for *in vivo* application as the balance between high polyplex stability and dissociation can be achieved. The prediction of cytotoxicity and transfection efficiency remains still challenging, but a few conclusions, in particular concerning the molar mass, can be drawn. Usually, high molar masses of 10 to 20 kDa lead to an increased transfection efficiency but also to a high cytotoxicity. Interestingly, in the case of graft and star polymers higher molar masses up to 100 kDa were presented without affecting the cytotoxicity and still showing high efficiency (Fig. 7). The interaction between the polymers and the cellular membrane probably differs, but this should be further investigated in detail. The open question, which architecture or system is the most promising one, cannot be answered up to now as every system has its pro and contra and further investigations are required.

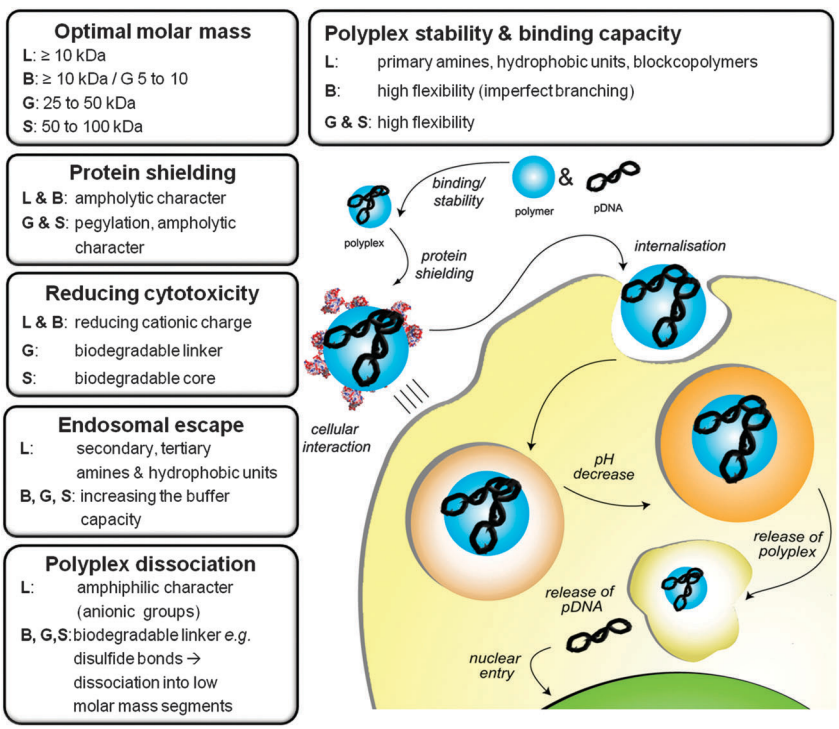

Fig. 7 Critical design parameter for an increased transfection efficiency and low cytotoxicity (L = linear polymers, B = branched polymers, G = graft polymers, S = star polymers).

However, in our opinion the graft- and star-based systems seem to be the most promising ones as with these systems high transfection efficiency and low cytotoxicity can be achieved. Moreover, with regard to the *in vivo* application, these systems provide the opportunity to synthesize biodegradable polymers in a defined way. The limited number of self-assembled systems like preformed spherical micelles or worm like structures were demonstrated as very efficient. Unfortunately, a few studies do not allow a conscience conclusion and further research is required. In the last few years, the research on different polymer-based pDNA transfection agents has led to numerous new insights of possible design rules for the optimized polymer, implicating the continuous progress in this field (Fig. 7).

Abbreviations

AEMA	Aminoethyl methacrylate
BAC	*N*,*N*-Bis(acryloyl cystamine)
BADS	Bis(2-acryloyl)oxyethyl disulfide
BMA	Butyl methacrylate
bPEI	Branched poly(ethylene imine)
CD	Cyclodextrin
CMC	Critical micelle concentration
DP	Degree of polymerisation
EGDMA	Ethylene glycol dimethacrylate
HEGMA	Hexa(ethylene glycol)methacrylate
HEMA	Hydroxyethyl methacrylate
lPEI	Linear poly(ethylene imine)
PASP	Poly(aspartamide)
PAsp(DET)	Poly(*N*-(*N*-(2-aminoethyl)-2-aminoethyl)aspartamide)
PAMAM	Poly(amidoamine)
PBuA	Poly(*n*-butyl acrylate)
PCI	Photochemical internalisation
PCL	Poly(3-caprolactone)
pDNA	Plasmid DNA
PDMAEMA	Poly(2-(dimethylamino)ethyl methacrylate)
PEG	Poly(ethylene glycol)
PEGEEMA	Poly(ethylene glycol)ethyl ether methacrylate
PEI	Poly(ethylene imine)
PEtOx	Poly(2-ethyl-2-oxazoline)
PEHA	Pentaethylenehexamine
PGEA	Ethanolamine functionalised poly(glycidyl methacrylate)
P(GMA)	Poly(glycidyl methacrylate)
PIC	Polyionic
PLL	Poly(L-lysin)
PMAA	Poly(methacrylic acid)
PMOXA	Poly(2-methyl-2oxazoline)
PMPC	Poly(2-methacryloyloxethyl phosphorylcholine)
PMPDSAH	Poly(*N*-(3-(methacryloylamino)propyl)-*N*,*N*-dimethyl-*N*-(3-sulfopropyl)ammonium hydroxide)
POSS	Poly(hedral oligomeric silesquioxane)
PPA	Poly(phoramidate)
PPI	Poly(propylenimine)
PS	Poly(styrene)
siRNA	Small interfering RNA
TEPA	Tetraethylenepentamine
TREN	Tris(2-aminoethyl)amine

Acknowledgements

We acknowledge funding from the Carl-Zeiss Foundation (Strukturantrag JCSM) and the Thuringian Ministry for Education, Science, and Culture (TMBWK; grants #B514-09051, NanoConSens and ProExzellence II, NanoPolar) as well as the German Federal Ministry of Education and Research (BMBF) (grants #13N13416, smart-dye-livery). Furthermore, we want to thank Dr. Christian Pietsch for discussions.

References

1 M. A. Mintzer and E. E. Simanek, *Chem. Rev.*, 2009, **109**, 259–302.
2 H. Buning, *EMBO Mol. Med.*, 2013, **5**, 1–3.
3 C. Sheridan, *Nat. Biotechnol.*, 2011, **29**, 121–128.
4 E. Check, *Nature*, 2002, **420**, 116–118.
5 http://www.ema.europa.eu/ema/index.jsp?curl=pages/medicines/human/medicines/002145/human_med_001480.jsp&mid=WC0b01ac058001d124, acessed 06.07.2015.
6 H. Yin, R. L. Kanasty, A. A. Eltoukhy, A. J. Vegas, J. R. Dorkin and D. G. Anderson, *Nat. Rev. Genet.*, 2014, **15**, 541–555.
7 O. Samsonova, C. Pfeiffer, M. Hellmund, O. M. Merkel and T. Kissel, *Polymers*, 2011, **3**, 693–718.
8 A. Akinc, M. Thomas, A. M. Klibanov and R. Langer, *J. Gene Med.*, 2005, **7**, 657–663.
9 A. Aied, U. Greiser, A. Pandit and W. X. Wang, *Drug Discovery Today*, 2013, **18**, 1090–1098.
10 E. V. van Gaal, R. van Eijk, R. S. Oosting, R. J. Kok, W. E. Hennink, D. J. Crommelin and E. Mastrobattista, *J. Controlled Release*, 2011, **154**, 218–232.
11 M. Lee and S. W. Kim, *Pharm. Res.*, 2005, **22**, 1–10.
12 M. Ogris, S. Brunner, S. Schuller, R. Kircheis and E. Wagner, *Gene Ther.*, 1999, **6**, 595–605.
13 S. Mishra, P. Webster and M. E. Davis, *Eur. J. Cell Biol.*, 2004, **83**, 97–111.
14 G. F. Walker, C. Fella, J. Pelisek, J. Fahrmeir, S. Boeckle, M. Ogris and E. Wagner, *Mol. Ther.*, 2005, **11**, 418–425.
15 J. G. Cai, Y. A. Yue, D. Rui, Y. F. Zhang, S. Y. Liu and C. Wu, *Macromolecules*, 2011, **44**, 2050–2057.
16 M. Wagner, A. C. Rinkenauer, A. Schallon and U. S. Schubert, *RSC Adv.*, 2013, **3**, 12774–12785.
17 L. Y. Qiu and Y. H. Bae, *Pharm. Res.*, 2006, **23**, 1–30.
18 M. Bray and T. W. Geisbert, *Int. J. Biochem. Cell Biol.*, 2005, **37**, 1560–1566.
19 T. K. Georgiou, *Polym. Int.*, 2014, **63**, 1130–1133.
20 X. Jiang, W. Qu, Y. Ren, J.-M. Williford, D. Pan, E. Luijten and H.-Q. Mao, *Adv. Mater.*, 2013, **25**, 227–232.

21 V. P. Chauhan, Z. Popovic, O. Chen, J. Cui, D. Fukumura, M. G. Bawendi and R. K. Jain, *Angew. Chem., Int. Ed.*, 2011, **50**, 11417–11420.
22 Y. Yue and C. Wu, *Biomater. Sci.*, 2013, **1**, 152–170.
23 S. K. Samal, M. Dash, S. Van Vlierberghe, D. L. Kaplan, E. Chiellini, C. van Blitterswijk, L. Moroni and P. Dubruel, *Chem. Soc. Rev.*, 2012, **41**, 7147–7194.
24 J. Ziebarth and Y. Wang, *Biophys. J.*, 2009, **97**, 1971–1983.
25 C. L. Grigsby and K. W. Leong, *J. R. Soc., Interface*, 2010, **7**, 67–82.
26 S. Xiang, H. Tong, Q. Shi, J. C. Fernandes, T. Jin, K. Dai and X. Zhang, *J. Controlled Release*, 2012, **158**, 371–378.
27 D. Fischer, Y. Li, B. Ahlemeyer, J. Krieglstein and T. Kissel, *Biomaterials*, 2003, **24**, 1121–1131.
28 K. M. Fichter, N. P. Ingle, P. M. McLendon and T. M. Reineke, *ACS Nano*, 2013, **7**, 347–364.
29 J. Rejman, A. Bragonzi and M. Conese, *Mol. Ther.*, 2005, **12**, 468–474.
30 D. Lechardeur, A. S. Verkman and G. L. Lukacs, *Adv. Drug Delivery Rev.*, 2005, **57**, 755–767.
31 A. Akinc, M. Thomas, A. M. Klibanov and R. Langer, *J. Gene Med.*, 2005, **7**, 657–663.
32 A. K. Varkouhi, M. Scholte, G. Storm and H. J. Haisma, *J. Controlled Release*, 2011, **151**, 220–228.
33 T. Merdan, K. Kunath, D. Fischer, J. Kopecek and T. Kissel, *Pharm. Res.*, 2002, **19**, 140–146.
34 R. V. Benjaminsen, M. A. Mattebjerg, J. R. Henriksen, S. M. Moghimi and T. L. Andresen, *Mol. Ther.*, 2013, **21**, 149–157.
35 Z. U. Rehman, D. Hoekstra and I. S. Zuhorn, *ACS Nano*, 2013, **7**, 3767–3777.
36 Y. W. Cho, J. D. Kim and K. Park, *J. Pharm. Pharmacol.*, 2003, **55**, 721–734.
37 W. T. Godbey, M. A. Barry, P. Saggau, K. K. Wu and A. G. Mikos, *J. Biomed. Mater. Res.*, 2000, **51**, 321–328.
38 J. D. Larsen, N. L. Ross and M. O. Sullivan, *J. Gene Med.*, 2012, **14**, 580–589.
39 M. Gillard, Z. Jia, J. J. Hou, M. Song, P. P. Gray, T. P. Munro and M. J. Monteiro, *Biomacromolecules*, 2014, **15**, 3569–3576.
40 D. A. Dean, D. D. Strong and W. E. Zimmer, *Gene Ther.*, 2005, **12**, 881–890.
41 P. van de Wetering, E. E. Moret, N. M. E. Schuurmans-Nieuwenbroek, M. J. van Steenbergen and W. E. Hennink, *Bioconjugate Chem.*, 1999, **10**, 589–597.
42 F. J. Xu and W. T. Yang, *Prog. Polym. Sci.*, 2011, **36**, 1099–1131.
43 K. Matyjaszewski and N. V. Tsarevsky, *Nat. Chem.*, 2009, **1**, 276–288.
44 K. Matyjaszewski, *Science*, 2011, **333**, 1104–1105.
45 Z. H. Liu, Z. Y. Zhang, C. R. Zhou and Y. P. Jiao, *Prog. Polym. Sci.*, 2010, **35**, 1144–1162.
46 A. C. Rinkenauer, L. Tauhardt, F. Wendler, K. Kempe, M. Gottschaldt, A. Traeger and U. S. Schubert, *Macromol. Biosci.*, 2015, **15**, 414–425.
47 K. Knop, R. Hoogenboom, D. Fischer and U. S. Schubert, *Angew. Chem., Int. Ed.*, 2010, **49**, 6288–6308.
48 N. Hadjichristidis, M. Pitsikalis, S. Pispas and H. Iatrou, *Chem. Rev.*, 2001, **101**, 3747–3792.
49 K. Berg, P. K. Selbo, A. Weyergang, A. Dietze, L. Prasmickaite, A. Bonsted, B. O. Engesaeter, E. Angell-Petersen, T. Warloe, N. Frandsen and A. Hogset, *J. Microsc.*, 2005, **218**, 133–147.
50 D. Ma, Y. Zhao, X. Y. Zhou, Q. M. Lin, Y. Zhang, J. T. Lin and W. Xue, *Macromol. Biosci.*, 2013, **13**, 1221–1227.
51 T. Nomoto, S. Fukushima, M. Kumagai, K. Machitani, A. Arnida, Y. Matsumoto, M. Oba, K. Miyata, K. Osada, N. Nishiyama and K. Kataoka, *Nat. Commun.*, 2014, **5**, 3545.
52 D. Ma, H.-B. Zhang, Y.-Y. Chen, J.-T. Lin and L.-M. Zhang, *J. Colloid Interface Sci.*, 2013, **405**, 305–311.
53 Y. Hu, W. Yuan, N. N. Zhao, J. Ma, W. T. Yang and F. J. Xu, *Biomaterials*, 2013, **34**, 5411–5422.
54 H. Petersen, K. Kunath, A. L. Martin, S. Stolnik, C. J. Roberts, M. C. Davies and T. Kissel, *Biomacromolecules*, 2002, **3**, 926–936.
55 R. Namgung, J. Kim, K. Singha, C. H. Kim and W. J. Kim, *Mol. Pharmaceutics*, 2009, **6**, 1826–1835.
56 K. Ladewig, Z. P. Xu, P. Gray and G. Q. Max Lu, *J. Biomed. Mater. Res.*, 2013, **102**, 2137–2146.
57 D. Ma, Z. H. Liu, Q. Q. Zheng, X. Y. Zhou, Y. Zhang, Y. F. Shi, J. T. Lin and W. Xue, *Macromol. Rapid Commun.*, 2013, **34**, 548–552.
58 M. Byrne, D. Victory, A. Hibbitts, M. Lanigan, A. Heise and S.-A. Cryan, *Biomater. Sci.*, 2013, **1**, 1223–1234.
59 Y. Y. Yang, X. Wang, Y. Hu, H. Hu, D. C. Wu and F. J. Xu, *ACS Appl. Mater. Interfaces*, 2013, **22**, 1044–1052.
60 A. Schallon, C. V. Synatschke, V. Jerome, A. H. E. Müller and R. Freitag, *Biomacromolecules*, 2012, **13**, 3463–3474.
61 K. M. Xiu, J. J. Yang, N. N. Zhao, J. S. Li and F. J. Xu, *Acta Biomater.*, 2013, **9**, 4726–4733.
62 C. V. Synatschke, A. Schallon, V. Jerome, R. Freitag and A. H. E. Müller, *Biomacromolecules*, 2011, **12**, 4247–4255.
63 J. J. Deng, N. Li, K. J. Mai, C. A. Yang, L. Yan and L. M. Zhang, *J. Mater. Chem.*, 2011, **21**, 5273–5281.
64 B. Liang, J. J. Deng, F. Yuan, N. Yang, W. Li, J. R. Yin, S. X. Pu, L. C. Xie, C. Gao and L. M. Zhang, *Carbohydr. Polym.*, 2013, **94**, 185–192.
65 Y. Hu, Y. Zhu, W. T. Yang and F. J. Xu, *ACS Appl. Mater. Interfaces*, 2013, **5**, 703–712.
66 T. K. Georgiou, M. Vamvakaki, C. S. Patrickios, E. N. Yamasaki and L. A. Phylactou, *Biomacromolecules*, 2004, **5**, 2221–2229.
67 T. K. Georgiou, M. Vamvakaki, L. A. Phylactou and C. S. Patrickios, *Biomacromolecules*, 2005, **6**, 2990–2997.
68 T. K. Georgiou, L. A. Phylactou and C. S. Patrickios, *Biomacromolecules*, 2006, **7**, 3505–3512.
69 H. Y. Cho, S. E. Averick, E. Paredes, K. Wegner, A. Averick, S. Jurga, S. R. Das and K. Matyjaszewski, *Biomacromolecules*, 2013, **14**, 1262–1267.
70 X. J. Cai, C. Y. Dong, H. Q. Dong, G. M. Wang, G. M. Pauletti, X. J. Pan, H. Y. Wen, I. Mehl, Y. Y. Li and D. L. Shi, *Biomacromolecules*, 2012, **13**, 1024–1034.

71 F. Y. Dai, P. Sun, Y. J. Liu and W. G. Liu, *Biomaterials*, 2010, **31**, 559–569.
72 Y. Y. Mai and A. Eisenberg, *Chem. Soc. Rev.*, 2012, **41**, 5969–5985.
73 P. P. Kundu and V. Sharma, *Curr. Opin. Solid State Mater. Sci.*, 2008, **12**, 89–102.
74 S. Agarwal, Y. Zhang, S. Maji and A. Greiner, *Mater. Today*, 2012, **15**, 388–393.
75 Y. Lee and K. Kataoka, *Adv. Polym. Sci.*, 2012, **249**, 95–134.
76 M. Mannisto, S. Vanderkerken, V. Toncheva, M. Elomaa, M. Ruponen, E. Schacht and A. Urtti, *J. Controlled Release*, 2002, **83**, 169–182.
77 I. Richard, M. Thibault, G. De Crescenzo, M. D. Buschmann and M. Lavertu, *Biomacromolecules*, 2013, **14**, 1732–1740.
78 B. Brissault, A. Kichler, C. Guis, C. Leborgne, O. Danos and H. Cheradame, *Bioconjugate Chem.*, 2003, **14**, 581–587.
79 H. Yu, V. Russ and E. Wagner, *AAPS J.*, 2009, **11**, 445–455.
80 J. M. Layman, S. M. Ramirez, M. D. Green and T. E. Long, *Biomacromolecules*, 2009, **10**, 1244–1252.
81 A. C. Rinkenauer, A. Vollrath, A. Schallon, L. Tauhardt, K. Kempe, S. Schubert, D. Fischer and U. S. Schubert, *ACS Comb. Sci.*, 2013, **15**, 475–482.
82 C. Zhu, S. Jung, G. Si, R. Cheng, F. Meng, X. Zhu, T. G. Park and Z. Zhong, *J. Polym. Sci., Part A: Polym. Chem.*, 2010, **48**, 2869–2877.
83 S. Han, H. Wan, D. Lin, S. Guo, H. Dong, J. Zhang, L. Deng, R. Liu, H. Tang and A. Dong, *Acta Biomater.*, 2014, **10**, 670–679.
84 J. H. Jeong, S. H. Song, D. W. Lim, H. Lee and T. G. Park, *J. Controlled Release*, 2001, **73**, 391–399.
85 F. J. Verbaan, C. Oussoren, C. J. Snel, D. J. Crommelin, W. E. Hennink and G. Storm, *J. Gene Med.*, 2004, **6**, 64–75.
86 J. P. Lai, Z. Y. Xu, R. P. Tang, W. H. Ji, R. Wang, J. Wang and C. Wang, *Polymer*, 2014, **55**, 2761–2771.
87 F. Y. Dai and W. G. Liu, *Biomaterials*, 2011, **32**, 628–638.
88 J. B. Zhou, J. Liu, C. J. Cheng, T. R. Patel, C. E. Weller, J. M. Piepmeier, Z. Z. Jiang and W. M. Saltzman, *Nat. Mater.*, 2012, **11**, 82–90.
89 L. Novo, E. V. B. van Gaal, E. Mastrobattista, C. F. van Nostrum and W. E. Hennink, *J. Controlled Release*, 2013, **169**, 246–256.
90 D. Sprouse and T. M. Reineke, *Biomacromolecules*, 2014, **15**, 2616–2628.
91 Z. Kadlecova, Y. Rajendra, M. Matasci, L. Baldi, D. L. Hacker, F. M. Wurm and H. A. Klok, *J. Controlled Release*, 2013, **169**, 276–288.
92 D. G. Anderson, A. Akinc, N. Hossain and R. Langer, *Mol. Ther.*, 2005, **11**, 426–434.
93 M. Neu, D. Fischer and T. Kissel, *J. Gene Med.*, 2005, **7**, 992–1009.
94 P. Y. Teo, C. Yang, J. L. Hedrick, A. C. Engler, D. J. Coady, S. Ghaem-Maghami, A. J. T. George and Y. Y. Yang, *Biomaterials*, 2013, **34**, 7971–7979.
95 J. Sun, F. Zeng, H. L. Jian and S. Z. Wu, *Polym. Chem.*, 2013, **4**, 5810–5818.
96 T. Zhao, H. Zhang, B. Newland, A. Aied, D. Zhou and W. Wang, *Angew. Chem., Int. Ed.*, 2014, **53**, 6095–6100.
97 S. Sevenson and D. A. Tomalia, *Adv. Drug Delivery Rev.*, 2012, **64**, 102–115.
98 X. F. Hu, H. B. Wang, J. H. Yang, W. G. Liu and W. Wang, *J. Appl. Polym. Sci.*, 2014, **131**, 1–9.
99 J. F. KukowskaLatallo, A. U. Bielinska, J. Johnson, R. Spindler, D. A. Tomalia and J. R. Baker, *Proc. Natl. Acad. Sci. U. S. A.*, 1996, **93**, 4897–4902.
100 S. P. Hong, A. U. Bielinska, A. Mecke, B. Keszler, J. L. Beals, X. Y. Shi, L. Balogh, B. G. Orr, J. R. Baker and M. M. B. Holl, *Bioconjugate Chem.*, 2004, **15**, 774–782.
101 P. T. Wong, K. Tang, A. Coulter, S. Tang, J. R. Baker, Jr. and S. K. Choi, *Biomacromolecules*, 2014, **15**, 4134–4145.
102 M. X. Tang, C. T. Redemann and F. C. Szoka, *Bioconjugate Chem.*, 1996, **7**, 703–714.
103 Z. Kadlecova, L. Baldi, D. Hacker, F. M. Wurm and H.-A. Klok, *Biomacromolecules*, 2012, **13**, 3127–3137.
104 C. Feng, Y. J. Li, D. Yang, J. H. Hu, X. H. Zhang and X. Y. Huang, *Chem. Soc. Rev.*, 2011, **40**, 1282–1295.
105 X. Jiang, M. C. Lok and W. E. Hennink, *Bioconjugate Chem.*, 2007, **18**, 2077–2084.
106 R. Q. Li, Y. Hu, B. R. Yu, N. N. Zhao and F. J. Xu, *Bioconjugate Chem.*, 2014, **25**, 155–164.
107 Z.-H. Wang, Y. Zhu, M.-Y. Chai, W.-T. Yang and F.-J. Xu, *Biomaterials*, 2012, **33**, 1873–1883.
108 H. Wei, J. A. Pahang and S. H. Pun, *Biomacromolecules*, 2013, **14**, 275–284.
109 M. Zhang, M. Liu, Y. N. Xue, S. W. Huang and R. X. Zhuo, *Bioconjugate Chem.*, 2009, **20**, 440–446.
110 X. P. Duan, J. S. Xiao, Q. Yin, Z. W. Zhang, S. R. Mao and Y. P. Li, *Int. J. Nanomed.*, 2012, **7**, 4961–4972.
111 X. Q. Liu, J. Z. Du, C. P. Zhang, F. Zhao, X. Z. Yang and J. Wang, *Int. J. Pharm.*, 2010, **392**, 118–126.
112 J. M. Benns, J.-S. Choi, R. I. Mahato, J.-S. Park and S. W. Kim, *Bioconjugate Chem.*, 2000, **11**, 637–645.
113 C. Scholz, P. Kos and E. Wagner, *Bioconjugate Chem.*, 2014, **25**, 251–261.
114 T. von Erlach, S. Zwicker, B. Pidhatika, R. Konradi, M. Textor, H. Hall and T. Luhmann, *Biomaterials*, 2011, **32**, 5291–5303.
115 J. Shi, J. L. Choi, B. Chou, R. N. Johnson, J. G. Schellinger and S. H. Pun, *ACS Nano*, 2013, **7**, 10612–10620.
116 R. N. Johnson, D. S. H. Chu, J. Shi, J. G. Schellinger, P. M. Carlson and S. H. Pun, *J. Controlled Release*, 2011, **155**, 303–311.
117 X. C. Yang, M. Y. Chai, Y. Zhu, W. T. Yang and F. J. Xu, *Bioconjugate Chem.*, 2012, **23**, 618–626.
118 J. Liu, Y. L. Xu, Q. Z. Yang, C. Li, W. E. Hennink, R. X. Zhuo and X. L. Jiang, *Acta Biomater.*, 2013, **9**, 7758–7766.
119 X. J. Loh, Z. X. Zhang, K. Y. Mya, Y. L. Wu, C. B. He and J. Li, *J. Mater. Chem.*, 2010, **20**, 10634–10642.
120 J. S. Li, Z. Z. Guo, J. Y. Xin, G. L. Zhao and H. N. Xiao, *Carbohydr. Polym.*, 2010, **79**, 277–283.
121 F. J. Xu, Z. X. Zhang, Y. Ping, J. Li, E. T. Kang and K. G. Neoh, *Biomacromolecules*, 2009, **10**, 285–293.

122 H. Cabral and K. Kataoka, *Sci. Technol. Adv. Mater.*, 2010, **11**, 1–9.
123 M. S. Aw, M. Kurian and D. Losic, *Chem. – Eur. J.*, 2013, **19**, 12586–12601.
124 C. Liu, F. Liu, L. Feng, M. Li, J. Zhang and N. Zhang, *Biomaterials*, 2013, **34**, 2547–2564.
125 N. Nishiyama, Y. Bae, K. Miyata, S. Fukushima and K. Kataoka, *Drug Discovery Today: Technol.*, 2005, **2**, 21–26.
126 K. Kataoka, H. Togawa, A. Harada, K. Yasugi, T. Matsumoto and S. Katayose, *Macromolecules*, 1996, **29**, 8556–8557.
127 N. Wiradharma, Y. Zhang, S. Venkataraman, J. L. Hedrick and Y. Y. Yang, *Nano Today*, 2009, **4**, 302–317.
128 M. H. Dufresne, M. Elsabahy and J. C. Leroux, *Pharm. Res.*, 2008, **25**, 2083–2093.
129 M. Oba, *Biol. Pharm. Bull.*, 2013, **36**, 1045–1051.
130 T. C. Lai, K. Kataoka and G. S. Kwon, *Colloids Surf., B*, 2012, **99**, 27–37.
131 A. M. Alhoranta, J. K. Lehtinen, A. O. Urtti, S. J. Butcher, V. O. Aseyev and H. J. Tenhu, *Biomacromolecules*, 2011, **12**, 3213–3222.
132 Y. Wang, L.-S. Wang, S.-H. Goh and Y.-Y. Yang, *Biomacromolecules*, 2007, **8**, 1028–1037.
133 J.-L. Zhu, H. Cheng, Y. Jin, S.-X. Cheng, X.-Z. Zhang and R.-X. Zhuo, *J. Mater. Chem.*, 2008, **18**, 4433–4441.
134 Y. Li, X. Lei, H. Dong and T. Ren, *RSC Adv.*, 2014, **4**, 8165–8176.
135 M. J. Manganiello, C. Cheng, A. J. Convertine, J. D. Bryers and P. S. Stayton, *Biomaterials*, 2012, **33**, 2301–2309.
136 A. C. Rinkenauer, A. Schallon, U. Gunther, M. Wagner, E. Betthausen, U. S. Schubert and F. H. Schacher, *ACS Nano*, 2013, **7**, 9621–9631.
137 A. Tschiche, S. Malhotra and R. Haag, *Nanomedicine*, 2014, **9**, 667–693.
138 O. Onaca, R. Enea, D. W. Hughes and W. Meier, *Macromol. Biosci.*, 2009, **9**, 129–139.
139 C. LoPresti, H. Lomas, M. Massignani, T. Smart and G. Battaglia, *J. Mater. Chem.*, 2009, **19**, 3576–3590.
140 M. Massignani, H. Lomas and G. Battaglia, *Adv. Polym. Sci.*, 2010, **229**, 115–154.
141 H. Lomas, I. Canton, S. MacNeil, J. Du, S. P. Armes, A. J. Ryan, A. L. Lewis and G. Battaglia, *Adv. Mater.*, 2007, **19**, 4238–4243.

Publication P2

Opposites attract: Influence of the molar mass branched poly(ethylene imine) on biophysical characteristics of siRNA-based polyplexes

M. Wagner, A. C. Rinkenauer, A. Schallon, U. S. Schubert

RSC Adv. **2013**, *3*, 12774–12785

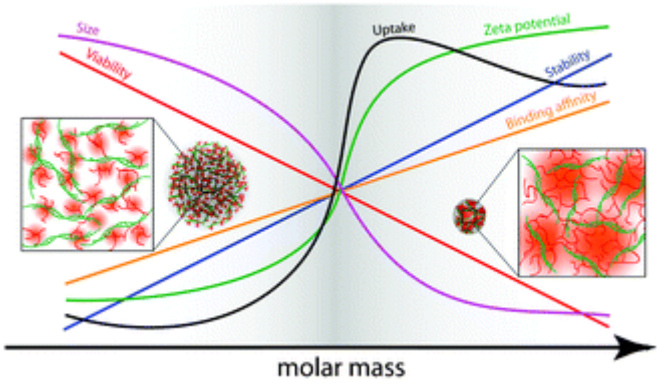

RSC Advances

RSC Publishing

PAPER

View Article Online
View Journal | View Issue

Cite this: *RSC Advances*, 2013, **3**, 12774

Opposites attract: influence of the molar mass of branched poly(ethylene imine) on biophysical characteristics of siRNA-based polyplexese

Michael Wagner,[ab] Alexandra C. Rinkenauer,[ab] Anja Schallon[ab] and Ulrich S. Schubert*[ab]

Received 26th February 2013,
Accepted 15th May 2013

DOI: 10.1039/c3ra42069h

www.rsc.org/advances

Polymer-based carriers, in particular polycations, represent an interesting alternative to viral vectors, as they form so-called polyplexes with nucleic acids by entropic driven, electrostatic interactions. In this study, we investigate in detail polyplexes based on small interfering RNA (siRNA), the delivery of which into eukaryotic cells represents an attractive route for treating genetic diseases by inhibition of harmful gene expression. Although plasmid DNA (pDNA) based polyplexes are well characterized, we show that not all knowledge can be adopted from pDNA, as siRNA is around 250 times smaller and shows a higher rigidity. The used polymer component is the polycation branched poly(ethylene imine) (B-PEI) of a high range of molar masses (0.6, 1.8, 10, 25 kDa), which are further analyzed by potentiometric titration and cytotoxicity tests. The formation, size, and net-charge of the polyplexes are examined at different ratios of nitrogen of the different polymers and phosphates of the RNA (N/P). Moreover, the stability of siRNA polyplexes against heparin and time was investigated. The obtained physicochemical parameters were then correlated to the cellular internalization of polyplexes. A strong dependency of the molar mass on the polyplex characteristics of the used B-PEI was found. Thereby, high molar mass B-PEI $\geqslant$ 10 kDa forms smaller polyplexes of around 50 nm radius with zeta potentials $>$ 25 mV, increased long-term stability, and enhanced cellular uptake compared to low molar mass ones. To gain deeper insight into the differences and characteristics of siRNA based polyplexes, the characterization by analytical and preparative ultracentrifugation (AUC, PUC) is applied on siRNA polyplexes for the first time and referred to conventional characterization methods such as DLS. AUC was also used to identify non-complexed PEI in the polyplex solutions. A virtual N/P of 1.3 for siRNA was measured, independent of the used molar masses of B-PEI. Additionally, differences in cellular uptakes of siRNA and pDNA based polyplexes were found. The results of this study will help to understand the properties of siRNA-based polyplexes and could lead to more efficient polymer design.

Introduction

Since the discovery of the RNA interference mechanism by Fire *et al.* in 1998,[1] siRNA delivery represents an attractive route for treating genetic diseases by inhibition of the expression of harmful genes. Compared to the delivery of pDNA, siRNA only needs to be delivered into the cytoplasm of the cells but not into the nucleus, which avoids the need for transport of the delivered molecules across the nuclear membrane. There are, however, two serious limitation of siRNA as a therapeutic agent. One of them is its high negative net-charge, which renders its delivery through the also negatively charged cell membrane difficult.[2] Beside this, genetic material, in particular siRNA, is not stable under physiological conditions but will be rapidly degraded by RNAses.[3] Thus, the half-life time of siRNA in blood serum varies from several minutes to an hour.[4] Both problems make the application of siRNA for *in vitro* and *in vivo* gene delivery challenging. To overcome them, non-viral polymeric carriers, in particular polycations, can be applied for the delivery of the genetic material into the cells and the subsequent expression of foreign genes,[5–7] as has been shown by recent intense research.[8–10] Although the transfection efficiencies of polymeric vectors, the so-called polyplexes, are lower compared to viral vectors, they have substantial advantages,[11,12] as their easy large-scale production, their safety for clinical uses,[13,14] and their potential for chemical modifications.[15–17] Among the polymers applied, the commercially available poly(ethylene imine) (PEI), which is intensively characterized in literature, is the most popular one and is

[a]*Laboratory of Organic and Macromolecular Chemistry (IOMC), Friedrich Schiller University Jena, Humboldtstrasse 10, Jena D-07743, Germany. E-mail: ulrich.schubert@uni-jena.de*
[b]*Jena Center for Soft Matter (JCSM), Friedrich Schiller University Jena, Philosophenweg 7, Jena D-07743, Germany*

widely investigated for the delivery of pDNA as well as siRNA.[18–22] Despite the broad interest, the polyplex formation of siRNA and PEI and their characteristics are only partially understood and not yet investigated in detail.

The primary driving force for complexation of nucleic acids by PEI is entropy. The ionic interactions between the negative phosphates in the nucleic acids and the protonated amine groups in the polymer induce a release of counter ions, which leads to an increase of translational entropy.[12,23] The gain of entropy is of course significantly smaller for siRNA than for pDNA, due to its shorter chain length. This results in a weaker binding in the polyplexes. The complexation is influenced also by other factors, like the 3-D structure of the polymers (linear or branched),[24] their molar mass,[25] or further intermolecular forces *e.g.* hydrophobic interactions. While linear PEI (L-PEI) contains mainly secondary amines, branched PEI (B-PEI) consists of primary, secondary, and tertiary amines. The resulting degree of protonation is essential for polyplex formation and for the release of the polyplexes from the endosome according to the postulated proton sponge effect.[5] Non-complexed PEI also influences the transfection efficiencies of polyplexes as well as the toxicity.[26] Besides the polymer itself, also the complexation conditions, *e.g.* buffer components, pH value, or ionic strength play an important role. Added salts can interact with the polyplexes or screen electrostatic forces. It was shown that, *e.g.*, low ionic strength promotes the formation of smaller pDNA polyplexes.[27]

An efficient gene carrier has to combine two features. On the one hand, the complexation has to be sufficiently strong to protect against degradation and to transport the siRNA through the cell membrane. On the other hand, the cellular uptake should be promoted and the release of the genetic material from the polyplex in the cytosol has to be possible. The development of polymers that offer a balance between the two features is an important goal. Above all, of course, the perfect gene carrier should be non-toxic.

For the detailed biophysical and physicochemical characterization of nanoparticles in general, different techniques and methods were established, in the first place light scattering (in particular dynamic light scattering) for measuring the translational diffusion coefficient and the hydrodynamic radius, respectively. Other hydrodynamic methods, *e.g.*, analytical ultracentrifugation (AUC), were up to now not used for analyzing siRNA-based polyplexes. AUC is well-known as a means for the characterization of the molar mass and size of proteins[28–30] but can be also applied for studying nanoparticles and synthetic polymers.[31–33] The efficiency of gene delivery depends on the molar mass of the polymer applied. For B-PEI, the best results for transfection of pDNA were obtained up to now with molar masses of 25 kDa.[34] Beside this, an increase in the molar mass of B-PEI and various other polymers often caused higher cytotoxic effects.[35,36] However, with siRNA 25 kDa B-PEI did not yield an efficient delivery of the nucleic acid, without any obvious reason.[34] This accentuates the importance of a detailed understanding of the polyplex properties.

Herein, the importance of a wide range of molar masses of B-PEI used for siRNA delivery will be presented. Therefore, the influence of the polymer on the formation, stability, size, and net-charge of the polyplexes at different N/P ratios (ratio of nitrogen in the polymer and phosphates in the RNA) will be elucidated in detail. As the knowledge of siRNA polyplexes based on results obtained with pDNA, we also focus on the differences of both genetic materials concerning their stiffness, amount of free PEI, and cellular uptake behavior. In addition, AUC will be applied for the characterization of such polyplexes and the obtained results compared to the revealed data by conventional methods. The potential of this powerful technique for detailed analysis of free and complexed PEI will be demonstrated.

Experimental

Materials

B-PEI of molar masses of 0.6, 1.8, and 10 kDa was purchased from Polysciences (Eppelheim, Germany), and 25 kDa B-PEI as well as heparin were purchased from Sigma Aldrich (Steinhausen, Germany). B-PEI was dissolved in sterile 20 mM 4-(2-hydroxethyl) piperazine-1-ethanesulfonic acid (HEPES) and 5% (w/w) glucose buffer (HBG, pH 7.2) to obtain stock solutions of 0.2 mg mL^{-1}. The quality of B-PEI was checked by dynamic light scattering and analytical ultracentrifugation to exclude an influence on the polyplex experiments later on. Control siRNA duplex negative control with 19 bp and Cy3 labeled siRNA was obtained from Eurogentech (Cologne, Germany). Stock solutions of siRNA were prepared by dissolving solid siRNA in sterile RNase free water to yield a concentration of 20 μM. Ethidium bromide solution 1% was purchased from Carl Roth (Karlsruhe, Germany). AlamarBlue and YOYO-1 was obtained from Life Technologies (Darmstadt, Germany). Cell culture materials, cell culture media, and solutions were obtained from PAA (Pasching, Austria). All other chemicals were purchased from Sigma Aldrich and are of analytical grade or better and used without further purification.

Polyplex preparation

Polyplexes of siRNA and B-PEI were prepared by mixing stock solutions of siRNA and B-PEI at a certain N/P ratio. The indicated amounts of B-PEI were added to a certain volume of 20 μM siRNA solution. Subsequently, the solutions were vortexed for 5 s at 2500 rpm. After incubation at room temperature for 20 min the mixture was diluted with HBG to a total volume of 1 mL and an overall siRNA concentration of 15 μg mL^{-1}.

Potentiometric titration

For potentiometric titration, 6 mg B-PEI were dissolved in 6 mL pure water. Titration experiments were performed using a Metrohm 765 Dosimat (Filderstadt, Germany) and a Greisinger GMH 3530 pH meter (Regenstauf, Germany), using 0.1 M hydrochloric acid or 0.1 M sodium hydroxide as titrant. The titration was started at pH $>$ 11. For this, a defined

amount of 0.1 M sodium hydroxide solution was added. Then, the solution was titrated against 0.1 M hydrochloric acid. The titration was stopped at pH 2. Each experiment was carried out in triplicate at 25 °C as described in the literature.[37]

Ethidiumbromide quenching assay (EBA)

The polyplex formation of siRNA and B-PEI was detected by quenching of the ethidium bromide (EB) fluorescence as described previously.[38] Briefly, 15 μg mL^{-1} siRNA in a total volume of 100 μL HBG was incubated with EB (0.4 μg mL^{-1}) for 10 min at room temperature, and then polyplexes with increasing amounts of B-PEI were formed in black 96-well plates (Nunc, Langenselbold, Germany). The samples were equilibrated for 20 min before the fluorescence was measured using a Tecan Genios Pro fluorescence microplate reader (Tecan, Crailsheim, Germany); the excitation and emission wavelength were 525 and 605 nm, respectively. A sample containing only siRNA and EB was used to calibrate the device to 100% fluorescence against a background of 0.4 μg mL^{-1} of EB in HBG solution. The percentage of dye displaced upon polyplex formation was calculated using eqn (1):

$$\mathrm{RFU} = \frac{F_{\mathrm{sample}} - F_0}{F_{\mathrm{siRNA}} - F_0} \quad (1)$$

Here, RFU is the relative fluorescence and F_{sample}, F_0, and F_{siRNA} are the fluorescence intensities of a given sample, the EB in HBG alone, and the EB intercalated into siRNA alone.

Heparin dissociation assay

To investigate the release of siRNA from polyplexes, the heparin dissociation assay was used.[24] For this purposee, 15 μg mL^{-1} siRNA were incubated for 10 min with EB (0.4 μg mL^{-1}) in a total volume of 100 μL HBG before polyplexes at N/P 10 were formed. After 15 min the polyplexes were transferred into black 96-well plates and heparin at the indicated concentrations was added. The solution was mixed and incubated for further 30 min at 37 °C. The fluorescence of EB (Ex 525 nm/Em 605 nm) was measured, and the percentage of intercalated EB was calculated as described before (1).

Dynamic light scattering

Dynamic light scattering (DLS) was performed on an ALV-CGS-3 system (ALV, Langen, Germany) equipped with a He–Ne laser operating at a wavelength of λ = 633 nm. The counts were detected at an angle of 90°. All measurements were carried out at 25 °C after an equilibration time of 120 s. For analyzing the autocorrelation function (ACF), the cumulant analysis and the CONTIN algorithm[39] were applied. Apparent hydrodynamic radii were calculated according to the Stokes–Einstein Equation (eqn (2)):

$$R_{\mathrm{H}} = \frac{kT}{6\pi\eta D_0} \quad (2)$$

Here, R_{H} is the hydrodynamic radius, k the Boltzmann constant, T the absolute temperature, η the viscosity of the sample, and D_0 the translational diffusion coefficient.

Electrophoretic light scattering

Electrophoretic light scattering was used to measure the electrokinetic potential, also known as zeta potential. The measurements were performed on a Zetasizer Nano ZS (Malvern Instruments, Herrenberg, Germany) by applying laser Doppler velocimetry.[40] For each measurement, 20 runs were carried out using the slow-field reversal and fast-field reversal mode at 150 V. Each experiment was performed in triplicate at 25 °C. The zeta potential (ζ) was calculated from the electrophoretic mobility (μ) according to the Henry Equation (eqn (3)) with $f(ka)$ = 1.5 (Smoluchowski model):

$$\zeta = \frac{3\eta\mu}{2\varepsilon f(ka)} \quad (3)$$

Here, η is the viscosity of the solution, ε the dielectric constant, and $f(ka)$ the Henry constant.

Analytical and preparative ultracentrifugation

Analytical ultracentrifugation was performed on a Beckman XL-I analytical ultracentrifuge (Krefeld, Germany). Experiments were carried out in double-sector aluminum centerpieces with optical path length of 12 mm in a four holes rotor setup. Each cell was filled with 0.42 mL of solvent (HBG) and 0.4 mL of sample. A rotor speed between 1000 to 40 000 rpm was used, depending on the sample. The system was equilibrated for 40 min at 25 °C in the centrifuge. Sedimentation data were recorded by absorbance or interference optics, depending on the sample. Data analysis was done by the Sedfit software.[41] For $c(s)$ analysis of sedimentation data, the partial specific volume of the compound was determined *via* AUC using the ''density variation method'' as described by Mächtle.[42] The partial specific volume (υ) of pure siRNA was taken from the literature.[43] For calculating the hydrodynamic radius (R_{H}) and the molar mass (M), the Svedberg equation was transformed into eqn (4) and (5), respectively.[44]

$$R_{\mathrm{H}} = \frac{3}{2}(2[s]\upsilon)^{1/2} \quad (4)$$

$$M = 9\pi\sqrt{2}N_{\mathrm{A}}\left[[s]\left(\frac{f}{f_{\mathrm{sph}}}\right)\right]^{\frac{3}{2}}\upsilon^{\frac{1}{2}} \quad (5)$$

Here, N_{A} is Avogadro's constant, $[s]$ the intrinsic sedimentation coefficient, f the frictional coefficient of the solute, and f_{sph} that of a hard sphere. Preparative ultracentrifugation (PUC) in combination with photometric detection of PEI by forming a copper complex was used to determine the amount of non complexed PEI. Therefore the polyplex solutions were formed in a volume of 2.5 mL at the stoichiometry of N/P 10 and centrifuged at 20 000 rpm for 2 h on a Beckmann Optima L-XP to remove the polyplexes. Afterwards the supernatant was collected. The concentration of PEI was determined by mixing of 100 μL supernatant and 100 μL copper acetate solution (20 mM) in a clear 96-well plate and determination of the absorbance at 285 nm of the copper–PEI complex.[45] The

concentration was determined from a calibration, which was recorded in the same way as the samples. Each measurement was repeated three times.

Cytotoxicity

For L929 cells (CCL-1, ATCC), the cytotoxicity assay was performed as described by ISO10993-5. In detail, cells were seeded at 10 000 cells per well in a 96-well plate and incubated for 24 h. No cells were seeded in the outer wells. Afterwards, polymers at the indicated concentrations were added, and the cells were incubated at 37 °C for further 24 h. Subsequently, the medium was replaced by D-PBS and AlamarBlue as recommended by the supplier. After incubation for 4 h, the fluorescence was measured at Ex 570/Em 610 nm, with untreated cells on the same well plate serving as controls.

Cellular uptake studies

For cellular uptake HEK-293 cells (CRL-1573, ATCC) were seeded at 10^5 cells per mL in a 12-well plate with 500 μL growth media (RPMI 1640 media, 10% fetal calf serum (FCS), 100 μg mL^{-1} streptomycin, 100 IU mL^{-1} penicillin, and 2 mM L-glutamine). The cells were cultured at 37 °C in a humidified 5% CO_2 atmosphere for 24 h. The media was changed by OptiMEM 1 h before polyplexes were added. Polyplexes containing siRNA were prepared at a final Cy3 labeled siRNA concentration of 15 μg mL^{-1} in HBG as described before. The labeling of pDNA was realized 1 h before polyplex formation. Therefore, 0.026 μL YOYO-1 (1 mM) per 1 μg pDNA were mixed in a small amount of pure water. Afterwards, HBG was added to a final concentration of 15 μg mL^{-1} pDNA Polymers were added at the indicated N/P ratio, and the polyplex solution was treated as described before and added to the cells. After 4 h of incubation, the cells were harvested and 10% trypan blue was added to quench the outer fluorescence of cells and identify only cells, taken up the genetic material. To determine the relative uptake of NPs, 10 000 cells were quantified by flow cytometry using a Cytomics FC 500 (Beckman Coulter).

Statistical analysis

Group data are reported as mean ± SD. To determine the significance of more than two groups of data, ANOVA was used.

Results and discussion

Cytotoxicity of the polymers used

As cationic polymers are known to cause toxic effects, the influence of the B-PEI molar mass on the cytotoxicity was investigated. The current ''gold standard'' for transfection of pDNA is 25 kDa PEI.[5] Here, the investigated polyplexes were formed with siRNA that is 250 times smaller compared to pDNA; therefore the use of PEIs with molar masses much lower than 25 kDa seemed to be adequate. The toxicity was tested in a worst case scenario, where only the polymers were used instead of the less toxic polyplexes. The polymers were incubated for 24 h and analyzed by AlamarBlue.[46] The relative viability of cells incubated with PEI compared to non-treated cells is shown in Fig. 1, where a strong correlation between

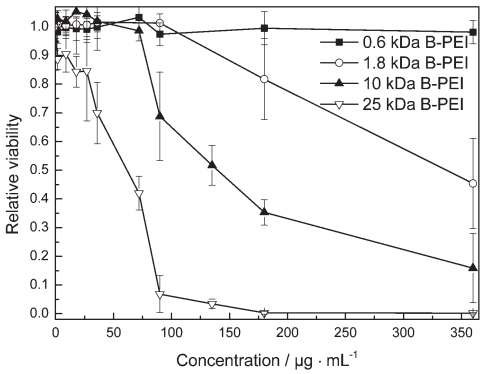

Fig. 1 Cytotoxicity of B-PEI with different molar masses at increasing concentration. The IC_{50} of 1.8, 10 and 25 kDa B-PEI was 335 μg ml^{-1}, 140 μg ml^{-1} and 62 μg ml^{-1}, respectively.

molar mass and toxicity can be seen. The IC_{50}-value (the concentration of polymer where only 50% of the cells are viable) distinctly decreases with higher molar mass, meaning a toxic effect at lower compound concentration. Furthermore, the smallest B-PEI (0.6 kDa) shows no significant toxicity up to 360 μg mL^{-1} (ANOVA). The investigated concentration range of PEI is adequate, keeping in mind that 360 μg mL^{-1} PEI corresponds to a N/P ratio above 200 (15 μg mL^{-1} siRNA) and all experiments were carried out below this ratio. It should be noted that all polymers investigated by us are not toxic (>80% viability) at N/P ratios up to 20. Polyplexes of B-PEI with molar masses higher than 25 kDa will not be investigated here, due to their high toxicity which makes them unsuitable for *in vitro* and *in vivo* studies.[47]

Potentiometric titration of branched PEI

One of the major postulated advantages of PEI as gene carrier is its high buffer capacity, which leads to osmotic swelling under the acidic conditions in the endosome and the release of the polyplexes into the cytosol.[48,49] Beside this, the degree of protonation can also have an impact on the stability and formation of the siRNA polyplexes. To study the influence of molar mass on the pK_a and the degree of protonation, titration curves of all four B-PEIs, at the same nitrogen (monomer unit) concentration, were measured by potentiometric titration. It must be mentioned that the titration behavior as well as the pK_a values strongly depend on the ionic strength and the polymer concentration itself, as reported first by Suh *et al.*[37] The data shown in Fig. 2 represents only apparent values, due to the fact that at lower pH value the protonated amines electrostatically suppress further protonation of neighboring amines. The corresponding apparent pK_a values were listed in Table 1. Values of $pK_a{}^b$ correspond mainly to protonation of secondary amines, whereas $pK_a{}^a$ is probably based on protonation of tertiary ones.[50] It was found that the titration behavior as well as the pK_a values of 10 and 25 kDa B-PEI do not differ significantly, whereas the protonation of 0.6 and 1.8 kDa B-PEIs differ (Fig. 2, Table 1). Both pK_a values decrease with increasing molar mass from 5.7 to 4.8 and 9.8 to 8.3, respectively, which is in good accordance with values reported by others for PEI polymers.[6,18] Even if there are small

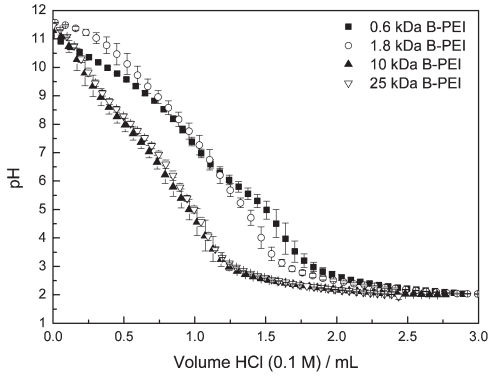

Fig. 2 Titration curves of 1 mg ml^{-1} B-PEI of indicated molar mass in water against HCl.

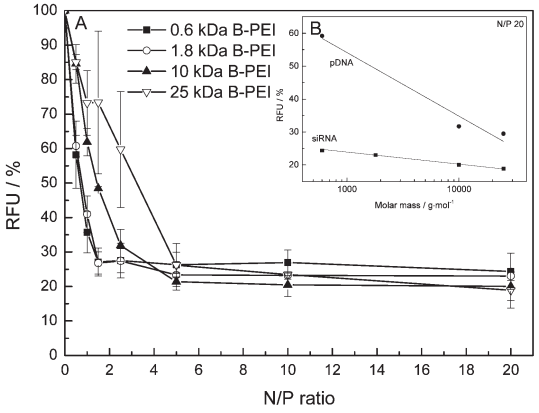

Fig. 3 Binding affinity of siRNA to B-PEI according to EBA (n = 3). A: different molar masses of B-PEI at different N/P ratios. B: binding affinity at N/P 20. The fluorescence of pure siRNA (N/P 0) is normalized to 100%.

differences in the pK_a values, this probably does not influence polyplex formation. One reason is that these values only represent apparent ionization data as mentioned above. In addition, the buffer capacity at pH 7.2, where the polyplexes were prepared, is very similar for all commercial B-PEIs as well as the ratio of primary, secondary, and tertiary amines as reported in the literature.[47] It is, however, not known which nitrogen atoms of the branched polymer are accessible for siRNA interaction during polyplex formation.

Polyplex formation and binding affinity

Polyplexes can be formed in different buffer solutions or non-buffered 150 mM NaCl. It was reported that the kind of buffer used has an influence on the polyplex characteristics, *e.g.* size.[51] Therefore, the polyplexes were always prepared in HBG (20 mM HEPES, 5% (w/v) glucose) to circumvent any influence due to changes of the solution conditions, like ionic strength or adsorption of ions. In contrast to saline buffers or physiological NaCl, the ionic strength is relatively low, which minimizes electrolysis during electrophoretic light scattering. The sugar content provides the physiological osmolarity for biological applications. A dependence of the results on the mixing protocol was not observed (data not shown).

To characterize the polyplex formation of siRNA and PEI, the ethidium bromide quenching assay (EBA) was used. The fluorescence intensity of ethidium bromide (EB) increases significantly when it intercalates into the double stranded siRNA.[52] After complexation of the siRNA with polymers like PEI, EB is excluded from the nucleic acid, which leads to a decrease of the fluorescence signal, as seen in Fig. 3. This displacement is probably caused by electrostatic and hydrophobic interactions of the polymer and the genetic material. Polyplex formation was observed for all B-PEIs, as indicated by RFU (eqn (1)) below 35%. At small N/P ratios (<2), 0.6 kDa and 1.8 kDa B-PEI show a higher affinity to siRNA compared to the 10 and 25 kDa analogues. Between N/P ratios of 2 and 5, no significant differences between data for different molar masses of B-PEI could be found. At N/P > 5, a constant fluorescence level is reached for all B-PEIs, indicating a complete complexation of the siRNA with the polymers. The fluorescence for higher molar mass B-PEI is slightly lower (Fig. 3B), indicating that the binding affinity increases with increasing molar mass of B-PEI. The dependency of binding affinity on the molar mass of B-PEI is stronger if pDNA was used as genetic material.

From these results, it can be concluded that a N/P ratio of 5 or higher is necessary for a complete complexation of the siRNA. The binding affinity of the polyplexes seems to increases with increasing molar mass of the polymer. A slightly decreased affinity of a 0.8 kDa B-PEI in comparison to the 25 kDa analogue was also reported in the literature;[24,25] this tendency was confirmed here over a wide range of molar masses.

Table 1 pK_a values determined by potentiometric titration against HCl

Polymer	pK_a [a]	pK_a [b]
0.6 kDa	5.7	9.8
1.8 kDa	5.3	9.5
10 kDa	4.9	8.2
25 kDa	4.8	8.3

[a] protonation of tertiary amines. [b] protonation of secondary amines.

Surface charge density-electrokinetic potential

As siRNA is negatively charged, it needs to be complexed by cationic polymers to be transported through the negatively charged cell membrane. The electrokinetic potential, also known as zeta potential, can serve as an indicator of the surface charge density of the complexes; it is one of the characteristics measured by electrophoretic light scattering and can be calculated from it by applying the Henry equation. We have used it for measuring the net-charge of the siRNA/B-PEI polyplexes at different N/P ratios. The results are shown in Fig. 4. At N/P ratios <1, no zeta potential could be measured as there was no detectable Doppler shift during the experiment. Binding between siRNA and B-PEI could, however, be detected even at low N/P ratios by EBA. This could indicate the formation of rather small polyplexes or the formation of a loosely bound network. All polyplexes at small N/P ratios (1 to

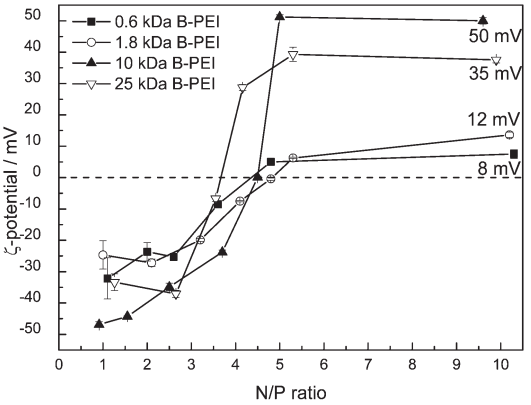

Fig. 4 Zeta potential of siRNA and B-PEI of different molar masses at different N/P ratios (n = 3).

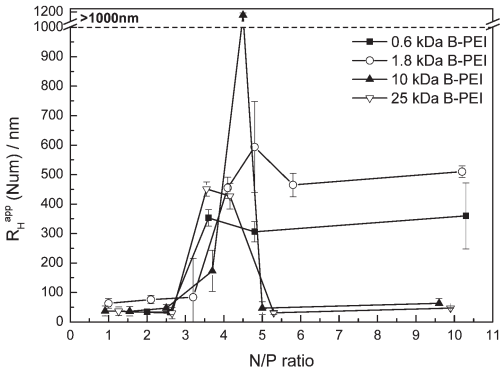

Fig. 5 Apparent hydrodynamic radius of the main population of polyplexes containing B-PEI of different molar masses at different N/P ratios, as obtained by CONTIN analysis. Radii larger than 1000 nm are presented as ''>1000'', due to the fact that the values determined are outside the reliable measuring range (n = 3).

3) show a negative zeta potential, ranging from −50 to −25 mV. At a N/P ratio of around 4, the zeta potential increases and shifts to positive values. At N/P 5, a nearly constant positive value of 35, 50, 12, and 5 mV for 25, 10, 1.8, and 0.6 kDa B-PEI polyplexes is reached, respectively. Obviously, a higher molar mass of the B-PEI leads to a higher zeta potential. A zeta potential of around 25 mV indicates stable polyplexes with positive charge density, whereas at 10 mV the complexes seem to be less stable. Higher values of the zeta potential are, however, difficult to interpret since the Helmholtz–Smoluchowski model is not valid any more.[40] Nevertheless, there is no further significant change in zeta potential at N/P > 5. These findings are in agreement with the binding affinities, where also a constant plateau is reached at those N/P ratios.

Investigation of polyplex size by DLS

It is well-known that the uptake of nanoparticles[53] as well as polyplexes[54] is influenced by their size. The internalization route resulting in successful gene expression therefore depends not only on the cell line but also on the PEI polyplex type.[55] Large polyplexes interact with the membrane, but the uptake is rather inefficient. Because of the importance of polyplex size for biological applications, the hydrodynamic radius of the polyplexes was analyzed in detail by DLS.

The hydrodynamic radii of polyplexes made of siRNA and the four different B-PEIs studied, at different N/P ratios, are presented in Fig. 5. For the calculations, the CONTIN algorithm was used. Radius measurements were unsuccessful for polyplexes at N/P ratios <1 due to a counting rate too small for application of the CONTIN algorithm, probably caused by the presence of very small polyplexes or of a loosely bound network only (see above). At N/P ratios from 1 to 3, hydrodynamic radii <100 nm were found: 30 to 50 nm for 0.6, 10, and 25 kDa B-PEI, and 60 up to 90 nm for 1.8 kDa B-PEI polyplexes, respectively. An increase in the B-PEI concentration and, thus, in the N/P ratio causes an increase in the hydrodynamic radius for all B-PEIs used. At N/P ratios of approximately 4 ± 0.5, maxima were observed: at 350 nm for 0.6 kDa, 600 nm for 1.8 kDa, >1000 nm for 10 kDa, and 450 nm for 25 kDa B-PEI polyplexes. At N/P ratios ⩾5, again a constant value was reached. For polyplexes of high molar mass B-PEIs (10 and 25 kDa), the hydrodynamic radius decreases to around 40 nm and 50 nm for 25 and 10 kDa B-PEI, respectively. The 0.6 and 1.8 kDa B-PEI formed larger polyplexes, with radii at around 350 nm and 500 nm, respectively. Taking all facts together, smaller polyplexes were formed using high molar mass B-PEI. As the uptake of large polyplexes into cells is less efficient, this could be one reason, why low molar mass B-PEI is less efficient for gene delivery.[56]

Fig. 6A–D shows, analogous to Fig. 5, the distributions of the hydrodynamic radii (linear number weighted) *versus* N/P. It should be noted that, according to Fig. 6, for all B-PEIs and investigated N/P ratios also some larger aggregates with high polydispersity are present besides the main polyplex population. For polyplexes of 0.6 kDa B-PEI, the amount of aggregates increases at higher N/P ratio (Fig. 6A). In addition, the radius of the aggregates increases from around 100 nm (N/P 2) to above 400 nm at N/P ratio 3. Polyplexes of 1.8 kDa B-PEI (Fig. 6B) show a similar behavior. For polyplexes of 10 kDa (Fig. 6C) and 25 kDa (Fig. 6D) B-PEI, the results are more complex. At N/P < 4, the behavior is comparable to that described above, which means that the amount of aggregates increases with increasing N/P ratio. At N/P 4 ± 0.5, only large aggregates (around 1000 nm for 10 kDa B-PEI, 400 nm for 25 kDa B-PEI) are present, whereas at N/P ratio of ⩾5 also polyplexes with small hydrodynamic radii (<50 nm) and only a low amount of aggregates with a radius of around 150 nm were observed. This confirms the previous results that N/P ⩾ 5 is necessary for complete complexation of the siRNA and the formation of compact nanocomplexes. In general, this is in accordance with literature, but it has to be kept in mind that often different buffers, concentrations and N/P ratios were investigated.[25]

Furthermore, the pure B-PEI polymers were also measured by DLS at concentrations between 5 to 20 mg mL^{-1}. For 25 and 10 kDa B-PEI a hydrodynamic radius of around 4 and 2 nm was found, respectively. For 1.8 and 0.6 kDa B-PEI no DLS measurements could be performed as the molar mass of the

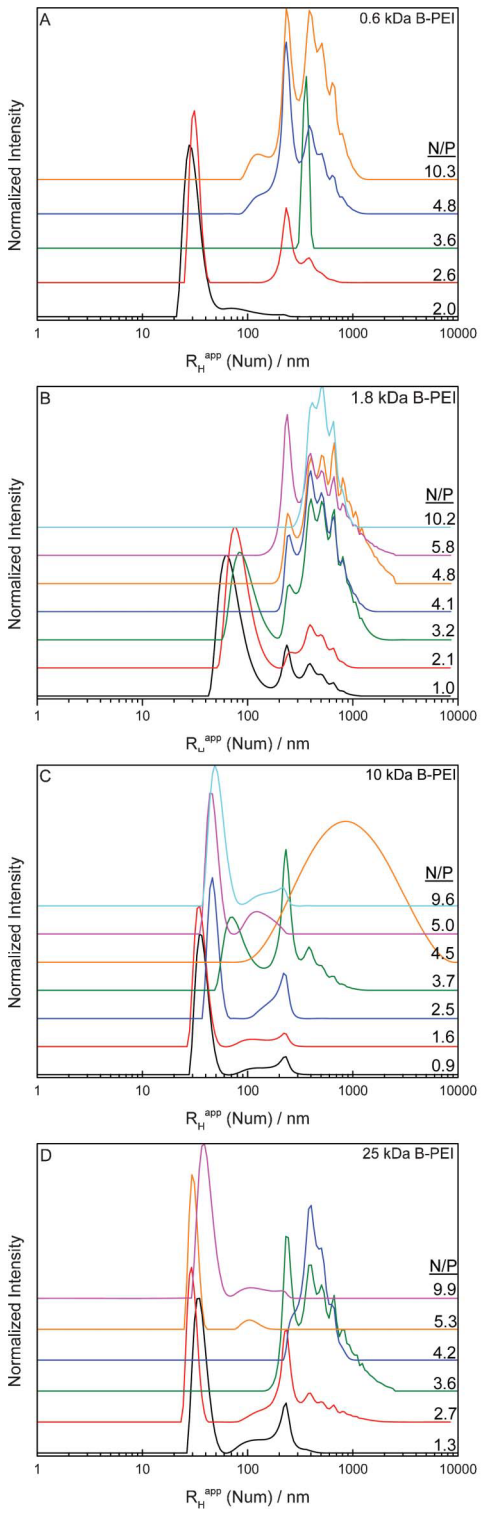

Fig. 6 Distribution of the hydrodynamic radii of siRNA/B-PEI polyplexes at different N/P ratios. The CONTIN algorithm was used for analyzing the ACF. The B-PEI molar masses were A) 0.6, B) 1.8, C) 10, and D) 25 kDa.

polymer, or to be more precisely, oligomer, is too low to yield any reliable data. At the concentrations, used for formation of polyplexes, no autocorrelation function could be obtained for all B-PEI samples. Therefore, an influence of the free PEI on the DLS results of the polyplex solutions can be excluded.

A comparison of zeta potential and hydrodynamic radii of the polyplexes reveals a good correlation. At N/P ratios <3, where the zeta potential is highly negative, small radii for polyplexes of all four tested B-PEIs were observed. Large aggregates occur for all B-PEI polyplexes at N/P ratio of 4 ± 0.5, where the zeta potential is around 0 mV. At higher N/P ratios, the radius decreases for polyplexes of higher molar mass B-PEI (10, 25 kDa), whereas the zeta potential reaches high positive values (>25 mV). In addition, polyplexes formed of low molar mass B-PEI (0.6, 1.8 kDa) showed only low positive zeta potentials (<15 mV) and a high tendency to form larger aggregates. From the results, it becomes clear that the electrostatic repulsion, indicated by the zeta potential, dominates the polyplex size and stability in solution. High repulsive interactions stabilize the polyplexes which results in small polyplexes with only low amounts of larger aggregates. In contrast, the presence of low or no repulsive interactions leads to fast aggregation and complexes with high hydrodynamic radius. Both, zeta potential and hydrodynamic radius also correlate with the relative fluorescence of the EBA, where a higher affinity for high molar mass B-PEI was found. To sum up, the binding affinity, the zeta potential as well as the hydrodynamic radius reaches a constant value at N/P ratio >5. With increasing molar mass of B-PEI, smaller, more positively charged polyplexes with a high binding affinity are formed. These are all arguments that the stability of the polyplexes increases with increasing molar mass of the used B-PEI. A schematic visualization of this situation can be seen in Scheme 1. It is assumed that with low molar mass B-PEI (left) a network-like polyplex is formed, where the polymer acts as a kind of linker. The result is a large, fast aggregating polyplex with only a low excess of positive charges, indicated by low zeta potential. In contrast, high molar mass B-PEI (right) forms smaller polyplexes, and the high excess of positive charges stabilizes the polyplexes electrostatically. Moreover, it becomes also clear that not all nitrogen atoms in the polymer are

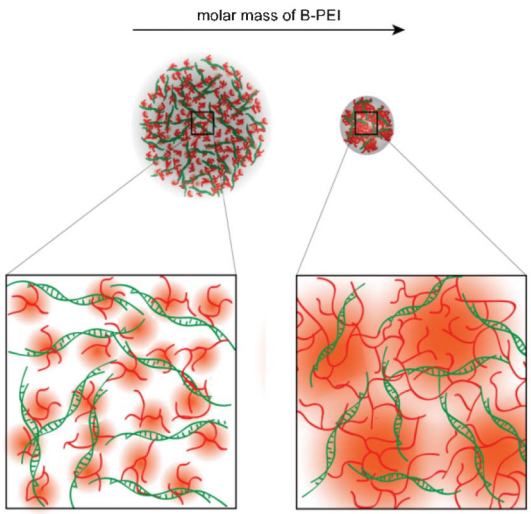

Scheme 1 Model of the polyplex formation by PEI of different molar masses.

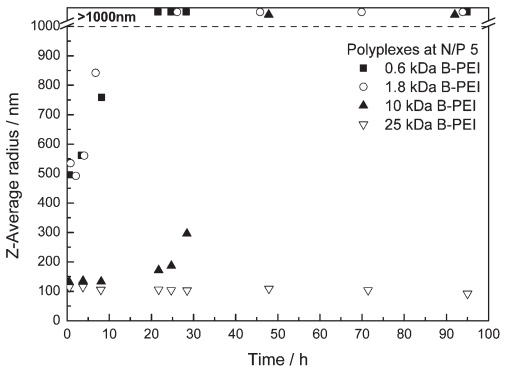

Fig. 7 Time dependency of the *z*-average radius, as obtained by cumulant analysis of polyplexes of siRNA and B-PEI of different molar masses at N/P 5. Radii larger than 1000 nm are presented as ''>1000'' in the upper part of the graphic, due to the fact that they are at the limit of the measurement range.

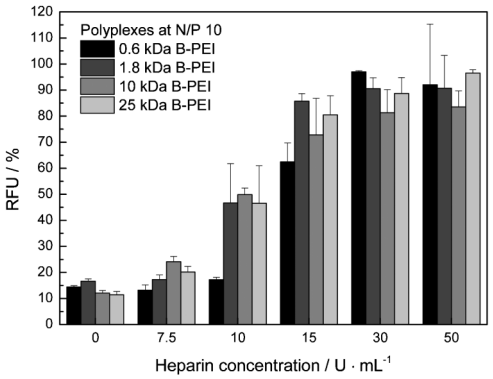

Fig. 8 Heparin-induced dissociation of polyplexes formed from siRNA and B-PEI of different molar masses, at N/P 10.

accessible to siRNA due to its rigidity in comparison with pDNA and the branched structure of PEI.[57] However, this first assumption should be investigated further in future.

Long-term stability of polyplexes

For the qualitative comparison of the polyplex solutions, the cumulant analysis and the z-average are powerful tools, since the whole system can be described by one single parameter which is sensitive to any changes occurring in the solution. The correct calculation of distributions of the hydrodynamic radius, as shown in Fig. 7, is more difficult. In this case, the analysis of the autocorrelation function (ACF) requires application of a multiple Γ algorithm (*e.g.* CONTIN). The cumulant analysis would reflect the distribution very inaccurately in this case, due to the strong influence of a relatively low amount of aggregates on the obtained *z*-average and PDI value.

In this study, the cumulant analysis of DLS measurements is used to record the long-term stability of the polyplexes (Fig. 7). It can be seen that the long-term stability of the polyplexes increases with increasing molar mass of the B-PEI used. The polyplexes of 0.6 and 1.8 kDa B-PEI, where already aggregates are present in the solutions, further aggregate within a few hours. Polyplexes of 10 kDa B-PEI are stable for approximately 24 h, whereas 25 kDa polyplexes are stable for more than 4 days. The time-dependent aggregation of the low molar mass B-PEI polyplexes can also be due to their low zeta potential, but this will not explain the aggregation of the 10 kDa B-PEI after one day, since its zeta potential is comparable to that of the 25 kDa B-PEI polyplexes. Even if the stability of all polyplexes is sufficient to carry out the physicochemical experiments, it is questionable, if the stability is high enough for transfections.

Polyplex dissociation (heparin assay)

A suitable polymer for gene delivery should form stable and small polyplexes but also release its genetic material inside the cell. To investigate the dissociation of the polyplex and the release of siRNA, the well-known heparin dissociation assay was applied.[24] Heparin is a sulfated glycosaminoglycan with high negative charge density that is widely used in medicine as anticoagulant. Due to its anionic character, heparin serves as competitor to siRNA and interacts with the cationic polymer.

With increasing amount of heparin, the polyplexes of siRNA and PEI dissolve. To measure the release of siRNA, again EB was used as described before. The polyplexes were prepared at N/P 10, because the polyplex is fully formed at this N/P ratio (compare EBA, zeta potential and size measurements). Fig. 8 clearly shows that it was possible to dissociate all polyplexes studied here. At heparin concentration of 30 U mL^{-1} nearly 100% of the siRNA present is free. The low molar mass PEI polyplex shows a higher stability against heparin at 10 U mL^{-1} than the other ones. This can be explained be a weaker affinity to anionic substances than the high molar mass ones. So, B-PEI with a weak binding to anionic substances like siRNA, as shown in the EB assay, should also show weaker binding to heparin. Furthermore, no significant difference between B-PEI of higher molar masses on the release of siRNA can be found.

Analytical and preparative ultracentrifugation experiments

AUC is a powerful technique for characterization of polymers, both biological and synthetic, and of nanoparticles. To the best of our knowledge, AUC has not been applied so far to investigate the solution behavior of siRNA-based polyplexes.

As it is known, that for DLS the intensity of scattered light scales with r^6, the amount of aggregates is overestimated in the intensity distribution. The calculation of number weighted distributions tries to correct this effect, but the obtained distributions cannot be interpreted quantitatively. Therefore, we apply analytical ultracentrifugation to proof whether the DLS results are precise.

At first, all polyplexes which were analyzed by DLS, were also investigated by AUC to compare both methods. The distribution of hydrodynamic radii of polyplexes formed with 10 kDa B-PEI at different N/P ratios is shown in Fig. 9. The results are in good agreement with those obtained by DLS (Fig. 6C). At N/P ratios below and above 4 ± 0.5, the polyplex radius is around 30 to 50 nm; some larger aggregates are also present. At N/P 3.7, the radius shifts to higher values of around 150 nm. At N/P 4.5, it was not possible to obtain any reliable sedimentation data. The reason for this is the formation of large aggregates and their extremely fast sedimentation, even

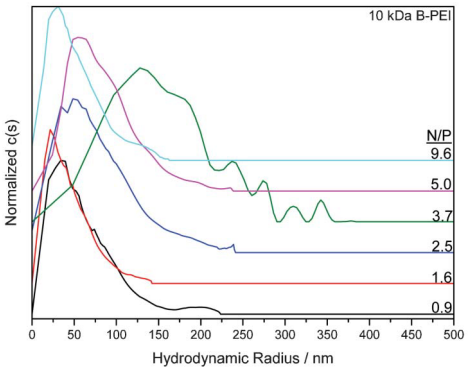

Fig. 9 Distribution of the hydrodynamic radii calculated from the distribution of sedimentation coefficents (eqn (4)) obtained by AUC of polyplexes of 10 kDa B-PEI and siRNA in HBG at 25 °C.

at a rotor speed of only 1000 rpm. This was also the case for other polyplex solutions and explains why the fraction of larger aggregates cannot be detected by AUC and why no reliable sedimentation data could be obtained for most N/P ratios of 0.6 and 1.8 kDa B-PEI polyplexes.

Typical sedimentation profiles of polyplexes formed of 10 kDa B-PEI at N/P 3.7, together with the corresponding residual plots, are shown in Fig. 10. The large contribution from noise is mainly due to the high sedimentation velocity of the particles. Consequently, the lowest possible rotor speed (1000 rpm) and a high radial step size (for each scan) of 0.1 mm had to be chosen to obtain sufficient data (note: in AUC resolution increases with speed[58]). With polyplex samples containing 10 and 25 kDa B PEI at N/P $>$ 5, after sedimentation of the polyplexes at 1000 rpm, the supernatants of the solution were centrifuged at 40 000 rpm. This revealed the presence of a second particle population. Its molar mass was calculated according to eqn (5) as 10.9 and 25.6 kDa for 10 kDa B-PEI and 25 kDa B-PEI polyplex solutions, respectively; it thus represents free B-PEI. Free siRNA could not be detected in the polyplex solution, which is in accordance with gel electrophoresis experiments in literature.[16]

As there are hints that free PEI is necessary for cellular uptake[26] the amount was quantified by preparative ultracentrifugation and photometrically determination of the copper chelate complex. In principle the amount of excess PEI can also be determined by AUC, but for the used N/P ratios and

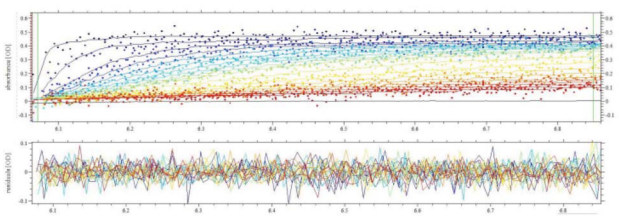

Fig. 10 Sedimentation velocity data of polyplexes of siRNA and 10 kDa B-PEI at N/P 3.7 in HBG at 25 °C. Rotor speed was 1000 rpm; scans were collected every minute. Top: Sedimentation profiles obtained by absorbance optics at 257 nm. Bottom: Corresponding plot of the residuals.

concentrations, the amount of PEI was too low to give accurate results. Nevertheless, quantification *via* the copper chelate method[45] shows that at N/P 10 around 85% of the PEI is free and not complexed. This corresponds to a virtual N/P ratio of around 1.3 for the polyplexes. Interestingly, this amount depends not on the molar mass of the used polymer. This correlates well to the small differences found in the EB assay and support the theory that only few amine groups of the polymer interact with the polymer whereas the other amines are responsible for the positive surface charge and interaction with other polyplexes.[59] Even if all polyplexes contain the same amount of positive charges, they have different zeta potentials (surface charge densities). This is probably due to their different radii and the different distribution of the charges in the polyplexes (Scheme 1). These results highlight the difference between complexation of siRNA and pDNA, where a value of 2.5 was described.[26] It is also known that polyplexes containing siRNA are slightly larger than pDNA polyplexes.[24,27] Both can be explained by a higher flexibility of pDNA compared to the stiff siRNA. While pDNA consists of more than thousand base pairs, siRNA has only 19 to 23 ($\sim$5 nm). With respect to the persistence length of RNA (the length where the chain behaves as a rigid rod) of $\sim$70 nm (260 bp),[57] it becomes obvious that short siRNA cannot condense and behaves as a rigid rod. Fitting of the frictional ratio f/f_{sph} from sedimentation velocity data ($f/f_{sph} \geqslant 2$, data not shown) also indicates a rod-like molecule. For this structure it is more difficult to become fully complexed. This can explain the already mentioned high N/P ratios required for complete complexation and lower virtual NP ratio of siRNA based polyplexes compared to pDNA ones and shows that not all insights gathered from pDNA can be adopted for siRNA.

Uptake study

The uptake behavior of the used B-PEIs of different molar masses was investigated using a Cy3 labeled siRNA. Therefore, the amount of internalized siRNA was detected with flow cytometry after 4 h, as this time is common for changing the transfection media to growth media during transfection procedure. Here, two N/P ratios were studied, in detail 1.3 and 10, what represent the virtual N/P and fully complexed siRNA (Fig. 3). For the virtual N/P ratio no significant uptake was achieved for B-PEI at all molar masses (Fig. 11). Besides, a significant uptake was detected using higher molar mass (10 and 25 kDa) B-PEI at N/P 10. This shows the potential of B-PEI $\geqslant$ 10 kDa and the necessity of an excess of polymer for cellular uptake of polyplexes. Taken the previous results into account, the inability of low molar mass PEI could be a consequence of increased polyplex sizes within 4 h, next to less stability indicated by lower zeta potentials, and lower pK_a values. Furthermore these results draw attention to the importance of size and zeta potential for efficient uptake, next to the potential of polymers to bind and release genetic material. To gain deeper insights into the mechanism of siRNA delivery in contrast to pDNA, the uptake of the latest was investigated using YOYO-1 labeled pDNA (Fig. 11). Again, higher molar masses at N/P 10 lead to a cellular uptake, but in comparison to siRNA, also B-PEI $\geqslant$ 10 kDa at N/P 1.3 showed internalization. This could be explained by the different molecular ratios

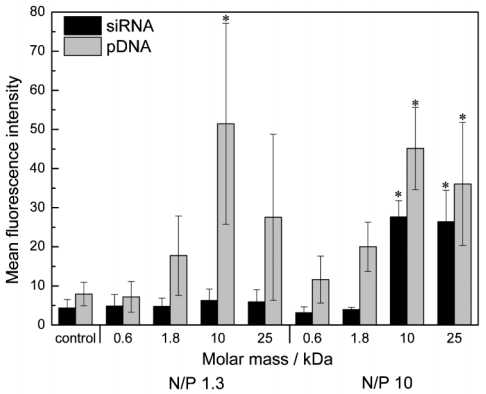

Fig. 11 Mean fluorescence intensity of HEK cells transfected with Cy3 labeled siRNA and YOYO-1 labeled pDNA after 4 h. Values represent mean ± S.D. $n \geqslant 3$; * indicate significant difference compared to control.

(polymer/nucleic acid). While around 54 molecules of 10 kDa B-PEI for one pDNA molecule represents N/P 1.3, this ratio is around 0.23 for siRNA (or 4.4 siRNA molecules per polymer) due to its 250 times shorter length. Obvious, the complexation of ~4 siRNA molecules by one B-PEI molecule is more difficult.

Additionally the question arises, how far the phosphates of a stiff molecule like siRNA (in contrast to pDNA) are accessible for branched PEI. Here, linear PEI with higher chain flexibility might be more effective. Since, this issue concerning the uptake and length/stiffness of the genetic material still remains to be unclear, it will be part of further investigations. However, using both genetic materials, the molar mass showed a strong impact onto cellular internalization, indicating a critical molar mass for efficient polyplex formation and therefore better cellular uptake.

Conclusions

In this study, the influence of the molar mass of B-PEI on the stability, formation, and uptake of siRNA-based polyplexes was investigated. We show that the stability of such polyplexes strongly depends on the molar mass of the used B-PEI. Taking the results from EBA, dynamic, and electrophoretic light scattering into account, it becomes clear that complete complexation of siRNA is reached at N/P > 5. No significant differences in the binding affinity and release of siRNA were observed using different molar masses of B-PEI. A high correlation between net charge (zeta potential) and hydrodynamic radius of the polyplexes was found. At high values of the zeta potential, regardless if negative or positive, small radii occur, whereas at low zeta potential we observe large aggregates. Small hydrodynamic radii and high values of zeta potential were observed at N/P < 3 for all molar masses of B-PEI and at N/P ⩾ 5 for 10 and 25 kDa B-PEI.

For the first time, we have successfully applied AUC for the characterization of siRNA polyplexes, suitable for polyplexes with radii smaller than 150 nm. Limitations occur due to the high sedimentation velocity of the polyplexes and the aggregates which requiring low rotor speeds and limited time for data collection only and, thus, leads to low resolution. To assess the problem of accurate size distributions of polyplex systems, containing different species, the establishment of asymmetric flow field-flow fractionation for such samples is currently under investigation.

Nevertheless, AUC represents a powerful technique for characterizing polyplexes in detail, in particular since also free PEI beside the polyplexes can be detected, which is not possible by DLS. By using PUC, a virtual N/P ratio of 1.3 was found. This decreased value compared to pDNA indicates differences of siRNA based polyplexes compared to pDNA based ones due to their shorter length and higher rigidity. Further differences, regarding the genetic material used, were found in cellular uptake. Whereas both, siRNA and pDNA, can be efficiently delivered into cells using B-PEI ⩾ 10 kDa at N/P 10, no siRNA uptake was detected at N/P 1.3. B-PEI with a molar mass higher 10 kDa seems to be the most promising candidates for siRNA-based polyplexes at N/P > 5, as the resultant polyplexes show a positive net charge, complete complexation of siRNA, a radius between 20 and 150 nm, necessary for internalization by endocytosis, and a significant cellular uptake.[60,61] Unfortunately, in terms of biological application these two polymers have higher toxicity than the low molar mass ones. Whereas most previous studies used 25 kDa PEI and a single low molar mass PEI (<1 kDa), our work shows the optimal molar mass is in between these values. *E.g.*, the 10 kDa B-PEI, which was not investigated for gene silencing before, is less toxic compared to the 25 kDa one and forms stable polyplexes with optimal net-charge and size for efficient cellular uptake. Furthermore, the influence of branching can be elucidated in future studies by investigation of linear, branched or star-shaped architectures of PEI. Moreover, statistical copolymers of PEI and poly(2-ethyl-2-oxazoline) might be interesting for gene delivery and polyplex formation, regarding reduced cytotoxicity.

Not all of the insights gathered for pDNA-based polyplexes can be adopted for siRNA, because of a 250 times lower molar mass, a higher rigidity and less flexibility. This study highlights the importance of a detailed analysis of polyplexes in the field of siRNA gene delivery as it not behaves identical as pDNA in all aspects.

Acknowledgements

This project was funded by the Carl-Zeiss Foundation (Strukturantrag JCSM). Furthermore, the authors would like to thank Dr Stephanie Schubert and Prof. Dr Dieter Schubert for helpful comments and Carolin Fritzsche for performing cytotoxicity assays.

Notes and references

1 A. Fire, S. Q. Xu, M. K. Montgomery, S. A. Kostas, S. E. Driver and C. C. Mello, *Nature*, 1998, **391**, 806–811.
2 M. A. Behlke, *Mol. Ther.*, 2006, **13**, 644–670.
3 J. J. Turner, S. W. Jones, S. A. Moschos, M. A. Lindsay and M. J. Gait, *Mol. BioSyst.*, 2007, **3**, 43–50.
4 D. M. Dykxhoorn, D. Palliser and J. Lieberman, *Gene Ther.*, 2006, **13**, 541–552.
5 O. Boussif, F. Lezoualch, M. A. Zanta, M. D. Mergny, D. Scherman, B. Demeneix and J. P. Behr, *Proc. Natl. Acad. Sci. U. S. A.*, 1995, **92**, 7297–7301.
6 S. Choosakoonkriang, B. A. Lobo, G. S. Koe, J. G. Koe and C. R. Middaugh, *J. Pharm. Sci.*, 2003, **92**, 1710–1722.
7 D. Störkle, S. Duschner, N. Heimann, M. Maskos and M. Schmidt, *Macromolecules*, 2007, **40**, 7998–8006.
8 W. J. Kim and S. W. Kim, *Pharm. Res.*, 2009, **26**, 657–666.
9 D. W. Pack, A. S. Hoffman, S. Pun and P. S. Stayton, *Nat. Rev. Drug Discovery*, 2005, **4**, 581–593.
10 J. B. Lee, J. Hong, D. K. Bonner, Z. Poon and P. T. Hammond, *Nat. Mater.*, 2012, **11**, 316–322.
11 K. A. Howard and J. Kjems, *Expert Opin. Biol. Ther.*, 2007, **7**, 1811–1822.
12 K. A. Howard, *Adv. Drug Delivery Rev.*, 2009, **61**, 710–720.
13 C. M. Varga, N. C. Tedford, M. Thomas, A. M. Klibanov, L. G. Griffith and D. A. Lauffenburger, *Gene Ther.*, 2005, **12**, 1023–1032.
14 F. Y. Xie, M. C. Woodle and P. Y. Lu, *Drug Discovery Today*, 2006, **11**, 67–73.
15 Y. Liu, O. Samsonova, B. Sproat, O. Merkel and T. Kissel, *J. Controlled Release*, 2011, **153**, 262–268.
16 S. R. Mao, M. Neu, O. Germershaus, O. Merkel, J. Sitterberg, U. Bakowsky and T. Kissel, *Bioconjugate Chem.*, 2006, **17**, 1209–1218.
17 M. S. Shim and Y. J. Kwon, *Biomacromolecules*, 2008, **9**, 1355–1355.
18 A. von Harpe, H. Petersen, Y. X. Li and T. Kissel, *J. Controlled Release*, 2000, **69**, 309–322.
19 Z. Dai and C. Wu, *Macromolecules*, 2012, 120508154954007.
20 B. Brissault, A. Kichler, C. Guis, C. Leborgne, O. Danos and H. Cheradame, *Bioconjugate Chem.*, 2003, **14**, 581–587.
21 M. Ogris, P. Steinlein, M. Kursa, K. Mechtler, R. Kircheis and E. Wagner, *Gene Ther.*, 1998, **5**, 1425–1433.
22 M.-E. Bonnet, P. Erbacher and A.-L. Bolcato-Bellemin, *Pharm. Res.*, 2008, **25**, 2972–2982.
23 J. Ziebarth and Y. M. Wang, *Biophys. J.*, 2009, **97**, 1971–1983.
24 A. Kwok and S. L. Hart, *Nanomed.: Nanotechnol., Biol. Med.*, 2011, **7**, 210–219.
25 A. C. Richards Grayson, A. M. Doody and D. Putnam, *Pharm. Res.*, 2006, **23**, 1868–1876.
26 S. Boeckle, K. von Gersdorff, S. van der Piepen, C. Culmsee, E. Wagner and M. Ogris, *J. Gene Med.*, 2004, **6**, 1102–1111.
27 D. J. Gary, N. Puri and Y.-Y. Won, *J. Controlled Release*, 2007, **121**, 64–73.
28 X. Mao, Z. Y. Ren, G. N. Parker, H. Sondermann, M. A. Pastorello, W. Wang, J. S. McMurray, B. Demeler, J. E. Darnell and X. M. Chen, *Mol. Cell*, 2005, **17**, 761–771.
29 P. Schuck, *Anal. Biochem.*, 2003, **320**, 104–124.
30 D. G. Myszka, R. W. Sweet, P. Hensley, M. Brigham-Burke, P. D. Kwong, W. A. Hendrickson, R. Wyatt, J. Sodroski and M. L. Doyle, *Proc. Natl. Acad. Sci. U. S. A.*, 2000, **97**, 9026–9031.
31 G. M. Pavlov, A. M. Breul, M. D. Hager and U. S. Schubert, *Macromol. Chem. Phys.*, 2012, **213**, 904–916.
32 B. Schulze, C. Friebe, S. Hoeppener, G. M. Pavlov, A. Winter, M. D. Hager and U. S. Schubert, *Macromol. Rapid Commun.*, 2012, **33**, 597–602.
33 I. Perevyazko, A. Vollrath, S. Hornig, G. M. Pavlov and U. S. Schubert, *J. Polym. Sci., Part A: Polym. Chem.*, 2010, **48**, 3924–3931.
34 S. Sundaram, L. K. Lee and C. M. Roth, *Nucleic Acids Res.*, 2007, **35**, 4396–4408.
35 E. Wagner, M. Cotten, R. Foisner and M. L. Birnstiel, *Proc. Natl. Acad. Sci. U. S. A.*, 1991, **88**, 4255–4259.
36 C. V. Synatschke, A. Schallon, V. Jerome, R. Freitag and A. H. E. Müller, *Biomacromolecules*, 2011, **12**, 4247–4255.
37 J. Suh, H. J. Paik and B. K. Hwang, *Bioorg. Chem.*, 1994, **22**, 318–327.
38 M. X. Tang and F. C. Szoka, *Gene Ther.*, 1997, **4**, 823–832.
39 S. W. Provencher, *Comput. Phys. Commun.*, 1982, **27**, 229–242.
40 A. V. Delgado, F. Gonzalez-Caballero, R. J. Hunter, L. K. Koopal and J. Lyklema, *J. Colloid Interface Sci.*, 2007, **309**, 194–224.
41 P. Schuck, *Biophys. J.*, 2000, **78**, 1606–1619.
42 W. Mächtle, *Makromol. Chem.*, 1984, **185**, 1025–1039.
43 G. F. Bonifacio, T. Brown, G. L. Conn and A. N. Lane, *Biophys. J.*, 1997, **73**, 1532–1538.
44 G. M. Pavlov, I. Y. Perevyazko, O. V. Okatova and U. S. Schubert, *Methods*, 2011, **54**, 124–135.
45 F. Ungaro, G. De Rosa, A. Miro and F. Quaglia, *J. Pharm. Biomed. Anal.*, 2003, **31**, 143–149.
46 R. Hamid, Y. Rotshteyn, L. Rabadi, R. Parikh and P. Bullock, *Toxicol. in Vitro*, 2004, **18**, 703–710.
47 D. Fischer, T. Bieber, Y. X. Li, H. P. Elsasser and T. Kissel, *Pharm. Res.*, 1999, **16**, 1273–1279.
48 T. Merdan, K. Kunath, D. Fischer, J. Kopecek and T. Kissel, *Pharm. Res.*, 2002, **19**, 140–146.
49 A. Akinc, M. Thomas, A. M. Klibanov and R. Langer, *J. Gene Med.*, 2005, **7**, 657–663.
50 M. Borkovec and G. J. M. Koper, *Macromolecules*, 1997, **30**, 2151–2158.
51 E. V. B. van Gaal, G. Spierenburg, W. E. Hennink, D. J. A. Crommelin and E. Mastrobattista, *J. Controlled Release*, 2010, **141**, 328–338.
52 M. J. Waring, *J. Mol. Biol.*, 1965, **13**, 269–282.
53 W. Jiang, B. Y. S. Kim, J. T. Rutka and W. C. W. Chan, *Nat. Nanotechnol.*, 2008, **3**, 145–150.
54 J. Rejman, M. Conese and D. Hoekstra, *J. Liposome Res.*, 2006, **16**, 237–247.
55 K. von Gersdorff, N. N. Sanders, R. Vandenbroucke, S. C. De Smedt, E. Wagner and M. Ogris, *Mol. Ther.*, 2006, **14**, 745–753.
56 O. M. Merkel, D. Librizzi, A. Pfestroff, T. Schurrat, K. Buyens, N. N. Sanders, S. C. De Smedt, M. Béhé and T. Kissel, *J. Controlled Release*, 2009, **138**, 148–159.
57 P. Kebbekus, D. E. Draper and P. Hagerman, *Biochemistry*, 1995, **34**, 4354–4357.
58 K. L. Planken and H. Cölfen, *Nanoscale*, 2010, **2**, 1849–1869.

59 A. Schallon, C. V. Synatschke, D. V. Pergushov, V. Jerome, A. H. E. Müller and R. Freitag, *Langmuir*, 2011, **27**, 12042–12051.
60 H. Aoki, M. Satoh, K. Mitsuzuka, A. Ito, S. Saito, T. Funato, M. Endoh, T. Takahashi and Y. Arai, *FEBS Lett.*, 2004, **567**, 203–208.
61 H. Gao, W. Shi and L. B. Freund, *Proc. Natl. Acad. Sci. U. S. A.*, 2005, **102**, 9469–9474.

Publication P3

A cationic poly(2-oxazonline) with high *in vitro* transfection efficiency identified by a library approach

A. C. Rinkenauer, L. Tauhardt, F. Wendler, K. Kempe, M. Gottschaldt, A. Traeger, U. S. Schubert

Macromol. Biosci. **2015**, *15*, 414-425.

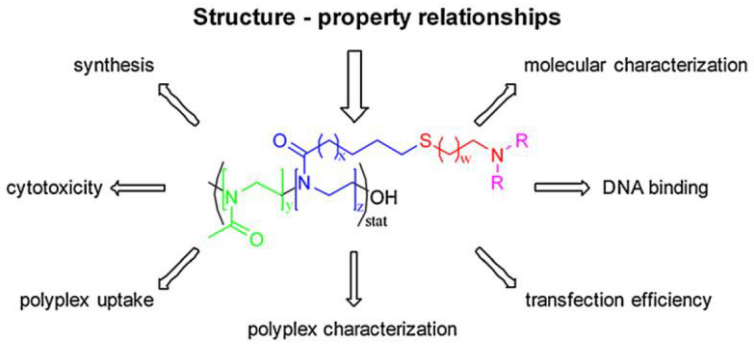

A Cationic Poly(2-oxazoline) with High In Vitro Transfection Efficiency Identified by a Library Approach[a]

Alexandra C. Rinkenauer, Lutz Tauhardt, Felix Wendler, Kristian Kempe, Michael Gottschaldt, Anja Traeger,* Ulrich S. Schubert*

To date, cationic polymers with high transfection efficiencies (TE) often have a high cytotoxicity. By screening an 18-membered library of cationic 2-oxazoline-based polymers, a polymer with similar TE as linear poly(ethylene imine) but no detectable cytotoxicity at the investigated concentrations could be identified. The influence of the polymer side chain hydrophobicity and the type and content of amino groups on the pDNA condensation, the TE, the cytotoxicity, the cellular membrane interaction as well as the size, charge, and stability of the polyplexes was studied. Primary amines and an amine content of at least 40% were required for an efficient TE. While polymers with short side chains were non-toxic up to an amine content of 40%, long hydrophobic side chains induced a high cytotoxicity.

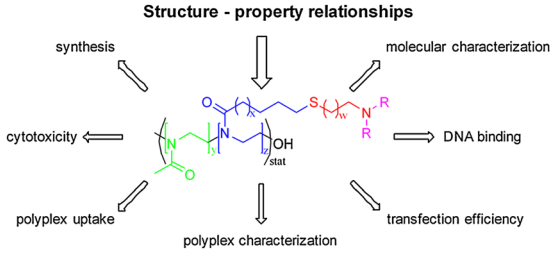

1. Introduction

Nanomaterials and their applications are of great interest for scientists of different disciplines such as biology, pharmacy, chemistry, biotechnology, physics, and medicine.[1] Within the field of nanomedicine, non-viral gene delivery has a high potential for the treatment of a large variety of diseases.[2,3] Although many problems have been solved during the last three decades, the ideal delivery agent, i.e., vector, still has to be found.[4] To design successful non-viral vectors for genetic materials, several bottlenecks have to be overcome.[5,6]

Non-viral vectors, in particular synthetic polymers, offer the advantage of being tailor-made systems, which can be produced in large scale and stored without further complications. Due to their good interaction with negatively charged genetic material such as plasmid DNA (pDNA) or small interfering RNA (siRNA), cationic polymers play an important role within the field of gene delivery.[1,7–12] Prominent examples of this polymer class are poly(ethylene imine) (PEI),[13–16] poly(L-lysine) (PLL),[17] and poly(methacrylate)s (e.g., PDMAEMA)[18–20] in which PEI represent the "gold standard" for in vitro transfections. Previous studies on structure–property relationships revealed the influence of molar mass, pK_a value, polymer end groups, side chain substitution, and polyplex size on the transfection efficiency (TE).[21–23] However, comprehensive structure–property relationships are rare[24] and the results of the different studies often cannot be transferred to other polymer classes leading to the necessity to perform detailed analyses for every material.

A. C. Rinkenauer,[†] L. Tauhardt,[†] F. Wendler, K. Kempe,[[+]] M. Gottschaldt, A. Traeger, U. S. Schubert
Laboratory of Organic and Macromolecular Chemistry (IOMC), Friedrich Schiller University Jena, Humboldtstrasse 10, 07743 Jena, Germany
Jena Center for Soft Matter (JCSM), Friedrich Schiller University Jena, Philosophenweg 7, 07743 Jena, Germany
E-mail: anja.traeger@uni-jena.de; ulrich.schubert@uni-jena.de
U. S. Schubert
Dutch Polymer Institute (DPI), John F. Kennedylaan 2, 5612 AB Eindhoven, The Netherlands
[[+]]Current address: Department of Chemical and Biomolecular Engineering, The University of Melbourne, Victoria 3010, Australia.
[†]These authors contributed equally to this work.

[a]**Supporting Information** is available from the Wiley Online Library or from the author.

DOI: 10.1002/mabi.201400334

The main requirement for transfection agents is an efficient delivery, combined with a low cytotoxicity. However, most cationic polymers are either efficient in delivering the genetic material but cytotoxic or they are non-toxic and fail in their delivery potential.[25,26] An often used method to overcome this drawback is the functionalization with non-toxic and biocompatible compounds such as carbohydrates or non-ionic polymers, e.g., poly(ethylene glycol) (PEG) and poly(2-oxazoline)s (POx).[27–35] Due to the so called ''stealth effect'', the polymers reduce the nonspecific interactions with blood components, e.g., by shielding of positive charges. Moreover, a prolonged blood circulation time leading to an enhanced permeability and retention (EPR) effect as well as a reduced cytotoxicity can be observed and the water solubility is increased.[31] POx, in particular poly(2-ethyl-2-oxazoline) (PEtOx) and poly(2-methyl-2-oxazoline) (PMeOx), have been intensively investigated as PEG alternative.[36–46] Compared to PEG, the synthesis of POx by a living cationic ring-opening polymerization (CROP) is rather undemanding, but also leads to well-defined polymers.[47–50] The preparation of cationic PEtOx copolymers with primary amine units,[51] and their usage in DNA binding hydrogels has been reported earlier.[52] However, the 2-(4-aminobutyl)-2-oxazoline/EtOx copolymers showed no TE (unpublished data). In addition, it was reported that partially hydrolyzed POxs, i.e., P(Ox-*stat*-EI), show less cytotoxicity but also less TE with increasing POx concentrations.[32,34] Further studies described a correlation between the polyplex stability and the amount of positive charges. Often, a decrease of the positive charge goes along with a reduction of the polyplex stability and, hence, leads to an inefficient cellular uptake and endosomal release. Moreover, the functionalization with PEG or hydrophilic POx (e.g., PMeOx, PEtOx) can result in an inefficient delivery, due to a reduced interaction with the genetic material and the cellular membranes caused by the cell- and protein-repellent character of the polymers, the so called PEG dilemma.[53–58] To solve this problem, additional polymer features have to be considered. Besides modifying polycations with ''stealth'' polymers,[31,37] the introduction of more neutral or hydrophobic characteristics have been discussed for gene delivery applications.[59,60] It is known from the development of antimicrobial POx that the introduction of long alkyl spacers leads to an enhanced membrane interaction.[61] Hence, it is assumed that the cellular uptake of modified cationic polymers, which is often reduced due to the ''stealth effect'', can be improved by introducing hydrophobic moieties.

In this study, the influence of hydrophobicity, type of amine, and amine content of 2-oxazoline-based polymers on the transfection behavior was systematically investigated. In detail, copolymers of alkene containing 2-oxazolines, namely 2-(9-decenyl)-2-oxazoline (DecEnOx) or 2-(3-butenyl)-2-oxazoline (ButEnOx), and 2-methyl-2-oxazoline (MeOx) were synthesized and further functionalized by thiol-ene photoaddition.[62–66] MeOx was chosen as comonomer to improve the water-solubility, which is limited for P(EtOx-*co*-ButEnOx) and P(EtOx-*co*-DecEnOx) due to the LCST behavior of PEtOx.[67] These copolymers were further systematically investigated with regard to: i) their ability to interact with pDNA and the cellular membrane, ii) their cellular uptake, iii) cytotoxicity, and iv) the TE.

2. Experimental Section

See Supporting Information.

3. Results and Discussion

3.1. Synthesis of a Cationic Poly(2-oxazoline) Library

To investigate the influence of the type of amine (primary or tertiary), the amine content, and the side chain hydrophobicity, a library of 18 new cationic POx copolymers has been synthesized (Scheme 1). Starting from MeOx and ButEnOx as well as DecEnOx, a series of copolymers containing up to 50 mol% of the double bond bearing comonomer has been prepared. In a straightforward approach, these double bonds have been functionalized with different amines (primary or tertiary) using the thiol-ene photoaddition procedure. For clarity, the final products have been labeled according to the following pattern: **s**, for all copolymers based on a ''short'' side chain of ButEnOx; **l**, for all polymers based on a ''long'' side chain of DecEnOx; the amine content is given as number in mol%; **p** or **t**, characterize the type of amine, namely primary (**p**) or tertiary amine (**t**) (Scheme 1). If not stated otherwise, there is a C_2H_4 spacer between the sulfur and the final amine group. In case of a hexamethylene spacer the term **h** is added to the compound abbreviation.

3.2. Synthesis of P(MeOx-*co*-ButEnOx) and P(MeOx-*co*-DecEnOx)

In order to synthesize well defined P(MeOx-*co*-ButEnOx), a kinetic study was performed for this copolymer system. The linearity of the first-order kinetic plots shows the living character of the copolymerization (Figure S1, Supporting Information). Having a higher polymerization rate, MeOx ($k_p = 0.097\,L\,mol^{-1}\,s^{-1}$) is incorporated faster into the polymer chain than ButEnOx ($k_p = 0.052\,L\,mol^{-1}\,s^{-1}$) indicative for the formation of a gradient copolymer. Characterization by size exclusion chromatography (SEC) showed an increasing molar mass with increasing conversion (Table S1, Supporting Information). Similar results

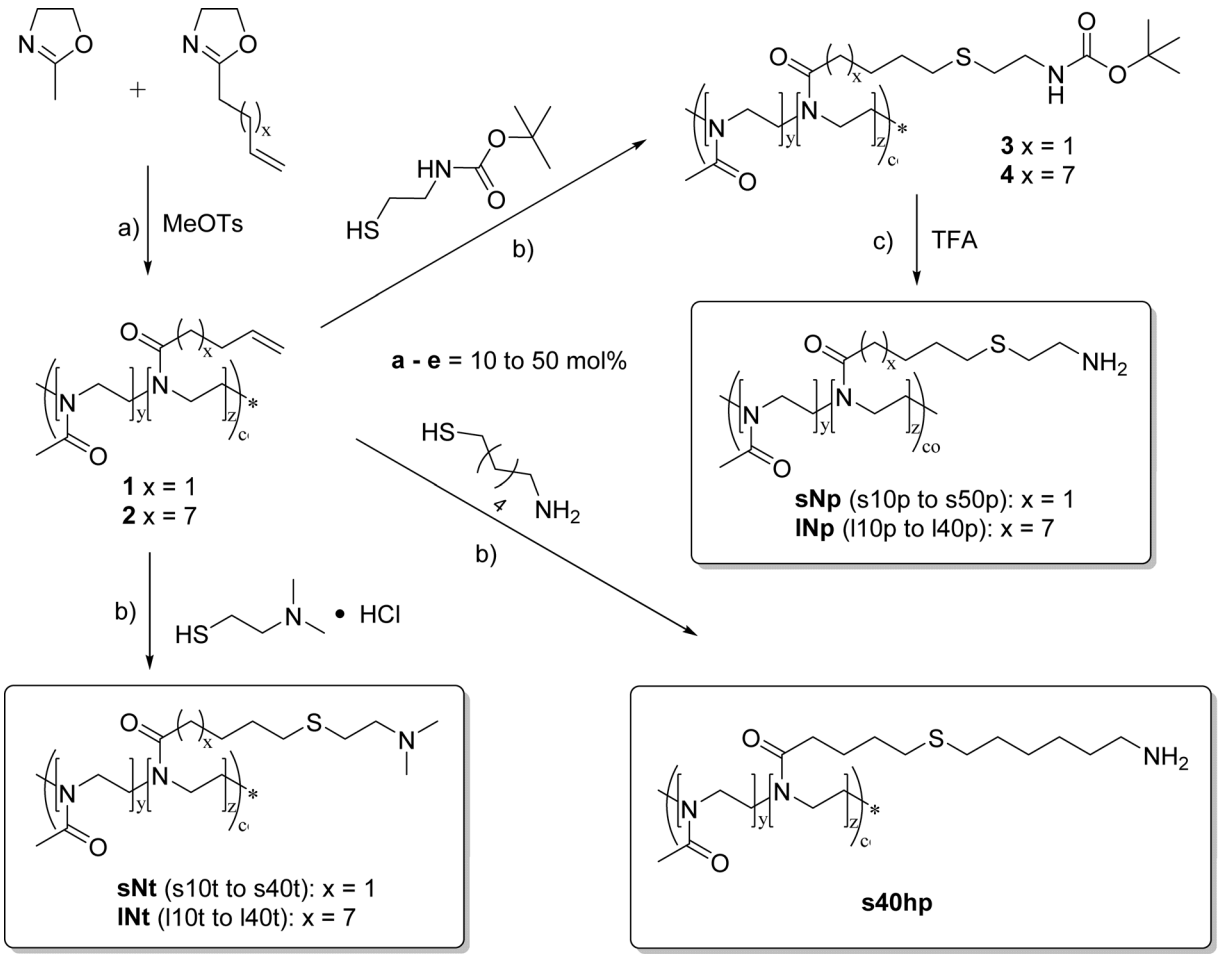

Scheme 1. Schematic representation of the synthesis of cationic poly(2-oxazoline)s. Reaction conditions: a) 140 °C, microwave reactor, acetonitrile, b) room temperature, overnight, methanol, catalyst: 0.1 mol% 2,2-dimethoxy-2-phenylacetophenone with respect to contained double bonds, c) room temperature, overnight, dichloromethane/trifluoroacetic acid. Product terms: **s** = short butyl side chain, **l** = long decenyl side chain, N = amine content in mol%, **h** = hexamethylene spacer, **p** = primary amine, **t** = tertiary amine.

were obtained for P(MeOx-*co*-DecEnOx), as reported elsewhere.[68]

To achieve a sufficient binding with the genetic material and a low cytotoxicity, an overall degree of polymerization (DP) of 200 was chosen. Copolymers with a ButEnOx/DecEnOx content of 10, 20, 30, and 40 mol%, respectively, have been prepared. Full conversion of the monomers was proven by ^{1}H NMR investigations. Copolymers with dispersity ($Đ_M$) values between 1.43 and 1.63 (Table S2, Supporting Information) were obtained. The rather high $Đ_M$ values for a living cationic polymerization can be attributed to two aspects: i) The different hydrodynamic volumes and column interactions of the polymers compared to the used poly(styrene) standard and ii) the occurrence of chain-transfer,[69,70] commonly observed for PMeOx systems with DP values higher than 100.[50] Due to the monomodality of the obtained SEC curves (exemplarily shown for the P(MeOx-*co*-ButEnOx) copolymer in Figure S2, Supporting Information), it is assumed that no chain coupling or "long chain branching"[70] reactions occurred, since those would lead to a shoulder at lower elution volumes, i.e., higher molar masses. Instead tailing of the SEC curves is observed, indicating the existence of low molar mass polymer chains, originating from chain-transfer and termination reactions. The extent of chain transfer reactions might have been reduced using EtOx as comonomer (more controlled reaction up to a DP of 200). However, to avoid low critical solution temperature (LCST) behavior known of PEtOx-containing copolymers, MeOx was chosen as comonomer.[62,67,71]

The ^{1}H NMR spectra showed that both monomers are incorporated (Figure 1, Figure S3, Supporting Information). In each case, two signals for the double bonds are visible around 5.86 and 5.00 ppm. The polymer backbone signal is found around 3.52 ppm. The signals of the side chain

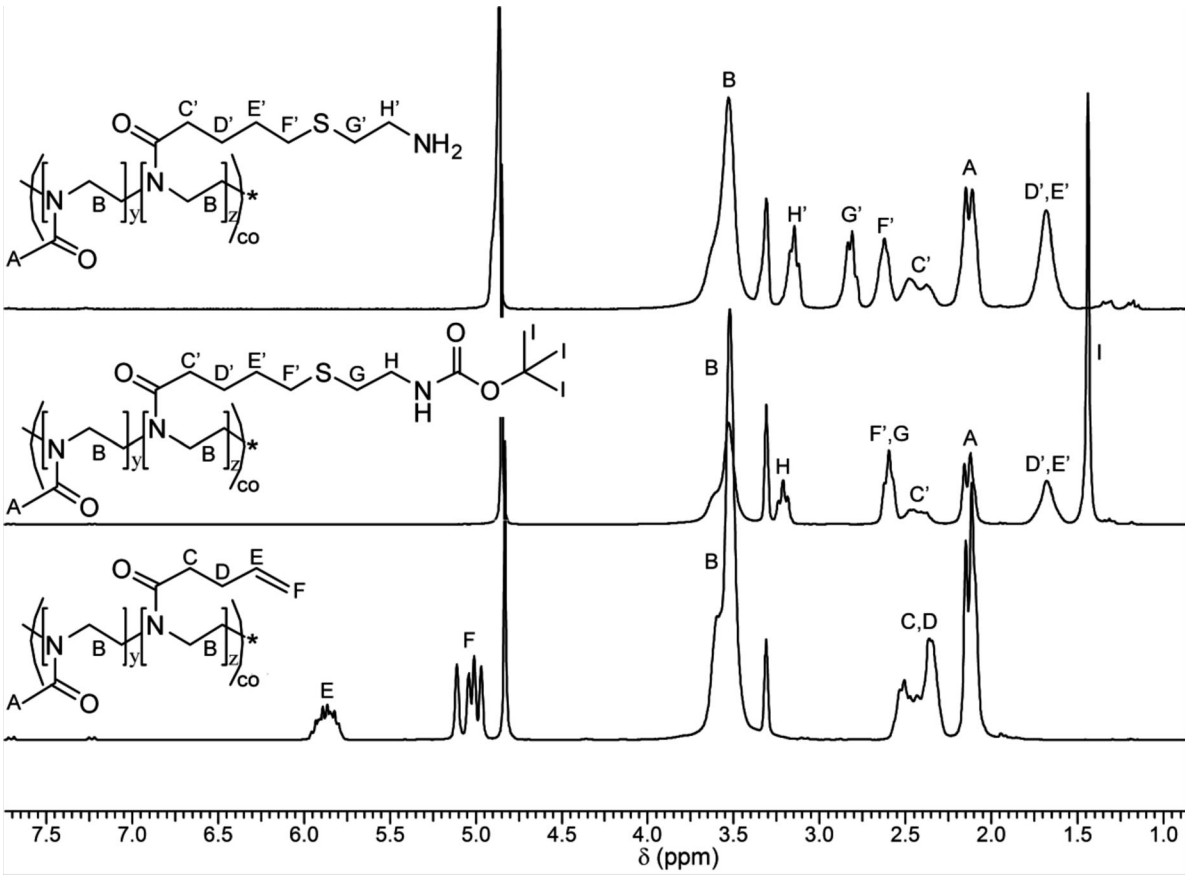

Figure 1. ^{1}H NMR spectra of **1d** (bottom), **3d** (middle), **s40p** (top) (250 MHz, solvent: CD_3OD).

protons occur between 1.00 and 2.60 ppm. By correlating the proton signal of the double bond at 5.86 ppm with the backbone signal, the monomer ratios within the polymer could be calculated. They were found to be in agreement with the ratios aimed for.

In general two different end groups are possible, namely a hydroxyl or an ester end group.[72] Unfortunately, the end group analysis, e.g., by ESI- or MALDI-TOF-MS, is not possible due to the high DP. However, at this high molar mass the influence of the end group should be only marginal or even negligible.

3.3. Thiol-ene Functionalization of P(MeOx-*co*-ButEnOx) and P(MeOx-*co*-DecEnOx) with Different Amines

To obtain a cationic character, required for DNA-binding, primary and tertiary amino groups were introduced into the copolymers by thiol-ene photoaddition reaction (Scheme 1). The primary amines were obtained by reaction of the copolymers with 2-(boc-amino)ethanethiol under UV irradiation ($\lambda = 365$ nm) and subsequent deprotection with trifluoroacetic acid. Characterization by ^{1}H NMR spectrometry showed that for both copolymer types (**3** and **4**) the double bond signals of the starting materials at 5.86 and 5.00 ppm disappeared after the photoaddition, indicating the complete functionalization with the thiol (Figure 1, Figure S3, Supporting Information). Moreover, a singlet of the boc protecting group at 1.44 ppm was obtained. For both **3** and **4**, the signals of the CH_2 next to the boc protected nitrogen can be found around 3.21 ppm. The protons signals at 2.60 ppm can be assigned to the CH_2 groups adjacent to the sulfur atom. After treatment with TFA and precipitation into ice-cold diethyl ether, the singlet of the boc protecting group disappeared, indicating the successful deprotection. SEC characterization of the MeOx/ButEnOx systems revealed a growing molar mass (lower elution volume) after the photoaddition of 2-(boc-amino)ethanethiol (Figure 2, Table S2, Supporting Information). After deprotection, the molar mass decreases further. For the MeOx/DecEnOx systems, SEC measurements were performed for the starting materials **2** and the final products **lNp**. A growing molar mass of the end products **lNp** compared to the starting materials **2** was observed. This is in accordance with the MeOx/ButEnOx systems. In all cases the $Đ_M$ values changed only slightly.

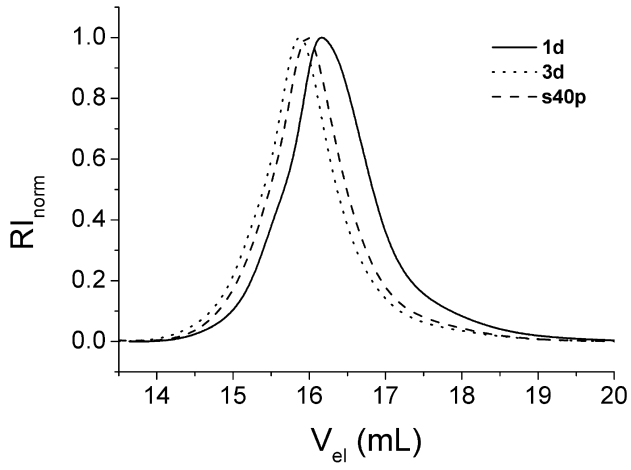

Figure 2. SEC curves of the copolymers **1d** (straight), **3d** (dotted), and **s40p** (dashed) (eluent: DMAc + 0.21% LiCl; calibration: PS).

In addition, copolymers with a tertiary amino group were prepared from **1** and **2** by UV-initiated thiol-ene reaction with dimethylaminoethanethiol hydrochloride. The ^{1}H NMR spectra of **sNt** and **lNt** showed a broad peak around 2.92 ppm belonging to the two CH_3 groups of the amino thiol (Figure S3, Supporting Information). The double bond signals of the starting materials disappeared, indicating a complete conversion. Although in theory the molar mass should increase after thiol-addition, analysis by SEC revealed lower molar masses of the cationic **sNt** polymers compared to the neutral starting material (Table S2, Supporting Information). Depending on the particular compound, the **lNt** polymers showed both increasing and decreasing molar masses. This is ascribed to the different hydrodynamic volumes of the cationic polymers in DMAc, but also to the different column interactions compared to the neutral PS standards used for calibration. It also explains the large variation in the molar masses and $Đ_M$ values, e.g., of **s40p** ($\overline{M}_n$ = 29,100 g mol^{-1}, $Đ_M$ = 1.52) and **s40t** ($\overline{M}_n$ = 20,180, $Đ_M$ = 1.35), which are both synthesized from the same starting material and only differ by the type of amine.

3.4. Binding of Genetic Material

An essential requirement for non-viral vectors is their interaction with negatively charged nucleic acids, resulting in the formation of interelectrolyte complexes, also known as polyplexes. The resulting pDNA condensation caused by the interaction with the polymers was analyzed using the ethidium bromide quenching assay (EBA). Due to electrostatic and hydrophobic interactions between polymer and pDNA, ethidium bromide (EB) is excluded from a preformed pDNA/EB complex and the decrease in the EB fluorescence intensity can be detected. All 16 polymers (**sNp**, **sNt**, **lNp**, and **lNt**) led to a decrease in the fluorescence intensity of EB and, thus, showed interaction with the pDNA (Figure S6, Supporting Information). As positive control, linear PEI (lPEI) with a DP of 200 was used, decreasing the fluorescence intensity to 44.9 ± 3.1% (Figure S7, Supporting Information). Higher relative fluorescence intensities of 65–80% were observed for the **sNp** polymers without significant differences concerning their amine content.

For the investigated copolymers, three tendencies can be observed: i) In the case of the polymers with long side chains, primary amines bind better than tertiary, ii) the amine content correlates with the pDNA condensation, and iii) the pDNA condensation increases with the side chain length (Figure 3A,B). The latter can be probably ascribed to stronger hydrophobic interaction with the pDNA, caused by the higher number of CH_2 groups in the side chains.[49]

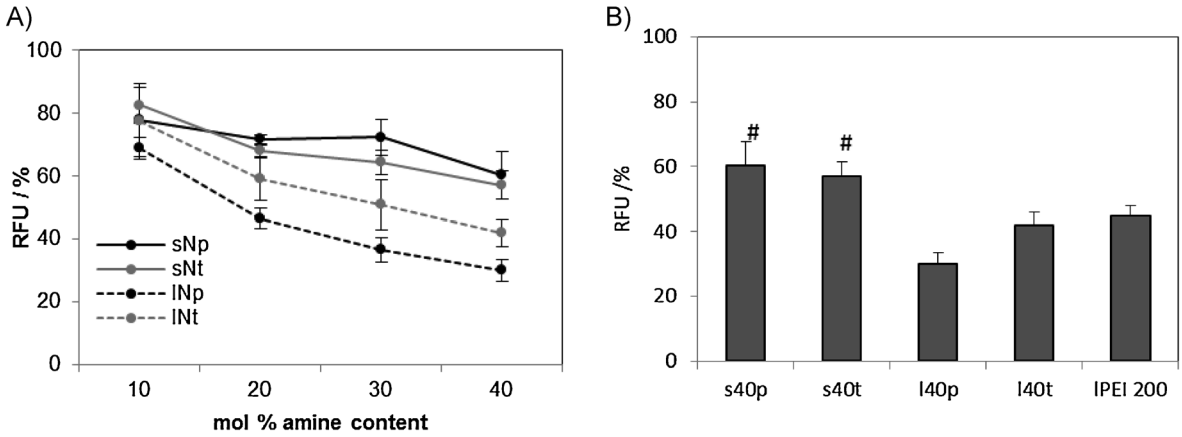

Figure 3. Ethidium bromide quenching assay of all 16 polymers with pDNA measured at physiological pH. A) Comparison at N/P ratio 40. B) Comparison of 40 mol% amine content (N/P 40) polymers. Values represent the mean ± SD (n = 3); #represents a significant difference ($p < 0.05$) to **l40p**.

However, based on the obtained data it is evident that the influence of the type of alky side chain (long vs. short) is more pronounced. In detail, up to 30% difference in the relative fluorescence intensity of **s40p** and **l40p** compared to 10% of **l40p** and **l40t** were found (Figure 3B). This observation emphasizes the importance of understanding the physicochemical interactions between the polymer and the genetic material, and not only the influence of electrostatic interactions for the polyplex formation mainly discussed in literature.[73,74]

3.5. Transfection Efficiency

Since an interaction with the pDNA could be observed, the polymer library was analyzed regarding the TE. To this end, human embryonic kidney cells (HEK) and pDNA, encoding the reporter gene EGFP, were used. As transfection outcome, the percentage of cells successfully expressing EGFP was identified using flow cytometry. Interestingly, one polymer, the **s40p**, showed a TE ($30.5 \pm 7.6\%$) comparable to that of lPEI ($31.2 \pm 1.7\%$) (Figure 4, Figure S18 and Table S3, Supporting Information), whereas all other polymers showed lower TEs (below 10%). The comparable TE of **s40p** and lPEI is surprising, since the same DP was used and, hence, **s40p** exhibits a much lower amine content (only 80 of 200 repeating units bear an amino group).

The observed differences in TE of 2-oxazoline-based polymers lead to the assumption that primary amino groups in the side chain in combination with small spacers to the backbone are beneficial. These results were not expected and highlight the influence of the polymer constitution for the biological properties. Only slight changes in the amine type, the amine content, or the side chain length can have a great impact on the TE. To gain a deeper insight into the structure–property relationship and find an answer to the question, why the other comparable polymers are less efficient, further investigations were performed. Subsequently, the polymers were studied concerning their polyplex properties, their cytotoxicity, and their membrane interaction.

3.6. Size and Charge of Polyplexes

For a fast and efficient internalization by endocytosis, polyplex sizes between 100 and 200 nm and a positive surface charge are beneficial.[6,75] It was found that all polymers, except **s10p**, form polyplexes with diameters below 200 nm (Table 1). Moreover, with increasing amine content a tendency to form smaller polyplexes was observed. The polyplexes prepared from the four 10 mol% amine-containing polymers exhibited a negative zeta potential, indicating an insufficient polyplex formation and, thus, explaining the insufficient TE (Figure 4 and Table S3). All other polymers formed polyplexes with a positive zeta potential (Table 1).

Furthermore, neither the hydrophobicity of the side chain nor the amine type showed an influence on the size and zeta potential of the investigated polyplexes. In conclusion, a critical amine content of 20 mol% is necessary for an efficient polyplex formation, indicated by a positive zeta potential.

3.7. Cytotoxicity of Polymers and Interaction with Cellular Membranes

In a next step, the biocompatibility of the polymers was investigated. To study the interactions between polymers and cellular membranes a hemolysis assay was performed.

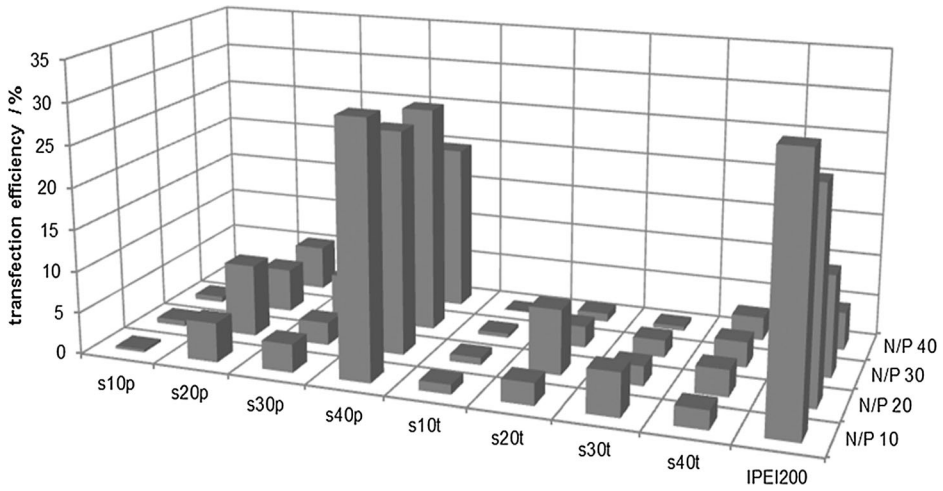

Figure 4. Transfection efficiency of all polymers with short side chains (**sNp** and **sNt**) and $lPEI_{200}$ for adherent HEK cells in serum reduced media at different N/P ratios. Values represent the mean ($n = 3$), SD can be found in the Supporting Information.

Table 1. Polyplex properties and hemolysis assay: polyplexes of indicated polymers and pDNA were formed at N/P ratio 20 in HBG buffer at pH 7.4 (PDI^P see Figure S8, Supporting Information).

			Polyplex properties		Hemolysis [%]		
					Concentration		
			Zeta potential [mV]	Diameter [nm]	10 μg mL^{-1}	50 μg mL^{-1}	100 μg mL^{-1}
Short hydrophobic side chain	Primary amines	**s10p**	−4.3 ± 2.1	255 ± 57	0.09	0.05	0.2
		s20p	22 ± 2.7	178 ± 2.6	0.4	1.5	2.6
		s30p	40 ± 1.6	110 ± 11	0.09	0.2	0.2
		s40p	23 ± 2.7	94 ± 3.4	0.6	1.6	2.9
	Tertiary amines	**s10t**	−5.5 ± 2.5	151 ± 14.7	0.5	0.6	0.7
		s20t	19 ± 1.7	158 ± 0.4	0.8	0.6	0.5
		s30t	29 ± 4.7	124 ± 3.5	0.6	0.6	0.7
		s40t	29 ± 1.7	105 ± 1.2	0.8	0.7	0.8
Long hydrophobic side chain	Primary amines	**l10p**	−17 ± 1.1	152 ± 3.1	0.9	18	17
		l20p	28 ± 1.8	105 ± 3.2	83	107	107
		l30p	29 ± 1.3	84 ± 0.5	105	124	102
		l40p	34 ± 1	97 ± 3	106	104	108
	Tertiary amines	**l10t**	−9 ± 1.2	152 ± 3.5	0.7	0.6	0.7
		l20t	26 ± 0.7	113 ± 3.6	10	50	86
		l30t	30 ± 2.7	84 ± 0.5	62	101	95
		l40t	27 ± 3	67 ± 1.8	102	100	100

Hemolysis assay of the whole polymer library using blood of three different donors ($n = 3$). 1% Triton X-100 was used as positive control and values were set to 100% hemolysis. Values represent the mean ($n = 3$) (SD can be found in the Supporting Information).

It was found that the polymers with short side chains (**sNp** and **sNt**) exhibit a hemolysis below 3%, indicative of no hemolytic activity (Table 1). In contrast, the polymers with long side chains (**lNp** and **lNt**) showed high hemolytic activity even at low concentrations (Table 1). This finding can be ascribed to strong membrane interaction of the more hydrophobic side chains leading to membrane destruction, as also reported elsewhere.[61] Moreover, the **lNp** polymers are more hemolytic compared to **lNt**, which also indicates an enhanced interaction of primary amines with the negative cellular membrane or their proteins. Due to their low amine chain content and insufficient polyplex formation, **l10p** and **l10t** did not cause any hemolytic effect (1.8%) (Table 1). The results show that the interaction between the polymers and membranes is much more influenced by the hydrophobic nature of the polymers than by the amine type and content. This is in accordance with the results of the pDNA condensation (EBA) study (Figure 3).

Besides the hemolytic activity, the cytotoxicity was investigated. It is a well-known problem that cationic polymers, such as high molar mass PEI or PDMAEMA, lead to low cell viabilities.[19,76] Both, PMeOx and PEtOx were postulated to decrease the cytotoxicity. Hence, the cytotoxicity of the 16 PMeOx-containing copolymers was analyzed using the AlamarBlue assay (Figure 5). This assay is based on a non-fluorescent indicator dye (resazurin) that is converted into a fluorescent dye by metabolically active cells. While the **sNp** and **sNt** polymers caused no cytotoxicity at concentrations up to 200 μg mL^{-1} (Figure 5A), lPEI showed an IC_{50} (concentration where 50% of cells are viable) at 3.6 μg mL^{-1} (data not shown). In this context, it has to be noted that **s40p** shows the same TE as lPEI but without any cytotoxic effects. In contrast, higher cytotoxicities were observed for polymers with long side chains (**lNp** and **lNt**), showing furthermore a dependency on the amine content, amine type, and the used concentration (Figure 5B). IC_{50} values of 4–14 μg mL^{-1} were obtained, meaning they have a cytotoxicity comparable to lPEI. In contrast to the **lNp** polymers, where **l40p** showed a lower cytotoxicity than **l30p**, an increasing cytotoxicity with increasing amine content was observed for the **lNt** polymers. The decreased toxicity of **l40p** might be caused by (electrostatic) interactions with serum

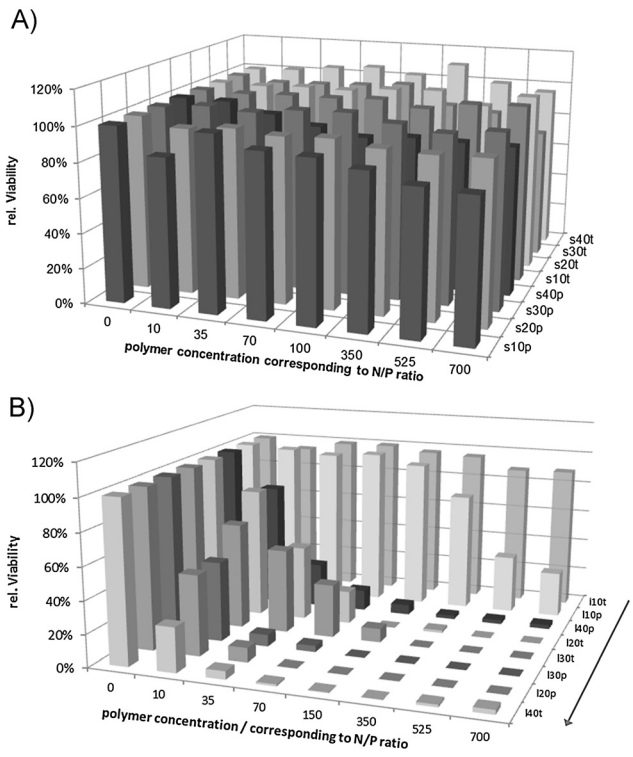

Figure 5. Cytotoxicity of indicated polymers (A, short side chains; B, long side chains) using AlamarBlue and L929 cells. A) Cells treated with **sNp** polymers and **sNt** polymers. B) Cells treated with **lNp** polymers and with **lNp** polymers. Arrow represents the increased cytotoxicity of **lNp** polymers. Values represent the mean ($n = 3$), SD can be found in the Supporting Information.

components and will be investigated in further studies. In summary, the alkyl content and the hydrophobicity of the side chains showed again a high impact on the interaction of the polymers with cellular membranes.

To further investigate the reason for the different cytotoxicity of the polymers, in particular **s40p** and **s40t** or **l40p**, a lactate dehydrogenase (LDH) assay was performed with all four 40 mol% amine containing polymers (Figure 6). Due to the possibility to determine the released cellular LDH in a sensitive way, the LDH assay is used to detect membrane destruction.[77]

In contrast to the hemolysis assay, the LDH assay can be performed with HEK cells, which are also used for transfection studies. Consequently, the membrane destruction ability of both, the polymers and the polyplexes, can be analyzed. It was observed that the polymers **s40p** and **s40t** as well as their polyplexes showed no membrane destruction, at an N/P ratio of 20. In case of **l40p**, the polyplex is less toxic than the corresponding polymer, which was also observed for PEI. This was already reported in literature and was ascribed to the shielding of the cationic charges of PEI by interactions with the genetic material.[78] It is assumed

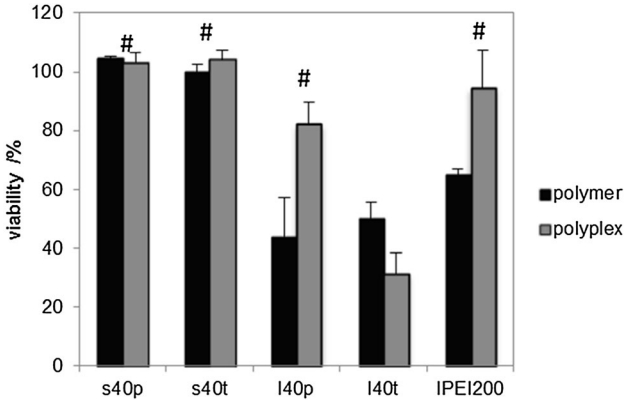

Figure 6. LDH assay of HEK cell. Cells were incubated with polyplexes of indicated polymers for 1 h at N/P 20. Values represent the mean ($n = 3$), SD can be found in the Supporting Information; #represents a significant difference ($p < 0.05$) compared to **l40t**.

that this is also valid for **l40p**, since this polymer strongly interacts with the pDNA (Figure 3). Interestingly, the polyplexes of **l40t** showed a slightly higher membrane destruction activity compared to the non-complexed polymers. A possible explanation can be an enhanced internalization of polyplexes compared to the polymers resulting in high intracellular cytotoxicity.

A possible reason for the higher cytotoxicity of **l40t** compared to **l40p** is the more hydrophobic character of the tertiary amine compared to the primary counterpart. In addition, the sterically demanding methyl groups of the tertiary amine possibly reduce the pDNA binding (Figure 3) and shield the cationic charges, as observed for **l40t**. Thus, the LDH assay confirms the assumption that an increased side chain hydrophobicity enhances the interaction with the membrane. In the case of **s40p** an optimum between the amount of "stealth" (MeOx) units for high biocompatibility, the amount and type of cationic groups for pDNA interaction, and the ideal length of the hydrophobic segment for membrane interactions was found, making **s40p** the best performing polymer.

3.8. Uptake of Polyplexes

Hitherto, the performed experiments could not explain the differences between the good performer **s40p** and the bad performer **s40t** regarding its transfection mechanism. Therefore, the uptake behavior was investigated using YOYO-1 labeled pDNA. The uptake of the fluorescent polyplexes was determined by flow cytometry.[79] To focus on the influence of amine type and hydrophobicity, only the 40 mol% polymers were studied (Figure 7). Polyplexes based on **l40p** showed a time-dependent uptake, similar to that of lPEI. Compared to this, the **s40p**-based polyplexes, which

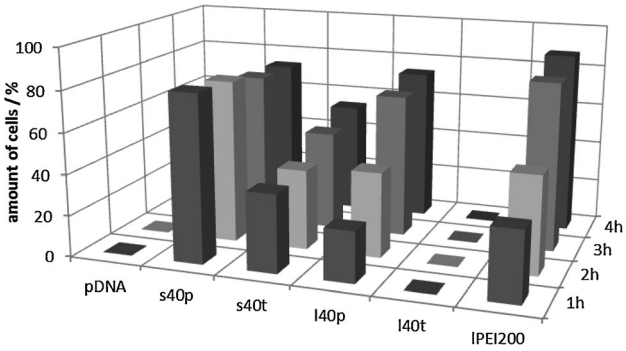

Figure 7. Uptake study: amount of cells transfected with YOYO-1 labeled pDNA for indicated time points using the polymers with 40 mol% amine content and pDNA and $lPEI_{200}$ (N/P ratio 20) as controls. Values represent the mean ($n = 3$), SD can be found in the Supporting Information.

showed the highest TE, were taken up much faster and more efficiently. Seventy percent of the HEK cells internalized **s40p** polyplexes already after 1 h of incubation (LPEI: 34%). In contrast to the **s40p** polyplexes, its corresponding polymer with tertiary amines (**s40t**) showed the lowest polyplex internalization. Only 60% of the cells internalized polyplexes, even after 4 h. For **l40t** polyplexes, no analysis was possible since the cytotoxicity was too high to obtain any reliable data, as also observed by the AlamarBlue and the LDH assay (Figure 5 and 6). The reduced uptake of polymers with tertiary amine side chains (**s40t)** and/or their high cytotoxicity (**l40t**) can explain their insufficient TE, compared to **s40p**. The bad TE of polymers with tertiary amines coupled to long hydrophobic side chains is in contrast to the poly(amine-*co*-ester) terpolymers systems reported by Zhou et al.,[80] where polymers with long hydrophobic domains and tertiary amines in the main chain revealed an excellent transfection behavior and low cytotoxicity. This once more highlights the importance of the polymer hydrophobicity for gene delivery applications. However, it also shows that results from different studies cannot easily be transferred to other polymer classes. Therefore, it is necessary to perform detailed analyses for each compound.

3.9. Polyplex Stability

To understand, why some polymers perform better than others, different bottlenecks were analyzed, starting from the polyplex itself to the cellular mechanisms. Another critical parameter is the polyplex stability. On one hand, the pDNA has to be protected against digestion, on the other hand, it has to be released inside cells. Hence, an optimum between strong and weak binding has to be found. The polyplex stability was analyzed using the heparin assay, in which negatively charged heparin competes with the pDNA. In Figure 8, the heparin concentration necessary for complete polyplex dissociation is presented (data of all compounds see Figure S9, Supporting Information). Compared to the polyplexes formed from polymers with short side chains (**sNp** and **sNt**), the ones of long side chain (**lNp** and **lNt**) are more stable, as indicated by higher heparin concentrations required to release the pDNA. This is particularly the case for **l40p**, where 50 U mL^{-1} heparin are required for the polyplex dissociation, which is in good correlation with the strong pDNA condensation (Figure 3). In contrast, the **s40p** polyplexes release the pDNA already at heparin concentration of 10 U mL^{-1}. This indicates a stronger binding of **l40p** and could result in an inefficient release of pDNA in the cytoplasm and, hence, a low TE (Figure 4 and 7). For the **sNt** and **lNt** polyplexes, only a small amount of heparin leads to dissociation. This is another indication that tertiary amines interact less strongly with genetic material and, hence, are not able to protect the pDNA at physiological pH 7 (Figure 3). As a consequence, the pDNA could be degraded due to the polyplex instability during the incubation in the transfection media or inside the cell (pH 7). The latter could also explain their inefficient uptake and the low amount of internalized pDNA.

3.10. Influence of the Thioether Position and Higher Amine Content

The type of polymer side chain showed a high impact on the cytotoxicity and the TE. To test whether the location of the sulfur within the side chain has an influence on the properties another polymer (**s40hp**, Scheme 1), having a hexamethylene spacer between the sulfur and the amine, was prepared by thiol-ene photoaddition. The polymer

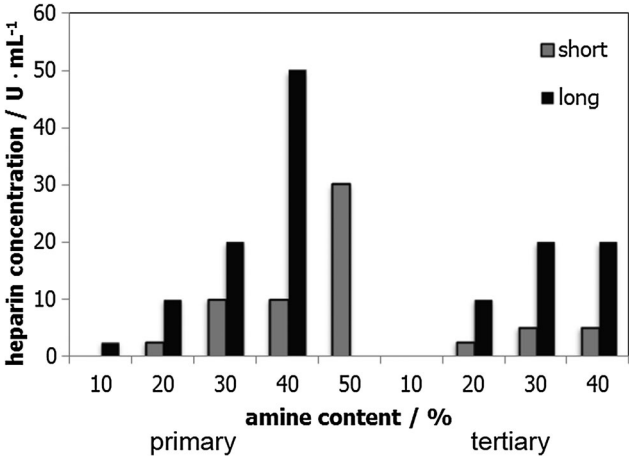

Figure 8. Polyplex stability: dissociation assay of polyplexes formed at N/P 20. The bars represent the heparin concentration at which the polyplexes are dissociated.

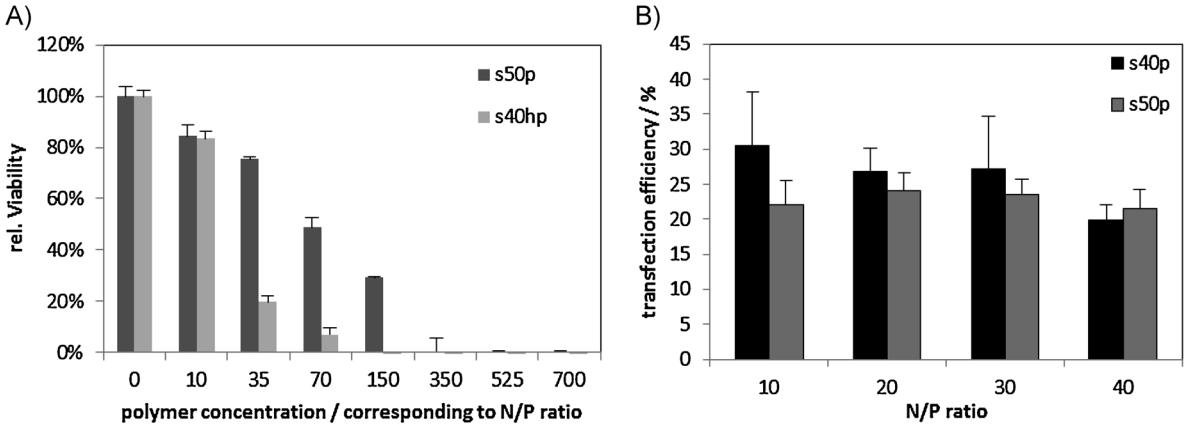

Figure 9. A) Cytotoxicity of indicated polymers (**s50p** and **s40hp**) using AlamarBlue and L929 cells ($n = 3$) and B) transfection efficiency of indicated polymers for adherent HEK cells in serum reduced media at different N/P ratios.

exhibits the same total number of CH_2 groups in the side chain but a different position of the thioether group. Analysis of the TE (data not shown) and the cytotoxicity (Figure 9A) yielded similar results as for the analogous **l40p** polymer. In detail, no TE and high cytotoxicity was observed. This proves that the cytotoxicity and TE is influenced by the side chain length and not by the location of the thioether group in the side chain.

Another question that arises is, if a higher amine content will lead to a further increased TE. Thus, a polymer with a short side chain and 50 mol% of primary amines was synthesized (**s50p**) according to the procedure described for the other **sNp** polymers (Scheme 1). Again, the TE and the cytotoxicity were investigated. For this polymer (**s50p**), the TE was slightly lower but showed no significant differences to the **s40p** polymer (Figure 9B). However, it was cytotoxic at higher concentration (Figure 9A), whereas for **s40p** no cytotoxicity was observed up to N/P ratio 700 (Figure 5A). Since a higher amine content showed no advantage for the transfection process and an increased cytotoxity, the **s50p** was not investigated further. Obviously, the polymer **s40p** represents an optimal combination of cationic charges, hydrophobicity and biocompatible monomers for enhanced cellular interaction and TE as well as reduced cytotoxicity.

4. Conclusion

Understanding the interplay between different parameters represents an important prerequisite for the development of non-toxic cationic polymers used as non-viral vectors in gene delivery applications. Here, we presented the synthesis and biological screening of an 18-membered 2-oxazoline-based copolymer library. Different parameters, such as the polymer side chain hydrophobicity, the type, and content of amine groups were systematically varied. MeOx as biocompatible "stealth" comonomer and DecEnOx or ButEnOx, respectively, have been copolymerized with varying ratios. Subsequent functionalization of the double bonds by thiol-ene photoaddition yielded cationic polymers with primary and tertiary amine groups. The influence of the different parameters on the pDNA condensation, the TE, the cytotoxicity, and cellular membrane interaction as well as the size, charge, and stability of the polyplexes was investigated (Figure 10).

It was found that independent of the amine content, long hydrophobic side chains enhance the pDNA condensation to the genetic material but interrupt the cellular membranes, leading to a higher cytotoxicity, hemolysis, and LDH release. Poly(2-oxazoline)s with short side chains and an amine content below 50 mol% were found to be biocompatible at all studied concentrations.

In addition, it was observed that primary amines are more suitable for an efficient binding and protection of pDNA. Here, an amine content of at least 40 mol% is necessary, since lower amine mol% revealed a decreased pDNA condensation. In case of tertiary amines, the binding with pDNA was too weak for all investigated polymers. Hence, the pDNA was released into the transfection media or inside the endosomes, which resulted in a reduced TE.

In the end, we could identify one polymer, namely **s40p**, which showed superior properties over lPEI. High transfection efficiencies similar to that of lPEI and a faster internalization were found. Most importantly, no cytotoxicity was observed in the tested concentration range. The presented study demonstrates the high potential of cationic poly(2-oxazoline)s for gene delivery and shows that it is possible to design cationic polymers having a high TE while being non-toxic. Further investigations will be executed, in particular on the best

		mol%	EBA [%]	Size [nm]	ZP [mV]	Toxic	Hemolytic	LDH-Release	Uptake [%]	Heparin [U mg^{-1}]	TE [%]	comments
Short hydrophobic side chain (x = 1)	primary amines	10	80	255	-4	no	no	-	-	0	0	no polyplex formation
		20	72	178	22	no	no	-	-	3	8	labile polyplex
		30	72	110	40	no	no	-	-	10	6	low TE
		40	60	94	23	no	no	no	90	10	31	**best performer!**
		50	60	51	47	yes	-	-	-	30	24	increased toxicity
	teriary amines	10	82	151	-6	no	no	-	-	0	1	no polyplex formation
		20	68	158	19	no	no	-	-	3	8	labile polyplex
		30	64	124	29	no	no	-	-	5	5	low TE
		40	57	105	29	no	no	no	60	5	3	inefficient uptake
x = 1		40	-	-	-	yes	-	-	-	-	8	hexamethylene spacer, toxic
Long hydrophobic side chain (x = 7)	primary amines	10	69	152	-17	yes	no	-	-	3	0	no polyplex formation
		20	46	105	28	yes	yes	-	-	10	6	toxic
		30	36	84	29	yes	yes	-	-	20	4	toxic
		40	30	97	34	yes	yes	yes	80	50	6	toxic
	teriary amines	10	76	152	-9	no	no	-	-	0	0	no polyplex formation
		20	60	113	26	yes	yes	-	-	10	3	toxic
		30	50	84	30	yes	yes	-	-	20	6	toxic
		40	41	67	27	yes	yes	yes	-	20	2	toxic
LPEI200			45	-	-	yes	-	no	90	-	31	good performer but toxic

Figure 10. Overview of all polymers regarding their characteristics and bottlenecks for the transfection process. Probable reasons for transfection failure or drawbacks are described as comments. Toxicity (AlamarBlue), hemolysis and LDH were classified with 0 for no effect, 0.5 for middle occurrence, and 1 for high occurrence.

performing polymer, to gain a deeper insight into the transfection mechanism.

Acknowledgements: The authors want to thank the Dutch Polymer Institute (DPI, Technology area HTE). The Carl-Zeiss Foundation (JCSM Strukturantrag) is gratefully acknowledged. We like to thank Cornelia Bader and Anette Kuse for the scale-up synthesis of ButEnOx and DecEnOx. Furthermore, Carolin Fritzsche is gratefully acknowledged for the performance of the hemolysis, AlamarBlue, and EBA assays. Dr. Kristian Kempe is grateful to the Alexander von Humboldt-foundation for financial support.

Received: July 17, 2014; Revised: October 4, 2014; Published online: November 18, 2014; DOI: 10.1002/mabi.201400334

Keywords: gene delivery; hydrophobic side chain; poly(2-oxazoline)s; primary amine; structure–property relationship; tertiary amine; viability

[1] R. Duncan, R. Gaspar, *Mol. Pharm.* **2011**, *8*, 2101.
[2] K. Itaka, K. Kataoka, *Eur. J. Pharm. Biopharm.* **2009**, *71*, 475.
[3] R. J. Christie, N. Nishiyama, K. Kataoka, *Endocrinology* **2010**, *151*, 466.
[4] K. Miyata, N. Nishiyama, K. Kataoka, *Chem. Soc. Rev.* **2012**, *41*, 2562.
[5] K. A. Whitehead, R. Langer, D. G. Anderson, *Nat. Rev. Drug Discov.* **2009**, *8*, 129.
[6] A. Aied, U. Greiser, A. Pandit, W. Wang, *Drug Discov. Today* **2013**, *18*, 1090.
[7] S. Barua, J. Ramos, T. Potta, D. Taylor, H. C. Huang, G. Montanez, K. Rege, *Comb. Chem. High Throughput Screen.* **2011**, *14*, 908.
[8] A. Basarkar, J. Singh, *Int. J. Nanomed.* **2007**, *2*, 353.
[9] S. C. De Smedt, J. Demeester, W. E. Hennink, *Pharm. Res.* **2000**, *17*, 113.
[10] D. W. Pack, A. S. Hoffman, S. Pun, P. S. Stayton, *Nat. Rev. Drug Discov.* **2005**, *4*, 581.
[11] R. Duncan, *Nat. Rev. Drug Discov.* **2003**, *2*, 347.
[12] M. A. Mintzer, E. E. Simanek, *Chem. Rev.* **2008**, *109*, 259.
[13] M. Breunig, U. Lungwitz, R. Liebl, J. Klar, B. Obermayer, T. Blunk, A. Goepferich, *Biochim. Biophys. Acta (BBA) – Gen. Subj.* **2007**, *1770*, 196.
[14] W. T. Godbey, K. K. Wu, A. G. Mikos, *J. Control. Release* **1999**, *60*, 149.
[15] M. Jäger, S. Schubert, S. Ochrimenko, D. Fischer, U. S. Schubert, *Chem. Soc. Rev.* **2012**, *41*, 4755.
[16] O. M. Merkel, D. Librizzi, A. Pfestroff, T. Schurrat, K. Buyens, N. N. Sanders, S. C. De Smedt, M. Béhé, T. Kissel, *J. Control. Release* **2009**, *138*, 148.
[17] R. J. Christie, K. Miyata, Y. Matsumoto, T. Nomoto, D. Menasco, T. C. Lai, M. Pennisi, K. Osada, S. Fukushima, N. Nishiyama, Y. Yamasaki, K. Kataoka, *Biomacromolecules* **2011**, *12*, 3174.
[18] P. van de Wetering, J. Y. Cherng, H. Talsma, D. J. A. Crommelin, W. E. Hennink, *J. Control. Release* **1998**, *53*, 145.
[19] C. V. Synatschke, A. Schallon, V. Jerome, R. Freitag, A. H. E. Muller, *Biomacromolecules* **2011**, *12*, 4247.
[20] S. Agarwal, Y. Zhang, S. Maji, A. Greiner, *Mater. Today* **2012**, *15*, 388.

[21] D. G. Anderson, A. Akinc, N. Hossain, R. Langer, *Mol. Ther.* **2005**, *11*, 426.
[22] P. van de Wetering, E. E. Moret, N. M. E. Schuurmans-Nieuwenbroek, M. J. van Steenbergen, W. E. Hennink, *Bioconjugate Chem.* **1999**, *10*, 589.
[23] D. J. Chen, B. S. Majors, A. Zelikin, D. Putnam, *J. Control. Release* **2005**, *103*, 273.
[24] Y. Yue, C. Wu, *Biomater. Sci.* **2013**, *1*, 152.
[25] S. Choksakulnimitr, S. Masuda, H. Tokuda, Y. Takakura, M. Hashida, *J. Control. Release* **1995**, *34*, 233.
[26] H. Lv, S. Zhang, B. Wang, S. Cui, J. Yan, *J. Control. Release* **2006**, *114*, 100.
[27] M. Lee, S. W. Kim, *Pharm. Res.* **2005**, *22*, 1.
[28] T. G. Park, J. H. Jeong, S. W. Kim, *Adv. Drug Deliv. Rev.* **2006**, *58*, 467.
[29] J. Dai, S. Zou, Y. Pei, D. Cheng, H. Ai, X. Shuai, *Biomaterials* **2011**, *32*, 1694.
[30] A. Mathew, H. Cao, E. Collin, W. Wang, A. Pandit, *Int. J. Pharm.* **2012**, *434*, 99.
[31] K. Knop, R. Hoogenboom, D. Fischer, U. S. Schubert, *Angew. Chem. Int. Ed.* **2010**, *49*, 6288.
[32] J. C. Fernandes, X. P. Qiu, F. M. Winnik, M. Benderdour, X. L. Zhang, K. R. Dai, Q. Shi, *Int. J. Nanomed.* **2013**, *8*, 4091.
[33] G.-H. Hsiue, H.-Z. Chiang, C.-H. Wang, T.-M. Juang, *Bioconjugate Chem.* **2006**, *17*, 781.
[34] J. H. Jeong, S. H. Song, D. W. Lim, H. Lee, T. G. Park, *J. Control. Release* **2001**, *73*, 391.
[35] Z. Zhong, J. Feijen, M. C. Lok, W. E. Hennink, L. V. Christensen, J. W. Yockman, Y.-H. Kim, S. W. Kim, *Biomacromolecules* **2005**, *6*, 3440.
[36] N. Adams, U. S. Schubert, *Adv. Drug Deliv. Rev.* **2007**, *59*, 1504.
[37] M. Bauer, C. Lautenschlaeger, K. Kempe, L. Tauhardt, U. S. Schubert, D. Fischer, *Macromol. Biosci.* **2012**, *12*, 986.
[38] J. Kronek, Z. Kroneková, J. Lusto, E. Paulovičová, L. Paulovičová, B. Mendrek, *J. Mater. Sci.: Mater. Med.* **2011**, *22*, 1725.
[39] R. Luxenhofer, G. Sahay, A. Schulz, D. Alakhova, T. K. Bronich, R. Jordan, A. V. Kabanov, *J. Control. Release* **2011**, *153*, 73.
[40] A. Mero, G. Pasut, L. D. Via, M. W. M. Fijten, U. S. Schubert, R. Hoogenboom, F. M. Veronese, *J. Control. Release* **2008**, *125*, 87.
[41] T. X. Viegas, M. D. Bentley, J. M. Harris, Z. Fang, K. Yoon, B. Dizman, R. Weimer, A. Mero, G. Pasut, F. M. Veronese, *Bioconjugate Chem.* **2011**, *22*, 976.
[42] S. Zalipsky, C. B. Hansen, J. M. Oaks, T. M. Allen, *J. Pharm. Sci.* **1996**, *85*, 133.
[43] M. Bauer, S. Schroeder, L. Tauhardt, K. Kempe, U. S. Schubert, D. Fischer, *J. Polym. Sci. A: Polym. Chem.* **2013**, *51*, 1816.
[44] R. Hoogenboom, *Angew. Chem. Int. Ed.* **2009**, *48*, 7978.
[45] H. Schlaad, C. Diehl, A. Gress, M. Meyer, A. L. Demirel, Y. Nur, A. Bertin, *Macromol. Rapid Commun.* **2010**, *31*, 511.
[46] J. Ulbricht, R. Jordan, R. Luxenhofer, *Biomaterials* **2014**, *35*, 4848.
[47] R. Hoogenboom, M. W. M. Fijten, H. M. L. Thijs, B. M. van Lankvelt, U. S. Schubert, *Des. Monomers Polym.* **2005**, *8*, 659.
[48] R. Hoogenboom, R. M. Paulus, Å. Pilotti, U. S. Schubert, *Macromol. Rapid Commun.* **2006**, *27*, 1556.
[49] F. Wiesbrock, R. Hoogenboom, M. Leenen, S. F. G. M. van Nispen, M. van der Loop, C. H. Abeln, A. M. J. van den Berg, U. S. Schubert, *Macromolecules* **2005**, *38*, 7957.
[50] F. Wiesbrock, R. Hoogenboom, M. A. M. Leenen, M. A. R. Meier, U. S. Schubert, *Macromolecules* **2005**, *38*, 5025.
[51] S. Cesana, J. Auernheimer, R. Jordan, H. Kessler, O. Nuyken, *Macromol. Chem. Phys.* **2006**, *207*, 183.
[52] M. Hartlieb, D. Pretzel, K. Kempe, C. Fritzsche, R. M. Paulus, M. Gottschaldt, U. S. Schubert, *Soft Matter* **2013**, *9*, 4693.
[53] R. Konradi, B. Pidhatika, A. Muhlebach, M. Textor, *Langmuir* **2008**, *24*, 613.
[54] L. Tauhardt, K. Kempe, M. Gottschaldt, U. S. Schubert, *Chem. Soc. Rev.* **2013**, *42*, 7998.
[55] I. Banerjee, R. C. Pangule, R. S. Kane, *Adv. Mater.* **2011**, *23*, 690.
[56] J. Blümmel, N. Perschmann, D. Aydin, J. Drinjakovic, T. Surrey, M. Lopez-Garcia, H. Kessler, J. P. Spatz, *Biomaterials* **2007**, *28*, 4739.
[57] H. Hatakeyama, H. Akita, H. Harashima, *Adv. Drug Deliv. Rev.* **2011**, *63*, 152.
[58] Y. Ikeda, Y. Nagasaki, *J. Appl. Polym. Sci.* **2014**, *131*, 40293(1).
[59] J. A. Fortune, T. I. Novobrantseva, A. M. Klibanov, *J. Drug Deliv.* **2011**, *2011*, 204058.
[60] S. T. Kim, K. Saha, C. Kim, V. M. Rotello, *Acc. Chem. Res.* **2013**, *46*, 681.
[61] C. J. Waschinski, V. Herdes, F. Schueler, J. C. Tiller, *Macromol. Biosci.* **2005**, *5*, 149.
[62] A. Gress, A. Völkel, H. Schlaad, *Macromolecules* **2007**, *40*, 7928.
[63] K. Kempe, A. Vollrath, H. W. Schaefer, T. G. Poehlmann, C. Biskup, R. Hoogenboom, S. Hornig, U. S. Schubert, *Macromol. Rapid Commun.* **2010**, *31*, 1869.
[64] C. Diehl, H. Schlaad, *Macromol. Biosci.* **2009**, *9*, 157.
[65] K. Kempe, R. Hoogenboom, M. Jaeger, U. S. Schubert, *Macromolecules* **2011**, *44*, 6424.
[66] K. Kempe, R. Hoogenboom, U. S. Schubert, *Macromol. Rapid Commun.* **2011**, *32*, 1484.
[67] K. Kempe, T. Neuwirth, J. Czaplewska, M. Gottschaldt, R. Hoogenboom, U. S. Schubert, *Polym. Chem.* **2011**, *2*, 1737.
[68] T. R. Dargaville, R. Forster, B. L. Farrugia, K. Kempe, L. Voorhaar, U. S. Schubert, R. Hoogenboom, *Macromol. Rapid Commun.* **2012**, *33*, 1695.
[69] M. Litt, A. Levy, J. Herz, *J. Macromol. Sci. A: Pure Appl. Chem.* **1975**, *9*, 703.
[70] J. M. Warakomski, B. P. Thill, *J. Polym. Sci. A: Polym. Chem.* **1990**, *28*, 3551.
[71] K. Kempe, C. Weber, K. Babiuch, M. Gottschaldt, R. Hoogenboom, U. S. Schubert, *Biomacromolecules* **2011**, *12*, 2591.
[72] A. Baumgaertel, E. Altuntaş, K. Kempe, A. Crecelius, U. S. Schubert, *J. Polym. Sci. A: Polym. Chem.* **2010**, *48*, 5533.
[73] K. A. Howard, *Adv. Drug Deliv. Rev.* **2009**, *61*, 710.
[74] J. Ziebarth, Y. M. Wang, *Biophys. J.* **2009**, *97*, 1971.
[75] J. Rejman, V. Oberle, I. S. Zuhorn, D. Hoekstra, *Biochem. J.* **2004**, *377*, 159.
[76] D. Fischer, T. Bieber, Y. Li, H. P. Elsasser, T. Kissel, *Pharm. Res.* **1999**, *16*, 1273.
[77] H. Kim, S. C. Yoon, T. Y. Lee, D. Jeong, *Toxicol. Lett.* **2009**, *184*, 13.
[78] A. Schallon, V. Jérôme, A. Walther, C. V. Synatschke, A. H. E. Mueller, R. Freitag, *React. Funct. Polym.* **2010**, *70*, 1.
[79] M. Ogris, E. Wagner, P. Steinlein, *Biochim. Biophys. Acta – Gen. Subj.* **2000**, *1474*, 237.
[80] J. Zhou, J. Liu, C. J. Cheng, T. R. Patel, C. E. Weller, J. M. Piepmeier, Z. Jiang, W. M. Saltzman, *Nat. Mater.* **2012**, *11*, 82.

Supporting Information

A cationic poly(2-oxazoline) with high *in vitro* transfection efficiency identified by a library approach

Alexandra C. Rinkenauer,[1,2‡] Lutz Tauhardt,[1,2‡] Felix Wendler,[1,2] Kristian Kempe,[1,2 †] Michael Gottschaldt,[1,2] Anja Träger,[1,2] Ulrich S. Schubert [1,2,3]**

[‡] *both authors contributed equally*

[1]Laboratory of Organic and Macromolecular Chemistry (IOMC), Friedrich Schiller University Jena, Humboldtstrasse 10, 07743 Jena, Germany

[2]Jena Center for Soft Matter (JCSM), Friedrich Schiller University Jena, Philosophenweg 7, 07743 Jena, Germany

[3]Dutch Polymer Institute (DPI), John F. Kennedylaan 2, 5612 AB Eindhoven, The Netherlands.

[†]Current address: Department of Chemical and Biomolecular Engineering, The University of Melbourne, Victoria 3010, Australia

*Address correspondence to: ulrich.schubert@uni-jena.de; anja.traeger@uni-jena.de

Results Section

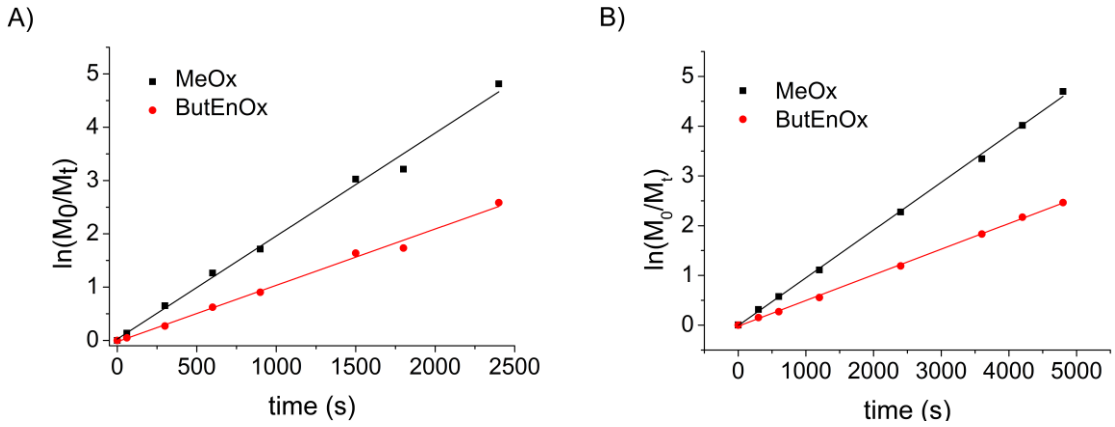

Figure S1. First-order kinetic plots of the copolymerization of MeOx and ButEnOx in acetonitrile at 140 °C for A) MeOx : ButEnOx = 90 : 10(kp_{MeOx} = 0.095 L mol^{-1} s^{-1}; $kp_{ButEnOx}$ = 0.052 L mol^{-1} s^{-1}) and for B) MeOx : ButEnOx = 180 : 20 (kp_{MeOx} = 0.097 L mol^{-1} s^{-1}; $kp_{ButEnOx}$ = 0.052 L mol^{-1} s^{-1}). The conversion was determined by gas chromatography.

Table S1. Kinetic and SEC Data for the copolymerization of MeOx and ButEnOx.

$MeOx_{90}$-*co*-$ButEnOx_{10}$				$MeOx_{180}$-*co*-$ButEnOx_{20}$			
Time [s]	MeOx : ButEnOx [%][a)]	M_n [g mol^{-1}][b)]	$Đ_M$[b)]	Time [s]	MeOx : ButEnOx [%][a)]	M_n [g mol^{-1}][b)]	$Đ_M$[b)]
60	13 : 5	2,200	1.10	1	1 : 0	-	-
300	48 : 24	5,780	1.11	300	27 : 14	6,510	1.20
600	72 : 46	7,400	1.13	600	44 : 24	8,690	1.28
900	82 : 59	8,310	1.14	1200	67 : 43	11,560	1.34
1500	95 : 80	9,190	1.15	2400	90 : 70	14,690	1.39
1800	96 : 82	9,470	1.16	3600	96 : 84	15,650	1.43
2400	99 : 92	9,550	1.16	4200	98 : 89	16,470	1.43
				4800	99 : 91	16,140	1.40

[a)]Conversion determined by gas chromatography. [b)]Determined by SEC.

Table S2. SEC Data of the different copolymers.

MeOx-*co*-ButEnOx				MeOx-*co*-DecEnOx			
Sample	MeOx : ButEnOx	M_n (g/mol)	$Đ_M$	Sample	MeOx : DecEnOx	M_n (g/mol)	$Đ_M$
1a	180 : 20	22,800	1.43	**2a**	180 : 20	19,800	1.47
1b	160 : 40	23,300	1.46	**2b**	160 : 40	25,500	1.47
1c	140 : 60	23,300	1.49	**2c**	140 : 60	19,800	1.45
1d	120 : 80	22,200	1.56	**2d**	120 : 80	22,900	1.63
1e	100 : 100	20,300	1.48				
3a	180 : 20	26,000	1.43	**4a**	180 : 20	-	-
3b	160 : 40	29,000	1.46	**4b**	160 : 40	-	-
3c	140 : 60	29,500	1.47	**4c**	140 : 60	-	-
3d	120 : 80	32,000	1.50	**4d**	120 : 80	-	-
3e	100 : 100	27,700	1.47				
s10p	180 : 20	24,100	1.44	**l10p**	180 : 20	23,600	1.51
s20p	160 : 40	23,200	1.40	**l20p**	160 : 40	31,600	1.43
s30p	140 : 60	27,400	1.40	**l30p**	140 : 60	30,500	1.54
s40p	120 : 80	29,100	1.52	**l40p**	120 : 80	38,100	1.62
s50p	100 : 100	28,500	1.26				
s10t	180 : 20	20,440	1.43	**l10t**	180 : 20	20,300	1.49
s20t	160 : 40	19,560	1.43	**l20t**	160 : 40	28,100	1.47
s30t	140 : 60	18,120	1.45	**l30t**	140 : 60	23,900	1.37
s40t	120 : 80	20,180	1.35	**l40t**	120 : 80	30,300	1.57
s40hp	120 : 80	34,200	1.31				

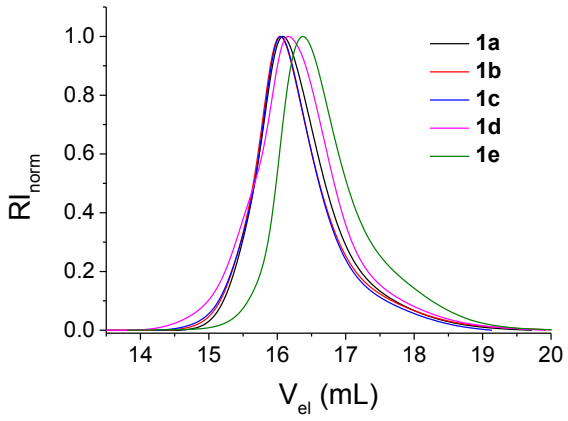

Figure S2. SEC curves of the P(MeOx-*grad*-ButEnOx).

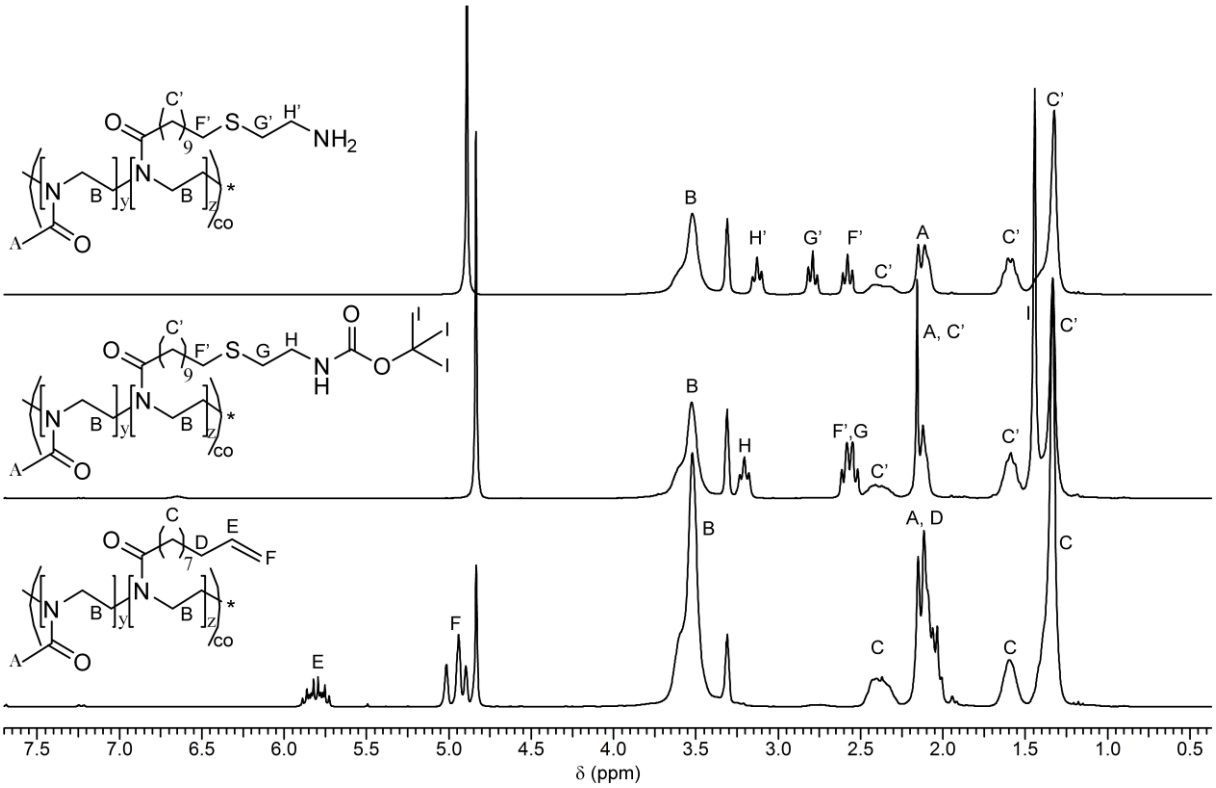

Figure S3. ^{1}H NMR spectra of **2d** (bottom), **4d** (middle), and **l40p** (top) (250 MHz, solvent: CD_3OD).

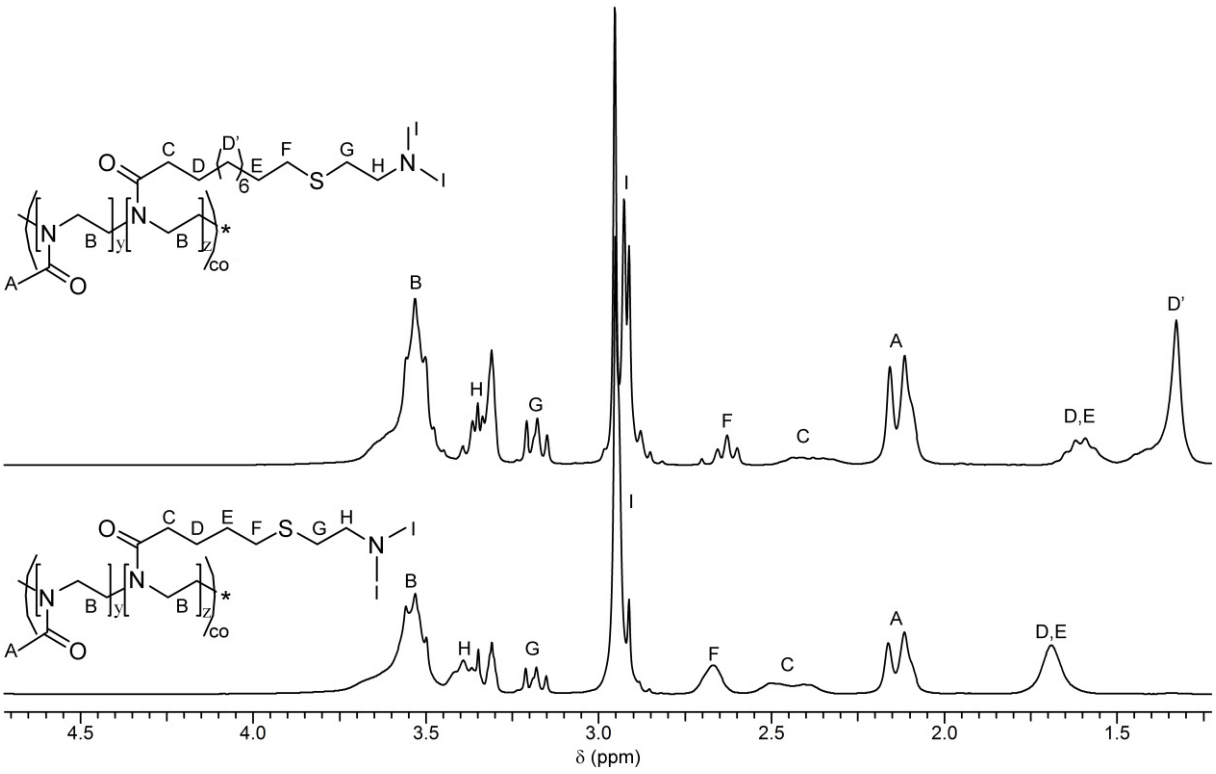

Figure S4. ^{1}H NMR spectra of **s40t** (bottom) and **l40t** (top) (250 MHz, solvent: CD_3OD).

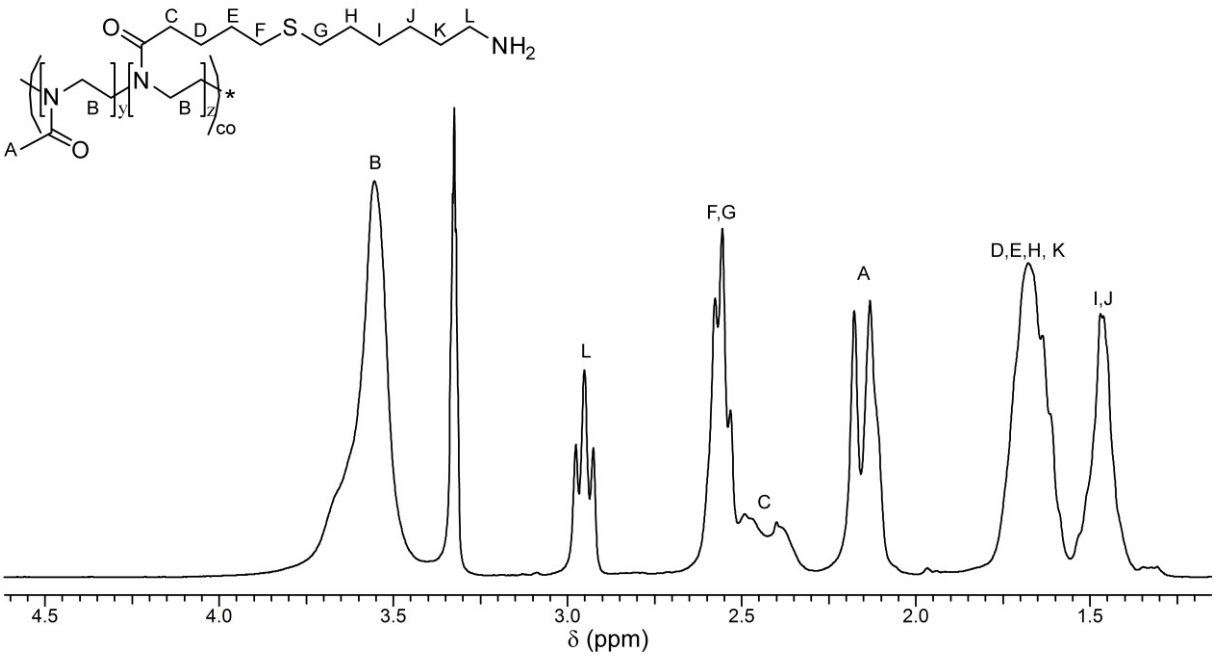

Figure S5. ^{1}H NMR spectrum of **s40hp** (300 MHz, solvent: CD_3OD).

Ethidium bromide binding assay

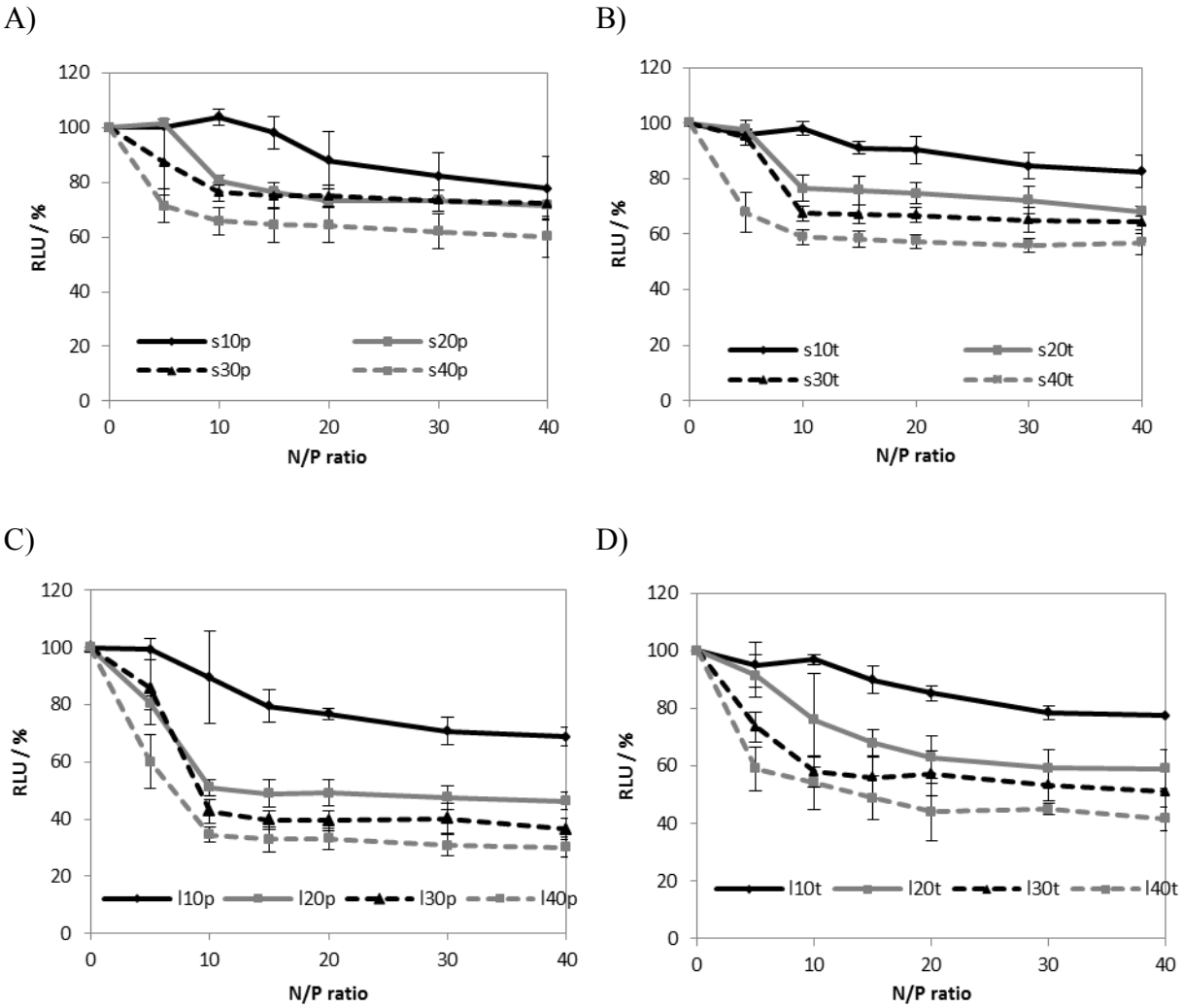

Figure S6. pDNA condensation of all 16 polymers with pDNA measured at physiological pH *via* EBA at indicated N/P ratios (n = 3).

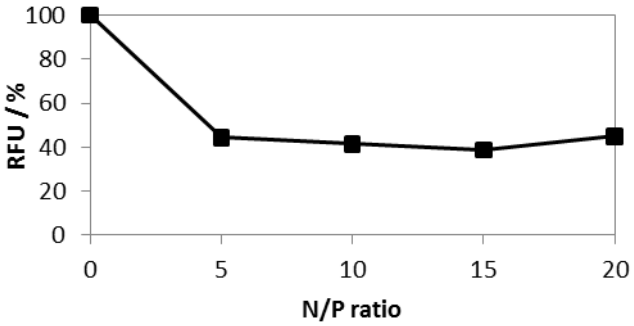

Figure S7. pDNA condensation of lPEI (DP = 200) with pDNA measured at physiological pH *via* EBA (n = 3).

Transfection efficiency

Table S3. Transfection efficiency: Raw data and standard derivation of all polymer at the indicated N/P ratio (n = 3).

N/P ratio	Sample	TE / %	SD	Sample	TE / %	SD	Sample	TE / %	SD	Sample	TE / %	SD
10	**s10p**	0.33	0.57	**s10t**	1.15	1.63	**l10p**	0	0	**l10t**	0.33	0.58
20		0.67	0.57		0.85	1.2		0	0		0	0
30		0.67	0.57		0.5	0.71		0	0		0.17	0.29
40		0	0		0	0		0	0		0.77	0.40
10	**s20p**	4.73	3.59	**s20t**	2.65	3.75	**l20p**	3.65	3.89	**l20t**	0.43	0.35
20		8.7	8.16		7.8	0.99		4.2	4.53		2.1	1.51
30		5.27	2.34		2.55	0.07		3.75	0.21		1.37	0.49
40		5.33	1.38		1	0		6.1	0		2.52	1.35
10	**s30p**	3.4	0.2	**s30t**	5.15	4.31	**l30p**	2.4	2.26	**l30t**	6.48	3.76
20		2.73	1.16		2.35	1.91		3.95	3.04		2.98	2.4
30		5.33	2.97		2.05	1.77		2.65	1.63		1	0
40		5.77	2.91		0.5	0		2.7	2.97		1	0
10	**s40p**	30.5	7.64	**s40t**	2.25	1.77	**l40p**	2.7	0.85	**l40t**	1.33	0.58
20		26.77	3.30		3.2	1.56		5.85	3.89		1	0
30		27.17	7.51		3.05	2.19		7.4	3.25		0.67	0.58
40		19.93	2.15		2.8	0		8.8	5.52		0.33	0.58
10	**s50p**	22.1	3.55	**lPEI200**	31.27	1.75						
20		24.07	2.54		25.23	8.81						
30		23.63	2.17		12.17	11.6						
40		21.6	2.63		4.57	6.18						

Polyplex properties PDI^P

Besides size and zeta potential, also the PDI^P was measured.

A) B)

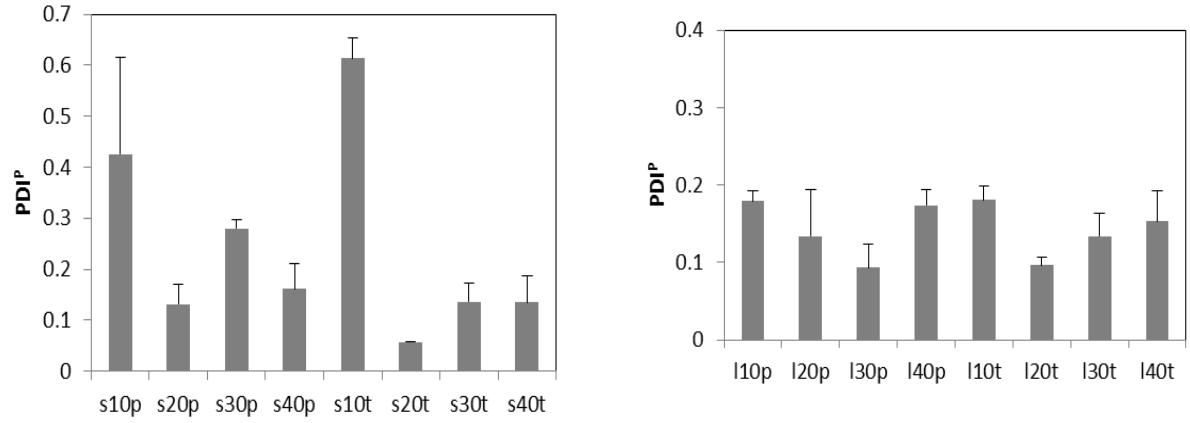

Figure S8. PDIs of the polyplexes prepared at NP ratio of 20.

Cytotoxicity and hemolysis assay

Table S4. Raw data with standard derivation for cytotoxicity (IC50) and hemolysis assay at the indicated polymer concentration.

			Toxicity		**Hemolysis**					
					raw data			STAB		
			IC_{50}	STAB	**10 µg/mL**	**50 µg/mL**	**100 µg/mL**	**10 µg/mL**	**50 µg/mL**	**100 µg/mL**
Short hydrophobic side chain	**primary amines**	**10**	0	-	0.0999	0.0544	0.1872	0.0269	0.0059	0.0642
		20	0	-	0.402	1.5459	2.5634	0.144	0.2172	0.4657
		30	0	-	0.0938	0.1925	0.188	0.0143	0.0291	0.0539
		40	0	-	0.5647	1.6672	2.8517	0.1148	0.0924	0.3764
		50	1	-	-	-	-	-	-	-
	teriary amines	**10**	0	-	0.47	0.57	0.71	3E-05	1E-07	3E-07
		20	0	-	0.76	0.56	0.47	4E-07	2E-07	7E-08
		30	0	-	0.55	0.57	0.69	0.5488	0.572	0.6938
		40	0	-	0.80	0.68	0.80	0.7989	0.6844	0.796
Long hydrophobic side chain	**primary amines**	**10**	0	0	0.8589	1.802	1.6973	0.1767	0.544	0.6171
		20	5	0.0794	83.206	107.42	107.07	27.032	44.606	45.089
		30	4.7127	0.0157	105	124.21	102.13	40.686	43.969	41.632
		40	34.853	0.0619	106.8	104.16	108.75	44.857	43.014	43.779
	teriary amines	**10**	0	0	0.6555	0.6133	0.7276	0.0616	0.0185	0.045
		20	13.795	0.059	10.204	50.688	85.833	0.4399	3.4895	3.3771
		30	13.795	0.0393	62.046	101.21	94.963	5.8019	5.557	17.997
		40	4.5983	0.1263	102.47	100.68	99.833	1.0602	3.8171	2.8269

Uptake studies

Table S5. Raw data and standard derivation of time dependent uptake kinetic.

	1 h		2 h		3 h		4 h	
	amount of cells / %	STAB	amount of cells / %	STAB	amount of cells / %	STAB	amount of cells / %	STAB
pDNA	0.3	0.2646	0.25	0.2121	0.65	0.495	0.4666667	0.1155
s40p	81.233333	7.9223	70	19	74.2	4.3841	73.4	3.2512
s40t	37.85	2.6163	38.9	0	48.05	16.9	53.7	4.1328
l40p	24.666667	6.8712	41.25	6.1518	69.65	16.051	74	14.47
l40t	0	0	0	0	0	0	0	0
lPEI200	33.8	0.8485	47.45	0.2121	81.85	13.647	88.033333	6.3058

Dissociation assay

A)

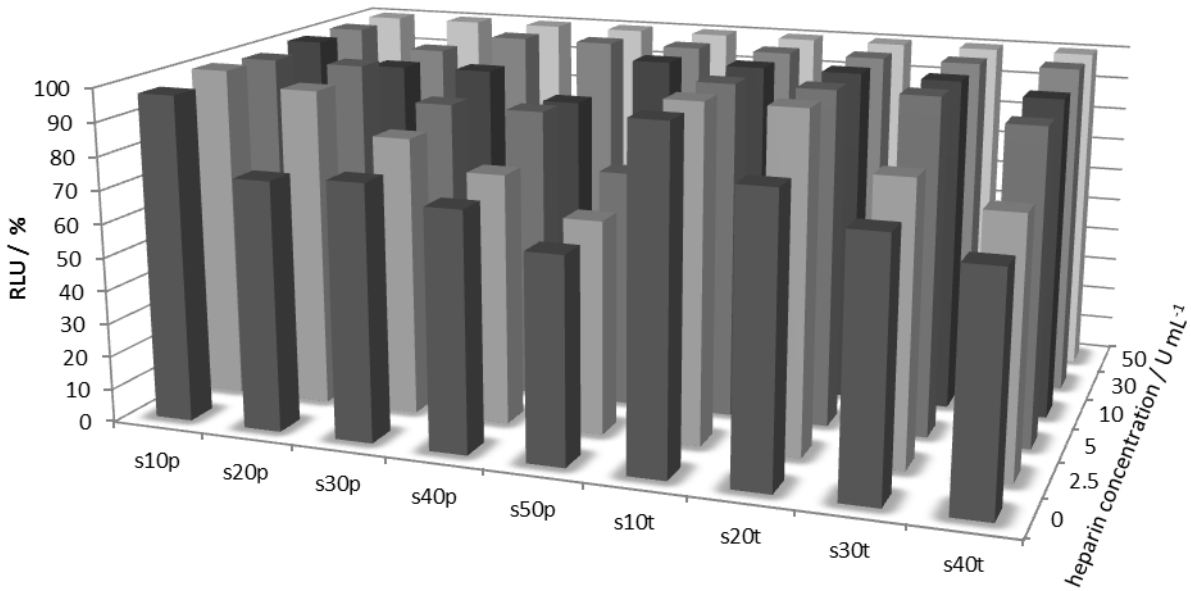

B)

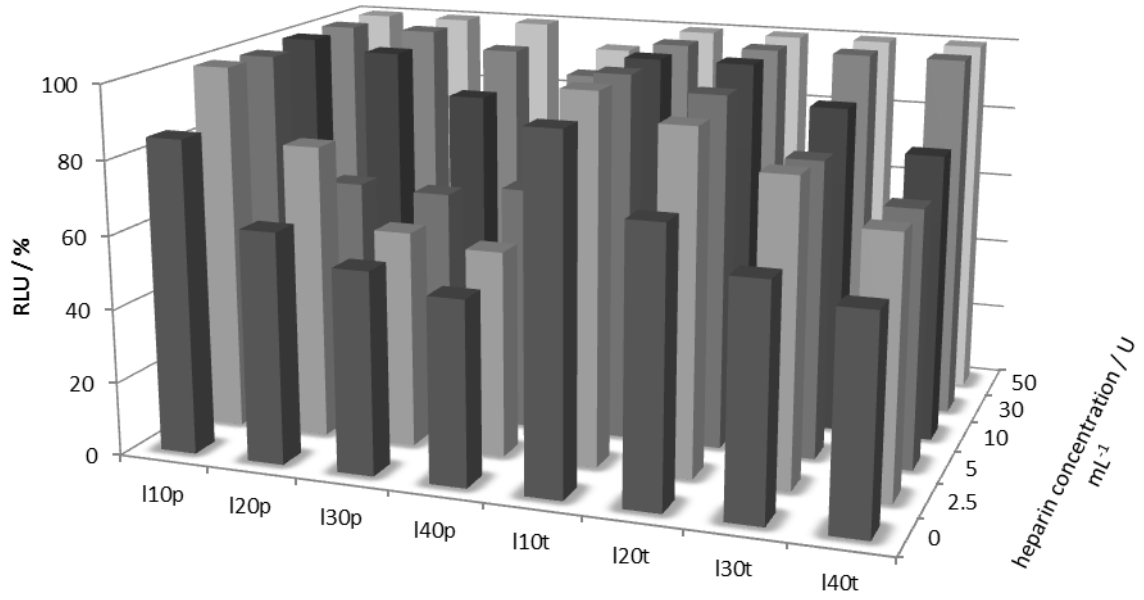

Figure S9. Dissociation assay with the indicated heparin concentration.

Experimental Section

Chemicals and instrumentation

Dry acetonitrile, MeOx and methyl tosylate (MeOTs) were obtained from Acros Organics. ButEnOx[1] and DecEnOx[2] were prepared according to literature procedure. All compounds were distilled to dryness over barium oxide (BaO), and stored under nitrogen. 2-(Boc-amino)ethanethiol and 2-dimethylaminoethanethiol hydrochloride were purchased from Sigma Aldrich.

Ethidium bromide solution 1% was purchased from Carl Roth (Karlsruhe, Germany). AlamarBlue and YOYO-1 was obtained from Life Technologies (Darmstadt, Germany). If not stated otherwise, cell culture materials, cell culture media, and solutions were obtained from PAA (Pasching, Austria). Plasmid pEGFP-N1 (4.7 kb, Clontech, USA) was isolated using Qiagen Giga plasmid Kit (Hilden, Germany). The CytoTox-One homogenous membrane integrity assay (LDH) was purchased from Promega (Mannheim, Germany) All other chemicals were purchased from Sigma Aldrich (Steinhausen, Germany) and are of analytical grade or better and used without further purification.

The Initiator Sixty single-mode microwave synthesizer from Biotage, equipped with a noninvasive IR sensor (accuracy: ±2%), was used for polymerizations microwave irradiation. Prior to use, the microwave vials were heated to 110 °C overnight and allowed to cool to room temperature under a nitrogen atmosphere. Proton (^{1}H) nuclear magnetic resonance (NMR) spectra were recorded on a Bruker AC 250 MHz at 298 K. Chemical shifts are reported in parts per million (ppm, δ scale) relative to the residual signal of the deuterated solvent. Size exclusion chromatographies (SEC) were measured on an Agilent Technologies 1200 Series gel permeation chromatography system equipped with a G1329A autosampler, a G131A isocratic pump, a G1362A refractive index detector, and both a PSS Gram 30 and a PSS Gram 1000 column placed in series. As eluent a 0.21% LiCl solution in *N,N*-

dimethylacetamide (DMAc) was used at 1 mL min-1 flow rate and a column oven temperature of 40 °C. Molar masses were calculated against poly(styrene).

Gas chromatography (GC) was measured on a Shimadzu GC-2010 VP equipped with an AOC-20s autosampler, an AOC-20i injector, a FID detector, a Restek Rtx-5 column (30 m length, 0.25 mm inner diameter, 0.25 μm film thickness, stationary phase: 5% diphenyl/95% dimethyl polysiloxane), and chloroform as solvent.

Kinetic investigation of the synthesis of P(MeOx-*co*-ButEnOx)

For the kinetic studies, a stock solution containing initiator (MeOTs), monomer (MeOx and ButEnOx), and solvent (acetonitrile) was prepared. The total monomer concentration was adjusted to 2 M with a total monomer to initiator ratio ([M]/[I]) = 100 with 10 mol% of ButEnOx. The stock solution was divided over seven microwave vials and capped under argon. For the calculation of the conversion a t_0 samples was taken. The vials were heated in the microwave synthesizer at 140 °C for different times. After cooling, the reaction was quenched. The monomer conversion was determined GC using the polymerization solvent as internal standard.

Synthesis of P(MeOx-*co*-ButEnOx) (1a-d) and P(MeOx-*co*-DecEnOx) (2a-d)

A solution of initiator (MeOTs), monomers (MeOx, and ButEnOx or DecEnOx), and solvent (acetonitrile) was prepared. The total monomer to initiator ratio was [M]/[I] = 200, with a ButEnOx/DecEnOx amount of 10, 20, 30, and 40 mol%, respectively (corresponding to 20, 40, 60, and 80 repeating units). For MeOx/ButEnOx also a 50 mol% solution was prepared (corresponding to 100 ButEnOx repeating units). The total monomer concentration was adjusted to of 4 M. The solution was heated in a microwave synthesizer for a predetermined time at 140 °C. After cooling to room temperature a sample was taken and the conversion was determined by ^{1}H NMR. The solvent was removed under reduced pressure.

The residue was dissolved in dichloromethane and precipitated into ice-cold diethyl ether. After filtration the polymer was dried at 40 °C for 3 days under reduced pressure.

Thiol-ene functionalization of P(MeOx-*co*-ButEnOx) with 2-(boc-amino)ethanethiol (3a-d)

A 5% solution of P(MeOx-*stat*-ButEnOx), 0.1 mol% 2,2-dimethoxy-2-phenylacetophenone (DMPA) per double bond, and a 10-fold excess per double bond of 2-(boc-amino)ethanethiol in ethanol was prepared. After degassing with nitrogen for 30 min, the reaction mixture was stirred in a UV chamber (λ = 365 nm) overnight, and the polymer was precipitated in ice-cold diethyl ether. After filtration the polymer was dried under reduced pressure for 3 days at 40 °C.

Thiol-ene funtionalization of P(MeOx-*co*-DecEnOx) with 2-(boc-amino)ethanethiol (4a-d)

A 5% solution of P(MeOx-*stat*-DecEnOx), 0.1 mol% 2,2-dimethoxy-2-phenylacetophenone (DMPA) per double bond, and a 10-fold excess per double bond of 2-(boc-amino)ethanethiol in tetrahydrofurane was prepared. After degassing with nitrogen for 30 min, the reaction mixture was stirred in a UV chamber (λ = 365 nm) overnight, and the polymer was precipitated in ice-cold diethyl ether. After filtration the polymer was dried under reduced pressure for 3 days at 40 °C.

Deprotection of P(MeOx-*co*-bocAmButEnOx) (sNp) and P(MeOx-*co*-bocAmDecEnOx) (lNp)

The polymer dissolved in dichloromethane (3 mL). Trifluoracetic acid was added (5 mL) and the reaction mixture was stirred overnight at room temperature. After the addition of methanol, the polymer was precipitated in ice-cold diethyl ether. The precipitate was filtered,

dissolved in methanol and stirred over night with Amberlyst® A21 (free base). The solvent was removed and polymer dried at 40 °C under reduced pressure for 3 days.

Thiol-ene funtionalization of P(MeOx-*co*-ButEnOx) (sNt) and P(MeOx-*co*-DecEnOx) (lNt) with 2-dimethylaminoethanethiol hydrochloride

A 5% solution of P(MeOx-*stat*-ButEnOx) or P(MeOx-*stat*-DecEnOx), respectively, 0.1 mol% 2,2-dimethoxy-2-phenylacetophenone (DMPA) per double bond, and a 10-fold excess per double bond of 2-dimethylaminoethanethiol hydrochloride in methanol was prepared. After degassing with nitrogen for 30 min, the reaction mixture was stirred in a UV chamber (λ = 365 nm) overnight. The reaction mixture was concentrated and purified by size exclusion chromatography using Sephadex® LH-20 running with methanol. The product was dried at 40 °C for 3 days.

Thiol-ene funtionalization of P(MeOx-co-ButEnOx) with 6-amino-1-hexanethiol hydrochloride (s40hp)

A 5% solution of P(MeOx-*stat*-ButEnOx) (**1d**), 0.1 mol% 2,2-dimethoxy-2-phenylacetophenone (DMPA) per double bond, and a 2-fold excess per double bond in methanol was prepared. After degassing with nitrogen for 30 min, the reaction mixture was stirred in a UV chamber (λ = 365 nm) overnight. The reaction mixture was concentrated and purified by size exclusion chromatography using Sephadex® LH-20 running with methanol. The product was dried at 40 °C for 3 days.

Polyplex preparation

Polyplexes of pDNA and polymers were prepared by mixing stock solutions of pDNA and polymers at a certain N/P ratio (nitrogen of polymer to phosphate of pDNA ratio) with 15 µg mL^{-1} pDNA solution in HBG buffer (20 mM 4-(2-hydroxethyl) piperazine-1-ethanesulfonic

acid (HEPES) and 5% (w/v) glucose, pH 7.2). Subsequently, the solutions were vortexed for 10 sec at maximal speed, and incubated at room temperature for 20 min.

Ethidium bromide quenching assay

The polyplex formation of pDNA and polymers was detected by quenching of the ethidium bromide (EB) fluorescence as described previously.[3] Briefly, 15 µg mL^{-1} pDNA in a total volume of 100 µL HBG (hepes buffered glucose) were incubated with EB (0.4 µg mL^{-1}) for 10 min at room temperature. Then, polyplexes with increasing amounts of indicated polymers were prepared in black 96-well plates (Nunc, Langenselbold, Germany). The samples were equilibrated for 10 min before the fluorescence was measured using a Tecan Genios Pro fluorescence microplate reader (Tecan, Crailsheim, Germany); the excitation and emission wavelength were 525 and 605 nm, respectively. A sample containing only pDNA and EB was used to calibrate the device to 100% fluorescence against a background of 0.4 µg mL^{-1} of EB in HBG solution. The percentage of dye displaced upon polyplex formation was calculated using equation (1):

$$\text{RFU}\,[\%] = \frac{F_{sample} - F_0}{F_{pDNA} - F_0} \qquad (1)$$

Here, RFU is the relative fluorescence and F_{sample}, F_0, and F_{pDNA} are the fluorescence intensities of a given sample, the EB in HBG alone, and the EB intercalated into pDNA alone.

Cytotoxicity

The cytotoxicity was tested with L929 cells, as this sensitive cell line is recommended by ISO10993-5. In detail, cells were seeded at 10^4 cells per well in a 96-well plate and incubated for 24 h. No cells were seeded in the outer wells. After exchanging the media with fresh one and 30 min incubation, polymers at the indicated end concentrations were added, and the cells were incubated at 37 °C for further 24 h. Subsequently, the medium was replaced by fresh

media and AlamarBlue as recommended by the supplier. After incubation for 4 h, the fluorescence was measured at Ex 570/Em 610 nm, with untreated cells on the same well plate serving as controls. The experiments were performed independently three times.

Dynamic and electrophoretic light scattering

Dynamic light scattering (DLS) was performed on an ALV-CGS-3 system (ALV, Langen, Germany) equipped with a He-Ne laser operating at a wavelength of $\lambda = 633$ nm. The counts were detected at an angle of 90°. All measurements were carried out at 25 °C after an equilibration time of 120 sec. For analyzing the autocorrelation function (ACF), the CONTIN algorithm[4] was applied. Apparent hydrodynamic radii were calculated according to the Stokes–Einstein equation.

Electrophoretic light scattering was used to measure the electrokinetic potential, also known as zeta potential. The measurements were performed on a Zetasizer Nano ZS (Malvern Instruments, Herrenberg, Germany) by applying laser Doppler velocimetry.[5] For each measurement, 20 runs were carried out using the slow-field reversal and fast-field reversal mode at 150 V. Each experiment was performed in triplicate at 25 °C. The zeta potential (ζ) was calculated from the electrophoretic mobility (μ) according to the Henry Equation. Henry coefficient f(ka) was calculated according to Oshima.[6]

Transfection of adherent cells

HEK-293 cells (CRL-1573, ATCC) cells were maintained in RPMI 1640 culture medium, L929 cells (CCL-1, ATCC) in DMEM culture medium. Both media were supplemented with 10% fetal calf serum (FCS), 100 µg mL^{-1} streptomycin, 100 IU mL^{-1} penicillin, and 2 mM L-glutamine. Cells were cultivated at 37 °C in a humidified 5% CO_2 atmosphere.

For transfection of the adherent cell lines, cells were seeded at a density of 10^4 cells per well in 24-well plates one day before transfection. One hour prior to transfection, cells were

rinsed with PBS and supplemented with 1 mL OptiMEM (Life Technologies) or fresh serum containing growth media (without antibiotics). After polyplexes formation (as described above), the polyplexes (100 µL) were added to the cells and the plates were incubated for 4 h in the incubator. Afterwards, the supernatant was replaced by1 mL of fresh growth medium, and the cells were further incubated for 20 h. For analysis, adherent cells were harvested by trypsinization.

For determination of the viability during flow cytometry, dead cells were identified via counterstaining with propidium iodide. The relative expression of EGFP fluorescence of 10^4 cells was quantified via flow cytometry using a Cytomics FC 500 (Beckman Coulter). For determination of the transfection efficiency viable cells expressing EGFP were gated. The experiments were performed independently three times.

Hemolysis assay

The membrane damaging properties of the polymers were quantified by analyzing the release of hemoglobin from human erythrocytes. The hemolysis assay was performed as described before.[7] Briefly, blood from sheep was centrifuged at 4.500 × g for 5 min and the pellet was washed three times with cold DPBS. The stock solutions were diluted in HBG of indicated pH, and polymer solutions were prepared in HBG buffer as well. 100 µL of each solution were mixed and further incubated for 60 min at 37 °C. The release of hemoglobin in the supernatant was determined at 580 nm after centrifugation (2,400 g for 5 min). The absorbance was measured using a plate reader (Genios Pro, Tecan, Germany). For comparison, collected erythrocytes were washed with DPBS and either lysed with 1% Triton X-100 yielding the 100% lysis control value (A_{100}) or resuspended in DPBS as reference (A_0). The analysis was repeated with blood from at least six independent donors. The hemolytic activity of the polycations was calculated as follow (2):

$$\% \text{ Hemolysis} = 100 * \frac{(A_{sample} - A_0)}{(A_{100} - A_0)} \quad (2)$$

Here, A_{sample}, A_0, and A_{100} are the absorbance intensities of a given sample, erythrocytes incubated with DPBS, and erythrocytes lysed with Titon X-100.

Lactate dehydrogenase (LDH) assay

For the LDH assay the CytoTox-ONE homogenouse membrane integrity assay was used. The assay was performed as recommended by the supplier. The samples (polymer as well as polyplexes) were incubated for 1 h with adHEK cells.

Plasmid DNA labeling

For labeling of a 1 µg pDNA, 0.026 µL of 1M YOYO-1 solution was mixed with pDNA in 20 µL of pure water. The solution was incubated for 1 h at room temperature protected from light, before HBG was added to the used pDNA concentration described before. Polymers were added at the indicated N/P ratio, and the polyplex solution was treated as described before and added to the cells. After the indicated time points of incubation, the cells were harvested and 10% trypan blue was added to quench the outer fluorescence of cells and identify only those cells, which have taken up the genetic material. To determine the relative uptake of NPs, 10,000 cells were measured by flow cytometry and the amount of viable cells showing YOYO-1 signal were gated. For measuring the mean fluorescence intensity, all viable cells were measured.

Heparin dissociation assay

To investigate the release of pDNA from polyplexes, the heparin dissociation assay was used. For this purpose, 15 µg mL^{-1} pDNA were incubated for 10 min with EB (0.4 µg mL^{-1}) in a total volume of 100 µL HBG before polyplexes at N/P 20 were formed. After 15 min in the dark the polyplexes were transferred into black 96-well plates, and heparin was added at the indicated concentrations. The solution was mixed and incubated for further 30 min at 37 °C in the dark. The fluorescence of EB (Ex 525 nm / Em 605 nm) was measured, and the percentage of intercalated EB was calculated as described before (1).

Statistical analysis

The values represent the mean ± SD. For the calculation of the standard derivation of two different groups the two sample t-test (student's t-test) was used. Statistical significant was defined with p-values of < 0,05.

References

[1] A. Gress, A. Völkel, H. Schlaad, *Macromolecules* **2007**, *40*, 7928.

[2] K. Kempe, A. Vollrath, H. W. Schaefer, T. G. Poehlmann, C. Biskup, R. Hoogenboom, S. Hornig, U. S. Schubert, *Macromol. Rapid Commun.* **2010**, *31*, 1869.

[3] A. Schallon, C. V. Synatschke, D. V. Pergushov, V. Jerome, A. H. E. Müller, R. Freitag, *Langmuir* **2011**, *27*, 12042.

[4] S. W. Provencher, *Comput. Phys. Commun.* **1982**, *27*, 229.

[5] A. V. Delgado, F. Gonzalez-Caballero, R. J. Hunter, L. K. Koopal, J. Lyklema, *J. Colloid Interface Sci.* **2007**, *309*, 194.

[6] H. Ohshima, *J. Colloid Interf. Sci.* **1994**, *168*, 269.

[7] A. Vollrath, D. Pretzel, C. Pietsch, I. Perevyazko, S. Schubert, G. M. Pavlov, U. S. Schubert, *Macromol. Rapid Commun.* **2012**.

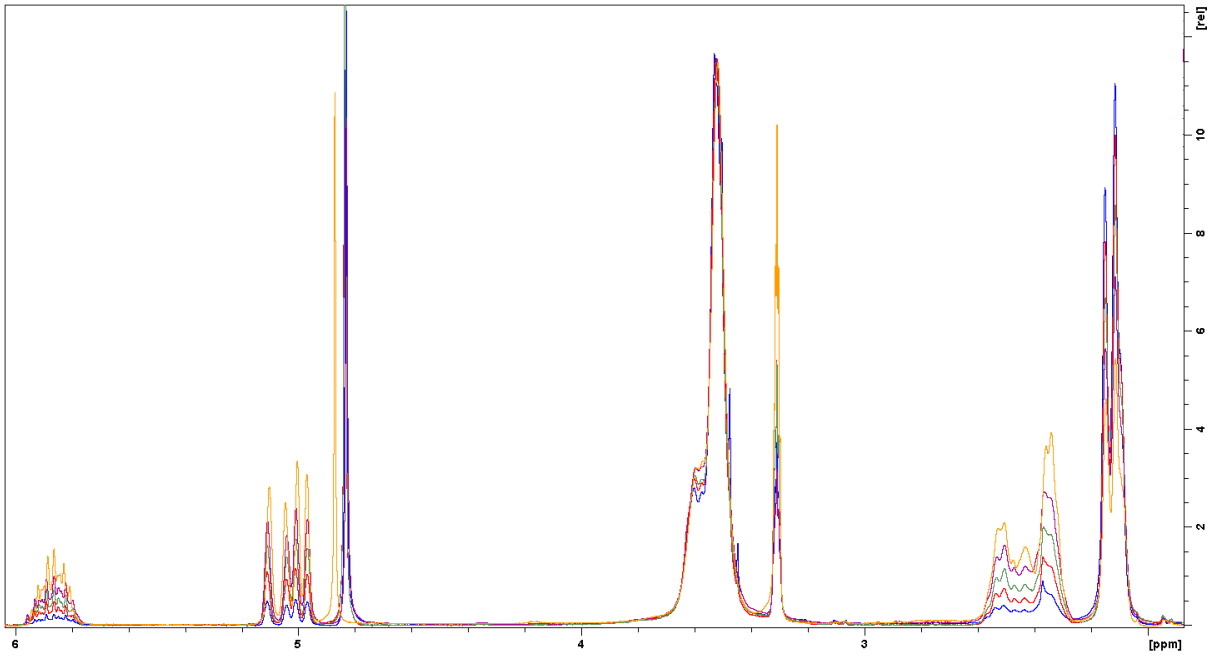

Figure S10. Overlay of the ^{1}H NMR spectra of **1a** (blue), **1b** (red), **1c** (green), **1d** (purple), and **1e** (orange). The signal intensities of the spectra were normalized to the peak of the polymer backbone signal at around 3.5 ppm (250 MHz, solvent: CD_3OD).

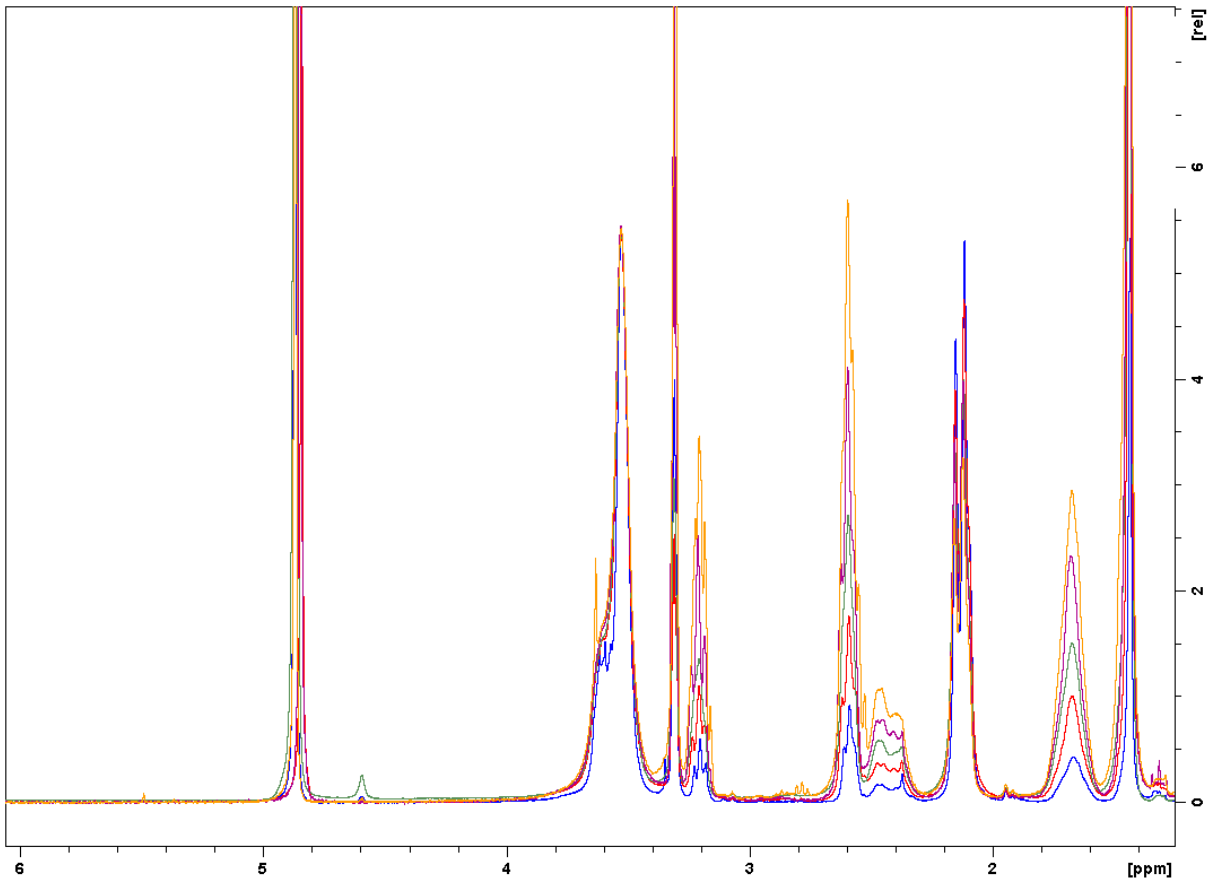

Figure S11. Overlay of the ^{1}H NMR spectra of **3a** (blue), **3b** (red), **3c** (green), **3d** (purple), and **3e** (orange). The signal intensities of the spectra were normalized to the peak of the polymer backbone signal at around 3.5 ppm (250 MHz, solvent: CD_3OD).

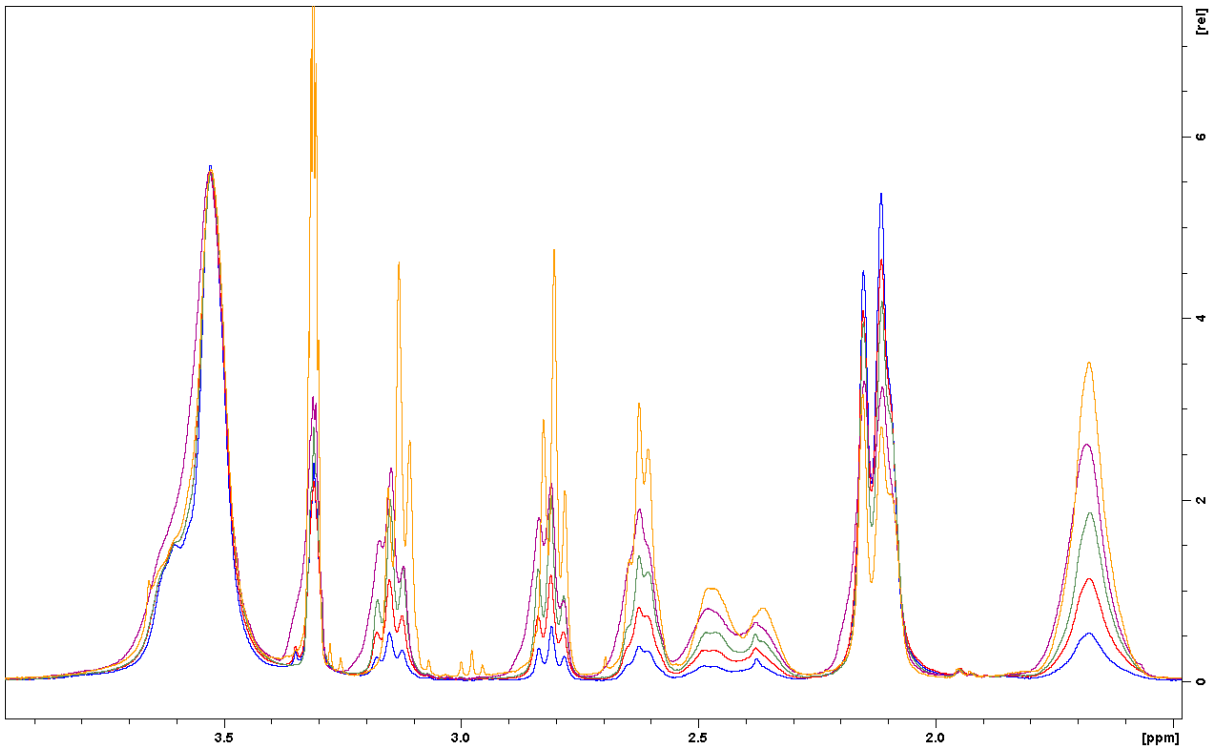

Figure S12. Overlay of the ^{1}H NMR spectra of **s10p** (blue), **s20p** (red), **s30p** (green), **s40p** (purple), and **s50p** (orange). The signal intensities of the spectra were normalized to the peak of the polymer backbone signal at around 3.5 ppm (250 MHz, solvent: CD_3OD).

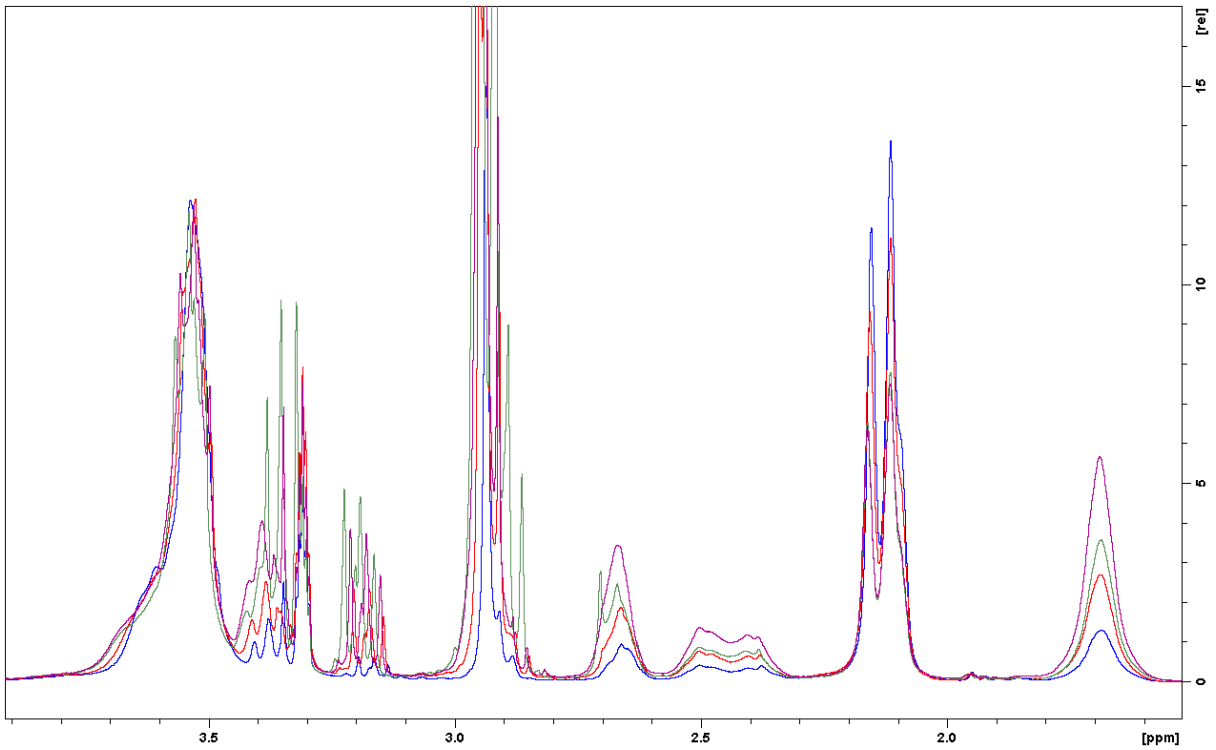

Figure S13. Overlay of the ^{1}H NMR spectra of **s10t** (blue), **s20tp** (red), **s30t** (green), and **s40t** (purple). The signal intensities of the spectra were normalized to the peak of the polymer backbone signal at around 3.5 ppm (250 MHz, solvent: CD_3OD).

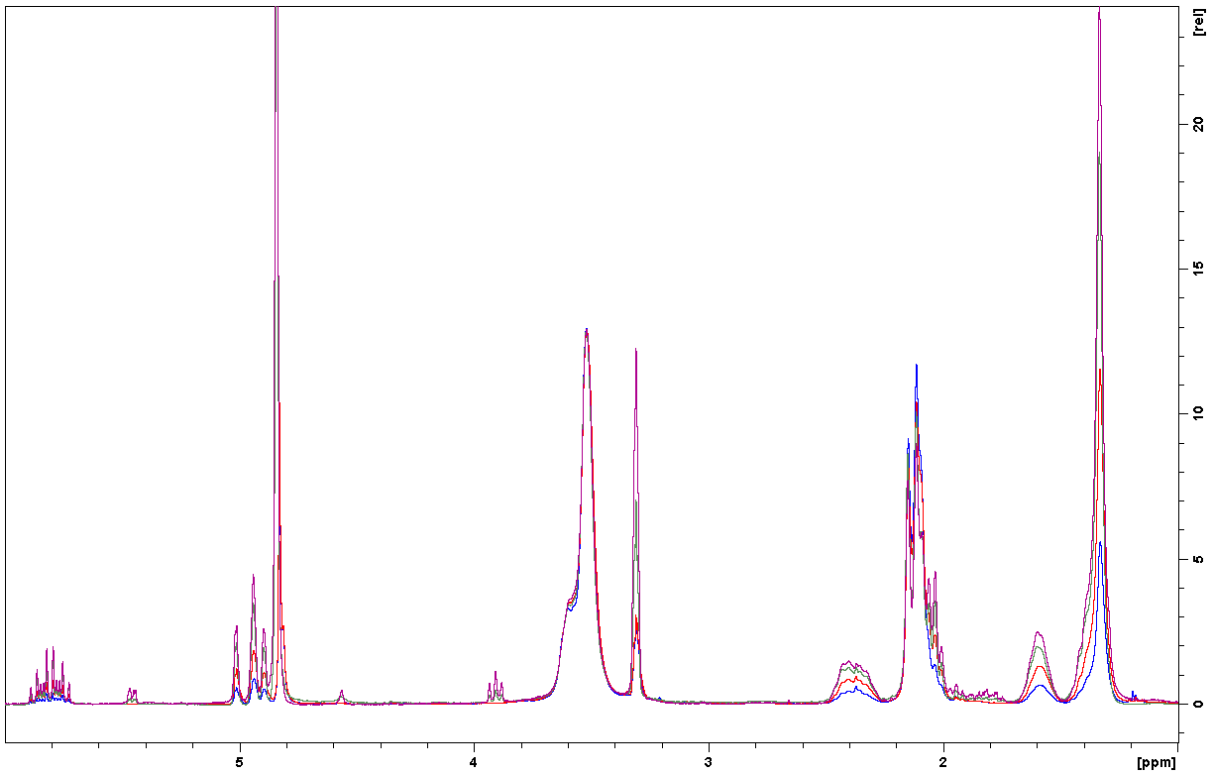

Figure S14. Overlay of the ^{1}H NMR spectra of **2a** (blue), **2b** (red), **2c** (green), and **2d** (purple). The signal intensities of the spectra were normalized to the peak of the polymer backbone signal at around 3.5 ppm (250 MHz, solvent: CD_3OD).

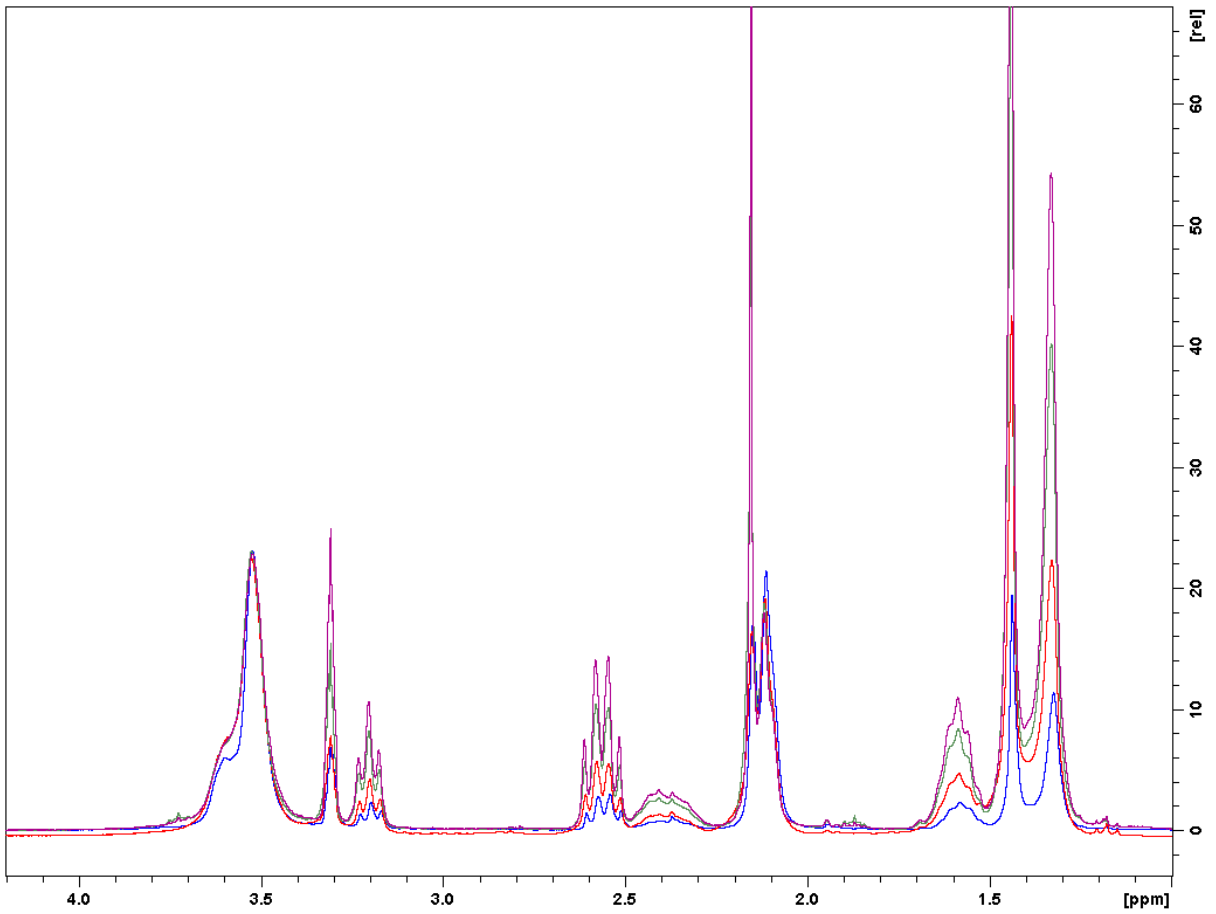

Figure S15. Overlay of the ^{1}H NMR spectra of **4a** (blue), **4b** (red), **2c** (green), and **4d** (purple). The signal intensities of the spectra were normalized to the peak of the polymer backbone signal at around 3.5 ppm (250 MHz, solvent: CD_3OD).

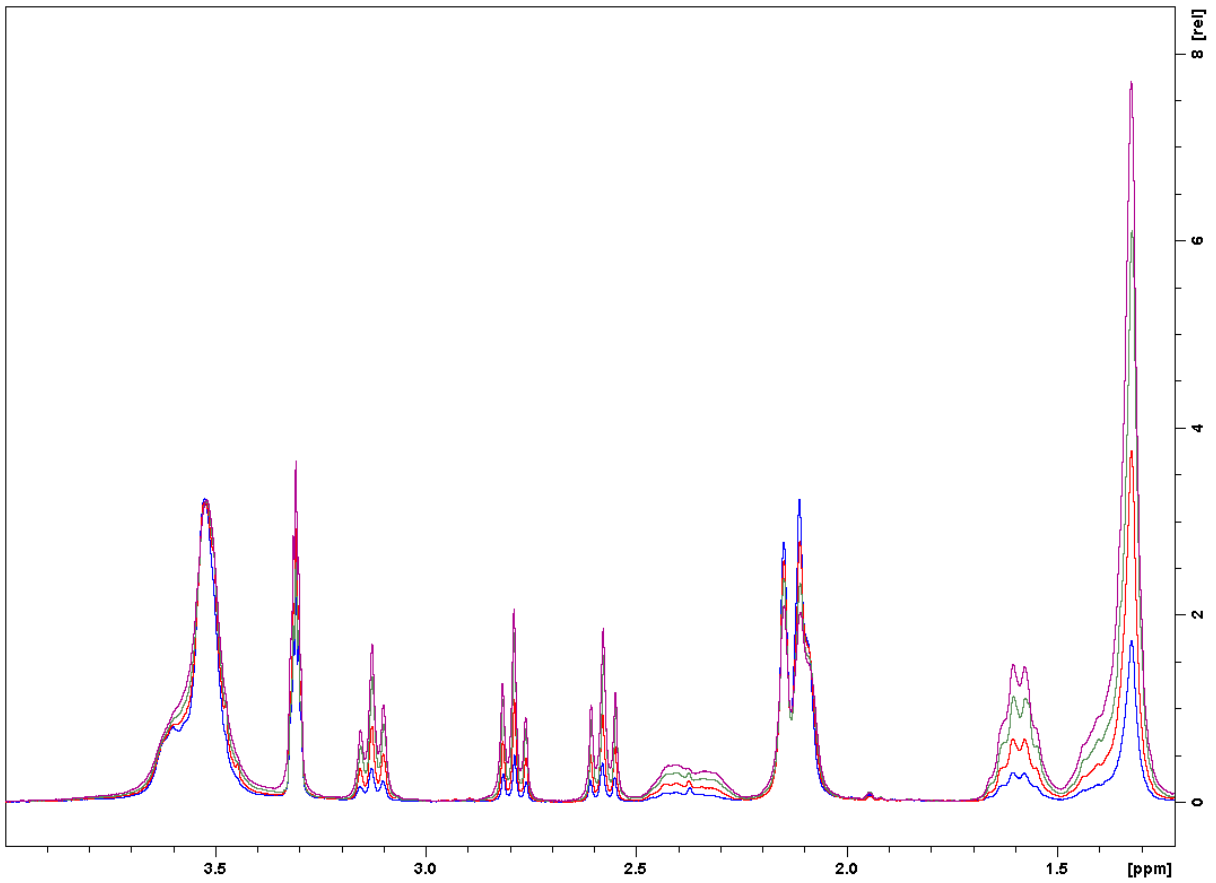

Figure S16. Overlay of the ^{1}H NMR spectra of **l10p** (blue), **l20p** (red), **l30p** (green), and **l40p** (purple). The signal intensities of the spectra were normalized to the peak of the polymer backbone signal at around 3.5 ppm (250 MHz, solvent: CD_3OD).

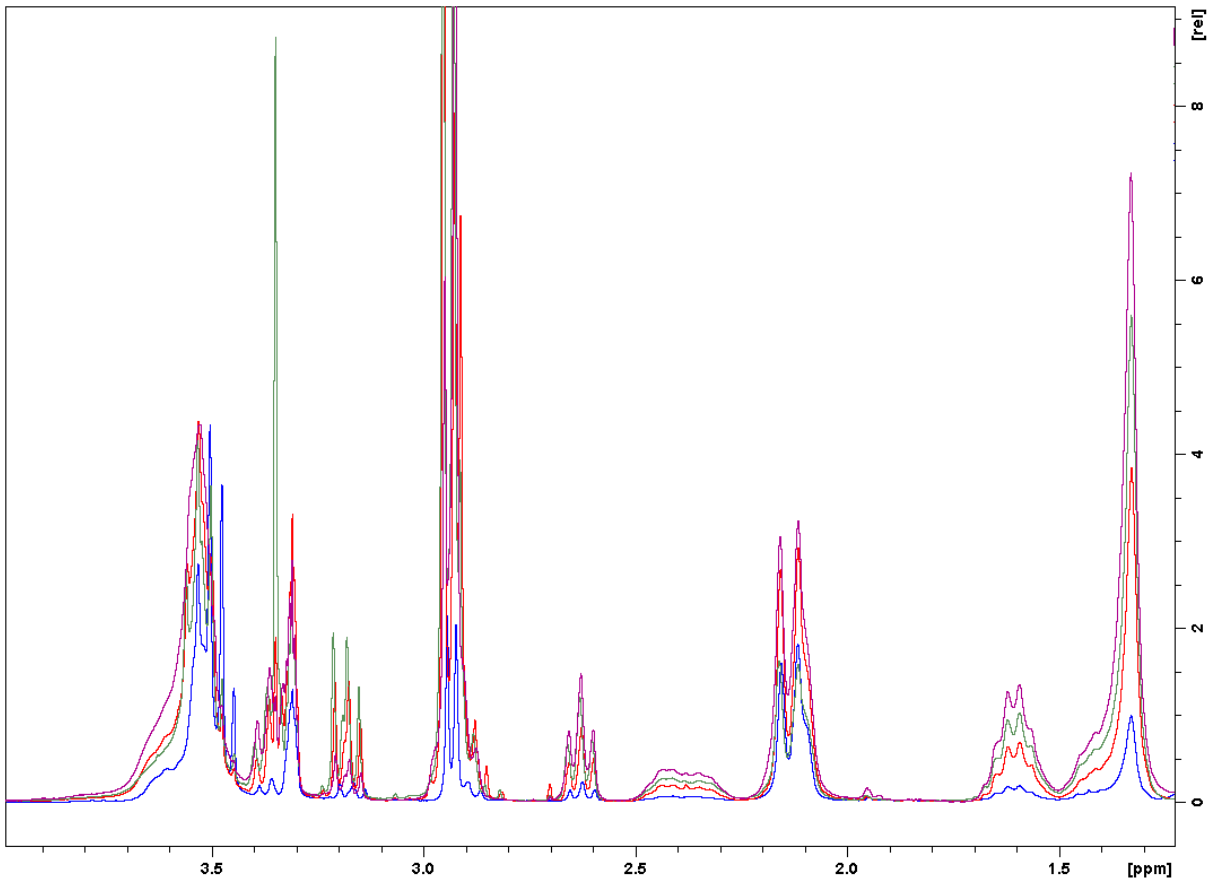

Figure S17. Overlay of the ^{1}H NMR spectra of **l10t** (blue), **l20t** (red), **l30t** (green), and **l40t** (purple). The signal intensities of the spectra were normalized to the peak of the polymer backbone signal at around 3.5 ppm (250 MHz, solvent: CD_3OD).

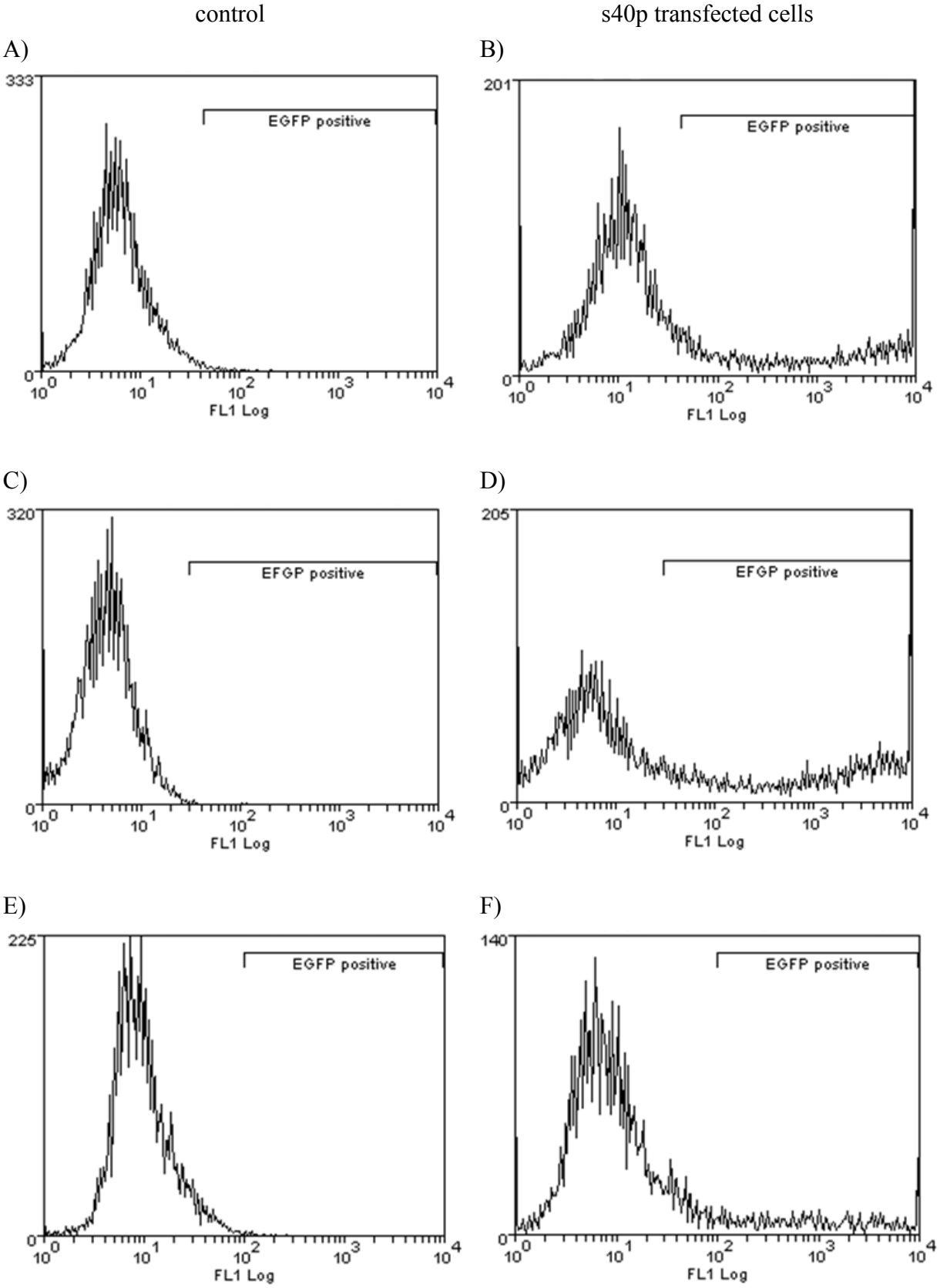

Figure S18. Histograms of non-transfected cells (A, C, E) and the corresponding HEK cell transfected with s40p (B, D, F) (NP 20). FL1 represents green fluorescence by EGFP expression.

Table S6. Mean fluorescence intensities (MFI) of non-transfected cells (control cells) and corresponding HEK cells transfected with s40p or lPEI (NP20). The values represent the MFI of the gated EGFP positive area (s. Figure S18).

	MFI control cells	MFI transfected cells s40p	MFI transfected cells lPEI
Sample A, B	0,682	381	389
Sample C, D	4,37	317	297
Sample D, E	11,3	226	257

Publication P4

Parallel high-throughput screening of polymer vectors for nonviral gene delivery: evaluation of structure-property relationships of transfection

A. C. Rinkenauer, A. Vollrath, A. Schallon, L. Tahuhardt, K. Kempe, S. Schubert, D. Fischer,

U. S. Schubert

ACS Comb. Sci. **2013**, *15*, 475-482.

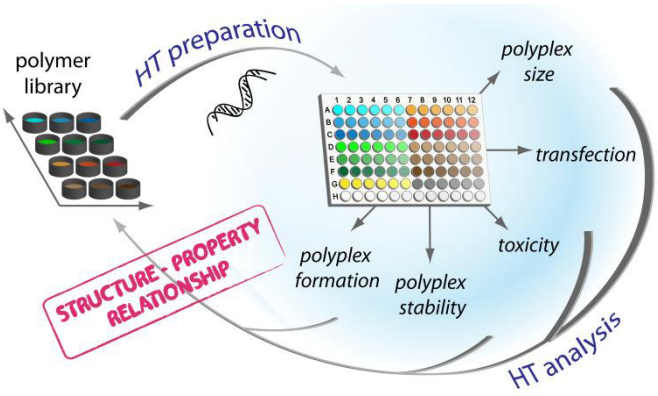

ACS Combinatorial Science

Research Article

pubs.acs.org/acscombsci

Parallel High-Throughput Screening of Polymer Vectors for Nonviral Gene Delivery: Evaluation of Structure–Property Relationships of Transfection

Alexandra C. Rinkenauer,[†,‡] Antje Vollrath,[†,‡] Anja Schallon,[†,‡] Lutz Tauhardt,[†,‡] Kristian Kempe,[†,‡] Stephanie Schubert,[‡,§] Dagmar Fischer,[§] and Ulrich S. Schubert*[,†,‡,∥]

[†]Laboratory of Organic and Macromolecular Chemistry (IOMC), Friedrich Schiller University Jena, Humboldtstraße 10, 07743 Jena, Germany

[‡]Jena Center for Soft Matter (JCSM), Friedrich Schiller University Jena, Philosophenweg 7, 07743 Jena, Germany

[§]Institute of Pharmacy, Department of Pharmaceutical Technology, Friedrich Schiller University Jena, Otto-Schott-Straße 41, 07745 Jena, Germany

[∥]Dutch Polymer Institute, P.O. Box 902, 5600 AX Eindhoven, the Netherlands

Supporting Information

ABSTRACT: In recent years, "high-throughput" (HT) has turned into a keyword in polymer research. In this study, we present a novel HT workflow for the investigation of cationic polymers for gene delivery applications. For this purpose, various poly(ethylene imine)s (PEI) were used as representative vectors and investigated via HT-assays in a 96-well plate format, starting from polyplex preparation up to the examination of the transfection process. In detail, automated polyplex preparation, complex size determination, DNA binding affinity, polyplex stability, cytotoxicity, and transfection efficiency were performed in the well plate format. With standard techniques, investigation of the biological properties of polymers is quite time-consuming, so only a limited number of materials and conditions (such as pH, buffer composition, and concentration) can be examined. The approach described here allows many different polymers and parameters to be tested for transfection properties and cytotoxicity, giving faster insights into structure–activity relationships for biological activity.

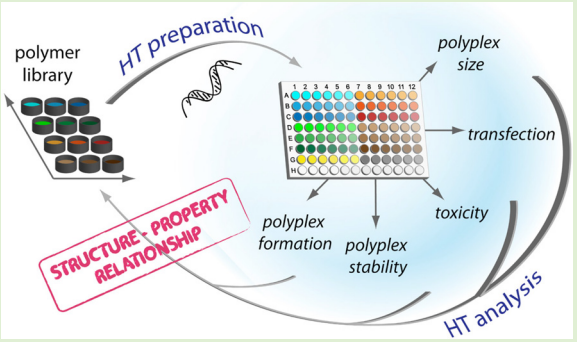

KEYWORDS: *high-throughput screening, transfection, nonviral gene delivery, polyplex stability, poly(ethylene imine), heparin, combinatorial workflow*

INTRODUCTION

Nonviral gene delivery (transfection) methods are of great interest for research and clinical applications. The use of cationic polymers as nonviral vectors to form complexes (polyplexes) with negatively charged plasmid DNA (pDNA) has long been explored as a safer and more controllable alternative to the use of possible infectious viral vectors.[1,2] For the evaluation of polymers as transfection agents, two main aspects must be considered: the efficiency of gene delivery with subsequent reporter gene expression and cytotoxicity.[3] Biophysical properties, such as polyplex size, surface charge, and binding affinity between the polymer and the genetic material play crucial roles in the required cellular uptake.[4,5] The binding within the interelectrolyte complex of polymer and pDNA has to be strong enough to protect the pDNA but must be reversible to release the pDNA inside the cells.[6,7] While much progress has been made, there is still an insufficient knowledge of how polymers should be constructed to be highly efficient and safe gene delivery vectors.[8,9]

This lack of predictability results in part from the great diversity of polymer classes and methods reported in the literature, which are difficult to compare to each other. For instance, transfection protocols differ notably for different cells and media, and different polymer solutions and buffers are used in the preparation of polyplexes.[10,11] While some examples have been used for in vitro applications and biotechnology research for decades, no polymer-based transfection agent has been approved for clinical use.[12−14]

The development of robotic techniques for the preparation of polymeric materials provides an opportunity for the high-throughput (HT) synthesis and characterization of cationic polymers in this context.[15−20] Using this synthetic approach, polymer properties such as molar mass, functional groups, architecture, and the combination of different monomers in

Received: February 21, 2013
Revised: June 20, 2013
Published: July 25, 2013

Scheme 1. Workflow of the High-Throughput Transfection Studies for Structure−Property Evaluations Concerning Molar Ratio, Size, Polyplex Formation, Polyplex Stability, Release, Transfection Efficiency, and Cytotoxicity

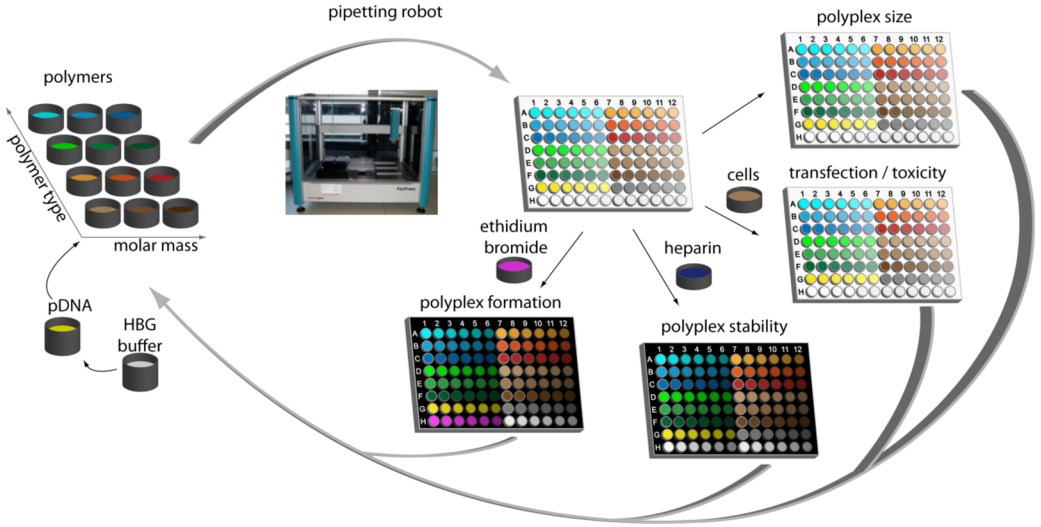

statistic or block copolymers can be altered, yielding systematic polymer libraries, which enable the elucidation of structure−property relationships.[15−23] Unfortunately, rapid methods for biological evaluation have not been hyphenated with efficient automated synthesis to construct a combinatorial HT workflow.[24−27] For example, binding affinity and polyplex stability have commonly been assessed by agarose gel electrophoresis, which is not well suited to HT screening. The use of an intercalating dye to establish binding affinities can provide an alternative compatible with a microtiter plate format.[28] Transfection and cytotoxicity assays can be similarly performed in multiwell plates with repeating samples to reduce measurement mistakes. Pioneers in this type of HT screening of a wide range of polymers as transfection agents have been Langer and co-workers (synthesis and transfection efficiency)[29] and Massing and co-workers (lipofection transfection efficiency and toxicity).[30]

We describe here a simple and powerful combinatorial high-throughput workflow that combines polyplex formation and biological screening (Scheme 1). It starts with the automated polyplex preparation via pipetting robots and continues with a parallel and HT analysis of analytical and biological properties of size, binding affinity, stability, transfection efficiency, and toxicity. We show that the novel workflow is applicable to a variety of polymer systems and conditions, allowing for fast and efficient screening of important vector parameters, such as polyplex formation, pDNA release, cytotoxicity, and transfection.

RESULTS AND DISCUSSION

Poly(ethylene imine) (PEI), the most prominent cationic polymer and most efficient transfection agent for pDNA in vitro, was used to validate the method.[31,14] Linear PEI (LPEI), obtained from poly(2-ethyl-2-oxazoline)s of different molar masses, was prepared.[32,33] By application of automated microwave synthesizers, poly(2-ethyl-2-oxazoline)s can be obtained within 10 min and converted into PEI within 1 h by acidic hydrolysis.[32] These cationic PEI polymers offer the advantage to be molecularly designed in a highly reproducible manner for specific applications in pharmacy or biotechnology. Commercially available branched PEI (BPEI) materials were also used in this study.

Evaluation of an Appropriate Buffer System. The formation of polyplexes from cationic polymers and anionic genetic material is driven by electrostatic interactions and a gain of entropy.[34] Thus, ionic strength, pH, and the final polyplex concentration have a major impact on the complexation behavior and the resulting polyplex size.[35,36] For the ex cellular characterization, polyplexes are often prepared in high ionic strength buffers, such as 150 mM sodium chloride (NaCl) or buffer systems using phosphate (PBS) or TRIS (TBS). Such high ionic strength media can have a negative impact on particle size and stability and lead to fast polyplex aggregation.[36,37] Thus, a low ionic strength 20 mM HEPES buffer with 5% glucose for physiological osmolarity (HBG buffer) was examined for polyplex preparation in a HT manner, as has been previously done for transfection.[37] Preliminary studies with linear PEI_{600} revealed that smaller polyplexes were formed in HBG.[35] A lower tendency to aggregate over time compared to physiological salt solutions (150 mM NaCl) was observed if the polyplexes were prepared in HBG.[38−40] Our measurements showed $LPEI_{600}$ polyplexes to exhibit no aggregation over 2 h in HBG (see Supporting Information), no aggregation or particle growth before and after the addition to serum containing culture media.[36−38] Furthermore, HBG buffer can be used for zeta potential measurements[41] in this concentration range as well as for electron microscopic evaluations, where salts cause electrophoresis or artifacts, respectively. Consequently, HBG was selected as most appropriate buffer system for HT studies and was used here for all polyplex preparations and analytical investigations.

Polyplex Preparation Using Pipetting Robots. A standard liquid handling robot was used for automated preparation of polyplexes from cationic polymers and DNA, similar to reports of robotic production of polymeric nanoparticles.[42] The benefit of such pipetting systems is the ability to systematically alter different parameters, such as polymer concentration, pH, or buffer composition.[43] Automated deposition of a buffered pDNA solution into wells containing various buffered cationic polymer solutions at desired concentrations was performed. While the reverse

dx.doi.org/10.1021/co400025u | ACS Comb. Sci. 2013, 15, 475−482

addition (pipetting polymer to DNA solution, vortexing after polymer addition) is the more conventional method,[1] giving better transfection results,[44] we observed similar outcomes in preliminary experiments using $LPEI_{600}$ and $BPEI_{600}$ (see Supporting Information) and in scattered tests of the HT method (data not shown). This may be due to more reversible interelectrolyte formation in the low ionic strength HBG buffer compared to high ionic strength buffers used previously.

To evaluate the dependence of polyplex properties on the nature of the polymers and preparation conditions, various cationic LPEI and BEI with varied degree of polymerization (DP = 20, 200, and 600) were used to form polyplexes with pDNA. Besides the molar mass and architecture, several nitrogen (polymer) to phosphate (DNA) ratios (N/P = 2.5, 5, 10, and 20) were applied. To this end, pDNA solution was added to a dilution series of polymer solutions, and the resulting suspensions were directly mixed by repetitive suction and release. After polyplex formation, the prepared suspensions were distributed automatically into different well plates for parallel analysis studies.

Investigation of Polyplex Size and Stability. The polyplex size allows a first hint of the polymer's capability to be used as a transfection agent, since polyplexes larger than 500 nm are known to show relatively poor uptake.[45] For this purpose, the polyplexes were first analyzed on a dynamic light scattering (DLS) plate reader.[46] As shown in Figure 1, all

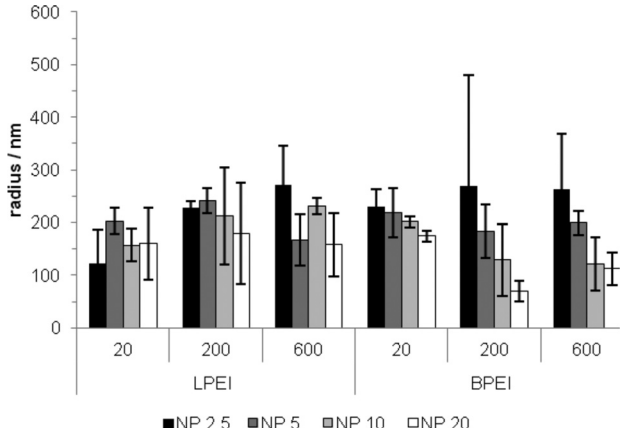

Figure 1. Hydrodynamic radii of polyplexes prepared using the pipetting robot. The values represent the mean ($n \geq 3$) of each polymer at different N/P ratios. PDI^P values of 0.09 to 0.5 were found.

polyplexes exhibited an average radius of less than 270 nm, with materials mixed at N/P ratios above 5 showing smaller radii. The smallest size (70 nm radius) was obtained for $BPEI_{200}$. It should be noted that the HT-DLS analysis data tended to report larger radii than measurements performed with a single-beam DLS instrument (see Supporting Information). HT-DLS results should be always considered with care, and we consider them informative only in a relative sense, to establish the potential of polymers to form nanoscaled polyplexes and gain information about their stability in comparison to standard polymer controls. Our data revealed three tendencies, also described in the literature: (i) increasing N/P ratios gave rise to smaller polyplexes, (ii) BPEI with higher DPs showed a stronger size dependency compared to LPEI, and (iii) BPEI condensed DNA into smaller particles compared to LPEI.[31] Interestingly, no systematic influence of the degree of polymerization or the molar mass on polyplex size was observed under the chosen conditions.

Fluorescence Displacement Assay. Considering the interpretation of transfection results the determination of the binding affinity of the polymers to the genetic material is of vital importance. As previously mentioned, the binding of a polyplex is at its optimal state when having a strong and reversible interaction. The required N/P ratio to form polyplexes were either done by usage of gel retardation assays or by fluorescence measurement of intercalating dyes, such as ethidium bromide (EB) or Pico Green. For an HT screening application, the gel retardation method is not suitable in a 96-well plate format, thus, the fluorescence displacement assay with EB (EBA) was chosen. Commonly, the binding of EB with pure pDNA leads to a high fluorescence signal. However, provided that the pDNA forms interelectrolyte complexes with the polymers, the displacement of dyes leads to a decrease of fluorescence signals. In Figure 2, the fluorescence signals

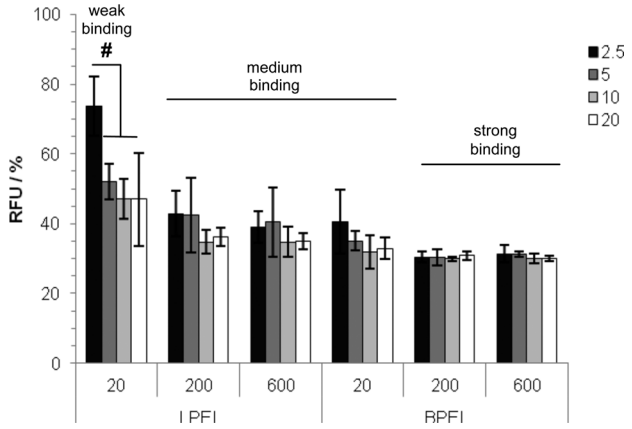

Figure 2. Fluorescence displacement assay using LPEI and BPEI with varying DP. The RFU of pure pDNA represent 100% RFU. N/P ratios of 2.5 up to 20 were studied using EB as intercalating agent. The values represent the mean ± S.D., $n \geq 3$, # indicate significant statistical difference (ANOVA, $p < 0.05$).

(RFU) of all PEI polymers with increasing N/P ratio are illustrated. It was found that $BPEI_{200}$ and $BPEI_{600}$ reached a comparable RFU of around 30.5 ± 1.4% ($p > 0.5$) indicating a strong DNA binding. Furthermore, the higher molar mass LPEIs ($LPEI_{200}$ and $LPEI_{600}$) along with $BPEI_{20}$ revealed comparable RFUs in the range of 37.1 ± 6.2% ($p > 0.1$). The weakest binding was obtained with $LPEI_{20}$ also showing the strong dependence of N/P. In particular, polyplexes formed at N/P 20 revealed a mediate RFU of 48.7 ± 8% ($p > 0.5$) in comparison to 73.8 ± 8.5% at N/P 5. The findings accredit that the binding affinity depends on the molar mass and the architecture of the polymer as well as on the N/P ratio applied. The relationship between the binding affinity and the molar mass of the polymer increases in a proportional manner. In addition, a higher binding affinity of branched structures (BPEI) was detected in comparison to linear architectures.[8,31] The literature[47,48] reports similar trends and confirms the possible analysis of polyplexes by this HT assay. Moreover, identical tendencies were obtained for this particular handmade assay using polyplexes of linear PEIs (see Supporting Information). At this point of the workflow, one should note that after performing size measurements and binding affinity assays, it is possible to exclude nonsuitable polymers as

dx.doi.org/10.1021/co400025u | ACS Comb. Sci. 2013, 15, 475−482

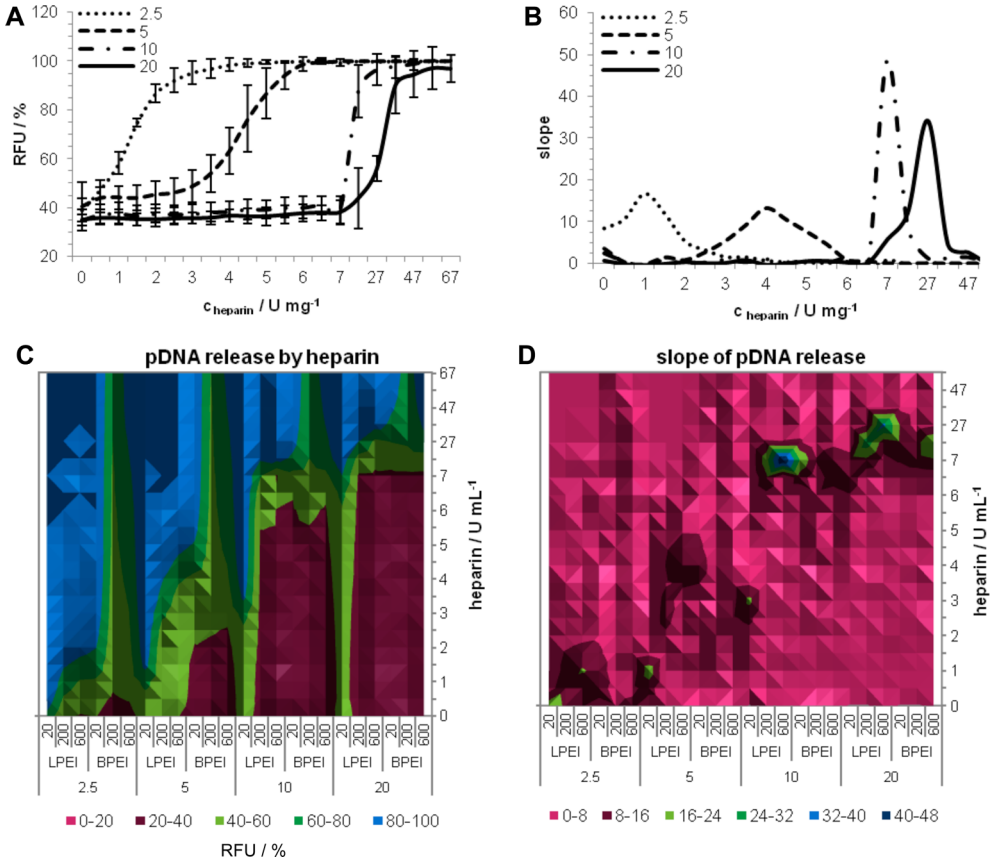

Figure 3. pDNA release of polyplexes after titration with heparin. Release of pDNA was measured by incubation of polyplexes with increasing heparin concentrations. (A) RFU of polyplexes prepared from $LPEI_{600}$ at different N/P ratios and increasing heparin concentrations. (B) Slope of RFU of $LPEI_{600}$ polyplexes at different N/P ratios. (C) RFU of all polyplexes at different N/P ratios and increasing heparin concentrations. Color represents the RFU. (D) Slope of RFU of all polyplexes at different N/P ratios. Color represents the slope. The values represent the mean ± S.D., $n \geq 3$.

transfection agents, which showed undesired interaction such as aggregation or no polyplex formation.

DNA Release. Subsequent to the determination of binding affinity, the release of pDNA from the polyplexes was investigated using the heparin assay. Heparin is a polyanion and it was reported to be a good competitor to negatively charged pDNA.[48] As a result of the polymer-heparin interaction, the pDNA is released and EB is repeatedly intercalating into pDNA leading to increased fluorescence intensities. Studies using heparin are often quantified via gel retardation assays or applying only one N/P ratio, which would potentially lead to misinterpretations. In particular for in vitro cultivations of adherent cells, the polyplex concentration at the cell membrane at the beginning of the transfection and after incubation differs. The explanation for this behavior could be justified by the polyplex sedimentation process.[8,49,50] For a more trustworthy outcome, all polyplex suspensions were titrated automatically against two heparin stock solutions to determine the critical heparin concentration at different N/P ratios. Using this approach, a wide range of heparin concentrations (n = 20) could be tested for one sample. The results obtained from the performed assay are displayed in detail for $LPEI_{600}$ (Figure 3A) and for all polymers and N/P ratios in (Figure 3C). As expected, the release of pDNA detected by RFU was dependent on the heparin concentration. Moreover, it was explored that for the release of total pDNA at higher N/P ratios, an increased amount of heparin was required. This can be explained by the fact that the amount of noncomplexed free polymer was increased at high N/P ratios, whereas the amount of complexed polymer remained constant.[51] Thus, by the addition of heparin to polyplex suspensions at high N/P ratios, first the free polymers complex with the heparin and no pDNA was released. Unless the critical concentration of heparin was met, the pDNA was not released. For an improved comparability, the inflection point of the titration curves in Figure 3A and C was defined as the critical heparin concentration (HC_{50}) and implemented as a representative value of the concentration at which 50% of the complexed pDNA was released (Figure 3B and D). The correlation between the N/P ratio and the heparin concentration was an apparent observation and confirmed already published trends.[48] However, our findings underline the relation between the architecture of PEI and the ability to release pDNA.

Polyplexes prepared from BPEIs showed higher HC_{50} values in comparison to the LPEIs (indicated by larger purple areas in particular at N/P 2.5 and 5, Figure 3C and D). Furthermore, the polyplexes prepared with the $LPEI_{20}$ exhibited an early release of the pDNA at low heparin concentration in contrast to its branched analog ($BPEI_{20}$) and the linear PEIs with higher molar masses ($LPEI_{200}$ and $LPEI_{600}$). A flagrant correlation could be made of these with the weak binding affinity (Figure 2).

dx.doi.org/10.1021/co400025u | ACS Comb. Sci. 2013, 15, 475−482

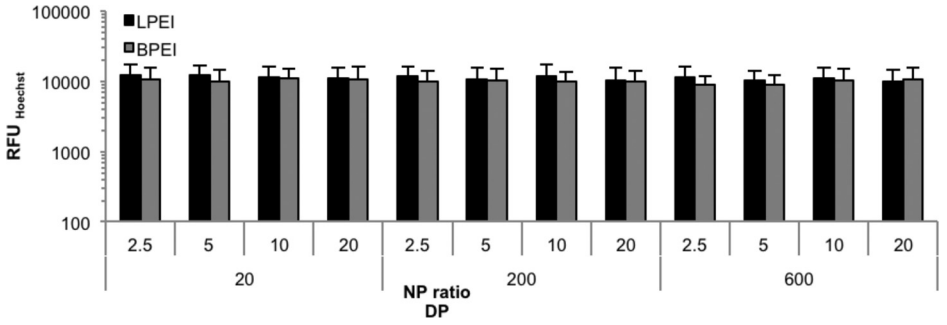

Figure 4. Investigation of cytotoxicity. The viability of cells after incubation of the polyplexes up to N/P 20. Nontreated cells served as controls and gave comparable results. The bottom of 96-well plates were measured at Em_{350}/Ex_{461} (Hoechst 33324).

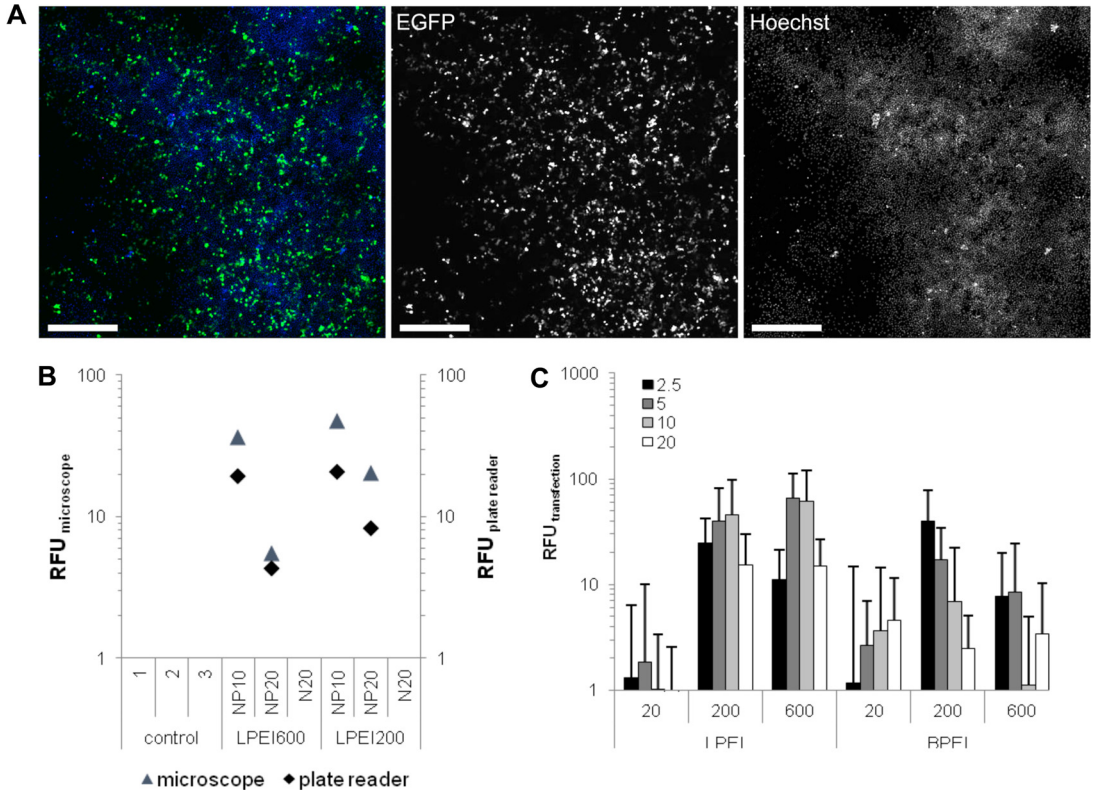

Figure 5. Transfection efficiency by microscopic evaluation and fluorescence intensity measurements. (A) HEK cells transfected with EGFP coding pDNA and $LPEI_{600}$ at N/P 10. Cell nuclei were stained with Hoechst 33324 (blue). Scale bare indicates 500 μm. (B) Correlation of the microscopic evaluation of EGFP content determined ($RFU_{microscope}$) and bottom measurements using a plate reader ($RFU_{plate\ reader}$). Three control wells, where cells were not transfected, as well as cells only incubated with the polymer at concentrations correspond N/P 20 (N20) showed no RFU. (C) Transfection efficiency and number of cells transfected with a pipetting robot in a 96-well plate. Values represent the mean ± S.D., $n \geq 3$.

Cytotoxicity. To study the cytotoxicity of the polyplexes, HEK cells used as for transfection experiments, were seeded in 96-well plates and incubated for 24 h with the prepared polyplex suspensions. Afterward, the viability of the cells was detected by staining with Hoechst 33324. This dye crosses of the cell membrane and stains the chromosomal DNA of attached cells. Subsequently, the fluorescence was measured utilizing the fluorescence plate reader. The obtained RFU signals of Hoechst of all treated cells are presented in Figure 4. No indication for cytotoxic effects of the polyplexes was found considering the fact that the obtained values were comparable to nontreated cells (ANOVA, $p > 0.05$).

As the polyplexes exhibited a lower cytotoxicity than the single polymers, due to neutralized cationic groups, the toxicity of these polyplexes at N/P 20 would be a criterion for knock out. However, for a comprehensive analysis, the polymers were also screened with concentrations up to 72 μg mL^{-1}, correlating to N/P 500 (DP 20 and 600, see Supporting Information). A relationship was elucidated between the increasing DP of the cationic polymers and the higher cytotoxicity level, which is in accordance to literature where no significant difference between linear and branched PEI was observed.[3,31] Interestingly, the polymers with the lowest DP showed no cytotoxicity at all investigated concentrations (see Supporting Information).

Transfection Efficiency. The transfection efficiency of the polyplexes was quantified using EGFP as reporter protein. For HT screening, the studies regarding the transfection efficiency were performed with a fluorescence plate reader by automatic scanning of the bottom area of the wells and complemented by

dx.doi.org/10.1021/co400025u | ACS Comb. Sci. 2013, 15, 475−482

microscope analysis. In Figure 5A, a representative overview of the cells (blue) transfected with $LPEI_{600}$ (green) is portrayed. Microscopic analysis and, in particular, subsequent data processing is not appropriate and efficient enough for a rapid HT screening, thus the quantification of EGFP using a fluorescence plate reader were compared to the mean fluorescence in each picture (Figure 5B). Thereby, a good correlation between the microscopic analysis and the fluorescence plate reader results was demonstrated, proving the capability to screen the EGFP amount in a fast and facile manner, in contrast to flow cytometry or microscopy. In general, it can be stated that there are some decent advantages of a fluorescence screening with a plate reader compared to luciferase or galactose based assays, namely, (i) an easy and cheap detection, (ii) the possibility to perform afterward single cell analysis by flow cytometry or microscopy of the same cells, and (iii) the fact that EGFP is a stable reporter protein.

The EGFP expression for all investigated PEI polymers are shown in Figure 5C. The polymers can be ranked from high to low transfection efficiency: $LPEI_{600}$ > $LPEI_{200}$ > $BPEI_{200}$ > $BPEI_{600}$ > $BPEI_{20}$ > $LPEI_{20}$, whereby the obvious increase in the standard deviation compared to flow cytometry measurements (see Supporting Information) must be taken into account. However, the HT investigation showed clear trends confirming a suitable approach to spot high potential candidates and to be subsequently investigated in depth. Thus, $LPEI_{20}$ revealed no transfection efficiency, while $LPEI_{600}$ shows the highest one, also confirmed by handmade polyplexes and the detection of EGFP by flow cytometry (see Supporting Information). This observation further verifies the potential of such a HT screening using a fluorescent plate reader for determination of the transfection efficiencies of polymers.

CONCLUSION

Since HT synthesis and characterization of polymers could be managed by synthetic robots and microwave synthesizers combined with subsequent automated characterization of the molecular properties, polymer libraries for biological applications can be prepared in a rapid manner.[15−20] So far, an efficient and fast HT screening of these polymers for gene delivery purposes regarding structure−property relationship was not possible. Herein, a solution for the biological screening for gene delivery applications has been presented. The discussed HT workflow enables a rapid analysis of polymer vectors in an automated way with respect to important polymer characteristics, such as molar mass, architecture, and N/P ratio. This supports the identification and evaluation of polymers with regard to their capability of efficient complexation, protection, and transfection efficiency. For instance, the described heparin assay can be used for 23 polymers at four different N/P ratios resulting in 92 samples plus controls (n = 1). Furthermore, the HT approach was applied and demonstrated the possible screening of the cytotoxicity and the transfection efficiency of the polyplexes. As expected, the study of the different PEI model polymers revealed that linear and branched PEI are noncytotoxic at the investigated concentrations, but with rising molar mass and polymer concentration the cytotoxic effect was increasing.[31] The polymeric architecture itself showed thereby no influence on the cell viability.[3] As per literature, at low molar masses the DNA binding affinity is influenced by the polymeric architecture, since $BPEI_{20}$ revealed a stronger pDNA binding than $LPEI_{20}$.[15,26] The obtained results indicated that PEIs with branched architectures and small molar masses have the highest potential to be used as gene vectors in vitro, as they offer the advantage of low cytotoxicity combined with high pDNA binding affinity. Beyond, the best transfection results were obtained for $LPEI_{600}$ and the $BPEI_{200}$.

In comparison with literature and handmade performances proof was established that the developed workflow is applicable for polymer systems. Furthermore, conditions enabling a fast and efficient screening in terms of important vector parameters, such as polyplex formation, transfection, and release were found. The possible screening of polymer libraries for the best transfection candidate will help to elucidate main polymer characteristics and to understand why some polymers are high performers and others not. Thus, an enhanced development of more efficient polymers and polyplexes can be realized.

EXPERIMENTAL PROCEDURES

Material. Ethidium bromide solution 1% was purchased from Carl Roth (Karlsruhe, Germany). AlamarBlue was obtained from Life Technologies (Darmstadt, Germany). If not otherwise stated, cell culture materials, cell culture media, and solutions were obtained from PAA (Pasching, Austria). Plasmid pEGFP-N1 (4.7 kb, Clontech, Mountain View, CA, U.S.A.) was isolated using Qiagen Giga plasmid Kit (Hilden, Germany). All other chemicals were purchased from Sigma Aldrich (Steinhausen, Germany) and are of analytical grade or better and used without further purification. Linear PEI was synthesized according to procedure described in literature.[32]

Polyplex Preparation Using Pipetting Robot. For an automated polyplex preparation, 100 μL buffered DNA solution (c = 15 μg mL^{-1}) were injected into wells that contain 300 μL of the desired polymer solution. As cationic polymers, linear PEI with a DP of 20, 200, and 600, as well as branched PEI with a DP of 20, 200, and 600 were applied. To achieve different polymer to DNA ratios (N/P ratios), a dilution series in HBG of four different polymer concentrations (N/P ratio 2.5, 5, 10, 20) was prepared using a pipetting robot from a polymer stock solution of c = 72 μg mL^{-1}. After addition of the DNA solution, the polyplex suspension was mixed five times by suction and release using 200 μL tips and incubated at least 20 min. Subsequently, 100 μL of each polyplex suspension were transferred into three different well plates for a detailed analysis studies. The following assays were performed up to 2 h after polyplex preparation.

ASSOCIATED CONTENT

Supporting Information

Additional experimental details, tables of SEC data and hydrodynamic radii of polyplexes, comparison of the conventional handmade ployplexes and HT polyplexes, figures showing transfection efficiency, fluorescence displacement and cytotoxicity, and hydrodynamic radii and PDI^{P}, and additional references. This material is available free of charge via the Internet at http://pubs.acs.org.

AUTHOR INFORMATION

Corresponding Author

*E-mail: ulrich.schubert@uni-jena.de.

Present Address

Kristian Kempe: Department of Chemical and Biomolecular Engineering, The University of Melbourne, Victoria 3010, Australia

Author Contributions

A.C.R. and A.V. contributed equally.

Funding

The financial support from the Thuringian Ministry for Education, Science and Culture (Grant B514-09051, NanoConSens), the Dutch Polymer Institute (DPI, technology area HTE, project 729), and the Carl-Zeiss Foundation (JCSM Strukturantrag) are gratefully acknowledged.

Notes

The authors declare no competing financial interest.

■ ACKNOWLEDGMENTS

We express our gratitude to Caroline Fritzsche for assistance in the cell culture, Dr. David Pretzel for assistance at the microscope, Michael Wagner for helpful discussions, and Sarah Crotty for corrections of the manuscript.

■ REFERENCES

(1) Schlenk, F.; Grund, S.; Fischer, D. Recent developments and perspectives on gene therapy using synthetic vectors. *Ther. Delivery* **2013**, *4* (1), 95−113.

(2) Pezzoli, D.; Chiesa, R.; De Nardo, L.; Candiani, G. We still have a long way to go to effectively deliver genes! *J. Appl. Biomater. Funct. Mater.* **2012**, *10* (2), e82−91.

(3) Breunig, M.; Lungwitz, U.; Liebl, R.; Goepferich, A. Breaking up the correlation between efficacy and toxicity for nonviral gene delivery. *Proc. Natl. Acad. Sci. U. S. A.* **2007**, *104* (36), 14454−9.

(4) Kunath, K.; von Harpe, A.; Fischer, D.; Petersen, H.; Bickel, U.; Voigt, K.; Kissel, T. Low-molecular-weight polyethylenimine as a non-viral vector for DNA delivery: comparison of physicochemical properties, transfection efficiency and in vivo distribution with high-molecular-weight polyethylenimine. *J. Controlled Release* **2003**, *89* (1), 113−125.

(5) Pereira, P.; Jorge, A. F.; Martins, R.; Pais, A. A.; Sousa, F.; Figueiras, A. Characterization of polyplexes involving small RNA. *J. Colloid Interface Sci.* **2012**, *387* (1), 84−94.

(6) Dai, Z.; Wu, C. How does DNA complex with polyethylenimine with different chain lengths and topologies in their aqueous solution mixtures? *Macromolecules* **2012**, *45* (10), 4346−4353.

(7) Itaka, K.; Harada, A.; Yamasaki, Y.; Nakamura, K.; Kawaguchi, H.; Kataoka, K. In situ single cell observation by fluorescence resonance energy transfer reveals fast intra-cytoplasmic delivery and easy release of plasmid DNA complexed with linear polyethylenimine. *J. Gene Med.* **2004**, *6* (1), 76−84.

(8) Neu, M.; Fischer, D.; Kissel, T. Recent advances in rational gene transfer vector design based on poly(ethylene imine) and its derivatives. *J. Gene Med.* **2005**, *7* (8), 992−1009.

(9) Patil, S. D.; Rhodes, D. G.; Burgess, D. J. DNA-based therapeutics and DNA delivery systems: a comprehensive review. *AAPS J.* **2005**, *7* (1), E61−77.

(10) Jiang, X.; Qu, W.; Pan, D.; Ren, Y.; Williford, J. M.; Cui, H.; Luijten, E.; Mao, H. Q. Plasmid-templated shape control of condensed DNA-block copolymer nanoparticles. *Adv. Mater.* **2013**, *25* (2), 227−32.

(11) Iwai, R.; Haruki, R.; Nemoto, Y.; Nakayama, Y. Enhanced transfection efficiency of poly(*N*,*N*-dimethylaminoethyl methacrylate)-based deposition transfection by combination with tris-(hydroxylmethyl)aminoethane. *Bioconjugate Chem.* **2013**, *29*, 29.

(12) Derouazi, M.; Girard, P.; Van Tilborgh, F.; Iglesias, K.; Muller, N.; Bertschinger, M.; Wurm, F. M. Serum-free large-scale transient transfection of CHO cells. *Biotechnol. Bioeng.* **2004**, *87* (4), 537−45.

(13) Florian, M. W. Production of recombinant protein therapeutics in cultivated mammalian cells. *Nat. Biotechnol.* **2004**, No. 22, 1393−1398.

(14) Boussif, O.; Lezoualch, F.; Zanta, M. A.; Mergny, M. D.; Scherman, D.; Demeneix, B.; Behr, J. P. A versatile vector for gene and oligonucleotide transfer into cells in culture and in-vivo—Polyethylenimine. *Proc. Natl. Acad. Sci. U. S. A.* **1995**, *92* (16), 7297−7301.

(15) Hoogenboom, R.; Fijten, M. W. M.; Thijs, H. M. L.; Van Lankvelt, B. M.; Schubert, U. S. Microwave-assisted synthesis and properties of a series of poly(2-alkyl-2-oxazoline)s. *Des. Monomers Polym.* **2005**, *8* (6), 659−671.

(16) Hoogenboom, R.; Schubert, U. S. Microwave-assisted polymer synthesis: Recent developments in a rapidly expanding field of research. *Macromol. Rapid Commun.* **2007**, *28* (4), 368−386.

(17) Hoogenboom, R.; Wiesbrock, F.; Huang, H. Y.; Leenen, M. A. M.; Thijs, H. M. L.; van Nispen, S. F. G. M.; Van der Loop, M.; Fustin, C. A.; Jonas, A. M.; Gohy, J. F.; Schubert, U. S. Microwave-assisted cationic ring-opening polymerization of 2-oxazolines: A powerful method for the synthesis of amphiphilic triblock copolymers. *Macromolecules* **2006**, *39* (14), 4719−4725.

(18) Wiesbrock, F.; Hoogenboom, R.; Abeln, C. H.; Schubert, U. S. Single-mode microwave ovens as new reaction devices: Accelerating the living polymerization of 2-ethyl-2-oxazoline. *Macromol. Rapid Commun.* **2004**, *25* (22), 1895−1899.

(19) Wiesbrock, F.; Hoogenboom, R.; Leenen, M.; van Nispen, S. F. G. M.; van der Loop, M.; Abeln, C. H.; van den Berg, A. M. J.; Schubert, U. S. Microwave-assisted synthesis of a 4(2)-membered library of diblock copoly(2-oxazoline)s and chain-extended homo poly(2-oxazoline)s and their thermal characterization. *Macromolecules* **2005**, *38* (19), 7957−7966.

(20) Wiesbrock, F.; Hoogenboom, R.; Leenen, M. A. M.; Meier, M. A. R.; Schubert, U. S. Investigation of the living cationic ring-opening polymerization of 2-methyl-, 2-ethyl-, 2-nonyl-, and 2-phenyl-2-oxazoline in a single-mode microwave reactor. *Macromolecules* **2005**, *38* (12), 5025−5034.

(21) Meier, M. A. R.; Hoogenboom, R.; Schubert, U. S. Combinatorial methods, automated synthesis and high-throughput screening in polymer research: The evolution continues. *Macromol. Rapid Commun.* **2004**, *25* (1), 21−33.

(22) Hoogenboom, R.; Meier, M. A. R.; Schubert, U. S. Combinatorial methods, automated synthesis and high-throughput screening in polymer research: Past and present. *Macromol. Rapid Commun.* **2003**, *24* (1), 16−32.

(23) Potyrailo, R.; Rajan, K.; Stoewe, K.; Takeuchi, I.; Chisholm, B.; Lam, H. Combinatorial and high-throughput screening of materials libraries: Review of state of the art. *ACS Comb. Sci.* **2011**, *13* (6), 579−633.

(24) Abeylath, S. C.; Ganta, S.; Iyer, A. K.; Amiji, M. Combinatorial-designed multifunctional polymeric nanosystems for tumor-targeted therapeutic delivery. *Acc. Chem. Res.* **2011**, *44* (10), 1009−1017.

(25) Akinc, A.; Lynn, D. M.; Anderson, D. G.; Langer, R. Parallel synthesis and biophysical characterization of a degradable polymer library for gene delivery. *J. Am. Chem. Soc.* **2003**, *125* (18), 5316−5323.

(26) Peters, A.; Brey, D. M.; Burdick, J. A. High-throughput and combinatorial technologies for tissue engineering applications. *Tissue Eng., Part B* **2009**, *15* (3), 225−239.

(27) Hook, A. L.; Chang, C. Y.; Yang, J.; Luckett, J.; Cockayne, A.; Atkinson, S.; Mei, Y.; Bayston, R.; Irvine, D. J.; Langer, R.; Anderson, D. G.; Williams, P.; Davies, M. C.; Alexander, M. R. Combinatorial discovery of polymers resistant to bacterial attachment. *Nat. Biotechnol.* **2012**, *30* (9), 868−U99.

(28) Batchelor, R.; Hagen, D.; Johnson, I.; Beechem, J. A fluorescent high-throughput assay for double-stranded DNA: the RediPlate PicoGreen assay. *Comb. Chem. High Throughput Screen.* **2003**, *6* (4), 287−291.

(29) Anderson, D. G.; Lynn, D. M.; Langer, R. Semi-automated synthesis and screening of a large library of degradable cationic polymers for gene delivery. *Angew. Chem., Int. Ed.* **2003**, *42* (27), 3153−3158.

(30) Regelin, A. E.; Fernholz, E.; Krug, H. F.; Massing, U. High throughput screening method for identification of new lipofection reagents. *J. Biomol. Screen* **2001**, *6* (4), 245−54.

(31) Parhamifar, L.; Larsen, A. K.; Hunter, A. C.; Andresen, T. L.; Moghimi, S. M. Polycation cytotoxicity: a delicate matter for nucleic acid therapy-focus on polyethylenimine. *Soft Matter* **2010**, *6* (17), 4001−4009.
(32) Tauhardt, L.; Kempe, K.; Knop, K.; Altuntas, E.; Jager, M.; Schubert, S.; Fischer, D.; Schubert, U. S. Linear polyethyleneimine: Optimized synthesis and characterization—On the way to "pharma-grade" batches. *Macromol. Chem. Phys.* **2011**, *212* (17), 1918−1924.
(33) Adams, N.; Schubert, U. S. Poly(2-oxazolines) in biological and biomedical application contexts. *Adv. Drug Delivery Rev.* **2007**, *59* (15), 1504−1520.
(34) Schallon, A.; Synatschke, C. V.; Pergushov, D. V.; Jerome, V.; Müller, A. H. E.; Freitag, R. DNA melting temperature assay for assessing the stability of DNA polyplexes intended for nonviral gene delivery. *Langmuir* **2011**, *27* (19), 12042−12051.
(35) van Gaal, E. V. B.; Spierenburg, G.; Hennink, W. E.; Crommelin, D. J. A.; Mastrobattista, E. Flow cytometry for rapid size determination and sorting of nucleic acid containing nanoparticles in biological fluids. *J. Controlled Release* **2010**, *141* (3), 328−338.
(36) van Gaal, E. V. B.; van Eijk, R.; Oosting, R. S.; Kok, R. J.; Hennink, W. E.; Crommelin, D. J. A.; Mastrobattista, E. How to screen non-viral gene delivery systems in vitro? *J. Controlled Release* **2011**, *154* (3), 218−232.
(37) Wightman, L.; Kircheis, R.; Rossler, V.; Carotta, S.; Ruzicka, R.; Kursa, M.; Wagner, E. Different behavior of branched and linear polyethylenimine for gene delivery in vitro and in vivo. *J. Gene Med.* **2001**, *3* (4), 362−72.
(38) Breunig, M.; Lungwitz, U.; Liebl, R.; Klar, J.; Obermayer, B.; Blunk, T.; Goepferich, A. Mechanistic insights into linear polyethylenimine-mediated gene transfer. *Biochim. Biophys. Acta, Gen. Subj.* **2007**, *1770* (2), 196−205.
(39) Goula, D.; Remy, J. S.; Erbacher, P.; Wasowicz, M.; Levi, G.; Abdallah, B.; Demeneix, B. A. Size, diffusibility and transfection performance of linear PEI/DNA complexes in the mouse central nervous system. *Gene Ther.* **1998**, *5* (5), 712−7.
(40) Wightman, L.; Kircheis, R.; Rossler, V.; Carotta, S.; Ruzicka, R.; Kursa, M.; Wagner, E. Different behavior of branched and linear polyethylenimine for gene delivery in vitro and in vivo. *J. Gene Med.* **2001**, *3* (4), 362−72.
(41) Wagner, M.; Rinkenauer, A. C.; Schallon, A.; Schubert, U. S. Opposites attract: Influence of the molar mass of branched poly(ethylene imine) on biophysical characteristics of siRNA-based polyplexese. *RSC Adv.* **2013**, *3*, 12774−12785.
(42) Perevyazko, I.; Vollrath, A.; Hornig, S.; Pavlov, G. M.; Schubert, U. S. Characterization of poly(methyl methacrylate) nanoparticles prepared by nanoprecipitation using analytical ultracentrifugation, dynamic light scattering, and scanning electron microscopy. *J. Polym. Sci., Part A: Polym. Chem.* **2010**, *48* (18), 3924−3931.
(43) Perevyazko, I. Y.; Delaney, J. T.; Vollrath, A.; Pavlov, G. M.; Schubert, S.; Schubert, U. S. Examination and optimization of the self-assembly of biocompatible, polymeric nanoparticles by high-throughput nanoprecipitation. *Soft Matter* **2011**, *7* (10), 5030−5035.
(44) Gebhart, C. L.; Kabanov, A. V. Evaluation of polyplexes as gene transfer agents. *J. Controlled Release* **2001**, *73* (2−3), 401−416.
(45) Rejman, J.; Bragonzi, A.; Conese, M. Role of clathrin- and caveolae-mediated endocytosis in gene transfer mediated by lipo- and polyplexes. *Mol. Ther.* **2005**, *12* (3), 468−474.
(46) Rejman, J.; Oberle, V.; Zuhorn, I. S.; Hoekstra, D. Size-dependent internalization of particles via the pathways of clathrin-and caveolae-mediated endocytosis. *Biochem. J.* **2004**, *377*, 159−169.
(47) Grayson, A. C.; Doody, A. M.; Putnam, D. Biophysical and structural characterization of polyethylenimine-mediated siRNA delivery in vitro. *Pharm. Res.* **2006**, *23* (8), 1868−76.
(48) Kwok, A.; Hart, S. L. Comparative structural and functional studies of nanoparticle formulations for DNA and siRNA delivery. *Nanomedicine* **2011**, *7* (2), 210−9.
(49) Luo, D.; Saltzman, W. M. Enhancement of transfection by physical concentration of DNA at the cell surface. *Nat. Biotechnol.* **2000**, *18* (8), 893−895.
(50) Tros de Ilarduya, C.; Sun, Y.; Duzgunes, N. Gene delivery by lipoplexes and polyplexes. *Eur. J. Pharm. Sci.* **2010**, *40* (3), 159−70.
(51) Perevyazko, I. Y.; Bauer, M.; Pavlov, G. M.; Hoeppener, S.; Schubert, S.; Fischer, D.; Schubert, U. S. Polyelectrolyte complexes of DNA and linear PEI: Formation, composition and properties. *Langmuir* **2012**, *28* (46), 16167−16176.

Supporting information:

Parallel high-throughput screening of polymer vectors for non-viral gene delivery: Evaluation of structure-property-relationships of transfection

*Alexandra C. Rinkenauer,[+,§,#] Antje Vollrath,[+,§,#] Anja Schallon,[+,§] Lutz Tauhardt,[+,§] Kristian Kempe,[+,§,∫] Stephanie Schubert,[§,&] Dagmar Fischer,[&] Ulrich S. Schubert[+,§,‡,]**

[#]equal contribution

[+]Laboratory of Organic and Macromolecular Chemistry (IOMC), Friedrich Schiller University Jena, Humboldtstraße 10, 07743 Jena, Germany

[§]Jena Center for Soft Matter (JCSM), Friedrich Schiller University Jena, Philosophenweg 7, 07743 Jena, Germany

[&]Institute of Pharmacy, Department of Pharmaceutical Technology, Friedrich Schiller University Jena, Otto-Schott-Str. 41, 07745 Jena, Germany

[‡]Dutch Polymer Institute, P.O. Box 902, 5600 AX Eindhoven, The Netherlands

[∫] Current address: Department of Chemical and Biomolecular Engineering, The University of Melbourne, Victoria 3010, Australia

* Address correspondence to: ulrich.schubert@uni-jena.de

1. Experimental section

Synthesis of LPEI

LPEIs were synthesized from the corresponding poly(2-ethyl-2-oxazoline)s (PEtOx) by acidic hydrolysis as described in literature.[1] Briefly, PEtOx (2 g) was dissolved in 6 M aqueous hydrochloric acid (15 mL) and heated at 130 °C for 1 h in a Initiator Sixty single-mode microwave synthesizer from Biotage, equipped with a noninvasive IR sensor (accuracy: ± 2%). The acid was removed under reduced pressure. The residue was dissolved in water and 3 M aqueous NaOH was added until precipitation occurred. The precipitate was filtered off, recrystallized from water, filtered, dissolved in methanol, and precipitated into ice-cold diethyl ether. Subsequently, the LPEI was dried for 3 day at 40 °C. The degrees of hydrolysis were determined by ^{1}H NMR spectroscopy and found to be 99% for all LPEIs. A detailed characterization of the short $LPEI_{20}$ can be found elsewhere.[1-2] ^{1}H NMR (300 MHz, CD_3OD): δ = 3.65 (t, CH_2-OH), 2.73 (br., N-CH_2), 2.39 (s, CH_3-N). IR (FT-IR): ν = 3217 (NH), 2 873 (CH_3), 2804 (CH), 1 446 (CH_2/CH_3), 1330 (C-N), 1134 (C-N), 1103 (C-N) cm^{-1}.

Table S1. SEC-Data of the PEtOx precursors.

PEtOx precursor	Repeating units[a)]	M_n (g/mol)[b)]	PDI[b)]
$PEtOx_{20}$	20	3,600	1.11
$PEtOx_{200}$	200	58,200	1.14
$PEtOx_{600}$	600	40,600	1.79

[a)]Calculated from ^{1}H NMR; [b)]Determined by size exclusion chromatography (solvent: chloroform/triethylamine/ iso-propanol [94/4/2]; calibration standard: PS)

Investigation of polyplex size and stability

For first studies, the polyplex sizes were studied by utilization of a Zetasizer Nano ZS (Malvern Instruments, Herrenberg, Germany). The measurements were carried out in a minimal volume cuvette ZEN 0040 (BRAND GmbH, Wertheim, Germany) with a laser beam at 633 nm and a

scattering angle of 173° at 25 °C. The viscosity (0.89 mPa s) and refractive index (1.33) of purified water at 25 °C were used for data analysis. 40 µL of polyplex suspensions were measured five times for 20 sec. The mean particle size was approximated as the effective (Z average) diameter and calculated with the General purpose (normal resolution) algorithm using the Malvern software 6.20. For the polyplex size analysis by dynamic light scattering, a DynaPro Plate Reader Plus (Wyatt Technology Corporation, Santa Barbara, CA) equipped with a 60 mV linearly polarized gallium arsenide (GaAs) laser of $\lambda = 832.5$ nm and operating at an angle of 156° was utilized. Again, the viscosity (0.89 mPa s) and refractive index (1.33) of purified water at 25 °C were used for data analysis. The data were analyzed with the Dynamics software ver. 6.10 by the method of cumulants as previously described for nanoparticle analysis.[3] The measurement time was set to 10 seconds per run and 10 acquisitions were collected five times per well and repeated 3 times in independent experiments.

Polyplex preparation: conventional methode

Polyplexes of pDNA and polymer were prepared by adding polymers at a certain N/P ratio to stock solutions of pDNA with 15 µg mL^{-1} in HBG buffer (20 mM 4-(2-hydroxethyl) piperazine-1-ethanesulfonic acid (HEPES) and 5% (w/v) glucose, pH 7.2). Subsequently, the solutions were vortexed for 10 sec at maximal speed, and incubated at room temperature for 10 min.

Binding affinity

The polyplex formation and binding affinity responsible for complexation of pDNA and polymers were detected by quenching of the ethidium bromide (EB) fluorescence as described previously.[4] After the polyplex preparation via pipetting robot or per hand, 100 µL of the polyplex solution were incubated with EB (0.4 µg mL^{-1}) for 10 min at room temperature in black 96-well plates (Nunc, Langenselbold, Germany). The fluorescence was measured using a Tecan

Genios Pro fluorescence microplate reader (Tecan, Crailsheim, Germany) with excitation and emission wavelength at 525 and 605 nm, respectively. A sample containing only pDNA and EB was used to calibrate the device to 100% fluorescence. The percentage of dye displaced upon polyplex formation was calculated using equation (1):

$$\text{RFU}\,[\%] = \frac{F_{\text{sample}}}{F_{\text{pDNA}}} \qquad (1)$$

Here, RFU represent the relative fluorescence. F_{sample} and F_{siRNA} indicate the fluorescence intensities of a given sample and the EB intercalated into pDNA alone, respectively.

DNA release by heparin

To investigate the release of pDNA from polyplexes, the heparin dissociation assay was used. For this purpose, 100 µL of polyplex solution were incubated for 10 min with EB (0.4 µg mL^{-1}) in a black 96-well plate. After transferring into the Tecan Genios Pro fluorescence microplate reader, heparin solutions were automatically added at the indicated concentrations. Therefore, 20 cycles of the following procedure were used: 5 µL of heparin stock solutions (10 U mL^{-1} or 200 U mL^{-1}) were dropped to each well. Afterwards the plate was shaked (orbital, 10 sec, 2 mm) and incubated for 5 min at 37 °C. After each cycle, the fluorescence of EB was measured, and the percentage of intercalated EB was calculated as described before (1).

Cell Culture

HEK-293 (CRL-1573, ATCC) cells were maintained in RPMI 1640 culture medium, L929 (CCL-1, ATCC) in DMEM culture medium. Both media were supplemented with 10% fetal calf serum (FCS), 100 µg/mL streptomycin, 100 IU mL^{-1} penicillin, and 2 mM L-glutamine. Cells were cultivated at 37 °C in a humidified 5% CO_2 atmosphere.

Cytotoxicity

The cytotoxicity of the single polymers was tested with L929 cells, as this cell line is recommended by ISO10993-5. In detail, cells were seeded at 10^4 cells per well in a 96-well plate and incubated for 24 h. No cells were seeded in the outer wells. Afterwards, polymers at the indicated endconcentrations were added, the plates were slued, and incubated at 37 °C for further 24 h. Subsequently, the medium was replaced by PBS and AlamarBlue as recommended by the supplier. After incubation for 4 h, the fluorescence was measured at Ex 570 / Em 610 nm, with untreated cells on the same well plate serving as controls (2).

$$\text{viability [\%]} = \frac{F_{sample} - F_0}{F_{control} - F_0} \quad (2)$$

Here, viability is the relative fluorescence and F_{sample}, F_0, and $F_{control}$ are the fluorescence intensities of a given sample, the blank wells without cells, and the control cells without polymer treatment.

Transfection of cells: HT manner

HEK 293 cells were maintained in RPMI 1640 culture medium, supplemented with 10% fetal calf serum (FCS), 100 µg mL^{-1} streptomycin, 100 IU mL^{-1} penicillin, and 2 mM L-glutamine. Cells were cultivated at 37 °C in a humidified 5% CO_2 atmosphere.

For transfection experiments, HEK cells were seeded at a density of 10^4 cells per well in 96-well plates 24 h before transfection. In order to avoid any misleading measurement results and to prevent a systematic mistake, the polyplexes were always placed and measured at different positions in the 96-well plate to avoid alterations due to differences in the gas exchange between outer and inner wells and 25 measuring points per well were taken. One hour prior transfection, cells were washed with PBS and supplemented with 100 µL OptiMEM (Life Technologies). Polyplex solutions were added (10 µL) to the cells and the plates were slued and incubated for 4 h at 37 °C. Afterwards, the supernatant was replaced by 100 µL of fresh growth medium (RPMI1640 based), and the cells were further incubated for 20 h. Before analysis, the cells were

incubated with 1 μg mL^{-1} Hoechst 33324 for 10 min at 37 °C, washed twice with PBS, and the plates were transferred to the plate reader. The expression of EGFP fluorescence (Ex 475 nm / Em 509 nm) and viability (Hoechst, Em 350 nm / Ex 461 nm) was quantified by using the fluorescence measured from the bottom of the plates. The transfection efficiency was calculated relative to cell number and control cells using the following equation (3), where and $EGFP_{sample}$, $EGFP_{control}$, $Hoechst_{sample}$, $Hoechst_{control}$ are the fluorescence signal of EGFP and Hoechst of treated (sample) and non treated (control) cells, respectively. Experiments were repeated 3 times independently.

$$\text{transfection efficiency} = \frac{EGFP_{sample} - EGFP_{control}}{Hoechst_{sample}/Hoechst_{control}} \quad (3)$$

Transfection of cells: conventional method

For transfection of the HEK 293 cell lines, cells were seeded at a density of 10^5 cell mL^{-1} in 12-well plates one day before transfection. One hour prior to transfection, cells were rinsed with PBS and supplemented with 1 mL OptiMEM (Life Technologies). Polyplexes (100 μL) were added to the cells and the plates were incubated for 4 h in the incubator. Afterwards, the supernatant was replaced by1 mL of fresh growth medium, and the cells were further incubated for 20 h. For analysis, adherent cells were harvested by trypsinization.

For determination of, dead cells, they were counterstained with propidium iodide. The relative expression of EGFP fluorescence of 10^4 cells was quantified via flow cytometry using a Cytomics FC 500 (Beckman Coulter). For determination of the transfection efficiency viable cells expressing EGFP were gated using non-treated cells as negative control. Experiments were repeated ≥ 3 times independently.

2. Results and Discussions

2.1 Comparison of conventional handmade polyplexes and polyplexes prepared by HT workflow

For examination of the presented HT screening workflow, selected experiments were performed with conventional methods, also called handmade.

2.1.1 Investigations of polyplex size and stability

In order to compare the preparation of the polyplexes *via* pipetting robot with the conventional vortexing method, $lPEI_{600}$ and $bPEI_{600}$ polymers were chosen for polyplex formation with DNA applying both techniques, pipetting and vortexing. As shown in Table S2, similar polyplex sizes and polydispersities were observed proving that the pipetting approach is suitable for the preparation of polyplexes.

Table S2. Hydrodynamic radii of polyplexes prepared by conventional preparation (vortexed for 10 sec, incubated for at least 15 min) and pipetting. Radii were measured with Zetasizer Nano ZS (Malvern Instruments, Herrenberg, Germany).

	METHOD	PEI (μL)	DNA (µL)	HB (µL)	Z Average (r, nm)	PDI
$lPEI_{600}$	pipetted 3x mix	100	50	50	80	0.40
	vortexed 10s	100	50	50	79	0.38
$bPEI_{600}$	pipetted 3x mix	100	50	50	68	0.23
	vortexed 10s	100	50	50	75	0.43

2.1.2 Transfection efficiency and binding affinity

Exemplary the transfection efficiency of the linear PEIs were performed handmade and analyzed with flow cytometer. The same tendencies obtained as with the platereader can be observed: enhanced transfection efficiencies with increased molar mass. This demonstrates the potential of using the platereader in a HT screening manner

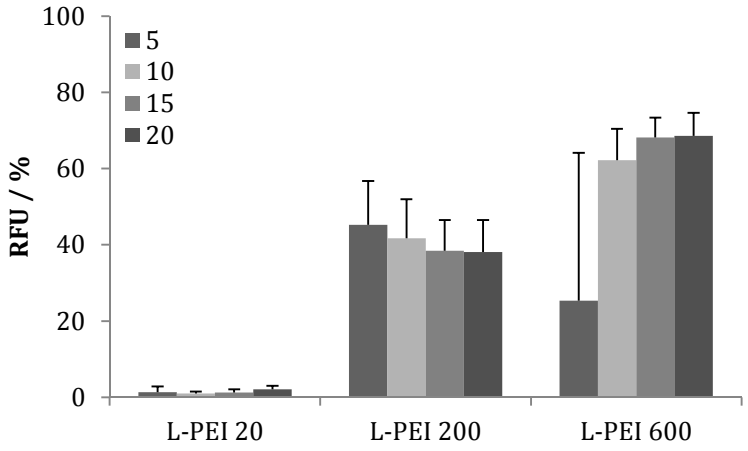

Figure S1. Transfection efficiency of linear PEIs: Polyplexes were formed handmade and analyzed via flow cytometer (n=3).

Moreover the binding affinity was analyzed. In this case the polyplexes were formed per hand and afterwards measured like in HT manner.

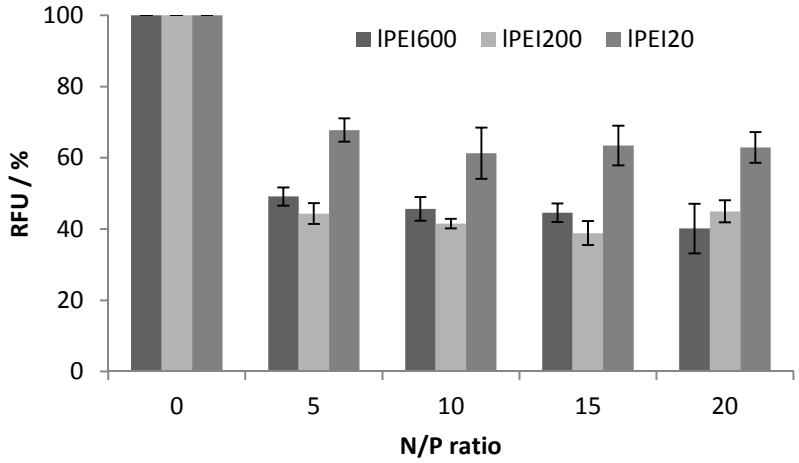

Figure S2. Fluorescence displacement assay of linear PEIs. EBA were performed handmade (n=3).

2.1.4 Cytotoxicity

Moreover the proof of the AlamarBlue as cytotoxicity test system was proven. Thus the high and low molecular weight PEIs were exemplary used. As shown in figure S3 the high molecular weight PEIs show the excepted cytotoxicity in contrast to the low molecular weight one. Demonstrating the possibility to use the AlamarBlue assay as test sytem.

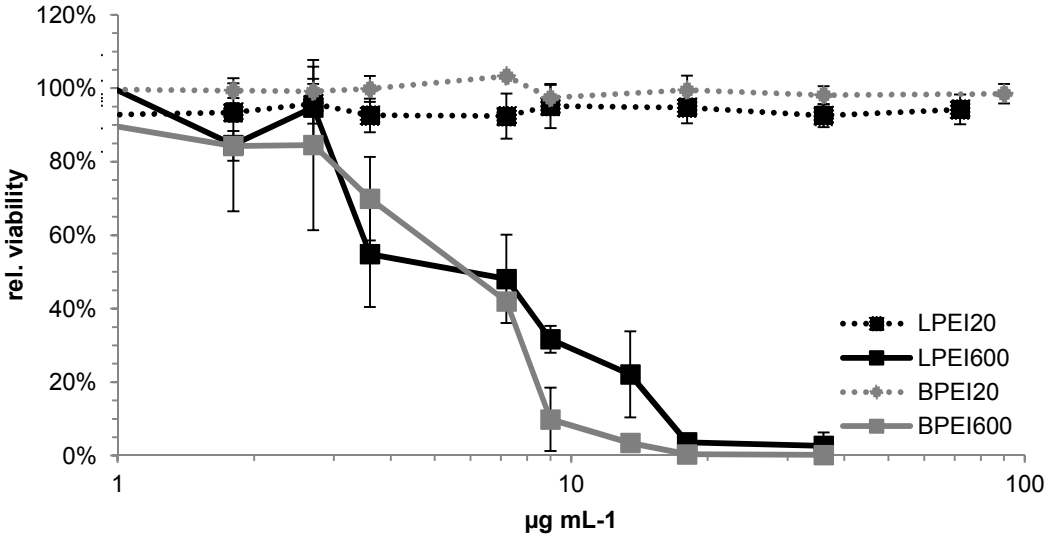

Figure S3. Cytotoxicity of the high and low molecular PEIs using the AlamarBlue assay (n=3)

2.2 Time-dependent stability of polyplexes

Additionally, selected polyplexes were studied over 2 h and revealed no occurance of aggregation (Table S3), which further confirmed the formation of stable polyplexes by utilization of the pipetting robot.

Table S3. Hydrodynamic radii of polyplexes prepared from $lPEI_{600}$ at NP 20 measured with Zetasizer Nano ZS (Malvern Instruments, Herrenberg, Germany).

Time [min]	Radius [nm]	PDI^P
30	82	0.400
60	58	0.325
120	59	0.395

2.3 Comparison of HT-DLS investigations with conventional single DLS measurements using NanoZetasizer, Malvern

To evaluate the reliability of the HT-DLS instrument, the polyplex sizes were measured manually using the Zetasizer (Malvern) (Figure S4). Polyplexes for all N/P ratios and all PEIs revealed thereby radii between 33 to 100 nm with PDI^Ps in a range of 0.2 to 0.6. Throughout this study, the values obtained by the Zetasizer were smaller compared to the ones measured by HT-DLS

reader. This could be due to the different measurement procedures, in particular in the case of the HT-DLS reader, where aggregates, often sediment during measurements, are taken much more into account. In the Zetasizer the laser beam passes the solution from one side in a defined height, where as the laser beam in the HT-DLS reader passes from the bottom.

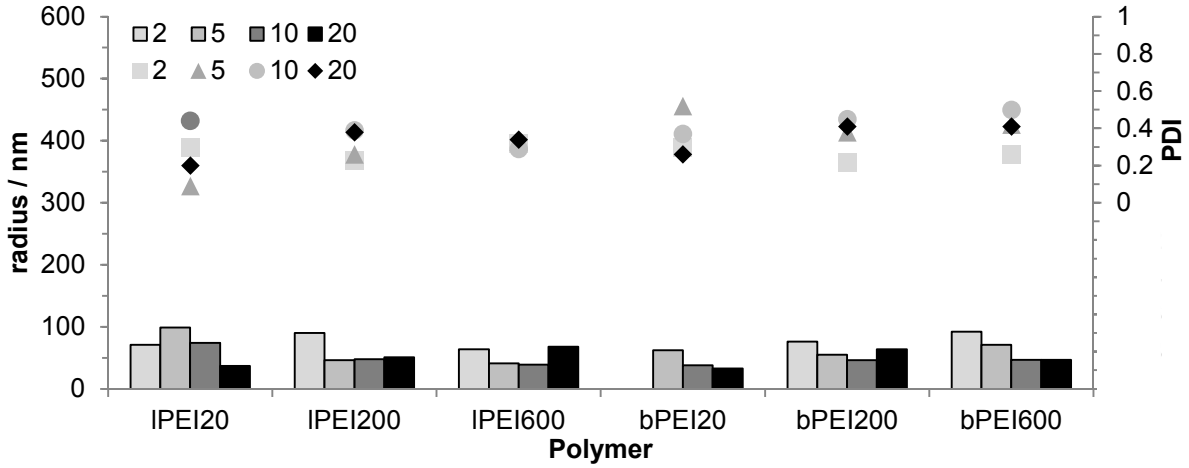

Figure S4. Hydrodynamic radii and PDI^P of polyplexes prepared from various linear and branched PEIs (number indicate the DP) at indicated NP ratios (2, 5, 10, 20) prepared by pipetting robot and measured with Zetasizer Nano ZS.

1. Tauhardt, L.; Kempe, K.; Knop, K.; Altuntaş, E.; Jäger, M.; Schubert, S.; Fischer, D.; Schubert, U. S., Linear Polyethyleneimine: Optimized Synthesis and Characterization – On the Way to "Pharmagrade" Batches. *Macromol. Chem. Phys.* **2011,** *212* (17), 1918-1924.
2. Altuntaş, E.; Knop, K.; Tauhardt, L.; Kempe, K.; Crecelius, A. C.; Jäger, M.; Hager, M. D.; Schubert, U. S., Tandem mass spectrometry of poly(ethylene imine)s by electrospray ionization (ESI) and matrix-assisted laser desorption/ionization (MALDI). *J. Mass Spec.* **2012,** *47* (1), 105-114.
3. Perevyazko, I. Y.; Delaney, J. T.; Vollrath, A.; Pavlov, G. M.; Schubert, S.; Schubert, U. S., Examination and optimization of the self-assembly of biocompatible, polymeric nanoparticles by high-throughput nanoprecipitation. *Soft Matter* **2011,** *7* (10), 5030-5035.
4. Tang, M. X.; Szoka, F. C., The influence of polymer structure on the interactions of cationic polymers with DNA and morphology of the resulting complexes. *Gene Ther.* **1997,** *4* (8), 823-832.

Publication P5

A paradigm change: Efficient transfection of human leukemia cells by stimuli-responsive multicompartment micelles

A. C. Rinkenauer, A. Schallon, U. Günther, M. Wagner, E. Betthausen, U. S. Schubert, F. H. Schacher,

ACS Nano **2013**, *7*, 9624-9631.

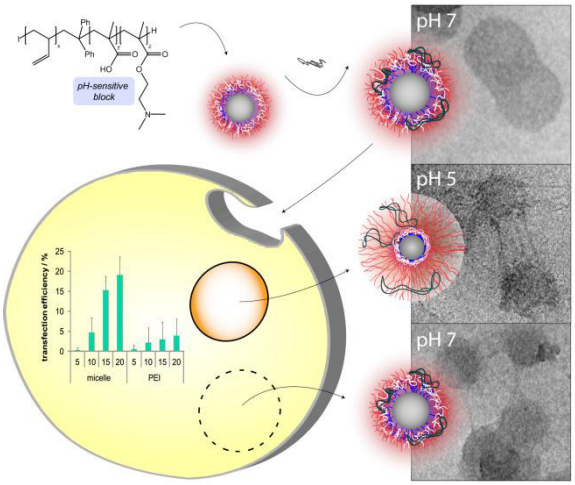

A Paradigm Change: Efficient Transfection of Human Leukemia Cells by Stimuli-Responsive Multicompartment Micelles

Alexandra C. Rinkenauer,[†,‡] Anja Schallon,[†,‡] Ulrike Günther,[†,‡] Michael Wagner,[†,‡] Eva Betthausen,[§] Ulrich S. Schubert,[†,‡,*] and Felix H. Schacher[†,‡,*]

[†]Laboratory of Organic and Macromolecular Chemistry (IOMC), Friedrich Schiller University Jena, Humboldtstrasse 10, 07743, Jena, Germany, [‡]Jena Center for Soft Matter (JCSM), Friedrich Schiller University Jena, Philosophenweg 7, 07743 Jena, Germany, and [§]Macromolecular Chemistry II, Bayreuth Center for Colloids and Interfaces, University Bayreuth, 95440 Bayreuth, Germany

ABSTRACT The controlled nonviral delivery of genetic material using cationic polymers into cells has been of interest during the past three decades, yet the ideal delivery agent featuring utmost transfection efficiency and low cytotoxicity still has to be developed. Here, we demonstrate that multicompartment micelles from stimuli-responsive triblock terpolymers, polybutadiene-*block*-poly(methacrylic acid)-*block*-poly(2-(dimethylamino)ethyl methacrylate) (BMAAD), are promising candidates. The structures exhibit a patchy shell, consisting of amphiphilic (interpolyelectrolyte complexes, MAA and D) and cationic patches (excess D), generating a surface reminiscent to those of certain viruses and capable of undergoing pH-dependent changes in charge stoichiometry. After polyplex formation with plasmid DNA, superior transfection efficiencies can be reached for both adherent cells and human leukemia cells. Compared to the gold standard PEI, remarkable improvements and a number of advantages were identified for this system, including increased cellular uptake and an improved release of the genetic material, accompanied by fast and efficient endosomal escape. Furthermore, high sedimentation rates might be beneficial regarding *in vitro* applications.

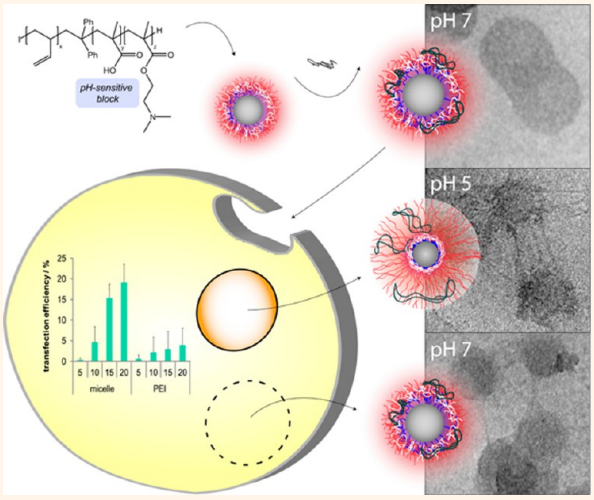

KEYWORDS: multicompartment micelles · interpolyelectrolyte complexes · nonviral gene transfection · polyplexes · human leukemia cells

The controlled delivery of genetic material into eukaryotic cells has been the focus of interdisciplinary scientific activities during the last three decades.[1,2] Within the field of nanomedicine, successful nonviral gene delivery holds great promise for the treatment of a wide variety of diseases, as a suitable transfection agent,[3] once identified, might be used in different approaches. Besides evolutionary qualified and very efficient viral transfection, nonviral delivery is of high interest, reflected in the large number of nonviral transfection agents being proposed. Thereby, among polymeric materials, poly(ethylene imine) (PEI) represents the "gold standard" for *in vitro* applications.[4]

The efficient protection of nucleic acids like plasmid DNA (pDNA) during delivery while maintaining utmost biocompatibility is one of the key requirements for such materials. In general, cationic polyelectrolytes are capable of forming polyplexes with negatively charged pDNA, the main driving forces being electrostatic interactions and a gain in entropy for the whole system.[5,6] Polyplexes with an excess of positive charges support both protection against degradation and uptake *via* the negatively charged cell membrane. Several studies show that the polymer architecture and the overall molar mass have a major influence on the transfection efficiency (TE).[7,8] Nevertheless, it is still

* Address correspondence to ulrich.schubert@uni-jena.de, felix.schacher@uni-jena.de.

Received for review April 25, 2013 and accepted October 22, 2013.

Published online October 22, 2013
10.1021/nn402072d

challenging to design systems comprising high TE and low cytotoxicity for gene delivery applications, as in the case of most cationic polymers, like PEI, high TEs are accompanied by increasing cytotoxicity. The use of poly(ethylene glycol) (PEG) as, *e.g.*, biocompatible shell is one straightforward approach to decrease the cytotoxicity but usually leads to lower TE.[9,10]

In addition, up to now most nonviral transfection agents fail in case of suspension cells, *e.g.*, Jurkat T cells, a model cell line for human leukemia cells. This has been attributed to the fact that 3D cultivation decreases the contact probability between cells and polyplexes in general, if compared to the mechanism proposed for the transfection of adherent cells.[11,12] Hence, designing polymers that are capable of efficient gene transfer into suspension cells would allow targeting immune cells for the therapy of immune defects (*e.g.*, HIV), for cancer (*e.g.*, leukemia), or to improve transient transfection in biotechnological approaches.[13] All these issues are further impeded by the fact that the underlying transfection mechanism for pDNA in contrast to siRNA (short interfering RNA) is far from being completely understood, rendering the design of efficient transfection agents for this purpose extraordinarily difficult.[14,15]

Here, we demonstrate for the first time the advantage of pH-responsive multicompartment micelles formed *via* self-assembly of a stimuli-responsive triblock terpolymer, polybutadiene-*block*-poly(methacrylic acid)-*block*-poly(2-(dimethylamino)ethyl methacrylate) (BMAAD, PB_{800}-*b*-$PMAA_{200}$-*b*-$PDMAEMA_{285}$; the subscripts denote the degrees of polymerization; the overall molar mass of BMAAD is 105 300 g/mol), as promising transfection agents for pDNA. Multicompartment structures represent a unique class of materials where either core, shell, or corona are further subdivided. Several strategies have been used to induce compartmentalization in block copolymer derived materials, including combinations of highly incompatible segments, kinetic control, or stepwise self-assembly by applying solvent mixtures.[16−18] Although multicompartment architectures have been in the focus for more than two decades, applications have been scarcely demonstrated. One very elegant example, however, was shown by Lodge and co-workers, where the segregated domains within micellar cores could be used to store two different hydrophobic guest molecules.[19] Regarding pH-responsive micellar carriers as gene delivery vehicles, pioneering work was performed by Kataoka and co-workers. For example, they used ABC triblock terpolymers with two cationic segments of different pK_a, facilitating the disruption of the endosome upon decrease of the pH[20] or, in another example, segments which underwent charge conversion during the uptake process.[21] Also, the use of pH-sensitive linkers between unlike segments of AB diblock copolymers has proven to be advantageous.[22]

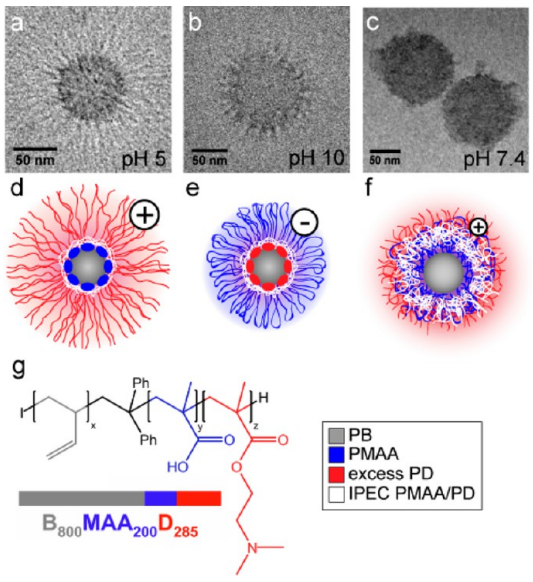

Figure 1. Cryo-TEM micrographs and schematic depictions of BMAAD micelles at pH 5 (a, d), pH 10 (b, e), and pH 7.4 (c, f). Structure and block lengths of the used BMAAD triblock terpolymer (g). Cryo-TEM images of pure BMAAD (a, b, c) and schematic illustrations thereof (d, e, f).

The aim of this work was to investigate how the rather heavy and voluminous BMAAD micelles can be used as efficient and pH-responsive nonviral gene transfection agents for adherent cells and human T-lymphocytes. We were interested whether the presence of different surface patches, also known from viral structures (*e.g.*, alpha viruses),[23−25] influences important process bottlenecks such as cytotoxicity or carrier/serum interaction. Further, insights into the underlying mechanism for pDNA transfection (which is far from being completely understood) by using a combination of different analytical techniques including asymmetric flow field-flow fractionation (AF4), cryogenic electron microscopy (cryo-TEM), analytical ultracentrifugation (AUC), and confocal laser scanning microscopy (CLSM) are presented.

RESULTS AND DISCUSSION

In our case, for BMAAD (PB_{800}-*b*-$PMAA_{200}$-*b*-$PDMAEMA_{285}$), the hydrophobic PB forms the micellar core, which, at low pH, is surrounded by a PMAA shell and a PDMAEMA corona (Figure 1). Such micelles are dynamic and show a strong pH-dependence concerning their shape, size, and surface charge.[26] At endosomal pH (~ 5), PMAA is uncharged, and PDMAEMA forms a cationic corona (Figure 1a and d), whereas at pH 10, PDMAEMA is uncharged and partially collapsed, and merely PMAA now forms a negatively charged corona (Figure 1b and e). Under physiological conditions (pH ~ 7.4) both blocks are charged, leading to the formation of an intramicellar interpolyelectrolyte complex (*im*-IPEC) shell (Figure 1c and f). Hence, the micellar surface is patchy, featuring both charge neutral (*im*-IPEC) and

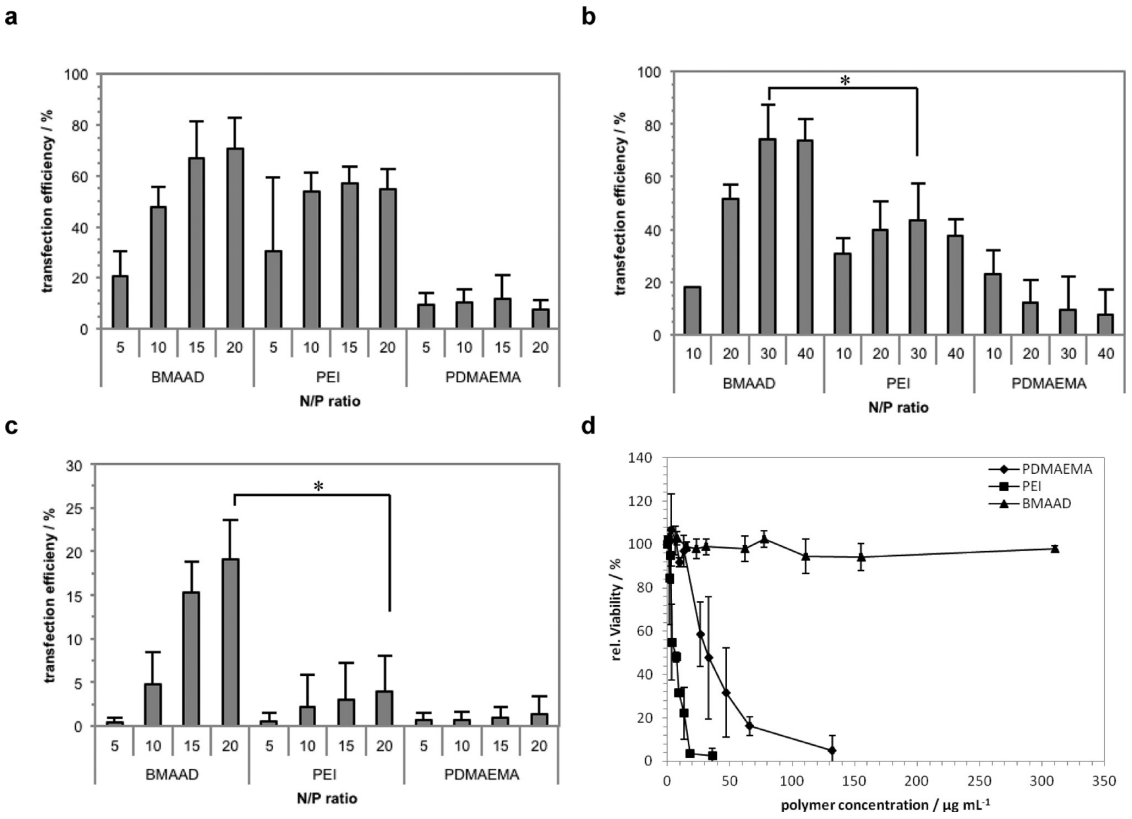

Figure 2. Transfection efficiencies of BMAAD, PEI_{570}, and $PDMAEMA_{191}$ for adherent HEK cells in serum-reduced (a) and serum-containing media (b) and human leukemia cells (c) at different N/P ratios. An EGFP (pEGFP-N1) was used as reporter gene. Cytotoxicity tests using L929 cells (d). Values represent the mean ± S.D; * represents a significant difference ($p < 0.01$).

cationic domains (the DP of PDMAEMA is higher than for the PMAA segment, resulting in an excess positive net charge). These IPEC patches may lead to an increased polycation density within parts of the corona, and this in turn favors the formation of patchy structures upon further complex formation.[27]

First, transfection studies of BMAAD with pDNA under serum-reduced conditions as well as with media containing 10% serum were performed with adherent HEK293 cells, using linear PEI_{570} (25 kDa) and $PDMAEMA_{191}$ (30 kDa) as comparison. The BMAAD micelles showed very high TE, even compared to PEI (BMAAD: 70 ± 12% at N/P 20; PEI: 55 ± 8% at N/P 20) under serum-reduced conditions (Figure 2a and Figure S1, Supporting Information). In contrast, linear PDMAEMA reaches only 12 ± 9% at N/P 15. This increased TE for adherent cells by using BMAAD micelles is in agreement with earlier studies on star-shaped PDMAEMA or micelles with a PDMAEMA corona.[28] In the presence of serum even superior results were obtained for BMAAD (74 ± 8% at N/P 30), comparable to Lipofectamine 2000,[29] whereas the TE decreased significantly for PEI (43 ± 7% at N/P 30; Figure 2b). The fact that BMAAD performs even better under serum conditions is remarkable as in general serum leads to unspecific interactions and lower TEs in case of cationic polymers.[28,30]

As the next step, the transfection of Jurkat T suspension cells with pDNA was evaluated. Figure 2c shows a TE of up to 19 ± 6% with polyplexes formed from BMAAD and pDNA (N/P 20), whereas both PEI and PDMAEMA show a significantly reduced TE, which is in agreement with literature.[31] The fact that BMAAD micelles reach a 5-fold higher TE compared to PEI highlights the potential of these structures as powerful transfection agents. It should be noted that the presence of PMAA within the *im*-IPEC shell does not decrease the TE. Moreover, transfection experiments under non static conditions (shaking) resulted in similar transfection efficiencies (Figure S8, Supporting Information). We also found no detectable cytotoxicity of BMAAD using sensitive L929 cells (Figure 2d) for concentrations up to 320 μg mL^{-1}, in contrast to PDMAEMA and PEI, which show IC_{50} values of 30 and 6 μg mL^{-1}, respectively. Even polyplexes of PEI/pDNA show lower values ($IC_{50} \sim 10$ μg mL^{-1}).[32] We propose that the PMAA block of BMAAD is responsible for the decreased cytotoxicity, without decreasing the TE in contrast to PEG.[10,33] Hence, the patchy micellar surface featuring cationic domains and neutral *im*-IPECs might serve as leverage to circumvent what is often called the "PEG-dilemma" (decreasing TE in the presence of a shielding PEG corona). The outstanding biocompatibility in combination with high TE values for

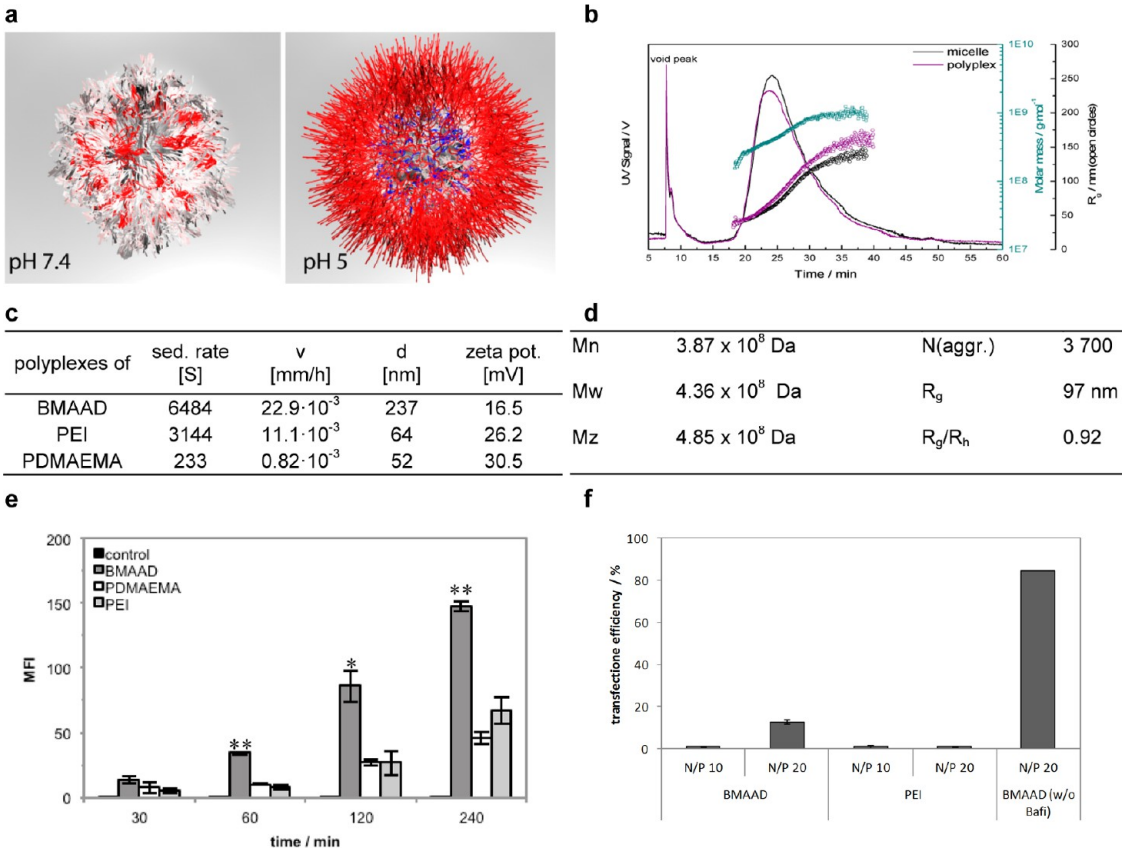

polyplexes of	sed. rate [S]	v [mm/h]	d [nm]	zeta pot. [mV]
BMAAD	6484	$22.9 \cdot 10^{-3}$	237	16.5
PEI	3144	$11.1 \cdot 10^{-3}$	64	26.2
PDMAEMA	233	$0.82 \cdot 10^{-3}$	52	30.5

Mn	3.87×10^8 Da	N(aggr.)	3 700
Mw	4.36×10^8 Da	R_g	97 nm
Mz	4.85×10^8 Da	R_g/R_h	0.92

Figure 3. Proposed surface characteristics of the BMAAD micelle (color code: red, positive charges/PDMAEMA; blue, negative charges/PMAA; white, neutral *im*-IPEC domains; a). Detailed characteristics of BMAAD micelles obtained by asymmetric flow field flow fractionation (AF4) at pH 7 (b, d). Sedimentation velocity, hydrodynamic diameter, and zeta potential of polyplexes formed at N/P 20 (c). Mean fluorescence intensity (MFI) of cells transfected with YOYO-1 labeled pDNA for indicated time points using BMAAD, PEI_{570}, and $PDMAEMA_{191}$ (e). Values represent the mean ± S.D; * represents a significant difference ($p < 0.05$) to PEI_{570} and $PDMAEMA_{191}$; ** represents a significant difference ($p < 0.01$) to PEI_{570} and $PDMAEMA_{191}$, # represents a significant difference ($p < 0.01$) to $PDMAEMA_{191}$. Transfection efficiencies using EGFP as reporter gene of BMAAD and PEI for adherent HEK cells treated with Bafilomycin (f).

BMAAD is impressive, as generally increases in efficiency are accompanied by higher cytotoxicity for transfection agents.[7,34] Thus, using an ampholytic triblock terpolymer containing both a cationic and an anionic segment allows constructing efficient nonviral gene delivery agents even though the cationic part, PDMAEMA, is usually regarded as being not very efficient.[35]

As such an outstanding performance was not anticipated for BMAAD, we were interested in the underlying mechanism. Therefore, all formed polyplexes were investigated with an ethidium bromide exclusion assay (EBA)[36] and dynamic light scattering (DLS) experiments. Both BMAAD and PDMAEMA show similar binding affinities to pDNA, but the values are lower compared to PEI (Figure S2, Supporting Information). This indicates the successful formation of polyplexes in all cases, as EBA only provides a qualitative assessment.[37] In addition, we performed a DNA gel migration assay, confirming the successful pDNA complexation at N/P 5 as no free pDNA could be detected (Figure S3, Supporting Information).

All polyplexes investigated exhibit a positive net charge at physiological pH, as shown in zeta-potential measurements (Figure 3c). Hydrodynamic diameters of 64 nm (PEI), 237 nm (BMAAD), and 52 nm (PDMAEMA) can be observed (Figure 3c). For BMAAD, the formed polyplexes are of comparable size as the "bare" micelles (212 nm),[26] which can be explained by a rather tight wrapping of pDNA around the particles.[38] pH-dependent surface characteristics of BMAAD are schematically presented in Figure 3a. At physiological pH (7.4) most of the PDMAEMA forms *im*-IPECs with PMAA (white), whereas a slightly positive surface charge is caused by excess protonated PDMAEMA (DP PDMAEMA > DP PMAA).[26] At endosomal pH (~5), PDMAEMA is highly protonated and stretched, whereas PMAA partially collapses. This is supported by pH-dependent zeta potential measurements. The appearance of neutral *im*-IPECs, cationic patches on the polyplex surface, and strong changes as a response to variations of the pH are also known from clusters of viral particles.[23−25]

The results could also be confirmed by asymmetric flow field-flow fractionation (AF4, Figure 3b), where an R_g of 97 nm was obtained for BMAAD and 111 nm for the corresponding polyplex; the obtained molar

masses were $M_n = 3.87 \times 10^8$ g mol^{-1} and $M_w = 4.36 \times 10^8$ g mol^{-1} for the micelle (Figure 3b and d). From the molar mass of the single triblock terpolymer (105 300 g mol^{-1}) the aggregation number can be calculated to roughly 3 700. Combining these results with the DLS data, the general ratio R_g/R_h, which provides information about the shape and the conformation of the sample, can be calculated. Typical values are 0.775 for a hard sphere, 1.0 for a soft sphere, or 1.78 for a monodisperse linear polymer chain in a good solvent.[39] In this study a value of 0.92 for the micelle and 0.94 for the corresponding polyplex were obtained, which both fit to the expected model of a soft sphere. With decreasing pH, the zeta potential as well as the hydrodynamic diameter increases from 16.5 mV and 237 nm to 30.3 mV and 420 nm (Figures 3c and 5). In addition, the stability of the BMAAD polyplexes in the presence of serum after 4 h was analyzed, and no significant changes could be observed (hydrodynamic diameter 230 nm), suggesting that no protein based aggregation takes place.

To achieve successful transfection in case of human leukemia cells, the binding affinity between polymer and pDNA, size, and zeta potential of the polyplexes is crucial. However, this has to be complemented by an enhanced recognition and uptake by the cells. The uptake is mainly influenced by the charge and a high concentration of polyplexes at the cell surface.[40] The latter can be accessed *via* the sedimentation rate of the polyplexes, as determined by analytical ultracentrifugation (AUC). Presumably, larger particles with higher sedimentation coefficients lead to an increased particle uptake in case of *in vitro* transfection.[41,42] Indeed, the trends observed from DLS studies (Figure 3c) can be confirmed, as polyplexes from BMAAD micelles revealed a higher sedimentation rate (6480 S) compared to PEI (3140 S) and PDMAEMA (230 S), most probably due to the rather dense PB core. This leads to longer and more intensive interactions between the cells and the polyplexes and, hence, an increased internalization.

To investigate the time-dependent cellular uptake of polyplexes, YOYO-1 labeled pDNA was used (Figure 3e and S8, Supporting Information). An enhanced uptake can be clearly achieved with BMAAD micelles compared to PEI or PDMAEMA. Already after 1 h the majority of cells internalized the labeled polyplexes with BMAAD, whereas 4 h are necessary in case of PEI (Figure S8, Supporting Information). Even more impressive, the overall amount of labeled pDNA taken up by all viable cells (mean fluorescence intensity, MFI, Figure 3e) is almost doubled for BMAAD at all indicated time points, demonstrating the enormous potential of these structures.

One previously identified bottleneck during transfection studies is the endosomal escape of polyplexes. For PEI, a rather high buffer capacity is known, causing the so-called proton sponge effect.[43] In contrast to PEI, PDMAEMA has lower buffer capacities,[26,44] which might explain a lower TE of linear PDMAEMA but not the high TE of BMAAD. Therefore, the behavior of BMAAD at endosomal pH ($\sim$ 5) was studied in more detail. Here, a rather stretched PDMAEMA corona and a partially collapsed PMAA shell can be anticipated.[26] The increased amount of positive charges lead to strong interactions with cellular membranes and, potentially, destabilization. This was confirmed both for the polymers and the polyplexes by a hemolysis assay at different pH values (Figure 4a and Figure S7, Supporting Information). While both PEI and PDMAEMA did not exhibit any hemolytic activity (Figure S7, Supporting Information), a strong pH-dependence with up to 30 and 8% at pH 5 was found for the BMAAD micelles and polyplexes, respectively. This supports our assumption that BMAAD destabilizes the endosomal membrane under acidic conditions and that the polyplex is released into the cytoplasm. The fact that this endosomal disruption is pH-dependent demonstrates the unique potential of such structures to react on subtle environmental changes and thereby induce endosomal escape.[45] To confirm the endosomal uptake and the necessity of acidification for an efficient transfection using BMAAD, transfections with bafilomycin were performed. Bafilomycin is known to inhibit the ATPases in the endosomes and therefore prevents acidification. The TEs of BMAAD and PEI are significantly decreased (Figure 3f) to 13 and 1%, respectively. It supports our assumption that endosomal pH facilitates destabilization and destruction of the endosomal membrane by shape/surface charge changes of the proposed BMAAD polyplexes. In addition, transfections were performed at 4 °C (Figure S8, Supporting Information), also significantly reducing the TE. To prove the fast and efficient endosomal escape, the colocalization of transported pDNA was investigated using confocal laser scanning microscopy (CLSM, Figure 4c). Therefore YOYO-1 labeled pDNA (green, Figure 4c) and LysoTracker Red (red, Figure 4c) were used to visualize the polyplexes as well as the late endosomes and lysosomes, respectively. Even after 1 h, a strong correlation of pDNA from PEI and PDMAEMA polyplexes and endosomes could be detected (yellow signal, Figure 4c) in contrast to BMAAD-based polyplexes. To verify the uptake of the BMAAD polyplexes *via* endocytosis, the colocalization of BMAAD polyplexes and early endosomes was demonstrated (Figure S8, Supporting Information).

Once the polyplexes are released into the cytoplasm, their dissociation is of great importance and was investigated using heparin, a negatively charged polysaccharide (Figure 4b). Typically, heparin concentrations of 10 U mL^{-1} are necessary to achieve a total release of pDNA from PEI-based polyplexes,[4] whereas 50 U mL^{-1} were needed for linear PDMAEMA, which is

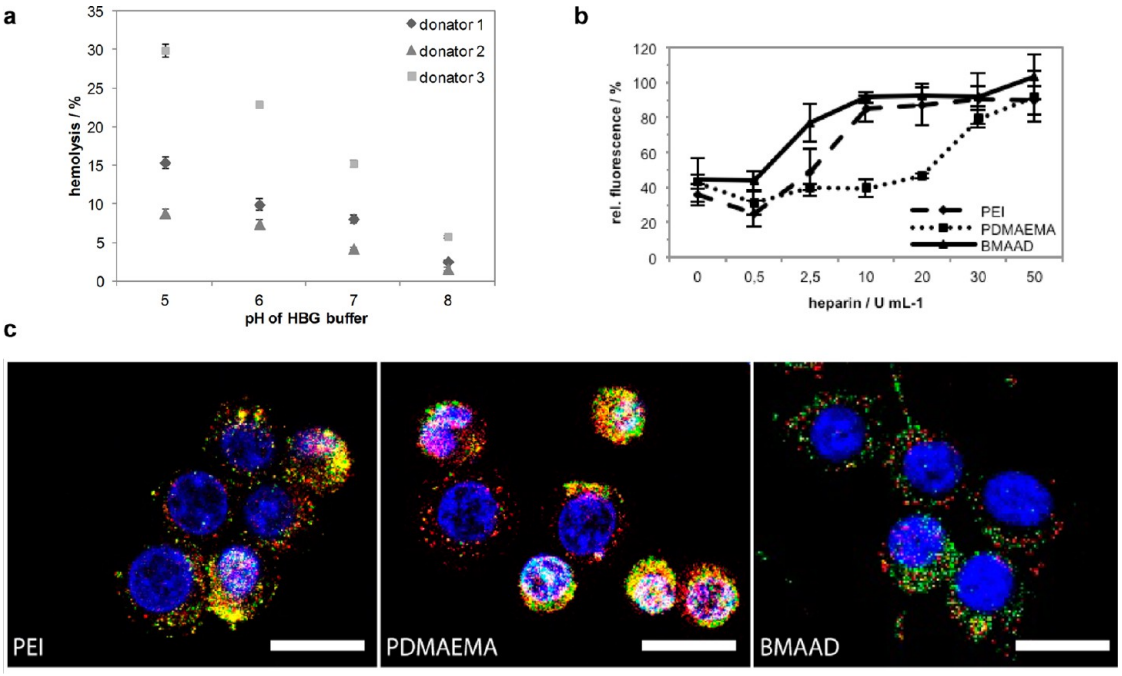

Figure 4. pH-dependent hemolysis assay of BMAAD of three different donators, each n = 3 (a). Dissociation assay of polyplexes formed at N/P 10 with increasing heparin concentrations (b). CLSM images of HEK cells transfected with indicated polymer based polyplexes and YOYO-1 labeled pDNA (green); late endosomes/lysosomes were stained with LysoTracker Red (red), and cell nuclei were stained with Hoechst 33342 (blue); each scale bar represents 20 μm; colocalization of pDNA and endosomal compartments are depicted in yellow (c).

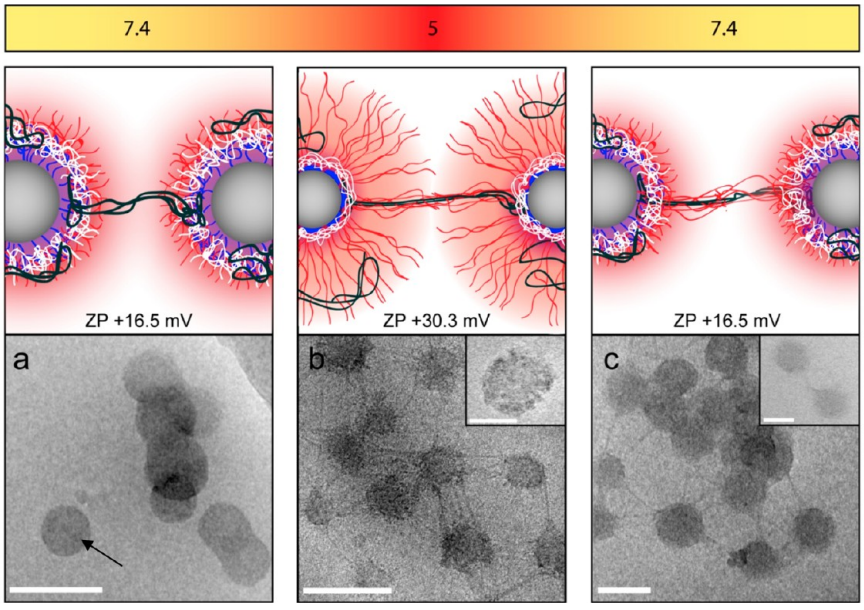

Figure 5. Schematic depiction of the proposed polyplex structure and the corresponding cryo-TEM micrographs at pH 7.4; the black arrow indicates the presence of *im*-IPECs (a), pH 5 (b), and pH 7.4 (c). Zeta potentials (ZP) of BMAAD polyplexes at pH 7.4 (16.5 mV) and pH 5 (30.3 mV). Color code: gray (PB), blue (PMAA), red (PDMAEMA), white (*im*-IPEC), and black (pDNA-polyplex). Scale bars indicate 200 nm and 50 nm in the insets.

a reason for the lower TE. Although BMAAD and PDMAEMA showed comparable binding affinities, the addition of only 10 U mL^{-1} of heparin led to an almost complete release of pDNA from BMAAD-based polyplexes. We attribute this to the PMAA block acting as a competing polyanion. In addition, the dissociation assay performed at pH 5 (Figure S5, Supporting Information) demonstrated a higher binding to pDNA, and thus, no polyplex dissociation in the endosome can be assumed.

The structure of the formed polyplexes was further investigated using cryo-TEM measurements at different pH-values (Figure 5). At pH 7.4, the BMAAD micelles are close to their isoelectric point,[26] and polyplex

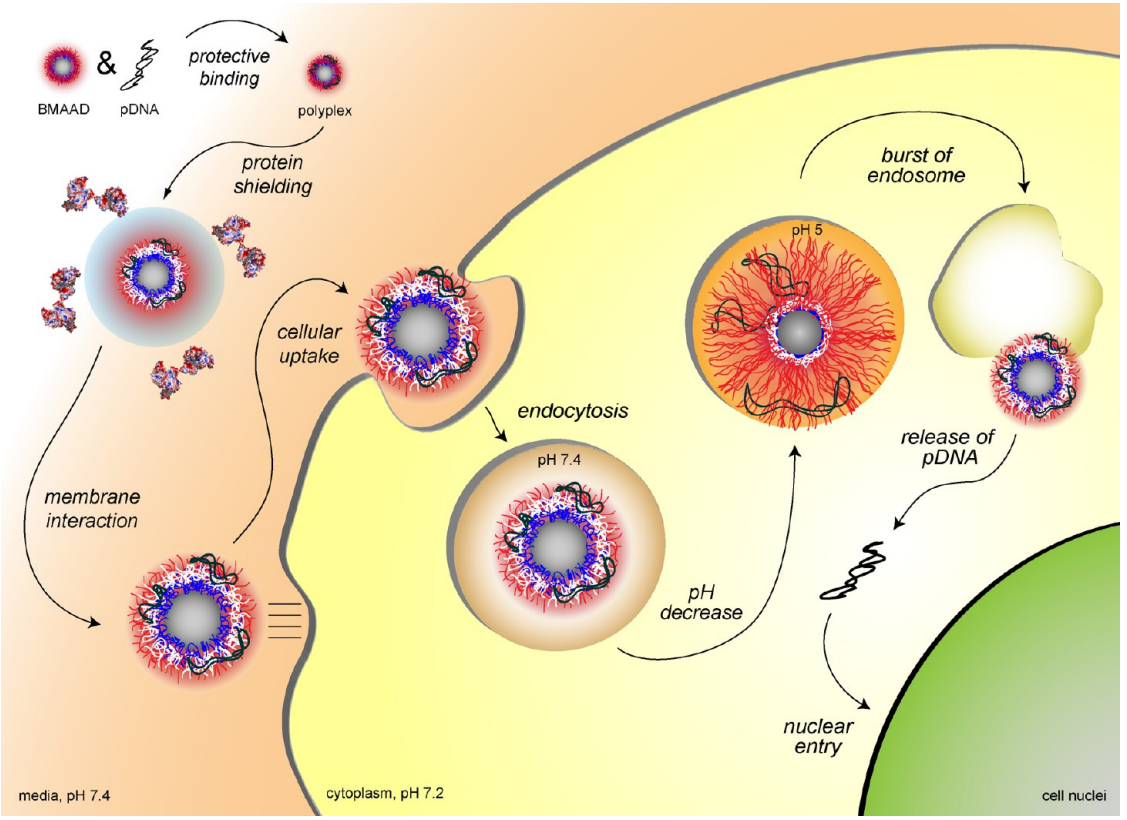

Figure 6. Schematic illustration of the proposed transfection mechanism for BMAAD-based polyplexes, with respect to the biological hurdles. The BMAAD micelle protects the genetic material (pDNA), prevents aggregation, and the cationic corona enables a fast and efficient cellular binding and uptake. Inside the endosomes, a decrease in pH leads to a swelling of the cationic corona and to a destabilization of the endosomal membrane. The release of the genetic material inside the cytoplasm is promoted by the middle block, PMAA, acting as a competing polyanion.

formation with pDNA leads to rather homogeneous structures of spherical shape (cryo-TEM, Figure 5a). The observed clustering can be explained by the rather low zeta potential of 16.5 mV. A decrease in pH within the endosome was simulated by the titration with dilute HCl until a pH of 5 was reached. This leads to full protonation and stretching of the PDMAEMA corona ($pK_a \sim 7.7$, zeta potential of 30.3 mV). Afterward, severe structural changes occur, as shown in Figure 5b: parts of the micellar core are covered by collapsed PMAA patches (blue), and in addition, the polyplexes formed of PDMAEMA (red) and pDNA (black) appear more dense and rigid, as seen in the protrusions connecting several micellar structures.[26]

These observations support our assumption of an endosomal burst occurring under these conditions and the data provided by hemolysis (Figure 4a). Subsequently, if the polyplex leaves the endosome, the pH within the cytoplasm rises to approximately 7.4, which was simulated for the same polyplex solution (Figure 5c). The cryo-TEM micrograph now shows polyplexes with the combined characteristics of Figure 5a and b: PMAA is resolubilized *via* deprotonation, leading to a more homogeneous overall appearance, and the rather rigid PDMAEMA/pDNA strands are still present, interconnecting several micelles. The latter can be explained by a closer look at the linear homopolymer of PDMAEMA, showing a rather strong binding between PDMAEMA and pDNA (linear PDMAEMA in Figure 4b). Since the polyplex is formed, neither an increase in pH (4 to 9, data not shown) nor the addition of heparin facilitated an easy release of pDNA. Hence, in the case of the BMAAD the negatively charged PMAA block acts as a competing polyelectrolyte, presumably reduces the binding between PDMAEMA and pDNA, and enables the release of genetic material in the cytoplasm. Comparable structural rearrangements induced by changes in pH have been reported for the Sindbis virus.[25]

So far, the use of BMAAD led to high TE and was accompanied by surprisingly low cytotoxicity and a facilitated release of pDNA. To highlight the advantage of this system, the proposed transfection mechanism with respect to the biological hurdles was schematically illustrated in Figure 6. After polyplex formation with pDNA, the internalization of the resulting structures crucially depends on the interaction with proteins and the cellular membrane. As we observed high transfection efficiency in the presence of serum proteins (Figure 2b) and no protein dependent aggregation, a good shielding behavior can be assumed. On the other hand, extremely fast cellular uptake

(Figure 3e and S8, Supporting Information) is caused by the presence of cationic surface patches, reminiscent to the surface clusters of certain viruses.[46,47] After internalization *via* endocytosis, prompt escape of the polyplexes from the endosome is facilitated by an increase in size and zeta potential due to protonation and swelling of the PDMAEMA segments (Figure 3a and Figure 5), avoiding both digestion and exocytosis (Figure 4c). In the cytoplasm, the release of the genetic material is supported by the presence of the middle block, PMAA, acting as a competing polyanion, resulting in an efficient expression of the reporter gene.

CONCLUSION

The successful design of powerful gene delivery agents imposes a range of bottlenecks,[15] but research efforts are justified by the potential applications within medicine and biotechnology.[48] Here, we presented a first study on the use of multicompartment micelles from stimuli-responsive triblock terpolymers as a new class of potential transfection agents. We propose that this might be the first step of a paradigm change for nonviral gene transfection agents as low cytotoxicity can be combined with outstanding TE for both adherent cells and rather hard-to-transfect human leukemia cells. In particular in the latter case, remarkable improvements compared to PEI and linear PDMAEMA were shown.

Detailed investigations of the underlying mechanism revealed a number of advantages for this system: the dense core of the BMAAD micelles leads to higher sedimentation rates and a superior cellular uptake. Furthermore, the interaction of two oppositely charged weak polyelectrolytes (PMAA and PDMAEMA) leading to *im*-IPECs and charge-neutral patches is to our opinion responsible for the reduced serum aggregation, unaffected viability, enhanced cellular uptake, and an improved pDNA release. In addition, under acidic conditions PDMAEMA provokes an increase in size and zeta potential, responsible for membrane destabilization and the release of the polyplex from the endosome.

Moreover, we believe that our results may aid in a profound understanding of the transfection mechanism of pDNA. Our mechanism was developed based on a combination of hemolysis data, cryo-TEM investigations (which provide structural insight into a model system), and microscopic images. All this is supported by pH-dependent zeta potential and size measurements.

In consequence, these effects render BMAAD a powerful advanced carrier for pDNA transfection studies, outperforming the "gold standard" PEI while maintaining superior biocompatibility. This work shows that by adopting certain design concepts from viruses (defined and responsive surface patches[23−25]) *via* the synthesis of well-defined block copolymers and the corresponding self-assembled aggregates superior control over (mainly) interface-dominated processes can be achieved. Of course, the next step would be to perform electron microscopy under cell culture conditions at different stages of the transfection process. To achieve this, we are currently working on strategies targeting the *in situ* immobilization of cells during different stages of transfection using fast gelation processes in aqueous media.

METHODS

Materials. Linear 25 kDa PEI was purchased from Polysciences (Eppelheim, Germany). Ethidium bromide solution 1% was purchased from Carl Roth (Karlsruhe, Germany). AlamarBlue, cell light early endosomes-RFP, BacMAM and YOYO-1 were obtained from Life Technologies (Darmstadt, Germany). If not stated otherwise, cell culture materials, cell culture media, and solutions were obtained from PAA (Pasching, Austria). Plasmid pEGFP-N1 (4.7 kb, Clontech, USA) was isolated using Qiagen Giga plasmid Kit (Hilden, Germany). All other chemicals were purchased from Sigma Aldrich (Steinhausen, Germany) and are of analytical grade or better and used without further purification. 2-Cyano-2-butyl dithiobenzoate (CBDB) was purchased from Aldrich and used without further purification. Azobis(isobutyronitrile) (AIBN, Aldrich) was recrystallized from methanol. 2-(Dimethylamino)-ethyl methacrylate (DMAEMA) was purchased from Aldrich and passed over a column filled with inhibitor remover prior to usage.

Synthesis of BMAAD Micelles. Synthesis and characterization of the BMAAD micelles were described previously.[26] Briefly, linear BTD triblock terpolymers were synthesized *via* sequential living anionic polymerization of the corresponding monomers in THF at low temperatures using *sec*-BuLi as initiator. Prior to the reaction, freshly distilled THF (600 mL) was treated with *sec*-BuLi at −20 °C, followed by stirring overnight at room temperature to produce alkoxides to stabilize the living polybutadienyl chain ends during the polymerization. In a typical reaction, 1,3-butadiene (20.5 mL, 13.3 g, 0.246 mol) was initiated with *sec*-BuLi (0.2 mL, 0.3 mmol) at −70 °C in THF and polymerized at −10 °C for 8 h. After polymerization of the first block, the living butadienyl chain ends were end-capped with 1,1-diphenylethylene (0.11 mL, 0.11 g, 0.6 mmol) for 1 h at −50 °C to attenuate the nucleophilicity. In this way, transfer reactions upon addition of the second monomer, *t*BMA, could be suppressed. Subsequently, *t*BMA (9.3 mL, 8.2 g, 0.057 mol) was added to the reaction mixture *via* syringe and stirred for 1 h at −40 °C. After polymerization of the second block, DMAEMA (20.2 mL, 18.9 g, 0.12 mol) was added *via* syringe.

Hydrolysis of the PtBMA Block. The BTD terpolymers were dissolved in dioxane at a concentration of 1 g L^{-1}. A spatula of the stabilizer 2,6-di-*tert*-butyl-*p*-cresol (BHT) and a 10-fold excess of hydrochloric acid relative to the ester moieties were added and the reaction mixture was refluxed at 120 °C for 24 h. Afterward, the excess of HCl was removed by dialysis against deionized water. After dialysis, micellar stock solutions in deionized water with concentrations of approximately 0.5 g L^{-1} were obtained. From these stock solutions changes in pH or salinity were performed by dialyzing against the corresponding buffer solutions.

Polyplex Preparation. Polyplexes of pDNA and polymers were prepared by mixing stock solutions of pDNA and polymers at a certain N/P ratio with 15 μg mL^{-1} of pDNA solution in HBG buffer (20 mM 4-(2-hydroxethyl) piperazine-1-ethanesulfonic acid (HEPES) and 5% (w/v) glucose, pH 7.2). Subsequently, the solutions were vortexed for 10 s at maximal speed and incubated at room temperature for 20 min.

Transfection of Adherent and Suspension Cells. HEK-293 cells (CRL-1573, ATCC) and Jurkat (TIB-152, ATCC) cells were maintained in RPMI 1640 culture medium, L929 cells (CCL-1, ATCC) in DMEM culture medium. Both media were supplemented with 10% fetal calf serum (FCS), 100 μg mL^{-1} of streptomycin, 100 IU mL^{-1} of penicillin, and 2 mM L-glutamine. Cells were cultivated at 37 °C in a humidified 5% CO_2 atmosphere.

For transfection of the adherent cell lines, cells were seeded at a density of 10^5 cells per well in 12-well plates one day before transfection. One hour prior to transfection, cells were rinsed with PBS and supplemented with 1 mL of OptiMEM (Life Technologies) or fresh serum-containing growth media (without antibiotics). Polyplexes (100 μL) were added to the cells, and the plates were incubated for 4 h in the incubator. Afterward, the supernatant was replaced by 1 mL of fresh growth medium, and the cells were further incubated for 20 h. For analysis, adherent cells were harvested by trypsinization. In the case of the Bafilomycin experiments, 175 nM Bafilomycin was added briefly before polyplex addition to OptiMEM.

For transfection of suspension cells (Jurkat), 0.25×10^5 cells were seeded in 0.25 mL of OptiMEM in 24-well plates, one hour prior to transfection. The polyplex solutions (50 μL) were added, and the plates were incubated for 4 h in the incubator. Afterward, 0.25 mL of growth medium were added, and the cells were incubated for further 20 h. For determination of the viability during flow cytometry, dead cells were identified *via* counterstaining with propidium iodide. The relative expression of EGFP fluorescence of 10^4 cells was quantified *via* flow cytometry using a Cytomics FC 500 (Beckman Coulter). For determination of the transfection efficiency viable cells expressing EGFP were gated. The experiments were performed independently three times. Confocal laser scanning microscopy (CLSM) was performed using as LSM510 (Carl Zeiss).

Plasmid DNA Labeling. For labeling of 1 μg pDNA, 0.026 μL of 1 M YOYO-1 solution was mixed with pDNA in 20 μL of pure water. The solution was incubated for 1 h at room temperature protected from light, before HBG was added to the used pDNA concentration described before. Polymers were added at the indicated N/P ratio, and the polyplex solution was treated as described before and added to the cells. After 4 h of incubation, the cells were harvested and 10% trypan blue was added to quench the outer fluorescence of cells and identify only those cells, which have taken up the genetic material. To determine the relative uptake of NPs, 10 000 cells were measured by flow cytometry, and the amount of viable cells showing YOYO-1 signal were gated. For measuring the mean fluorescence intensity, all viable cells were measured.

Cytotoxicity. The cytotoxicity was tested with L929 cells, as this sensitive cell line is recommended by ISO10993-5. In detail, cells were seeded at 10^4 cells per well in a 96-well plate and incubated for 24 h. No cells were seeded in the outer wells. Afterward, polymers at the indicated concentrations were added, and the cells were incubated at 37 °C for further 24 h. Subsequently, the medium was replaced by D-PBS and AlamarBlue as recommended by the supplier. After incubation for 4 h, the fluorescence was measured at Ex 570/Em 610 nm, with untreated cells on the same well plate serving as controls. The experiments were performed independently three times.

Analytical Ultracentrifugation. Analytical ultracentrifugation (AUC) was performed on a Beckman XL-I analytical ultracentrifuge (Krefeld, Germany). Experiments were carried out in double-sector aluminum centerpieces with an optical path length of 12 mm in a four holes rotor setup. Each cell was filled with 0.42 mL of solvent (HBG) and 0.4 mL of sample. A rotor speed between 1000 to 10 000 rpm was used, depending on the sample. The system was equilibrated for 40 min at 25 °C in the centrifuge. Sedimentation data were recorded by absorbance optics. Data analysis was done by the Sedfit software.[49]

Asymmetric Flow Field-Flow Fractionation (AF4). Asymmetric flow field-flow fractionation (AF4) was performed on an AF2000 MT System (Postnova Analytics, Landsberg, Germany) coupled to a UV (PN3211, 260 nm), RI (PN3150), and MALLS (PN3070, 633 nm) detector. The eluent is delivered by three different pumps (tip, focus, cross-flow), and the sample is injected by an autosampler (PN5300) into the channel. The channel has a trapezoidal geometry and an overall area of 31.6 cm^2. The nominal height of the spacer was 500 μm, and a regenerated cellulose membrane with a molar mass cutoff of 10 kDa was used as accumulation wall. All experiments were carried out at 25 °C, and the eluent was degassed water containing 0.02% NaN_3 to avoid bacterial growth. To prevent attractive interactions between the negative surface of the membrane and the positive charges in the corona of the micelle, the membrane surface was saturated by injection of 100 μg of pure PDMAEMA with the same procedure as for the micellar systems described below. Twenty microliters of samples were injected with an injection flow rate of 0.2 mL min^{-1} and a cross-flow rate of 0.9 mL min^{-1} for 7 min (detector flow rate was set to 1 mL min^{-1}). After a focusing step, the cross-flow rate was reduced under an exponential gradient (0.3) within 15 min to 0.05 mL min^{-1} and kept constant for 25 min. Afterward the cross-flow rate was reduced to 0 mL min^{-1} for 15 min to ensure complete elution. The refractive index increment for BMAAD was measured by manual injection of a known concentration directly into the channel without any focusing or cross-flow. Integration of the RI signal gives a dn/dc of 0.156 mL g^{-1}. For calculation of the molar mass and the radius of gyration the Berry plot was used.[50] All measurements were repeated 5 times.

Cryo-TEM Measurements. For cryo-TEM, 5 μL of the sample solution (in HBG) were applied to copper grids covered with a holey carbon film (Quantifoil R3.5/1 Micro Tools GmbH, Jena, Germany). The excess of the solution was automatically blotted with a filter paper (1 s), and the grid was then plunged rapidly into liquid ethane (−180 °C) in a cryobox (Carl Zeiss NTS GmbH). After removing excess ethane with a filter paper, the samples were transferred with a cryotransfer unit (Gatan 626-DH, Gatan GmbH, Munich, Germany) into the precooled cryoelectron microscope operated at 120 kV (Philips CM 120, Eindhoven, Netherlands) and viewed under low dose conditions with a bottom-mounted 1k CCD camera.

Conflict of Interest: The authors declare no competing financial interest.

Acknowledgment. We acknowledge funding from the Carl-Zeiss Foundation and the Thuringian Ministry for Education, Science, and Culture (TMBWK; grants #B514-09051, NanoConSens, and #B515-10065, ChaPoNano). E.B. gratefully acknowledges funding by the state of Bavaria through a BayEFG scholarship and support by the Elite Network of Bavaria. F. H. S. is grateful for a fellowship from the Fonds der chemischen Industrie (FCI). Moreover, we thank C. Fritzsche for hemolysis studies and Alamar Blue assays, A. Krieg for the synthesis of PDMAEMA, and A. Press for microscopic investigations. We would further like to thank reviewers #1 and #3 for helpful and critical comments.

Supporting Information Available: Additional experimental section. Flow cytometer analysis, ethidium bromide quenching assays, agarose gel migration assays, additional cryo-TEM measurements, heparin dissociation assays, polyplex stability in the presence and absence of serum, pH-dependent hemolysis assays, as well as further data regarding the uptake mechanism of the polyplexes. This material is available free of charge *via* the Internet at http://pubs.acs.org.

REFERENCES AND NOTES

1. Miyata, K.; Nishiyama, N.; Kataoka, K. Rational Design of Smart Supramolecular Assemblies for Gene Delivery: Chemical Challenges in the Creation of Artificial Viruses. *Chem. Soc. Rev.* **2012**, *41*, 2562–2574.
2. Ringsdorf, H. Hermann Staudinger and the Future of Polymer Research Jubilees—Beloved Occasions for Cultural Piety. *Angew. Chem., Int. Ed.* **2004**, *43*, 1064–1076.
3. Itaka, K.; Kataoka, K. Recent Development of Nonviral Gene Delivery Systems with Virus-like Structures and Mechanisms. *Eur. J. Pharm. Biopharm.* **2009**, *71*, 475–483.
4. Breunig, M.; Lungwitz, U.; Liebl, R.; Goepferich, A. Breaking up the Correlation Between Efficacy and Toxicity for Nonviral Gene Delivery. *Proc. Natl. Acad. Sci. U. S. A.* **2007**, *104*, 14454–14459.

5. Howard, K. A. Delivery of RNA Interference Therapeutics Using Polycation-Based Nanoparticles. *Adv. Drug Delivery Rev.* **2009**, *61*, 710–720.
6. Pergushov, D. V.; Müller, A. H. E.; Schacher, F. H. Micellar Interpolyelectrolyte Complexes. *Chem. Soc. Rev.* **2012**, *41*, 6888–6901.
7. Synatschke, C. V.; Schallon, A.; Jerome, V.; Freitag, R.; Müller, A. H. E. Influence of Polymer Architecture and Molecular Weight of Poly(2-(dimethylamino)ethyl methacrylate) Polycations on Transfection Efficiency and Cell Viability in Gene Delivery. *Biomacromolecules* **2011**, *12*, 4247–4255.
8. Majewski, A. P.; Schallon, A.; Jerome, V.; Freitag, R.; Müller, A. H. E.; Schmalz, H. Dual-Responsive Magnetic Core-Shell Nanoparticles for Nonviral Gene Delivery and Cell Separation. *Biomacromolecules* **2012**, *13*, 857–866.
9. Nguyen, J.; Xie, X.; Neu, M.; Dumitrascu, R.; Reul, R.; Sitterberg, J.; Bakowsky, U.; Schermuly, R.; Fink, L.; Schmehl, T.; *et al.* Effects of Cell-Penetrating Peptides and Pegylation on Transfection Efficiency of Polyethylenimine in Mouse Lungs. *J. Gene Med.* **2008**, *10*, 1236–1246.
10. Mishra, S.; Webster, P.; Davis, M. E. PEGylation Significantly Affects Cellular Uptake and Intracellular Trafficking of Nonviral Gene Delivery Particles. *Eur. J. Cell Biol.* **2004**, *83*, 97–111.
11. Behr, J. P. Synthetic Gene Transfer Vectors II: Back to the Future. *Acc. Chem. Res.* **2012**, *45*, 980–984.
12. Jordan, M.; Wurm, F. Transfection of Adherent and Suspended Cells by Calcium Phosphate. *Methods* **2004**, *33*, 136–143.
13. Keller, H.; Yunxu, C.; Marit, G.; Pla, M.; Reiffers, J.; Theze, J.; Froussard, P. Transgene Expression, But Not Gene Delivery, Is Improved by Adhesion-Assisted Lipofection of Hematopoietic Cells. *Gene Ther.* **1999**, *6*, 931–938.
14. Gary, D. J.; Puri, N.; Won, Y. Y. Polymer-Based siRNA Delivery: Perspectives on the Fundamental and Phenomenological Distinctions from Polymer-Based DNA Delivery. *J. Controlled Release* **2007**, *121*, 64–73.
15. Whitehead, K. A.; Langer, R.; Anderson, D. G. Knocking Down Barriers: Advances in siRNA Delivery. *Nat. Rev. Drug Discovery* **2009**, *8*, 129–138.
16. Moughton, A. O.; Hillmyer, M. A.; Lodge, T. P. Multicompartment Block Polymer Micelles. *Macromolecules* **2011**, *45*, 2–19.
17. Cui, H.; Chen, Z.; Zhong, S.; Wooley, K. L.; Pochan, D. J. Block Copolymer Assembly *via* Kinetic Control. *Science* **2007**, *317*, 647–650.
18. Gröschel, A. H.; Schacher, F. H.; Schmalz, H.; Borisov, O. V.; Zhulina, E. B.; Walther, A.; Müller, A. H. E. Precise Hierarchical Self-Assembly of Multicompartment Micelles. *Nat. Commun.* **2012**, *3*, 710.
19. Lodge, T. P.; Rasdal, A.; Li, Z.; Hillmyer, M. A. Simultaneous, Segregated Storage of Two Agents in a Multicompartment Micelle. *J. Am. Chem. Soc.* **2005**, *127*, 17608–17609.
20. Fukushima, S.; Miyata, K.; Nishiyama, N.; Kanayama, N.; Yamasaki, Y.; Kataoka, K. PEGylated Polyplex Micelles from Triblock Cationers with Spatially Ordered Layering of Condensed pDNA and Buffering Units for Enhanced Intracellular Gene Delivery. *J. Am. Chem. Soc.* **2005**, *127*, 2810–2811.
21. Lee, Y.; Miyata, K.; Oba, M.; Ishii, T.; Fukushima, S.; Han, M.; Koyama, H.; Nishiyama, N.; Kataoka, K. Charge-Conversion Ternary Polyplex with Endosome Disruption Moiety: A Technique for Efficient and Safe Gene Delivery. *Angew. Chem., Int. Ed.* **2008**, *47*, 5163–5166.
22. Oishi, M.; Sasaki, S.; Nagasaki, Y.; Kataoka, K. pH-Responsive Oligodeoxynucleotide (ODN)−Poly(Ethylene Glycol) Conjugate through Acid-Labile β-Thiopropionate Linkage: Preparation and Polyion Complex Micelle Formation. *Biomacromolecules* **2003**, *4*, 1426–1432.
23. Huang, Q.; Sivaramakrishna, R. P.; Ludwig, K.; Korte, T.; Bottcher, C.; Herrmann, A. Early Steps of the Conformational Change of Influenza Virus Hemagglutinin to a Fusion Active State: Stability and Energetics of the Hemagglutinin. *Biochim. Biophys. Acta* **2003**, *1614*, 3–13.
24. Dimitrov, D. S. Virus Entry: Molecular Mechanisms and Biomedical Applications. *Nat. Rev. Microbiol.* **2004**, *2*, 109–122.
25. Paredes, A. M.; Ferreira, D.; Horton, M.; Saad, A.; Tsuruta, H.; Johnston, R.; Klimstra, W.; Ryman, K.; Hernandez, R.; Chiu, W.; *et al.* Conformational Changes in Sindbis Virions Resulting from Exposure to Low pH and Interactions with Cells Suggest that Cell Penetration May Occur at the Cell Surface in the Absence of Membrane Fusion. *Virology* **2004**, *324*, 373–386.
26. Betthausen, E.; Drechsler, M.; Förtsch, M.; Schacher, F. H.; Müller, A. H. E. Dual Stimuli-Responsive Multicompartment Micelles from Triblock Terpolymers with Tunable Hydrophilicity. *Soft Matter* **2011**, *7*, 8880–8891.
27. Schacher, F.; Betthausen, E.; Walther, A.; Schmalz, H.; Pergushov, D. V.; Müller, A. H. E. Interpolyelectrolyte Complexes of Dynamic Multicompartment Micelles. *ACS Nano* **2009**, *3*, 2095–2102.
28. Schallon, A.; Synatschke, C. V.; Jerome, V.; Müller, A. H. E.; Freitag, R. Nanoparticulate Nonviral Agent for the Effective Delivery of pDNA and siRNA to Differentiated Cells and Primary Human T Lymphocytes. *Biomacromolecules* **2012**, *13*, 3463–3474.
29. Keeney, M.; Ong, S.-G.; Padilla, A.; Yao, Z.; Goodman, S.; Wu, J. C.; Yang, F. Development of Poly(β-amino ester)-Based Biodegradable Nanoparticles for Nonviral Delivery of Minicircle DNA. *ACS Nano* **2013**, *7*, 7241–7250.
30. Fischer, D.; Bieber, T.; Li, Y.; Elsasser, H. P.; Kissel, T.; Novel Non-Viral, A. Vector for DNA Delivery Based on Low Molecular Weight, Branched Polyethylenimine: Effect of Molecular Weight on Transfection Efficiency and Cytotoxicity. *Pharm. Res.* **1999**, *16*, 1273–1279.
31. Wang, D. A.; Narang, A. S.; Kotb, M.; Gaber, A. O.; Miller, D. D.; Kim, S. W.; Mahato, R. I. Novel Branched Poly-(ethylenimine)-Cholesterol Water-Soluble Lipopolymers for Gene Delivery. *Biomacromolecules* **2002**, *3*, 1197–1207.
32. Schallon, A.; Jerome, V.; Walther, A.; Synatschke, C. V.; Müller, A. H. E.; Freitag, R. Performance of Three PDMAEMA-Based Polycation Architectures as Gene Delivery Agents in Comparison to Linear and Branched PEI. *React. Funct. Polym.* **2010**, *70*, 1–10.
33. Vollrath, A.; Schallon, A.; Pietsch, C.; Schubert, S.; Nomoto, T.; Matsumoto, Y.; Kataoka, K.; Schubert, U. S. A Toolbox of Differently Sized and Labeled PMMA Nanoparticles for Cellular Uptake Investigations. *Soft Matter* **2013**, *9*, 99–108.
34. Kwok, A.; Hart, S. L. Comparative Structural and Functional Studies of Nanoparticle Formulations for DNA and siRNA Delivery. *Nanomedicine* **2011**, *7*, 210–219.
35. van de Wetering, P.; Moret, E. E.; Schuurmans-Nieuwenbroek, N. M.; van Steenbergen, M. J.; Hennink, W. E. Structure-Activity Relationships of Water-Soluble Cationic Methacrylate/Methacrylamide Polymers for Nonviral Gene Delivery. *Bioconjugate Chem.* **1999**, *10*, 589–597.
36. Waring, M. J. Complex Formation between Ethidium Bromide and Nucleic Acids. *J. Mol. Biol.* **1965**, *13*, 269–282.
37. Schallon, A.; Synatschke, C. V.; Pergushov, D. V.; Jerome, V.; Müller, A. H. E.; Freitag, R. DNA Melting Temperature Assay for Assessing the Stability of DNA Polyplexes Intended for Nonviral Gene Delivery. *Langmuir* **2011**, *27*, 12042–12051.
38. Alhoranta, A. M.; Lehtinen, J. K.; Urtti, A. O.; Butcher, S. J.; Aseyev, V. O.; Tenhu, H. J. Cationic Amphiphilic Star and Linear Block Copolymers: Synthesis, Self-Assembly, and *in Vitro* Gene Transfection. *Biomacromolecules* **2011**, *12*, 3213–3222.
39. Burchard, W. Solution Properties of Branched Macromolecules. *Polym. Sci.* **1999**, *143*, 113–194.
40. Florian, M. W. Production of Recombinant Protein Therapeutics in Cultivated Mammalian Cells. *Nat. Biotechnol.* **2004**, 1393–1398.
41. Luo, D.; Saltzman, W. M. Enhancement of Transfection by Physical Concentration of DNA at the Cell Surface. *Nat. Biotechnol.* **2000**, *18*, 893–895.
42. Tros de Ilarduya, C.; Sun, Y.; Duzgunes, N. Gene Delivery by Lipoplexes and Polyplexes. *Eur. J. Pharm. Sci.* **2010**, *40*, 159–170.

43. Akinc, A.; Thomas, M.; Klibanov, A. M.; Langer, R. Exploring Polyethylenimine-Mediated DNA Transfection and the Proton Sponge Hypothesis. *J. Gene Med.* **2005**, *7*, 657–663.
44. Cherng, J. Y. Investigation of DNA Spectral Conformational Changes and Polymer Buffering Capacity in Relation to Transfection Efficiency of DNA/Polymer Complexes. *J. Pharm. Pharm. Sci.* **2009**, *12*, 346–356.
45. Lee, Y.; Miyata, K.; Oba, M.; Ishii, T.; Fukushima, S.; Han, M.; Koyama, H.; Nishiyama, N.; Kataoka, K. Charge-Conversion Ternary Polyplex with Endosome Disruption Moiety: a Technique for Efficient and Safe Gene Delivery. *Angew. Chem., Int. Ed.* **2008**, *47*, 5163–5166.
46. Penin, F.; Combet, C.; Germanidis, G.; Frainais, P. O.; Deleage, G.; Pawlotsky, J. M. Conservation of the Conformation and Positive Charges of Hepatitis C Virus E2 Envelope Glycoprotein Hypervariable Region 1 Points to a Role in Cell Attachment. *J. Virol.* **2001**, *75*, 5703–5710.
47. Karlin, S.; Brendel, V. Charge Configurations in Viral Proteins. *Proc. Natl. Acad. Sci. U. S. A.* **1988**, *85*, 9396–9400.
48. Christie, R. J.; Nishiyama, N.; Kataoka, K. Minireview: Delivering the Code: Polyplex Carriers for Deoxyribonucleic Acid and Ribonucleic Acid Interference Therapies. *Endocrinology* **2010**, *151*, 466–473.
49. Schuck, P. Size-Distribution Analysis of Macromolecules by Sedimentation Velocity Ultracentrifugation and Lamm Equation Modeling. *Biophys. J.* **2000**, *78*, 1606–1619.
50. Andersson, M.; Wittgren, B.; Wahlund, K. G. Accuracy in Multiangle Light Scattering Measurements for Molar Mass and Radius Estimations. Model Calculations and Experiments. *Anal. Chem.* **2003**, *75*, 4279–4291.

Supporting Information:

A Paradigm Change: Efficient Transfection of Human Leukemia Cells by Stimuli-Responsive Multicompartment Micelles

Alexandra C. Rinkenauer, Anja Schallon, Ulrike Günther, Michael Wagner, Eva Betthausen,

Ulrich S. Schubert*, Felix H. Schacher*

Laboratory of Organic and Macromolecular Chemistry (IOMC), Friedrich-Schiller-University Jena, Humboldtstrasse 10, Jena D-07743, Germany

Jena Center for Soft Matter (JCSM), Friedrich-Schiller-University Jena, Philosophenweg 7, Jena D-07743, Germany

E-Mail: felix.schacher@uni-jena.de; ulrich.schubert@uni-jena.de

Experimental section

Synthesis of PDMAEMA

A solution of 1.54 mL DMAEMA (1.43 g, 9.1 mmol), 8.5 mg CBDB (0.03 mmol) and 1 mg AIBN (0.0061 mmol) in 4 mL anisole was prepared in a microwave vial. The reaction vessel was capped, flushed with argon for 30 minutes and placed in an oil bath at 70 °C for 15 hours. Afterwards, the reaction solution was cooled down to ambient temperature and precipitated into 30 mL hexane to receive the final polymer. The dried polymer was characterized by size exclusion chromatography (SEC), providing its molar mass (M_n) of 27,600 and a PDI value of 1.28.

Size exclusion chromatography

SEC was measured on a Shimadzu system equipped with a SCL-10A system controller, a LC-10AD pump, and a RID-10A refractive index detector using a solvent mixture containing chloroform, triethylamine, and isopropanol (94:4:2) at a flow rate of 1 mL min^{-1} on a PSS-SDV-linear M 5 µm column at 40 °C. The system was calibrated with polystyrene (370 to 67,500 g mol^{-1}) and PMMA (2000 to 88,000 g mol^{-1}) standards.

Ethidium bromide quenching assay

The polyplex formation of pDNA and polymers was detected by quenching of the ethidium bromide (EB) fluorescence as described previously.[1] Briefly, 15 µg mL^{-1} pDNA in a total volume of 100 µL HBG were incubated with EB (0.4 µg mL^{-1}) for 10 min at room temperature. Then, polyplexes with increasing amounts of indicated polymers were prepared in black 96-well plates (Nunc, Langenselbold, Germany). The samples were equilibrated for 20 min before the fluorescence was measured using a Tecan Genios Pro fluorescence microplate reader (Tecan, Crailsheim, Germany); the excitation and emission wavelength were 525 and 605 nm, respectively. A sample containing only pDNA and EB was used to calibrate the device to 100% fluorescence against a background of 0.4 µg mL^{-1} of EB in HBG solution. The percentage of dye displaced upon polyplex formation was calculated using equation (1):

$$\mathrm{RFU}\ [\%] = \frac{F_{sample} - F_0}{F_{pDNA} - F_0} \mathrm{RFU}\ [\%] = \frac{F_{sample} - F_0}{F_{pDNA} - F_0} \quad (1)$$

Here, RFU is the relative fluorescence and F_{sample}, F_0, and F_{DNA} are the fluorescence intensities of a given sample, the EB in HBG alone, and the EB intercalated into pDNA alone.

Gel migration assay

The polyplexes were formed as described before in a volume of 50µL at the indicated N/P ratios and after 15 minutes incubation 5µL loading buffer (0.25% Bromphenolblue, 40% saccharose) was added. Afterwards the solutions were loaded to an 1% agarose gel, electrophorese (Bio-Rad, Munich, Germany, Mini-Sub Cell GT System) was carried out with a current of 80 V (PowerPac^{TM} Basic as power supply) for 1 h in TBE running buffer solution (107,8 g/L trise-base, 7,4g/L EDTA, 55g/L borate). Subsequently the agarose gel was incubated 30 min in TBE containing ethidium-bromid.

Heparin dissociation assay

To investigate the release of pDNA from polyplexes, the heparin dissociation assay was used. For this purpose, 15 µg mL^{-1} pDNA were incubated for 10 min with EB (0.4 µg mL^{-1}) in a total volume of 100 µL HBG (pH 7 and 5) before polyplexes at N/P 10 were formed. After 15 min in the dark the polyplexes were transferred into black 96-well plates, and heparin was added at the indicated concentrations. The solution was mixed and incubated for further 30 min at 37 °C in the dark. The fluorescence of EB (Ex 525 nm / Em 605 nm) was measured, and the percentage of intercalated EB was calculated as described before (1).

Hemolysis assay

The membrane damaging properties of the polymers were quantified by analyzing the release of hemoglobin from human erythrocytes. The hemolysis assay was performed as described before.[2] Briefly, blood from sheep was centrifuged at 4.500 × g for 5 min and the pellet was washed three times with cold DPBS. The stock solutions were diluted in HBG of indicated pH, and polymer solutions were prepared in HBG buffer as well. 100 µL of each solution were mixed and further incubated for 60 min at 37 °C. The release of hemoglobin in the supernatant was determined at 580 nm after centrifugation (2,400 g for 5 min). The absorbance was measured using a plate reader (Genios Pro, Tecan, Germany). For comparison, collected erythrocytes were washed with DPBS and either lysed with 1% Triton X-100 yielding the 100% lysis control value (A_{100}) or resuspended in DPBS as reference (A_0). The analysis was repeated with blood from at least six independent donors. The hemolytic activity of the polycations was calculated as follow (2):

$$\%\ \mathrm{Hemolysis} = 100 * \frac{(A_{sample} - A_0)}{(A_{100} - A_0)} \%\ \mathrm{Hemolysis} = 100 * \frac{(A_{sample} - A_0)}{(A_{100} - A_0)} \quad (2)$$

Here, A_{sample}, A_0, and A_{100} are the absorbance intensities of a given sample, erythrocytes incubated with DPBS, and erythrocytes lysed with Titon X-100.

Dynamic and electrophoretic light scattering

Dynamic light scattering (DLS) was performed on an ALV-CGS-3 system (ALV, Langen, Germany) equipped with a He-Ne laser operating at a wavelength of $\lambda = 633$ nm. The counts were detected at an angle of 90°. All measurements were carried out at 25 °C after an equilibration time of 120 sec. For analyzing the autocorrelation function (ACF), the CONTIN algorithm[3] was applied. Apparent hydrodynamic radii were calculated according to the Stokes–Einstein equation.

Electrophoretic light scattering was used to measure the electrokinetic potential, also known as zeta potential. The measurements were performed on a Zetasizer Nano ZS (Malvern Instruments, Herrenberg, Germany) by applying laser Doppler velocimetry.[4] For each measurement, 20 runs were carried out using the slow-field reversal and fast-field reversal mode at 150 V. Each experiment was performed in triplicate at 25 °C. The zeta potential (ζ) was calculated from the electrophoretic mobility (μ) according to the Henry Equation. Henry coefficient f(ka) was calculated according to Oshima.[5]

Serum stability by DLS

Polyplexes were incubated with serum containing growth media in a micro-cuvette for 4h at 37°C under a CO2 atmosphere. Afterwards the cuvette was closed and directly transferred to the DLS device (Malvern Zetasizer). Measurements were done at 37 °C, detection at scattering angle of 173° and laser wavelength of 633 nm. Cumulant analysis and a non-negative least-square algorithm were used to obtain distribution of hydrodynamic radius, z-average and PDI.

Results section

Flow Cytometer Analysis

The transfection efficiency was determined by measuring the amount of cells that express EGFP (encoded on the transported pDNA). Therefore, non-transfected cells serve as controls and were analyzed by flow cytometry. The histogram of control cells was used to define the amount of EGFP expressing cells (see Figure S1, control). The percentage of cells in the specific area was defined as transfection efficiency in percentage.

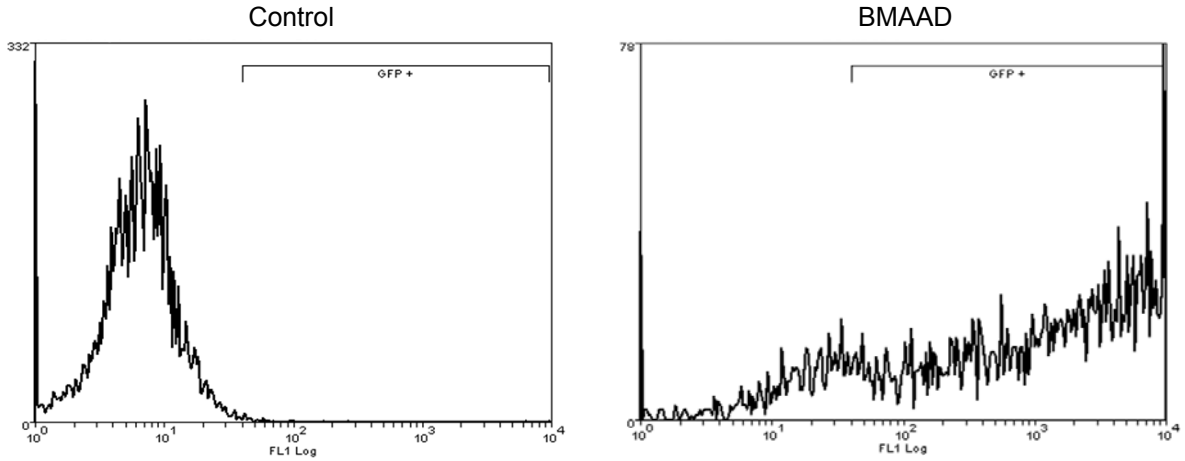

Figure S1. Histograms of non-transfected cells (control) and HEK cell transfected with BMAAD (N/P20). FL1 Log represents green fluorescence by EGFP expression.

Interaction between used polymers and genetic material

Indicated by the decrease of ethidium bromide fluorescence it is obvious that all polymers lead to a full complexation of the pDNA. Nevertheless, there are differences in the binding affinity. PEI shows a stronger interaction compared to PDMAEMA and BMAAD. The dependence of EBA on the chemical nature of the monomer was previously described.[1]

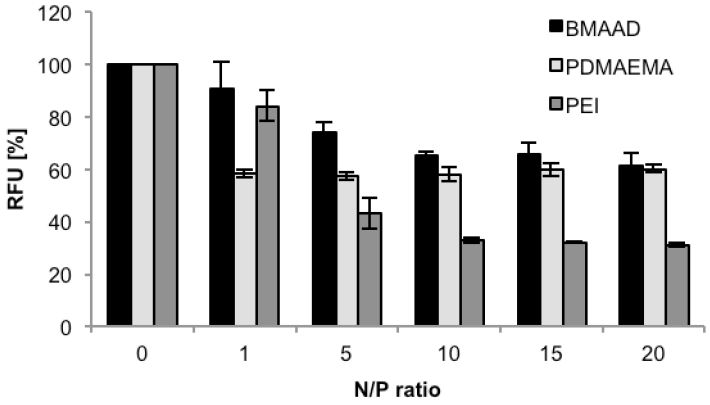

Figure S2. Ethidium bromide quenching assay of pDNA complexed with the indicated polymers. Binding of polymer to the pDNA results in a decrease in fluorescence intensity. The binding affinity was investigated dependent on the N/P ratio.

The agarose gel migration assay was performed with the BMAAD micelle to confirm the full complexation of the pDNA. The results confirm the previous investigations (Figure S2) of the EBA. At an N/P ratio of 5 the pDNA is fully complexed with BMAAD micelles and no free pDNA is detectable.

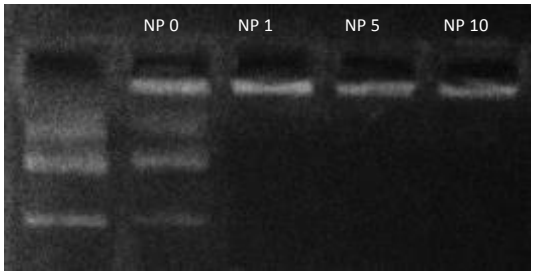

Figure S3. Agarose gel migration assay. Polyplexes were formed at indicated N/P ratio with BMAAD and 15 µg pDNA

pDNA release at pH 5

To investigate the polyplex dissociation and, thus, the pDNA release both cryo-TEM investigations (at pH 5 and 7) and a heparin dissociation assay at pH5 were performed.

Cryo-TEM

The polyplexes were formed as described at a N/P ratio of 20, after 10 min incubation heparin (10 U/mL) was added and incubated for another 10 min. As can be seen in the micrographs, at pH 5 the polyplex surface remains patchy (Figure S4b), although less protrusions can be observed. For pH 7, in both cases the polyplex surface is rather smooth.

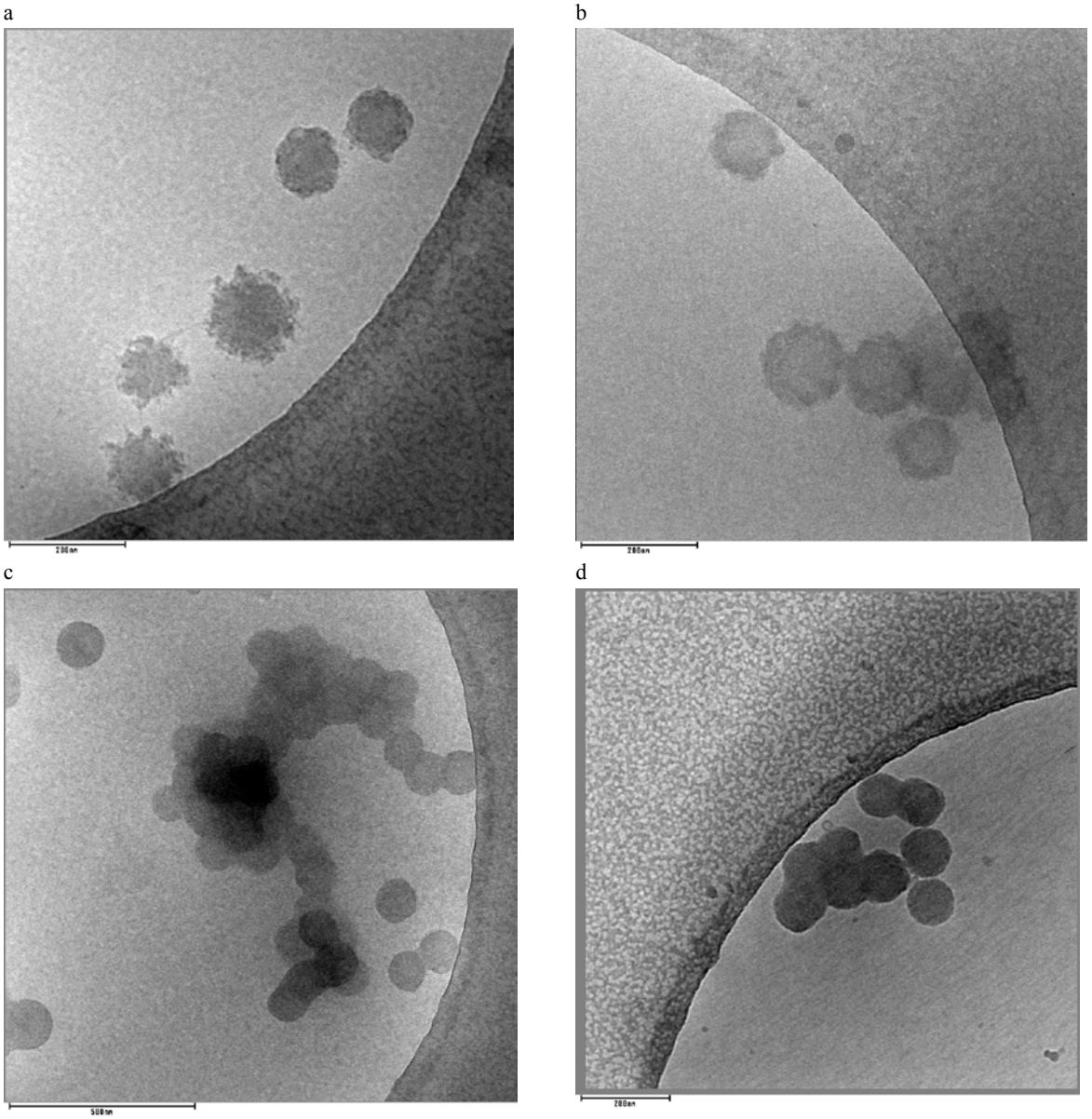

Figure S4. Cryo-TEM micrographs of BMAAD polyplexes incubated without (a, c) and with 10 U/mL heparin (b, d) at pH 5 (a, b) and pH 7 (c, d).

Heparin dissociation assay

Besides the cryo-TEM investigations a heparin dissociation assay was performed at pH 5. In contrast to the release assay at pH 7 no full decomplexation of the pDNA could be achieved. Moreover at heparin concentration of 2.5 U/mL no fluorescence changes compared to 0.5 U/mL heparin could be detected. Thus, the BMAAD micelles have a much higher binding to the pDNA at pH 5, indicating no polyplex dissociation in the endosome occurring.

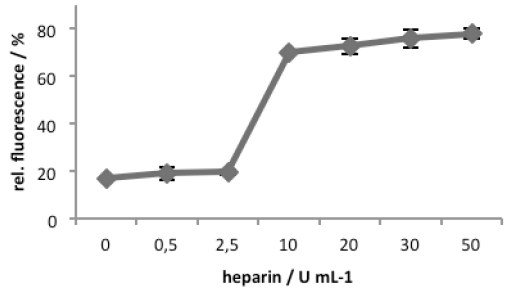

Figure S5: Dissociation assay of polyplexes formed at N/P 10 in pH 5 with increasing heparin concentrations (n=2)

Polyplex stability in presence and absence of serum

To analyze the aggregation behavior of the BMAAD polyplexe in HBG, their size was investigated over several hours. As obvious no changes in size were detected and thus no aggregation occured.

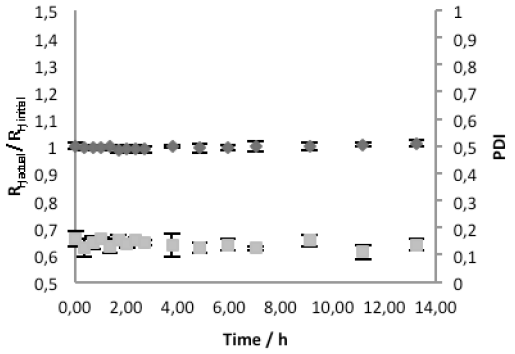

Figure S6: BMAAD polyplex stability in HBG (pH7). The relative diameters are demonstrated over 15 h.

pH dependent hemolysis assay of polyplexes

The hemolysis assay of the polyplexes confirms the results of the hemolysis assay using the single polymers. The BMAAD polyplexes shows, membrane-perturbing activity at pH 5 (endosomal pH), in contrast to physiological pH. PEI shows no dependency of pH, regarding its hemolysis activity.

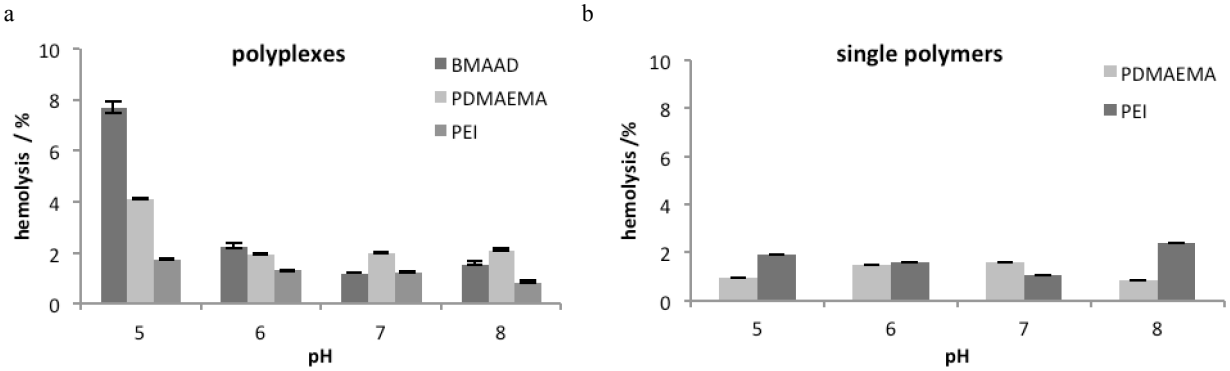

Figure S7. pH-dependent hemolysis assay of polyplexes (a) and single indicated polymers (b). Polyplexes of BMAAD, PDMAEMA, and PEI were formed at N/P ratio 20 and the values represent the mean of three different donators.

Analysis of polyplex uptake mechanism

To analyze the uptake mechanism of the BMAAD polyplexes in more detail the transfection were performed at 4 °C as endocytosis is energy dependent and should be reduced at this temperature (figure S8b)

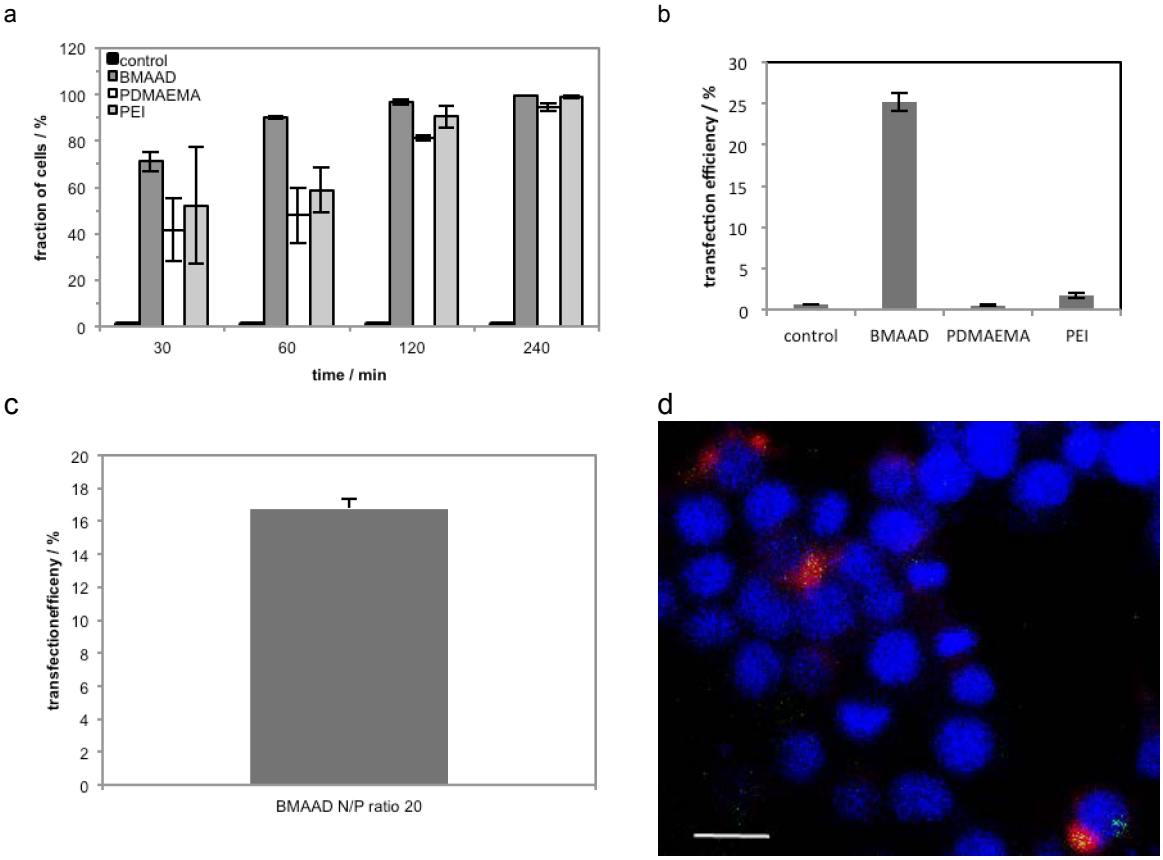

Figure S8: Fraction of cells with Yoyo-1 labled pDNA for indicated time points using BMAAD, PEI and PDMAEMA (a). Transfection efficiencies with EGFP as reporter gen of BMAAD and PEI for adherent HEK cells performed at 4°C at N/P ratio 20 (b). Transfection efficiencies of Jurkat T cells under non-static conditions (c). CLSM images of HEK cells transfected with indicated BMAAD based polyplexes and YOYO-1 labeled pDNA (green), the early endosomes were stained by cell light early endosome BacMAM2.0 (red), and cell nuclei were stained with Hoechst 33342 (blue). Values represent the mean ± S.D; * represents a significant difference ($p < 0.01$).

The transfection efficiency of BMAAD as well as PEI is significant decreased when incubated for 4 h at 4 C°. This indicates an energy dependent uptake of BMAAD. The remaining TE of 25 % yielded with BMAAD can be explained by a very efficient binding to the cellular membrane.

References

1. Schallon, A.; Synatschke, C. V.; Pergushov, D. V.; Jerome, V.; Müller, A. H. E.; Freitag, R., DNA Melting Temperature Assay for Assessing the Stability of DNA Polyplexes Intended for Nonviral Gene Delivery. *Langmuir* **2011**, *27*, 12042-12051.
2. Vollrath, A.; Pretzel, D.; Pietsch, C.; Perevyazko, I.; Schubert, S.; Pavlov, G. M.; Schubert, U. S., Preparation, Cellular Internalization, and Biocompatibility of Highly Fluorescent PMMA Nanoparticles. *Macromol. Rapid Commun.* **2012**, *33*, 1791-1797.
3. Provencher, S. W., CONTIN - A General-Purpose Constrained Regularization Program for Inverting Noisy Linear Algebraic and Integral-Equations. *Comput Phys Commun* **1982**, *27*, 229-242.
4. Delgado, A. V.; Gonzalez-Caballero, F.; Hunter, R. J.; Koopal, L. K.; Lyklema, J., Measurement and Interpretation of Electrokinetic Phenomena. *J. Colloid Interface Sci.* **2007**, *309*, 194-224.
5. Ohshima, H., A Simple Expression for Henrys Function for the Retardation Effect in Electrophoresis of Spherical Colloidal Particles. *J Colloid Interf Sci* **1994**, *168*, 269-271.

Publication P6

Small but powerful: Co-assembly of polyether-based triblock terpolymer into sub-30 nm micelles and synergistic effects on cellular interactions

M. J. Barthel, A. C. Rinkenauer, M. Wagner, U. Mansfeld, S. Höppner, J. A. Czaplewska, M. Gottschaldt, A. Traeger, F. H. Schacher, U. S. Schubert

Biomacromolecules **2014**, *15*, 2426-2439.

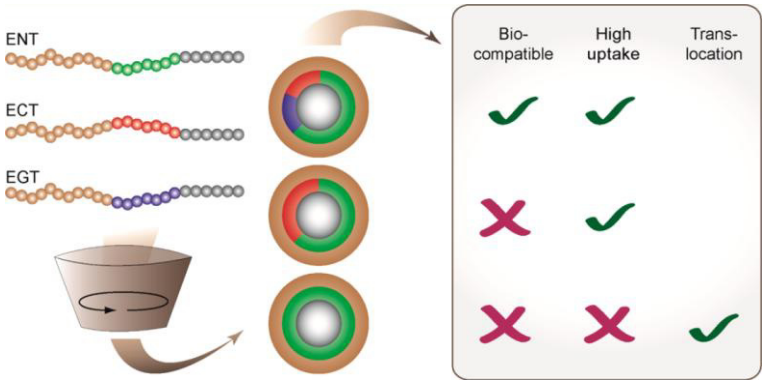

Article

pubs.acs.org/Biomac

Small but Powerful: Co-Assembly of Polyether-Based Triblock Terpolymers into Sub-30 nm Micelles and Synergistic Effects on Cellular Interactions

Markus J. Barthel,[†,‡,§,∥] Alexandra C. Rinkenauer,[†,‡,§] Michael Wagner,[‡,§] Ulrich Mansfeld,[‡,§] Stephanie Hoeppener,[‡,§] Justyna A. Czaplewska,[‡,§] Michael Gottschaldt,[‡,§] Anja Träger,[‡,§] Felix H. Schacher,*[,‡,§] and Ulrich S. Schubert*[,‡,§,∥]

[‡]Laboratory of Organic and Macromolecular Chemistry (IOMC), Friedrich Schiller University Jena, Humboldtstrasse 10, 07743 Jena, Germany

[§]Jena Center for Soft Matter (JCSM), Friedrich Schiller University Jena, Philosophenweg 7, 07743 Jena, Germany

[∥]Dutch Polymer Institute (DPI), P.O. Box 902, 5600 AX Eindhoven, The Netherlands

Supporting Information

ABSTRACT: We introduce a versatile ABC triblock terpolymer platform based on poly(ethylene oxide)-*block*-poly(allyl glycidyl ether)-*block*-poly(*tert*-butyl glycidyl ether) (PEO-*b*-PAGE-*b*-P*t*BGE) and subsequent functionalization of the PAGE segment with thiogalactose (hydroxyl), cysteamine (amino), and 2-mercaptopropionic acid (carboxy) by thiol−ene chemistry. These materials are used to prepare core-shell-corona micelles with a P*t*BGE core, a PAGE shell, and a PEO corona and sizes below 30 nm in aqueous media. We investigate the influence of different functional groups on micelle formation and cellular uptake. Moreover, co-assembly of differently functionalized materials allows to create micelles with a mixed shell and adjustable charge and, in that way, important characteristics such as cell uptake or cytotoxicity can be controlled. Furthermore, we demonstrate that even the uptake mechanism depends on the substitution pattern of the underlying triblock terpolymer.

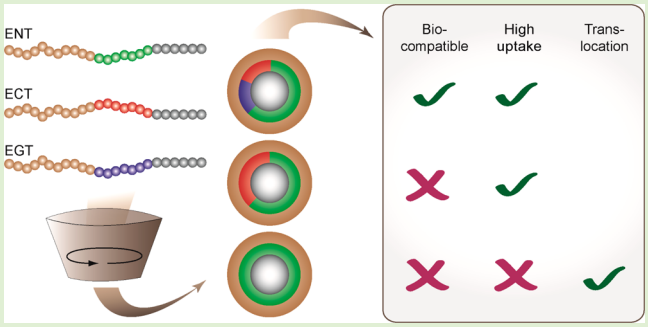

INTRODUCTION

The synthesis and self-assembly of amphiphilic block copolymers into micellar structures of defined size, shape, and composition represents a very active field of research and such nanostructures show high potential for their use in potential biomedical and pharmaceutical applications.[1,2] The introduction of further functionalities or stimuli-responsive segments as well as the morphological variety being accessible benefit from the introduction of a third segment (C) resulting in ABC triblock terpolymers.[3] Since first attempts in the 1980s and the pioneering work of Stadler and co-workers later in the 1990s, increasing research efforts have been devoted to the preparation and application of such materials.[4−7] One intriguing aspect of ternary materials is that multicompartment micelles can be realized, structures which are further subdivided in core, shell, or corona. As a consequence of their architecture, multicompartment micelles can be used to simultaneously store two different payloads within one micellar core or to implement several responsive segments.[8−11] In this context, we recently reported that multicompartment micelles with pH-dependent charge and morphology bear enormous potential as nonviral gene transfection agents, enabling high delivery efficiency in combination with low cytotoxicities.[12,13]

Typically, each segment of ABC triblock terpolymers is attributed a specific "task" in solution: One block (e.g., A) ensures solubility in the desired environment. In water, often poly(ethylene oxide) (PEO) is used as this material is water-soluble, nontoxic, and prevents unspecific protein interactions ("stealth" effect).[14−17] Another segment (B) can be used to introduce functional groups or the possibility to carry out postpolymerization functionalization reactions (e.g., allyl glycidyl ether) to further fine-tune the material properties or to attach targeting moieties.[18−21] The third block (C) often is utilized as solvophobic block, resulting in amphiphilic triblock terpolymers in the case of hydrophobic segments. Related to this, we recently reported that hydrophobic glycidyl ethers, for example, *tert*-butyl glycidyl ether or furfuryl glycidyl ether, can be used as core forming segments in micellar aggregates.[18,19,22,23] These micellar cores can be applied, for example,

Received: February 24, 2014
Revised: May 27, 2014
Published: May 29, 2014

to encapsulate hydrophobic guest compounds such as drugs or dyes.[24] If suitable building blocks are realized, the response of block copolymer nanostructures toward changes in temperature or pH value can be easily realized.[25,26] This often induces quite drastic changes of the material properties and can be used to trigger the controlled release of encapsulated cargo or to enable endosomal release after cell internalization.[12,27,28] Nevertheless, to date, the number of solution applications involving ABC triblock terpolymers is rather low, probably due to high synthetic efforts that often involve the combination of different polymerization techniques, modification sequences, or stepwise assembly procedures.

An alternative approach for the design of complex block copolymer micelles is the simple mixing of block copolymers. For instance, AB and AC diblock copolymers, where A represents identical hydrophobic blocks, which are mixed in nonselective solvents and then transferred to a solvent or solvent mixture selective for B and C. It is generally believed that comparable degrees of polymerization (DP) for block A are beneficial. This could be shown, for example, for PEO-*b*-PLA and PNIPAM-*b*-PLA diblock copolymers. Co-assembly in aqueuos solution leads to the formation of micelles with a PLA core and a mixed PEO/PNIPAM shell. These materials showed potential as smart carriers in drug delivery processes.[29−32] In this context, Kabanov and co-workers have demonstrated that comicelles prepared from mixtures of amphiphilic and cationic copolymers based on Pluronics can be applied for an efficient delivery of oligonucleotide sequences.[33] Such concepts have also been employed for the preparation of multicompartment micelles.[34,35]

Besides efforts to design structures of increased complexity for drug delivery applications, Kataoka et al. demonstrated that size does indeed matter and showed that micelles with diameters below 100 nm are highly interesting candidates in such approaches.[36] Commonly, nanostructures with diameters between 50 to 200 nm are used because endocytosis as predominant internalization process can be assumed, the interaction with the immune system is reduced, and renal clearance can be avoided.[37,38] In contrast, polymeric micelles with sizes far below 100 nm are scarce in literature and, up to now, rarely studied with regard to interactions with biological matter.[37] In this context, spherical core−shell micellar structures of approximately 30 nm were found to effectively penetrate poorly permeable tumor membranes.[36] Besides size, also charge significantly influences cell interactions of polymeric micelles, as well as their cytotoxicity and hemocompatibility. In general, the presence of cationic charges leads to increased interactions with the negatively charged cell membrane. Although this is advantageous for uptake, it also favors membrane destabilization and increases cytotoxicity. These side effects can be circumvented by using PEO as corona, but often at the cost of decreased cell interaction.[39,40] As an alternative, the presence of negatively charged segments allows to decrease both the cytotoxicity and nonspecific interactions with serum proteins.[41] Hence, direct control over the charge balance in (block co-) polymer nanostructures seems to be a promising strategy to balance cellular interactions, efficient uptake, and simultaneously suppress nonspecific interactions and lower cytotoxicity. This can be achieved, e.g., via the combination of positively and negatively charged blocks in block copolymers and has been recently demonstrated for multicompartment micelles from polybutadiene-*block*-poly(methacrylic acid)-*block*-poly(2-dimethylaminoethyl methacrylate) (BMAAD) triblock terpolymers. These structures comprise a polybutadiene core, a patchy shell consisting of *intra*-micellar interpolyelectrolyte complexes (*im*-IPEC) between PMAA and PDMAEMA, and a cationic corona of excess PDMAEMA.[12] We could demonstrate that the presence of the *im*-IPECs and the inherent pH-dependent dynamics of the system favor cellular uptake, while the PMAA middle segment acts as competing polyelectrolyte during delivery of pDNA and, at the same time, reduces cytotoxicity and facilitates release of the genetic material. Nevertheless, this approach suffers from a severe drawback: Preparation conditions, micellar size, and pH-dependent characteristics depend strongly on the terpolymer composition and, thus, have to be investigated and optimized for each new material being synthesized. This motivated us to probe a different, more versatile and general approach: Co-assembly of a small library of structurally similar ABC triblock terpolymers with different functional groups being present within the segment B.

We therefore introduce a triblock terpolymer platform based on poly(ethylene oxide)-*block*-poly(allyl glycidyl ether)-*block*-poly(*tert*-butyl glycidyl ether) (PEO-*b*-PAGE-*b*-P*t*BGE), synthesized by sequential living anionic ring-opening polymerization (AROP), as versatile carriers for hydrophobic compounds. The pendant double bonds of the PAGE block were functionalized by thiol−ene chemistry to introduce model ligands (thiogalactose), amine groups to provide positive charges (cysteamine), as well as carboxylic groups to generate negative charges (3-mercapto propionic acid). The obtained triblock terpolymers are subsequently used for the co-assembly into well-defined spherical core-shell-corona micelles with diameters below 30 nm and precisely adjustable charge and composition. Depending on the latter, we found synergistic effects regarding cellular uptake and cytotoxicity. In addition, the internalization efficiency (and pathway) was analyzed under serum-reduced and serum-containing conditions, showing an effective shielding by the PEO corona and providing first insights into the underlying uptake mechanism.

EXPERIMENTAL SECTION

Instruments and Methods. ^{1}H NMR spectra were recorded on a Bruker AC 300 MHz spectrometer in deuterated chloroform.

Size Exclusion Chromatography (SEC). Size exclusion chromatography (SEC) was performed on a Shimadzu SCL-10A system (with a LC-10AD pump, a RID-10A refractive index detector, and a PL gel 5 μm mixed-D column at RT), the eluent was a mixture of chloroform/triethylamine/isopropanol (94:4:2) with a flow rate of 1 mL/min. The system was calibrated with poly(ethylene glycol) standards from PSS (M_n = 1470 to 42000 g/mol).

Matrix Assisted Laser Desorption Ionization - Time of Flight Mass Spectrometry (MALDI-ToF). MALDI−ToF mass spectra were obtained using an Ultraflex III ToF/ToF mass spectrometer (Bruker Daltonics) with *trans*-2-[3-(4-*tert*-butylphenyl)-2-methyl-2-propenylidene] malononitrile (DCTB) or 2,5-dihydroxybenzoic acid (DHB) as matrix in reflector as well as in linear mode. The instrument was calibrated prior to each measurement with an external PMMA standard from PSS Polymer Standards Services GmbH.

Dynamic Light Scattering (DLS). Dynamic light scattering (DLS) was performed at a scattering angle of 90° on an ALV CGS-3 instrument and a He−Ne laser operating at a wavelength of λ = 633 nm at 25 °C. The CONTIN algorithm was applied to analyze the obtained correlation functions. Apparent hydrodynamic radii were calculated according to the Stokes−Einstein equation. All CONTIN plots are number-weighted.

Cryogenic Transmission Electron Microscopy (cryo-TEM). Cryo-TEM measurements were carried out at 120 kV using a Philips-CM

120 equipped with a 1k × 1k CCD camera. Sample preparation was performed on Quantifoil grids (holey carbon R2/2) after plasma cleaning. Vitrification of the samples was carried out in a home-built system with a temperature control unit. A drop of the polymer solution (5 μL) was placed on the grid, which was blotted and subsequently plunged into a cryogen reservoir containing liquid ethane. The samples were afterward stored in liquid nitrogen and were transferred to the TEM keeping the temperature below −176 °C to avoid the formation of crystalline ice layers.

Asymmetric Flow Field-Flow Fractionation (AF4). Asymmetric flow field-flow fractionation (AF4) was performed on an AF2000 MT System (Postnova Analytics, Landsberg, Germany) coupled to an UV (PN3211, 260 nm), RI (PN3150), MALLS (PN3070, 633 nm), and DLS (ZetaSizer Nano ZS) detector. The eluent is delivered by three different pumps (tip, focus, cross-flow) and the sample is injected by an autosampler (PN5300) into the channel. The channel has a trapezoidal geometry and an overall area of 31.6 cm^2. The nominal height of the spacer was 500 μm and a regenerated cellulose membrane with a molar mass cutoff of 10 kg/mol was used as accumulation wall. All experiments were carried out at 25 °C and the eluent was degassed water containing 20 mM NaCl. The detector flow rate was set to 0.5 mL/min for all samples and 20 μL (5 mg/mL) were injected with an injection flow rate of 0.2 mL/min for 7 min. For EAT the cross-flow was set to 2 mL/min and decreased under an exponential gradient (0.5) to 0 within 20 min. For EGT the cross-flow was set to 2 mL/min and decreased under a linear gradient to 0 within 20 min. For ECT the cross-flow was set to 2 mL/min and decreased under an exponential gradient (0.5) to 0 within 25 min. For ENT the cross-flow was set to 1.3 mL/min and decreased under an exponential gradient (0.7) to 0 within 25 min. For $(ENT/ECT)^{1:2.6}$ the cross-flow was set to 2 mL/min and decreased under a linear gradient to 0 within 35 min. For $(ENT/ECT)^{1.2:1}$, the cross-flow was set to 2 mL/min and decreased under a linear gradient to 0 within 30 min. For $(ENT/ECT)^{3.5:1}$, $(ENT/ECT/EGT)^{3.5:1:0.5}$, and $(ENT/ECT/EGT)^{3.4:1:2.3}$, the cross-flow was set to 1.3 mL/min and decreased under an exponential gradient (0.7) to 0 within 25 min. After the cross-flow reaches zero, for all samples, the cross-flow was kept constant at zero for at least 30 min to ensure complete elution. For calculation of the molar mass and the radius of gyration a Berry plot was used.[42] All measurements were repeated three times. The refractive index increment (dn/dc) of all samples was measured by manual injection of a known concentration directly into the channel without any focusing or cross-flow. The dn/dc was calculated as the average of at least three injections from the area under the RI curve (AUC_{RI}).

Electrophoretic Light Scattering (ELS). Electrophoretic light scattering was used to measure the electrokinetic potential, also known as zeta potential. The measurements were performed on a Zetasizer Nano ZS (Malvern Instruments, Herrenberg, Germany) by applying laser Doppler velocimetry.[43] For each measurement, 20 runs were carried out using the slow-field reversal and fast-field reversal mode at 150 V. Each experiment was performed in triplicate at 25 °C. The zeta potential (ζ) was calculated from the electrophoretic mobility (μ) according to the Henry equation. Henry coefficient f(ka) was calculated according to Ohshima.[44]

Gel Migration Assay. The micelles (40 μg) were incubated with 5 μL loading buffer (0.25% bromphenolblue, 40% saccharose). Afterward, the solutions were loaded to an 1% agarose gel, electrophorese (Bio-Rad, Munich, Germany, Mini-Sub Cell GT System) was carried out with a current of 80 V (PowerPac Basic as power supply) for 30 min in TBE running buffer solution (107.8 g/L tris-base, 7.4 g/L EDTA, 55 g/L borate). Subsequently, the agarose gel was irradiated with an UV-lamp to induce fluorescence of the bands.

HEK-293 cells (CRL-1573, ATCC) were maintained in RPMI 1640 culture medium, L929 cells (CCL-1, ATCC) in DMEM culture medium, and HepG2 (HB-8065, ATCC) in DMEM-F12 culture medium. Both media were supplemented with 10% fetal calf serum (FCS), 100 μg/mL streptomycin, 100 IU/mL penicillin, and 2 mM L-glutamine. Cells were cultivated at 37 °C in a humidified 5% CO_2 atmosphere.

Cytotoxicity. For L929 cells, the cytotoxicity assay was performed as described by ISO10993-5. In detail, cells were seeded at 1×10^4 cells per well in a 96-well plate and incubated for 24 h. No cells were seeded in the outer wells. Afterward, polymers at the indicated concentrations were added, and the cells were incubated at 37 °C for further 24 h. Subsequently, the medium was replaced by fresh media and AlamarBlue, as recommended by the supplier. After incubation for 4 h, the fluorescence was measured at Ex 570/Em 610 nm, with untreated cells on the same well plate serving as controls.

Hemolysis Assay. The membrane damaging properties of the polymers were quantified by analyzing the release of hemoglobin from human erythrocytes. The erythrocyte-containing blood was centrifuged at 700 g for 10 min. The obtained pellet was washed three times with D-PBS pH 7.4 by centrifugation at 700 g for 10 min and resuspended in HBG buffer of pH 7. Polymer solutions were added to the erythrocytes (100 μL) and incubated for 60 min under constant shaking at 37 °C. After centrifugation (700 g, 10 min), the supernatant was analyzed for released hemoglobin at 580 nm. The absorbance was measured using a plate reader (Genios Pro, Tecan, Germany). For comparison, collected erythrocytes were washed with DPBS and either lysed with 0.2% Triton X-100, yielding the 100% lysis control value (A_{100}) or resuspended in DPBS as reference (A_0). The analysis was repeated with blood from at least six independent donors. The hemolytic activity of the polycations was calculated as follow:

$$\%\text{hemolysis} = 100 \times (A_{\text{sample}} - A_0)/(A_{100} - A_0) \quad (1)$$

Here, A_{sample}, A_0, and A_{100} are the absorbance intensities of a given sample, erythrocytes incubated with D-PBS, and erythrocytes lysed with Titon X-100.

Uptake Studies. For uptake of the adherent cell lines, cells were seeded at a density of 10^5 cells per well in 12-well plates 1 day before internalization experiment. A total of 1 h prior to addition of micelles, cells were rinsed with PBS and supplemented with 1 mL OptiMEM (Life Technologies) or fresh serum containing growth media. Micelles were added at indicated end concentration to the cells and the plates were incubated for 24 h in the incubator. For analysis, the cells were harvested by trypsinization and 10% trypan blue was added. Subsequently, the cells were analyzed via flow cytometry using a Cytomics FC 500 (Beckman Coulter). For determination of the viability during flow cytometry, dead cells were identified in the SSC/FSC dot plot. The relative uptake of encapsulated nile red fluorescence of 10^4 cells was quantified. For determination of the uptake efficiency, viable cells containing nile red were gated. The experiments were performed at least independently three times.

Materials. The triblock terpolymer precursor PEO_{42}-*b*-$PAGE_{15}$-*b*-$PtBGE_{12}$ (SEC: M_n = 3350 g/mol; M_w = 3500 g/mol; $Đ$ = 1.05; obtained with PEO calibration; NMR: M_n = 5122 g/mol) as well as 2,3,4,6-tetra-*O*-acetyl-1-thio-β-D-galactopyranose (acetylated thiogalactose) were synthesized as reported previously.[19,45,46] 2,2-Dimethoxy-2-phenylacetophenone (DMPA), cysteamine, 3-mercapto propionic acid, sodium methanolate (0.5 M in methanol), nile red, DOWEX 50WX8−200, methanol, *N*,*N*-dimethylformamide (DMF), tetrahydrofuran (THF), and ethanol were purchased from Aldrich and used as received. AlamarBlue was obtained from Life Technologies (Darmstadt, Germany). If not stated otherwise, cell culture materials, cell culture media, and solutions were obtained from PAA (Pasching, Austria). All other chemicals were purchased from Sigma-Aldrich (Steinhausen, Germany) and are of analytical grade or better and were used without further purification.

Cysteamine Functionalization of PEO_{42}-b-$PAGE_{15}$-b-$PtBGE_{12}$. A total of 300 mg (0.059 mmol, corresponding to 0.88 mmol of PAGE) of the triblock terpolymer were dissolved in 5 mL of a mixture of DMF, EtOH, and MeOH (ratio 1:0.3:1). Aliquots of 45 mg (0.18 mmol, 0.2 equiv) DMPA and 339 mg cysteamine (4.39 mmol, 5 equiv) were added to the mixture. The reaction mixture was degassed and stirred under UV irradiation (366 nm, 6 W) for 24 h. The increase of the molar mass (M_n) and the decrease of the signal intensity of the peaks of the double bond were monitored by SEC and ^{1}H NMR, respectively. The reaction mixture was purified by dialysis against

Scheme 1. Schematic Representation of the Thiol−Ene Modification of PEO_{42}-*b*-$PAGE_{15}$-*b*-P*t*BGE_{12} Using Cysteamine (N), 3-Mercapto Propionic Acid (C), and Acetylated Thiogalactose[a]

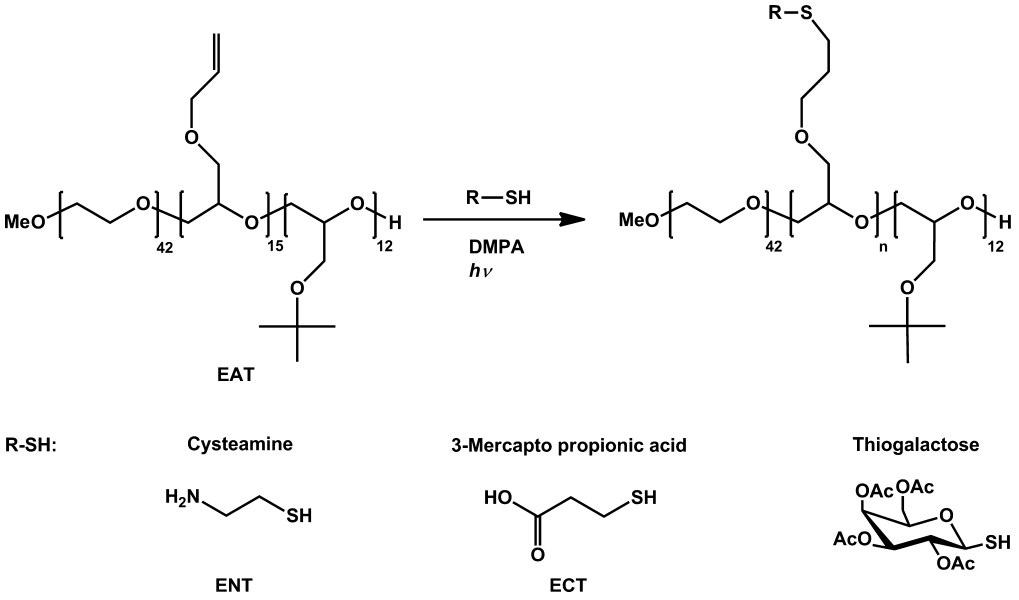

[a]The abbreviations (EAT, ENT, ECT) will be used later on for the nomenclature of the micelles generated via self-assembly of the modified triblock terpolymers.

water, a THF/water mixture (1:1) and pure THF. The solvent was removed by distillation under reduced pressure and the product dried under vacuum. Yield: 250 mg.

^{1}H NMR (300 MHz, $CDCl_3$-d_6, δ in ppm): 6.00−5.75 (m, 1H), 5.34−5.07 (m, 2H), 4.04−3.9 (m, 2H), 3.9−3.2 (m, PEO backbone), 2.74−1.94 (br, 4H, CH_2-CH_2-S), 2.74−1.93 (br, 2H, S-CH_2), 1.3−0.97 (s, 9H). f = 53%. SEC: M_n = 3500 g/mol, M_w = 3600 g/mol, $Đ$ = 1.06.

3-Mercapto Propionic Acid Functionalization of PEO_{42}-b-$PAGE_{15}$-b-$PtBGE_{12}$. A total of 450 mg (0.088 mmol, corresponding to 1.32 mmol of PAGE) of the triblock terpolymer was dissolved in 5 mL of a mixture of DMF/EtOH (ratio 3:1). Subsequently, 68 mg (0.27 mmol, 0.2 equiv) DMPA and 0.23 mL of 3-mercapto propionic acid (2.64 mmol, 2 equiv) were added. The reaction mixture was degassed and stirred under UV irradiation (366 nm, 6 W) for 24 h. The increase of the molar mass (M_n) and the decrease of the signal intensity of the peaks of the double bond were monitored by SEC and ^{1}H NMR, respectively. The reaction mixture was purified by dialysis against a THF/water mixture (5:1) and pure THF. The solvent was removed by distillation under reduced pressure and the product dried under vacuum. Yield: 600 mg.

^{1}H NMR (300 MHz, $CDCl_3$-d_6, δ in ppm): 3.94−3.24 (m, PEO backbone), 2.87−2.72 (m, 4H, CH_2 linker), 1.92−1.76 (m, 2H), 1.24−1.09 (s, 9H). Degree of functionalization: f = 100%. SEC: M_n = 3550 g/mol, M_w = 3700 g/mol, $Đ$ = 1.05.

Thiogalactose Functionalization of PEO_{42}-b-$PAGE_{15}$-b-$PtBGE_{12}$. A total of 450 mg (0.088 mmol, corresponding to 1.32 mmol of PAGE) of the triblock terpolymer were dissolved in 5 mL of a mixture of DMF/EtOH (ratio 3:1). To the mixture, 68 mg (0.27 mmol, 0.2 equiv) DMPA and 963 mg acetylated thiogalactose (2.64 mmol, 2 equiv) were added. The reaction mixture was degassed and stirred under UV irradiation (366 nm, 6 W) for 72 h. The increase of the molar mass (M_n) and the decrease of the signal intensity of the peaks of the double bond were monitored by SEC and ^{1}H NMR, respectively. The reaction mixture was purified by size exclusion chromatography (Biobeads SX-1) and the product was dried under vacuum. Yield: 600 mg.

^{1}H NMR (300 MHz, $CDCl_3$-d_6, δ in ppm): 6.00−5.76 (m, 1H), 5.7−4.9 (m, 3H, Gal), 4.56−4.43 (m, 1H, Gal), 4.40−4.21 (m, 3H, Gal), 4.20−3.03 (m, PEO backbone), 2.86−2.62 (m, 2H), 2.57−1.47 (m, 12H−Ac), 1.28−1.04 (s, 9H). Degree of functionalization: f = 70%. SEC: M_n = 4200 g/mol, M_w = 4350 g/mol, $Đ$ = 1.04.

Deprotection of PEO_{42}-b-($PAGE_5$-co-$PAGE_{10,Gal}$)-b-$PtBGE_{12}$. A total of 600 mg (0.066 mmol, corresponding to 2.64 mmol of acetyl groups) of the triblock terpolymer was dissolved in 15 mL of dry methanol. To the mixture, 7 mL (3.5 mmol, 1.3 equiv) of a 0.5 M sodium methanolate solution was added and the mixture was allowed to stir for 1 h. Afterward, a DOWEX 50WX8−200 ion-exchange resin was added and stirred for 15 min to neutralize the reaction mixture. The resin was filtered off, and the crude product was dialyzed against a water/THF mixture (5:1), pure water, and pure THF. The solvent was removed by distillation under reduced pressure and product was dried under vacuum. Yield: 250 mg.

^{1}H NMR (300 MHz, $CDCl_3$-d_6, δ in ppm): 6.0−5.76 (m, 1H), 5.5−4.84 (m, 3H-Gal), 4.10−2.80 (m, PEO backbone), 1.26−1.01 (s, 9H). SEC: M_n = 10400 g/mol, M_w = 11500 g/mol, $Đ$ = 1.10.

Preparation of Triblock Terpolymer Micelles. The following procedures with the respective stoichiometry were used for the preparation of all micellar nanostructures with a concentration of 10 g/L in aqueous solution.

A total of 100 mg of the corresponding triblock terpolymer was dissolved in 5 mL of THF, and 4 mg of nile red was added to the solution. To the mixture was then added slowly 10 mL of Milli-Q water via syringe, and the THF was allowed to evaporate by stirring overnight. Non-encapsulated dye was filtered off by a 0.45 μm nylon syringe filter. In case of evaporation of water, the solution was filled up again to a volume of 10 mL. After filtration, a clear pink solution could be obtained.

Binary Co-micelles. Here, the preparation of a 1.2:1 mixture of PEO_{42}-b-($PAGE_{8,NH2}$-co-$PAGE_7$)-b-P*t*BGE_{12} and PEO_{42}-b-$PAGE_{15,COOH}$-b-P*t*BGE_{12} is reported. Due to the different degrees of functionalization, a 2:1 ratio regarding the masses was used.

A total of 6.6 mg of PEO_{42}-b-($PAGE_{8,NH2}$-co-$PAGE_7$)-b-P*t*BGE_{12} and 3.3 mg of PEO_{42}-b-$PAGE_{15,COOH}$-b-P*t*BGE_{12} were dissolved in 0.3 mL of THF, and approximately 2 mg of nile red was added to the solution. The solution was then slowly added to 1 mL of Milli-Q water and the THF was allowed to evaporate by stirring overnight. Nonencapsulated dye remained as precipitate in the solution and was filtered off by a 0.45 μm nylon syringe filter. In case of evaporation of water, the solution was filled up again to a volume of 1 mL. After filtration, a clear pink solution could be obtained.

dx.doi.org/10.1021/bm5002894 | Biomacromolecules 2014, 15, 2426−2439

Table 1. Characterization Data of the Synthesized Triblock Terpolymers[a]

sample	abbreviation	SEC			^{1}H NMR	
		M_n (g/mol)	M_w (g/mol)	$Đ$	M_n (g/mol)	f (%)
PEO$_{42}$-*b*-PAGE$_{15}$-*b*-P*t*BGE$_{12}$	EAT	3350	3500	1.05	5100	
PEO$_{42}$-*b*-(PAGE$_{8,NH2}$-*co*-PAGE$_7$)-*b*-P*t*BGE$_{12}$	ENT	3500	3600	1.06	5750	53
PEO$_{42}$-*b*-PAGE$_{15,COOH}$-*b*-P*t*BGE$_{12}$	ECT	3550	3700	1.05	6700	100
PEO$_{42}$-*b*-(PAGE$_{10,AcGal}$-*co*-PAGE$_5$)-*b*-P*t*BGE$_{12}$		4200	4350	1.04	8800	70
PEO$_{42}$-*b*-(PAGE$_{10,Gal}$-*co*-PAGE$_5$)-*b*-P*t*BGE$_{12}$	EGT	10400	11500	1.10	7100	70

[a]The subscripts represent the degree of polymerization. The shown abbreviations are used later on when describing self-assembled structures of the materials.

Scheme 2. Schematic Representation of the Deprotection of Acetylated Thiogalactose (G) Attached to a PEO-*b*-PAGE-*b*-P*t*BGE Triblock Terpolymer[a]

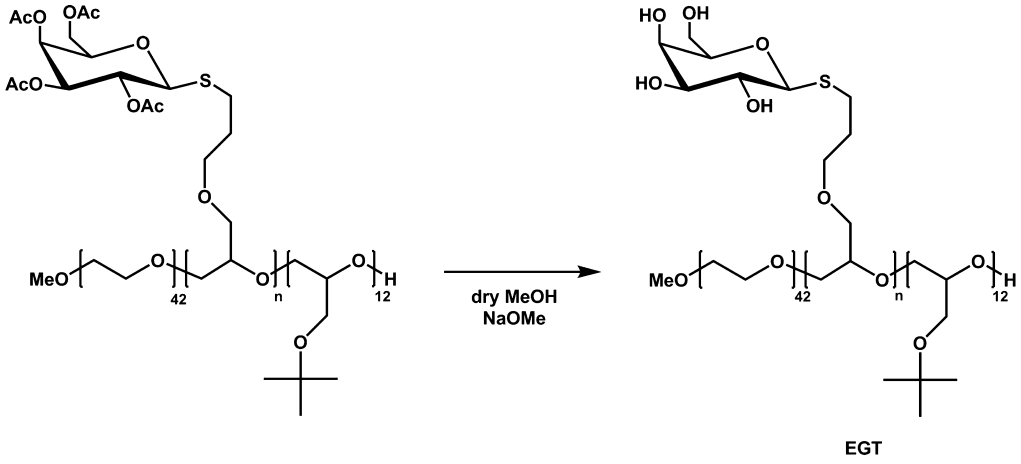

[a]The abbreviation EGT will be used later on for the nomenclature of micelles generated via self-assembly of the modified triblock terpolymer.

Ternary Comicelles. Here, the preparation of a 3.4:1:2.3 mixture of PEO$_{42}$-*b*-(PAGE$_{8,NH2}$-*co*-PAGE$_7$)-*b*-P*t*BGE$_{12}$, PEO$_{42}$-*b*-PAGE$_{15,COOH}$-*b*-P*t*BGE$_{12}$, and PEO$_{42}$-*b*-(PAGE$_{10,AcGal}$-*co*-PAGE$_5$)-*b*-P*t*BGE$_{12}$ is reported. Due to the different degrees of functionalization, a 6:1:3.5 ratio regarding the stoichiometry of the amino and carboxy functionalized triblock terpolymers was used.

A total of 12 mg of PEO$_{42}$-*b*-(PAGE$_{8,NH2}$-*co*-PAGE$_7$)-*b*-P*t*BGE$_{12}$, 2 mg of PEO$_{42}$-*b*-PAGE$_{15,COOH}$-*b*-P*t*BGE$_{12}$, and 7 mg PEO$_{42}$-*b*-(PAGE$_{10,AcGal}$-*co*-PAGE$_5$)-*b*-P*t*BGE$_{12}$ were dissolved in 0.4 mL of THF, and approximately 3 mg of nile red was added to the solution. The solution was then slowly added to 2.1 mL of Milli-Q water, and the THF was allowed to evaporate by stirring overnight. Non-encapsulated dye remained as precipitate in the solution and was filtered off by a 0.45 μm nylon syringe filter. In the case of evaporation of water, the solution was filled up again to a volume of 2.1 mL. After filtration, a clear pink solution could be obtained.

RESULTS AND DISCUSSION

Synthesis and Postpolymerization Functionalization of PEO$_{42}$-*b*-PAGE$_{15}$-*b*-P*t*BGE$_{12}$. Based on earlier studies regarding the synthesis and functionalization, we used a polyether-based triblock terpolymer, poly(ethylene oxide)-*block*-poly(allyl glycidyl ether)-*block*-poly(*tert*-butyl glycidyl ether) (PEO-*b*-PAGE-*b*-P*t*BGE), as starting material for the synthesis of triblock terpolymers with identical A and C segments but different functionalities present in the B block.[18,19] The synthesis of PEO$_{42}$-*b*-PAGE$_{15}$-*b*-P*t*BGE$_{12}$ by AROP has been described previously (the subscripts denote the degrees of polymerization of the respective segment).[19] To generate differently functionalized examples for co-assembly, PEO$_{42}$-*b*-PAGE$_{15}$-*b*-P*t*BGE$_{12}$ was modified by thiol−ene chemistry: Cysteamine (2-aminoethanethiol) was used to introduce NH$_2$ groups and the possibility to form cationic charges in aqueous media, 3-mercapto propionic acid enables the introduction of carboxylic acid moieties and, hence, negative charges, and thiogalactose represents a model targeting moiety to ensure selective cellular uptake in hepatocytes.[47,48] In the latter case, acetyl-protected thiogalactose was used initially (Scheme 1).

The reactions were performed in mixtures of DMF/EtOH for tetraacetyl thiogalactose and 3-mercapto propionic acid, whereas a mixture of DMF/EtOH/MeOH was used for cysteamine due to the rather low solubility of this compound. The reaction progress was monitored by size exclusion chromatography (SEC, shift to lower elution volumes in all cases) and ^{1}H NMR spectroscopy (Figures S1−S3). The degree of functionalization was determined by ^{1}H NMR spectroscopy through the decrease in intensity of the characteristic signals for the pendant double bonds of PAGE at 5.85 and 5.20 ppm compared to the *t*-butyl group of the P*t*BGE block at 1.15 ppm (Table 1). For the functionalization with 3-mercapto propionic acid, full conversion could be reached after 24 h of irradiation. In contrast, only 53% functionalization could be obtained for cysteamine despite probing longer reaction times, higher irradiation intensity, or different triblock terpolymer/thiol ratios. We attribute this to the lower solubility observed for cysteamine. Similarly, in case of the acetylated thiogalactose only 70% functionalization could be reached, presumably also due to solubility issues of either the starting material or the triblock terpolymer after modification. Therefore, PEO$_{42}$-*b*-(PAGE$_{8,NH2}$-*co*-PAGE$_7$)-*b*-P*t*BGE$_{12}$ (ENT), PEO$_{42}$-*b*-PAGE$_{15,COOH}$-*b*-P*t*BGE$_{12}$ (ECT),

dx.doi.org/10.1021/bm5002894 | Biomacromolecules 2014, 15, 2426−2439

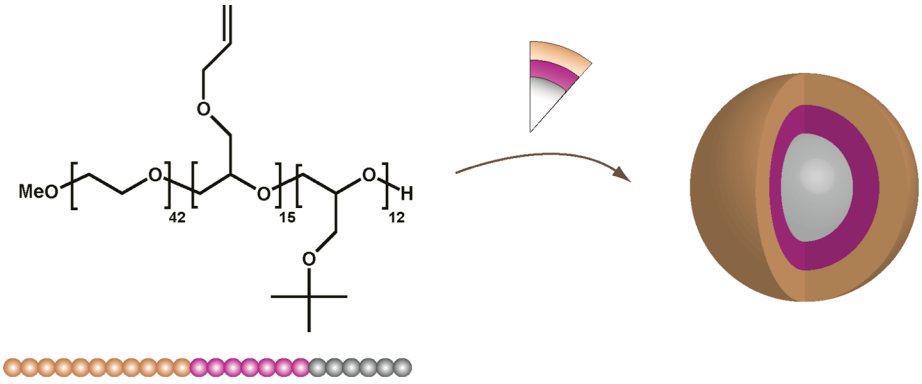

Figure 1. Schematic representation of a core−shell-corona micelle formed by PEO_{42}-*b*-$PAGE_{15}$-*b*-P*t*BGE_{12} in aqueous media with a P*t*BGE core (gray), a PAGE shell (purple), and a PEO corona (brown).

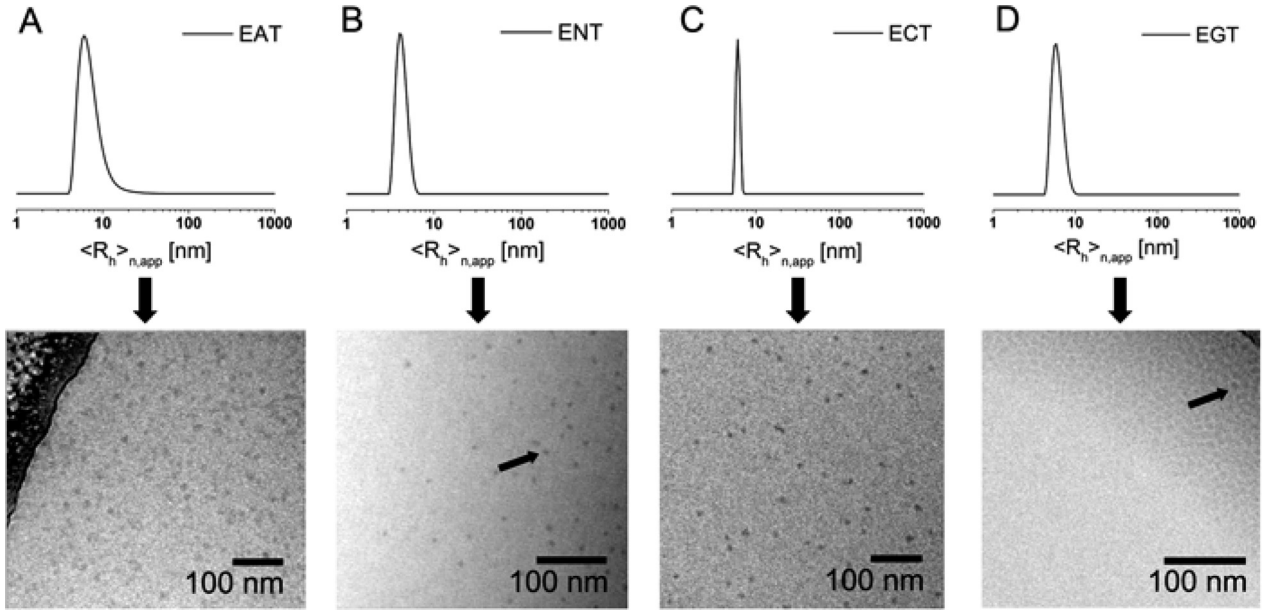

Figure 2. Number-weighted DLS CONTIN plots (upper section) for EAT (A, $\langle R_h \rangle_{n,app}$ = 7 nm), ENT (B, $\langle R_h \rangle_{n,app}$ = 4 nm), ECT (C, $\langle R_h \rangle_{n,app}$ = 6 nm), and EGT (D, $\langle R_h \rangle_{n,app}$ = 6 nm), as well as the corresponding cryo-TEM images (lower section) of the prepared micelles. Due to the rather low contrast an arrow highlights representative ENT (B) and EGT (D) micellar cores. All cryo-TEM images are displayed as recorded.

Table 2. DLS and AF4 Data for the Investigated Triblock Terpolymer Micelles and Co-Micelles[a]

sample	$M_n \times 10^{-5}$ (g/mol)	$\langle R_h \rangle_{n,app}$[b] (nm)	N_{agg}	$\langle R_g \rangle$ (nm)	$\langle R_h \rangle$[c] (nm)	$\langle R_g/R_h \rangle$[d]	$\langle R_h \rangle$[e] (nm)
EAT	11.48 ± 0.078	7.0	225 ± 2	10.1 ± 0.6	13.0 ± 0.4	0.777 ± 0.021	11.8 ± 0.1
ENT	18.58 ± 0.314	4.2	323 ± 56	15.8 ± 1.1	17.4 ± 1.8	0.916 ± 0.148	9.5 ± 0.3
ECT	10.45 ± 0.007	6.1	156 ± 1	12.2 ± 0.8	14.4 ± 0.1	0.844 ± 0.054	13.5 ± 0.3
EGT	2.224 ± 0.070	6.0	31 ± 1	5.4 ± 0.6	5.3 ± 0.3	1.018 ± 0.136	7.1 ± 0.3
$(ENT/ECT)^{3.5:1}$	11.97 ± 0.366	6.3	204 ± 6	12.3 ± 0.4	15.2 ± 0.5	0.810 ± 0.042	
$(ENT/ECT)^{1.2:1}$	7.323 ± 0.127	4.3	121 ± 2	8.9 ± 0.8	10.6 ± 1.5	0.844 ± 0.051	10.5 ± 0.2
$(ENT/ECT)^{1:2.6}$	6.192 ± 0.039	4.9	99 ± 1	9.0 ± 1.6	10.4 ± 0.5	0.875 ± 0.196	10.5 ± 0.1
$(ENT/ECT/EGT)^{3.5:1:0.5}$	11.34 ± 0.714	8.2	190 ± 12	13.6 ± 1.2	15.9 ± 0.1	0.856 ± 0.084	12.3 ± 0.5
$(ENT/ECT/EGT)^{3.4:1:2.3}$	9.654 ± 0.482	6.7	155 ± 8	13.5 ± 1.2	15.1 ± 0.1	0.899 ± 0.076	11.5 ± 0.5

[a]AF4 was performed using aqueous 20 mM NaCl solution. [b]Batch DLS in pure water. [c]Online DLS (AF4-DLS) in 20 mM NaCl. [d]R_h from AF4-DLS. [e]Batch DLS in 20 mM NaCl.

and PEO_{42}-*b*-($PAGE_{10,AcGal}$-*co*-$PAGE_5$)-*b*-P*t*BGE_{12} (EGT after deprotection) could be successfully prepared using thiol−ene chemistry.

In a second step, the acetylated galactose was deprotected by treatment with sodium methanolate (Scheme 2). For this purpose, the polymer was dissolved in dry methanol, an excess of sodium methanolate was added, and the solution was stirred for 1 h. The crude product was purified by dialysis and the complete deprotection was confirmed by ^{1}H NMR measurements (Figure S3, Table 1). As shown in Figure S3, an increase of the molar mass was detected, contrary to what would be expected. We assume that the deprotection and, therefore,

dx.doi.org/10.1021/bm5002894 | *Biomacromolecules* 2014, 15, 2426−2439

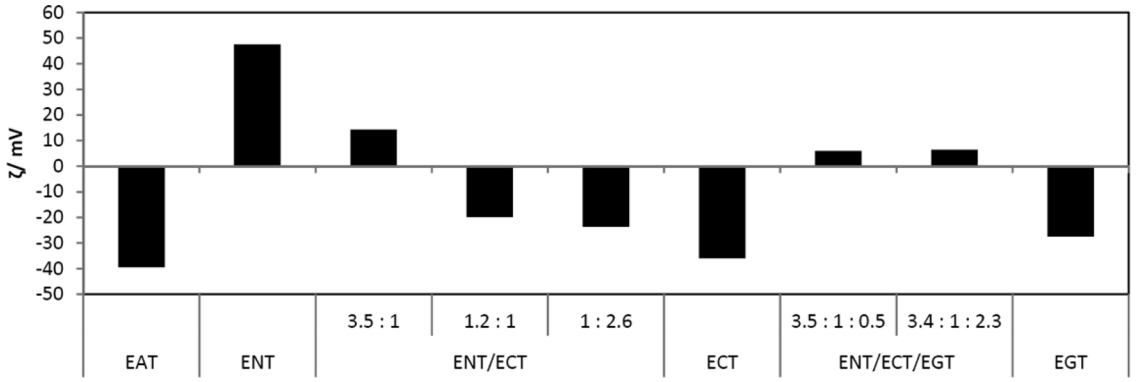

Figure 3. Zeta-potential measurements of different triblock terpolymer micelles and comicelles in water.

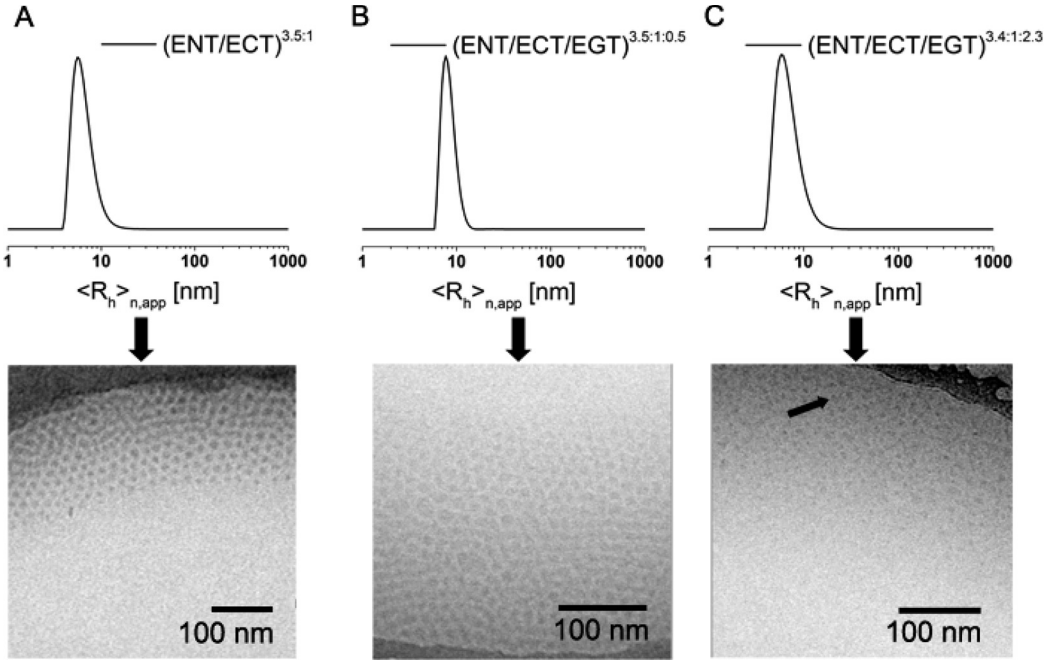

Figure 4. Number-weighted DLS CONTIN plots (upper row), for $(ENT/ECT)^{3.5:1}$ (A, $\langle R_h \rangle_{n,app}$ = 6 nm), $(ENT/ECT/EGT)^{3.5:1:0.5}$ (B, $\langle R_h \rangle_{n,app}$ = 8 nm), and $(ENT/ECT/EGT)^{3.4:1:2.3}$ (C, $\langle R_h \rangle_{n,app}$ = 7 nm), as well as the corresponding cryo-TEM images (lower row) of the prepared comicelles. Due to the low contrast, one micellar core is highlighted with an arrow for $(ENT/ECT/EGT)^{3.4:1:2.3}$ (C). All cryo-TEM images are displayed as recorded.

changes in solubility significantly influence the hydrodynamic radius, resulting in a shift to lower elution volume. This behavior has also been reported in earlier studies.[49]

For simplicity, the nomenclature ENT, ECT, and EGT will be used for micellar structures generated by self-assembly or co-assembly of these compounds.

Micelle Formation in Aqueous Media. We have shown earlier that PEO-*b*-PAGE-*b*-P*t*BGE triblock terpolymers as well as their thiogalactose-functionalized counterparts undergo self-assembly in aqueous media into micelles with a P*t*BGE core, a PAGE shell, and a PEO corona (Figure 1).[19] Prior to co-assembly studies, micelles separately formed by EAT (before thiol−ene modification), ENT, ECT, and EGT in aqueous solution were investigated.

Micellar solutions with a concentration of 10 g/L were prepared by the addition of THF solutions of the respective triblock terpolymer to water, followed by evaporation of the organic co-solvent. Subsequently, the solutions were analyzed by dynamic light scattering (DLS) and cryogenic transmission electron microscopy (cryo-TEM). In Figure 2, the number weighted hydrodynamic radii from DLS are depicted. For all samples, radii (R_h) in the range of 4 to 7 nm were detected in ultrapure water (pH = 7), and the results are summarized in Table 2. The corresponding intensity weighted DLS CONTIN plots of all samples are shown in Figure S7.

In addition to DLS experiments, also cryo-TEM measurements were performed. In that way, block copolymer nanostructures in aqueous solution can be visualized without drying artifacts.[50−52] As shown in Figure 2, spherical micelles were found for all samples discussed here. For micelles formed by ENT (Figure 2B) and EGT (Figure 2D) black arrows were added to highlight a representative micellar core. In some cases, a small distribution of worm-like structures was also found in cryo-TEM, presumably due to aggregation of spherical micelles (Figure S4). This phenomenon was also observed in our previous studies.[18,19] In general, for all samples micelles with a particle diameter ranging from 10 to 15 nm could be detected, confirming the results from DLS studies. To ensure the stability

dx.doi.org/10.1021/bm5002894 | *Biomacromolecules* 2014, 15, 2426−2439

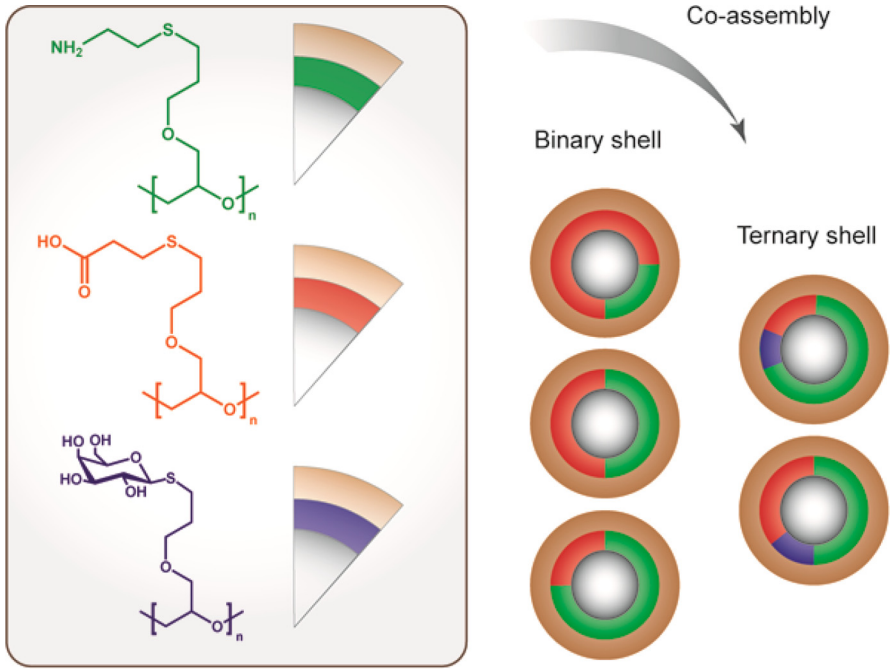

Figure 5. Schematic representation of the co-assembly of functionalized triblock terpolymers into binary and ternary core-shell-corona micelles with a mixed shell. The fractions of the modified PAGE shell (color code: green = cysteamine functionalized, red = 3-mercapto propionic acid functionalized, blue = thiogalactose functionalized) represent the mixing ratio during co-assembly.

of the prepared nanoparticles even at low concentrations, in particular for the later shown internalization tests, DLS measurements with diluted solutions of ECT were performed (Figure S5). For this purpose, a sample of 2.06 g/L was diluted stepwise up to a concentration of 0.005 g/L. Even at this concentration, micelles could be detected using DLS experiments. The sample was chosen, as this polymer showed the highest degree of functionalization and, therefore, also the highest hydrophilicity.

Mixed Micelles Formed via Co-Assembly of Triblock Terpolymers. We have recently shown that a combination of positively and negatively charged segments within triblock terpolymers (i.e., ampholytic materials) and the resulting multicompartment micelles in aqueous media led to pH-dependent interaction with cells, enhanced cellular uptake, and superior transfection efficiencies for pDNA.[12,28] However, in this particular case, one single material has been used, and it can be anticipated that the charge ratio (cationic/anionic) plays an important role. We were, therefore, interested in the co-assembly of different triblock terpolymers as an alternative strategy to control charge and functionality within such micelles.[29,30] In this context, the above-described triblock terpolymers (ENT, ECT, EGT) represent a versatile and highly flexible tool box. Co-assembly should again lead to the formation of core-shell-corona micelles, featuring a PEO corona and a hydrophobic P*t*BGE core formed by identical segments A and C. The shell (B segment), however, should now be composed of different functional groups, depending on which material combinations are used. As a first example, micelles with different charge ratios (NH_2/COOH) were prepared by co-assembly of ENT and ECT. For this purpose, mixtures of both triblock terpolymers were dissolved in THF and slowly added into water. Binary comicelles with an excess of positive charges $(ENT/ECT)^{3.5:1}$, a slight excess of positive charges $(ENT/ECT)^{1.2:1}$, and an excess of negative charges $(ENT/ECT)^{1:2.6}$ were assembled using this pathway. In all cases, the superscripts represent the mixing ratio regarding the functional groups of the involved triblock terpolymers. The micellar solutions were afterward analyzed by DLS and cryo-TEM (Figure 4, the DLS CONTIN plots for $(ENT/ECT)^{1.2:1}$ and $(ENT/ECT)^{1:2.6}$ can be found in Figure S6). A schematic representation of the co-assembly and the formation of comicelles is presented in Figure 5.

Again, spherical micelles with hydrodynamic radii of 4 to 6 nm were obtained by DLS and these results were confirmed by cryo-TEM measurements (diameters of 12−14 nm were observed). As both middle blocks of ENT (NH_2) and ECT (COOH) are weak polyelectrolytes, we anticipated that the pH value might have an influence during the assembly process. Therefore, the co-assembly was carried out under acidic (pH ∼ 4) as well as basic conditions (pH ∼ 12), and the results were compared to the data obtained under neutral conditions (pH ∼ 7). Additionally, also, the preparation pathway was changed, that is, addition of water to THF solutions instead of vice versa. In all cases, no significant influence on the micellar size and the dispersity was observed (Table S1) and, therefore, all subsequent co-assembly procedures were carried out at pH 7 and via the addition of the THF solution containing the triblock terpolymers into water.

Subsequently, a detailed characterization of the micelles and comicelles regarding charge was carried out using zeta-potential measurements. As structures of rather small size were obtained, it is at the same time highly demanding and crucial to investigate if, for example, comicelles of ENT and ECT or if two separate populations are formed. This is difficult to estimate using only DLS and cryo-TEM. For the zeta-potential measurements and, also, later, for AF4 measurements, gel electrophoresis, and cell uptake studies, nile red, a hydrophobic red fluorescent dye, was encapsulated into the hydrophobic P*t*BGE core. Nile red is poorly soluble in water and exhibits a strong fluorescence in hydrophobic environment.[53] Therefore, the respective triblock terpolymer (or mixtures) and a small

dx.doi.org/10.1021/bm5002894 | *Biomacromolecules* 2014, 15, 2426−2439

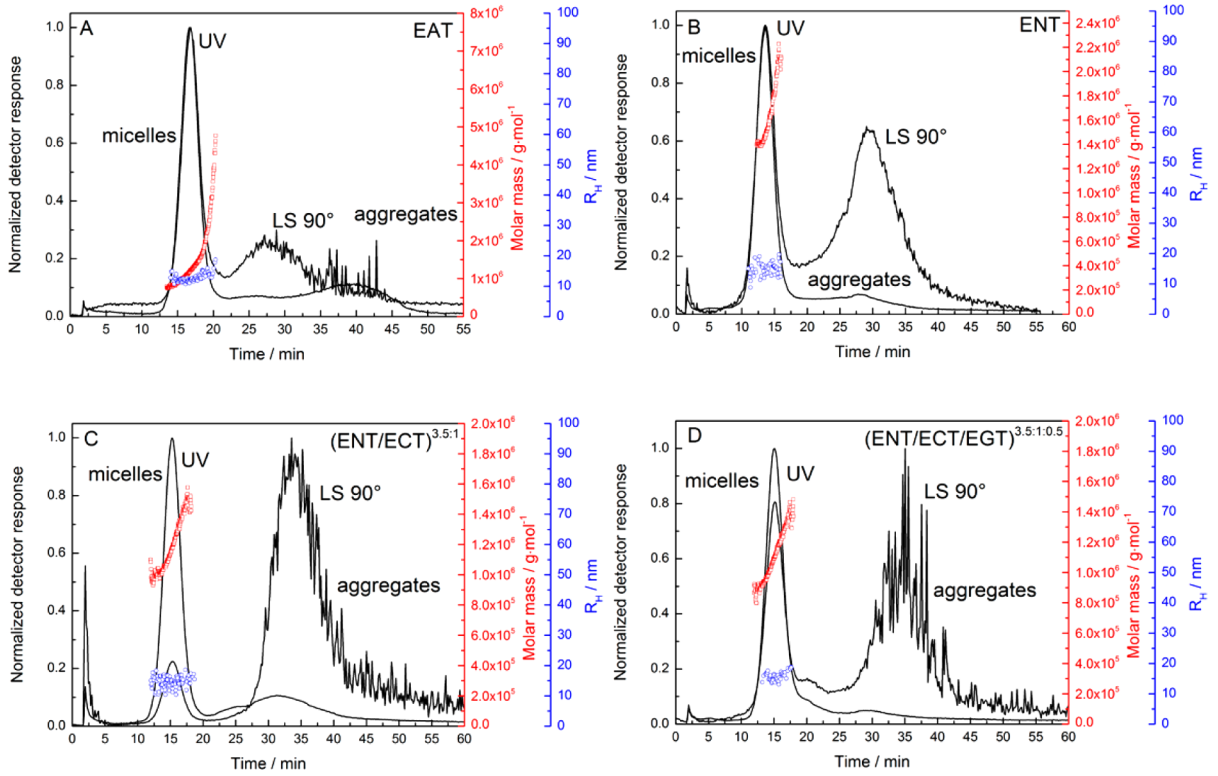

Figure 6. AF4 fractograms of triblock terpolymer micelles from EAT (A), ENT (B), $(ENT/ECT)^{3.5:1}$ (C), and $(ENT/ECT/EGT)^{3.5:1:0.5}$ (D) in 20 mM NaCl solution.

amount of the dye were dissolved in THF and slowly added into a defined amount of water (identical preparation pathway as has been described earlier). Afterward, the organic solvent was evaporated and the excess of non-encapsulated dye was filtered off.

In a first approach, the zeta potential of different micellar populations at a pH value of 7 was analyzed, and the results are depicted in Figure 3. As expected, a negative value is found for ECT (−36 mV) whereas the zeta potential for ENT is positive (47.5 mV). Both EAT and EGT revealed negative values (−39.5 and −27 mV), which can be attributed to the complexation of ions within the PEO corona or charge−dipole and dipole−dipole interactions, which are both known to influence the zeta potential.[43,54]

For binary comicelles (ENT/ECT), a clear dependence of the zeta potential on the mixing ratio can be observed, as with increasing amount of ENT the zeta potential increases (from −23.6 mV for $(ENT/ECT)^{1:2.6}$ to 14.2 mV for $(ENT/ECT)^{3.5:1}$). Thus, zeta potential measurements indicate that comicelles are formed. If the co-assembly in the case of, for example, $(ENT/ECT)^{3.5:1}$ would lead to two separate populations of ENT and ECT, aggregation of oppositely charged micelles due to electrostatic interactions might be expected. In this case, an increase of the aggregates size and, presumably, precipitation might occur. As an attempt to clarify this, mixtures of ENT and ECT micelles after self-assembly via the above-described protocol were prepared at comparable charge ratios and were investigated using time-dependent DLS measurements (Figure S10A), revealing an increase of the R_h from 4 to 10 nm within 2 h and partial precipitation of the material after 12 h (Figure S10B). As the comicelles proved to be stable over several weeks, as confirmed by zeta-potential measurements and the presence of a monomodal size distribution (DLS), an efficient preparation of comicelles by our protocol can be assumed.

Besides charge control in binary systems, also ternary systems were targeted where NH_2 groups (ENT), COOH moieties (ECT), and galactose as model targeting ligand (EGT) are combined. Galactose was chosen to enable selective cellular uptake into hepatocytes, which has been already demonstrated.[47,48] For the ternary systems, two ratios were prepared via co-assembly: $(ENT/ECT/EGT)^{3.5:1:0.5}$ and $(ENT/ECT/EGT)^{3.4:1:2.3}$, featuring almost identical charge ratios and mainly differing in the amount of incorporated galactose. The as-prepared micellar solutions were characterized by DLS and cryo-TEM, and the results are depicted in Figure 4B,C and Table 2. In both cases, spherical micelles with R_h = 8 nm for $(ENT/ECT/EGT)^{3.5:1:0.5}$ and 7 nm in the case of $(ENT/ECT/EGT)^{3.4:1:2.3}$ were found in DLS experiments. In cryo-TEM, again spherical micelles with diameters of 10 to 16 nm could be detected. A decreased contrast was observed for higher amounts of incorporated sugar moieties.

In all cases, evaluation by DLS and cryo-TEM led to comparable results regarding size and shape of both binary and ternary comicelles. Moreover, the ternary comicelles exhibit a decreased zeta potential if compared to the binary $(ENT/ECT)^{3.5:1}$ structures with 6 mV for $(ENT/ECT/EGT)^{3.5:1:0.5}$ and 6.5 mV for $(ENT/ECT/EGT)^{3.4:1:2.3}$, thus, indicating the presence of EGT within the structures (Figure 3). Also, in this case, the zeta potential measurements indicate that comicelles are formed.

Asymmetric Flow Field−Flow Fractionation of Triblock Terpolymer Micelles. To obtain further insights into size, shape, and aggregation number of micelles formed by different triblock terpolymers (and combinations), asymmetric flow field-flow fractionation (AF4) coupled online to multi-

dx.doi.org/10.1021/bm5002894 | Biomacromolecules 2014, 15, 2426−2439

angle light scattering (MALS) and DLS was applied. Here, a 10000 g/mol membrane of regenerated cellulose and an aqueous eluent containing 20 mM NaCl was used for all systems investigated. Fractograms are shown in Figures 6 and S8. For all samples, the main peak represents spherical micelles and, in addition, a small second aggregate population could be detected after the cross-flow reaches zero (labeled "aggregates" in Figure 6). We attribute this to the presence of a small fraction of worm-like structures in accordance with earlier observations and the cryo-TEM experiments.[18] In the case of EGT and $(ENT/ECT/EGT)^{3.4:1:2.3}$, also a small fraction of triblock terpolymer unimers could be identified. Number weighted molar masses M_n of the micelles and aggregation numbers N_{agg}, as well as the different radii (R_g, R_h) and the shape ratio (R_g/R_h) derived from AF4 measurements are listed in Table 2. Thereby, the ratio R_g/R_h provides information about the shape of a macromolecule or colloid. Typical values are 0.778 for a hard sphere, 1.0 for a soft sphere, or 1.78 for a monodisperse linear polymer chain in a good solvent.[55] Additional characteristics (dn/dc values, M_w, M_z, and $Đ$) can be found in Table S2. Aggregation numbers N_{agg} were calculated by dividing the molar mass (M_n) of the micelles by the molar mass (M_n, ^{1}H NMR) of the single triblock terpolymer chain. The hydrodynamic radii measured by AF4-MALS-DLS were significantly higher (around 10−15 nm) in contrast to batch DLS experiments for all samples. We attribute this to the different medium (20 mM NaCl) and, indeed, DLS measurements under these conditions could confirm the results from AF4. The increase in size in the presence of salt might originate from the complexation of sodium ions by the PEO corona or, in case of micelles prepared via co-assembly of ENT and ECT, an increase in ionic strength, and the screening of attractive electrostatic forces between differently charged side chains (COO^- for ECT; NH_3^+ for ENT) within the shell.[56] Nevertheless, in all cases the ratio R_g/R_h scales between 0.775 (hard sphere) and 1.0 (soft sphere), indicating a spherical shape.[55,57]

By AF4 experiments, also the absolute molar mass of the micelles could be detected: Comparable values (M_n) of 1000 to 2000 kg/mol were obtained for EAT, ENT, and ECT micelles, whereas only 220 kg/mol were found in the case of EGT. This corresponds to N_{agg} = 30 (EGT), 225 (EAT), 323 (ENT), and 156 (ECT), respectively. At this point, we attribute the lower values observed for EGT to the steric demand of the thiogalactose side chains within the PAGE shell, preventing a more compact assembly. This is also in good accordance with the observation of a small fraction of triblock terpolymer unimers in the AF4 fractograms (Figure S8B). The aggregation numbers N_{agg} of binary and ternary comicelles were calculated by consideration of the different molar masses of the terpolymers and under the assumption that the ratios of polymer chains in the micelles are the same as the mixing ratios of the triblock terpolymers.

Molar masses of binary and ternary comicelles are in between 620 kg/mol $[(ENT/ECT)^{1:2.6}$, N_{agg} = 99] and 1200 kg/mol $[(ENT/ECT)^{3.5:1}$, N_{agg} = 204]. This indicates the formation of more compact structures with increasing amounts of ENT for the investigated range of charge ratios.

Gel Electrophoresis. In addition to zeta potential measurements, another powerful method for the separation of charged macromolecules (e.g., DNA) is gel electrophoresis. Here, the samples are placed in an agarose gel and an electrical field is applied. The electrical field induces movement within the gel toward the positive or negative pole, depending on the charge of the sample investigated.

A small amount of labeled micelles and comicelles was placed in an agarose gel and an electric field was applied. We anticipated that comicelles should feature only one band, as additional confirmation of the zeta-potential measurements. As shown in Figure 7, micelles formed by ENT reveal the highest

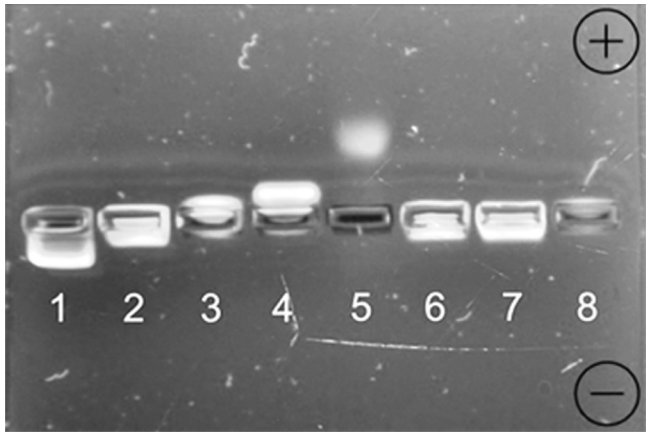

Figure 7. Gel electrophoresis using 1% agarose gel and TBE buffer (1 = ENT, 2 = $(ENT/ECT)^{3.5:1}$, 3 = $(ENT/ECT)^{1.2:1}$, 4 = $(ENT/ECT)^{1:2.6}$, 5 = ECT, 6 = $(ENT/ECT/EGT)^{3.5:1:0.5}$, 7 = $(ENT/ECT/EGT)^{3.4:1:2.3}$, 8 = EGT).

shift to the negative pole, whereas ECT moved toward the positive pole. The bands observed for ENT/ECT comicelles of different mixing ratios are, in accordance with their zeta-potential, in between. If two separate populations of ENT and ECT would be formed, two separate bands in gel electrophoresis toward opposite poles might be expected. As only one band is visible for all samples, we regard this as another indication for an efficient co-assembly. In addition, ternary ENT/ECT/EGT exhibited movement toward the negative pole, again confirming the results from zeta-potential measurements. EGT did not show any movement in gel electrophoresis. Contrary to the negative zeta potential of −39.5 mV, EAT micelles exhibited a clear shift to the negative pole (Figure S9). Up to now, we have no conclusive explanation for this behavior as also zeta potential measurements in comparable buffer solutions (the exact composition is given in the experimental part) yielded negative values.

Cellular Interactions. *Cytotoxicity and Hemolysis of Triblock Terpolymer Micelles.* Aiming for a later use of such triblock terpolymer micelles in targeting and/or delivery applications, their cytotoxicity was investigated using an Alamar blue assay. At first, triblock terpolymer micelles formed via the self-assembly of one single material were investigated. Micelles formed of EAT, ECT, or EGT did not show any cytotoxic effects for concentrations up to 0.5 mg/mL (cell viability was above 70%), only in case of ENT the situation was different (Figure 8A). Regarding EAT, ECT, and EGT, these results are in accordance with literature, as all structures exhibited negative zeta potentials.[39,58] For micelles based on ENT, the IC_{50} of 300 μg/mL can be explained by the presence of cationic charges within the shell (zeta potential of +47.5 mV), which could lead to stronger interactions with or even disruption of the cell membrane. These results can be taken as further proof that the functionalization of the middle block (PAGE) significantly influences interactions of such micelles with biological matter,

dx.doi.org/10.1021/bm5002894 | Biomacromolecules 2014, 15, 2426−2439

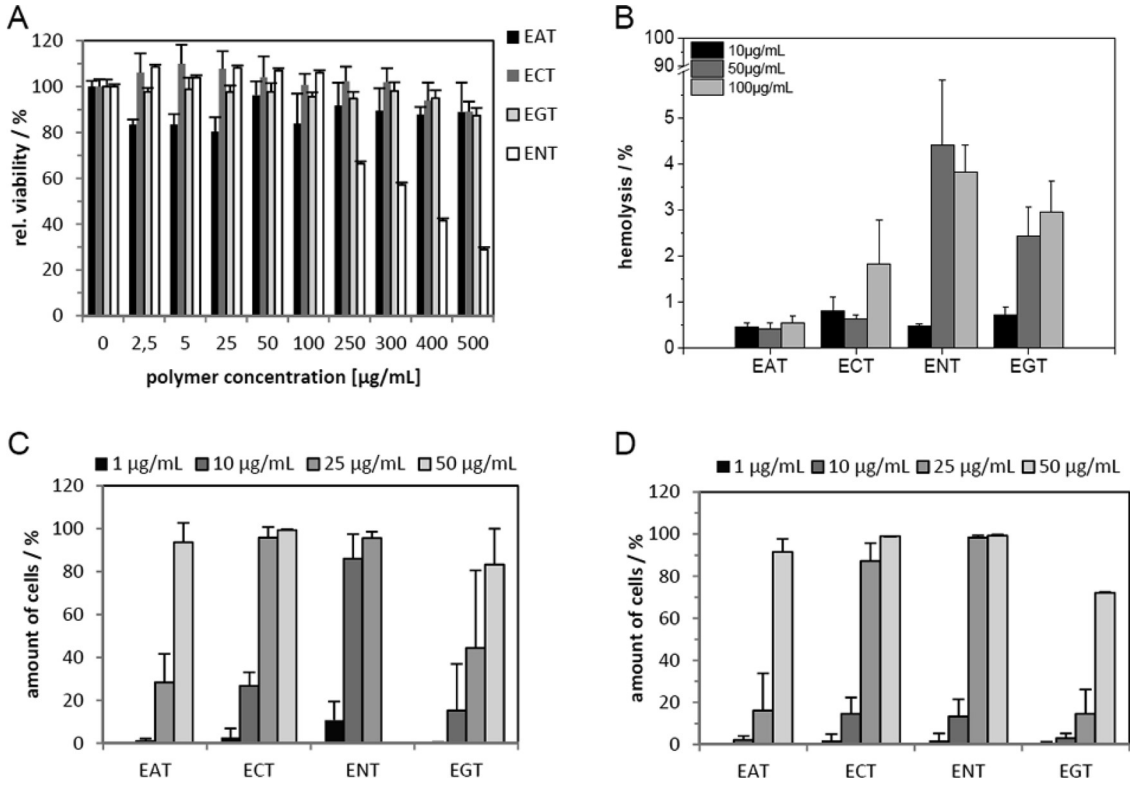

Figure 8. Cytotoxicity test of triblock terpolymer micelles using L929 cells (A) and hemolysis assay using three different donators (B). Cellular uptake under serum reduced (C) and serum containing conditions (D) in HEK cells. Values represent the mean ± SD.

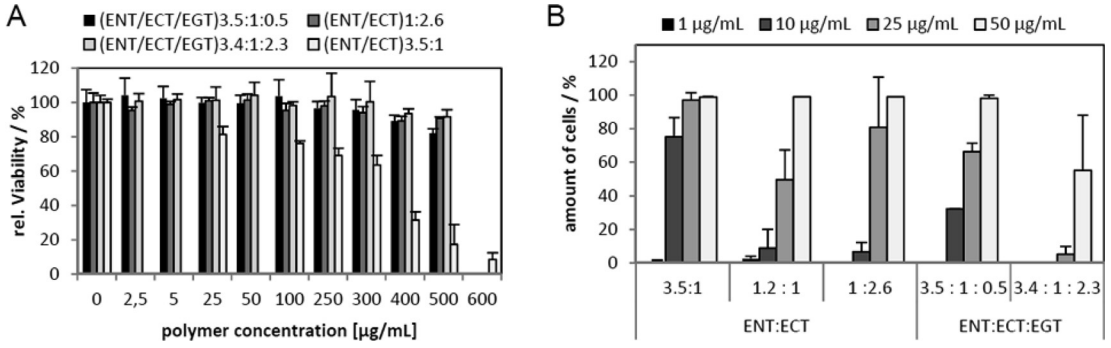

Figure 9. Cytotoxicity test of binary and ternary comicelles using L929 cells (A) and cellular uptake in HEK cells (B). Values represent the mean ± SD; $n = 3$.

even though all structures feature a rather long PEO corona (compared to the degrees of polymerization for PAGE and P*t*BGE).[59]

A hemolysis assay was performed to gain deeper insight into the interaction of EAT, ENT, ECT, and EGT micelles with negatively charged cell membranes: Here, ENT exhibited slight hemolytic activity at concentrations of 50 μg/mL (3.8 ± 0.6% hemolysis, Figure 8B). No hemolytic activity was found for both EAT and ECT. In contrast, 2.9 ± 0.6% hemolysis was observed for EGT micelles. We attribute this to hydrophobic interactions with the cell membrane, possibly even incorporation of EGT into the latter.

Internalization of Triblock Terpolymer Micelles. Furthermore, the internalization efficiency of micelles from EAT, ENT, ECT, and EGT into human embryonic kidney (HEK) cells, a model cell line for unspecific uptake studies, was analyzed under serum-reduced and serum-containing conditions. As nile red was encapsulated in the micelles, the internalization was analyzed by flow cytometry, at which untreated cells were applied as control (Figure S12). Under serum-reduced conditions the critical concentration, that is, the concentration where EAT shows nearly no uptake (1 ± 1.1%), was determined to be 10 μg/mL (Figure 8C). From this data set, it becomes obvious that ENT revealed the best uptake into 79.7 ± 4.5% (at 10 μg/mL) of the cells. This can be attributed to the presence of positive charges in the shell and an increased interaction with the cell membrane, also confirmed by the earlier discussed hemolysis assay. Higher concentrations of 50 μg/mL could not be analyzed as the cell viability was too low under serum reduced condition. Compared to ENT, the decreased uptake of ECT and EGT at a concentration of 10 μg/mL with 26.8 ± 6.3% and 15.3 ± 21.7%, respectively, can be explained by the negative zeta potential of these particles, resulting in decreased interactions with cells. Nevertheless, even ECT and EGT show significantly increased cellular uptake induced either by the introduction of charges (COOH) or

dx.doi.org/10.1021/bm5002894 | *Biomacromolecules* 2014, 15, 2426−2439

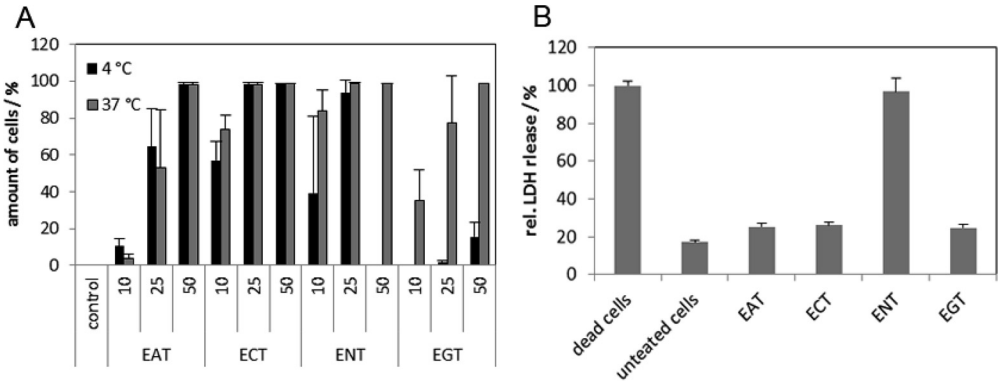

Figure 10. Cellular uptake of triblock terpolymer micelles at 4 and 37 °C in HEK cells after 4 h (A) and lactate dehydrogenase assay with HEK cells and 25 μg/mL of the micelles (B). Values represent the mean ± S.D; $n = 3$.

targeting units (thiogalactose) if compared to EAT at 10 μg/mL (1 ± 1.11%). As the presence of a PEO corona has been shown in many examples to prevent unspecific protein adsorption ("stealth effect"),[17] the uptake was also analyzed in the presence of serum (Figure 8D). Here, only the uptake of ENT decreased significantly from 86 ± 11% to 13 ± 0.6% at 10 μg/mL ($p < 0.005$), presumably due to stronger interactions with negatively charged serum proteins.[60,61] Nevertheless, the uptake of both ENT and ECT is significantly higher compared to EAT with 2 ± 0.5% ($p < 0.05$). The internalization of EGT is similar to EAT at 10 μg/mL, thus, also reduced from 15 to 2.9% in the presence of serum proteins. As the functionalization with thiogalactose is supposed to result in specific uptake into liver cells, we also incubated the EGT micelles with HepG2 cells.[47] Unfortunately, no increased uptake at low concentrations (3.9 ± 5% at 10 μg/mL) could be detected, which would hint toward a targeted internalization process (Figure S11). One explanation might be that the galactose side chains are not sufficiently exposed at the surface and, thus, the interaction with the asialoglycoprotein receptor, specific for galactose in HepG2 cells, is hampered. Further, the PEO corona might form hydrogen bonds with the galactose residues,[62] additionally reducing their accessibility.

Cytotoxicity and Internalization of Comicelles. As the up to now used triblock terpolymer micelles (EAT, ENT, ECT, and EGT) already showed significant differences regarding cellular uptake and cytotoxicity, the influence of the composition in binary and ternary comicelles on the cytotoxicity was studied (Figure 9A). $(ENT/ECT)^{3.5:1}$ exhibited a positive zeta potential and a similar cytotoxicity (IC_{50} of 350 μg/mL), if compared to ENT (Figure 8A). In the case of $(ENT/ECT)^{1.2:1}$ and $(ENT/ECT)^{1:2.6}$, no cytotoxicity was observed, in accordance with the negative zeta potential.

Interestingly, both the ternary comicelles, $(ENT/ECT/EGT)^{3.5:1:0.5}$ and $(ENT/ECT/EGT)^{3.4:1:2.3}$, which feature the same charge ratio as $(ENT/ECT)^{3.5:1}$ and exhibited positive zeta potentials, did not show any cytotoxicity at all tested concentrations. This is indeed remarkable, and we propose that this originates from the presence of EGT terpolymer chains in these structures. All prepared comicelles were further investigated regarding their internalization behavior. In this case, $(ENT/ECT)^{3.5:1}$ demonstrated outstanding uptake compared to all other samples as already at 10 μg/mL under serum-containing conditions 75 ± 11.5% of the cells showed internalization (Figure 9B). These results are comparable to ENT micelles under serum-reduced conditions, thus, indicating decreased nonspecific interactions of $(ENT/ECT)^{3.5:1}$ with serum proteins. For both $(ENT/ECT)^{1.2:1}$ and $(ENT/ECT)^{1:2.6}$, reduced uptake with 8.9 ± 11% and 6.7 ± 5.5% (compared to $(ENT/ECT)^{3.5:1}$) was found. In the case of ternary comicelles, $(ENT/ECT/EGT)^{3.5:1:0.5}$ exhibited decreased uptake compared to $(ENT/ECT)^{3.5:1}$, presumably due to the presence of EGT (Figure 9B). A further increase of the galactose content leads to even lower values, which is in accordance with lower uptake of EGT compared to ECT and ENT. Nevertheless, it should be noted that, in contrast to $(ENT/ECT)^{3.5:1}$, both $(ENT/ECT/EGT)^{3.5:1:0.5}$ and $(ENT/ECT/EGT)^{3.4:1:2.3}$ did not show any cytotoxicity. In summary, by adjusting the micellar composition via co-assembly of ENT, ECT, and EGT, both cellular uptake and cytotoxicity can be controlled and optimized (according to our results).

Further Investigations Regarding the Pathway for Cellular Uptake. We were also interested in a more detailed analysis of the internalization process. The size of the core−shell-corona micelles used in the present study is below 30 nm in diameter, a size where studies on the internalization process are rarely found, as normally nanostructures between 50 to 200 nm are used in drug delivery applications. Here, internalization via endocytosis is under debate, as this process is usually observed for structures with sizes between 50 to 500 nm.[63−65] As endocytosis is energy dependent, the uptake efficiencies were investigated at 4 °C, conditions which are known to inhibit energy-dependent mechanisms (Figure 10A).[66] Interestingly, no significant changes under these conditions were found for EAT, ECT, and ENT if compared to 37 °C. In contrast, the internalization efficiency for EGT decreased significantly to 15 ± 7.8% (at 50 μg/mL), indicating an energy-dependent mechanism.

Besides, ENT micelles are already cytotoxic at a concentration of 50 μg/mL at 4 °C, in contrast to 37 °C. The increased cytotoxicity at 4 °C might originate from the reduced fluidity of the cell membrane at low temperatures. Therefore, it might occur that cationically charged micelles lead to destabilization and local disruption of the membrane.[67] As the size of the micelles is rather small, these perforations can be easily closed at 37 °C at normal membrane fluidity. At 4 °C, however, this process is significantly slowed down, leading to cell leakage. It has been described in the literature that structures of a few nanometers in size can lead to pore formation and translocation through the cell membrane.[68,69] To evaluate if cell leakage is caused in our case, a lactate dehydrogenase (LDH) assay was performed,[70] which was used

dx.doi.org/10.1021/bm5002894 | Biomacromolecules 2014, 15, 2426−2439

to detect the release of cytosolic LDH into the surrounding media through membrane perforations. For ECT and EAT micelles, no significant LDH release could be observed in contrast to ENT (Figure 10B). This provides a first hint and supports our assumption that EAT and ECT micelles cross the cellular membrane by the formation of reversible membrane pores or penetrate the cell membrane via diffusion. ENT seems to cause larger pores, resulting in LDH release. These first investigations of the internalization process demonstrate that differences in shell composition and functionality of triblock terpolymer micelles influence not only cytotoxicity and uptake efficiency, but also alter the overall internalization process. In that respect, the herein presented toolbox of triblock terpolymers represents an ideal starting point for the purposeful variation of micellar composition and charge and more detailed investigations of the uptake mechanism will follow.

CONCLUSION

Multifunctional and well-defined triblock terpolymers represent very promising materials for the preparation of efficient drug delivery vehicles. Here, we introduce a concept for the co-assembly of ABC triblock terpolymers with identical A and C segments but different functionalities in the middle block (B) into core−shell-corona micelles with a mixed shell. In that way, sub-30 nm particles with superior control over charge and the location of targeting ligands with the micellar shell were formed. The materials employed are poly(ethylene oxide)-*block*-poly(allyl glycidyl ether)-*block*-poly(*tert*-butyl glycidyl ether) (PEO-*b*-PAGE-*b*-P*t*BGE) triblock terpolymers where the PAGE segments has been subsequently modified using thiol−ene chemistry to introduce $-NH_2$ (cysteamine, ENT), −COOH (3-mercaptopropionic acid, ECT), and thiolgalactose residues (EGT). Depending on whether binary (ENT/ECT) or ternary comicelles (ENT/ECT/EGT) were prepared, charge and, directly linked to that, cytotoxicity of the resulting nanoparticle could be adjusted. In the case of ENT/ECT/EGT comicelles, efficient cellular uptake (even in the presence of serum proteins) could be combined with low cytotoxicity. Different characterization methods, including dynamic light scattering (DLS), asymmetric flow field-flow fractionation (AF4), zeta potential measurements, and cryo-TEM indicate that indeed co-micellization occurs. Moreover, first insights into the internalization process of these sub-30 nm micelles could be provided and our results hint toward uptake via direct penetration through the cell membrane and not via endocytosis, offering interesting possibilities for further detailed studies.

ASSOCIATED CONTENT

Supporting Information

Size-exclusion chromatograms and ^{1}H NMR spectra for the synthesized materials. Further DLS CONTIN plots, TEM images, and information regarding the cellular uptake, as well as detailed data of the AF4 measurements. This material is available free of charge via the Internet at http://pubs.acs.org.

AUTHOR INFORMATION

Corresponding Authors

*E-mail: felix.schacher@uni-jena.de.
*E-mail: ulrich.schubert@uni-jena.de.

Author Contributions

†Both authors contributed equally to this work (M.J.B. and A.C.R.).

Notes

The authors declare no competing financial interest.

ACKNOWLEDGMENTS

The authors want to acknowledge C. Fritzsche for hemolysis studies and Alamar Blue assay. The work of M.J.B. forms part of the research programme of the Dutch Polymer Institute (DPI), Project #690. A.C.R., A.S., and M.W. thank the Carl Zeiss Foundation for financial support. F.H.S. is grateful for a fellowship from the Fonds der Chemischen Industrie (FCI). Furthermore, the authors want to acknowledge the Thuringian Ministry for Education, Science and Culture (TMBWK; #B515-10065, ChaPoNano; #B514-09051, NanoConSens).

REFERENCES

(1) Mai, Y. Y.; Eisenberg, A. *Chem. Soc. Rev.* **2012**, *41*, 5969−5985.
(2) Schacher, F. H.; Rupar, P. A.; Manners, I. *Angew. Chem., Int. Ed.* **2012**, *51*, 7898−7921.
(3) Barthel, M. J.; Schacher, F. H.; Schubert, U. S. *Polym. Chem.* **2014**, *5*, 2647−2662.
(4) Price, C.; Lally, T. P.; Stubbers, R. *Polymer* **1974**, *15*, 541−543.
(5) Arai, K.; Kotaka, T.; Kitano, Y.; Yoshimura, K. *Macromolecules* **1980**, *13*, 455−457.
(6) Mogi, Y.; Kotsuji, H.; Kaneko, Y.; Mori, K.; Matsushita, Y.; Noda, I. *Macromolecules* **1992**, *25*, 5408−5411.
(7) Auschra, C.; Stadler, R. *Macromolecules* **1993**, *26*, 2171−2174.
(8) Lodge, T. P.; Rasdal, A.; Li, Z. B.; Hillmyer, M. A. *J. Am. Chem. Soc.* **2005**, *127*, 17608−17609.
(9) Betthausen, E.; Drechsler, M.; Fortsch, M.; Schacher, F. H.; Müller, A. H. E. *Soft Matter* **2011**, *7*, 8880−8891.
(10) Gröschel, A. H.; Schacher, F. H.; Schmalz, H.; Borisov, O. V.; Zhulina, E. B.; Walther, A.; Müller, A. H. E. *Nat. Commun.* **2012**, *3*, 710.
(11) Gröschel, A. H.; Walther, A.; Löbling, T. I.; Schacher, F. H.; Schmalz, H.; Müller, A. H. E. *Nature* **2013**, *503*, 247−251.
(12) Rinkenauer, A. C.; Schallon, A.; Günther, U.; Wagner, M.; Betthausen, E.; Schubert, U. S.; Schacher, F. H. *ACS Nano* **2013**, *7*, 9621−9631.
(13) Schallon, A.; Synatschke, C. V.; Jerome, V.; Müller, A. H. E.; Freitag, R. *Biomacromolecules* **2012**, *13*, 3463−3474.
(14) Huang, X. Y.; Chen, S.; Huang, J. L. *J. Polym. Sci., Part A: Polym. Chem.* **1999**, *37*, 825−833.
(15) Arnal, M. L.; Balsamo, V.; Lopez-Carrasquero, F.; Contreras, J.; Carrillo, M.; Schmalz, H.; Abetz, V.; Laredo, E.; Müller, A. J. *Macromolecules* **2001**, *34*, 7973−7982.
(16) Jing, R. K.; Wang, G. W.; Zhang, Y. N.; Huang, J. L. *Macromolecules* **2011**, *44*, 805−810.
(17) Knop, K.; Hoogenboom, R.; Fischer, D.; Schubert, U. S. *Angew. Chem., Int. Ed.* **2010**, *49*, 6288−6308.
(18) Barthel, M. J.; Babiuch, K.; Rudolph, T.; Vitz, J.; Hoeppener, S.; Gottschaldt, M.; Hager, M. D.; Schacher, F. H.; Schubert, U. S. *J. Polym. Sci., Part A: Polym. Chem.* **2012**, *50*, 2914−2923.
(19) Barthel, M. J.; Mansfeld, U.; Hoeppener, S.; Czaplewska, J. A.; Schacher, F. H.; Schubert, U. S. *Soft Matter* **2013**, *9*, 3509−3520.
(20) Obermeier, B.; Frey, H. *Bioconjugate Chem.* **2011**, *22*, 436−444.
(21) Hruby, M.; Konak, C.; Ulbrich, K. *J. Controlled Release* **2005**, *103*, 137−148.
(22) Lin, S. L.; Zhu, W. J.; He, X. H.; Xing, Y. H.; Liang, L. Y.; Chen, T.; Lin, J. P. *J. Phys. Chem. B* **2013**, *117*, 2586−2593.
(23) Libera, M.; Trzebicka, B.; Kowalczuk, A.; Walach, W.; Dworak, A. *Polymer* **2011**, *52*, 250−257.
(24) Kataoka, K.; Harada, A.; Nagasaki, Y. *Adv. Drug Delivery Rev.* **2001**, *47*, 113−131.

(25) Sun, P. J.; Zhang, Y.; Shi, L. Q.; Gan, Z. H. *Macromol. Biosci.* **2010**, *10*, 621−631.
(26) Van Butsele, K.; Cajot, S.; Van Vlierberghe, S.; Dubruel, P.; Passirani, C.; Benoit, J. P.; Jerome, R.; Jerome, C. *Adv. Funct. Mater.* **2009**, *19*, 1416−1425.
(27) Fukushima, S.; Miyata, K.; Nishiyama, N.; Kanayama, N.; Yamasaki, Y.; Kataoka, K. *J. Am. Chem. Soc.* **2005**, *127*, 2810−2811.
(28) Lee, Y.; Miyata, K.; Oba, M.; Ishii, T.; Fukushima, S.; Han, M.; Koyama, H.; Nishiyama, N.; Kataoka, K. *Angew. Chem., Int. Ed.* **2008**, *47*, 5163−5166.
(29) Wu, C. L.; Ma, R. J.; He, H.; Zhao, L. Z.; Gao, H. J.; An, Y. L.; Shi, L. Q. *Macromol. Biosci.* **2009**, *9*, 1185−1193.
(30) Attia, A. B. E.; Ong, Z. Y.; Hedrick, J. L.; Lee, P. P.; Ee, P. L. R.; Hammond, P. T.; Yang, Y. Y. *Curr. Opin. Colloid Interface Sci.* **2011**, *16*, 182−194.
(31) Liu, X.; Liu, Y.; Zhang, Z. K.; Huang, F.; Tao, Q.; Ma, R. J.; An, Y. L.; Shi, L. Q. *Chem. Eur. J.* **2013**, *19*, 7437−7442.
(32) Lin, J. P.; Zhu, J. Q.; Chen, T.; Lin, S. L.; Cai, C. H.; Zhang, L. S.; Zhuang, Y.; Wang, X. S. *Biomaterials* **2009**, *30*, 108−117.
(33) Vinogradov, S. V.; Batrakova, E. V.; Li, S.; Kabanov, A. V. *J. Drug Targeting* **2004**, *12*, 517−526.
(34) Zheng, R.; Liu, G.; Yan, X. *J. Am. Chem. Soc.* **2005**, *127*, 15358−15359.
(35) Li, Z.; Hillmyer, M. A.; Lodge, T. P. *Macromolecules* **2006**, *39*, 765−771.
(36) Cabral, H.; Matsumoto, Y.; Mizuno, K.; Chen, Q.; Murakami, M.; Kimura, M.; Terada, Y.; Kano, M. R.; Miyazono, K.; Uesaka, M.; Nishiyama, N.; Kataoka, K. *Nat. Nanotechnol.* **2011**, *6*, 815−823.
(37) Dong, H.; Dube, N.; Shu, J. Y.; Seo, J. W.; Mahakian, L. M.; Ferrara, K. W.; Xu, T. *ACS Nano* **2012**, *6*, 5320−5329.
(38) Alexis, F.; Pridgen, E.; Molnar, L. K.; Farokhzad, O. C. *Mol. Pharmaceutics* **2008**, *5*, 505−515.
(39) Nguyen, J.; Xie, X.; Neu, M.; Dumitrascu, R.; Reul, R.; Sitterberg, J.; Bakowsky, U.; Schermuly, R.; Fink, L.; Schmehl, T.; Gessler, T.; Seeger, W.; Kissel, T. *J. Gene Med.* **2008**, *10*, 1236−1246.
(40) Mishra, S.; Webster, P.; Davis, M. E. *Eur. J. Cell. Biol.* **2004**, *83*, 97−111.
(41) Sun, J.; Zeng, F.; Jian, H.; Wu, S. *Biomacromolecules* **2013**, *14*, 728−736.
(42) Andersson, M.; Wittgren, B.; Wahlund, K. G. *Anal. Chem.* **2003**, *75*, 4279−4291.
(43) Delgado, A. V.; Gonzalez-Caballero, F.; Hunter, R. J.; Koopal, L. K.; Lyklema, J. *J. Colloid Interface Sci.* **2007**, *309*, 194−224.
(44) Ohshima, H. *J. Colloid Interface Sci.* **1994**, *168*, 269−271.
(45) Gottschaldt, M.; Koth, D.; Müller, D.; Klette, I.; Rau, S.; Görls, H.; Schafer, B.; Baum, R. P.; Yano, S. *Chem. Eur. J.* **2007**, *13*, 10273−10280.
(46) Ibatullin, F. M.; Shabalin, K. A.; Janis, J. V.; Shavva, A. G. *Tetrahedron Lett.* **2003**, *44*, 7961−7964.
(47) Babiuch, K.; Pretzel, D.; Tolstik, T.; Vollrath, A.; Stanca, S.; Foertsch, F.; Becer, C. R.; Gottschaldt, M.; Biskup, C.; Schubert, U. S. *Macromol. Biosci.* **2012**, *12*, 1190−1199.
(48) Yang, R.; Meng, F. H.; Ma, S. B.; Huang, F. S.; Liu, H. Y.; Zhong, Z. Y. *Biomacromolecules* **2011**, *12*, 3047−3055.
(49) Babiuch, K.; Becer, C. R.; Gottschaldt, M.; Delaney, J. T.; Weisser, J.; Beer, B.; Wyrwa, R.; Schnabelrauch, M.; Schubert, U. S. *Macromol. Biosci.* **2011**, *11*, 535−548.
(50) Cui, H.; Hodgdon, T. K.; Kaler, E. W.; Abezgauz, L.; Danino, D.; Lubovsky, M.; Talmon, Y.; Pochan, D. J. *Soft Matter* **2007**, *3*, 945−955.
(51) Holder, S. J.; Sommerdijk, N. A. J. M. *Polym. Chem.* **2011**, *2*, 1018−1028.
(52) Zhong, S.; Pochan, D. J. *Polym. Rev.* **2010**, *50*, 287−320.
(53) Greenspan, P.; Mayer, E. P.; Fowler, S. D. *J. Cell. Biol.* **1985**, *100*, 965−973.
(54) Wagner, M.; Reiche, K.; Blume, A.; Garidel, P. *Colloids Surf., A* **2012**, *415*, 421−430.
(55) Burchard, W. *Adv. Polym. Sci.* **1999**, *143*, 113−194.
(56) Benincasa, M. A.; Caldwell, K. D. *J. Chromatogr., A* **2001**, *925*, 159−169.
(57) Glantz, M.; Hakansson, A.; Mansson, H. L.; Paulsson, M.; Nilsson, L. *Langmuir* **2010**, *26*, 12585−12591.
(58) Vollrath, A.; Pretzel, D.; Pietsch, C.; Perevyazko, I.; Schubert, S.; Pavlov, G. M.; Schubert, U. S. *Macromol. Rapid Commun.* **2012**, *33*, 1791−1797.
(59) Verbaan, F. J.; Oussoren, C.; Snel, C. J.; Crommelin, D. J. A.; Hennink, W. E.; Storm, G. *J. Gene Med.* **2004**, *6*, 64−75.
(60) Ogris, M.; Brunner, S.; Schuller, S.; Kircheis, R.; Wagner, E. *Gene Ther.* **1999**, *6*, 595−605.
(61) Cherng, J. Y.; vandeWetering, P.; Talsma, H.; Crommelin, D. J. A.; Hennink, W. E. *Pharm. Res.* **1996**, *13*, 1038−1042.
(62) Belbekhouche, S.; Dulong, V.; Picton, L.; Le Cerf, D. *Colloids Surf., A* **2013**, *428*, 25−31.
(63) Albanese, A.; Tang, P. S.; Chan, W. C. *Annu. Rev. Biomed. Eng.* **2012**, *14*, 1−16.
(64) Rejman, J.; Oberle, V.; Zuhorn, I. S.; Hoekstra, D. *Biochem. J.* **2004**, *377*, 159−169.
(65) Lai, S. K.; Hida, K.; Man, S. T.; Chen, C.; Machamer, C.; Schroer, T. A.; Hanes, J. *Biomaterials* **2007**, *28*, 2876−2884.
(66) Steinman, R. M.; Mellman, I. S.; Muller, W. A.; Cohn, Z. A. *J. Cell Biol.* **1983**, *96*, 1−27.
(67) Leroueil, P. R.; Hong, S. Y.; Mecke, A.; Baker, J. R.; Orr, B. G.; Holl, M. M. B. *Acc. Chem. Res.* **2007**, *40*, 335−342.
(68) Ting, C. L.; Wang, Z. G. *Soft Matter* **2012**, *8*, 12066−12071.
(69) Ding, H. M.; Tian, W. D.; Ma, Y. Q. *ACS Nano* **2012**, *6*, 1230−1238.
(70) Choksakulnimitr, S.; Masuda, S.; Tokuda, H.; Takakura, Y.; Hashida, M. *J. Controlled Release* **1995**, *34*, 233−241.

Supporting information for

"Small but powerful: Co-assembly of polyether-based triblock terpolymers into sub-30nm micelles and synergistic effects on cellular interactions"

Markus J. Barthel[#,1,2,3] Alexandra C. Rinkenauer[#,1,2] Michael Wagner,[1,2] Ulrich Mansfeld,[1,2] Stephanie Hoeppener,[1,2] Justyna A. Czaplewska,[1,2] Michael Gottschald,[1,2] Anja Träger,[1,2] Felix H. Schacher,*[1,2] Ulrich S. Schubert*[1,2,3]

[#]Both authors contributed equally to this work.

[1] Laboratory of Organic and Macromolecular Chemistry (IOMC), Friedrich Schiller University Jena, Humboldtstrasse 10, 07743 Jena, Germany.

[2] Jena Center for Soft Matter (JCSM), Friedrich Schiller University Jena, Philosophenweg 7, 07743 Jena, Germany.

[3] Dutch Polymer Institute (DPI), P.O. Box 902, 5600 AX Eindhoven, the Netherlands.

Email: ulrich.schubert@uni-jena.de; felix.schacher@uni-jena.de

Table S1: Influence of the pH value of the solution on the self-assembly process.

Sample	$\langle R_h \rangle_{n,app}$ [nm]
$(ENT/ECT)^{3.5:1}$ pH = 7	6
$(ENT/ECT)^{3.5:1}$ pH = 3	7
$(ENT/ECT)^{3.5:1}$ pH = 11	7

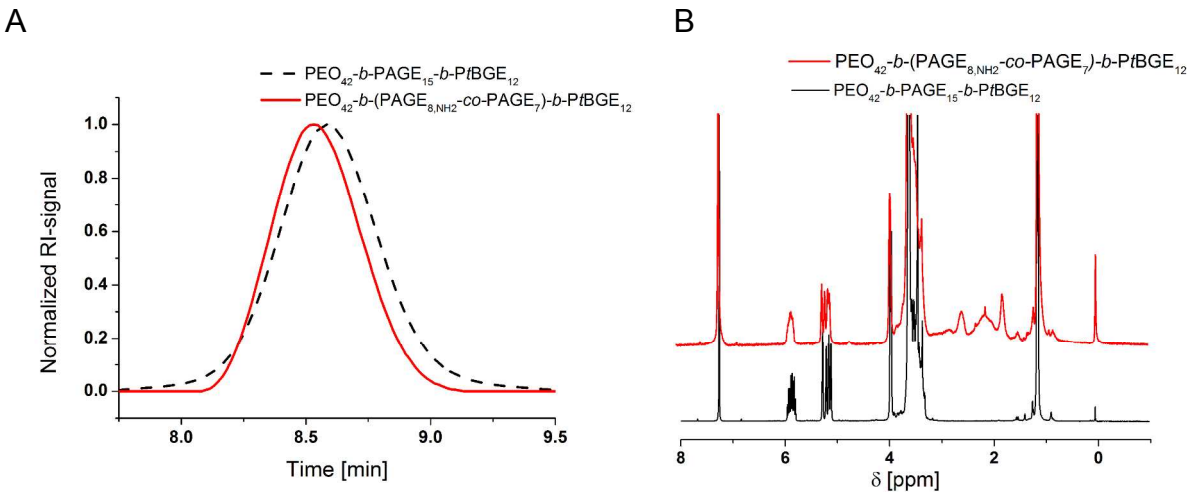

Figure S1: SEC traces (A) and ^{1}H NMR spectrum (B) of the PEO_{42}-*b*-$PAGE_{15}$-*b*-P*t*BGE_{12} precursor as well as the cysteamine functionalized triblock terpolymer.

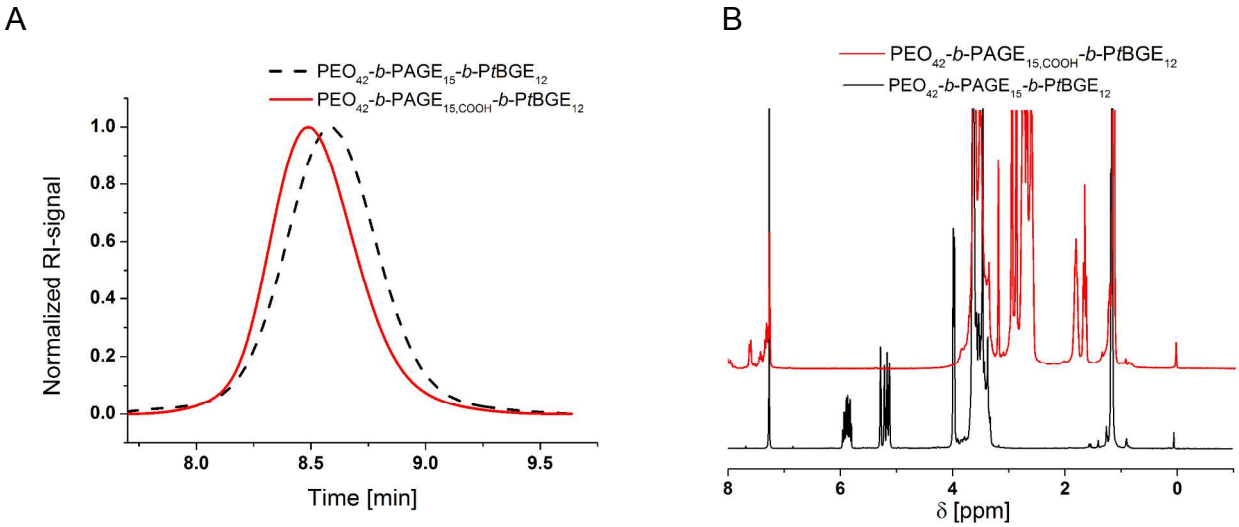

Figure S2: SEC traces (A) and ^{1}H NMR spectrum (B) of the PEO_{42}-*b*-$PAGE_{15}$-*b*-P*t*BGE_{12} precursor as well as the 3-mercapto propionic acid functionalized triblock terpolymer.

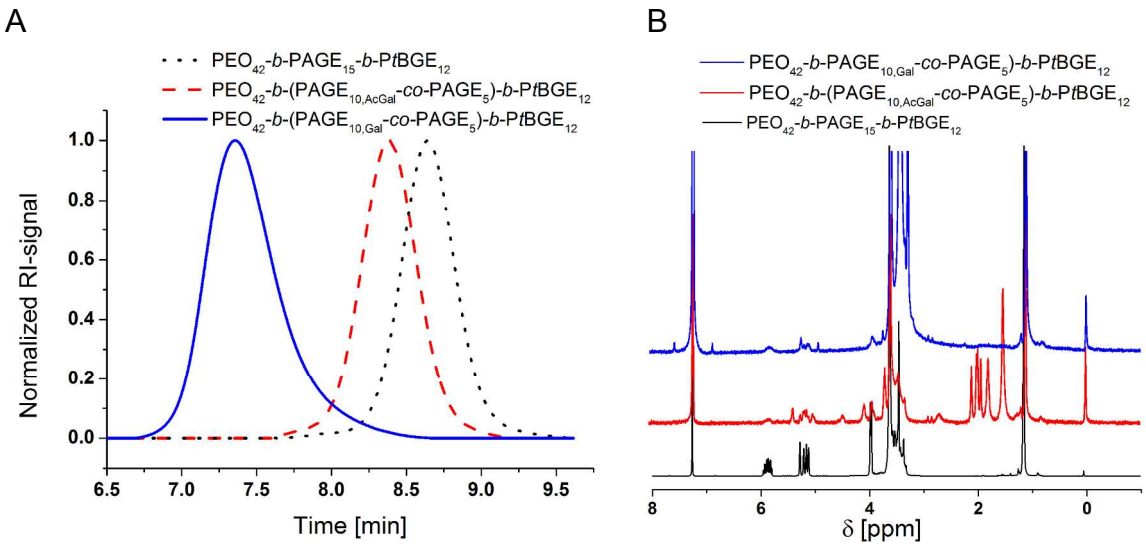

Figure S3: SEC traces (A) and ^{1}H NMR spectrum (B) of the PEO_{42}-*b*-$PAGE_{15}$-*b*-P*t*BGE_{12} precursor, the acetylated thiogalactose functionalized triblock terpolymer as well as the deprotected product.

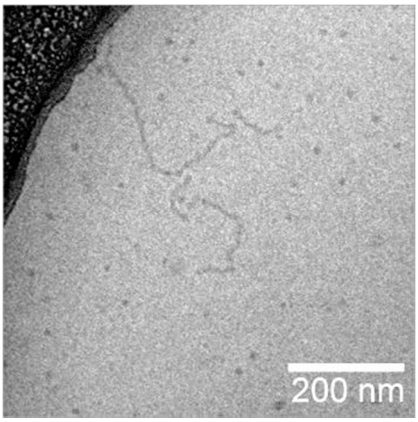

Figure S4: Cryo-TEM image of PEO_{42}-*b*-$PAGE_{15,COOH}$-*b*-P*t*BGE_{12} (ECT) as example displaying the minor distribution of worm-like structures.

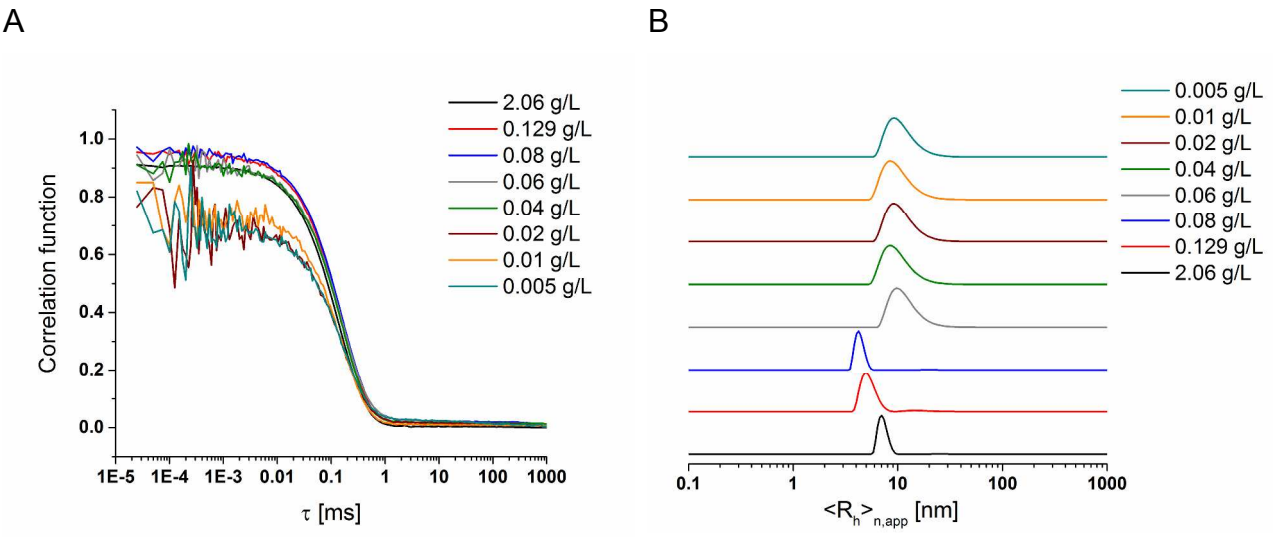

Figure S5: Correlation functions of the DLS measurements of the ECT sample at different concentrations (A) as well as the related number weighted CONTIN plots (B).

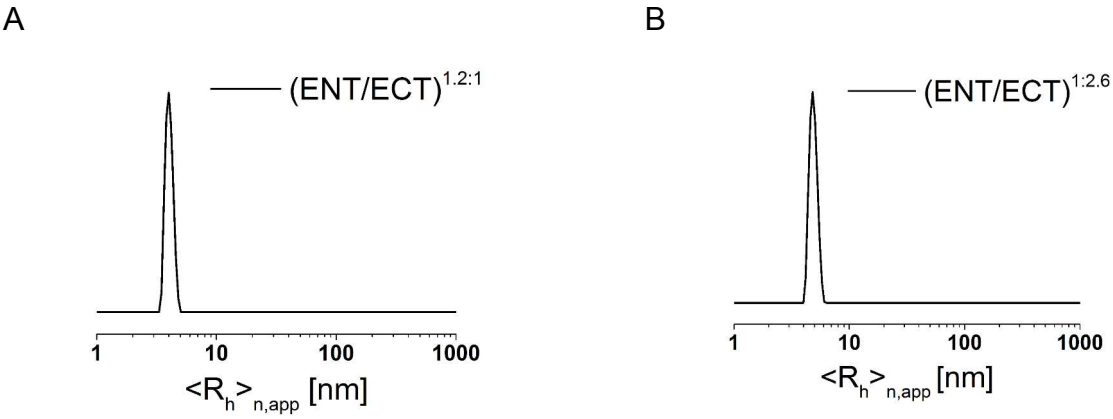

Figure S6: Number-weighted DLS CONTIN plots for the 1.2:1 (A) and 1:2.6 (B) mixture of PEO_{42}-*b*-($PAGE_{8,NH2}$-*co*-$PAGE_{7}$)-*b*-P*t*BGE_{12} / PEO_{42}-*b*-$PAGE_{15,COOH}$-*b*-P*t*BGE_{12} (ENT/ECT).

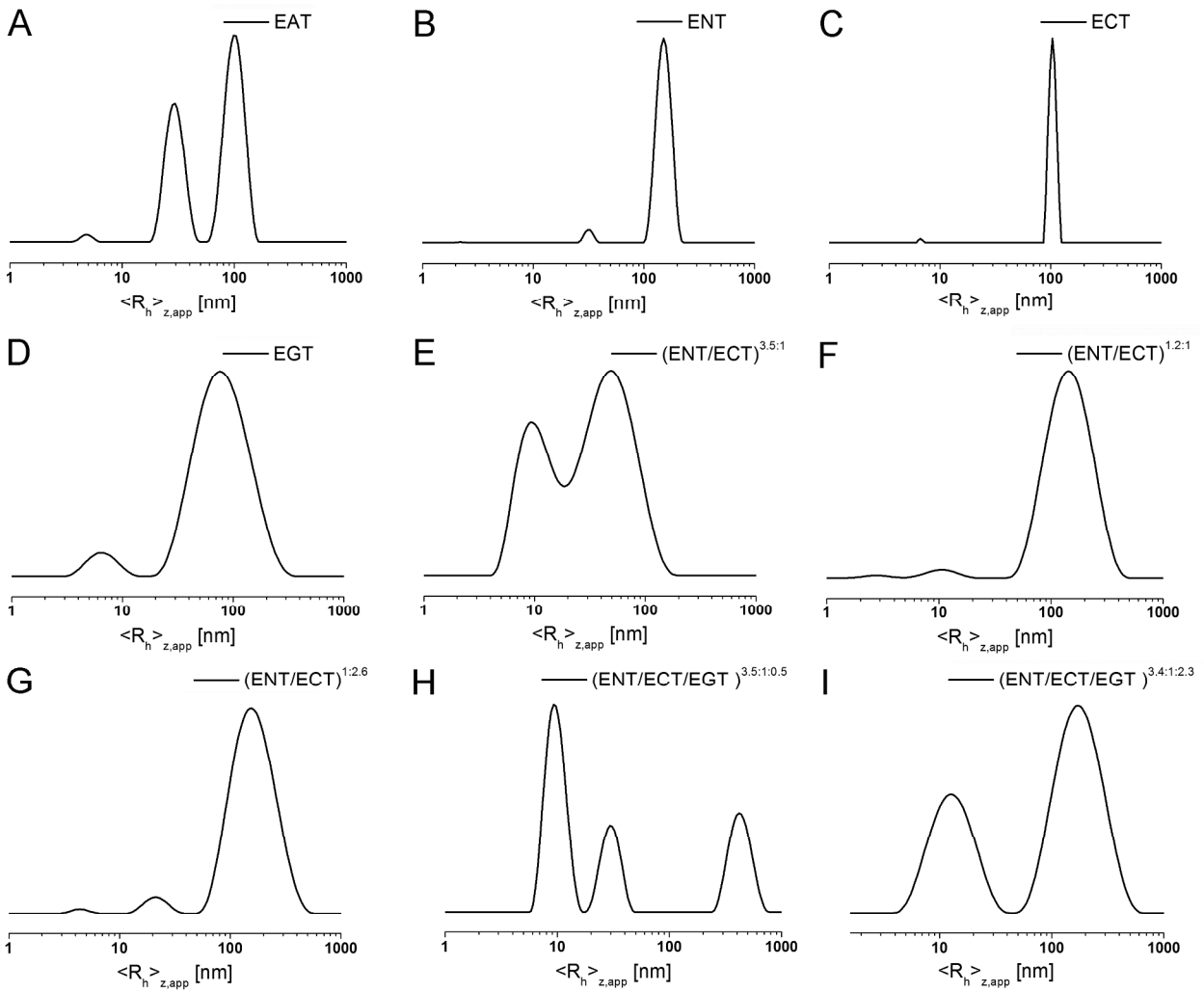

Figure S7: Intensity-weighted DLS CONTIN plots for PEO_{42}-*b*-$PAGE_{15}$-*b*-P*t*BGE_{12} (EAT, A), PEO_{42}-*b*-($PAGE_{8,NH2}$-*co*-$PAGE_7$)-*b*-P*t*BGE_{12} (ENT, B), PEO_{42}-*b*-$PAGE_{15,COOH}$-*b*-P*t*BGE_{12} (ECT, C), PEO_{42}-*b*-($PAGE_{10,Gal}$-*co*-$PAGE_5$)-*b*-P*t*BGE_{12} (EGT, D), PEO_{42}-*b*-($PAGE_{8,NH2}$-*co*-$PAGE_7$)-*b*-P*t*BGE_{12} / PEO_{42}-*b*-$PAGE_{15,COOH}$-*b*-P*t*BGE_{12} $((ENT/ECT)^{3.5:1}$, E), PEO_{42}-*b*-($PAGE_{8,NH2}$-*co*-$PAGE_7$)-*b*-P*t*BGE_{12} / PEO_{42}-*b*-$PAGE_{15,COOH}$-*b*-P*t*BGE_{12} $((ENT/ECT)^{1.2:1}$, F), PEO_{42}-*b*-($PAGE_{8,NH2}$-*co*-$PAGE_7$)-*b*-P*t*BGE_{12} / PEO_{42}-*b*-$PAGE_{15,COOH}$-*b*-P*t*BGE_{12} $((ENT/ECT)^{1:2.6}$, G), PEO_{42}-*b*-($PAGE_{8,NH2}$-*co*-$PAGE_7$)-*b*-P*t*BGE_{12} / PEO_{42}-*b*-$PAGE_{15,COOH}$-*b*-P*t*BGE_{12} / PEO_{42}-*b*-($PAGE_{10,Gal}$-*co*-$PAGE_5$)-*b*-P*t*BGE_{12} $((ENT/ECT/EGT)^{3.5:1:0.5}$, H) and PEO_{42}-*b*-($PAGE_{8,NH2}$-*co*-$PAGE_7$)-*b*-P*t*BGE_{12} / PEO_{42}-*b*-$PAGE_{15,COOH}$-*b*-P*t*BGE_{12} / PEO_{42}-*b*-($PAGE_{10,Gal}$-*co*-$PAGE_5$)-*b*-P*t*BGE_{12} $((ENT/ECT/EGT)^{3.4:1:2.3}$, I).

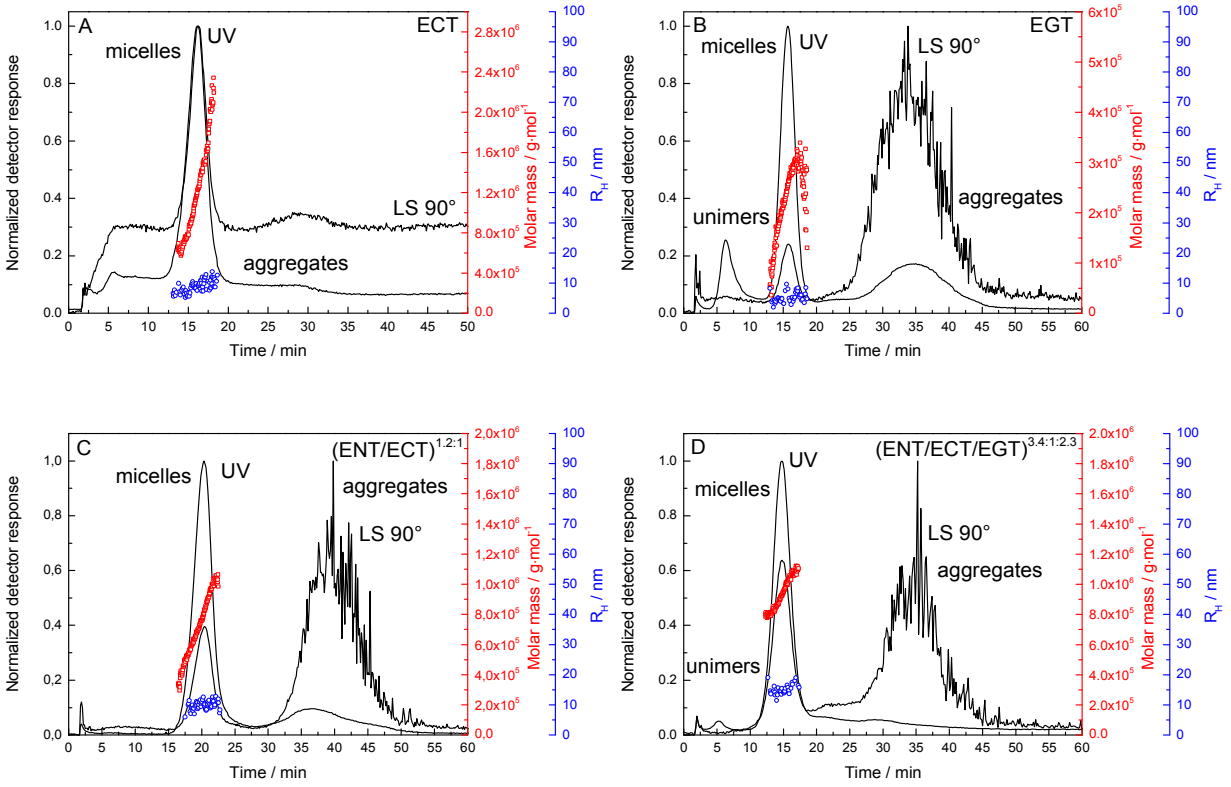

Figure S8: AF4 fractograms of self-assembled structures of PEO_{42}-*b*-$PAGE_{15,COOH}$-*b*-P*t*BGE_{12} (ECT, A), PEO_{42}-*b*-($PAGE_{10,Gal}$-*co*-$PAGE_5$)-*b*-P*t*BGE_{12} (EGT, B), PEO_{42}-*b*-($PAGE_{8,NH2}$-*co*-$PAGE_7$)-*b*-P*t*BGE_{12} / PEO_{42}-*b*-$PAGE_{15,COOH}$-*b*-P*t*BGE_{12} ($(ENT/ECT)^{1.2:1}$, C), PEO_{42}-*b*-($PAGE_{8,NH2}$-*co*-$PAGE_7$)-*b*-P*t*BGE_{12} / PEO_{42}-*b*-$PAGE_{15,COOH}$-*b*-P*t*BGE_{12} ($(ENT/ECT)^{1:2.6}$, D) and PEO_{42}-*b*-($PAGE_{8,NH2}$-*co*-$PAGE_7$)-*b*-P*t*BGE_{12} / PEO_{42}-*b*-$PAGE_{15,COOH}$-*b*-P*t*BGE_{12} / PEO_{42}-*b*-($PAGE_{10,Gal}$-*co*-$PAGE_5$)-*b*-P*t*BGE_{12} ($(ENT/ECT/EGT)^{3.4:1:2.3}$, C) in 20 mM NaCl.

Table S2: Experimental dn/dc values of the different polymer systems in 20 mM NaCl.

Sample	dn/dc (mL/g)	M_w (g/mol)	M_z (g/mol)	Đ
EAT	0.111±0.001	1.226E6±7,371	1.353E6±14,572	1.07±0.001
ENT	0.092±0.008	1.888E6±37,165	1.926E6±36,501	1.02±0.003
ECT	0.128±0.002	1.140E6±8,485	1.239E6±11,314	1.09±0.001
EGT	0.144±0.001	2.428E5±4,327	2.551E5±5,667	1.09±0.037
(ENT/ECT)3.5:1	0.116±0.001	1.213E6±36,638	1.230E6±36,638	1.01±0.001
(ENT/ECT)1.2:1	0.096±0.004	7.665E5±11,067	7.981E5±10,152	1.05±0.003
(ENT/ECT)1:2.6	0.114±0.001	6.386E5±2,113	6.569E5±2,223	1.03±0.004
(ENT/ECT/EGT)3.5:1:0.5	0.101±0.001	1.154E6±74,661	1.175E6±79,952	1.02±0.002
(ENT/ECT/EGT)3.4:1:2.3	0.113±0.002	9.743E5±48,431	9.820E5±46,701	1.01±0.001

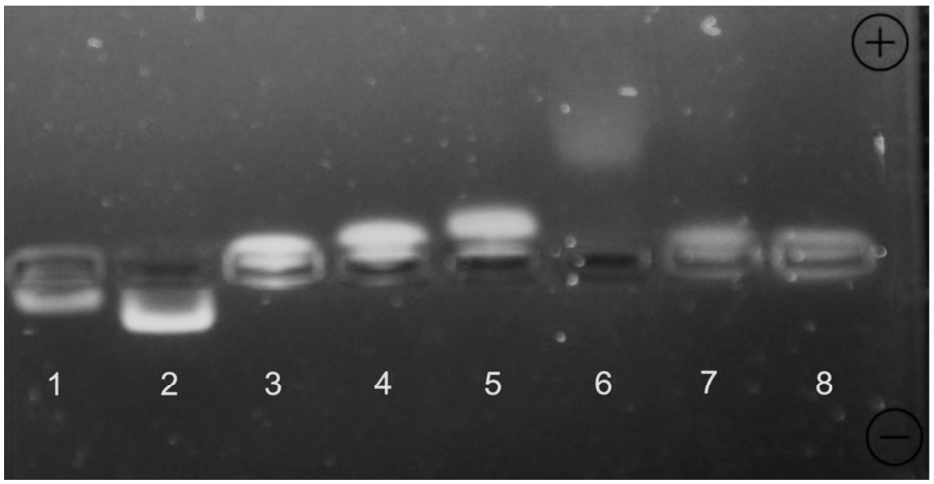

Figure S9: Gel-electrophoresis study of the as synthesized material EAT (1), ENT (2), mixtures of ENT and ECT in ratios of 3:1 (3), 1:1 (4), 1:3 (5), ECT (6), a mixture of ECT and EGT in a ratio of 1:1 (7) and EGT(8).

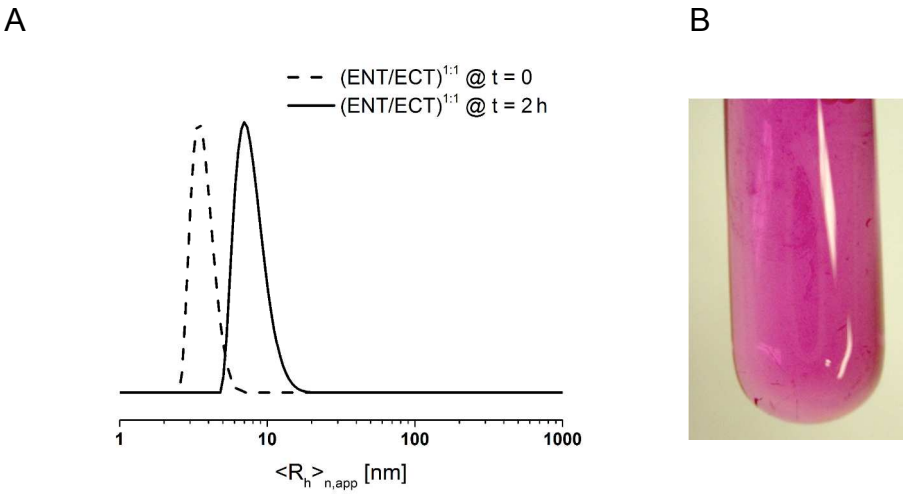

Figure S10: Number-weighted DLS CONTIN plots of a 1:1 mixture of PEO_{42}-*b*-($PAGE_{8,NH2}$-*co*-$PAGE_{7}$)-*b*-P*t*BGE_{12} (ENT) micelles with PEO_{42}-*b*-$PAGE_{15,COOH}$-*b*-P*t*BGE_{12} (ENT/ECT) directly after mixing and 2 h (ENT/ECT) (A) and a photograph of the solution after 12 h showing precipitated material (B).

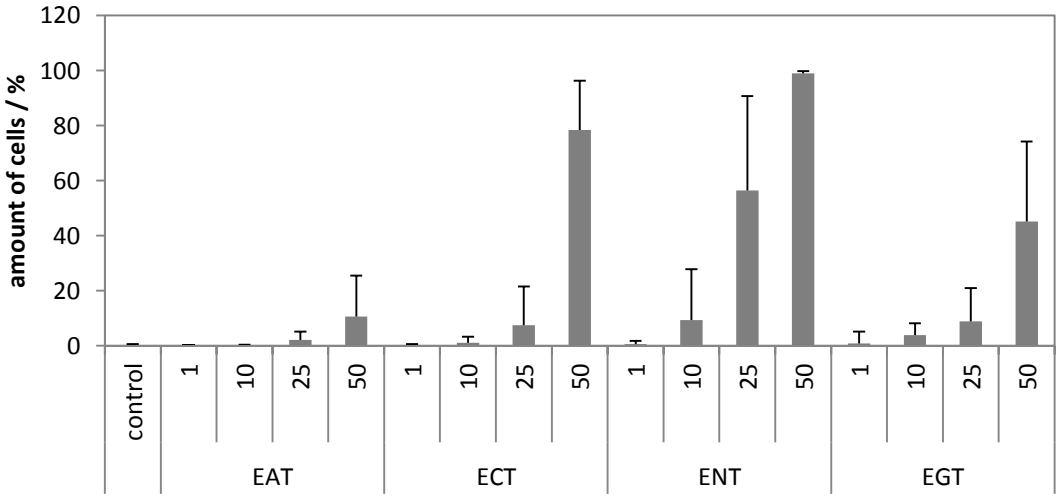

Figure S11: Internalization efficiency of triblock terpolymer micelles in HepG2 cells.

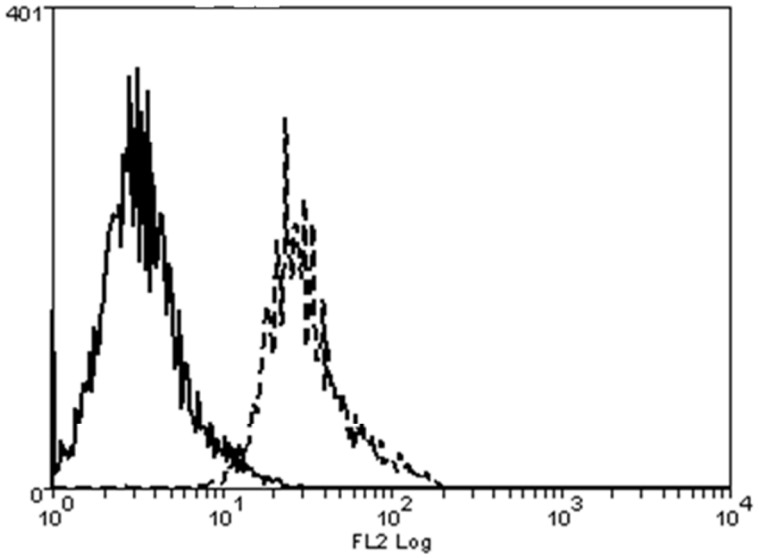

Figure S12: Flow cytometer histogram of control cells (continues line) and cell treated with $(ENT/ECT)^{3.5:1}$ micelles (dashed line).

Publication P7

RAFT made methacrylate copolymers for reversible pH-responsive nanoparticles

T. Yildrim, A. C. Rinkenauer, C. Weber, A. Traeger, S. Schubert, U. S. Schubert

J. Polym. Sci. Part A: Polym. Chem. **2015**, *53*, 2711-2721.

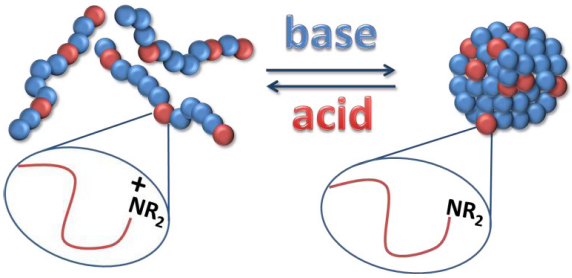

RAFT Made Methacrylate Copolymers for Reversible pH-Responsive Nanoparticles

Turgay Yildirim,[1,2] Alexandra C. Rinkenauer,[1,2] Christine Weber,[1,2] Anja Traeger,[1,2] Stephanie Schubert,[2,3] Ulrich S. Schubert[1,2]

[1]Laboratory of Organic and Macromolecular Chemistry (IOMC), Friedrich Schiller University Jena, Humboldtstr. 10, 07743 Jena, Germany
[2]Jena Center for Soft Matter (JCSM), Friedrich Schiller University Jena, Philosophenweg 7, 07743 Jena, Germany
[3]Institute of Pharmacy, Department of Pharmaceutical Technology, Friedrich Schiller University Jena, Otto-Schott-Str. 41, 07745 Jena, Germany
Correspondence to: U.S. Schubert; (E-mail: ulrich.schubert@uni-jena.de)

Received 1 May 2015; accepted 1 June 2015; published online 2 July 2015
DOI: 10.1002/pola.27734

ABSTRACT: In this study, we designed and investigated pH-responsive nanoparticles based on different ratios of monomers with primary, secondary or tertiary amino groups. For this purpose, copolymers of methyl methacrylate (MMA) with different compositions of amino methacrylates (2-(dimethylamino)ethyl methacrylate (DMAEMA), 2-(*tert*-butylamino)ethyl methacrylate (*t*BAEMA) and 2-aminoethyl methacrylate hydrochloride (AEMA·HCl)) were synthesized using the reversible addition-fragmentation chain transfer (RAFT) polymerization process. The controlled nature of the radical polymerization was demonstrated by kinetic studies. All copolymers show low dispersities ($Đ_M < 1.2$) with amino contents between 9 and 21 mol %. For the nanoparticle formation, nanoprecipitation with subsequent solvent evaporation was used. All suspensions were characterized by dynamic light scattering (DLS) and scanning electron microscopy (SEM). Different initial conditions of the formulations resulted in differently sized nanoparticles that have monomodal size distributions, relatively narrow polydispersity index (PDI) values and positive zeta potential values. The pH-stability test results demonstrated that, depending on the structure and amount of the amino content, the obtained nanoparticles reveal a reversible pH-response, such as dissolution at acidic pH values. The ability of the nanoparticles to encapsulate guest molecules was confirmed by pyrene fluorescence studies. The cytotoxicity assay results showed that the nanoparticles did not have any significant cytotoxic effect. © 2015 Wiley Periodicals, Inc. J. Polym. Sci., Part A: Polym. Chem. **2015**, *53*, 2711–2721

KEYWORDS: copolymerization; nanoparticles; nanoprecipitation; pH-responsive polymers; pH-responsive nanoparticles; polymerization kinetics; RAFT polymerization; self-assembly

INTRODUCTION Stimuli-responsive polymeric nanoparticles recently gained increasing attention due to their potential applications in numerous fields, in particular for pharmaceutical applications.[1–3] Depending on the chemical composition, such "smart" nanoparticles respond to external and/or internal stimuli by physicochemical changes driven by temperature,[4] light,[5] redox reaction,[6] ultrasound,[7] or pH value.[8] Among these, pH-responsive nanoparticles are regarded as highly promising vehicles for the selective delivery of pharmaceutical agents to the diseased tissues. Due to the fact that cancer cells have an abnormal acidic extracellular environment,[9] the pH-sensitivity of the matrix material can trigger the release of the encapsulated drugs. Several pH-responsive nanoparticle systems were reported to increase the efficacy of anticancer drugs in cancer therapy.[10–12] Moreover, a drug delivery vehicle with pH-responsive shedding would be useful for endosomal escape due to the acidification of the late endosome and lysosome.[13]

There are two main strategies to fabricate polymeric pH-responsive nanoparticle systems. The first category comprises the nanoparticles prepared from polymers that have pH-sensitive bonds, such as hydrazone or acetal bonds.[14,15] The second category involves the nanoparticle formation from polymers containing ionizable segments, such as amino and/or carboxyl groups.[16,17] Although there are several methodologies to prepare polymeric nanoparticles,[18] most of the pH-responsive structures in literature are based on the supramolecular self-assembly of copolymer micelles. However, the instability of the micelles below their critical micelle concentration represents a serious drawback.[19]

Additional Supporting Information may be found in the online version of this article.

Moreover, uniform size and morphology of the assembled structure is confined with block type copolymers that are harder to synthesize compared to statistical copolymers,[20] also in terms of upscaling.

In this study, a library of well-defined copolymers of methyl methacrylate (MMA) with three amino comonomers with ionizable segments (2-(dimethylamino)ethyl methacrylate (DMAEMA), 2-(*tert*-butylamino)ethyl methacrylate (*t*BAEMA) and 2-aminoethyl methacrylate hydrochloride (AEMA·HCl)) were synthesized via RAFT polymerization (Scheme 1) to obtain a novel pH-responsive drug delivery vehicle for the controlled release of loaded pharmaceutical agents in acidic environment.[21] MMA was used as main monomer in the copolymer chains due to the required hydrophobicity for the nanoparticle formation. DMAEMA, *t*BAEMA, and AEMA·HCl were used as comonomers since their polymers act as weak polybases with pKa values between 7.6 and 8.[22–24] All nanoparticles were prepared by means of nanoprecipitation[25,26] of the synthesized copolymers. To investigate a possible effect of the amino content on the pH-response of corresponding nanoparticles, the copolymer composition was varied by using different monomer feed ratios. Compared to the well-known pH-responsive systems, such as Eudragit E100,[27] the main advantage of our approach is the possibility to tune the nanoparticle's size, solubility, amino content and distribution of the amino moieties along the polymer chain, which could improve loading and release profiles of the pharmaceutical agents encapsulated.

EXPERIMENTAL SECTION

Materials

The monomers methyl methacrylate (MMA), 2-(*N,N*-dimethylamino)ethyl methacrylate (DMAEMA), 2-(*tert*-butylamino)ethyl methacrylate (*t*BAEMA) and 2-aminoethyl methacrylate hydrochloride (AEMA·HCl) were purchased from Sigma Aldrich and purified by stirring in the presence of inhibitor remover prior to use. 2,2′-Azobis(iso-butyronitrile) (AIBN) was purchased from Acros and recrystallized from methanol prior to use. 4-Cyano-4-(phenylcarbonothioylthio) pentanoic acid (CPADB), Amberlyst® A21, 1,3,5-trioxane, inhibitor remover and pyrene were purchased from Sigma Aldrich. AlamarBlue was obtained from Life Technologies. If not stated otherwise, cell culture materials, cell culture media, and solutions were obtained from PAA. All other chemicals were obtained from standard suppliers and used without purification unless specified.

Instruments and Methods

Proton nuclear magnetic resonance (^{1}H NMR) spectra were recorded at room temperature in $CDCl_3$ or CD_3OD on a Brucker Avance 300 MHz using the residual solvent resonance as an internal standard. The chemical shifts are given in ppm.

Gas chromatography (GC) measurements were performed on a Shimadzu GC-2010 instrument.

Size-exclusion chromatography (SEC) measurements were performed on two different setups: (SEC in $CHCl_3$) Shimadzu system equipped with a SCL-10A system controller, a LC-10AD pump, a RID-10A refractive index detector and a PSSSDV-linear S column (5 μm particle size; Polymer Standards Service GmbH, Mainz, Germany) at 40 °C using a chloroform, triethylamine and 2-propanol (94:4:2) mixture as eluent at a flow rate of 1 mL min^{-1}. The system was calibrated with PMMA standards ($M_p = 410$ to 88,000 g mol^{-1}); (SEC in DMAc) Agilent 1200 series equipped with a G1310A pump, a G1315D DA detector, a G1362A RI detector, and PSS GRAM 30 Å/1000 Å (10 μm particle size) columns in series at 40 °C using *N,N*-dimethylacetamide (DMAc) with 2.1 g L^{-1} LiCl as eluent at a flow rate of 1 mL min^{-1}. The system was calibrated with PMMA standards ($M_p = 505$ to 981,000 g mol^{-1}).

Chlorine analysis was carried out on a Titrator TLalpha 20 instrument.

Dynamic light scattering (DLS) was performed on a Zetasizer Nano ZS (Malvern Instruments, Herrenberg, Germany). After an equilibration time of 180 s, 3 × 30 runs were carried out at 25 °C ($\lambda = 633$ nm). The counts were detected at an angle of 173°. Each measurement was performed in triplicate. The mean particle size was approximated as the effective (Z-average) diameter and the width of the distribution as the polydispersity index of the particles (PDI) obtained by the cumulants method assuming a spherical shape.

Electrophoretic light scattering was used to measure the electrokinetic potential, also known as zeta potential. The measurements were performed on a Zetasizer Nano ZS (Malvern Instruments, Herrenberg, Germany) by applying laser Doppler velocimetry. For each measurement, 10 runs were carried out using the slow-field and fast-field reversal mode at 150 V. Each experiment was performed in triplicate at 25 °C.

For scanning electron microscopy (SEM), 5 μL of the suspensions were placed on a mica surface and dried overnight at room temperature under atmospheric pressure. Afterwards, images were taken using a Gemini 1530 type LEO field emission scanning electron microscope (Carl-Zeiss AG, Germany). The samples were coated with a thin layer (4 nm) of platinum via sputter coating using a Bal-TEC 020 HR Sputtering Coater.

For the cytotoxicity tests a Tecan Infinite 200 Pro fluorescence microplate reader (Crailsheim, Germany) was used.

The fluorescence spectra of pyrene solutions were recorded on a Jasco FP-6500 fluorometer applying an excitation wavelength of 335 nm. The emission spectra were recorded from 350 to 600 nm. The excitation and emission bandwidths were 3.0 and 3.0 nm, respectively. For the pH-response test of the nanoparticles a BioShake instrument (Analytik Jena AG, Germany) was used.

Synthesis

RAFT Polymerization

MMA was copolymerized with three different amino methacrylates (DMAEMA, *t*BAEMA and AEMA·HCl) using CPADB as chain transfer agent (CTA) and AIBN as initiator. The initial

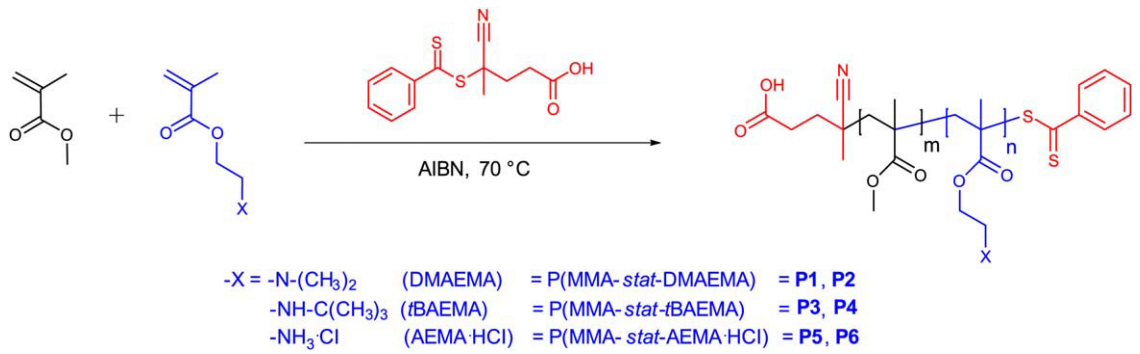

SCHEME 1 Schematic representation of the RAFT copolymerization of MMA with amino-functionalized methacrylates. [Color figure can be viewed in the online issue, which is available at wileyonlinelibrary.com.]

monomer feed ratios of the monomers were varied whereas the overall monomer to CTA ratio was kept constant at 100. All polymerizations were carried out at 70 °C in an oil bath. The copolymerizations with DMAEMA and *t*BAEMA (**P1–P4**) were performed in a 2 M ethanolic solution. Methanol was used as solvent for the copolymerizations with AEMA·HCl (**P5–P6**). The polymerization conditions are summarized in Table 1. An exemplary RAFT copolymerization procedure (Table 1, **P1**) is as follows: 30 g MMA (0.300 mol), 5.234 g DMAEMA (0.033 mol), 930 mg CPADB (3.329 mmol), and 137 mg AIBN (0.832 mmol) were dissolved in ethanol in a 250 mL two-necked round-bottom flask equipped with a magnetic stir bar. The total volume of the reaction mixture was 166 mL. After degassing for 4 h by argon purging, the t_0 sample for GC was taken and the flask was immersed in a preheated oil bath under stirring at 70 °C. After 10 h, the polymerization was stopped by cooling to room temperature and exposing to air. Monomer conversions were determined via GC by using the reaction solvent (ethanol) as internal standard. The polymer was purified by precipitating in cold hexane (approximately six times). The resulting pink colored polymer was dried under high vacuum at room temperature until constant weight to produce an overall yield of 40%. The number average molar mass (M_n) and molar mass dispersities were determined by two different SEC systems by using PMMA standards. SEC in $CHCl_3$: $M_n = 6100$ g mol^{-1} and $Đ_M = 1.16$. SEC in DMAc: $M_n = 6300$ g mol^{-1} and $Đ_M = 1.13$. ^{1}H NMR ($CDCl_3$, 300 MHz): $\delta = 7.87$, 7.52 and 7.36 (Ar-H, CPADB), 4.13 (—$OCH_2CH_2NH(CH_3)_2$), 3.60 (—OCH_3), 2.64 (—$OCH_2CH_2NH(CH_3)_2$), 2.4–0.7 (backbone) ppm.

The degree of polymerization (DP) for each polymer was calculated from the signal integrals in the ^{1}H NMR spectrum of the purified copolymer using the following equations:

$$\mathrm{DP_{MMA}} = \frac{I(\text{peak } a)/3}{I(\text{peak } c)/2} \quad (1)$$

$$\mathrm{DP_{DMAEMA}} = \frac{I(\text{peak } b)/2}{I(\text{peak } c)/2}, \quad (2)$$

with I(a) corresponding to the integral of methyl proton peaks of the MMA at 3.60 ppm, *I(b)* corresponding to the integral of methylene proton peaks of the DMAEMA at 4.13 ppm, and I(c) corresponding to the integral of two aromatic protons of the dithiobenzoate end group at 7.87 ppm. Molar mass values were calculated by using the following equation:

$$M_{n,NMR} = (\mathrm{DP_{MMA}} \times M_{MMA}) + (\mathrm{DP_{DMAEMA}} \times M_{DMAEMA}) + M_{CTA}, \quad (3)$$

in which the molar mass of the MMA, DMAEMA and RAFT agent are 100.12, 157.21, and 279.38 g mol^{-1}, respectively.

Kinetic Study of the Polymerizations

During each polymerization, aliquots of 0.2 mL were taken periodically from the reaction mixture by a syringe purged with argon. From each sample, conversions were calculated via GC (**P1-P4**) or ^{1}H NMR (**P5-P6**) by using the reaction solvents (**P1-P4**) or 1,3,5-trioxane (**P5-P6**) as internal standards. Molar masses and dispersities were determined via SEC analysis ($CHCl_3$, RI detection).

TABLE 1 RAFT Copolymerization Conditions of MMA (**M1**) and Corresponding Amino-Functionalized Methacrylates (**M2**)[a]

Entry	**M2**	**M1**/**M2**/CTA/AIBN	Solvent	Polymerization Time [h]
P1	DMAEMA	90/10/1/0.25	Ethanol	10
P2	DMAEMA	80/20/1/0.25	Ethanol	10
P3	*t*BAEMA	95/5/1/0.25	Ethanol	13
P4	*t*BAEMA	85/15/1/0.25	Ethanol	10
P5[b]	AEMA·HCl	90/10/1/0.25	Methanol	9
P6[b]	AEMA·HCl	80/20/1/0.25	Methanol	10

[a] All polymerizations were carried out at total monomer concentrations of 2 mol L^{-1}.

[b] Polymerization was carried out under reflux.

Deprotonation of the Polymers

Ion exchange resin Amberlyst A21® was used to deprotonate **P5** and **P6**. For a typical deprotonation reaction, **P5** was dissolved in methanol, mixed with Amberlyst® A21 and stirred for 1 h at room temperature. Subsequently, the corresponding polymer **P7** was obtained by filtration, precipitation into ice-cold hexane and by removal of the volatiles under reduced pressure at room temperature. ^{1}H NMR ($CDCl_3$, 300 MHz): $\delta = 7.87$, 7.52, and 7.36 (Ar-H, CPADB), 4.00 (—$OCH_2CH_2NH_2$), 3.60 (—OCH_3), 2.97 (—$OCH_2CH_2NH_2$), 2.5–0.7 (backbone) ppm. SEC in $CHCl_3$: $M_n = 5300$ g mol^{-1} and $Đ_M = 1.15$, SEC in DMAc: $M_n = 9000$ g mol^{-1} and $Đ_M = 1.10$. Elemental anal. found: C 58.31%, H 8%, N 1.73%, S 0.85%, Cl 1.01%.

Preparation of the Nanoparticle Suspensions

For nanoprecipitation, the corresponding polymers (**P1**, **P2**, **P3**, **P4**, **P7,** and **P8**) were dissolved in acetone at a concentration of 1 or 10 mg mL^{-1}, respectively, and subsequently added dropwise to deionized water under continuous stirring at 500 rpm (acetone to water, AW method). For the water to acetone (WA) method, deionized water was added drop-wise to the acetone polymer solution under stirring at 500 rpm. The acetone/water (solvent/nonsolvent) ratio was kept constant at 0.5 for all suspensions. After removal of the acetone by stirring overnight at room temperature (GC analysis ensured complete removal of acetone), all suspensions were diluted to the final volume of 10 mL. The nanoparticles were characterized by DLS (performed in pure water) and SEM without filtration.

pH-Response Test of the Nanoparticles

For the pH stability test of the nanoparticles ($c = 0.3$ mg mL^{-1}), 0.0667 M acetate buffer (pH values 3.4, 4, 5, 6) and 0.0667 M tris buffer (pH values 7, 8, 9) were used. 500 μL of nanoparticle suspensions were mixed with 500 μL of buffer solutions in Eppendorf tubes and stored at 37 °C while mixing at 200 rpm in a BioShake instrument. After 24 h, DLS and zeta potential measurements were performed (particle concentration of 0.15 mg mL^{-1} in all corresponding buffer systems).

Fluorescence Spectroscopic Study of the Nanoparticles

1 mL stock solution of pyrene (6×10^{-5} mol L^{-1}) in acetone was added to 1 mL nanoparticle suspensions (0.15 mg mL^{-1} polymer concentrations) at various pH values. The samples were incubated at 37 °C for 24 h to remove acetone and to give a final pyrene concentration of 3×10^{-5} mol L^{-1}.

Cell Lines, Culture Conditions, and Cytotoxicity Test of Nanoparticles

The L929 (CCL-1, ATCC) cell lines used in the cytotoxicity experiments were maintained in DMEM culture media supplemented with 10% fetal calf serum (FCS), 100 μg mL^{-1} streptomycin and 100 IU mL^{-1} penicilin. The cells were cultured at 37 °C in humidified 5% CO_2 atmosphere. The cytotoxicity was tested with L929 cells, as this sensitive cell line is recommended by ISO10993-5 ($n = 6$). In detail, cells were seeded at 10 cells per well in a 96-well plate and incubated for 24 h. No cells were seeded in the outer wells. Afterwards, the media were replaced by fresh media and incubated for 30 min. The nanoparticle suspensions were added in the end concentration range from 10 to 1000 μg mL^{-1}, and the cells were incubated at 37 °C for further 24 h. Subsequently, the medium was replaced by fresh media and AlamarBlue as recommended by the supplier. After incubation for 4 h, the fluorescence was measured at Ex 570/Em 610 nm, with untreated cells on the same well plate serving as controls.

RESULTS AND DISCUSSION

A series of amino-functionalized PMMA based copolymers was synthesized via RAFT polymerization due to its versatility and suitability for the synthesis of well-defined amino methacrylate copolymers.[28,29] Three different commercially available amino methacrylates that have tertiary (DMAEMA), secondary (*t*BAEMA) and protonated primary amine functionalities (AEMA·HCl) were used as comonomers. The utilized CTA CPADB has previously been successfully applied to mediate the RAFT polymerization of amino methacrylates.[29,30] [M]/[CTA] was kept constant at a ratio of 100/1 with a monomer concentration of 2 mol L^{-1} in order to obtain relatively low molar mass polymers, considering the increased toxicity of high molar mass polycations.[31] Depending on previous research in our group, the [CTA]/[AIBN] ratio was kept at 1/0.25 regarding polymerization rate and control over the molar mass.[32] All polymerizations were carried out in ethanol at 70 °C, except for **P5**-**P6**, where methanol under reflux was used as solvent because of the poor solubility of AEMA·HCl in ethanol. The primary amine containing monomer AEMA can easily rearrange to its thermodynamically more stable isomer 2-hydroxyethyl methacrylamide, and the dithiobenzoate moiety of the CTA is prone to an aminolysis reaction if the free amine monomer is used.[24] Thus, the hydrochloride salt of the monomer AEMA was used for the polymerization. Two different initial monomer feed ratios were applied for each copolymerization to vary the amino content in the copolymers. The amino methacrylate content in the copolymers was kept low (in between 9 and 21) due to the required hydrophobicity of the copolymers for the capability to form nanoparticles via nanoprecipitation.

Kinetic Studies

The distribution of the amine functionality among the PMMA chain might be an important parameter that could affect the particle formation or structure. To obtain information about the sequence arrangements of the monomers in the PMMA based copolymer chains, kinetic studies were performed for each copolymerization. The obtained data from the kinetic studies of the RAFT copolymerizations of MMA with 10 mol% comonomer (DMAEMA, *t*BAEMA and AEMA·HCl, respectively) are displayed in Figure 1. The corresponding data derived from the kinetic studies with 20 mol% comonomer content are given in the supporting information (Supporting

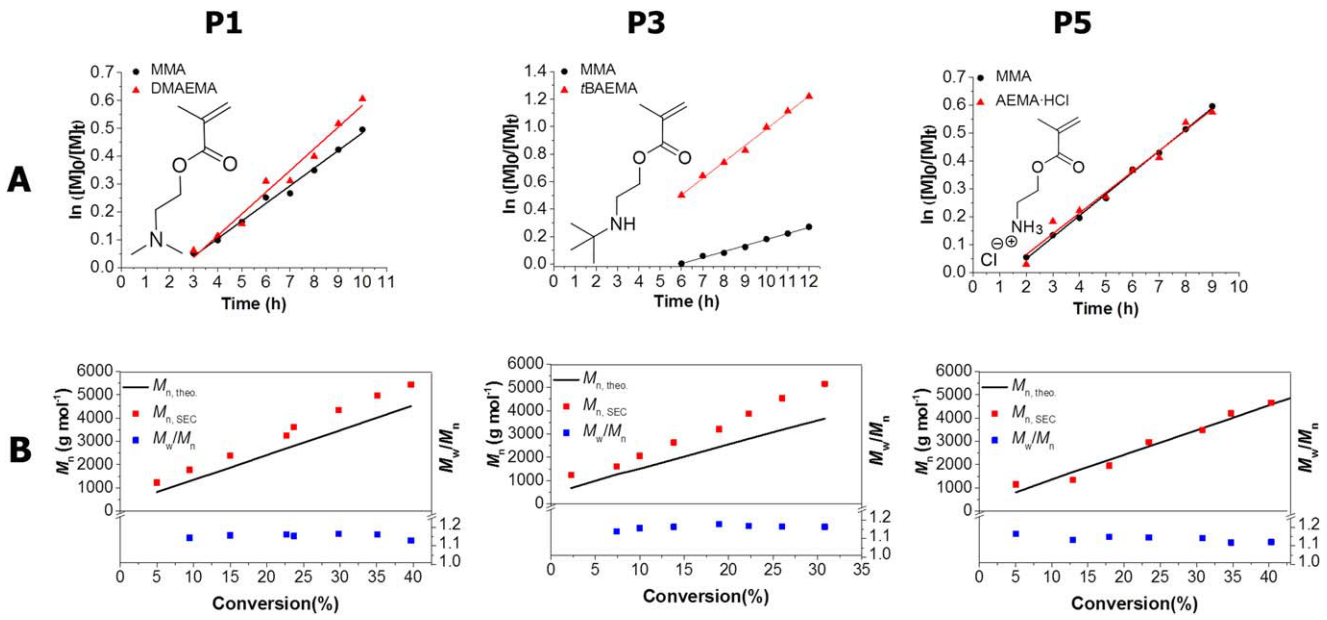

FIGURE 1 Kinetic studies of the RAFT copolymerization of MMA with 10 mol% comonomer DMAEMA (**P1**), *t*BAEMA (**P3**) and AEMA·HCl (**P5**). [M]/[CPADB]/[AIBN] = 100/1/0.25; $[M]_0 = 2$ mol L^{-1}. Polymerization conditions for (**P1** and **P3**): Solvent ethanol, $T = 70$ °C. Polymerization conditions for **P5**: Solvent methanol under reflux. (A) Semilogarithmic kinetic plots. (B) M_n and M_w/M_n evolution with total monomer conversion. [Color figure can be viewed in the online issue, which is available at wileyonlinelibrary.com.]

Information Fig. S2). Analysis of the kinetic samples by means of SEC in $CHCl_3$ revealed monomodal molar mass distributions that shift to lower elution volumes throughout the course of the polymerization (Supporting Information Fig. S1). The molar mass M_n was found to increase linearly with respect to the total monomer conversion (**B**, Fig. 1). These results indicate the controlled nature of the RAFT polymerization.

The semilogarithmic kinetic plots are linear (**A**, Fig. 1) for both monomers in each copolymerization, indicating a pseudo first order polymerization behaviour. At the beginning of the DMAEMA and AEMA·HCl polymerizations, induction periods of around 2 h were observed for each monomer, which is often reported for RAFT polymerizations.[33–36] However, for *t*BAEMA copolymerizations an increase in the induction period of the MMA was observed. This is due to the selective addition of the *t*BAEMA to the growing polymer chains at the beginning of the polymerizations.

The slopes of MMA and DMAEMA in the semilogarithmic plot, which are directly proportional to the polymerization rates of MMA and DMAEMA, respectively, are close to each other, which indicates that both monomers are consumed at close rates. In accordance to the results of the kinetic studies, the ratio of the monomers in the isolated copolymers is similar to the initial monomer feed ratio. These results are also in a good agreement with the reported reactivity ratios of MMA and DMAEMA for the RAFT and free radical copolymerizations ($r_{MMA} \sim 0.8$, $r_{DMAEMA} \sim 0.9$).[37,38] Therefore, it can be concluded that MMA and DMAEMA arrange in the polymer chain in a random sequence.

In contrast, the increased slope of the *t*BAEMA in the semilogarthmic plot reveals that *t*BAEMA is consumed faster than MMA. Indeed, the compositions in the isolated polymers deviated significantly from the initial monomer feed ratios in favor of *t*BAEMA at moderate monomer conversions. The reported relative reactivity ratios of MMA ($r_{MMA} \sim 0.7$) and *t*BAEMA ($r_{tBAEMA} \sim 1.4$)[39] for the free radical copolymerization are in a good agreement with these results. Thus, it can be concluded that the copolymers of MMA and *t*BAEMA display a gradient composition.[40,41]

To the best of our knowledge there are no relative reactivity ratios reported for the copolymerization of MMA and AEMA·HCl. However, almost identical slopes of MMA and AEMA·HCl in the semilogarithmic plot hint towards a random arrangement of the monomers along the polymer chain for both 10 as well as 20 mol% AEMA·HCl.

The kinetic plots for the copolymerizations of same monomers with different initial monomer feed ratios revealed similar results (Supporting Information Fig. S2).

Copolymer Synthesis and Characterization

Based on the results obtained from preliminary kinetic studies, the final copolymers were synthesized under similar conditions with a total M/CTA of 100 aiming at 10 as well as 20% amino content for each monomer. All polymerizations were stopped at moderate monomer conversions to exclude undesired coupling reactions that could take place at higher monomer conversions. Each purified polymer was characterized by ^{1}H NMR spectroscopy and SEC measurements on two systems (Table 2).

TABLE 2 Selected Characterization Data of the MMA (**M1**) Copolymers with Corresponding Amino Methacrylates (**M2**)

Entry	M2	f(M1/M2)[a]	F(M1/M2)[b,c]	Conv. (%) M1 M2	$M_{n,\,theo.}$[d] (g mol^{-1})	DP[c] M1 M2	M_n[c] (g mol^{-1})	M_n[e] (g mol^{-1})	$Đ_M$[e]	M_n[f] (g mol^{-1})	$Đ_M$[f]
P1	DMAEMA	9	7.4	39[g] 45[g]	4,500	41 5.5	5,200	6,100	1.16	6,300	1.13
P2	DMAEMA	4	4	42[g] 50[g]	5,200	40 10	5,900	7,600	1.17	7,800	1.15
P3	*t*BAEMA	19	9.5	29[g] 70[g]	3,700	35 3.7	4,500	5,200	1.19	7,100	1.17
P4	*t*BAEMA	5.7	3.8	36[g] 72[g]	5,300	35 9.2	5,500	7,900	1.15	11,900	1.16
P5	AEMA·HCl	9	9.1	45[c] 44[c]	5,000	42 4.6	5,200	5,100	1.13	9,200	1.15
P6	AEMA·HCl	4	3.7	48[c] 52[c]	5,900	30 8.2	4,600	4,500	1.19	11,000	1.15
P7[h]	AEMA		9			45 5	5,200	5,300	1.18	9,000	1.10
P8[i]	AEMA		3.6			35 9.8	5,000	4,800	1.18	10,000	1.15

[a] Initial monomer feed ratio.
[b] Monomer ratio in the isolated copolymer.
[c] Determined by ^{1}H NMR spectroscopy.
[d] Determined by the formula $M_{n,theo.} = [([M]_{M1}/[CTA] \times Conv. \times M_{M1}) + ([M]_{M2}/[CTA] \times Conv. \times M_{M2}) + (M_{CTA})]$.
[e] Determined by SEC in $CHCl_3$ analysis (RI detection, PMMA calibration).
[f] Determined by SEC in DMAc analysis (RI detection, PMMA calibration).
[g] Determined by GC.
[h] Deprotonated form of **P5**.
[i] Deprotonated form of **P6**.

The compositions of the isolated copolymers (F(M1/M2), Table 2) were calculated from the ^{1}H NMR spectra by using the integrals of appropriate signals derived from both comonomers (methyl proton signal "a" for MMA and methylene proton signal "b" for the amino monomers in Fig. 2, see the experimental section for details). Although DMAEMA and AEMA·HCl copolymers had close initial monomer feed ratios and monomer compositions in the polymers, *t*BAEMA copolymers revealed a composition drift. These results are in accordance with the kinetic studies of the corresponding monomers described above. However, by adjustment of the corresponding monomer feed ratios it was possible to obtain two sets of polymers that contained 10 and 20 mol% of amine comonomer, respectively. All ^{1}H NMR spectra clearly indicate the presence of the dithiobenzoate end-groups derived from the CTA (signals of the aromatic protons at 7.3–7.9 ppm) enabling an estimation of the DP for MMA and for each amino methacrylate. The according number average molar mass (M_n) values calculated by ^{1}H NMR are in good agreement with the theoretical values that were calculated from the [monomer] to [CTA] ratio and the monomer conversions. It should be noted that the ^{1}H NMR spectrum of **P6** was measured in methanol due to the insufficient solubility of **P6** in $CDCl_3$.

The isolated copolymers were analysed using two different SEC systems, which both revealed monomodal traces for all polymers with low dispersity values ($Đ_M < 1.2$) (Fig. 3, Supporting Information Fig. S3, Table 2). In general, higher M_n values were obtained from both SEC systems using PMMA calibration compared to the M_n values calculated from the ^{1}H NMR spectra. This is attributed to the difference in hydrodynamic volumes of the polymers in both eluents that

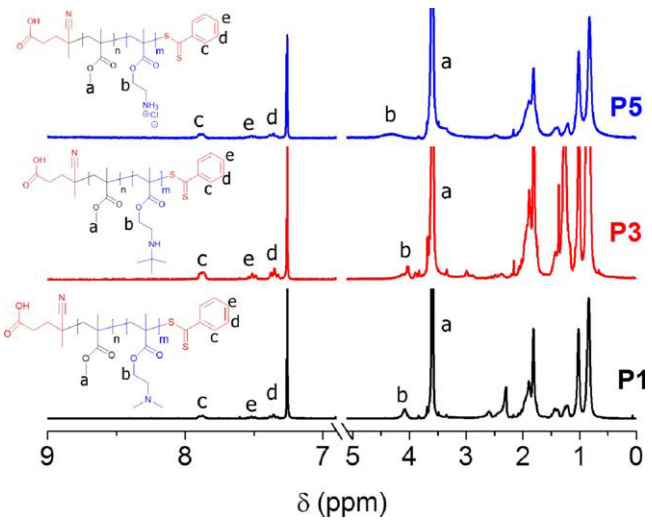

FIGURE 2 ^{1}H NMR spectra (300 MHz, $CDCl_3$) of **P1**, **P3,** and **P5** and the assignment of the peaks used to calculate the DP. [Color figure can be viewed in the online issue, which is available at wileyonlinelibrary.com.]

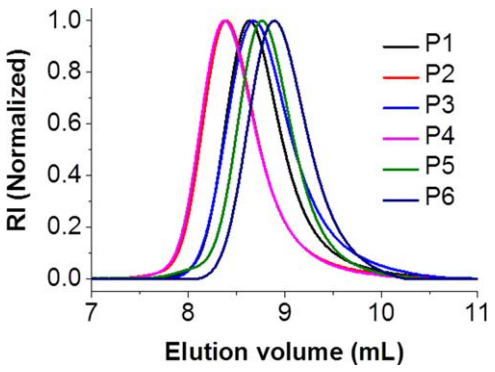

FIGURE 3 Normalized SEC traces in $CHCl_3$ (RI detection, eluent: $CHCl_3$) of isolated copolymers of **P1**-**P6**. [Color figure can be viewed in the online issue, which is available at wileyonlinelibrary.com.]

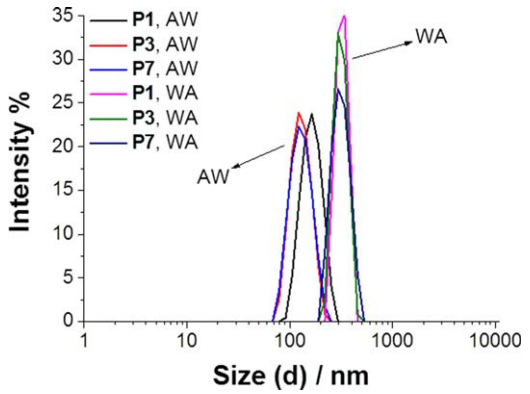

FIGURE 4 Intensity size distributions of nanoparticles in water (**P1**, **P3,** and **P7**) with the initial acetone-polymer concentration of 1 mg mL^{-1}, prepared by dropping acetone-polymer solution to water (AW) or dropping water to acetone-polymer solution (WA). [Color figure can be viewed in the online issue, which is available at wileyonlinelibrary.com.]

are used in these SEC systems compared to PMMA homopolymers. In particular the polar eluent of the SEC in DMAc apparently results in an increased hydrodynamic volume of the amine-containing polymers, which directly leads to an increased apparent molar mass.

Finally the charged copolymers that contain AEMA·HCl (**P5**-**P6**) were treated with Amberlyst® A21 to obtain the desired primary amino-functionalized copolymers (**P7**-**P8**). Elemental analysis results demonstrated a significant decrease in the chlorine content after the deprotonation reactions (Supporting Information Table S1). Both SEC systems revealed no change after the deprotonation reactions (Supporting Information Figs. S4–S7), which ensures the absence of disulfide bond formation, which could possibly occur subsequent to an end group cleavage of the polymers with Amberlyst® A21. It should also be noted that the ^{1}H NMR spectrum of **P8** (Supporting Information Fig. S15) was measured in $CDCl_3$ instead of MeOD since the polymer solubility after deprotonation changed dramatically, indicating the decreased polarity of the deprotonated polymer.

Preparation of Nanoparticle Suspensions

Polymeric nanoparticles were prepared from the synthesized tertiary (**P1**, **P2**), secondary (**P3**, **P4**) and primary (**P7**, **P8**) amino-functional MMA based copolymers by means of nanoprecipitation with subsequent solvent evaporation without any need of stabilizers/surfactants. The acetone/water ratio was kept at 0.5 for all suspensions. In order to obtain differently sized nanoparticles, two different initial acetone-polymer solution concentrations (1 mg mL^{-1}, 10 mg mL^{-1}) and two different dropping methods (dropping acetone polymer solution to water (AW) and dropping water to acetone polymer solution (WA)) were applied for each polymer. In general, smaller nanoparticles were obtained with dropping acetone polymer solution to water (AW) than dropping water to acetone polymer solution (WA) (Fig. 4), which is commonly observed for the nanoprecipitation method.[42] For the initial acetone-polymer solution concentration of 1 mg mL^{-1}, nanoparticles with monomodal size distributions (Fig. 4) and low polydispersity (PDI) values (Table 3) were obtained from all polymers.

However, with the initial acetone-polymer concentration of 10 mg mL^{-1}, nanoparticles with monomodal size distributions could only be obtained from the copolymers that contained DMAEMA and AEMA (**P1**, **P2**, **P7,** and **P8**), which both have a random comonomer distribution. In contrast, the gradient copolymers of *t*BAEMA (**P3**-**P4**) yielded nanoparticles and undefined aggregates which result in multimodal size distributions and high PDI values. This might be due to the tightly spaced amino groups along the polymer chain,

TABLE 3 Characterization Results of the Prepared Nanoparticles

		Z-average[b] [d, nm]		PDI[b]		Zeta potential[c] [mV]	
Polymer	Method[a]	$c = 1$ g L^{-1}	$c = 10$ g L^{-1}	$c = 1$ g L^{-1}	$c = 10$ g L^{-1}	$c = 1$ g L^{-1}	$c = 10$ g L^{-1}
P1	AW	152 ± 2	123 ± 1	0.16 ± 0.02	0.12 ± 0.01	+35 ± 4.4	+37 ± 0.3
	WA	340 ± 3	720 ± 18	0.11 ± 0.03	0.07 ± 0.05	+25 ± 4.3	+48 ± 1.1
P2	AW	184 ± 2	131 ± 2	0.16 ± 0.01	0.11 ± 0.04	+52 ± 0.4	+31 ± 0.7
	WA	473 ± 3	636 ± 4	0.18 ± 0.04	0.07 ± 0.05	+47 ± 0.4	+51 ± 0.7
P3	AW	126 ± 1	200 ± 1[d]	0.12 ± 0.02	0.19 ± 0.03[d]	+44 ± 3.3	+ 56 ± 9[d]
	WA	314 ± 3	1079 ± 28[d]	0.14 ± 0.04	0.26 ± 0.12[d]	+29 ± 0.4	+ 40 ± 3[d]
P4	AW	169 ± 2	158 ± 1[d]	0.15 ± 0.01	0.15 ± 0.03[d]	+36 ± 6.4	+ 41 ± 3[d]
	WA	331 ± 3	610 ± 12[d]	0.09 ± 0.05	0.14 ± 0.01[d]	+20 ± 2.1	+ 26 ± 2[d]
P7	AW	121 ± 1	110 ± 1	0.17 ± 0.01	0.14 ± 0.02	+56 ± 3.2	+59 ± 0.6
	WA	306 ± 2	339 ± 2	0.11 ± 0.02	0.10 ± 0.03	+61 ± 0.5	+64 ± 1.0
P8	AW	133 ± 1	182 ± 1	0.14 ± 0.02	0.08 ± 0.04	+54 ± 2.1	+59 ± 0.8
	WA	254 ± 3	582 ± 13	0.07 ± 0.05	0.17 ± 0.02	+53 ± 3.7	+61 ± 0.6

[a] AW, dropping acetone to water; WA, dropping water to acetone.
[b] Average values of three DLS measurements.
[c] Average values of three zeta potential measurements.
[d] Nanoprecipitation with acetate buffer (pH = 5) as nonsolvent.

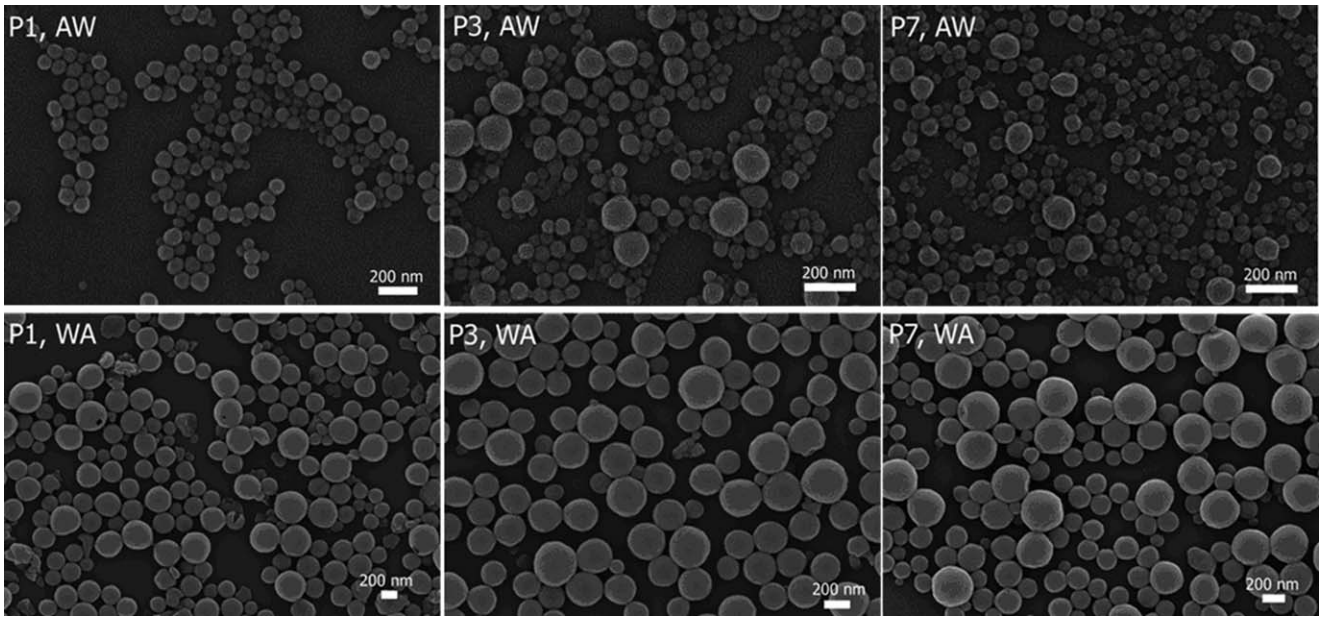

FIGURE 5 SEM images of nanoparticles that were prepared from **P1**, **P3,** and **P7** (1 mg mL^{-1}) by dropping acetone-polymer solution to water (AW) or dropping water to acetone-polymer solution (WA).

which result in strong intrachain electrostatic repulsion causing retardation of the protonation of the amino groups.[43] This would result in lower pKa values of gradient *t*BAEMA copolymers, although all used amino methacrylate monomers have similar pKa values[22–24] and prevent the nanoparticles from acquiring an appreciable cationic character at neutral pH values. Thus, favored van der Waals attraction results in particle aggregation. To support this assumption, instead of pure water an acetate buffer system with a pH value of 5 was used as nonsolvent for the nanoprecipitaion of **P3** and **P4** with an initial acetone-polymer concentration of 10 mg mL^{-1}. In this case, nanoparticles with monomodal size distributions and low PDI values could be obtained, presumably due to the electrostatic stabilization of the nanoparticles as a consequence of protonation of the closely spaced amino chains at acidic pH values. By dropping acetone-polymer solution to water (AW), small nanoparticles with comparable sizes (Z-average diameter between 110 and 184 nm) were obtained for both initial acetone-polymer concentrations ($c = 1$ mg mL^{-1}, $c = 10$ mg mL^{-1}, for **P3** and **P4** at pH 5). The acetone-polymer concentration did not affect the nanoparticle size significantly. However, by dropping water into acetone-polymer solution, relatively smaller nanoparticles (Z-average diameter between 254 and 473 nm) were formed at an initial acetone-polymer concentration of 1 mg mL^{-1} compared to 10 mg mL^{-1} (Z-average diameter between 339 and 720 nm) (Fig. 4). As intended, the zeta potential of all suspensions shows positive values in between +20 to +64 mV indicating a high colloidal stability. The long term stability of the nanoparticle suspensions was tested at room temperature for three weeks, showing no change in size and size distributions. SEM investigations revealed that all nanoparticles have spherical shapes (Fig. 5, Supporting Information Figs. S16–S18).

pH-Response Test of the Nanoparticles

The pH-responsive behavior behavior was tested by storing nanoparticle suspensions at various pH values. Dilute buffer systems were used to prevent salting out effects. The DLS measurements (**A**, Fig. 6) revealed that nanoparticles from **P1** at pH 7 to 8 were not stable and are significantly larger with higher PDI values compared to water suspensions. Undefined aggregates were also observed at pH 7 to 8. This can be explained by the low zeta potential of the nanoparticle suspensions (**B**, Fig. 6) at these pH values. At low zeta potential values, van der Waals attractions become stronger than electrostatic repulsions, which result in aggregation. In general, stable colloidal dispersions have zeta potentials beyond ±20 mV.[44] In agreement with this, **P1** nanoparticles are stable at pH values of 3.4, 4, 5, 6 and 9 with relatively high absolute zeta potentials. It should be noted that **P1** nanoparticles have negative zeta potentials at pH 9 as already reported for the p(DMAEMA) microgels above their isoelectric point.[45] Unlike **P1**, **P2** nanoparticles did not show any sign of instability at pH 7, only at pH values of 8 and 9 due to the higher DMAEMA content in **P2**, meaning a stronger cationic character. At pH values of 3.4 to 5, **P2** nanoparticles are protonated and dissolve as already reported for DMAEMA functional micelles at acidic conditions. The dissolution is also monitored by the significant decrease in the derived count rate obtained from DLS measurements that is directly proportional to the size and the number of the nanoparticles.[46] A subsequent increase of the pH value back to the initial pH value of 7.5 resulted in a significant increase in the derived count rate and a Z-average diameter slightly larger than the original nanoparticles (Z-average diameter = 180 nm, PDI = 0.38), which hints toward the reversible dissolution ability of the nanoparticles. Furthermore, the copolymer **P2** itself also revealed complete

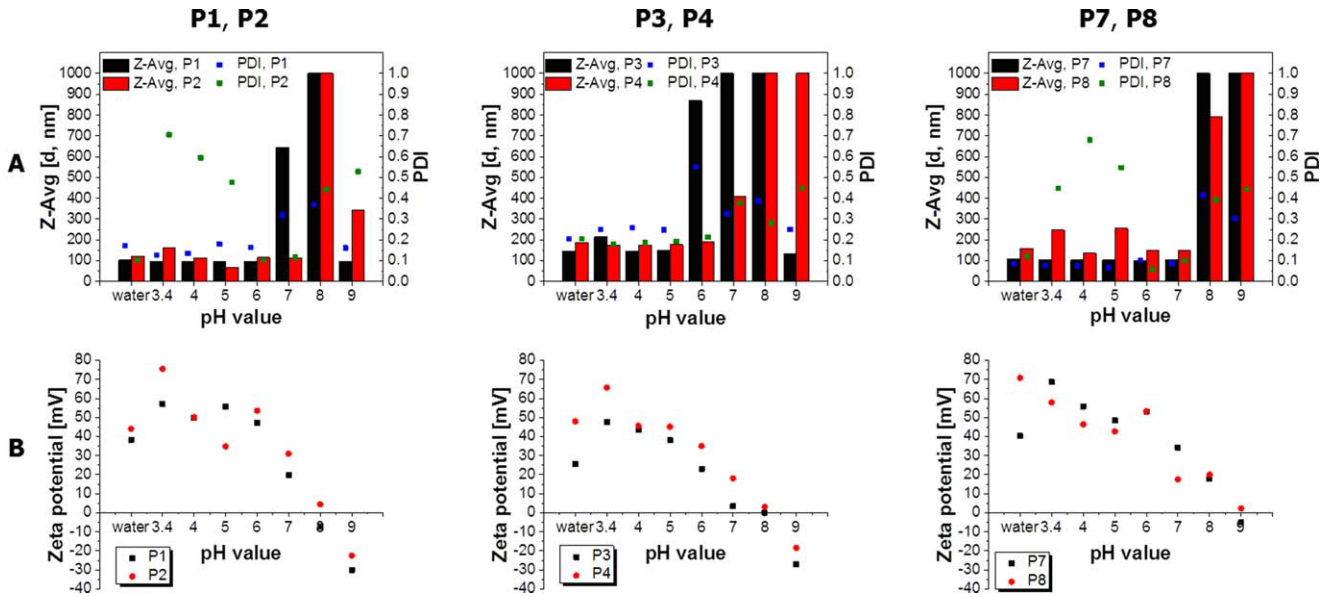

FIGURE 6 (A) Z-Average diameter (represented up to 1000 nm) and PDI values of nanoparticles as a function of the pH value. **(B)** Zeta potentials of the nanoparticles as a function of the pH value. [Color figure can be viewed in the online issue, which is available at wileyonlinelibrary.com.]

dissolution in aqueous media (0.3 mg/mL) at a pH value of 3.4. A dynamic increase of the pH value to the pH value of 7.5 resulted in spontaneous nanoparticle formation; DLS measurements ensured the nanoparticle formation (Z-average diameter = 124 nm, PDI = 0.34). In contrast, copolymer **P1** did not show any solubility in acidic aqueous media. Similar results were also obtained with nanoparticles prepared from Eudragit E100 as a reference pH-responsive material (Supporting Information Fig. S19).[27]

Due to the tightly spaced *t*BAEMA moieties that prevent protonation at neutral pH values, nanoparticles of **P3** and **P4** demonstrated less stability around neutral pH values compared to the DMAEMA functional nanoparticles. As shown in Figure 6, **P3** nanoparticles aggregate between pH 6 to 8 and **P4** nanoparticles aggregate between pH 7 to 9 as a consequence of the low zeta potential values. At acidic pH values, **P3** and **P4** nanoparticles were both stable due to the protonation of the *t*BAEMA. It should be noted that there was no nanoparticle dissociation observed even for **P4** that contains 21% *t*BAEMA.

Nanoparticles derived from the AEMA copolymers (**P7** and **P8**) revealed a higher stability compared to the DMAEMA and *t*BAEMA based nanoparticles around neutral pH values. Compared to the DMAEMA and *t*BAEMA nanoparticles, higher isoelectric points of the AEMA nanoparticles at a pH value around 9, as estimated from Figure 6(B), also support the higher stability of the AEMA based nanoparticles around neutral pH values. This can be explained by the primary amino structure of the AEMA that renders nanoparticles to protonate easily under neutral conditions. As shown in Figure 6, **P7** and **P8** nanoparticles are stable at pH values of 6 and 7 with relatively high zeta potential values. However, they tend to aggregate at pH values of 8 and 9 as a consequence of the low zeta potential values. Although **P7** nanoparticles are stable at pH values of 3.4, 4, and 5, **P8** nanoparticles with larger amino content were protonated and dissolved at these pH values.

Fluorescence Spectroscopic Study of the Nanoparticles

Pyrene as hydrophobic fluorescent probe was encapsulated as a model drug in **P2** and **P8** nanoparticles due to their dissolution ability at acidic pH values. The fluorescence emission spectra of pyrene against **P2** nanoparticles at various pH values are shown in Figure 7. Pyrene in pure water is

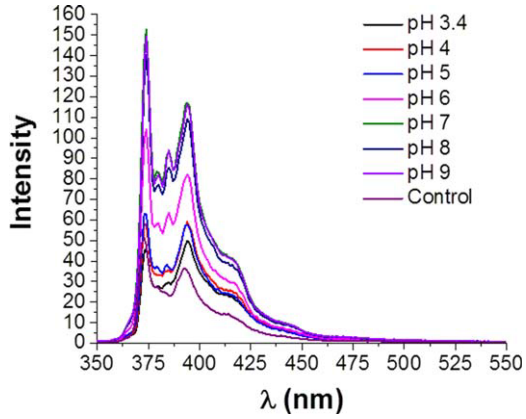

FIGURE 7 Fluorescence emission spectra of pyrene (6×10^{-5} mol L^{-1}) against **P2** nanoparticles (0.15 mg mL^{-1}) at various pH values. Pyrene in pure water was used as control. [Color figure can be viewed in the online issue, which is available at wileyonlinelibrary.com.]

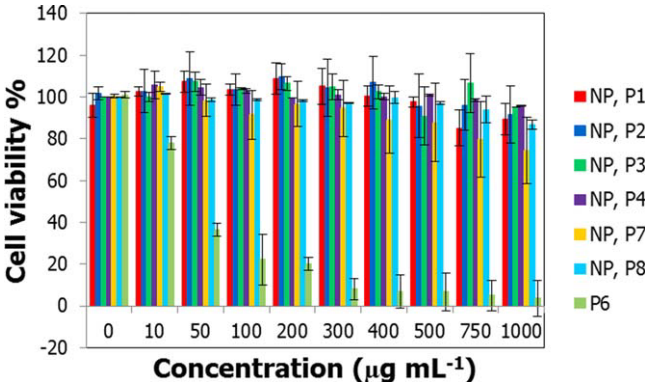

FIGURE 8 Cytotoxicity test of nanoparticles (NPs) that were prepared from **P1**, **P2**, **P3**, **P4**, **P7**, **P8** and water soluble polymer **P6** in L929 cells. The relative viability is expressed as percentage to control cells not treated with nanoparticles. Untreated cells on the same well plate were used as positive controls. Data represent means ± SD, $n \geq 6$. [Color figure can be viewed in the online issue, which is available at wileyonlinelibrary.com.]

used as control. The total intensities of the emission spectra of the nanoparticle suspensions at pH values from 7 to 9 are significantly higher compared to the emission intensity of the control. This indicates that pyrene is transferred into the hydrophobic domains of the nanoparticles and/or aggregates. However, at pH values of 3.4 to 5, the emission intensity of the pyrene is similar to the intensity of the control, which clearly reveals the dissolution of **P2** nanoparticles at these pH values. **P8** nanoparticles showed similar results (Supporting Information Fig. S20). However, compared to the same concentration of **P2** nanoparticles they have lower pyrene fluorescence intensities at pH values 7 to 9. This can be due to the lower hydrophobicity of the **P8** nanoparticles compared to the **P2** nanoparticles, meaning that **P2** might show in general higher encapsulation efficiencies for hydrophobic drugs.

Cytotoxicity of the Nanoparticles in L929 Cells

To evaluate the cytotoxicity of the nanoparticles, one nanoparticle sample of each copolymer prepared from 1 mg mL^{-1} AW technique and water soluble polymer **P6** was investigated at the indicated concentrations (Fig. 8). The cytotoxicity assay results showed that the nanoparticles did not have any significant cytotoxic effect on L929 cells after 24 h incubation at up to 1 mg mL^{-1}. These results are promising in comparison to the previous reports because cationic nanoparticles have frequently been associated with toxic effects in cell studies.[47,48] It should be noted that nanoparticles based on PMMA are known as nontoxic, whereas homopolymers based on PDMAEMA and PAEMA are known to be toxic.[49] **P6** showed a severe toxic effect on the cells, which is due to the primary amino functional AEMA moieties in the copolymer. However, nanoparticles, which are derived from **P8** (the deprotonated form of **P6**), are nontoxic. This might be due to the change of the cationic charge of the polymer. **P8** contains pH-responsive primary amines that are not fully protonated at the pH values applied. This leads to a decreased water solubility enabling nanoparticle formation. Due to the fact that the cationic charges are mainly responsible for cytotoxicity, the reduced charge content possibly also results in less destructive effects on the cell membrane.[50] Moreover, it was already demonstrated that cationic polyplexes with a comparable size to the nanoparticles show less cytotoxic effects in contrast to the free cationic polymer chains.[51] The cytotoxicity of single cationic polymer chains is based on the disruption of the lipid double layer by the formation of nanoscale pores or membrane thinning (2 to 5 nm).[52] Thus, the reduced cytotoxicity of the nanoparticle can be attributed to the combination of reduced cationic charge and less disruptive cell membrane interaction.

CONCLUSIONS

A library of well-defined copolymers of MMA with DMAEMA, *t*BAEMA and AEMA·HCl was synthesized via RAFT polymerization by varying the initial monomer feed ratios to alter the amino content in the copolymers and in the corresponding nanoparticle. The controlled nature of the polymerizations was certified by kinetic studies. By variation of the initial formulation conditions during the nanoprecipitation method, such as polymer concentration and dropping method, well-defined nanoparticles from the synthesized copolymers with varying sizes were successfully prepared. Moreover, pH-stability tests demonstrated that, depending on the structure and amount of the amino functionality in the copolymers, the corresponding nanoparticles reveal a pH response. Fluorescence spectroscopic studies of pyrene as model drug revealed the dissolution of two nanoparticle batches at acidic pH values. Moreover, none of these nanoparticles exhibited any cytotoxic effect on L929 cells.

The results encourage the use of these polymeric nanoparticles as novel carriers for the controlled release of loaded pharmaceutical agents in acidic environment, for example, cancer cells or endosomal cellular compartments. To optimize the release profile, the polymeric composition can be varied. Future investigations will deal with the controlled release of active payloads such as anticancer drugs but also with the delivery and release of genetic material, where the cationic moieties might favor the encapsulation efficiency and the burst release from endosome.

ACKNOWLEDGMENTS

We acknowledge funding from the Carl-Zeiss Foundation (JCSM Strukturantrag and fellowship for C.W.) and the Thüringer Ministerium für Wirtschaft, Wissenschaft, und Digitale Gesellschaft (TMWWDG, ProExzellenz II, NanoConSens). We also express our gratitude to Steffi Stumpf for help in the SEM investigations, Carolin Fritzsche for cell studies, and Dr. Michael Wagner, Dr. Antje Vollrath and Dr. Christian Pietsch for helpful discussion.

REFERENCES AND NOTES

1 R. Cheng, F. Meng, C. Deng, H.-A. Klok, Z. Zhong, *Biomaterials* **2013**, *34*, 3647–3657.

2 Y. Li, W. Xiao, K. Xiao, L. Berti, J. Luo, H. P. Tseng, G. Fung, K. S. Lam, *Angew. Chem. Int. Ed.* **2012**, *51*, 2864–2869.

3 M. Motornov, Y. Roiter, I. Tokarev, S. Minko, *Prog. Polym. Sci.* **2010**, *35*, 174–211.

4 B. Jeong, Y. H. Bae, S. W. Kim, *J. Control. Release* **2000**, *63*, 155–163.

5 B. Yan, J.-C. Boyer, D. Habault, N. R. Branda, Y. Zhao, *J. Am. Chem. Soc.* **2012**, *134*, 16558–16561.

6 J. Wang, X. Sun, W. Mao, W. Sun, J. Tang, M. Sui, Y. Shen, Z. Gu, *Adv. Mater.* **2013**, *25*, 3670–3676.

7 S.-F. Lee, X.-M. Zhu, Y.-X. J. Wang, S.-H. Xuan, Q. You, W.-H. Chan, C.-H. Wong, F. Wang, J. C. Yu, C. H. K. Cheng, K. C.-F. Leung, *ACS Appl. Mater. Interfaces* **2013**, *5*, 1566–1574.

8 R. Liu, D. Li, B. He, X. Xu, M. Sheng, Y. Lai, G. Wang, Z. Gu, *J. Control. Release* **2011**, *152*, 49–56.

9 N. E. Sounni, A. Noel, *Clin. Chem.* **2013**, *59*, 85–93.

10 Y. Lee, S. Fukushima, Y. Bae, S. Hiki, T. Ishii, K. Kataoka, *J. Am. Chem. Soc.* **2007**, *129*, 5362–5363.

11 E. S. Lee, K. Na, Y. H. Bae, *Nano Lett.* **2005**, *5*, 325–329.

12 S. Ganta, H. Devalapally, A. Shahiwala, M. Amiji, *J. Control. Release* **2008**, *126*, 187–204.

13 C. Clawson, L. Ton, S. Aryal, V. Fu, S. Esener, L. Zhang, *Langmuir* **2011**, *27*, 10556–10561.

14 Y. Bae, S. Fukushima, A. Harada, K. Kataoka, *Angew. Chem. Int. Ed.* **2003**, *42*, 4640–4643.

15 E. R. Gillies, J. M. J. Fréchet, *Bioconjugate Chem.* **2005**, *16*, 361–368.

16 J. Ko, K. Park, Y.-S. Kim, M. S. Kim, J. K. Han, K. Kim, R.-W. Park, I.-S. Kim, H. K. Song, D. S. Lee, I. C. Kwon, *J. Control. Release* **2007**, *123*, 109–115.

17 G.-H. Hsiue, C.-H. Wang, C.-L. Lo, C.-H. Wang, J.-P. Li, J.-L. Yang, *Int. J. Pharm.* **2006**, *317*, 69–75.

18 C. E. Mora-Huertas, H. Fessi, A. Elaissari, *Int. J. Pharm.* **2010**, *385*, 113–142.

19 A. W. Jackson, D. A. Fulton, *Polym. Chem.* **2013**, *4*, 31.

20 A. Honglawan, H. Ni, D. Weissman, S. Yang, *Polym. Chem.* **2013**, *4*, 3667.

21 G. Moad, E. Rizzardo, S. H. Thang, *Polymer* **2008**, *49*, 1079–1131.

22 S.-i. Yamamoto, J. Pietrasik, K. Matyjaszewski, *Macromolecules* **2008**, *41*, 7013–7020.

23 A. J. Morse, D. Dupin, K. L. Thompson, S. P. Armes, K. Ouzineb, P. Mills, R. Swart, *Langmuir* **2012**, *28*, 11733–11744.

24 L. He, E. S. Read, S. P. Armes, D. J. Adams, *Macromolecules* **2007**, *40*, 4429–4438.

25 H. Fessi, F. Puisieux, J. P. Devissaguet, N. Ammoury, S. Benita, *Int. J. Pharm.* **1989**, *55*, R1–R4.

26 S. Schubert, J. J. T. Delaney, U. S. Schubert, *Soft Matter* **2011**, *7*, 1581–1588.

27 D. Kohane, D. Anderson, C. Yu, R. Langer, *Pharm. Res.* **2003**, *20*, 1533–1538.

28 A. H. Alidedeoglu, A. W. York, C. L. McCormick, S. E. Morgan, *J. Polym. Sci., Part A: Polym. Chem.* **2009**, *47*, 5405–5415.

29 I. Kurtulus, G. Yilmaz, M. Ucuncu, M. Emrullahoglu, C. R. Becer, V. Bulmus, *Polym. Chem.* **2014**, *5*, 1593.

30 G. Moad, J. Chiefari, Y. K. Chong, J. Krstina, R. T. A. Mayadunne, A. Postma, E. Rizzardo, S. H. Thang, *Polym. Int.* **2000**, *49*, 993–1001.

31 J. M. Layman, S. M. Ramirez, M. D. Green, T. E. Long, *Biomacromolecules* **2009**, *10*, 1244–1252.

32 M. W. M. Fijten, R. M. Paulus, U. S. Schubert, *J. Polym. Sci., Part A: Polym. Chem.* **2005**, *43*, 3831–3839.

33 J. B. McLeary, J. M. McKenzie, M. P. Tonge, R. D. Sanderson, B. Klumperman, *Chem. Commun.* **2004**, 1950–1951.

34 J. Bigot, B. Charleux, G. Cooke, F. Delattre, D. Fournier, J. Lyskawa, F. Stoffelbach, P. Woisel, *Macromolecules* **2009**, *43*, 82–90.

35 A. J. D. Magenau, N. Martinez-Castro, D. A. Savin, R. F. Storey, *Macromolecules* **2009**, *42*, 8044–8051.

36 W. Zhang, L. Liu, X. Zhuang, X. Li, J. Bai, Y. Chen, *J. Polym. Sci. Part A: Polym. Chem.* **2008**, *46*, 7049–7061.

37 S. G. Roy, K. Bauri, S. Pal, A. Goswami, G. Madras, P. De, *Polym. Int.* **2013**, *62*, 463–473.

38 P. Cotanda, D. B. Wright, M. Tyler, R. K. O'Reilly, *J. Polym. Sci., Part A: Polym. Chem.* **2013**, *51*, 3333–3338.

39 S.H. Hong, V.M. McHung, Review of preparation and properties of polymers from copolymerization of aprotic acrylic monomers with protic acrylic monomers. Technical Report. Chemical Research, Development and Engineering Center, Aberdeen Proving Ground, MD. Available at: http://www.dtic.mil/cgibin/GetTRDoc?Location=U2&doc=GetTRDoc.pdf&AD=ADA197467; 1988, accessed on September 1, **2014**.

40 K. Matyjaszewski, M. J. Ziegler, S. V. Arehart, D. Greszta, T. Pakula, *J. Phys. Org. Chem.* **2000**, *13*, 775–786.

41 Y. K. Chong, T. P. T. Le, G. Moad, E. Rizzardo, S. H. Thang, *Macromolecules* **1999**, *32*, 2071–2074.

42 A. Vollrath, D. Pretzel, C. Pietsch, I. Perevyazko, S. Schubert, G. M. Pavlov, U. S. Schubert, *Macromol. Rapid. Commun.* **2012**, *33*, 1791–1797.

43 H. Lee, S. H. Son, R. Sharma, Y.-Y. Won, *J. Phys. Chem. B* **2011**, *115*, 844–860.

44 A. Shalviri, H. K. Chan, G. Raval, M. J. Abdekhodaie, Q. Liu, H. Heerklotz, X. Y. Wu, *Colloids Surf. B* **2013**, *101*, 405–413.

45 L. Hu, L.-Y. Chu, M. Yang, H.-D. Wang, C. Hui Niu, *J. Colloid Interface Sci.* **2007**, *311*, 110–117.

46 S. J. Wallace, J. Li, R. L. Nation, B. J. Boyd, *Drug Deliv. Transl. Res.* **2012**, *2*, 284–292.

47 H. Zhang, T. Xia, H. Meng, M. Xue, S. George, Z. Ji, X. Wang, R. Liu, M. Wang, B. France, R. Rallo, R. Damoiseaux, Y. Cohen, K. A. Bradley, J. I. Zink, A. E. Nel, *ACS Nano* **2011**, *5*, 2756–2769.

48 P. H. M. Hoet, L. Gilissen, B. Nemery, *Toxicol. Appl. Pharm.* **2001**, *175*, 184–190.

49 C. He, J. Liu, X. Ye, L. Xie, Q. Zhang, X. Ren, G. Zhang, C. Wu, *Langmuir* **2008**, *24*, 10717–10722.

50 N. M. Schaeublin, L. K. Braydich-Stolle, A. M. Schrand, J. M. Miller, J. Hutchison, J. J. Schlager, S. M. Hussain, *Nanoscale* **2011**, *3*, 410–420.

51 Y. Yue, F. Jin, R. Deng, J. Cai, Y. Chen, M. C. M. Lin, H.-F. Kung, C. Wu, *J. Control. Release* **2011**, *155*, 67–76.

52 S. Hong, P. R. Leroueil, E. K. Janus, J. L. Peters, M.-M. Kober, M. T. Islam, B. G. Orr, J. R. Baker, M. M. Banaszak Holl, *Bioconjug. Chem.* **2006**, *17*, 728–734.

Supporting Information

RAFT made methacrylate copolymers for reversible pH-responsive nanoparticles

Turgay Yildirim,[a,b] Alexandra C. Rinkenauer,[a,b] Christine Weber,[a,b] Anja Traeger,[a,b] Stephanie Schubert,[b,c] Ulrich S. Schubert[a,b]*

[a]Laboratory of Organic and Macromolecular Chemistry (IOMC), Friedrich Schiller University Jena, Humboldtstr. 10, 07743 Jena, Germany

[b]Jena Center for Soft Matter (JCSM), Friedrich Schiller University Jena, Philosophenweg 7, 07743 Jena, Germany

[c]Institute of Pharmacy, Department of Pharmaceutical Technology, Friedrich Schiller University Jena, Otto-Schott-Str. 41, 07745 Jena, Germany

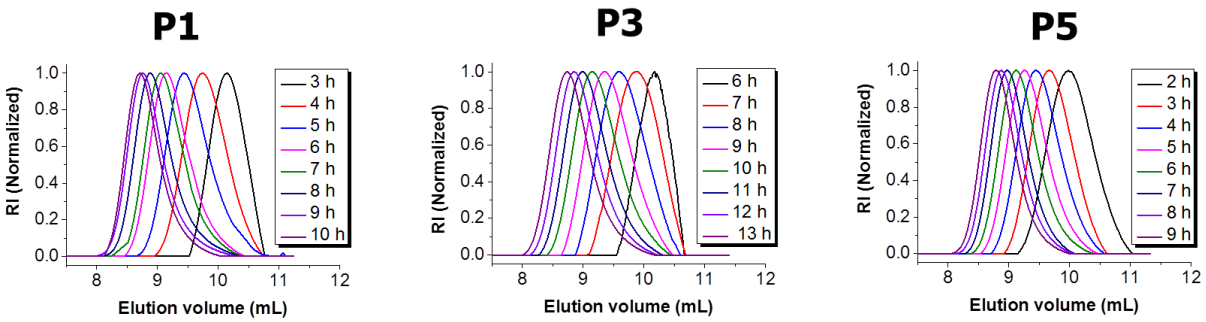

Figure SI-1 Overlay of the SEC traces ($CHCl_3$) from kinetic studies of the RAFT copolymerization of MMA with 10% comonomer: DMAEMA (**P1**), *t*BAEMA (**P3**) and AEMA·HCl (**P5**). [M]/[CPADB]/[AIBN] = 100/1/0.25; $[M]_0$ = 2 mol L^{-1}. Polymerization conditions for (**P1** and **P3**): Solvent ethanol, T = 70 °C. Polymerization conditions for **P5**: Solvent methanol under reflux.

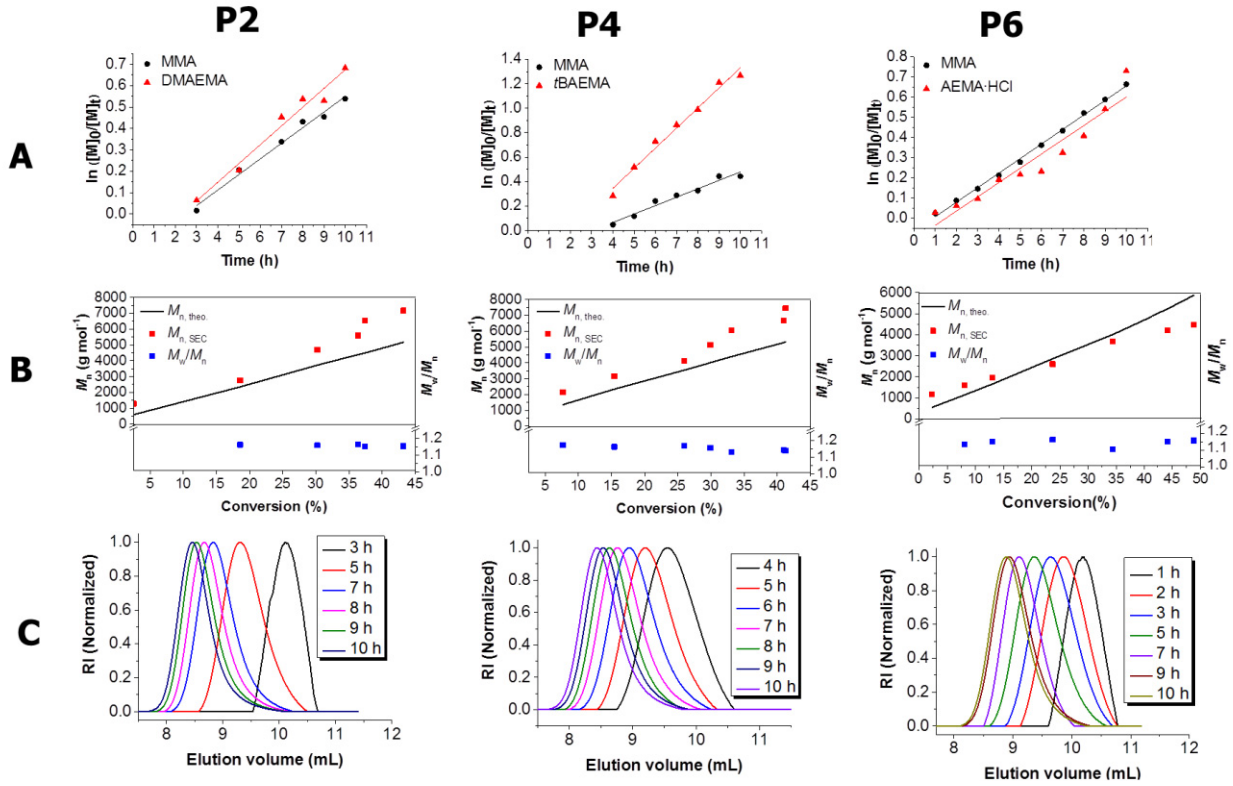

Figure SI-2 Kinetic studies of the RAFT copolymerization of MMA with 20 mol% comonomer DMAEMA (P2), *t*BAEMA (P4) and AEMA·HCl (P6). [M]/[CPADB]/[AIBN] = 100/1/0.25; $[M]_0$ = 2 mol L^{-1}. Polymerization conditions for (P2 and P4): Solvent ethanol, T = 70 °C. Polymerization conditions for P6: Solvent methanol under reflux. (A) Semilogarithmic kinetic plots. (B) M_n and M_w/M_n evolution with total monomer conversion. (C) SEC overlay traces ($CHCl_3$).

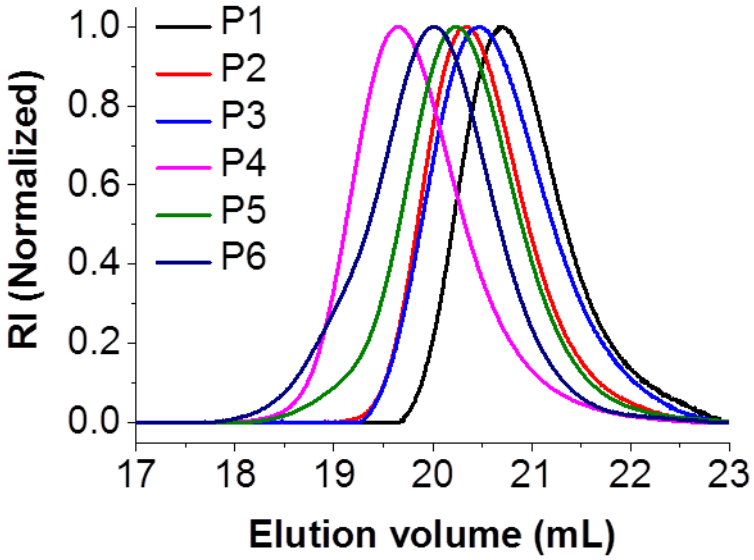

Figure SI-3 Normalized SEC traces (DMAc, RI detection) of the isolated copolymers of **P1**-**P6**.

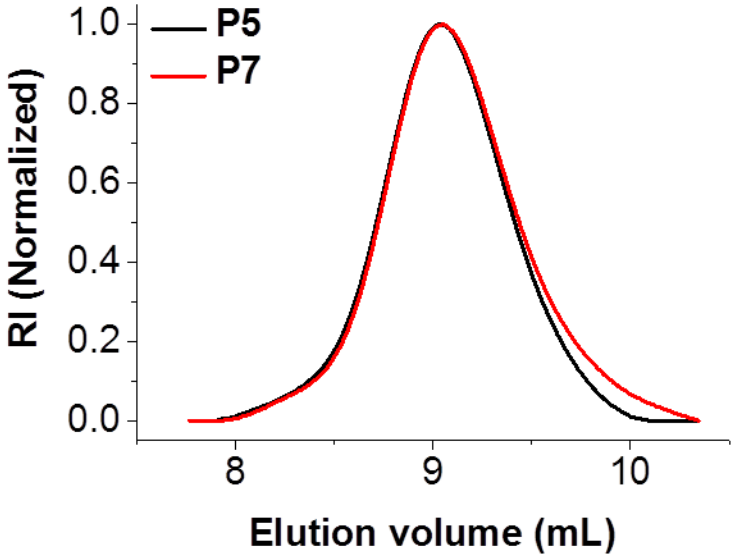

Figure SI-4 Normalized SEC traces ($CHCl_3$, RI detection) of the isolated copolymers **P5** and **P7**.

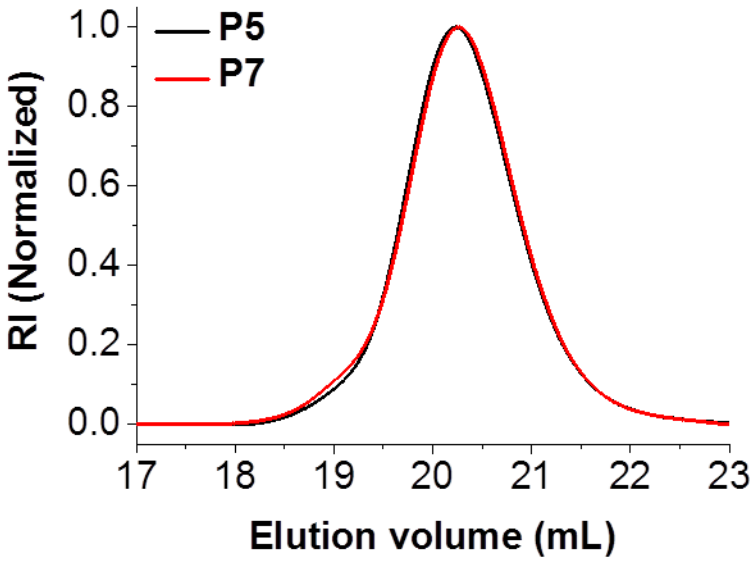

Figure SI-5 Normalized SEC traces (DMAc, RI detection) of isolated copolymers **P5** and **P7**.

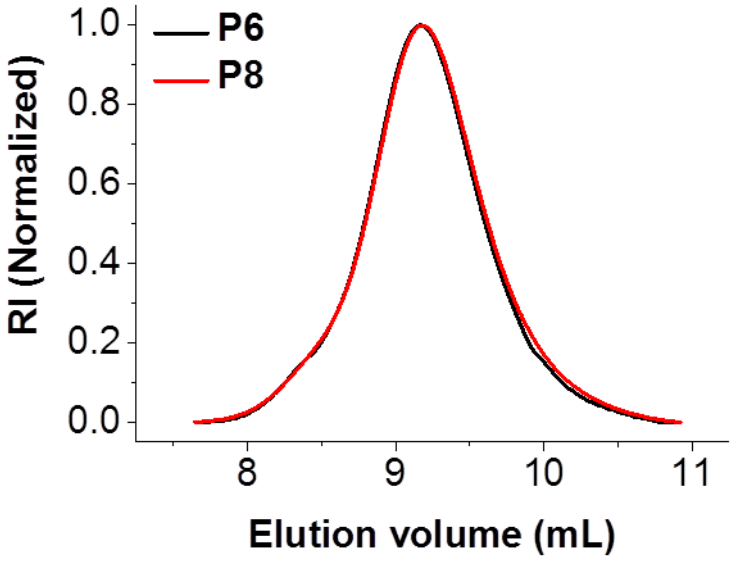

Figure SI-6 Normalized SEC traces ($CHCl_3$, RI detection) of isolated copolymers **P6** and **P8**.

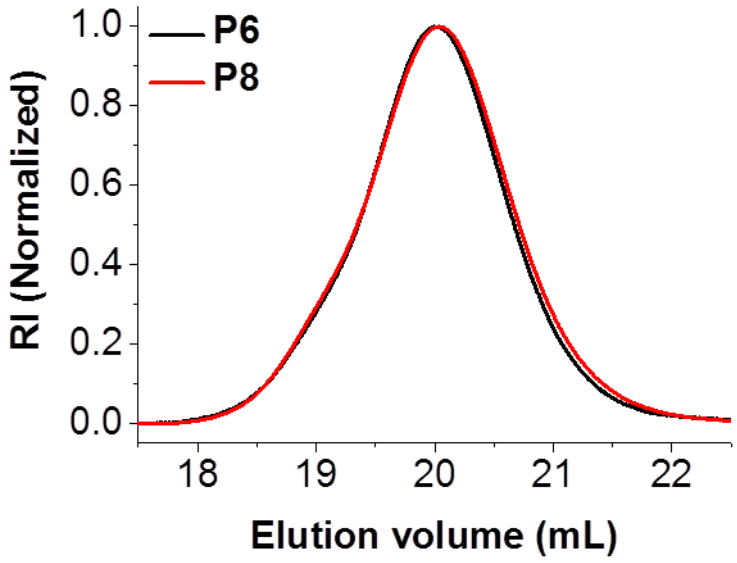

Figure SI-7 Normalized SEC traces (DMAc, RI detection) of isolated copolymers **P6** and **P8**.

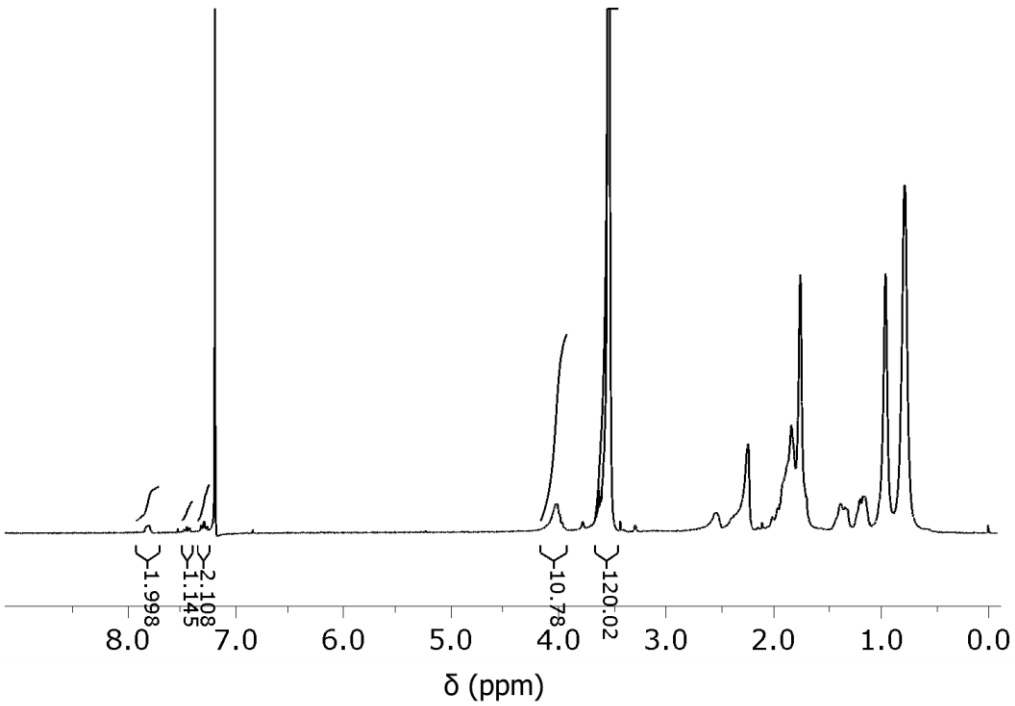

Figure SI-8 ^{1}H NMR spectrum (300 MHz, $CDCl_3$) of **P1**.

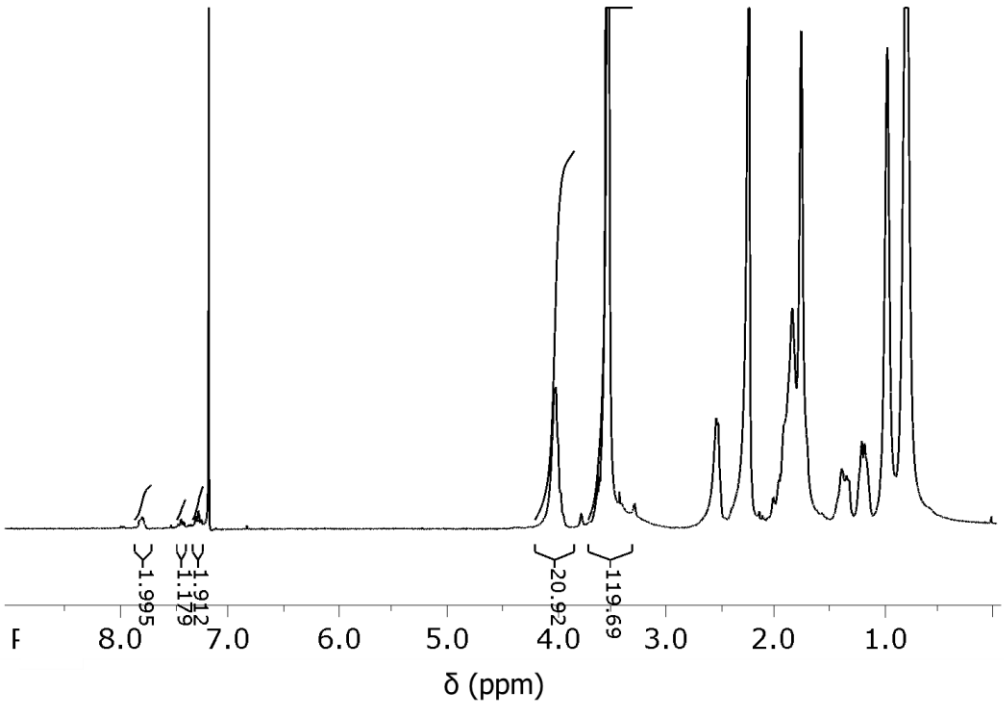

Figure SI-9 ^{1}H NMR spectrum (300 MHz, $CDCl_3$) of **P2**.

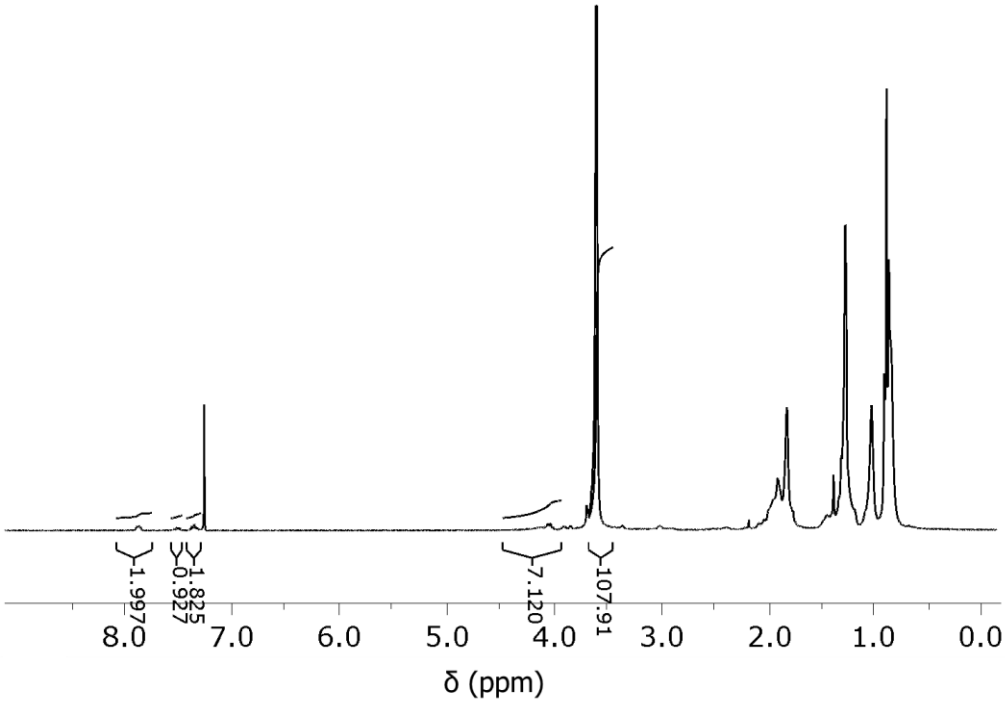

Figure SI-10 ^{1}H NMR spectrum (300 MHz, $CDCl_3$) of **P3**.

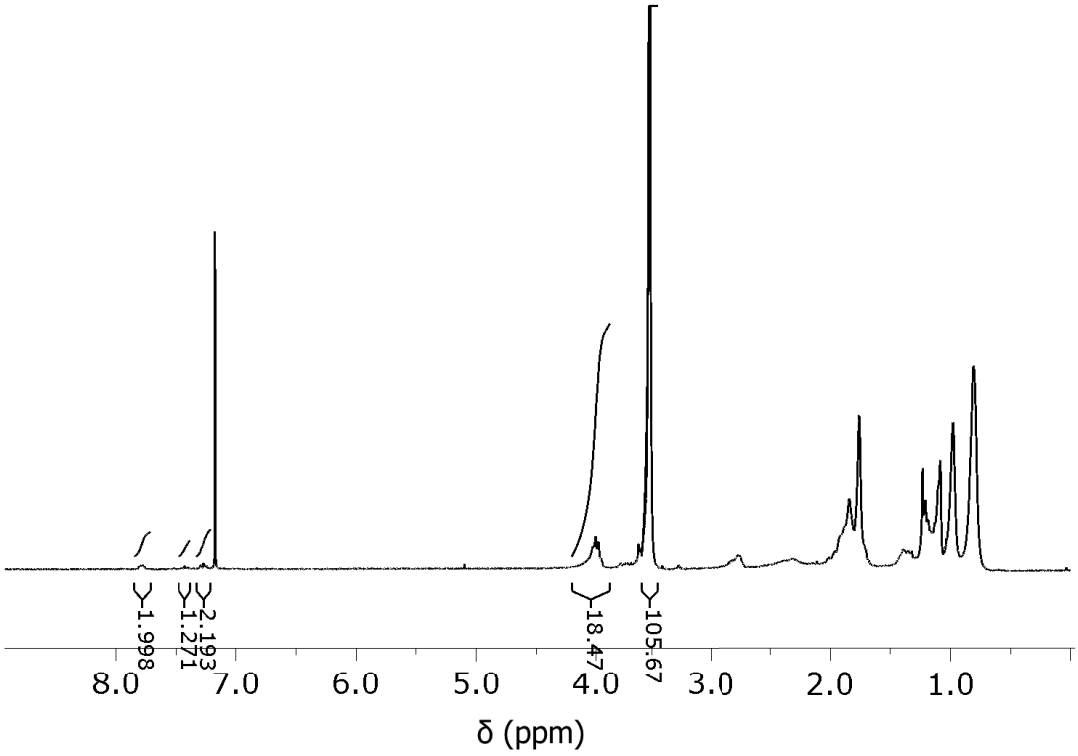

Figure SI-11 ^{1}H NMR spectrum (300 MHz, $CDCl_3$) of **P4**.

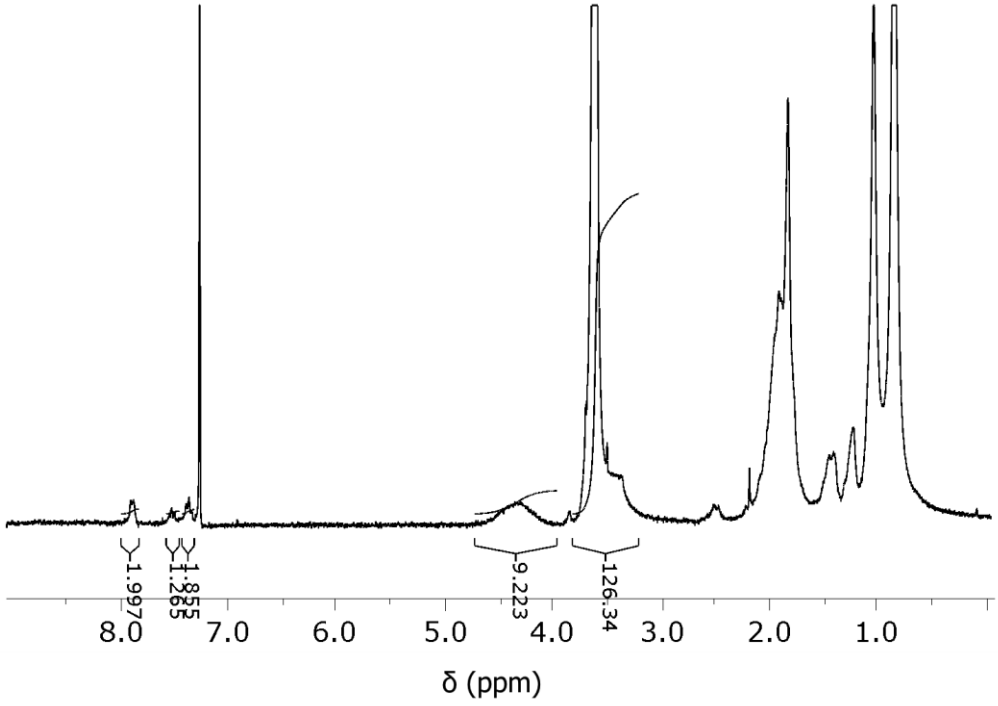

Figure SI-12 ^{1}H NMR spectrum (300 MHz, $CDCl_3$) of **P5**.

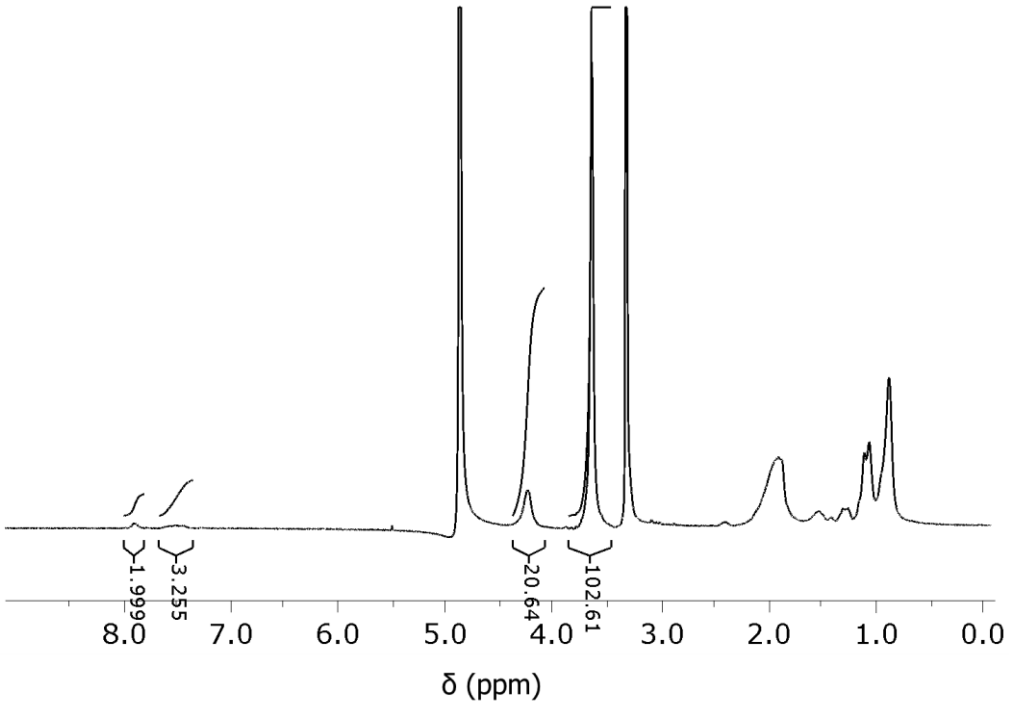

Figure SI-13 ^{1}H NMR spectrum (300 MHz, MeOD) of **P6**.

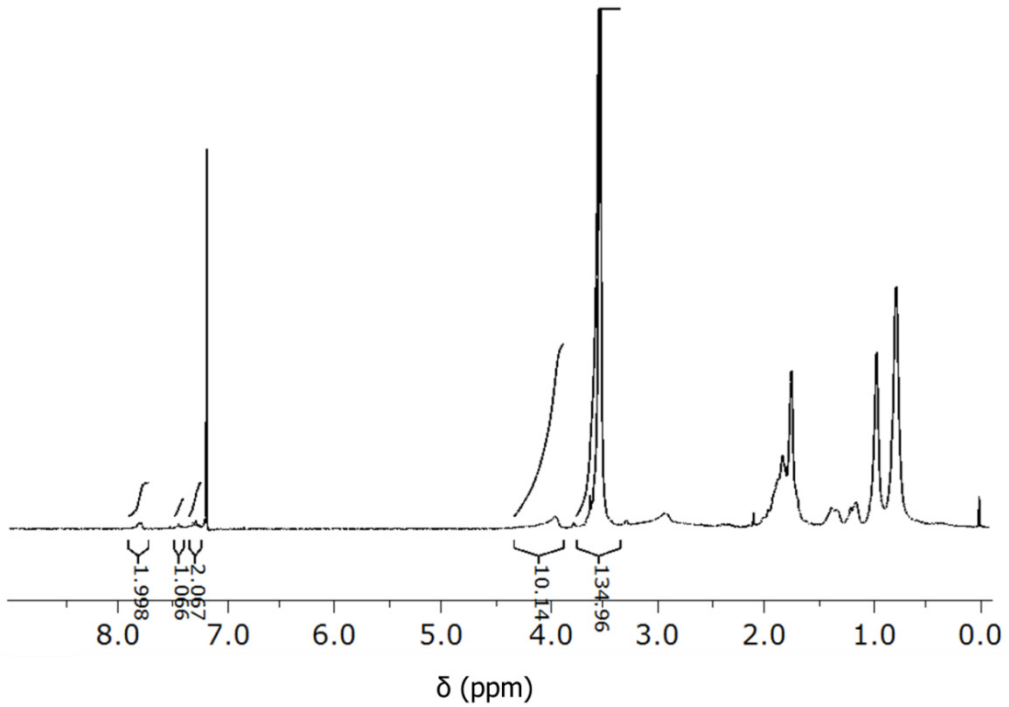

Figure SI-14 ^{1}H NMR spectrum (300 MHz, $CDCl_3$) of **P7**.

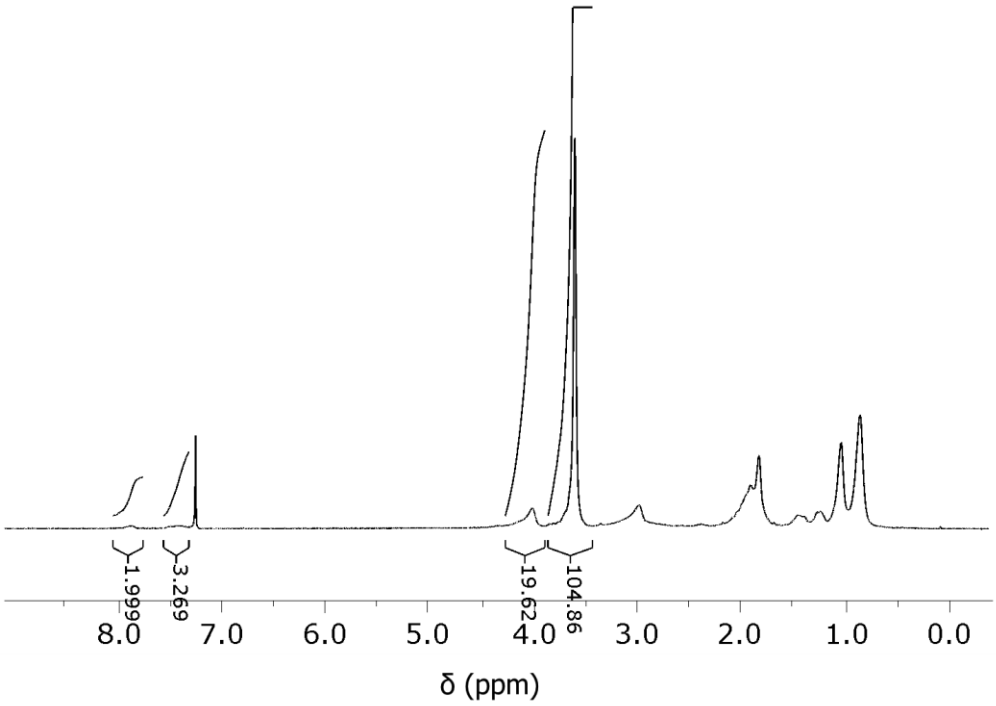

Figure SI-15 ^{1}H NMR spectrum (300 MHz, $CDCl_3$) of **P8**.

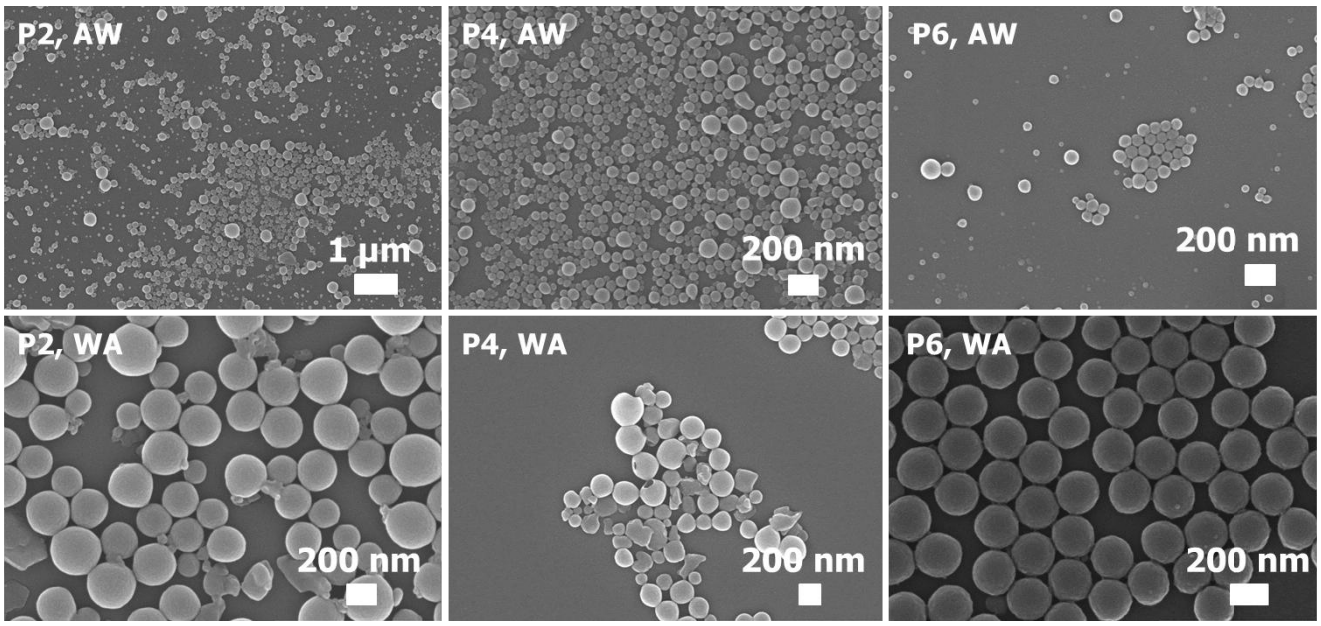

Figure SI-16 SEM images of nanoparticles that were prepared from **P2**, **P4** and **P8** (1 mg mL^{-1}) by dropping acetone-polymer solution to water (AW) or dropping water to acetone-polymer solution (WA).

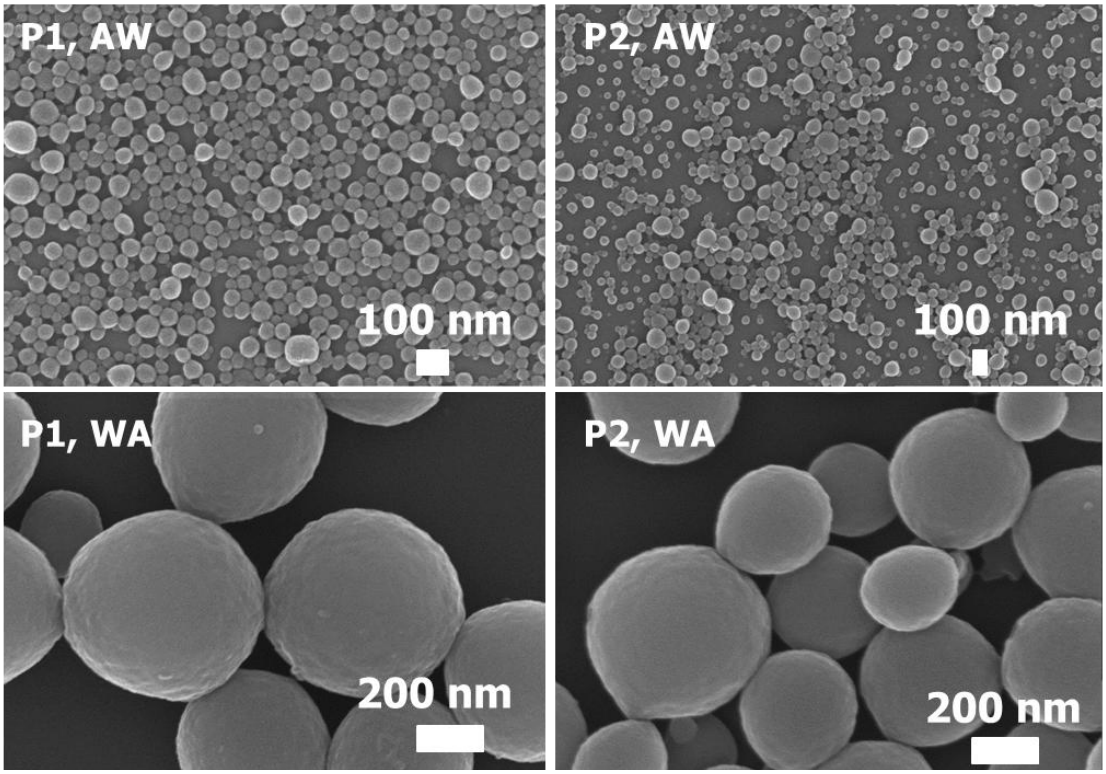

Figure SI-17 SEM images of nanoparticles that were prepared from **P1** and **P2** (10 mg mL^{-1}) by dropping acetone-polymer solution to water (AW) or dropping water to acetone-polymer solution (WA).

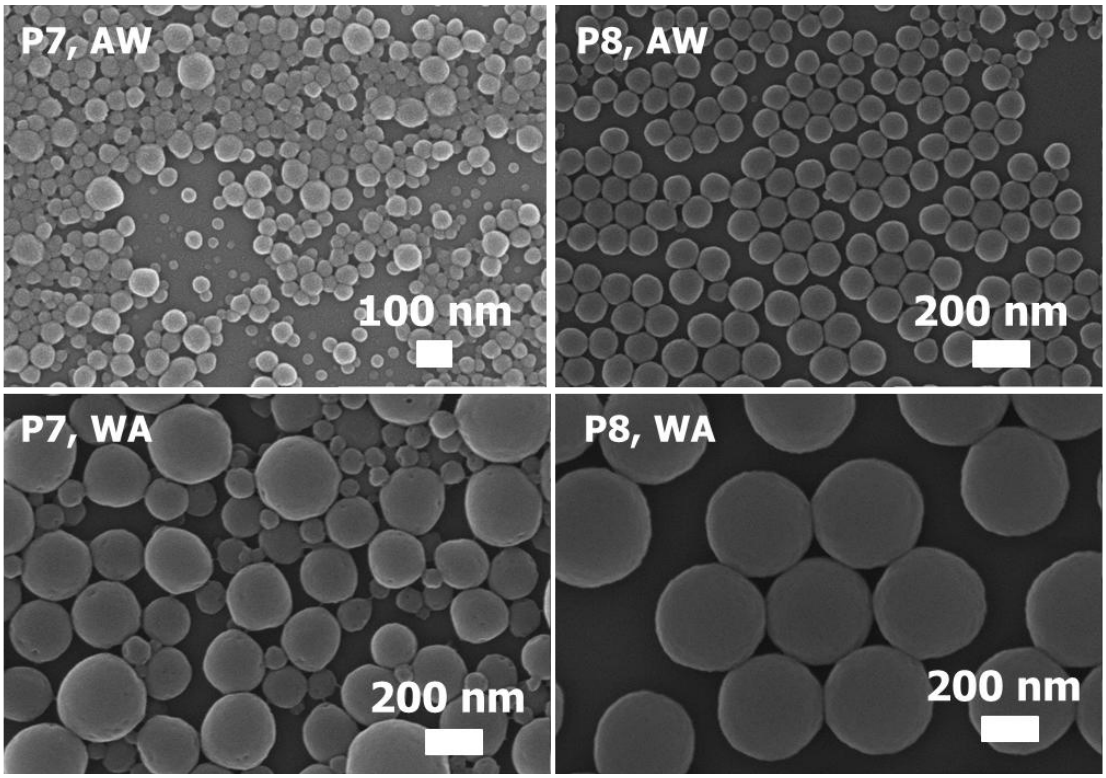

Figure SI-18 SEM images of nanoparticles that were prepared from **P7** and **P8** (10 mg mL^{-1}) by dropping acetone-polymer solution to water (AW) or dropping water to acetone-polymer solution (WA).

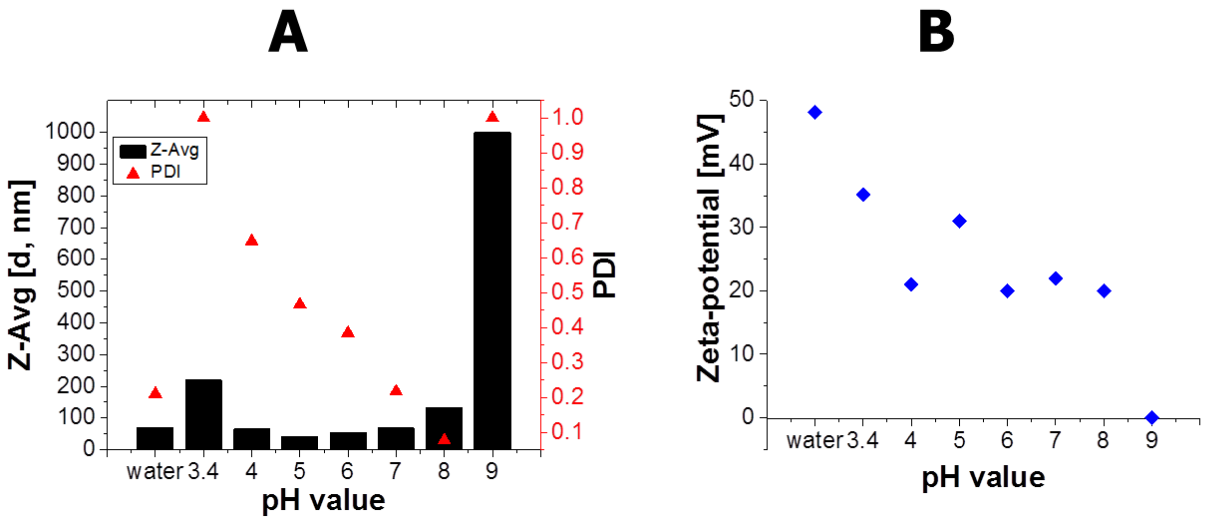

Figure SI-19 (A) Z-Average diameter (represented up to 1000 nm) and PDI values of Eudragit E100 nanoparticles as a function of the pH value. **(B)** Zeta potential of the Eudragit E100 nanoparticles as a function of the pH value.

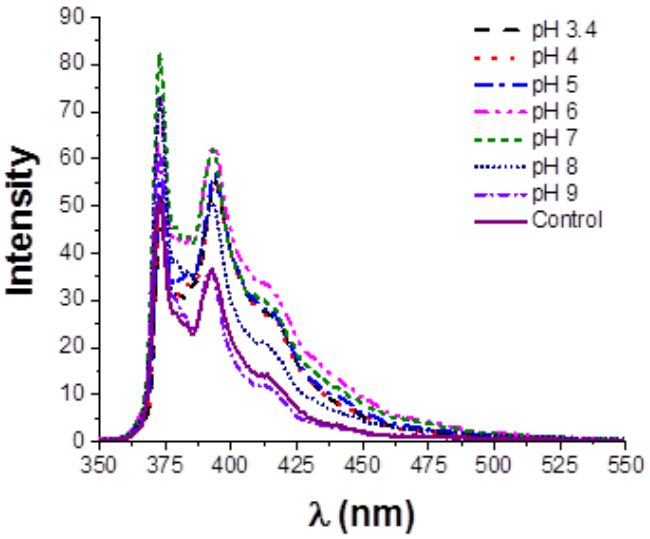

Figure SI-20 Fluorescence emission spectra of pyrene (6×10^{-5} mol L^{-1}) with **P8** nanoparticles (0.15 mg mL^{-1}) at various pH values. Pyrene in pure water was used as control.

Table SI-1 C, H, N, S and Cl contents (mass % in dry sample) in the copolymers of **P5**, **P6**, **P7** and **P8** that were determined by elemental analysis.

Polymer	C	H	N	S	Cl
P5	56.30	7.86	1.73	0.81	3.03
P7	58.31	8.00	1.73	0.85	1.01
P6	52.97	7.85	2.95	0.94	4.92
P8	55.80	7.75	3.02	0.89	0.92

Publication P8

Comparison of the uptake of methacrylate-based nanoparticles in static and dynamic *in vitro* systems as well as *in vivo*,

A. C. Rinkenauer, A. T. Press, M. Raasch, C. Pietsch, S. Schweizer, S. Schwörer, K. L. Rudolph, A. Mosig, M. Bauer, A. Traeger, U. S. Schubert,

J. Controll. Release **2015**, *261*, 158-168.

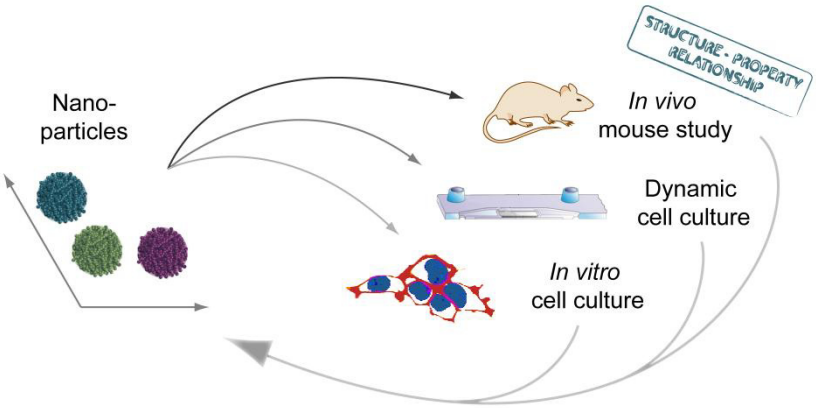

Journal of Controlled Release 216 (2015) 158–168

Contents lists available at ScienceDirect

Journal of Controlled Release

journal homepage: www.elsevier.com/locate/jconrel

Comparison of the uptake of methacrylate-based nanoparticles in static and dynamic *in vitro* systems as well as *in vivo*

Alexandra C. Rinkenauer [a,b,1], Adrian T. Press [b,c,1], Martin Raasch [c,d], Christian Pietsch [a], Simon Schweizer [a], Simon Schwörer [b,e], Karl L. Rudolph [b,e], Alexander Mosig [b,c,d], Michael Bauer [b,c], Anja Traeger [a,b,*], Ulrich S. Schubert [a,b,*]

[a] *Laboratory of Organic and Macromolecular Chemistry (IOMC), Friedrich Schiller University Jena, Humboldtstrasse 10, 07743 Jena, Germany*
[b] *Jena Center for Soft Matter (JCSM), Friedrich Schiller University Jena, Philosophenweg 7, 07743 Jena, Germany*
[c] *Center for Sepsis Control and Care (CSCC), Jena University Hospital, Erlanger Allee 101, 07747 Jena, Germany*
[d] *Institute of Biochemistry II, Jena University Hospital, Friedrich Schiller University Jena, Nonnenplan 2, 07743 Jena, Germany*
[e] *Leibniz Institute for Age Research, Fritz Lipmann Institute Jena, Beutenbergstrasse 11, 07745 Jena, Germany*

ARTICLE INFO

Article history:
Received 27 April 2015
Received in revised form 23 July 2015
Accepted 4 August 2015
Available online 12 August 2015

Keywords:
Methacrylate
Nanoparticle
In vivo
Shear stress
Microfluidics
Uptake
Pharmacokinetic

ABSTRACT

Polymer-based nanoparticles are promising drug delivery systems allowing the development of new drug and treatment strategies with reduced side effects. However, it remains a challenge to screen for new and effective nanoparticle-based systems *in vitro*. Important factors influencing the behavior of nanoparticles *in vivo* cannot be simulated in screening assays *in vitro*, which still represent the main tools in academic research and pharmaceutical industry. These systems have serious drawbacks in the development of nanoparticle-based drug delivery systems, since they do not consider the highly complex processes influencing nanoparticle clearance, distribution, and uptake *in vivo*. In particular, the transfer of *in vitro* nanoparticle performance to *in vivo* models often fails, demonstrating the urgent need for novel *in vitro* tools that can imitate aspects of the *in vivo* situation more accurate. Dynamic cell culture, where cells are cultured and incubated in the presence of shear stress has the potential to bridge this gap by mimicking key-features of organs and vessels. Our approach implements and compares a chip-based dynamic cell culture model to the common static cell culture and mouse model to assess its capability to predict the *in vivo* success more accurately, by using a well-defined poly((methyl methacrylate)-*co*-(methacrylic acid)) and poly((methyl methacrylate)-*co*-(2-dimethylamino ethylmethacrylate)) based nanoparticle library. After characterization in static and dynamic *in vitro* cell culture we were able to show that physiological conditions such as cell–cell communication of co-cultured endothelial cells and macrophages as well as mechanotransductive signaling through shear stress significantly alter cellular nanoparticle uptake. In addition, it could be demonstrated by using dynamic cell cultures that the *in vivo* situation is simulated more accurately and thereby can be applied as a novel system to investigate the performance of nanoparticle systems *in vivo* more reliable.

1. Introduction

Drug delivery *via* polymer-based nanoparticles has the potential to be used for novel treatment strategies offering improved pharmacological properties, higher efficiencies as well as reduced side effects, compared to direct drug application [1]. In order to develop optimized nanoparticle-based drug delivery systems, the investigation of key-factors influencing their pharmacokinetic and pharmacodynamic properties is necessary. Numerous factors affect the uptake of nanoparticles *in vitro*, including the protein corona, surface charge, size and shape [2–5]. For instance, it is well-known that nanoparticles with 50 to 200 nm in diameter are internalized by a wide variety of cells [6]. However, direct translation of their uptake efficiency *in vitro* to their behavior *in vivo* is challenging. In particular, the prediction concerning biodistribution and interaction with the reticuloendothelial system (RES) remains a challenge [7,8]. Thus, resource and time consuming *in vivo* experiments are applied to evaluate new nanoparticle systems and to answer the question, whether they improve the biodistribution and the availability of a compound to the target cell and whether a reduced uptake by off-target tissues and cells is realized to limit detrimental effects. As a consequence, different targeting moieties such as antibodies, aptamers, metabolites, and anti-genes were used to coat the nanoparticle surface, creating new cell-type specific nanotherapeutics, -diagnostics, and -theranostic systems. [9–13] The

* Corresponding authors at: Laboratory of Organic and Macromolecular Chemistry (IOMC), Friedrich Schiller University Jena, Humboldtstrasse 10, 07743 Jena, Germany.
E-mail addresses: anja.traeger@uni-jena.de (A. Traeger), ulrich.schubert@uni-jena.de (U.S. Schubert).
[1] Authors contribute equally to this work.

http://dx.doi.org/10.1016/j.jconrel.2015.08.008
0168-3659/

biodistribution of nanoparticles is influenced by the RES as nanoparticles once in the circulation interact with various plasma proteins such as opsonins (immune globulins and complement factor) as well as albumins influencing their fate in different manners [14,15]. The formed protein corona is strongly under investigation, but so far only a few interacting proteins were identified resulting in a predictable impact on the fate of nanoparticles [16,17]. Due to the complexity of the plasma protein composition with more than 3.700 proteins and several other factors, the corona is still rarely understood and its dynamic makes it difficult to analyze [14]. An important role in the RES for drug- and nanoparticle clearance plays the liver [18]. In particular Kupffer cells, the local tissue-macrophages but although their endothelial cells, possess phagocytic or endocytic activity against blood-borne materials entering the liver and contribute to tissue modulation and regulation of the immune system in response to stimulants [19–21]. Their close cellular interaction and communication was described as relevant for different diseases [22]. For a rational drug development, possible immune-modulatory effects as well as nanoparticle clearance are key factors that need to be investigated under physiological conditions [23].

Promising new developments to more accurately model the *in vivo* environments are dynamic (co)-cultures where cells are cultured and incubated under shear stress and different cell-types might interact with each other. Endothelial cells line the inner layer of the blood vessels and are in direct contact with the bloodstream. For this purpose, their cell biology as morphology, cytoskeleton, permeability, and the expression of important markers and surface proteins as well as cellular interactions are affected by shear stress [24,25]. This mechanical force evolved to an important factor investigating physiological processes in the context of endothelial substance interaction and internalization. Endothelial cells represent the first tissue barrier nanoparticles have to overcome to reach parenchymal target cells as it is often aimed. Not only endothelial cells but also local macrophages, in particular in the liver but also in other vessels, have direct contact to nanoparticles and might clear them, why we co-cultured primary macrophages with human umbilical vein endothelial cells (HUVECs) to better understand their influence on uptake. In particular new screening methods to test toxicity, permeability and transport of drugs are under investigation [23,26]. In a recent study, where liver-specific PLGA-based nanoparticles were used, the relevance of shear stress on nanoparticle-uptake in an artificial liver was presented [13]. To gain more insight into the impact of shear stress and co-culture of HUVECs and primary macrophages, well-known methacrylate-based nanoparticles can be applied. Methacrylates are non-biodegradable and, thus, particularly suited to analyze the internalization behavior depending on structural properties of nanoparticles, *e.g.*, surface charge or size. In addition, poly(methyl methacrylates) (PMMA) are proposed for vaccination [6,27].

Herein, we used a library consisting of co-polymers for nanoparticle preparation, poly((methyl methacrylate)-*co*-(methacrylic acid)) (P(MMA-*co*-MAA)) and poly((methyl methacrylate)-*co*-(2-dimethylamino ethyl-methacrylate)) (P(MMA-*co*-DMAEMA)) representing polymers with pH dependent anionic and cationic charges, respectively. Moreover, in the case of P(MMA-*co*-MAA) the amount of methacrylic acid was varied. Nanoparticles were formed *via* nanoprecipitation to circumvent the use of surfactants and to obtain narrow size distribution [28–30]. Previous results gathered from *in vitro* studies are only of limited use to screen nanoparticles for drug applications, since the results hardly represent the *in vivo* situation [31,32], revealing the lack of appropriate methods allowing investigation of nanoparticle uptake and clearance under physiological relevant conditions. In the case of the applied methacrylate-based nanoparticle library with comparable size we were able to demonstrate a different internalization. On one hand attributed to different charge density (3% PMAA *vs.* 13% PMAA) and on the other hand due to different charges (PMAA *vs.* PDMAEMA) were investigated under static *in vitro* and dynamic cell culture. The impact of particle charge and the influence of shear stress on nanoparticle internalization *in vitro* were systematically characterized. Finally, the results were compared to an *in vivo* mouse model verifying the dynamic co-cell culture as promising tool for screening nanoparticle uptake and clearance.

2. Results and discussion

2.1. Polymer and nanoparticle preparation and characterization

The co-polymers were synthesized *via* the reversible addition–fragmentation chain transfer (RAFT) polymerization technique [33,34] to obtain polymers with narrow molar mass distribution and tailored polymer properties, *i.e.*, a defined amount of carboxylic acid or amines and, therefore, a defined number of charges within the polymer. Here, pH dependent co-polymers were synthesized consisting on the one hand of negatively charged MAA units at basic conditions and on the other hand of cationic charges (DMAEMA units) at acidic conditions. The amount of charges of the polymer represents a crucial parameter for the nanoparticle formation and stability. Nanoparticles with zeta potentials above ± 20 mV are more stabilized by the repulsion forces compared to particles with zeta potentials below [35]. A fine-tuning of the pH dependency, which goes hand in hand with negative charges (–COOH groups), as well as the hydrophobicity (MMA units) was realized by synthesizing co-polymer libraries with a systematic variation in the compositions. Thus, MAA amounts of 3, 5, 8 and 13%, as well as 20% of DMAEMA were used as a co-monomer in the polymerization procedure. Both monomers MMA and MAA (or DMAEMA) were statistically distributed along the polymer chain due to the same reactivity ratio [36]. The low amounts of MAA or DMAEMA ensure the formation and stability of hydrophobic particles under physiological pH values. In the case of 20% PDMAEMA nanoparticles a swelling is assumed due to the protonation of the amine group at a decreased pH value (PDMAEMA $pK_a = 7.5$) [37,38] in endosomes/lysosomes [39].

Molar masses between $M_n = 11.700$ g mol^{-1} to 12.700 g mol^{-1} with dispersities lower than 1.2 were determined by size exclusion chromatography (SEC) for the final co-polymers (Table 1 and Fig. S1). The compositions (content of MMA and MAA or MMA and DMAEMA) were calculated using ^{1}H NMR spectroscopy. The observed values agree well with prospected theoretical amounts and are listed in Table 1. The benefit of these polymers for preparation of defined nanoparticles *via* nanoprecipitation was already demonstrated earlier [28,40,41]. An advantage of nanoprecipitation is the absence of surfactants, as they can influence the properties of nanoparticles and their biological impact [42,43]. Furthermore, nanoparticles with different diameters with narrow size distributions can easily be obtained. In this study nanoparticles of around 200 nm in diameter were chosen as at this size cellular internalization *via* endocytosis could be assumed [28]. The characterization of the nanoparticles was performed using dynamic light scattering (DLS) as well as scanning electron microscopy (SEM) measurements (Table 1, Figs. 1 and S2). The zeta potential measurements confirm the negative surface charges of nanoparticles consisting of PMMA-*co*-PMAA and positive charges for PMMA-*co*-PDMAEMA nanoparticles (Table S2).

2.2. Internalization of methacrylate-based nanoparticles in static cell cultures

Initially, the nanoparticles were investigated regarding their internalization in HEK293 cells. For this purpose, flow cytometry and confocal microscopy was used. Methacrylate-based particles are known to lead to an increased granularity or rather increased side scatter (SSC) in flow cytometry after internalization [28,44], To exclude the influence of cell size (forward scatter, FSC) the relative SSC/FSC was used as indication for successful nanoparticle internalization as it was also confirmed by nile red fluorescent intensity, encapsulated into different nanoparticles as a cargo. A clear correlation of cellular internalization rates depending on the PMAA amount of nanoparticles was observed.

Table 1
Polymer and nanoparticle characterization.

Polymer	M_n[a]	$Đ$[a]	Theo. ratio[b] MAA/D [%]	Exp. ratio[c] MAA/D [%]	Nanoparticle	D_H [nm][d]	PDI_P
P(MMA-*co*-MAA)	11.700	1.17	3.0	3.3	3% PMAA	196	0.061
P(MMA-*co*-MAA)	12.200	1.20	5.0	5.1	5% PMAA	193	0.097
P(MMA-*co*-MAA)	12.700	1.19	7.5	8.2	8% PMAA	207	0.099
P(MMA-*co*-MAA)	12.600	1.19	10.0	13.3	13% PMAA	205	0.079
P(MMA-*co*-DMAEMA)	11.000	1.10	20.0	20.8	20% PDMAEMA	207	0.101

[a] Calculated from SEC ($CHCl_3$), PMMA calibration.
[b] Molar ratio in the polymer feed solutions, MAA = methacrylic acid and D = dimethylamino ethyl methacrylate.
[c] Calculated from ^1H NMR spectroscopy. The homopolymer PMMA was used as reference (adjustment of the broad backbone integral from 0.5 to 2.5 ppm to exclude impurities like water) and all spectra were corrected with this ratio between $-OCH_3$ to the backbone signal of PMMA (correction factor 0.964).
[d] D_H represents the Z-average intensity weighted diameter.

Increasing amounts of PMAA resulted in an increased uptake of nanoparticles (Fig. 2A). In particular, the differences in the uptake behavior of 3% PMAA (rel. SSC/FSC = 1.2) and 13% PMAA (rel. SSC/FSC = 1.7) is remarkable. The differences in polymer composition and related negative charge increase of the particle surface as well as a decreased hydrophobicity appear to be beneficial for the cellular uptake. The cationic charged nanoparticles (20% PDMAEMA) displayed the highest cellular uptake (rel. SSC/FSC = 2). Increased internalization rate might be explained by the cationic charges that are known to be beneficial for interaction with the cell membrane [5]. Nanoparticles carrying negative as well as positive charges show an adsorption of serum proteins that impact their uptake efficiency [14,18]. The question arises whether the different cellular uptake of the methacrylate-based nanoparticles can be ascribed to the interaction with the cell membrane or rather to different protein coronas. Therefore, we tested the nanoparticle uptake of 3% PMAA, 13% PMAA and 20% PDMAEMA in the presence of fetal calf serum (FCS) in the cell culture medium (Fig. 2B). We found no impact of FCS on internalization of 13% PMAA and 20% PDMAEMA nanoparticles. In contrast, we observed a more efficient cellular uptake of 3% PMAA in the absence of FCS. Thus, we speculate that differences in cellular uptake of 3% and 13% PMAA nanoparticle are triggered by varying protein coronas depending on the exposed surface charges of nanoparticles and their interaction with the cell membrane. That the cellular uptake rates of 13% PMAA and 20% PDMAEMA are independent of the presence of proteins was not expected before, as in general a decreased uptake due to an increased protein interaction is assumed for nanoparticles formed of hydrophobic polymers [45,46]. Thus, further investigations are required to characterize the formation of the protein corona depending on surface charge density and the impact of its composition on cellular internalization. SDS-PAGE of nanoparticle bound proteins reveals a lack of distinct protein binding as well as a total reduction of bound proteins to the higher charged nanoparticles irrespectively if positively or negatively charged (Fig. S 3A, B).

As the sensitivity of relative SSC/FSC is limited and, moreover, restricted to flow cytometry analysis the hydrophobic dye nile red was encapsulated into the nanoparticles. The encapsulation efficiency varies depending on the hydrophobicity of the polymers. We tackled this obstacle by applying a correction factor determined for each nanoparticle batch (Table S3) [47]. To confirm the uptake measured by the relative SSC/FSC, the fluorescence intensity was also used showing a good correlation (Fig. S4). In addition, confocal microscopy was performed to verify the internalization of nanoparticles measured by flow cytometry (Fig. 3). All investigated nanoparticles were detectable inside the cells. 20% PDMAEMA shows higher fluorescence intensity and a more diffuse distribution compared to PMAA nanoparticle. This supports the assumption of swelling of nanoparticles under acidic conditions within the endosome.

The dependency of cellular uptake on charge amount and type were further confirmed in various cell types, including primary murine muscle cells (Table 2). Beside cell-type specific variations concerning the amount of internalized nanoparticles, two general trends were observed: With increasing negative charge, the cellular uptake was increased; however, the cationic charged nanoparticles were internalized more efficiently. Thus, the performance of the nanoparticles is mainly influenced by the particle composition depending on the polymer chemistry with an impact on the protein corona [48–50]. Therefore, the observed trends are independent of the used cell-types or if co-culture is used (Figs. 4 and S6). The nanoparticle uptake of HUVECs is significantly decreased due to cellular interactions. Further a significant decreased uptake in both cell-types was observed in contrast to the mono-culture.

Cytotoxicity is another highly relevant parameter for *in vivo* application of nanoparticles. Therefore, the hemo-compatibility of the nanoparticle library was tested using erythrocytes. We observed no release of hemoglobin or aggregation of erythrocytes promoting the nanoparticles suitable for *in vivo* investigations (Fig. S5).

Taken together, static *in vitro* studies depict relevant properties of nanoparticles: (i) Uptake effectiveness depending on nanoparticle characteristics, (ii) they enable crucial assays to understand the interaction of nanoparticles with soluble molecules of, *e.g.*, serum proteins, and (iii) they allow a first assessment of nanoparticle toxicity. In addition, by analyzing the cellular uptake in different cell types the same trend concerning an enhanced uptake of charged nanoparticles was observed. Interaction of particles and proteins were shown by SDS-PAGE,

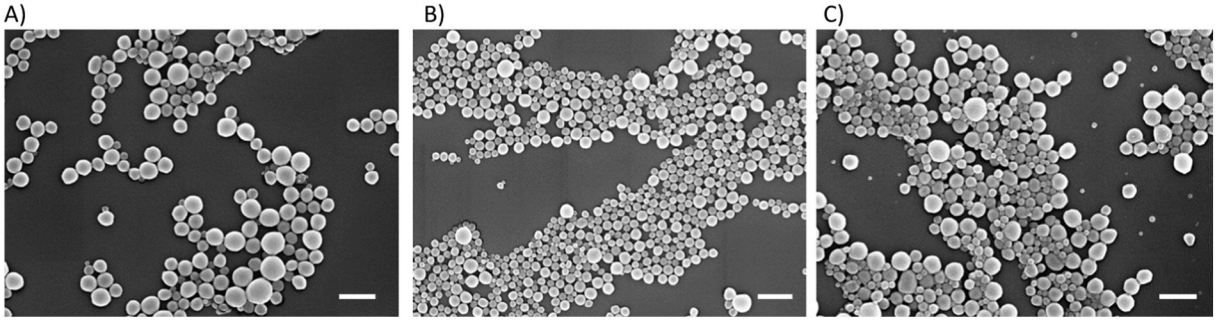

Fig. 1. SEM micrographs of methacrylate-based nanoparticles A (3% PMAA), B (13% PMAA) and C (20% PDMAEMA) confirm their spherical shape. Scale bar = 500 nm.

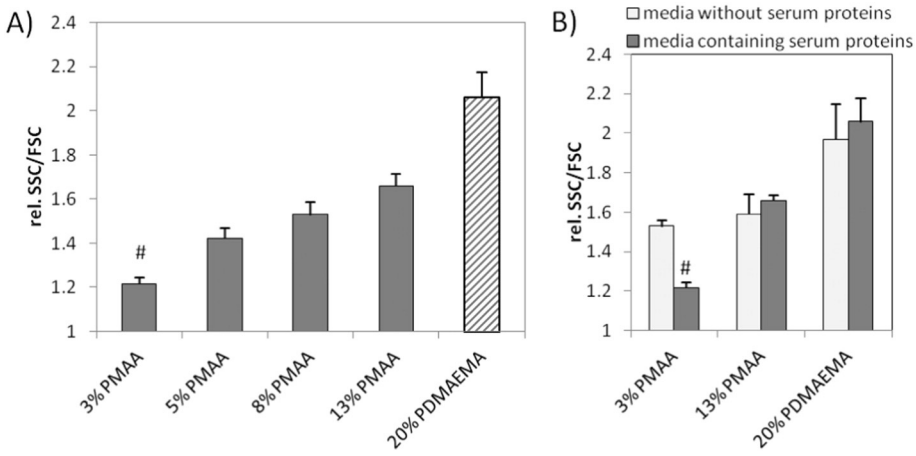

Fig. 2. Internalization of methacrylate-based nanoparticles in HEK293 cells treated for 24 h with 100 μg mL^{-1} nanoparticle in media containing FCS, rel. SSC/FSC regarding the control. A) Negative and cationic charged nanoparticle uptake, # represent significant differences compared to 20% PDMAEMA and B) comparison of nanoparticle uptake in media with and without serum. A, B) bars show mean + s.e.m of three independent experiments, significance tested using A) two-way ANOVA with Turkey's post-hoc test and using B) Kruskal-Wallis and Dunn's multiple comparison test, $p < 0.05$.

indicating serum interaction as one aspect of the internalization of nanoparticles, rising evidence for opsonization and RES interaction [16]. Common used *in vitro* blood compatibility tests like complement activation can be applied for first investigations, but these tests are also known to lead in false-positive results due to the optical properties of the nanoparticles [8]. In addition, static cell culture conditions provide sedimentation effects which are strongly altered under dynamic condition, *e.g.*, in the blood stream [51].

2.3. Internalization of methacrylate-based nanoparticles in dynamic cell cultures

Cell culture under dynamic conditions allows the investigation of nanoparticle binding and internalization under physiologically relevant *in vitro* conditions. In particular, the impact of different cell phenotypes of HUVECs [52] on the nanoparticle uptake under shear stress can be investigated in dynamic cell cultures [24,25]. Shear stress values from 0.7, 3.0, 6.0 and 10.0 dyn cm^{-2} were applied representing basal nutrient exchange with minimal mechanical stimulation observed *e.g.*, in hepatic sinusoids (0.7 dyn cm^{-2}) and shear stress values observed in human veins and venules (3.0 and 6.0 dyn cm^{-2}) [53], human suprarenal aorta (6.0 dyn cm^{-2}) and human common carotid artery (10.0 dyn cm^{-2}) [54]. Interestingly, increasing shear stress positively correlates with the total amount of internalized nanoparticles in mono-cultures (Fig. 5A, B). This indicates that nanoparticle-cell interactions are sufficient to induce adhesion and internalization even at high shear stress. In comparison, other studies investigating inorganic SiO_2-nanoparticles or polystyrene nanoparticles showed a reduced uptake under increasing shear stress conditions, even when antibodies where used as targeting moiety, suggesting that these nanoparticles would have sufficient target-cell interactions *in vivo* [25,55,56]. The findings of the methacrylate-based nanoparticle concerning shear stress can be attributed to a higher frequency of nanoparticle interaction per cell compared to static *in vitro* conditions. Dynamic cell culture revealed a different nanoparticle uptake as seen under static *in vitro* conditions: Uptake of 13% PMAA nanoparticles occurred more efficiently compared to 20% PDMAEMA, whereas the uptake of 3% PMAA was of significant lower efficiency (Fig. 4B). Shear stress higher than 6 dyn cm^{-2} does not increase the uptake of 20% PDMAEMA but reaches a plateau. Nanoparticles composed of 20% PDMAEMA differ from PMAA containing particles in respect to their ability of swelling under acidic conditions. A plateau for cellular uptake was reached at 3 dyn cm^{-2} for 20% PDMAEMA indicating a sufficient interaction of nanoparticles with the cell membrane, since the uptake was significantly decreased at even higher shear stress. Thus, tendencies between different nanoparticles, which were obtained under static conditions, differ under dynamic conditions. In particular, the uptake rate of the 20% PDMAEMA under flow conditions is reduced to comparable levels as 13% PMAA. This might be due to an activation of HUVEC under

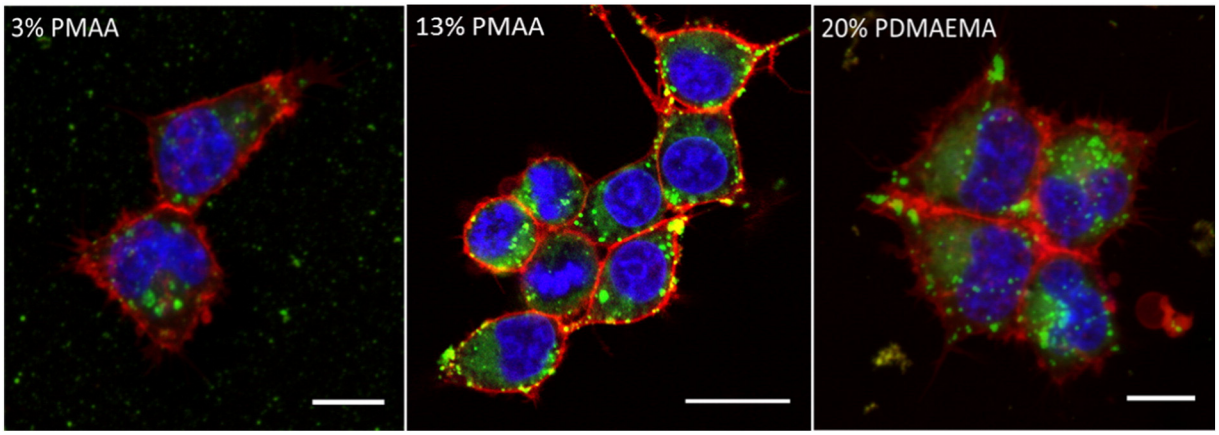

Fig. 3. Internalization of methacrylate-based nanoparticles. HEK293 cells were stained with Hoechst for DNA-staining (blue) and CellMask DeepRed (red) for plasma membrane staining previous to the addition of nanoparticles (green). Images were taken 25 to 30 min after addition of nanoparticles. Scale bar = 10 μm. (For interpretation of the references to color in this figure legend, the reader is referred to the web version of this article.)

Table 2
Internalization of methacrylate-based nanoparticles in cell lines of different origin analyzed after 24 h *via* flow cytometry. The MFI was used as readout (n = 3) and was rated into very low uptake (− = MFI < 15), media uptake (+ = 15 < MFI < 50), high uptake (++ = 50 < MFI < 150) and very high uptake (+++ = MFI > 150).

	Cell line	3% PMAA	13% PMAA	20% PDMAEMA
Immortal	HEK 293	−	+	+
	L929	−	+	++
	HepG2	−	−	+
primary	Primary muscle cells	−	+	++
	Differentiated muscle cells	+	++	+++
	HUVEC	−	+	++
	MΦ	−	+	++

dynamic conditions leading to a different surface receptor expression pattern [25,33].

Furthermore cell–cell interactions, known to influence cellular physiology, have to be taken into consideration. For this purpose, a co-culture composed of MΦ and HUVEC, assembled in a reproducible composition and cultured under standardized conditions, was used for dynamic cell culture experiments (Fig. 5). In particular, the contribution of macrophages for nanoparticle uptake with consideration to heterogeneous cell interactions between macrophages and the endothelial lining was investigated. MΦs are known to be responsible for clearance of circulating nanoparticles in the blood stream by phagocytosis [8]. In the presence of MΦ, a shear stress dependent increased uptake of nanoparticles in HUVECs was observed. MΦ in general exhibited a higher uptake rate compared to HUVEC. Compared to the HUVEC mono-culture, the presence of MΦ strongly decreased the nanoparticle uptake through HUVECs (Fig. 5B). It is not likely that reduced nanoparticle uptake by HUVECs is simply due to an increased uptake rate through MΦ. It can be assumed that the proportion of nanoparticles in the medium in relation to the perfused cell cluster of HUVEC and MΦ will outbalance possible local concentration gradients formed by elevated uptake kinetics. This gains importance in particular under high perfusion conditions, where most of the prominent differences in uptake rates have been observed. The presence of primary human MΦ in co-culture was accompanied by a decreased endothelial uptake observed for all applied nanoparticles. In addition, a release mechanism for 13% PMAA can be assumed as 13% PMAA as well as 20% PDMAEMA lead to a homogeneous staining of the cytoplasm (Figs. 3, 5A). The investigations in static and dynamic cell culture conditions lead to the assumptions that the 13% PMAA as well as the 20% PDMAEMA would be also taken up by macrophages *in vivo*. In addition, the uptake of 13% PMAA and 20% PDMAEMA nanoparticles should be enhanced compared to the 3% PMAA nanoparticle. Concerning the uptake-tendencies between the different nanoparticles in the co-culture experiments, similar patterns were obtained under static and dynamic conditions at 3 and 6 dyn cm^{-2}, respectively (Figs. 4, 5). However, at 0.7 dyn cm^{-2}, which is assumed to be present in hepatic sinusoids, the uptake of 13% PMAA and 20% PDMAEMA did not significantly differ in contrast to the results under static conditions.

2.4. Internalization of methacrylate-based nanoparticles in vivo

The liver is composed of four major cell types: endothelial cells, local macrophages (Kupffer cells), stellate cells and hepatocytes. The liver sinusoidal endothelial cells (LSECs) represent a specialized subset of endothelial cells, whereas HUVEC reflect endothelial cells of the vasculature [57]. A major obstacle in *in vitro* studies and their translation to the *in vivo* situation is the missing consideration of biodistribution within an organism. It is considered as necessary to avoid the accumulation of nanoparticles in the RES, however often it is hardly discriminated, which cell type is affected. While hepatocyte mainly function as metabolic and detoxifying cells, Kupffer cells are known to clear all kinds xenobiotics effectively and trigger local and global responses to these molecules. Using intravital microscopy we could observe the cellular-distribution of 3%, 13% PMAA and 20% PDMAEMA nanoparticles in the liver. *In vivo* Kupffer cells mainly cleared all tested nanoparticles in the liver. However to a lesser extend also LSECs — liver-specific endothelial cells — took up especially 13% PMAA and 20% PDMAEMA nanoparticles (Fig. 6A). Beside the differences in the cellular distribution also the speed and kinetic of nanoparticle-uptake varies between nanoparticles. 20% PDMAEMA were taken up fastest (4.6% per min) followed by 13% PMAA nanoparticles (3.8% per min). The slowest uptake had low-charged (3% PMAA) nanoparticles (1.9% per min) (Fig. 6B). These different uptake kinetics and cellular distribution represent the different ability to unspecifically interact with cellular membranes and subsequently activate endocytotic or phagocytotic pathways. The uptake of all nanoparticles reached a plateau after 30 to 60 min reflecting a saturation of the processes or a clearance of the nanoparticles in the

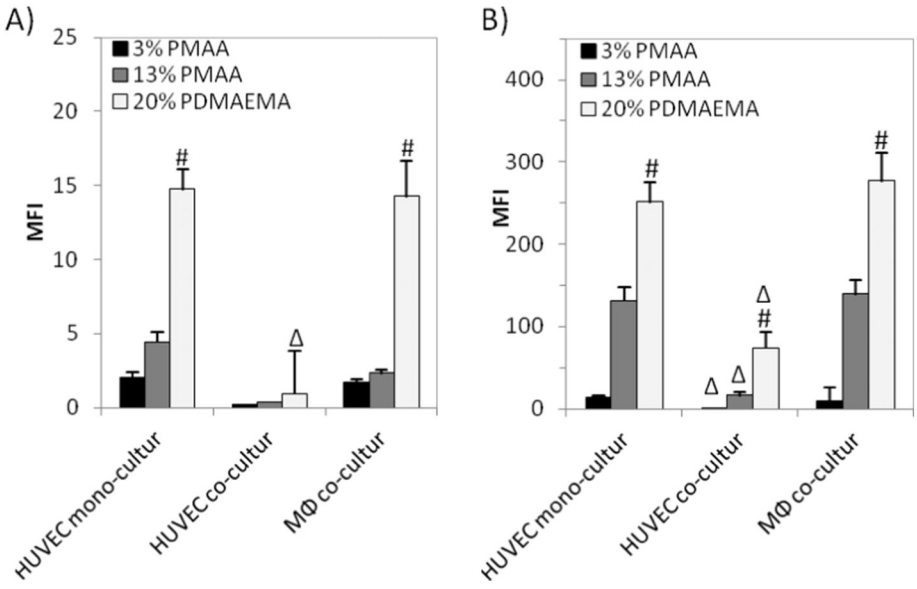

Fig. 4. Internalization of methacrylate-based nanoparticles in mono-culture and co-culture of HUVEC and MΦ treated for 1 h with 200 μg mL^{-1} nanoparticles. A) Analysis *via* flow cytometry and B) *via* microscopy # represent significant differences of 3 and 13% PMAA compared to 20% PDMAEMA within the different cultures, Δ represent significant differences of the cell types in co-culture compared to the corresponding mono-culture. The bars show mean + s.e.m of three independent experiments, significance using two-way ANOVA with Turkey's post-hoc test $p < 0.05$.

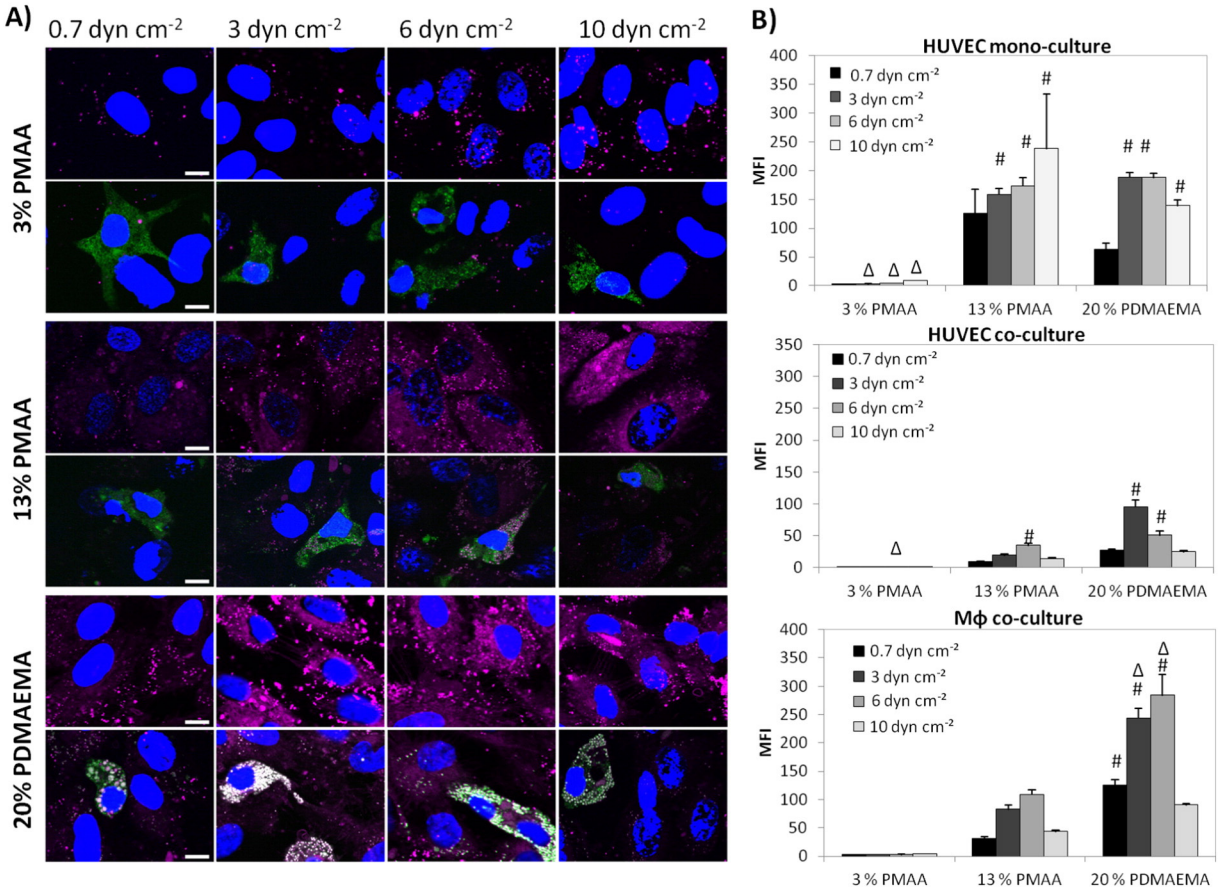

Fig. 5. Different nanoparticles in the dynamic cell culture. A, B) Uptake of different nanoparticles containing nile red in a HUVEC monoculture or a co-culture with MΦ which were subjected to different shear stress (0.7, 3, 6 or 10 dyn cm^{-2}) were analyzed after 60 min. A) Uptake and distribution of different nanoparticles (purple) in the HUVEC monoculture (upper panels) and co-culture (lower panels) with MΦ. Cells were subsequently stained with DAPI (blue) and macrophages were stained using CMFDA (green). All scale bars = 10 μm. B) Measured and analyzed MFI in HUVECs or MΦ. MFI were corrected using the calculated correction factor mentioned earlier. Differences between groups were analyzed using a two-way ANOVA with Tukey's post-hoc test performed on three independent experiments. #: $p < 0.05$ significant differences to 3% PMAA of corresponding dyn cm^{-2}. Δ: $p < 0.05$ for the differences between the 13% PMAA NP-uptake to the corresponding dyn cm^{-2}. (For interpretation of the references to color in this figure legend, the reader is referred to the web version of this article.)

body (Fig. 6B). The MFI of 20% PDMAEMA even decreased constantly by 0.5% per min after 30 min within the time of observation, implying a release of nile red from 20% PDMAEMA. Finally we also compared the uptake of the nanoparticles in Kupffer cells *in vivo* revealing that higher charged ones (13% PMAA and 20% PDMAEMA) are cleared more effective than the low charged 3% PMAA and that Kupffer cells showed a higher uptake than endothelial cells. However, higher charged nanoparticles excerpt a smaller difference between the uptake in Kupffer cells and endothelial lining (Fig. 6C). The uptake in the static cell culture clearly showed a significant increased uptake of 20% PDMAEMA, which was also present in the co-culture experiments at 3 and 6 dyn cm^{-2}. However, at 0.7 dyn cm^{-2} the differences between 13% PMAA and 20% PDMAEMA are less pronounced in the co-culture (Fig. 5B).

3. Conclusion

Studies on nanoparticle uptake and transferability from *in vitro* to *in vivo* are necessary but challenging. Thus, methods for pre-screening of nanoparticle-cell interaction under physiological relevant conditions are required. In particular, the interaction of nanoparticles with immune cells responsible for unwanted clearance is important but unknown after *in vitro* investigations. It was previously shown that static *in vitro* studies underestimate effects and effectiveness of nanoparticle uptake and clearance *in vivo* [13]. In this study, we could demonstrate that the dynamic cell culture mimics shear-stress as one key-factor influencing nanoparticle uptake in general and might represent an important screening option for cell-type specific nanoparticle uptake. In particular in the case of the HUVEC mono-culture the tendencies of nanoparticle uptake were different between static and dynamic conditions. The dynamic cell culture influences the uptake tendencies of the tested nanoparticles, leading to decreased uptake of 20% PDMAEMA whereas under static conditions 20% PDMAEMA showed the highest uptake. Previously it was shown that applying shear-stress results in different surface receptor expression patterns which might lead to an increased uptake of the 13% PMAA whereas the uptake of 20% PDMAEMA seems to be not influenced by this HUVEC activation.

Diminished cell-interactions of low-charged non-targeted nanoparticles (3% PMAA) might lead to reduced and unspecific uptake. However, insufficient cellular membrane interactions might also compromise the nanoparticle uptake resulting in a shear-stress dependent decrease of uptake efficiency, demonstrated by previous studies of CdTe-quantum dots and SiO_2-based nanoparticles [25]. Another study tested vascular cell adhesion molecule (VCAM)-1-antibodies as targeting moiety conjugated to the surface of inorganic nanoparticles to address only activated endothelial cells [55]. Despite an increased uptake in cells expressing VCAM-1 under static culture conditions, subjecting these cells to flow lead to a decrease of uptake effectiveness. However, nanoparticle carrying VCAM-1-conjugated antibodies still showed a significant higher uptake. These studies reveal the importance of balancing the interaction of nanoparticles to ensure a specific uptake under certain circumstances but preventing unspecific nanoparticle interaction.

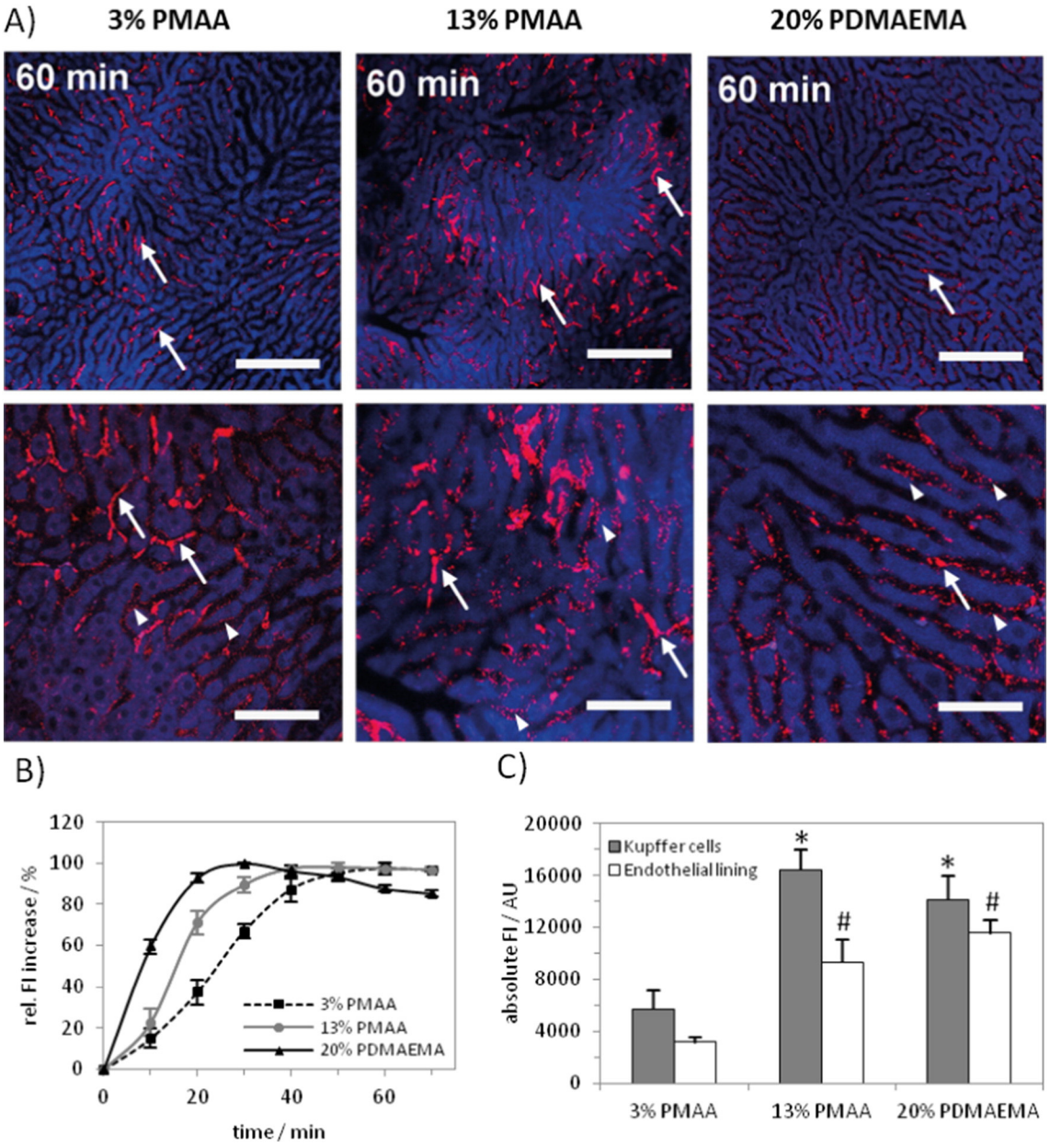

Fig. 6. A) Intravital microscopy of different nanoparticles in the liver (liver architecture: blue, nile red containing nanoparticles red) showing accumulation of nanoparticles mostly in Kupffer cells (examples marked with white arrows) and only little in endothelial cells (examples marked with a white triangle); scale bar for upper column is 250 μm, lower column is 50 μm. Contrast of all images were harmonized. B) Uptake kinetic of nile red containing nanoparticles in Kupffer cells *in vivo*; graph show mean ± s.e.m. of three independent experiments. C) Maximal fluorescence intensity of PMAA and PDMAEMA-nanoparticles containing nile red in murine Kupffer cells and endothelial lining in the liver 30 min (PDMAEMA) or 60 min (PMAAs) after administration. Significance was tested using a two-way ANOVA with Tukey's post-hoc test performed on three independent experiments; $p < 0.01$ between 13% PMAA or 20% PDMAEMA and 3% PMAA in * Kupffer cells or # endothelial lining. # $p < 0.01$ between both cell types of one nanoparticle. (For interpretation of the references to color in this figure legend, the reader is referred to the web version of this article.)

Beside the influence of shear stress, monocultures lack cell–cell interactions and the resulting impact on the nanoparticle uptake. Based on the cell culture and supported by *in vivo* investigations, we showed that co-cultured macrophages have a severe impact on endothelial uptake of all nanoparticles tested. Further studies are required to characterize the underlying mechanism and to design nanoparticles in a way to prevent this inhibitory effect on endothelial cells. Besides, the question arises if also tumor-associated macrophages play a role in modulating the nanoparticle uptake in cancer cells leading to a reduced efficacy of nanoparticle-based tumor therapy or whether this is an effect restricted by the vascular endothelium [58].

This study shows that static cell cultures represent a fast and useful tool to assess nanoparticle uptake in general. Assessing nanoparticle uptake in primary endothelial cells is significantly influenced by physiological shear stress. We therefore suggest that investigation of nanoparticle uptake in endothelial cells should be performed under dynamic conditions where physiological relevant shear stress conditions could be resembled. In macrophage rich environments the effects of endothelial cell activation seems to be overwhelmed, likely due to macrophage derived factors effecting endothelial nanoparticle uptake. Considering the applied shear stress of 0.7 dyn cm^{-2} less pronounced differences between the uptake of 13% PMAA and 20% PDMAEMA under dynamic conditions were obtained in contrast to static conditions. This demonstrates the importance of shear stress on nanoparticle uptake. Since animal experiments are resource and time consuming, new models and automated systems for dynamic cell culture should be developed for screening purposes to increase the success of new animal studies.

4. Experimental section

4.1. Materials

MMA, MAA and DMAEMA were purchased from Sigma Aldrich and purified with an inhibitor-remover before use. 2,2′-azobis-(isobutyronitrile) (AIBN) was recrystallized from methanol prior to use. The chain transfer agent 2-cyano-2-propyl dithiobenzoate (CPDB) and the dye nile red was purchased from Sigma Aldrich.

4.2. Polymer synthesis and characterization

The co-polymers P(MMA-*stat*-MAA), were prepared by co-polymerization of MMA with MAA using the RAFT polymerization method [33,34]. In a typical RAFT co-polymerization experiment (3 mol% MAA as example, all polymerization conditions are listed in the SI), 5.827 g of MMA monomer (58.2 mmol), 0.155 g of MAA monomer (1.8 mmol), 24.63 mg of AIBN initiator (0.15 mmol), 132.8 mg of CPDB RAFT agent (0.6 mmol) and 5.16 mL ethanol were mixed together in a 25 mL reaction vial. The monomer concentration was kept at 4 mol L^{-1}. Subsequently, the reaction solution was placed in a preheated oil bath at 70 °C for 10 h. The copolymer was purified by precipitation into a large volume of cold diethyl-ether and dried under reduced pressure. ^{1}H NMR (CD_2Cl_2, 300 MHz): $\delta = 7.89$ (d, Ar-H, CPDB), 7.57 (t, Ar-H, CPDB), 7.41 (t, Ar-H, CPDB), 3.60 (–OCH_3), 2.25–0.5 (backbone) ppm. SEC ($CHCl_3$, PMMA standard): M_n = 12.700 g mol^{-1}, $Đ = 1.17$. All RAFT polymerizations and polymer analysis by SEC and ^{1}H NMR can be found in the supplementary information.

4.3. Instrumentation

Size-exclusion chromatography (SEC) experiments were performed on a Shimadzu system equipped with a SCL-10A system controller, a LC-10AD pump, a RID-10A refractive index detector, a UVD SPD-10AD UV/Vis detector and a PSS SDV linear S, 5 μm column (8 × 300 mm) with chloroform/triethylamine/2-propanol (94:4:2) as eluent at 1 mL min^{-1}, and the column oven was set to 40 °C. A calibration with low dispersity polystyrene standards (ranging Mn from 376 to 128,000 g mol^{-1}) was used.

^{1}H NMR spectra were recorded on a Bruker AC 300 (300 MHz) spectrometer at 298 K. The chemical shifts are reported in parts per million (ppm, δ scale) relative to the signals from the NMR solvents.

4.4. Preparation and characterization of nanoparticles

The nanoparticles used in this study were prepared by nanoprecipitation [28]. For this purpose, 25 to 30 mg of the distinguished polymer was dissolved in 1 mL acetone. For the preparation of nile red containing nanoparticles, 1 mg mL^{-1} nile red was diluted in acetone as stock-solution. Then, 250 to 300 μg of nile red was added from the stock- to the polymer-solution. The obtained solution was dropped into 10 mL of type 1-water. A 120 × 0.8 mm syringe was used to drop 100 to 200 μL of the polymer-solution per minute into the 10 mL type 1-water under permanent stirring (300 to 500 rpm) on a magnetic stirrer (Magnetic Stirrer MR Hei-Standard). Afterwards, the nanoparticle-suspension was stirred overnight for evaporation of acetone. The acetone-free nanoparticles with encapsulated nile red were shortly centrifuged for 10 to 20 s at 1620 ×*g* to remove all non-encapsulated nile red. Finally, the supernatant was diluted with type 1-water to the desired concentration.

The sizes of the nanoparticles were characterized by DLS on a Zetasizer Nano ZS (Malvern Instruments, Germany) with a He–Ne laser operating at a wavelength of λ = 633 nm. The detection of the counts occurs at an angle of 173°. All measurements were carried out at 25 °C after an equilibration time of 120 s. For analyzing the autocorrelation function the CONTIN algorithm was applied [59]. The apparent hydrodynamic diameter was calculated according to the Stokes–Einstein equation. The zeta potential of the nanoparticles was analyzed using the Zetasizer Nano ZS by applying laser doppler velocimetry. 20 runs were performed for each measurement using the slow-field reversal and fast-field reversal mode at 150 V. The experiment was performed in triplicate at 25 °C. The zeta potential (ζ) was calculated from the electrophoretic mobility (μ) according to the Henry Equation. Henry coefficient f(ka) was calculated according to Oshima [60].

Scanning electron microscopy (SEM) characterization was performed as follow: Nanoparticle suspensions were diluted with deionized water (~1.0 mg mL^{-1}). One droplet of the suspension was placed on a mica surface and dried in vacuum. Finally, the samples were coated with platinum (4 nm), using a BAL-TEC MED020 sputtering device (Bal-Tec AG, Lichtenstein). SEM measurements were performed on a Zeiss SIGMA VP Field Emission SEM equipped with the GEMINI column (Carl-Zeiss AG, Germany) operating at 3 to 7 kV using the InLens or SE2 detector.

The encapsulation efficiency and thus the fluorescence intensity vary dependent on the used polymers. For comparison of the fluorescence intensities a correction factor was applied [47]. Therefore, the nanoparticle stock solutions were diluted to 0.2 μg mL^{-1}, 100 μg mL^{-1} and 200 μg mL^{-1} and the fluorescence intensity was analyzed at the GENios Pro fluorescence microplate reader (Tecan, Germany). The nanoparticles were excited at $\lambda_{Ex} = 488$ nm (bandwidth 9 nm) and the emission was measured at $\lambda_{Em} = 575$ nm (bandwidth 20 nm). The correction factor represents the relative values of the slope of the fluorescence intensity against the nanoparticle concentration [47].

4.5. Hemolysis assay and erythrocyte aggregation

The membrane damaging properties of the polymers were quantified by analyzing the release of hemoglobin from erythrocytes. The hemolysis assay was performed as described before [41]. Briefly, blood from sheep was centrifuged at 4 500 ×*g* for 5 min and the pellet was washed three times with cold Dulbecco-PBS (DPBS). The stock solutions were diluted in DPBS and 100 μL of each nanoparticle solution at the indicated concentration were mixed and further incubated for 60 min at 37 °C. The release of hemoglobin in the supernatant was determined at 580 nm after centrifugation (2 400 ×*g* for 5 min). The absorbance was measured using a plate reader. For comparison, the collected erythrocytes were washed with DPBS and either lysed with 1% Triton X-100 (Sigma Aldrich, Germany) yielding the 100% lysis control value (A_{100}) or re-suspended in DPBS as reference (A0). The hemolytic activity of the nanoparticles was calculated as follow (1):

$$Hemolysis = \frac{100 * (A_{sample} - A_0)}{(A_{100} - A_0)}. \quad (1)$$

Here, A_{sample}, A_0, and A_{100} are the absorbance intensities of a given sample, erythrocytes incubated with DPBS, and erythrocytes lysed with Titon X-100.

For the erythrocyte aggregation 100 μL of the suspension were mixed with nanoparticle solution of the same volume and incubated for 2 h at 37 °C. bPEI 25 kDa was used as negative control at a concentration of 50 μg mL^{-1}. The erythrocytes aggregation was evaluated by microscopy. The analysis of hemolysis and erythrocyte aggregation was repeated with blood from at least three independent donors.

4.6. Culture of immortal cells

If not stated otherwise, cell culture materials, cell culture media, and solutions were obtained from Biochrom GmbH (Germany). The cells were cultured at 37 °C in a humidified 5% CO_2 atmosphere. HEK293 cells (CLR-1573, ATCC) were maintained in RPMI 1640, L929 cells (CCL-1, ATCC) in Dulbecco's MEM with stable L-glutamine and HepG2

(DSMZ, Germany) were cultured in DMEM/Ham's F-12. The media were supplemented with 10% fetal calf serum, 100 μg mL^{-1} of streptomycin, 100 IU mL^{-1} of penicillin and in the case of the HEK293 cells 2 mM L-glutamine were added.

4.7. Human umbilical vein endothelial (HUVEC) cell culture

HUVEC were isolated from human umbilical cord veins through collagenase digestion as previously described [61]. Experiments were performed with HUVECs up to passage 4 cultured in Endothelial Cell Growth Medium MV (PromoCell, Germany).

4.8. Peripheral blood mononuclear cell (PBMC) culture and macrophage differentiation

PBMCs were freshly isolated immediately after collecting donor blood from healthy volunteers. The donors were informed about the aim of the study and gave written informed consent. Blood sample volume was diluted two times with PBS without calcium and magnesium (Biochrom AG, Germany) containing 0.1% bovine serum albumin (BSA, Carl Roth, Germany) and 2 mM EDTA (Sigma-Aldrich, Germany; isolation buffer). PBMCs were obtained from density gradient centrifugation using Biocoll separating solution (Biochrom AG, Germany). The cells were washed subsequently in isolation buffer for several times and were finally strained by a 40 μm molecular mesh (BD Bioscience, Germany). For monocyte enrichment 10^7 PBMCs per well were plated on a six well plate in 2 mL X-VIVO 15 (Lonza, Germany) supplemented with 10% autologous serum, 10 ng mL^{-1} GM-CSF (PeproTech, Germany), 100 units mL^{-1} penicillin, and 100 μg mL^{-1} streptomycin (Life Technologies, Germany). The cells were washed with plain X-VIVO 15 medium after 3 h of incubation and fresh medium with supplements (stated above) was added. Including the preparation time for flow culture nanoparticle experiments, macrophage (MΦ) differentiation was performed for five days.

4.9. Fluorescence activated cell sorting (FACS) of satellite cells and myotube differentiation

For the culture of primary myoblasts, satellite cells were purified by FACS as described elsewhere [62,63]. 8 to 12 weeks old C57BL/6 were sacrificed and the muscles from hind limbs were prepared and collected in PBS. Muscle tissue was washed in PBS, minced with scissors and digested in DMEM containing 650 U mL^{-1} collagenase-solution (Biochrom, Germany) for 90 min at 37 °C with agitation (70 rpm). Digested muscle tissue was washed with PBS supplemented with 10% fetal calf serum, triturated and incubated again in Collagenase (100 U mL^{-1}, Biochrom, Germany) and Dispase (2.4 U mL^{-1}, Life Technologies, Germany) for 30 min at 37 °C with agitation (100 rpm). The muscle slurry was further diluted with PBS supplemented with 10% fetal calf serum, filtered through 100 μm cell strainers and pelleted at 500 ×*g* for 5 min. Pellets were re-suspended in 10 mL FACS buffer (Hank's Balanced Salt Solution (HBSS), Life Technologies, Germany) containing 2% fetal calf serum (Biochrom, Germany) and filtered through 40 μm cell strainers and pelleted again at 500 ×*g* for 5 min. Pellets were re-suspended in 500 μL FACS buffer and stained with anti-mouse CD45 APC conjugate (30-F11, 1:200, eBioscience), anti-mouse CD11b APC conjugate (M1/70, 1:800, eBioscience, USA), anti-mouse Sca-1 APC conjugate (D7, 1:800, eBioscience, USA), anti-mouse/rat CD29 PE conjugate (ß1-Integrin, 1:400, Biolegend, USA) and biotinylated anti-mouse CD184 (CXCR4, 1:100, BD Bioscience, USA) for 20 min at 4 °C on a rotating wheel. Cells were washed with 5 mL FACS buffer and pelleted at 500 ×*g* for 5 min. Pellets were re-suspended in 500 μL FACS buffer and incubated with Streptavidin Cy7-PE conjugate (1:100, eBioscience, USA) for 20 min at 4 °C on a rotating wheel. Live cells were identified as calcein blue positive (1:1000, Life Technologies, Germany) and propidium iodide negative (1 μg mL^{-1}, BD Bioscience). Satellite cells were identified as $CD45^-$ $Sca\text{-}1^-CD11b^-CXCR4^+\beta1\text{-}integrin^+$ [63]. Cell sorting was performed on FACSAriaIII (BD Bioscience, USA) equipped with 405 nm, 488 nm and 633 nm lasers, respectively.

Satellite cells were sorted into growth medium comprised of F10 (Life Technologies, Germany) with 20% horse serum (PAA Laboratories), 500 U mL^{-1} penicillin/streptomycin (Life Technologies, Germany) and 5 ng mL^{-1} basic fibroblast growth factor (bFGF) (Sigma Aldrich, Germany) and maintained in 3% oxygen in collagen and laminin coated well-plates with fresh bFGF added daily. For the coating, well plates were incubated with collagen type I from rat tail (1 mg mL^{-1}, Sigma Aldrich, Germany) and laminin (10 mg mL^{-1}, Life Technologies, Germany) in type 1-water for at least 1 h at 37 °C and allowed to air-dry. To be considered as primary myoblasts, satellite cells were cultured for at least 1 week. For passaging, primary myoblasts were incubated with 0.5% trypsin (Life Technologies, Germany) in PBS for 3 min at 37 °C and collected in FACS buffer.

Primary myoblasts were passaged up to 70 to 80% confluence, and growth medium was replaced by differentiation medium comprised of DMEM with 2% horse serum and 500 U mL^{-1} penicillin/streptomycin (all Life Technologies, Germany). Myoblasts were allowed to differentiate into myotubes for five days.

4.10. Internalization of nanoparticles in static cell cultures

Cells were seeded with a density of 10^5 cells per well in 12-well plates. The growth medium was replaced by fresh medium 30 min before the addition of nanoparticles with indicated concentrations. After 24 h or 1 h incubation at 37 °C and with 5% CO_2, cells were analyzed *via* flow cytometry (FC 500, Beckman Coulter, Germany). Viable cells were identified by SSC/FSC and nanoparticle containing cells identified *via* their increased fluorescence (for nanoparticles with encapsulated nile red) or by increased side scatter (SSC). To avoid the detection of cells with attached nile red containing nanoparticles at the cell surface, 10% trypan blue (Sigma Aldrich, Germany) was added before the measurement to quench outer fluorescence. The relative SSC/FSC or mean fluorescence intensity (MFI) of at least 10^4 viable cells was used to quantify internalization of the nanoparticles. In case of the co-culture experiments (HUVECs and MΦ) the MΦ cells were stained with specific anti-human CD45 antibody (FITC-conjugated, ImmunoTools, Friesoythe, Germany). For this purpose, the cells were centrifuged at 200 *g* for 5 min at room temperature (RT), the pellet was washed with 200 μL DPBS and further centrifuged (300 *g*, 5 min, RT). Before adding 2 μL antibody, the pellet was suspended in 50 μL DPBS and afterwards incubated for 30 min on ice. Subsequently, the cells were centrifuged (300 *g*, 5 min, RT) and re-suspended in 500 μL DPBS for flow cytometry investigations. All experiments were performed independently for three times.

4.11. Confocal live-cell imaging

HEK293 cells were seeded in cell-view chamber slides (Greiner Bio-One, Germany) at a density of 10^5 cells per well and cultured as described above. After 24 h, cells were stained by adding 2 μg mL^{-1} bisBenzimide H 33258 (Sigma Aldrich, Germany) and 5 μg mL^{-1} CellMask DeepRed (Life Technologies, Germany). After 10 min under normal growth conditions cells were washed twice with pre-warmed HBSS (Life Technologies, Karlsruhe, Germany) twice and OptiMEM (Life Technologies, Germany) was added. Confocal live-cell imaging was performed on a laser scanning microscope (LSM-780, Zeiss AG, Germany) at 37 °C in a humidified 5% CO_2 atmosphere. H33258 was excited with a laser diode at 375 to 405 nm. Emitted light of 410 to 485 nm was collected on a photomultiplier tube. Different nanoparticles containing nile red at a concentration of 25 μg mL^{-1} were imaged through excitation at 488 nm (argon-ion laser) and fluorescence was detected using a gallium arsenide phosphide detector through a

500 nm long pass for 40 min. Fluorescence analysis of nanoparticle uptake were performed with ImageJ 1.46r (NIH, USA).

4.12. Internalization of nanoparticles in dynamic cell cultures

Rhombic chamber chips (RCC) were obtained from microfluidic ChipShop (Jena, Germany). Microfluidic cell culture experiments were performed under sterile environmental conditions of 5% CO_2, 70% air humidity and 37 °C. Monocytes were harvested 24 h after isolation by treatment with 4 mg mL^{-1} lidocaine (Sigma-Aldrich, Germany) and 5 mM EDTA. Confluent HUVECs were detached using trypsin. Monocytes were stained with 1 μM CellTracker green CMFDA (Life Technologies, Karlsruhe, Germany) for 45 min in serum-free X-VIVO 15. Subsequently monocytes and HUVECs were pooled 1:3 in Endothelial Growth Medium MV supplemented with 10% autologous serum, 10 ng mL^{-1} GM-CSF and 100 U mL^{-1} penicillin and 100 μg mL^{-1} streptomycin and seeded at a density of 1.3×10^5 HUVECs cm^{-2} and 0.43×10^5 monocytes cm^{-2} into RCC. Medium was changed on a daily basis. Mϕ differentiation was performed in presence of GM-CSF for 72 h under static culture conditions. HUVEC were perfused using peristaltic pumps (Ismatec REGLO digital MS-CA-4/12-100, Germany). Shear stress within RCC was calculated as previously described [24]. Shear stress of 0.7, 3.0, 6.0 and 10.0 dyn cm^{-2} was applied for 24 h following 60 min nanoparticle uptake at a concentration of 200 μg mL^{-1}. Negative charged nanoparticles containing nile red were solved in Endothelial Cell Growth Medium MV without additives. Cells were mounted with VectaShield Hard Set H-1500 with DAPI (Biozol, Germany).

Immunofluorescence microscopy was performed with Axio Observer.Z1 controlled by AxioVision 4.8.2 SP 3 software (both from Zeiss, Germany). Fluorescence analysis and quantification of nanoparticle uptake were performed with ImageJ 1.46r (NIH, USA).

4.13. Protein binding to nanoparticles and SDS-PAGE

To assess serum protein binding to nanoparticles, 0.5 mg nanoparticles were added to 1 mL RPMI 1640 containing 10% fetal calf serum, mixed gently by inverting the tube several times and incubate for 10 min at 37 °C and humidified 5% CO_2 atmosphere. Afterwards, nanoparticles were washed twice using centrifugation (10 600 ×*g*, 10 min). Medium was removed and nanoparticles were re-suspended in 2 mL PBS without calcium and magnesium.

4.14. Animals

Animal studies were conducted in accordance with animal welfare legislation under pathogen-free conditions in the animal facility of the Jena University Hospital. During all procedures and imaging methods, animals remained under deep general anesthesia using Desflurane (Baxter, USA) and pain-reflexes were assessed to gauge the depth of anesthesia. The body temperature further was permanently kept on 37 °C using feed-back controlled heating plates.

4.15. Intravital microscopy

A tail-vein catheter was made attaching the tip of a 30 gauge-needle to polyurethane tubing (inner diameter of 0.30 mm and an outer diameter of 0.64 mm) (AgnTho's, Sweden). The catheter was then sterilized by formaldehyde fumigation before placed in the tail-vein of male FVB/NRj mice. Afterwards the left lateral abdomen was shaved and opened by a 1 cm vertical incision. The ligamentum falciforme was further dissected and the left lateral liver lobe was exposed on a cover slip. It then was fixed with a drop of *n*-butyl-2-cyanoacrylat (Histoacryl, B. Braun Melsungen AG, Germany) on the cover slide to avoid movements. For the analysis an inverted confocal laser scanning microscope (LSM-780, Zeiss AG, Jena, Germany) was used.

The liver architecture was visualized using the NAD(P)H/H^+ autofluorescence of hepatocytes by excitation with a laser diode at 375 to 405 nm, and collecting emitted light of 410 to 485 nm with a photomultiplier tube. Different nanoparticles containing nile red were imaged as described above. After localizing ≥3 areas of interest of each liver, different nanoparticles containing nile red were administered *via* the tail-veil catheter. Then, images were taken every 5 min to monitor kinetics. Analysis of >30 Kupffer cells or of the endothelial lining from 3 areas of interest per mouse and three mice resulted in the mean gray values shown in the table. The analysis was done at 30 min (PDMAEMA) or 60 min (PMAA) when kinetic analysis showed a plateau in the fluorescence intensity. Fluorescence analysis of nanoparticle uptake was performed with ImageJ 1.46r (NIH, MD, USA).

4.16. Statistical analysis

All results are reported as average of the performed experiments with standard error of mean (s.e.m.). All tests were performed using a significance level of 0.05. Detailed test information is stated in the figure legends. The analysis was performed using GraphPad Prism 6 software (Graphpad Software, USA).

Acknowledgment

We acknowledge funding from Carl Zeiss Foundation (Strukturantrag JCSM) (grant #0563-2.8/335/4) and the Thuringian Ministry for Education, Science and Culture (TMBWK; grants #B514-09051, NanoConSens and ProExzellence II, NanoPolar) as well as the German Federal Ministry of Education and Research (BMBF) (grants #13N13416, SmartDyeLivery) and the Center for Sepsis Control and Care for providing the LSM-780. We thank U. Vetterling for assistance with the animal experiments. This work was further supported by the European Union (ERC advanced grant to K. L. Rudolph, grant 323136 — StemCellGerontoGenes) and the State of Thuringia (FZ-12001-514).

Appendix A. Supplementary data

Supporting information available: Additional experimental section, polymerization of copolymer as well as further data regarding polymer and nanoparticle characterization, hemolysis and aggregation assay. Supplementary data associated with this article can be found, in the online version, at http://dx.doi.org/10.1016/j.jconrel.2015.08.008.

References

[1] A.Z. Wang, R. Langer, O.C. Farokhzad, Annu. Rev. Med. 63 (2012) 185–198.
[2] L. Treuel, X.E. Jiang, G.U. Nienhaus, J. R. Soc. Interface 10 (2013) 1–9.
[3] A. Lesniak, A. Salvati, M.J. Santos-Martinez, M.W. Radomski, K.A. Dawson, C. Aberg, J. Am. Chem. Soc. 135 (2013) 1438–1444.
[4] Z. Zhang, C. Wang, Y. Zha, W. Hu, Z. Gao, Y. Zang, J. Chen, J. Zhang, L. Dong, ACS Nano 9 (2015) 2405–2419.
[5] J. Voigt, J. Christensen, V.P. Shastri, PNAS 111 (2014) 2942–2947.
[6] V. Mailander, K. Landfester, Biomacromolecules 10 (2009) 2379–2400.
[7] C. Chen Weihsu, X. Zhang Andrew, S.-D. Li, Eur. J. Nanomed. 4 (2012) 89–93.
[8] M.A. Dobrovolskaia, P. Aggarwal, J.B. Hall, S.E. McNeil, Mol. Pharm. 5 (2008) 487–495.
[9] B.B. Wang, C.V. Galliford, P.S. Low, Nanomedicine 9 (2014) 313–330.
[10] J. Xie, S. Lee, X.Y. Chen, Adv. Drug Deliv. Rev. 62 (2010) 1064–1079.
[11] O.C. Farokhzad, J.J. Cheng, B.A. Teply, I. Sherifi, S. Jon, P.W. Kantoff, J.P. Richie, R. Langer, PNAS 103 (2006) 6315–6320.
[12] M.E. Davis, J.E. Zuckerman, C.H.J. Choi, D. Seligson, A. Tolcher, C.A. Alabi, Y. Yen, J.D. Heidel, A. Ribas, Nature 464 (2010) 1067–1140.
[13] A.T. Press, A. Traeger, C. Pietsch, A. Mosig, M. Wagner, M.G. Clemens, N. Jbeily, N. Koch, M. Gottschaldt, N. Beziere, V. Ermolayev, V. Ntziachristos, J. Popp, M.M. Kessels, B. Qualmann, U.S. Schubert, M. Bauer, Nat. Commun. 5 (2014) 5565.
[14] P. Aggarwal, J.B. Hall, C.B. McLeland, M.A. Dobrovolskaia, S.E. McNeil, Adv. Drug Deliv. Rev. 61 (2009) 428–437.
[15] M. Lundqvist, J. Stigler, G. Elia, I. Lynch, T. Cedervall, K.A. Dawson, PNAS 105 (2008) 14265–14270.
[16] S. Tenzer, D. Docter, J. Kuharev, A. Musyanovych, V. Fetz, R. Hecht, F. Schlenk, D. Fischer, K. Kiouptsi, C. Reinhardt, K. Landfester, H. Schild, M. Maskos, S.K. Knauer, R.H. Stauber, Nat. Nanotechnol. 8 (2013) 772–1000.

[17] S. Ritz, S. Schottler, N. Kotman, G. Baier, A. Musyanovych, J. Kuharev, K. Landfester, H. Schild, O. Jahn, S. Tenzer, V. Mailander, Biomacromolecules 16 (2015) 1311–1321.
[18] M.J. Ernsting, M. Murakami, A. Roy, S.D. Li, J. Control. Release 172 (2013) 782–794.
[19] F. Alexis, E. Pridgen, L.K. Molnar, O.C. Farokhzad, Mol. Pharm. 5 (2008) 505–515.
[20] R. Kumar, I. Roy, T.Y. Ohulchanskky, L.A. Vathy, E.J. Bergey, M. Sajjad, P.N. Prasad, ACS Nano 4 (2010) 699–708.
[21] A.C. Anselmo, S. Mitragotri, J. Control. Release 190 (2014) 531–541.
[22] N.A. Hutchins, C.S. Chung, J.N. Borgerding, C.A. Ayala, A. Ayala, Am. J. Pathol. 182 (2013) 742–754.
[23] K.S. Vellonen, M. Malinen, E. Mannermaa, A. Subrizi, E. Toropainen, Y.R. Lou, H. Kidron, M. Yliperttula, A. Urtti, J. Control. Release 190 (2014) 94–114.
[24] M. Raasch, K. Rennert, T. Jahn, S. Peters, T. Henkel, O. Huber, I. Schulz, H. Becker, S. Lorkowski, H. Funke, A. Mosig, Biofabrication 7 (2015) 015013.
[25] S.P. Samuel, N. Jain, F. O'Dowd, T. Paul, D. Kashanin, V.A. Gerard, Y.K. Gun'ko, A. Prina-Mello, Y. Volkov, Int. J. Nanomedicine 7 (2012) 2943–2956.
[26] S.H. Au, M.D. Chamberlain, S. Mahesh, M.V. Sefton, A.R. Wheeler, Lab Chip 14 (2014) 3290–3299.
[27] J. Kreuter, J. Control. Release 16 (1991) 169–176.
[28] A. Vollrath, A. Schallon, C. Pietsch, S. Schubert, T. Nomoto, Y. Matsumoto, K. Kataoka, U.S. Schubert, Soft Matter 9 (2013) 99–108.
[29] I. Perevyazko, A. Vollrath, S. Hornig, G.M. Pavlov, U.S. Schubert, J. Polym. Sci. Polym. Chem. 48 (2010) 3924–3931.
[30] S. Hornig, T. Heinze, C.R. Becer, U.S. Schubert, J. Mater. Chem. 19 (2009) 3838–3840.
[31] J.W. Nichols, Y.H. Bae, Nano Today 7 (2012) 606–618.
[32] J.M. Lee, T.J. Yoon, Y.S. Cho, Biomed. Res. Int. 782041 (2013) 1–10.
[33] J. Chiefari, Y.K. Chong, F. Ercole, J. Krstina, J. Jeffery, T.P.T. Le, R.T.A. Mayadunne, G.F. Meijs, C.L. Moad, G. Moad, E. Rizzardo, S.H. Thang, Macromolecules 31 (1998) 5559–5562.
[34] G. Moad, E. Rizzardo, S.H. Thang, Aust. J. Chem. 62 (2009) 1402–1472.
[35] A. Shalviri, H.K. Chan, G. Raval, M.J. Abdekhodaie, Q. Liu, H. Heerklotz, X.Y. Wu, Colloids Surf. B 101 (2013) 405–413.
[36] J. Brandrup, E.H. Immergut, E.A. Grulke, Polymer Handbook, 4 ed.Wiley-Interscience, 1999.
[37] S. Agarwal, Y. Zhang, S. Maji, A. Greiner, Mater. Today 15 (2012) 388–393.
[38] P. van de Wetering, E.E. Moret, N.M.E. Schuurmans-Nieuwenbroek, M.J. van Steenbergen, W.E. Hennink, Bioconjug. Chem. 10 (1999) 589–597.
[39] T. Yildirim, A.C. Rinkenauer, C. Weber, A. Traeger, S. Schubert, U.S. Schubert, J. Polym. Sci. Polym. Chem. (2015), http://dx.doi.org/10.1002/pola.27734.
[40] I.Y. Perevyazko, A. Vollrath, C. Pietsch, S. Schubert, G.M. Pavlov, U.S. Schubert, J. Polym. Sci. Polym. Chem. 50 (2012) 2906–2913.
[41] A. Vollrath, D. Pretzel, C. Pietsch, I. Perevyazko, S. Schubert, G.M. Pavlov, U.S. Schubert, Macromol. Rapid Commun. 33 (2012) 1791–1797.
[42] L. Araujo, R. Lobenberg, J. Kreuter, J. Drug Target. 6 (1999) 373–385.
[43] A. Schrade, V. Mailander, S. Ritz, K. Landfester, U. Ziener, Macromol. Biosci. 12 (2012) 1459–1471.
[44] A. Palecanda, L. Kobzik, Methods 21 (2000) 241–247.
[45] G. Baier, C. Costa, A. Zeller, D. Baumann, C. Sayer, P.H.H. Araujo, V. Mailander, A. Musyanovych, K. Landfester, Macromol. Biosci. 11 (2011) 628–638.
[46] K. Xiao, Y.P. Li, J.T. Luo, J.S. Lee, W.W. Xiao, A.M. Gonik, R.G. Agarwal, K.S. Lam, Biomaterials 32 (2011) 3435–3446.
[47] S. Lerch, M. Dass, A. Musyanovych, K. Landfester, V. Mailander, Eur. J. Pharm. Biopharm. 84 (2013) 265–274.
[48] M. Luck, B.R. Paulke, W. Schroder, T. Blunk, R.H. Muller, J. Biomed. Mater. Res. 39 (1998) 478–485.
[49] M.A. Dobrovolskaia, S.E. Mcneil, Nat. Nanotechnol. 2 (2007) 469–478.
[50] R.A. Petros, J.M. DeSimone, Nat. Rev. Drug Discov. 9 (2010) 615–627.
[51] E.C. Cho, Q. Zhang, Y.N. Xia, Nat. Nanotechnol. 6 (2011) 385–391.
[52] E. Berthier, E.W.K. Young, D. Beebe, Lab Chip 12 (2012) 1224–1237.
[53] A.M. Malek, S.L. Alper, S. Izumo, JAMA-J. Am. Med. Assoc. 282 (1999) 2035–2042.
[54] C. Cheng, F. Helderman, D. Tempel, D. Segers, B. Hierck, R. Poelmann, A. van Tol, D.J. Duncker, D. Robbers-Visser, N.T.C. Ursem, R. van Haperen, J.J. Wentzel, F. Gijsen, A.F.W. van der Steen, R. de Crom, R. Krams, Atherosclerosis 195 (2007) 225–235.
[55] H. Yang, F.L. Zhao, Y. Li, M.M. Xu, L. Li, C.H. Wu, H. Miyoshi, Y.Y. Liu, Int. J. Nanomedicine 8 (2013) 1897–1906.
[56] A. Lin, A. Sabnis, S. Kona, S. Nattama, H. Patel, J.F. Dong, K.T. Nguyen, J. Biomed. Mater. Res. A 93 (2010) 833–842.
[57] Y. Kim, P. Rajagopalan, PLoS ONE 5 (2010).
[58] D. Alizadeh, L.Y. Zhang, J. Hwang, T. Schluep, B. Badie, Nanomed. Nanotechnol. 6 (2010) 382–390.
[59] S.W. Provencher, Comput. Phys. Commun. 27 (1982) 229–242.
[60] H. Ohshima, J. Colloid Interface Sci. 168 (1994) 269–271.
[61] E.A. Jaffe, R.L. Nachman, C.G. Becker, C.R. Minick, J. Clin. Invest. 52 (1973) 2745–2756.
[62] R.I. Sherwood, J.L. Christensen, I.M. Conboy, M.J. Conboy, T.A. Rando, I.L. Weissman, A.J. Wagers, Cell 119 (2004) 543–554.
[63] M. Cerletti, S. Jurga, C.A. Witczak, M.F. Hirshman, J.L. Shadrach, L.J. Goodyear, A.J. Wagers, Cell 134 (2008) 37–47.

Supporting Information

Microfluidically-supported cell culture as bridge between *in vitro* and *in vivo* investigations of well-defined nanoparticle libraries.

Alexandra C. Rinkenauer,[1,2,#] Adrian T. Press,[2,3,#] Martin Raasch,[3,4] Christian Pietsch,[1] Simon Schweizer,[1] Simon Schwörer,[2,5] Karl L. Rudolph,[2,5] Alexander Mosig,[2,3,4] Michael Bauer,[2,3] Anja Träger,[1,2] Ulrich S. Schubert [1,2]**

[1]Laboratory of Organic and Macromolecular Chemistry (IOMC), Friedrich Schiller University Jena, Humboldtstrasse 10, 07743 Jena, Germany

[2]Jena Center for Soft Matter (JCSM), Friedrich Schiller University Jena, Philosophenweg 7, 07743 Jena, Germany

[3]Center for Sepsis Control and Care (CSCC), Jena University Hospital, Erlanger Allee 101, 07747 Jena

[4]Institute of Biochemistry II, Jena University Hospital, Friedrich Schiller University Jena, Nonnenplan 2, 07743 Jena, Germany

[5]Leibniz Institute for Age Research, Fritz Lipmann Institute Jena, Beutenbergstrasse 11, 07745 Jena, Germany

[#]authors contribute equally to this work

*Address correspondence to: ulrich.schubert@uni-jena.de; anja.traeger@uni-jena.de

1 Polymerizations

Table S 1: Overview of the selected RAFT polymerization conditions.

Polymer sample	Feed ratio [a] MMA/MAA	Feed ratio CPDB/AIBN	m in g MMA	MAA	CPDB	AIBN	time [h]
PMMA	100/0	1/0.25	6.007	0	0.1328	0.0246	13
P(MMA-*co*-MAA)	97/3	1/0.25	5.827	0.155	0.1328	0.0246	13
P(MMA-*co*-MAA)	95/5	1/0.25	5.707	0.258	0.1328	0.0246	13
P(MMA-*co*-MAA)	92.5/7.5	1/0.25	5.557	0.387	0.1328	0.0246	13
P(MMA-*co*-MAA)	90/10	1/0.25	5.406	0.516	0.1328	0.0246	13
P(MMA-*co*-DMAEMA)	80/20	1/0.25	4.806	1.033	0.1328	0.0246	12.5

[a] Molar ratio in the polymer feed solutions between MMA and MAA or DMAEMA.

1.1 Polymer characterization:

SEC chromatograms and ^{1}H NMR spectra of the final copolymers.

PMMA:

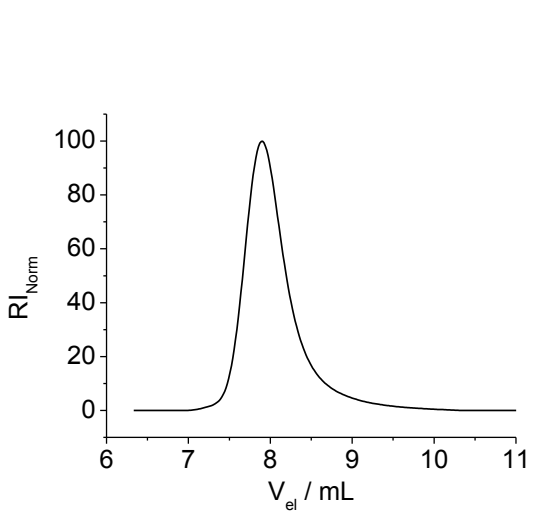

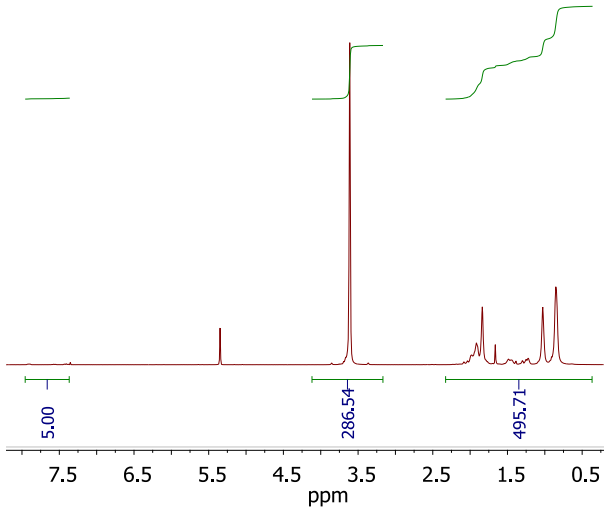

3% PMAA:

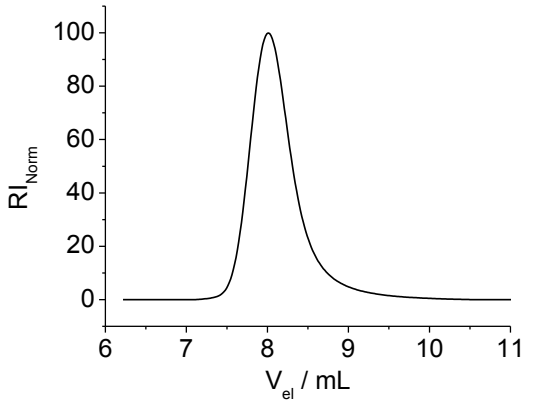

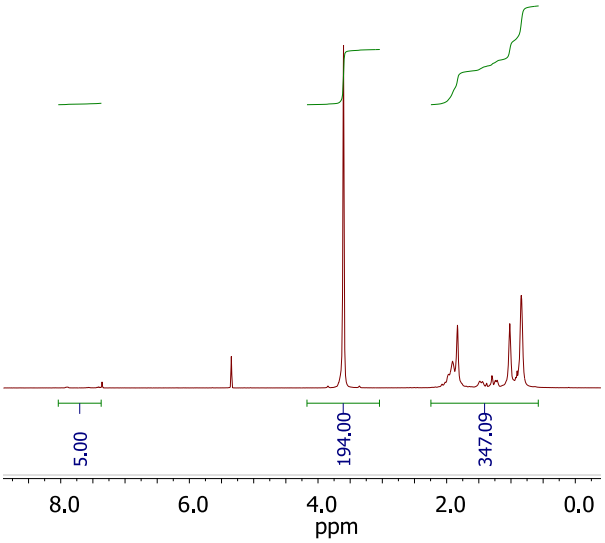

5% PMAA:

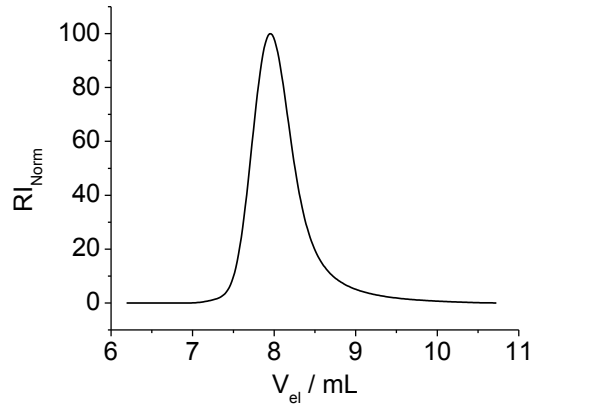
100
80
60
40
20
0
RI Norm
6
7
8
9
10
11
V el / mL

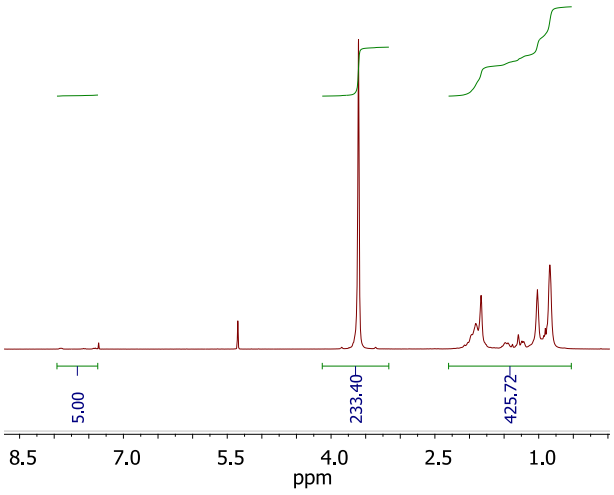
5.00
233.40
425.72
8.5
7.0
5.5
4.0
2.5
1.0
ppm

8% PMAA:

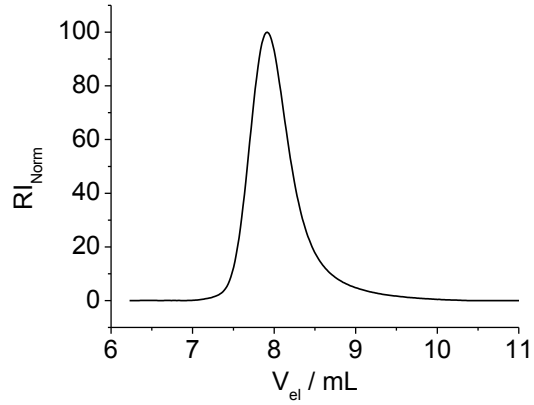
100
80
60
40
20
0
RI Norm
6
7
8
9
10
11
V el / mL

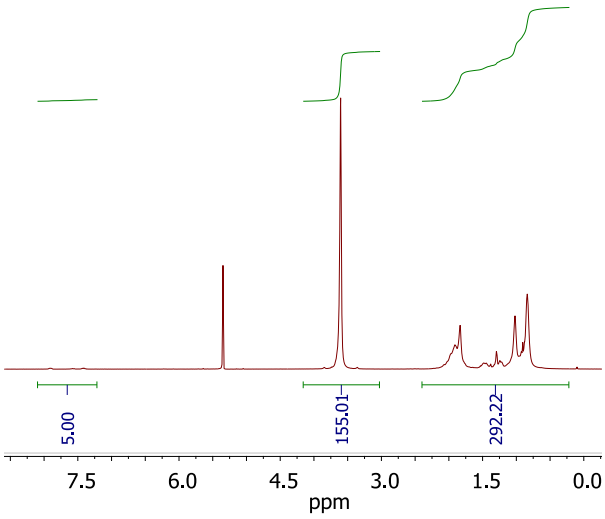
5.00
155.01
292.22
7.5
6.0
4.5
3.0
1.5
0.0
ppm

13% PMAA:

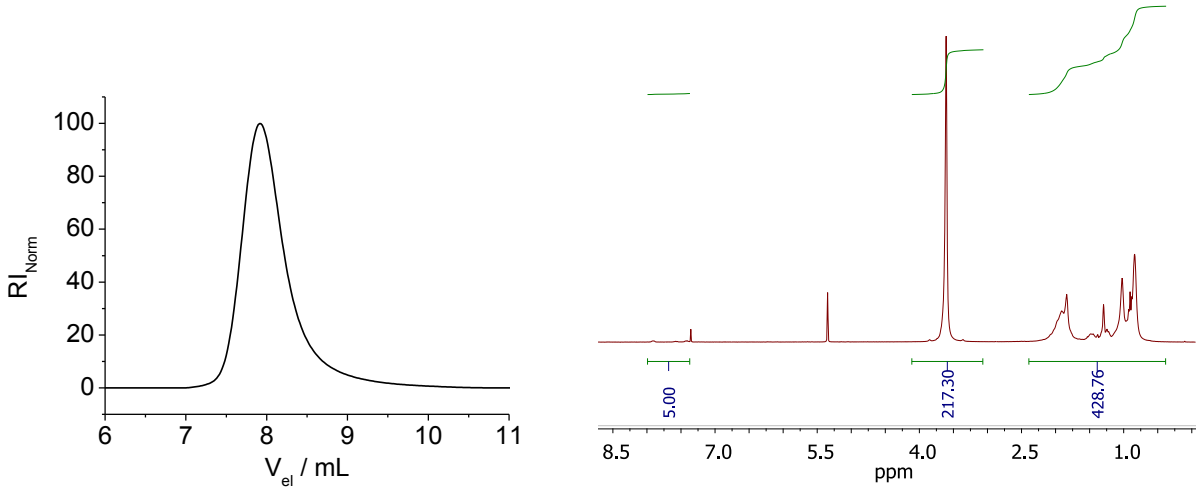

20% PDMAEMA:

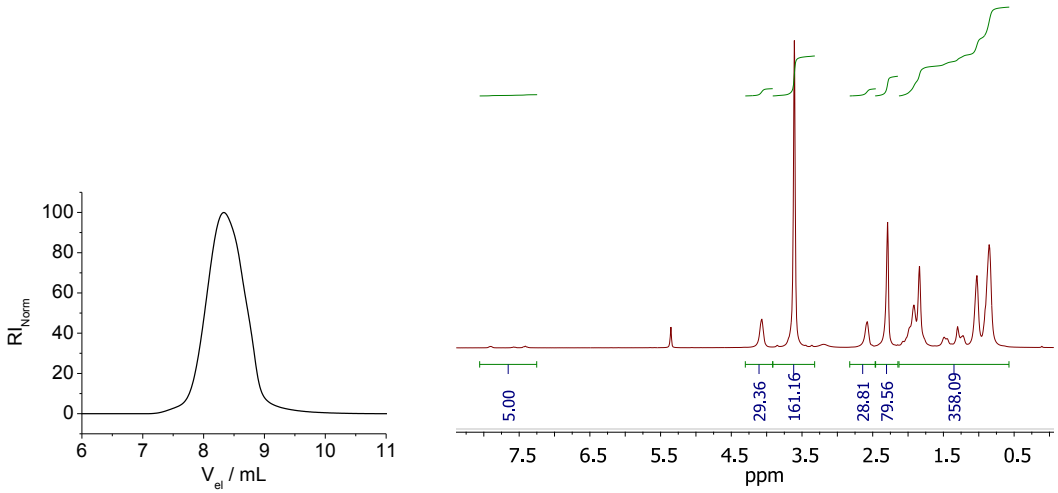

Figure S 1: SEC chromatograms and ^{1}H NMR spectra's of the final copolymers. The homopolymer PMMA was used as reference (adjustment of the broad backbone integral from 0.5 to 2.5 ppm to exclude impurities like water) and all spectra were corrected with this ratio between –OCH_3 and the backbone signal of PMMA (correction factor 0.964).

2 Nanoparticle characterization

Table S 2: Zeta potential of methacrylate-based nanoparticles with concentrations of 50 µg mL^{-1} in type 1-water.

Nanoparticle	Zeta potential [mV]
3% PMAA	– 43.3
5% PMAA	– 32.7
8% PMAA	– 32.5
13% PMAA	– 38.3
20% PDMAEMA	+ 31.3

Figure S 2: DLS curves of methacrylate-based nanoparticles with concentrations of 50 µg mL^{-1} in type 1-water.

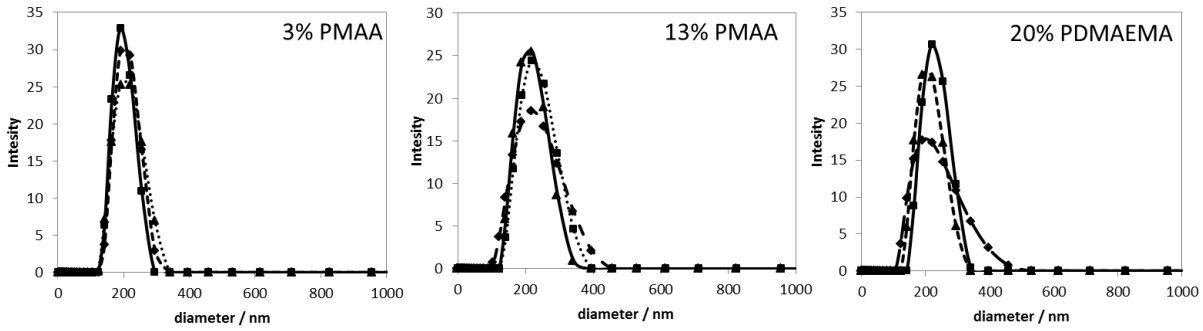

2.1 SDS-PAGE of nanoparticle incubated in serum containing media

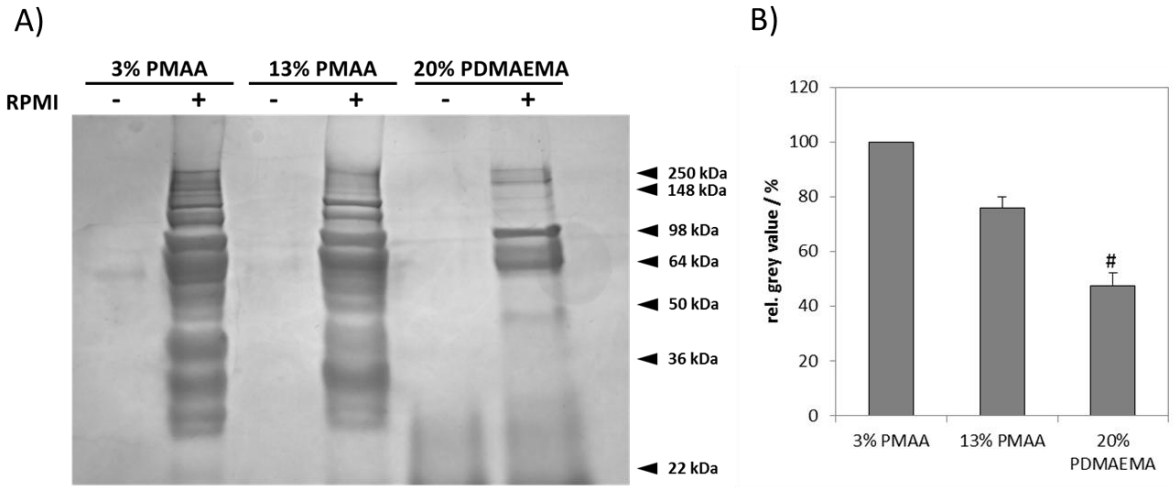

Figure S 3: ***In vitro*** **investigation of protein binding to nanoparticles. SDS-PAGE of serum proteins bound to nanoparticles and densitometric analysis of total protein binding revealed a trend of lower protein binding to 13% PMAA and 20%DMAEMA compared to 3%PMAA. Bars show mean + s.e.m of three independent experiments, significance tested using Kruskal-Wallis and Dunn's multiple comparison test,** $^{\#}p<0.05$.

2.2 Diameter and PDI of different nanoparticle batches

Table S 3: Nanoparticle batches containing nile red. Size and PDI_P **are determined by DLS. The applied correction factors are given.**

polymer	diameter / nm	PDI_P	correction factor
3% PMAA	206	0.099	0.49
3% PMAA	215	0.081	0.32
13% PMAA	188	0.064	1
13% PMAA	183	0.039	0.8
20% PDMAEMA	209	0.122	0.64
20% PDMAEMA	186	0.1	0.5

2.3 Correlation of SSC/FSC using nile red.

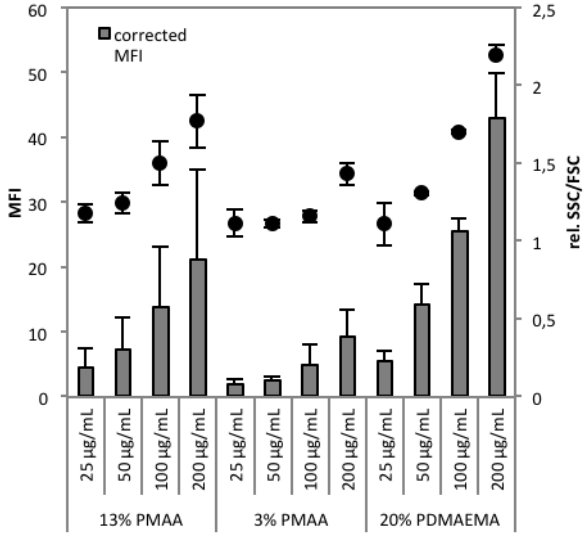

Figure S 4: Correlation of the uptake of methacrylate-based nanoparticle using rel. SSC/FSC and the corrected mean fluorescence intensity (MFI). HEK293 cells were incubated in media containing serum proteins for 24 h. Values represent the mean of three independent experiments ± SD.

2.4 Hemolysis and aggregation

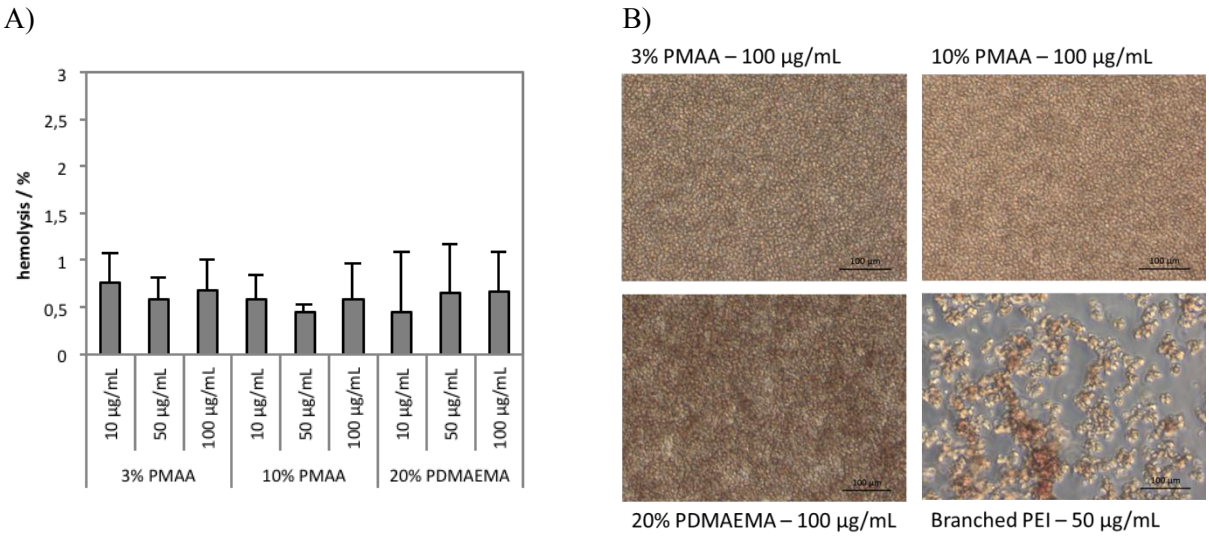

Figure S 5: Hemolysis and aggregation assay of the methacrylate-based nanoparticles.

2.5 Uptake investigations of methacrylate-based nanoparticles under static conditions

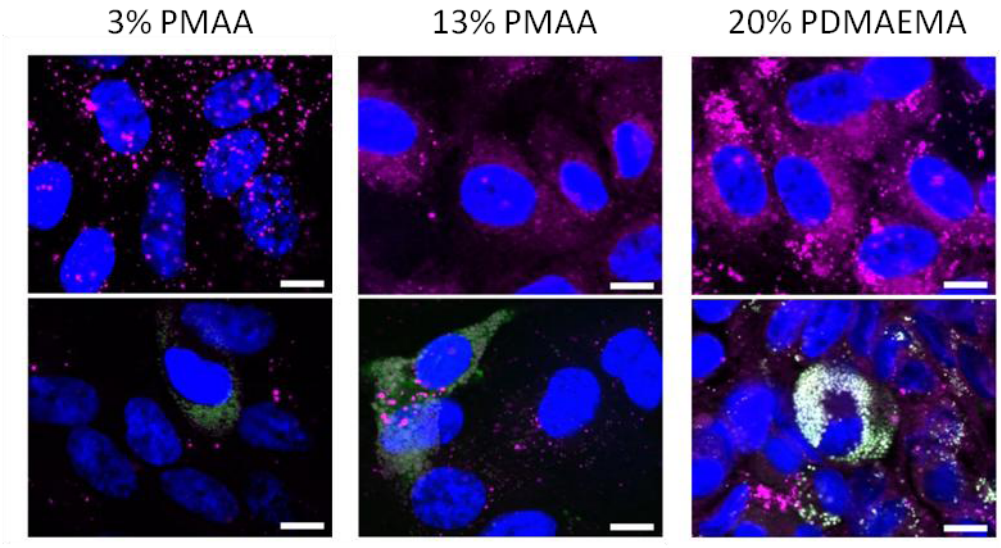

Figure S 6: Different nanoparticles in the microfluidically-assisted cell culture. Uptake of different nanoparticles containing nile red in a HUVEC monoculture or a co-culture with MΦ which were analyzed after 60 min. Uptake and distribution of different nanoparticles (purple) in the HUVEC monoculture (upper panels) and co-culture (lower panels) with MΦ. Cells were subsequently stained with DAPI (blue) and macrophages were stained using CMFDA (green). All scale bars = 10 µm.